DOE/NASA/0125-1
NASA CR-165480
ERC TR-8101

AC Propulsion System for an Electric Vehicle

Phase 1 Final Report

Steven Geppert
Eaton Corporation
Engineering & Research Center

August 1981

Prepared for
NATIONAL AERONAUTICS AND SPACE ADMINISTRATION
Lewis Research Center
Under Contract DEN 3-125

for
U.S. DEPARTMENT OF ENERGY
Conservation and Renewable Energy
Office of Vehicle and Engine R&D

NOTICE

DOE/NASA/0125-1
NASA CR-165480
ERC TR-8101

AC Propulsion System for an Electric Vehicle

Phase 1 Final Report

Steven Geppert
Eaton Corporation
Engineering & Research Center
Southfield, Michigan 48037

August 1981

Prepared for
National Aeronautics and Space Administration
Lewis Research Center
Cleveland, Ohio 44135
Under Contract DEN 3-125

for
U.S. DEPARTMENT OF ENERGY
Conservation and Renewable Energy
Office of Vehicle and Engine R&D
Washington, D.C. 20545
Under Interagency Agreement DE-AI01-77CS51044

ACKNOWLEDGEMENT

The following people made major contributions to this report:

M. P. Bujold
D. Gritter
M. R. Hoffmann
M. P. Jacobs
C. James
I. Kalns
D. C. Pasma
J. M. Slicker

TABLE OF CONTENTS

TABLE OF CONTENTS

LIST OF FIGURES

LIST OF FIGURES

LIST OF FIGURES

LIST OF FIGURES

LIST OF FIGURES

LIST OF FIGURES

LIST OF FIGURES

LIST OF FIGURES

LIST OF FIGURES

1. SUMMARY

The object of this program was to develop and test a functional prototype of an ac propulsion system for an over-the-road electric vehicle. It was designed and fabricated "from the ground up." The system consists of a two-speed, mechanically-shifted (hydraulic clutches) automatic transaxle, an 18.65 kw (25 hp) rated ac traction induction motor, a pulse-width-modulated (PWM) transistorized inverter, and an overall microprocessor-based vehicle/drive controller. It was shipped to LeRC September 2, 1980, where it will undergo further testing and evaluation on the Road Load Simulator.

The system is sized to allow a 1450 kg (3200 lb.) GVW vehicle to meet SAE J227a/D cycle and achieve a level road speed of 105 km/hr (65 mph). Prototype system weight is 185 kg (407 lb.). Design considerations and major developmental problems and solutions are described for each component. Both hardware and software descriptions are included.

Efficiency and performance test results for each system component are given. Technical feasibility is clearly demonstrated in meeting performance requirements. Overall system efficiency and performance tests, carried out on an instrumented test frame in both metering and regenerative modes, are described. A peak dc-to-mechanical system efficiency of 82% was achieved, and an average efficiency (based on total mechanical output energy/net inverter input energy) over the SAE 227a/D cycle of 79% was deduced from steady-state performance data. No attempt was made to mount this first generation system in a vehicle.

Although the emphasis of the work was hardware and software development and testing, several related areas were addressed. Computer models for the inverter, motor and representative vehicle fitted with the system were developed. Where possible, correlation tests between model and experiment were run. Overall agreement was good. The models can act as tools to further optimize system design. Examples of this design function are given, along with model descriptions and results.

A preliminary reliability model and failure-modes-criticality analysis are given. Reliability and maintainability goals are stated which are in keeping with the consumer requirement of a low service vehicle. Present predicted reliability does not meet the goal, and very careful packaging and diagnostic design will be needed to meet the maintainability goal in a production system. These goals impact hardest on the inverter, and it is this component which presents the main challenge.

Component and life cycle cost estimates are given. These estimates are rough due to the early stage of the design and due to the uncertainty of future inverter power transistor cost, which is a major factor in system cost. With $40.00 transistors and system annual production of 10,000 units, original equipment

manufacturer (OEM) system cost is estimated at $2320 and life cycle cost at $0.023/km (batteries not included, 1980 dollars).

The work was performed under NASA-Lewis Research Center (LeRC) Contract DEN3-125, from March 7, 1979, through February, 1981.

2. INTRODUCTION

2.1 Background

In early 1977, the Engineering & Research Center of Eaton Corporation began exploring new product opportunities for over-the-road vehicles with alternate power sources. The impetus was the growing importation cost of and risky dependence upon foreign petroleum in the United States, and the realization that in dealing with an entrenched, vast, complicated, and oil-dependent transportation system, any significant substitution demands very long lead times for orderly, evolutionary change. Petroleum is a finite resource, and as increasing scarcity drives the price up, more cost-effective means of personal transportation should be made available. Natural and synthesized liquid and gaseous fuels will be available for the foreseeable future. The internal combustion engine will continue to dominate for many years. But the technology and infrastructure for vehicles such as electric vehicles not dependent upon petroleum should be developed while the need is not urgent.

We concluded among alternative power sources--several novel and intriguing--that the electric option held significant growth potential in fulfilling certain transportation needs. It also became evident that economic and political forces were building support for an electric vehicle (EV) industry.

Commuting and shopping represents a large percentage of the total personal vehicle miles driven. The range requirements are in line with near-term battery technology. A practical EV serving a part of this transportation need would be an excellent first step in providing a personal transportation option. Even limited consumer acceptance (less than 5% of annual personal vehicle sales) would represent around half a million units per year in the United States alone. Although such penetration would not significantly reduce national oil consumption, it would provide the foundation for substantial market share as EV prices fall with production volume and experience, petroleum fuel prices continue to rise, and EV performance improves. The initially small penetration could still be good business for EV component suppliers. For these reasons, the study recommended that Eaton concentrate its development effort on an electric drive system serving the urban-suburban small commuter car market.

Through 1977, many propulsion concepts, both ac and dc, and possible electric and hybrid configurations were evaluated. Numerous existing experimental EV's were studied. By late 1977, the ac propulsion system concept took shape. The system was aimed at the post-1985 market, since its

refinement and cost reduction would take at least six years. Moreover, the present "market" was negligible.

During 1978, Eaton conceived the detailed designs for the induction motor, the power inverter, and the controller. A two-speed transaxle layout was decided upon after extensive study of alternatives. By the end of 1978, the motor was being fabricated at the Eaton Industrial Drives Operation, the controller hardware and first-cut software were completed, and tests on one leg of the inverter were underway in the laboratory. Transaxle design was in progress.

In mid 1978, Eaton presented the concept to the NASA-Lewis Research Center (LeRC). LeRC, as the administering arm to DOE for EV propulsion system and component development (under Public Law 94-413-1976, "Electric and Hybrid Vehicle Research, Development, and Demonstration Act of 1976"), expressed an interest in supporting the completion and testing of the ac propulsion system. The resultant contract effort commenced March 7, 1979. This report covers the work done under this contract.

2.2 Purpose of Project

The primary purpose of the contracted effort was to prove technical feasibility of the Eaton ac propulsion system concept through prototype construction and dynamometer testing on an instrumented test frame.

2.3 Scope of Project

Upon entering the contract, all components in the system were well along in design or actual hardware. The contract accelerated the effort to complete the functional prototype hardware. One complete system was built. Developmental and performance testing were major tasks. Subsidiary tasks included initial cost, reliability, maintainability, and computer modeling/simulation work.

2.4 Testing Overview

The testing approach consisted of three levels. Firstly, the transaxle, motor, inverter, and controller were each tested individually for function and efficiency. Secondly, the electrical subpackage (motor, inverter, and controller) was tested and debugged on a dynamometer test stand. Finally, the complete system was fitted to a special test frame for refinement and overall efficiency testing. Hardware and software improvements were continually being made throughout the test phases. The test frame with the system was delivered to LeRC for testing on the Road Load Simulator facility.

3. SYSTEM OVERVIEW

3.1 System Concept

It was decided at the outset that the Eaton system should advance vehicle traction drive technology, since product introduction would be at least six years away. Thus, an approach was selected which had long-term potential for vehicle traction. For consumer vehicles, the primary criteria are weight, efficiency, cost, size, ruggedness, and maintainability. Weighing these factors, and considering the favorable price trend of power electronic devices, the following major technical decisions were reached:

1. The drive would use a three-phase ac induction motor.

2. The inverter (converts battery dc current to motor ac current) would use transistors as the main switching devices.

3. The inverter would use the pulse-width modulation (PWM) technique for motor voltage control.

4. A two-speed transaxle assembly would provide a direct mechanical link from motor shaft to vehicle drive wheels. The shift would be automatic to prevent driver abuse and increase customer acceptance.

5. The controller would handle all aspects of the vehicle-motor control: shift commands, operator inputs, monitor functions, and regenerative braking.

6. The propulsion system would be independent of battery type. As long as the battery (or fuel cell) could provide a voltage and current within rather wide limits, the system would work. This requirement was deemed necessary in light of the battery advancements predicted.

7. The system would be sized for a small, all-electric car. Installation flexibility was important in order to allow fitting to a range of body designs.

8. All components would be considered together as a propulsion system, since optimum overall performance is then most likely to result.

References 1 and 2 expand on this system justification. A system block diagram is shown in Figure 3.1.1.

3.2 Component Specifications

Figure 3.2.1 lists the primary specifications for each component. Figure 3.2.2 is a photograph of the system shown with axle stubs. No attempt was made to package the inverter for minimum size and vehicle installation.

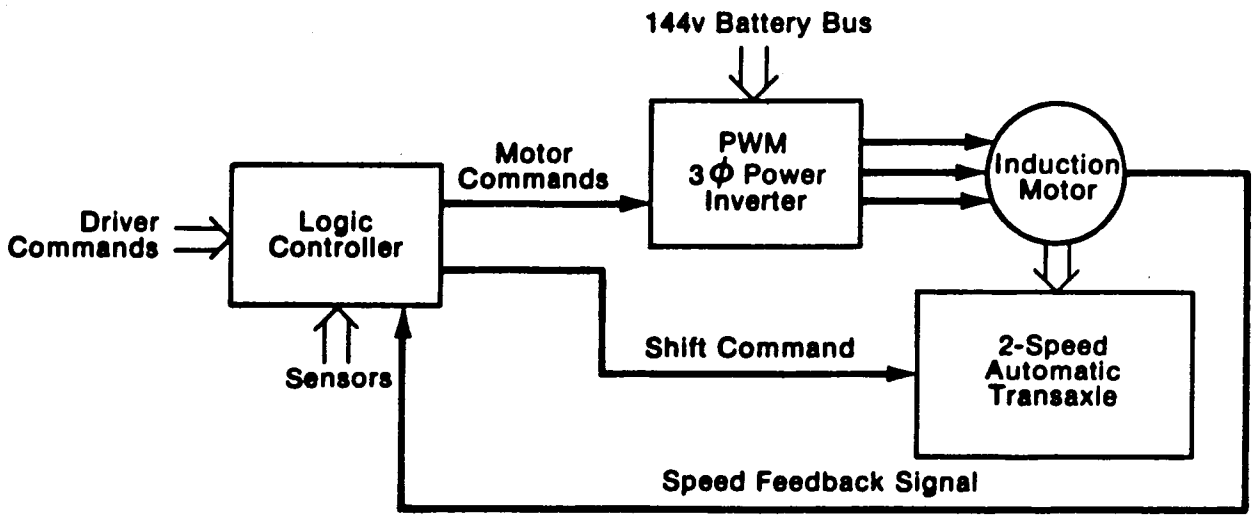

Figure 3.1.1 System Block Diagram

FIGURE 3.2.1
PRIMARY SYSTEM SPECIFICATIONS OF ENGINEERING DEVELOPMENT PROTOTYPE

TRANSAXLE

Input Power: 18.6 kw (25 hp) continuous (motoring or regen.)
33.6 kw (45 hp) intermittent
Max. Input Speed: 9000 rpm
Max. Input Torque: 54.2 Nm (40 lb.-ft.)
Reduction Ratios:
Morse Hy-VO® Chain Drive: 2.52:1
Planetary Gear: 2.4:1 Low
1:1 High
Final Drive Gear: 3.26:1 1360 kg (3000 lb.) vehicle
3.67:1 1815 kg (4000 lb.) vehicle
Overall Ratios:
Low Gear: 19.7:1 1360 kg vehicle
22.1:1 1815 kg vehicle
High Gear: 8.22:1 1360 kg vehicle
9.25:1 1815 kg vehicle
Max. Output Speed: 1095 rpm
Max. Output Torque: 1221 Nm (900 lb.-ft.) total
Weight incl. Pump, Valves, Oil: 48 kg (106 lbs.)
Design Life: 4000 hrs. (160,000 km)
Width (overall with motor): 55.2 cm (21.7 in.)
Width (axle flange to axle flange): 22.3 cm (8.8 in.)
Shift Means: Automatic with Two Hydraulic Clutch Packs
Case Material: Aluminum or Magnesium (prototype is aluminum)
Hydraulic System:
Pressure: 10.3 bar (150 psi) max.
Pump Power: 0.25 kw (1/3 hp)
Capacity: 3.8 l (4 qts.)
Fluid: GM Dexron II

MOTOR

Type: AC induction traction
Rating: 18.6 kw (25 hp) for one hour at base freq. and above
33.6 kw (45 hp) for two minutes at base frequency
29.8 kw (40 hp) for two minutes at max. frequency
Phases: 3
Poles: 2
Base Frequency: 94 Hz (5640 rpm nominal)
Max. Frequency: 150 Hz (9000 rpm nominal)
Voltage at Base Frequency: 100 vrms line-line
Design: Compatible with PWM inverter with up to 2 kHz equivalent switching rate. Nominal 144 v dc bus.
Frame: NEMA 180 special with face mounting AJ. Totally enclosed.
Diameter: 20 cm (8 in.)
Overall Length: 53.3 cm (21 in.)
Cooling: Oil flow over stator windings (oil also lubricates bearings) 0.03 l/sec.
Materials:
Rotor Bars: Aluminum
Stator Windings: Copper with Class H Insulation
Laminations: Transformer Silicon Steel
Case: Steel (first prototype)
Ambient Temperature: -40° to +45°C
Weight: 66.8 kg (147 lb.) (first prototype)

FIGURE 3.2.1 (continued)

INVERTER

Type: PWM transistorized, 3 phase. 300v, 400a monolithic Darlingtons
Rating: 30 kw. Current limited to lower power at slow speed
Bus Voltage: 94 to 160 volts dc
Protection: Transistor interlock within a phase leg
Power-up base drive inhibit
Back diode current sense
High-speed Hall-effect current sensors on each phase
High temperature sensor cutout
Overvoltage cutout
Isolation: Controller switching commands opto-coupled to local base drive logic
Cooling: Forced air over extruded aluminum heat sinks
Max. Equivalent Switching Rate: 2 kHz

CONTROLLER

Type: Microprocessor-based, slip control scheme. PWM voltage control strategy.
Inputs: Driver accel/decel demand
Motor speed
Bus voltage
Bus current
Battery pack temperature
Motor case temperature
Transistor heat sink temperature
Diagnostic control
Outputs: Inverter switching command signals
Gearshift command
Alarm warn and shutdown
Diagnostic readouts
Sample Data Rate: 38 Hz (except slip control response bandwidth)
Slip Control Bandwidth: Greater than 100 Hz

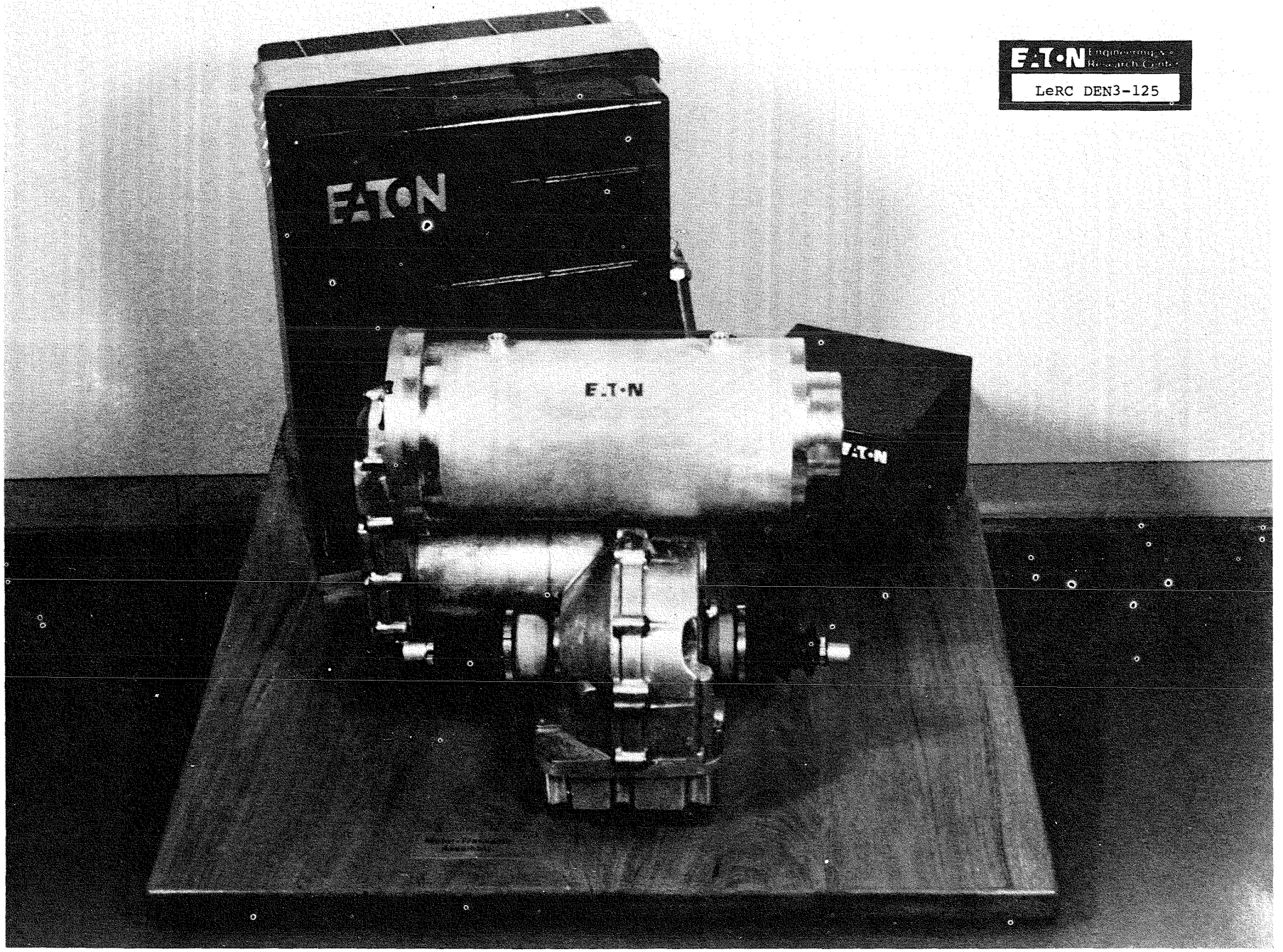

Figure 3.2.2 Prototype ac Propulsion System

A weight summary is given in Fig. 3.2.3. Total prototype system weight is 185 kg (407 lb.). The estimated production weight of 146.5 kg (322 lb.) is considered readily attainable with no exotic packaging or materials.

	First Functional Prototype	Product Version (est.)
Transaxle w/oil, pump, pump motor, hoses, external valves	48.0 kg (106 lbs.)	39.0 kg (86 lbs.)
Motor	67.0 kg (147 lbs.)	55.0 kg (121 lbs.)
Inverter w/enclosure	60.0 kg (131 lbs.)	45.0 kg (99 lbs.)
Controller	7.5 kg (17 lbs.)	5.0 kg (11 lbs.)
Motor and Misc. Cables	2.5 kg (5.5 lbs.)	2.5 kg (5.5 lbs.)
TOTALS	185.0 kg (407 lbs.)	146.5 kg (322 lbs.)

Fig. 3.2.3 AC Propulsion System Component Weight Data

4. TRANSAXLE

4.1 Design

The transaxle assembly, in addition to its basic function of transmitting mechanical power from the ac motor to the driving axles of the vehicle, also serves as structural support for the motor and a cooling means for much of the motor's rejected heat.

The transaxle is a two-speed, powershifted mechanical automatic, consisting of a chain drive reduction, a planetary gear and clutch assembly, a final drive gearset, a differential head assembly, and a hydraulic control system. A schematic of the powertrain is shown in Figure 4.1.1. A photograph of an assembly of the transaxle's internal components is shown in Figure 4.1.2.

Mechanical System

The chain drive reduction between the ac motor and the two-speed planetary transmission features a Morse Hy-Vo Lite(R) chain. It was selected for its high efficiency, low noise, compact design, low weight and cost (compared to gears spanning the same shaft center distance). Also, the reduction ratio is easier to select and so is the center distance (to accommodate a larger motor, for instance) by substituting an alternate chain housing. The chain drive is also less sensitive to component deflections and permits somewhat wider manufacturing tolerances.

The design details of the chain drive components were worked out in cooperation with application engineers from Morse Chain Division of Borg-Warner Company. The initial set of prototype parts has performed very satisfactorily throughout all tests.

The two-speed planetary gearset is a variation of the popular Ravigneaux arrangement. Referring to Figure 4.1.1, in high gear, the gearset is locked up (no relative motion within the carrier) by the "high" clutch which locks the input shaft to the output (carrier). In low gear, the larger sun gear is grounded by the low clutch, the smaller sun gear is driving, with the carrier the output, for a reduction ratio of 2.4:1. (See Appendix C for details on Ratio Determination.) The gearset and most clutch components were adapted from a current production car automatic transmission (GM's 180) with minor modifications such as improved lubrication of carrier bearings for continuous running in low ratio. The number of clutch plates in each disk clutch was increased in order to lower the operating apply pressures and reduce specific energy input to the plates during transient shifts. The gearset is designed to have adequate strength for input torque of

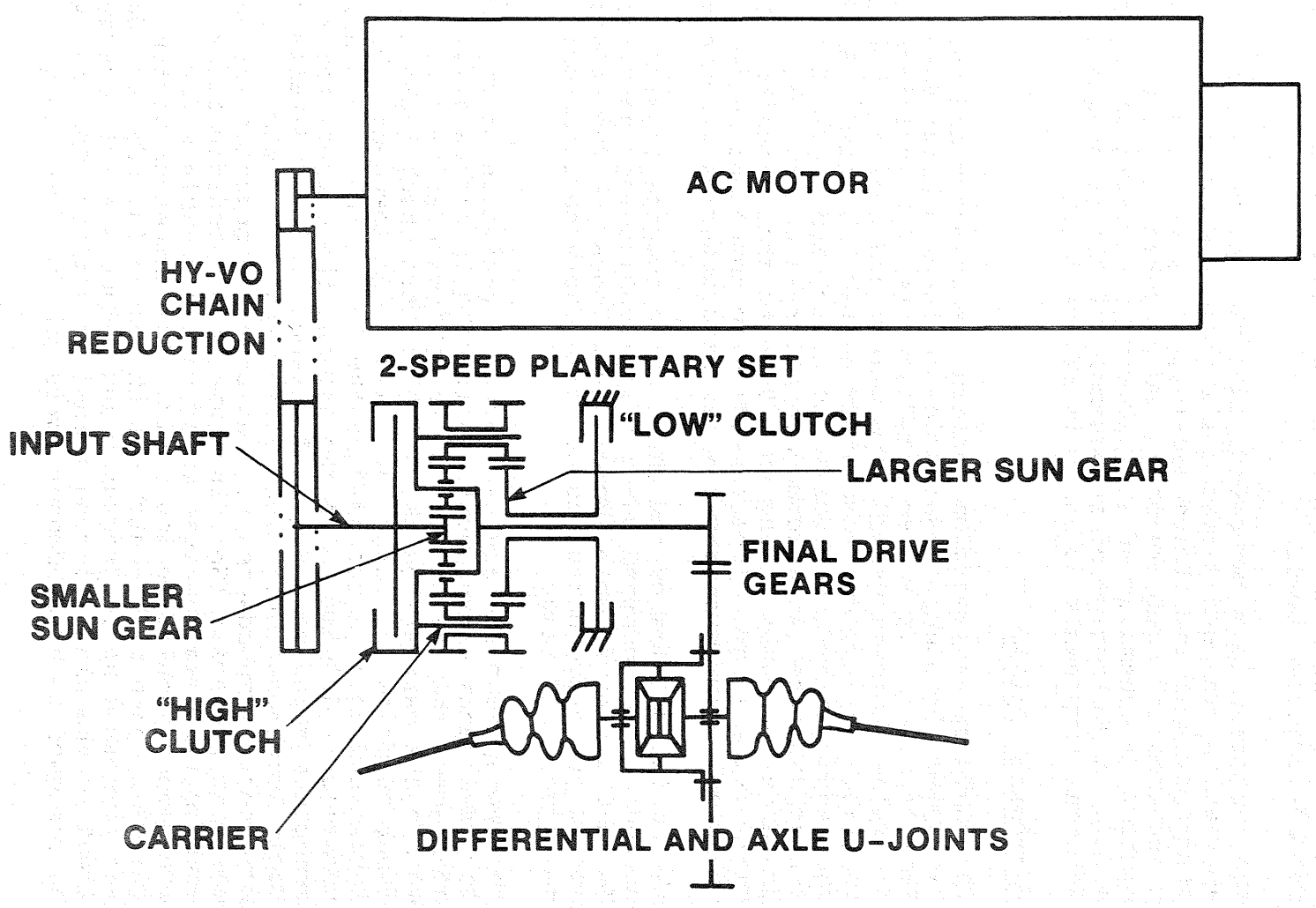

Figure 4.1.1. Drivetrain Schematic

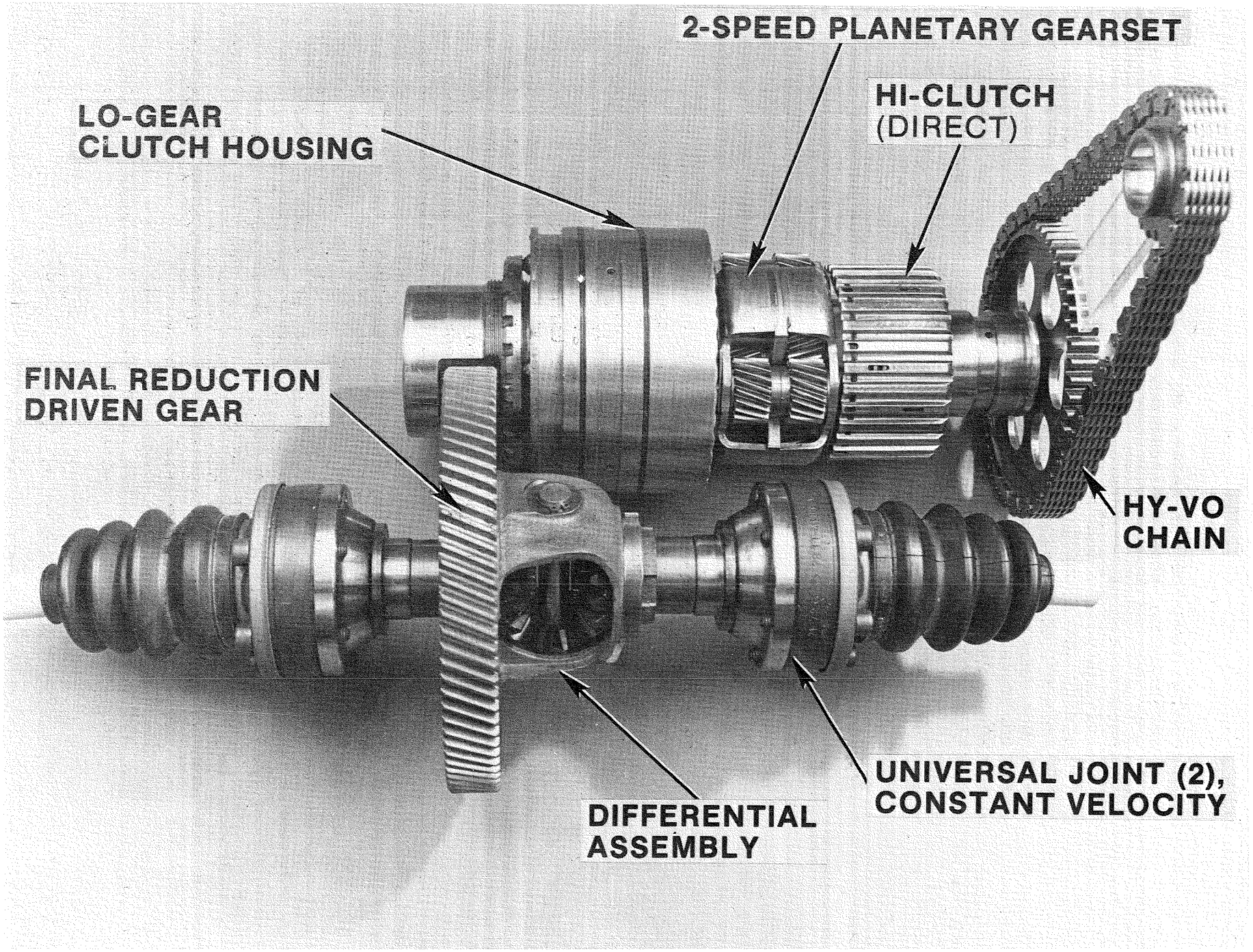

Figure 4.1.2 Internal Components of the Transaxle

352 Nm (260 lb-ft); hence, it has considerable over-capacity for this application.

Both disk clutches are oil pressure-applied. It was initially intended to have the low clutch applied by spring force and released by oil pressure. This would reduce pump power demand in low gear, provide a come-home gear in case of hydraulic failure, and also simplify controls. However, a study of failure modes revealed an unacceptable condition: namely, a hydraulic failure at high vehicle speeds in high gear would cause a downshift into low and subsequent excessive motor overspeed. Therefore, the final design uses oil pressure to apply both high and low clutches.

The disk packs of both clutches have performed very satisfactorily without a single failure or deterioration in performance through many inadvertent, harsh shifts during controls development testing. Clutch apply pressure presently used is 3.10-3.45 bar (45-50 psi); this provides a 50% safety margin over those pressures at which the clutches were slipped under static torque load.

The final reduction gearset is helical. Two discrete ratios are presently available, depending on gross vehicle weight. The higher reduction ratio of 3.67:1 favors the gradeability of a 1810 kg (4000 lb) vehicle at the expense of somewhat reduced maximum speed, 96 km/h (60 mph). The lower ratio of 3.26:1 provides favorable characteristics for a 1360 kg (3000 lb) vehicle throughout its performance spectrum. The gears were designed for minimum weight. For example, a 20.3 cm (8 in.) diameter bull gear weighs 1.8 kg (4 lbs). A B-10 surface durability fatigue life in excess of 5000 hrs was calculated, at rated load and speed. Bending stresses were kept below the endurance limit of the gear materials, SAE 8620 steel, carburized.

The differential head assembly is adapted without any modifications from the production transaxle of the Ford Fiesta. Its sufficient load capacity and low weight were the reasons for the selection. The differential assembly has not been used in testing, however, since a single output was desired for convenience in dynamometer installation. A solid shaft with an integral flange supporting the final reduction driven gear was substituted for the differential head assembly. The weight, inertia and drag of the substitute solid shaft closely approximate those of the differential assembly.

All bearings were sized to provide a B-10 life of over 5000 hrs. at rated load and speed.

The transaxle housing design incorporates features that make it particularly suitable for installation in electric

vehicles, where shape and size constraints are more varied and severe. The motor-supporting chain housing can be indexed about the centerline of the driven sprocket from nearly upright to an almost horizontal position, thus providing considerable flexibility in fitting the assembly into a confined space of a vehicle chassis. The two extreme locations of the motor relative to the transaxle assembly are illustrated in Figures 4.1.3 and 4.1.4. Three other intermediate positions at 20-degree increments are optional.

The housing design can also be modified to accept a motor by replacing two relatively inexpensive castings--the chain housing and its cover, plus a longer Hy-Vo® chain. The remainder of the transaxle assembly would be unaffected.

The five housing castings are A 356-T6 aluminum and weigh a total of 12.7 kg (28 lbs), machined.

Hydraulic System

The hydraulic system performs the clutch actuation functions and provides lube and cooling flow to the motor and transaxle.

A small 12 V dc motor drives a gear pump, generating 4.1 bar (60 psi) pressure. Oil flow beyond that required for the clutches is directed to the lube and cooling circuits. A schematic of the hydraulic circuit is shown in Figure 4.1.5.

An independently driven pump was chosen over a conventional, transmission input shaft-driven pump for the following reasons:

- substantial pumping power loss is avoided at high input speeds
- cooling of traction motor is provided after vehicle is stopped, if necessary
- pump-reversing is avoided when traction motor is reversed.

The hydraulic controls were breadboarded externally for flexibility during development. The development of a minimal hydraulic system compatible with ac motor characteristics and the electronic speed and power control system is expected to extend well into the vehicle testing phase. Vehicle startability, inching control and transient shift quality at different load and speed combinations will be fully addressed at that time.

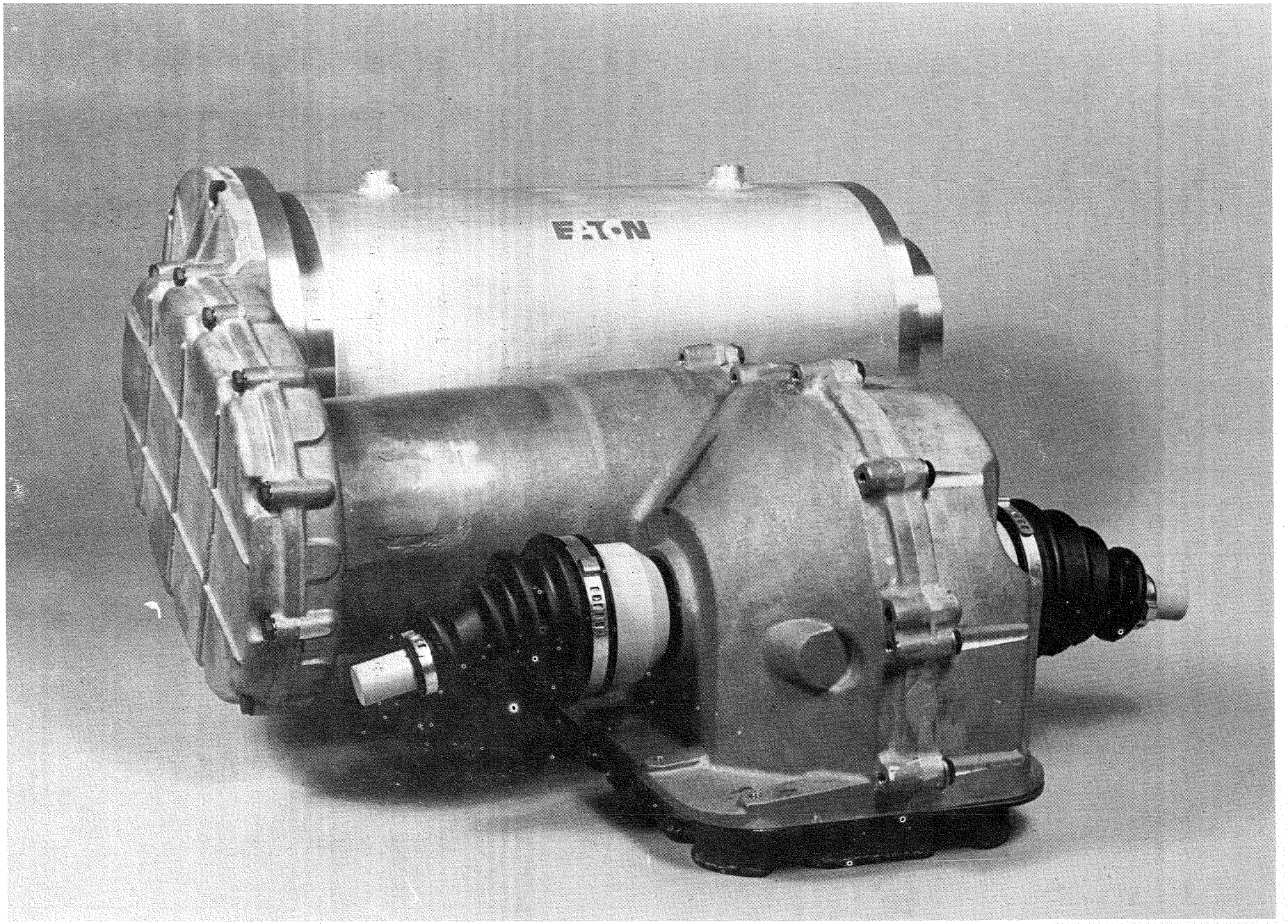

Figure 4.1.3 Two Speed Transaxle Shown In Flat Position

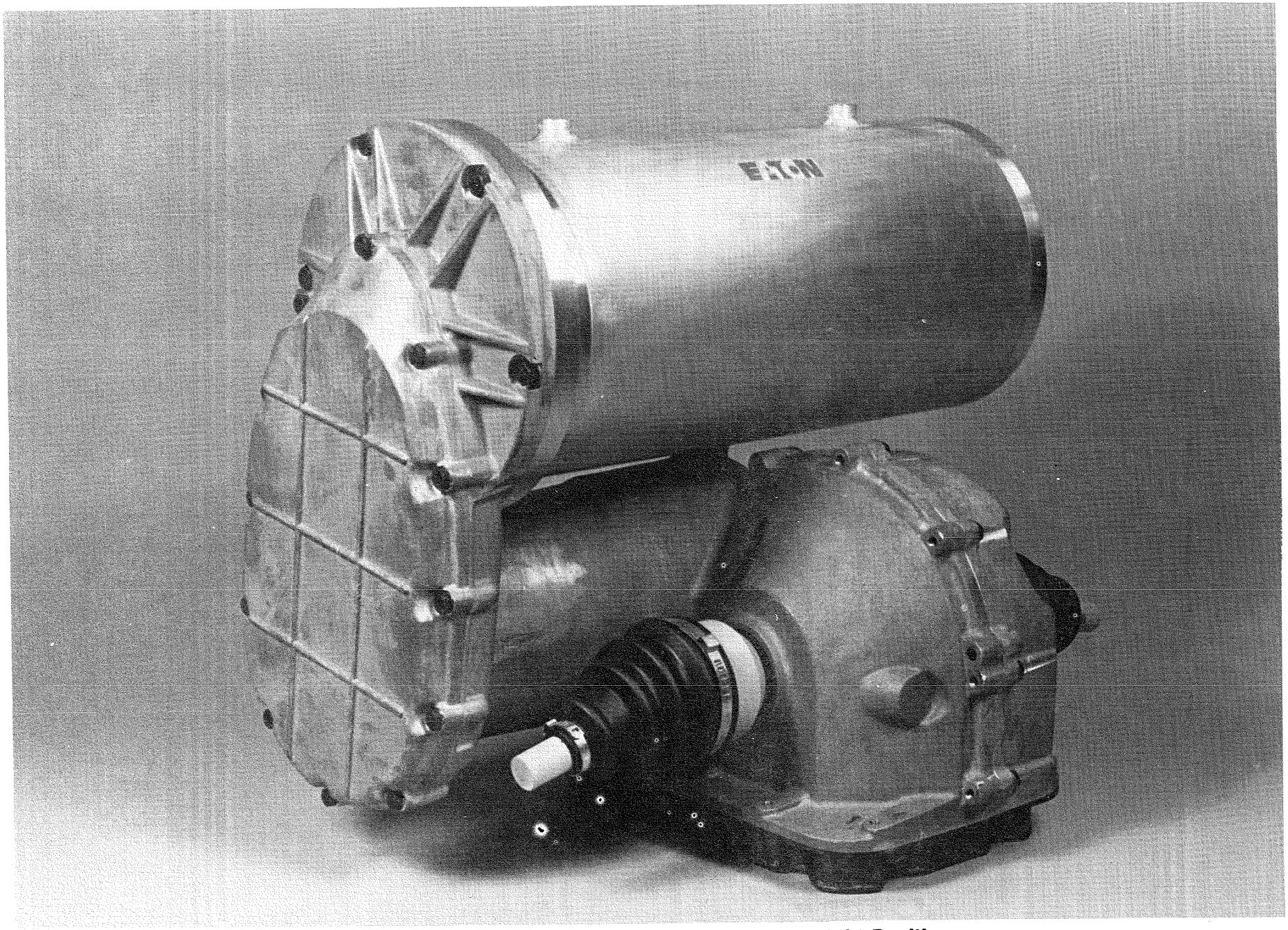

Figure 4.1.4 Two Speed Transaxle Shown in Upright Position

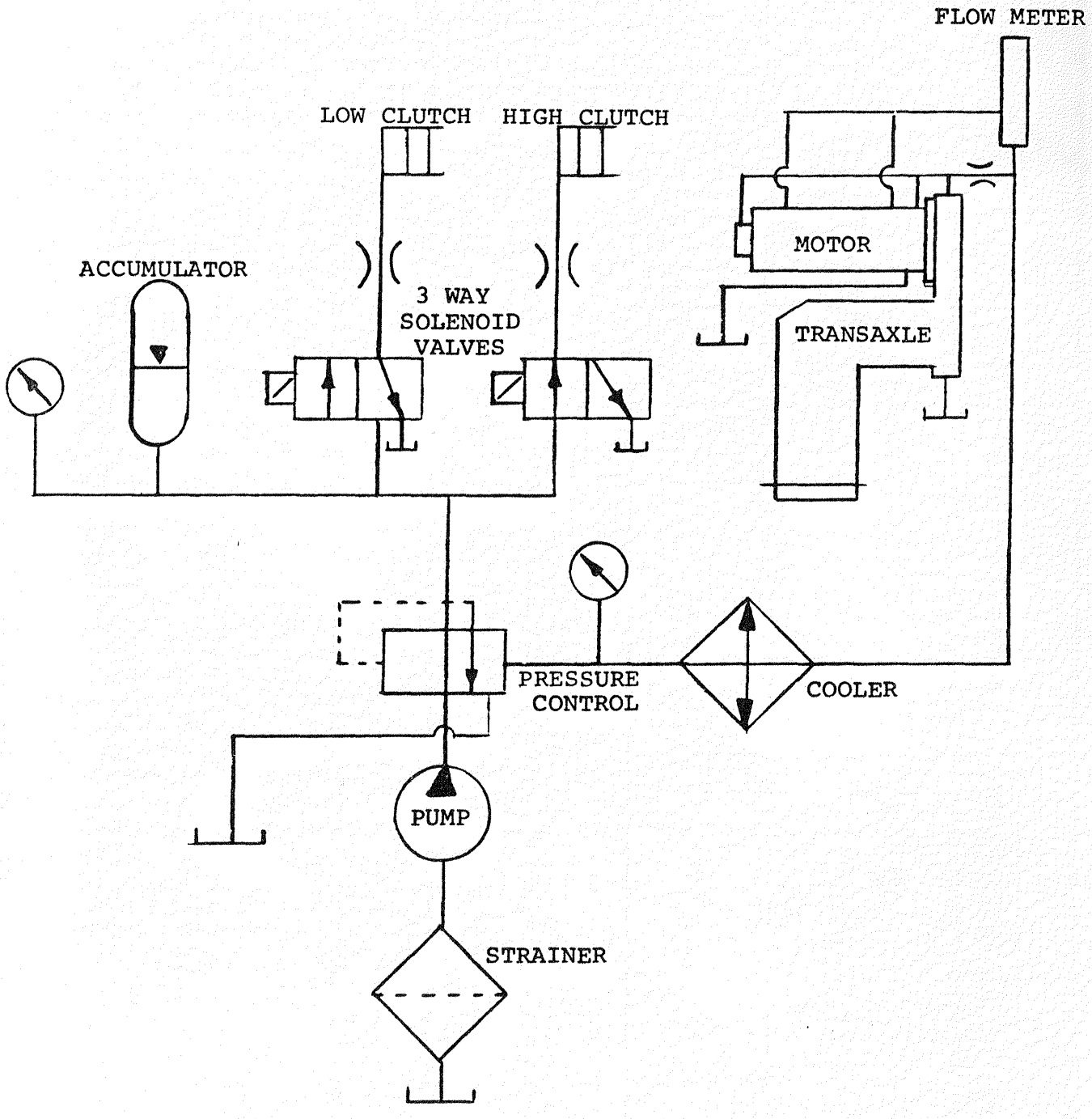

Figure 4.1.5

Transaxle Hydraulic System for Test-Bed Installation

The present hydraulic system only provides sufficient means to dynamometer-test the basic functions of the drivetrain. The system underwent some development, most of it involving the transition from the initial 60 Hz ac motor-powered pump and hand-actuated clutch-shift-valve system to the dc motored pump and automatic clutch actuation from the electronic control.

Several pump motor combinations were tried in an effort to minimize current draw. The final selection draws about 12 A (12 V) when pumping 4.5 bar (65 psi), 950 cc/min. (0.25 gpm). A 4-way solenoid valve initially used for clutch actuation was replaced by an individual 2-way solenoid valve for each clutch in order to provide clutch overlap capability.

Appendix B contains instructions for operating the present transaxle as installed on the test frame delivered to LeRC in September, 1980.

4.2 Testing

Shakedown Test

The transaxle was installed on a dynamometer equipped for no-load testing only. The unit was driven in coast mode (output shaft driving) in order to conveniently achieve full shaft speeds. A check was made throughout the speed range in each gear ratio for unusual noises, vibrations, overheating and lube circulation. No excessive noises or vibrations were observed. Somewhat high temperatures were noted on housing surfaces near the high range clutch. Also, lube return from disk clutch compartment and the chain housing was slow.

The unit was subsequently disassembled, inspected and reworked to eliminate the above shortcomings. Clearances between clutch plates of the high range clutch were substantially increased, and so were the lube return passages from the chain housing, the clutch compartment, and the low gear clutch pack.

The unit was reassembled. Static torque tests were performed in order to establish oil pressures at incipient clutch slip under maximum input torque. The operating clutch pressure range of 3.1-3.5 bar (45-50 psig) was thus established, representing a 1.5 safety factor over pressures at slip.

Efficiency Tests

The objective of these tests was to determine the mechanical efficiency of the transaxle alone, in the drive mode throughout its operational speed and load spectrum.

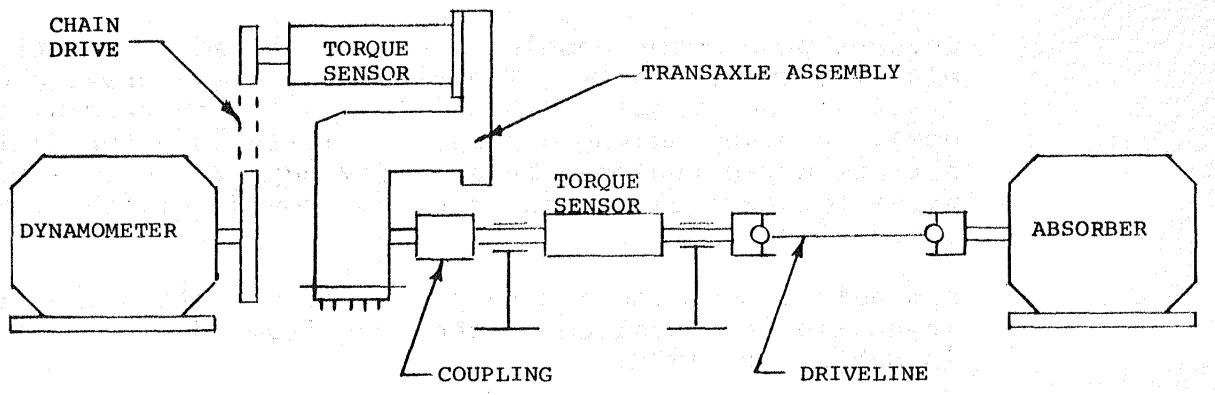

Figure 4.2.1 Setup for Drive Performance Test

The tests were run on the test setup shown in Figure 4.2.1. Figure 4.2.2 lists test equipment and instrumentation used. Figure 4.2.3 below lists the type of data acquired in these tests and the instrumentation used.

EQUIPMENT	PART NO.	MANUFACTURER
Driving Dynamometer	Model 26G308	General Electric
Flexible Coupling	226 SN	Thomas-Rexnord
Flexible Coupling	226 SN	Thomas-Rexnord
Absorber	1014DG	Dynamatic
Heat Exchanger	F-301-ER-2P	Young
Circulation Heater	NWHO-2	Chromalox
INSTRUMENTATION AND SENSORS		
Torque Sensor	MCRT6-02T(2-3)	Himmelstein
Torque Sensor	1648-5K	Lebow
Torque Signal Conditioner	878K	Daytronic
Torque Signal Conditioner	878	Daytronic
Speed Readout	76140010	Airpax
Temperature Conditioner	810	Daytronic
Thermocouples	6610WBA2	Applied Instruments

Figure 4.2.2 - Test Setup Components & Instrumentation

	ROOT MEAN SQUARE METHOD (% OF FULL SCALE)	SUM OF ERRORS METHOD (% OF FULL SCALE)	FULL SCALE
Torque Error (Lebow)	0.08%	0.15%	416 lb-ft
Torque Error (Himmelstein)	0.221%	0.31%	166 lb-ft
Speed Error	0.124%	0.223%	9000 RPM
Power Out Error	0.50%	0.70%	100%
Efficiency Error	0.58%	1.0%	

Figure 4.2.3 - Test Variables and Errors

A worst case system accuracy for the torque sensors, connecting cables and readouts was determined from the calibration charts. Following are the individual instrument accuracies:

TAPE RECORDER: Sangamo Model #3500

ACCURACY: $\pm$ 0.05% of full scale

TORQUE SENSOR: Lebow (1648-5K) + Daytronic (878A)

ACCURACY: (Calculated torque - measured)/(full scale torque) x (100) x (175.79-176.0)/(416.66) x (100) = $\pm$ 0.05% of full scale

TORQUE SENSOR: Himmelstein MCRT 6-62T(2-3) + Daytronic (878)

ACCURACY: (Calculated torque - measured)/(full scale torque x (100) x (56.26-55.9)/(166.66) x (100) = $\pm$ 0.21% of full scale

SPEED SENSOR: Speed pickup + Airpax counter

ACCURACY: Calibration was $\pm$ count (1/4000) x (100) = $\pm$ 0.025 of full scale

SPEED CONDITIONER: Frequency to voltage converter-Daytronic 840

ACCURACY: 0.05% of average dc voltage $\pm$ 0.10% of full scale

HEWLETT PACKARD ANALYZER: HP 5451B Fourier analyzer

ACCURACY: 12 bits = 2" = 2048 parts = 1 volt
(1/2048) x (100) = $\pm$ 0.048% of full scale
The resolution is determined by setting 1 volt at full scale and storing the actual reading in one of 2048 parts.

COMPUTER ROUND-OFF ACCURACY: 0.5% of full scale

System accuracy was determined from these instrument accuracies. Two generally accepted methods were used for calculating a system error, namely, the root mean square and the sum of the errors method. Both methods are tabulated in Figure 4.2.3 for torque, speed, power and efficiency readings.

Results

Test results indicate transaxle mechanical efficiencies above 90% through most of the load-speed spectrum. Figures 4.2.4, 5, 6, 7, and 8 show measured efficiencies in both gear ratios at 40%, 80% and 120% rated load and various output speeds.

The above efficiencies do not include the hydraulic pump loss of a constant 0.15 kw (0.2 HP).

The transaxle assembly performed satisfactorily throughout the above tests, with no malfunctions or degradation in function.

During complete system tests, covered in detail in Section 9, the transaxle assembly experienced two breakdowns, due to almost identical planetary carrier output shaft failures. In both cases the shaft failed due to stress concentration at a cross-hole resulting from original manufacture. Figure 4.2.9 shows one such failure.

Heat damage to planetary gears and carrier pins due to initial insufficient lube flow to the carrier planetary bearings is shown in Figure 4.2.10.

The carrier/shaft assembly was redesigned to have a two-piece shaft free of stress concentrations and to be electron beam welded to the larger-diameter section of the original carrier shaft. The lube path to the planetary carrier bearings was enlarged. There was no recurrence of the above failures in subsequent testing.

Discussion Of Results

The results of these lab tests indicate satisfactory function and acceptable performance of the transaxle assembly in the operational modes tested. Mechanical efficiency is close to the predicted efficiency and is generally satisfactory across the entire speed-load-ratio spectrum. These efficiency tests were performed in the drive mode only, due to equipment availability and program schedule. Regenerative mode efficiencies are expected to be only slightly lower than drive mode efficiencies.

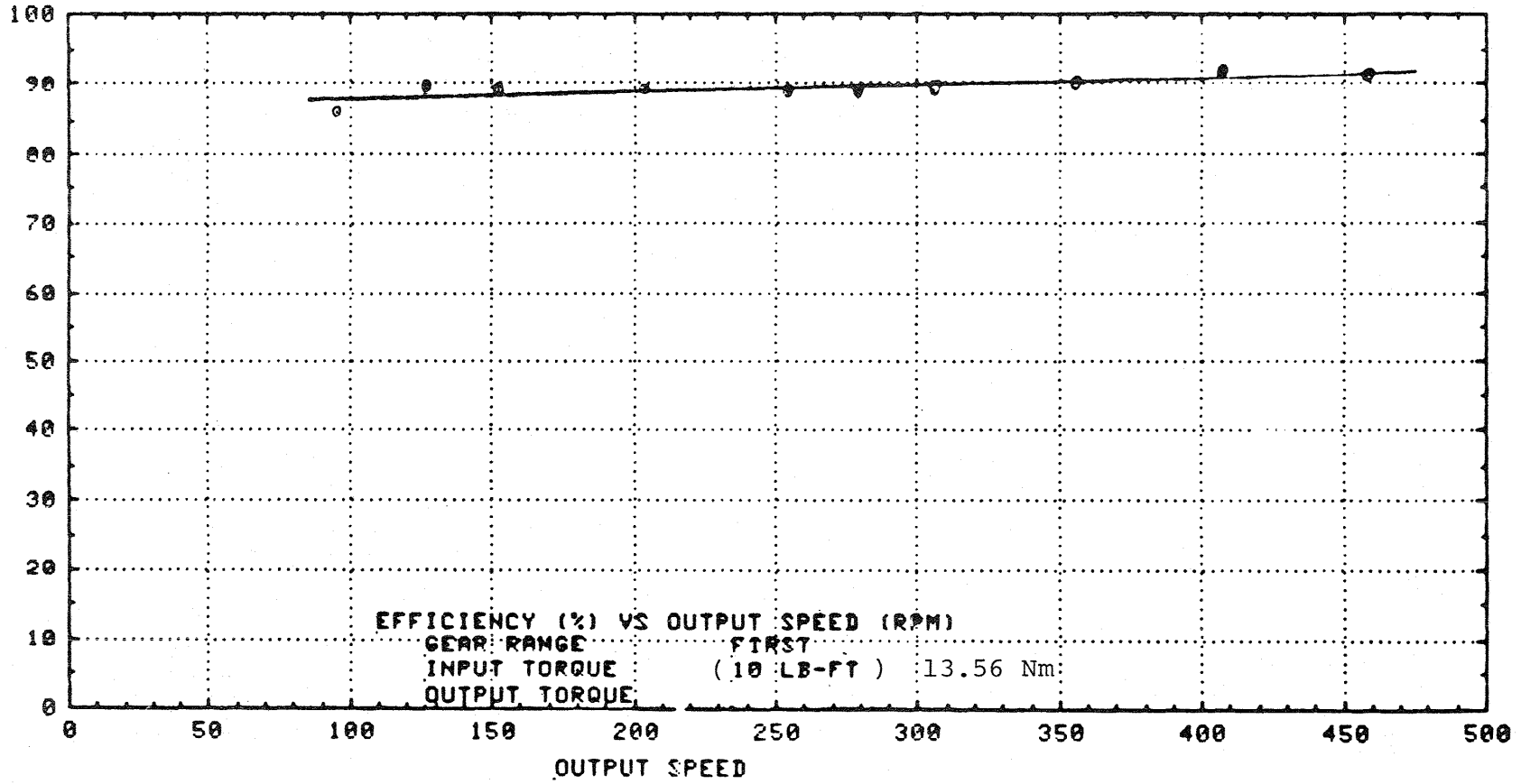
EFFICIENCY
100
90
80
70
60
50
40
30
20
10
0
0
50
100
150
200
250
300
350
400
450
500
OUTPUT SPEED
EFFICIENCY (%) VS OUTPUT SPEED (RPM)
GEAR RANGE FIRST
INPUT TORQUE (10 LB-FT) 13.56 Nm
OUTPUT TORQUE

Figure 4.2.4

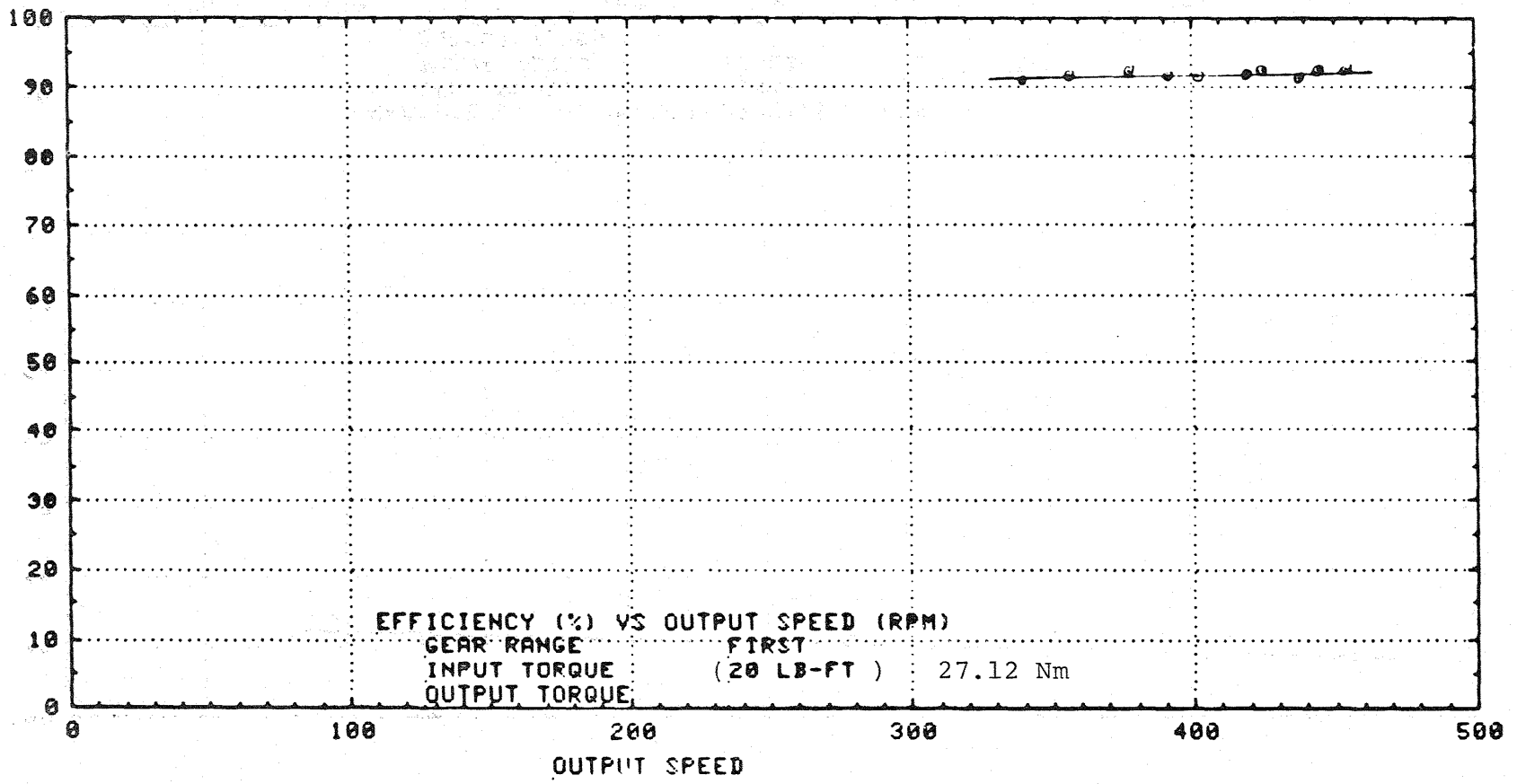
100
90
80
70
60
50
40
30
20
10
0
EFFICIENCY
EFFICIENCY (%) VS OUTPUT SPEED (RPM)
GEAR RANGE FIRST
INPUT TORQUE (20 LB-FT) 27.12 Nm
OUTPUT TORQUE
0
100
200
300
400
500
OUTPUT SPEED

Figure 4.2.5

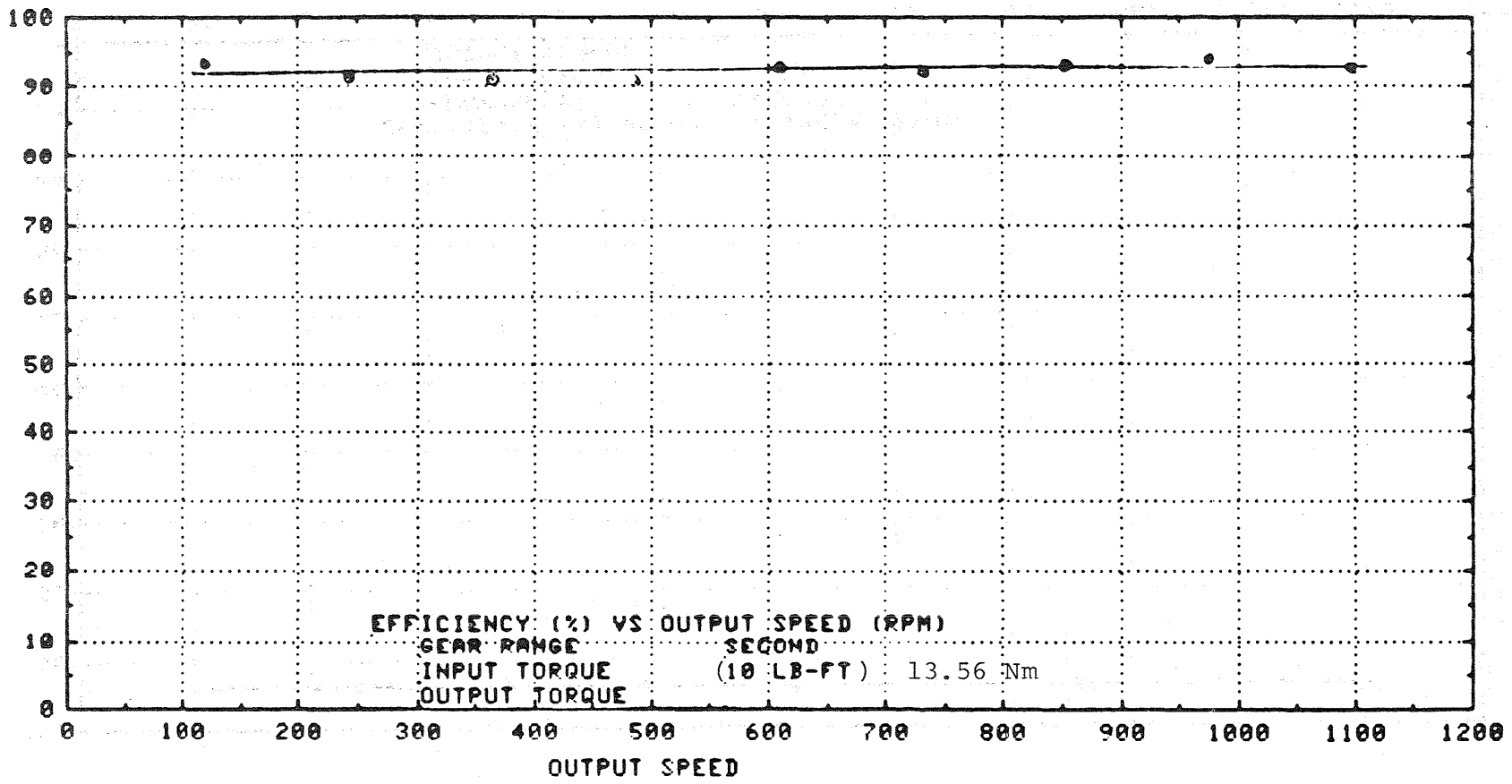
EFFICIENCY
100
90
80
70
60
50
40
30
20
10
0
0
100
200
300
400
500
600
700
800
900
1000
1100
1200
OUTPUT SPEED
EFFICIENCY (%) VS OUTPUT SPEED (RPM)
GEAR RANGE SECOND
INPUT TORQUE (10 LB-FT) 13.56 Nm
OUTPUT TORQUE

Figure 4.2.6

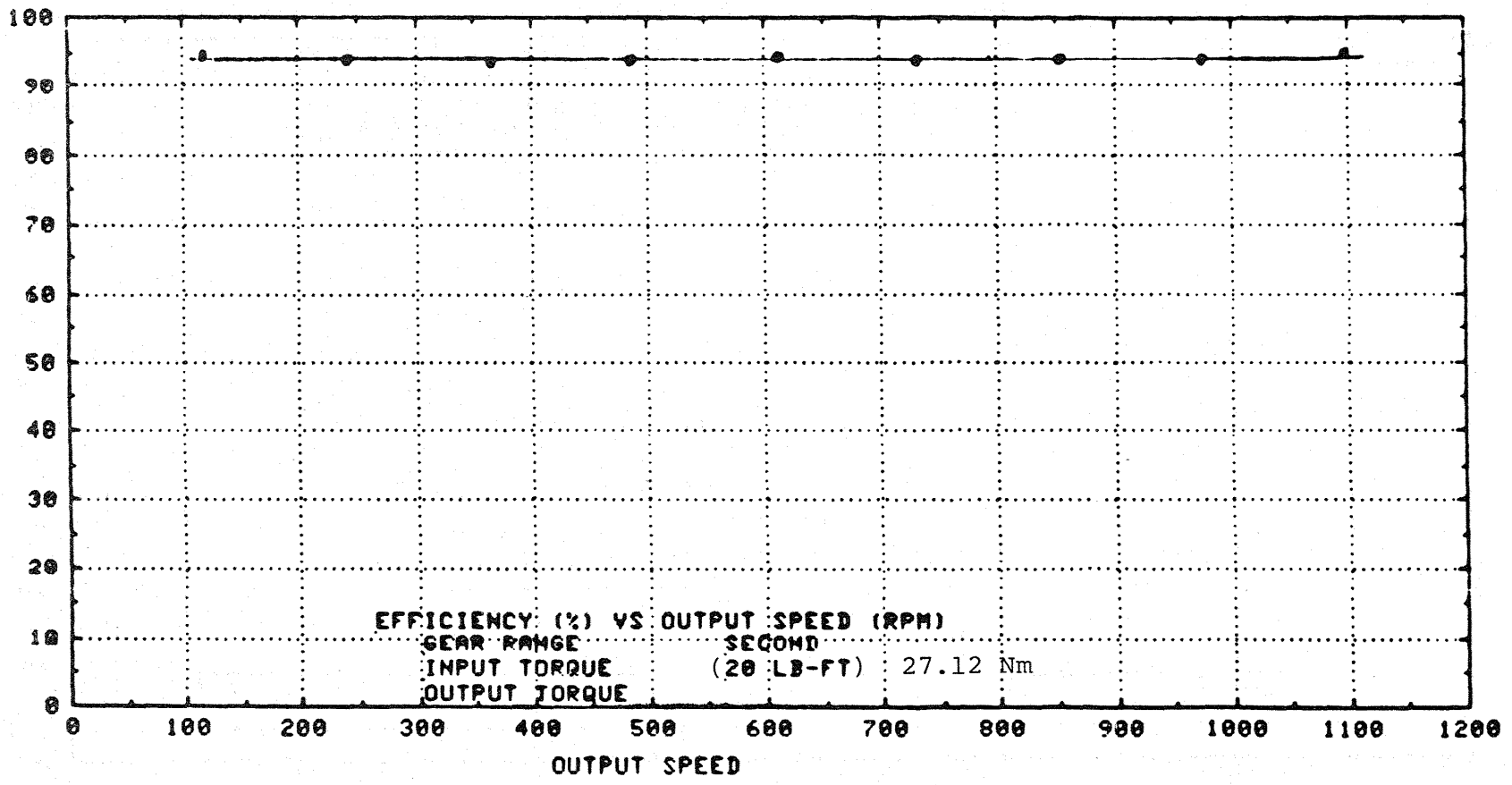
EFFICIENCY
100
90
80
70
60
50
40
30
20
10
0
0
100
200
300
400
500
600
700
800
900
1000
1100
1200
OUTPUT SPEED
EFFICIENCY (%) VS OUTPUT SPEED (RPM)
GEAR RANGE SECOND
INPUT TORQUE (20 LB-FT) 27.12 Nm
OUTPUT TORQUE

Figure 4.2.7

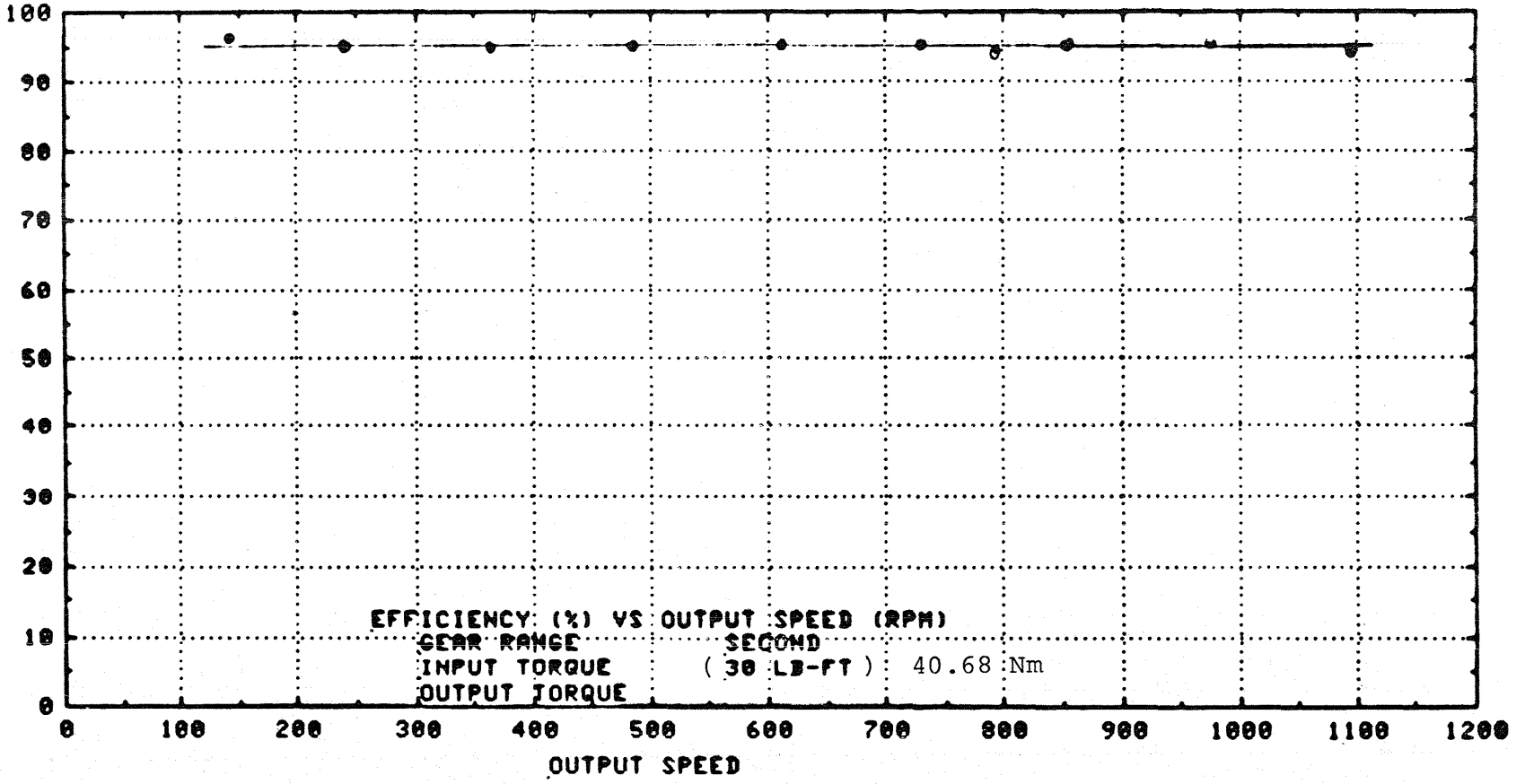
EFFICIENCY
100
90
80
70
60
50
40
30
20
10
0
EFFICIENCY (%) VS OUTPUT SPEED (RPM)
GEAR RANGE SECOND
INPUT TORQUE (30 LB-FT) 40.68 Nm
OUTPUT TORQUE
0
100
200
300
400
500
600
700
800
900
1000
1100
1200
OUTPUT SPEED

Figure 4.2.8

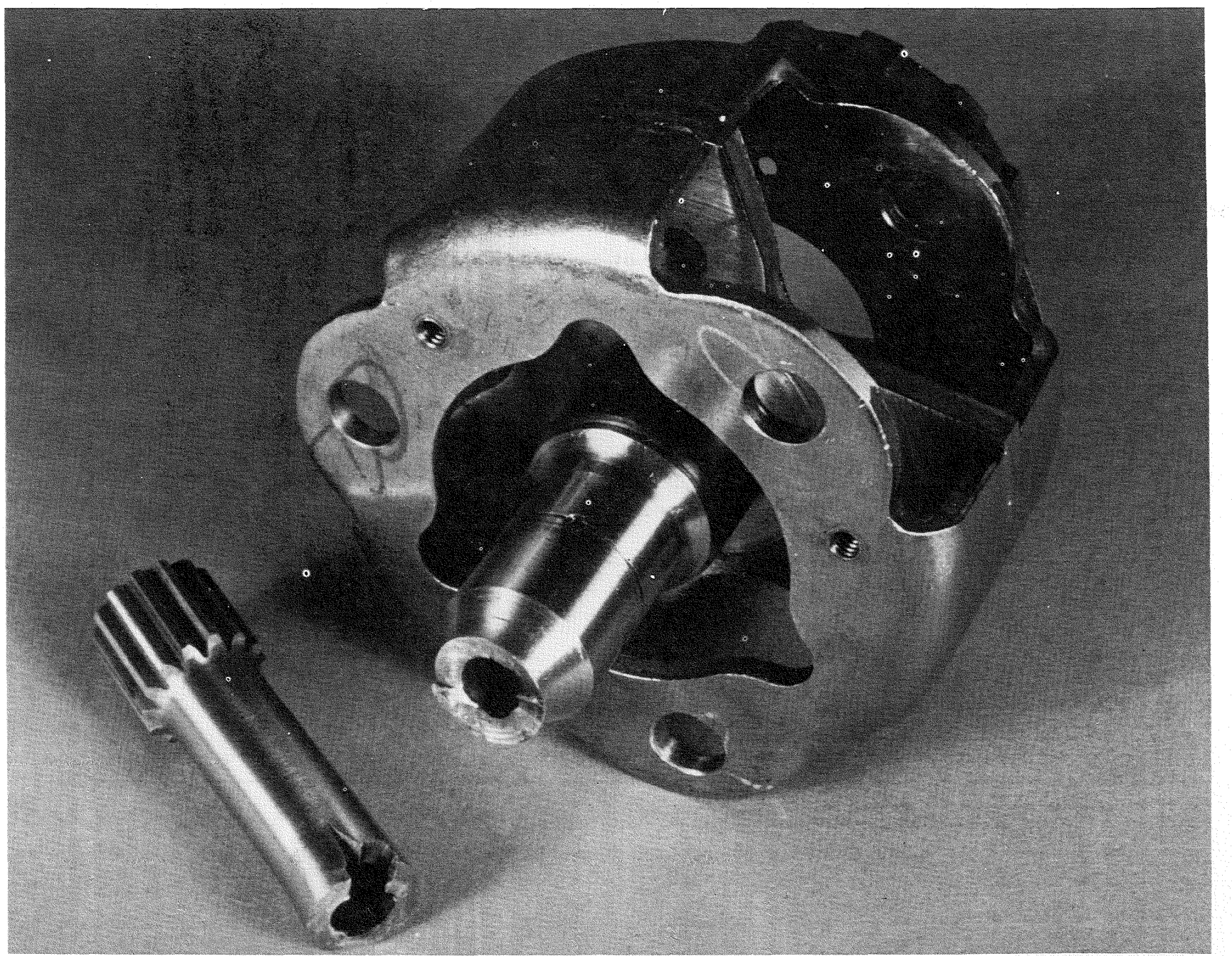

Figure 4.2.9 Failed Planetary Carrier Shaft

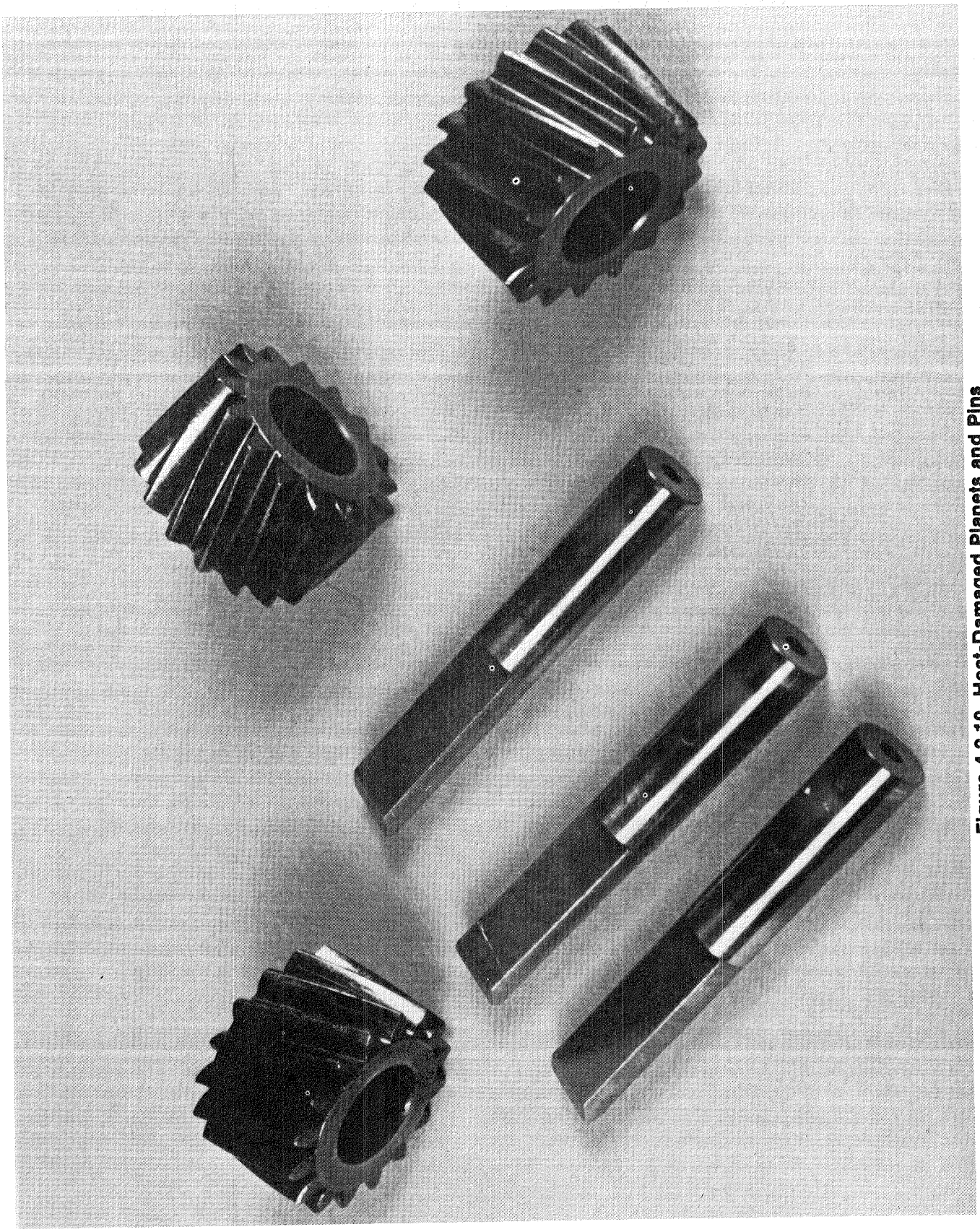

Figure 4.2.10 Heat-Damaged Planets and Pins

Noise or vibrations did not appear excessive in any of the operational modes, including regenerative mode, during shakedown tests.

Lubrication and cooling appeared adequate under laboratory conditions at final test.

The in-vehicle tests, scheduled for Phase II of this program, will confirm true adequacy of this design with regard to satisfactory function, durability, noise, vibrations, cooling and lubrication.

4.3 Future Improvements

Even though the transaxle assembly can be considered ready for installation in a vehicle for further development testing, certain aspects in the design already suggest potential improvements in weight, size, cost and function.

Considerable weight reduction (30%) is possible through the use of magnesium housings. Redesign can shorten the 2-speed section by about 3.8 cm (1.5 in). These two revisions are expected to give a total weight reduction of about 6.8 kg (15 lbs).

Revision of low clutch actuator and support design is expected to give further weight and cost reductions.

A functional improvement is contemplated in the area of oil return to sump from chain housing and from the planetary compartment.

The chain itself may be replaced by a timing belt, for further weight reduction.

A satisfactory parking latch design has to be worked out and integrated in the transaxle assembly.

Finally, hydraulic components such as the pump, valves and fluid passages will be integrated with the housings for more compact design and assembly simplification.

5. MOTOR

5.1 Design Consideration

The ac traction motor is designed for high efficiency, small size, low cost, and easy integration into a relatively simple drive train. This may require that trade-offs and compromises be made. The design decisions which were made in the development of the final motor specifications are described in the following paragraphs.

The motor specifications are as shown below (Figure 5.1.1). A phantom drawing of the motor is shown in Figure 5.1.2.

Rating: 18.6 kw for one hour at base frequency and above
29.8 kw for two minutes at maximum frequency.
Phases: 3
Poles: 2
Base Frequency: 94 Hz, 5640 RPM synchronous speed.
Maximum Frequency: 150 Hz (9000 RPM).
Voltage: 100 volts RMS line to line.
Frame: 180 special face mounted, totally enclosed.
Cooling: Oil cooled at 1.9 liters/minute, radiation, convection, and conduction from frame may also be utilized.
Ambient Temperature: -40° to +45°C.
Insulation: Class H (good to 180°C or better).
Efficiency Goal: 85% or higher at 18.6 kw, 94 Hz sine wave.
Power Factor Goal: 0.85 or higher 18.6 kw, 94 Hz.

Figure 5.1.1. Motor Specifications

Speed-Torque Selection

To provide efficient integration of the motor with the transaxle and inverter, the motor was specified to operate over the per unit speed-torque range shown in Figure 5.1.3.

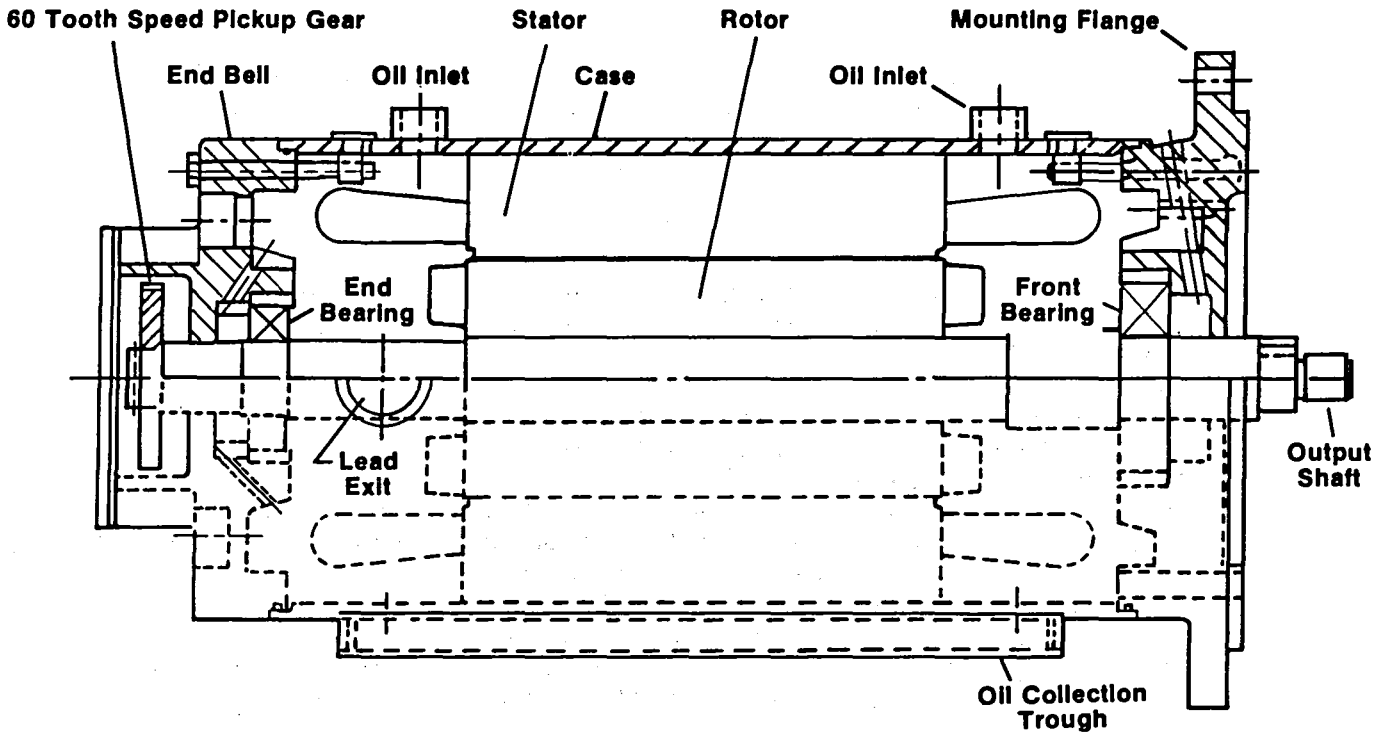

Figure 5.1.2 Motor

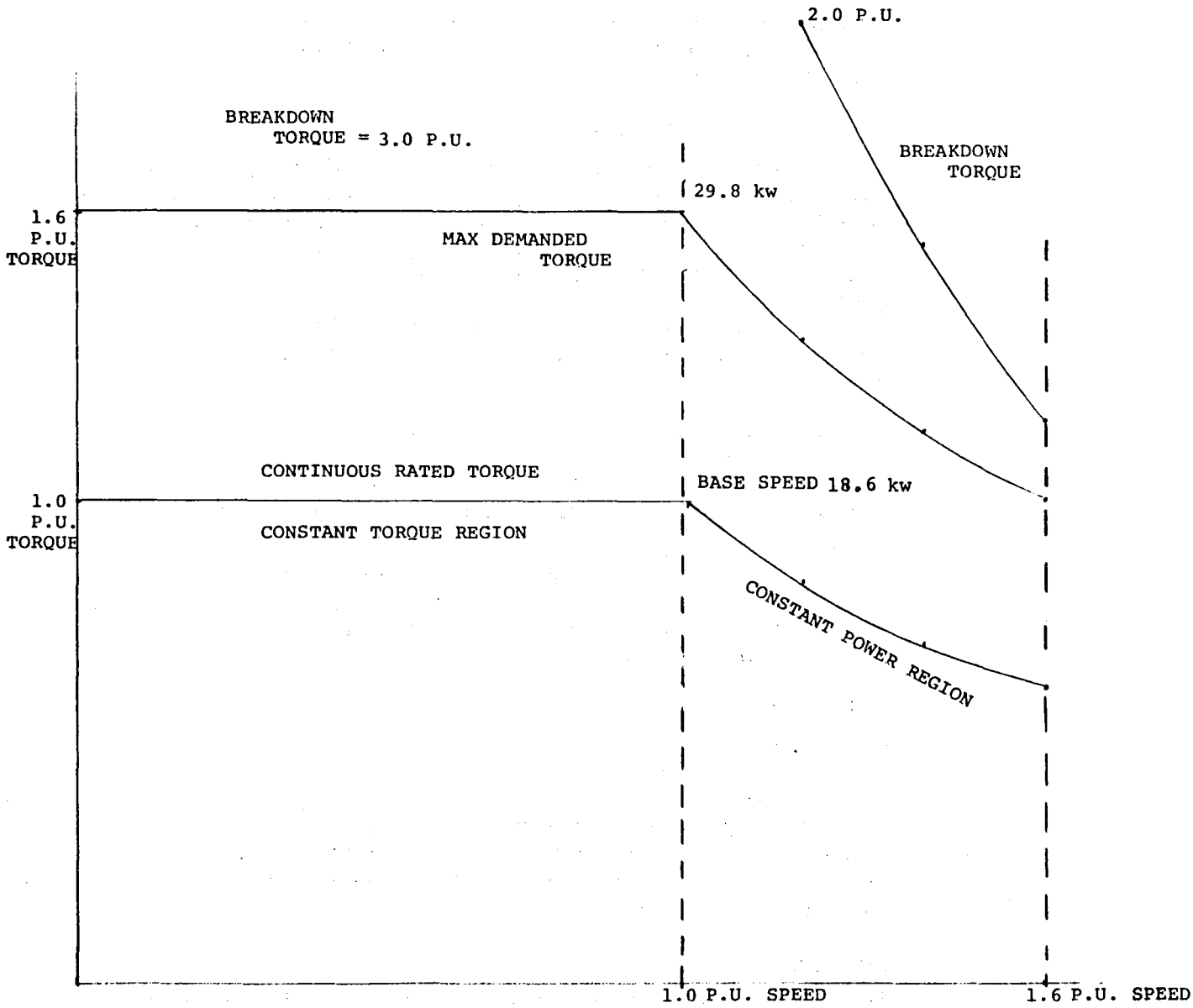

P.U. = Per Unit Value

Figure 5.1.3 Motor Speed-Torque Range

Continuous constant torque capability is provided from zero to base speed at a torque which produces 18.7 kw (25 hp) at base speed. Previous experience suggests a conservative constant power range of 1.6:1 above base speed will avoid the breakdown torque curve of the machine. Also, a moderate 1.6:1 ratio of maximum to continuous torque is specified, resulting in a peak output at base speed of 29.8 kw (40 hp) limited by the inverter current handling capability. The available motor

breakdown torque is considerably higher, ensuring that 29.8 kw may be achieved over the entire constant horsepower range.

Base speed selection

For a given power rating the size and weight of an ac machine decreases in proportion to the increase in base speed. Base speed is defined as the maximum speed in the constant torque range, or the speed at which rated motor V/Hz (rated motor voltage divided by rated stator frequency) requires the maximum inverter output voltage. Thus, it is desirable to specify as high a base speed as possible. As base speed increases, however, the higher electrical frequencies cause increased iron losses requiring better electrical steels and thinner laminations. In addition, the inverter switching losses increase and the gear reduction to the vehicle wheels becomes excessive. Also, top speed affects the criticality of balancing and bearing selection.

A maximum speed of 9000 rpm was chosen. This top speed is satisfactory for mechanical consideration of balancing and bearings. Higher speeds require a more complex reduction in the transaxle. The 1.6:1 constant power range then gives a base speed of 5640 rpm.

Pole number

For a given electrical frequency, rotor speed is determined by the motor pole number. A two-pole motor is preferable to the four pole: the two-pole approach halves the required stator frequency, allowing equal motor performance with less expensive iron. More importantly, the inverter switching stresses and losses are also reduced by employing a two-pole motor.

Voltage

The higher the system voltage, the lower the motor current and the more compact and efficient the inverter. Also, more flexibility is afforded in the motor design for optimum efficiency, since finer gradations in winding the stator are possible. The voltage rating results from the highest bus voltage that the inverter transistors can safely handle. The chosen transistor allowed a 144 vdc bus. The line-to-line motor RMS voltage rating is given by

$$(1.9\ \text{V/cell} \times 72\ \text{cells} - 3.5\ \text{V} - 4\ \text{V})\ \sqrt{6}/\pi - 0.4\ \text{V} = 100\ \text{VRMS}$$

where 1.9 V = cell voltage at rated power
3.5 V = cabling and shunt drop
4.0 V = two transistor on stator drops
$\sqrt{6}/\pi$ = conversion factor: square wave to equivalent L-L RMS
0.4 V = motor cable drop

In a small vehicle, space constraints quickly put a practical limit on voltage with current traction batteries.

Motor frame size

The two motor frame sizes under consideration were the NEMA 210 and 180 diameter. The 210 frame would result in a conventional motor with a fairly short stack and a large winding area, resulting in a motor which would be efficient and cool. The disadvantages of the 210 frame include large end bells which contribute unnecessary weight and a shape which is difficult to integrate into the transaxle.

Although conventional 180 frame geometry proved too small to provide 18 kw rated operation, a design with a much longer stack proved to provide rated power at a calculated efficiency no less than that of a 210 frame. Thus, a longer than usual 180 frame motor, which fits nicely to the transaxle results. The relatively shorter stator winding end turn paths, together with the long stack length, compensate for any disadvantage in a two-pole design. A secondary advantage of the long, small diameter design is a high torque-to-inertia ratio for rapid acceleration.

Thermal considerations

Forced air cooling was eliminated because a totally enclosed design was desired. The stator winding was identified as requiring extra cooling. To provide this, an arrangement to cause cooling oil to flow over the end turns was provided. A simple low pressure flow system is used rather than a high pressure spray system. A portion of the oil is used for bearing lubrication. A sump at the bottom of the motor collects the oil and returns it to the transaxle. The aluminum face mounting flange of the motor also provides heat transfer to the transaxle body.

Economics

The decision was made to employ standard lamination punchings, rotor shaft, and magnet wire in construction to reduce fabrication time and cost. A cast aluminum rotor without integral fan is employed to allow economical mass production. As a result, this first motor cannot be viewed as an optimum motor. Future changes using custom laminations, etc. to allow a larger winding area and an optimum air gap diameter may result in a noticeable improvement in performance. (See also Section 12.)

5.2 Detail Design

The motor was designed with the aid of a computer program. The program output includes the motor characteristics shown in Figure 5.2.1. As shown, the predicted sine wave efficiency is about 90% at full load and remains high down to 1/4 load. A large breakdown torque allows an adequate margin for 30 kw operation at 150 Hz (9000 rpm). The per-unit magnetizing reactance is low for a machine of this rating because of the small frame size, indicating the need for volts per Hertz modulation under lightly loaded conditions.

Primary mechanical parameters are shown below:

Active Material Weight:	66.8 kg
Stack Length:	203.2 mm
Air Gap:	0.7 mm
Coil Connection:	"Y"

Stator Frequency Hz	Torque P.U.	Power Output kw	Slip Hz	Current Amps	Efficiency %	Power Factor
94	1.0	18.7	1.52	130	91.3	0.901
94	1.6	29.9	2.58	207	89.9	0.923
150	0.62	18.7	1.543	125	91.7	0.935
150	1.0	29.9	2.77	210	89.7	0.913
94	3.45		12.49	Breakdown Torque		
150	1.51		7.89	Breakdown Torque		
94	0.25	4.65		53.8	87.4	0.572
94	0.5	9.35		75.4	90.8	0.786
94	0.75	14.02		101.8	91.5	0.867

Figure 5.2.1

Computer Predicted Performance

5.3 Motor Tests

Factory tests were performed to verify the performance and thermal capacity of the motor. The machine was first driven from a three-phase 60 Hz supply to provide sinusoidal excitation. The motor was coupled to the supply through an auto-transformer and a 112.5 KVA step-down transformer to provide the proper volts per hertz. Oil cooling was provided using Dexron #2 transmission oil. See Figure 5.3.1.

Operation at higher frequencies was checked by operating the motor through the transformer from a 50 KVA 230 VAC PWM inverter.

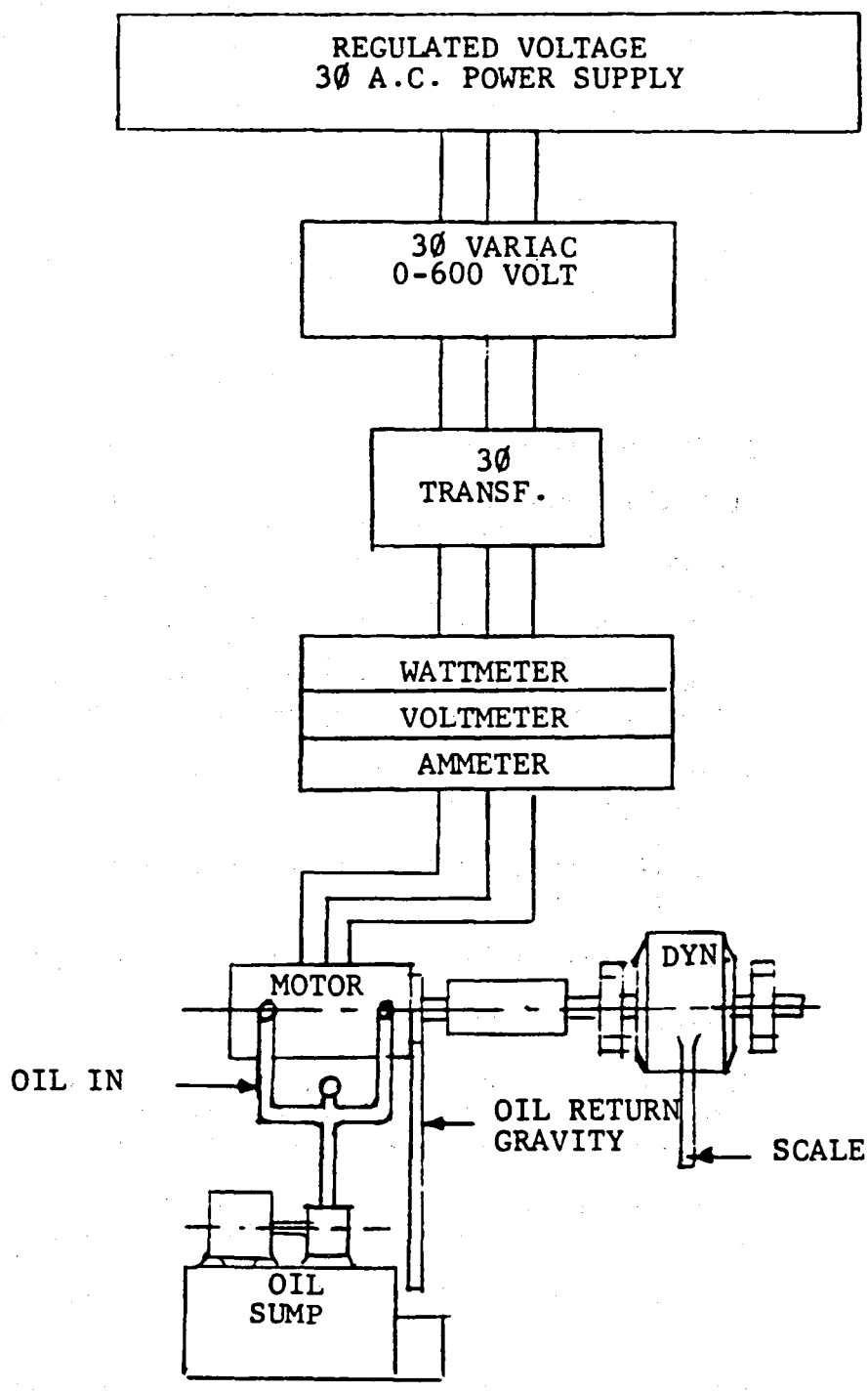

Figure 5.3.1 Factory Test Setup With Sinewave Excitation

Figure 5.3.2 tabulates the result for the full load sine wave test.

Locked rotor readings and breakdown torque could not be taken due to the limitations of the power supply.

A full load heat run was taken for one hour at 11.9 kw, 64 V and 60 Hz.

Data from this test are listed below.

KW	Volts	Amps	Watts In	Eff.	P.F.	Rise by Res.
11.84	64	136.8	13680	86.6	90.2	87.1°C

This test was run with 1.9 liters/min. of Dexron #2 transmission through the motor.

Noise and Vibration

With the motor running idle at 9000 rpm and being supplied by the inverter, vibration readings were taken using an IRD Model 306 Lab number 229 vibration meter. No readings were over 0.01 mm (0.4 mils) vibration in the horizontal or vertical plane on both front and back of motor.

Using a General Radio #1551-C, Lab number 522 sound level meter at the "A" weighing position, the noise data is:

- 0.92 meters (3 ft.) from side of motor - 76 dba background only
- 0.92 meters (3 ft.) from side of motor - 78 dba motor & background

These noise figures are considered acceptable

Analysis of Test Results

With the oil cooling in operation at 1.9 liters/min., temperature rises were recorded. The two test points are plotted on the following page in Figure 5.3.3.

Assuming an exponential relationship, the two 60 Hz, 11.94 kw data points were solved to yield:

$$T_r = 105.6° \ (1 - e^{-t/35.6})$$

T_r = °C rise
t = minutes

The thermal time constant T = 35.6 minutes, very close to the value predicted in a separate computer analysis of 34 minutes.

Figure 5.3.2 Motor Testing To Specifications

HP 25 RPM 5641/9000 VOLTS 100 PHASE 3 CYCLES 0-150
FRAME 180-SPL INSUL.CL. H WT. 147 LBS.
MOTOR WIND. RES. 0.0186 Ω @20°C

LINE SUPPLY FULL LOAD AT 60 Hz - 15 H.P. *REVISED FULL LOAD - 16 H.P.

	FULL LOAD		FULL LOAD			FULL LOAD		FULL LOAD		
TIME	10.45	11.15	8:25	8:55	9:25	9:35	10:05	1:20	1:50	2:20
SCALE	11.25	11.25	11.25	11.25	11.25	12	12	12	12	12
TORQUE	22.5	22.5	22.5	22.5	22.5	24	24	24	24	24
% OF RATED TORQUE	100	100	100	100	100	100*	100*	100*	100*	100*
MOTOR RPM	3518	3502	3524	3504	3430	3486	3470	3518	3494	3472
HP	15.08	15.01	15.10	15.02	14.96	15.94	15.86	16.08	15.97	15.87
VOLTAGE	64	64	64	64	64	64	64	64	64	64
AMMETER	3.27	3.26	3.2	3.23	3.2	3.45	3.45	3.37	3.39	3.42
MULT. X RATIO	40	40	40	40	40	40	40	40	40	40
AMPERES	130.8	130.4	128.0	129.2	128.0	138	138	134.8	135.6	136.8
WATTMETER	352	322	318	318	319	342	348	335	340	342
MULT. X RATIO	40	40	40	40	40	40	40	40	40	40
TOTAL (Watts)	13000	12880	12720	12720	12760	13680	13920	13400	13600	13680
EFFICIENCY MOTOR	86.5	86.9	88.6	88.1	87.5	86.9	91.0	89.7	90.5	90.2
P.F.% →	89.7	89.1	89.6	88.8	89.9	89.4	85	89.5	87.6	86.6
VOLTS/Hz	1.067	1.067	1.067	1.067	1.067	1.067	1.067	1.067	1.067	1.067
Hz	60	60	60	60	60	60	60	60	60	60
OIL TEMP. IN °C			22	29	37	38	43	28.5	32	40
OIL TEMP. OUT °C		33	23	33	43	42	48	28	34	43.5
GPM/PSI		1.06/	0.5/12.0	0.50/12.0	0.50/11.0	0.5/10.0	0.50/9.0	0.50/11.5	0.50/9.75	0.50/9.0
RES. Ω		1.2278	0.01858	0.0226	0.0242		0.02332	0.01901	0.02343	0.02533
RES. RATIO R_H/R_C		1.225	0.999	1.215	1.301		1.361	1.022	1.260	1.362
TEMP. RISE °C		53.8	0	51.7	73.6		88.9	1.1	61.2	87.1
AMBIENT AIR °C	23.5	23.5	22	23	23	23	23	24.5	25	25
HSG.TEMP. °C MOTOR	29.5	59.5	21.5	50	73	68	82	26.5	52	76

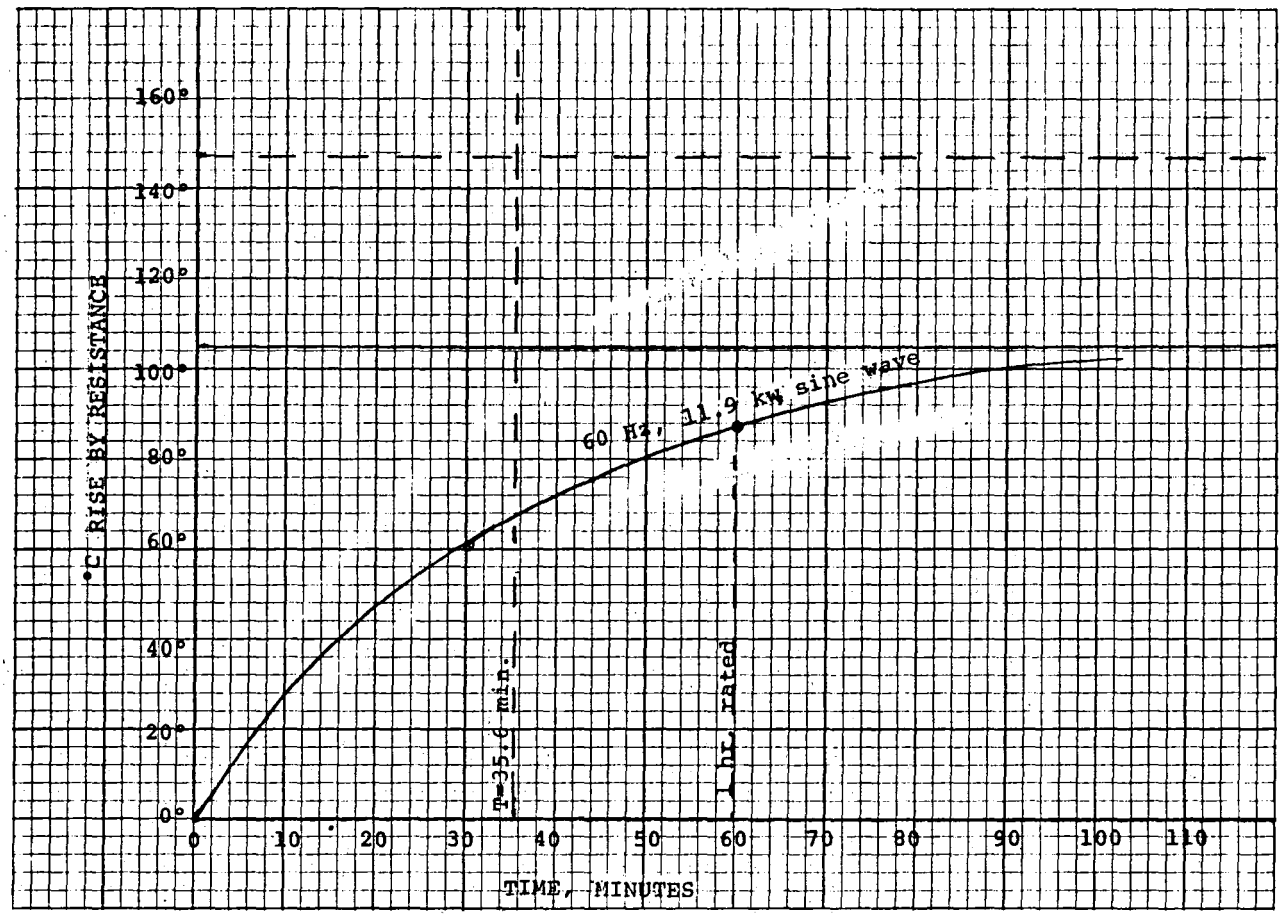

Figure 5.3.3 Measured Machine Temperature Rise By Resistance Method.

The 1 hour rise is 86°C. Even with a 45°C air ambient and a 52°C oil inlet temperature, the machine rise by resistance would be about 141°C. This allows a margin of 160° - 141° = 19°, assuming that 160°C is the maximum practical allowable by the resistance method for the 180°C maximum Class H insulation.

No Load Current

An idle saturation test was also run. The no load excitation current is higher than would be expected for an industrial machine.

Figure 5.3.4 shows that 47.2 amps at 60 Hz sine wave uncoupled excitation current is drawn at rated V/Hz.

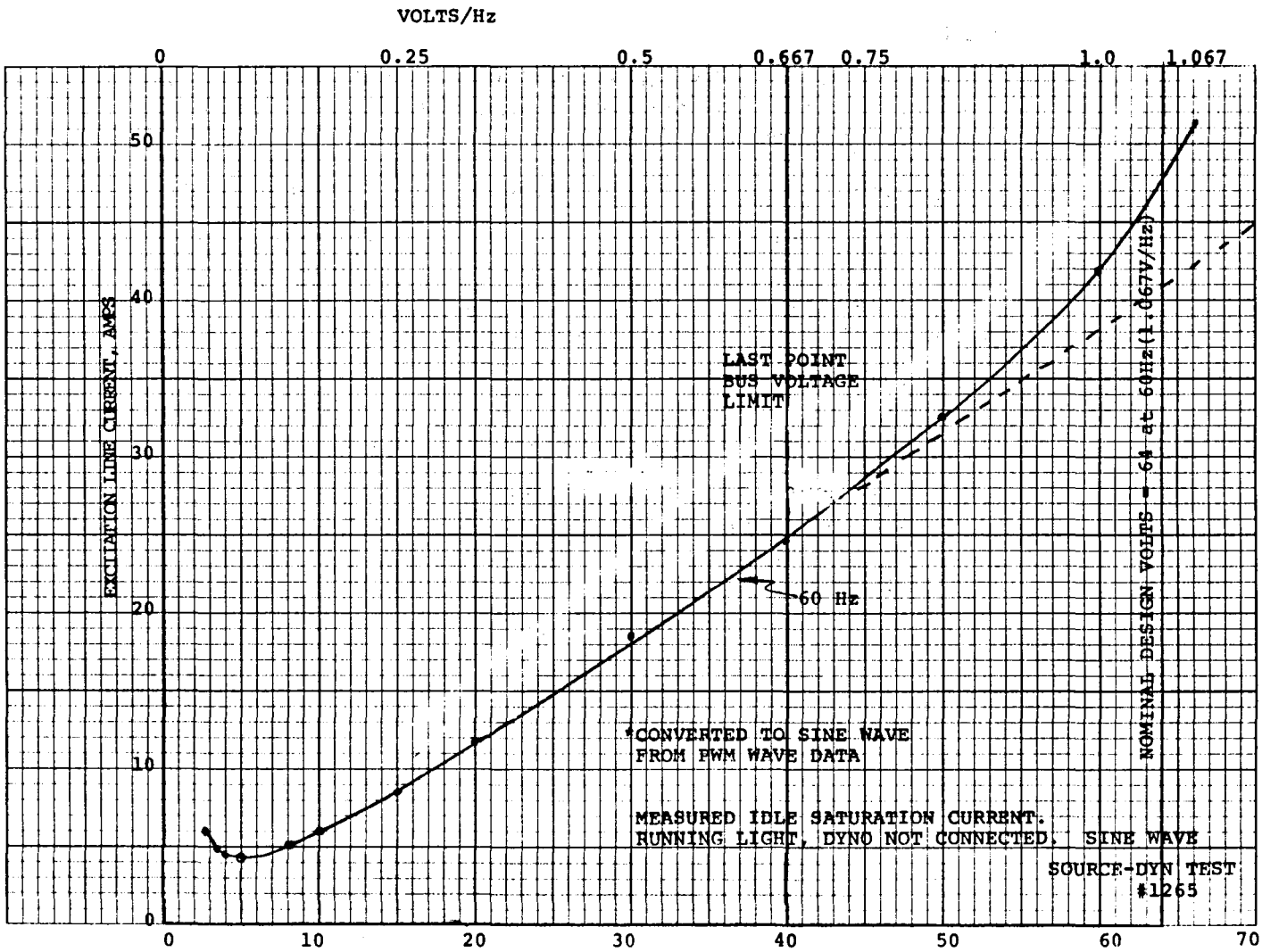

Figure 5.3.4. Motor No Load Excitation Current

	No load current on dyno	Current at 100% Load	Percent Excitation Current
60 Hz, sine	49.4	129.2	38.2%
60 Hz, PWM	52.6	-	-
94 Hz PWM	66	150	44%
150 Hz PWM	36.5	148	24.7%

This high percentage stresses the importance of the volts/Hz modulation proposed for light load operation.

Slip

The slip is somewhat higher than predicted by the design and contributes to the less than predicted efficiency. Results are shown below.

60 Hz sine, dyn on but no load.....2 rpm, 0.05%
60 Hz sine, 11.2 kw cold.....76 rpm, 2.11%
60 Hz sine, 11.2 kw hot.....110 rpm, 3.05%

60 Hz sine, 11.9 kw cold.....82 rpm, 2.28%
60 Hz sine, 11.9 kw hot.....128 rpm, 3.56%

Losses

The losses in the prototype motor are as follows:

Iron Losses	222
Stator Copper Loss	711
Rotor Copper Loss	489
Windage & Friction	13
Stray	406
Total Watts	1841

5.4 Motor Testing With PWM Traction Inverter

Prior to total system integration of the motor, inverter, and transaxle on the test frame, an initial test phase was performed with the motor and inverter alone. This phase was aimed at testing the motor and inverter under maximum expected power levels and at optimizing the efficiency of the system. Portions of this test phase referring to inverter results are included under the section on the inverter. Results pertaining to motor performance are given below.

Test Setup

Mechanical configuration

The motor was mounted upon a torque table accurate to 0.085 nm (0.75 lb-in). This accuracy is within 0.26% of the full load torque of the motor. The dynamometer is a 6000 rpm dc type and is capable of 33.6 kw (45 hp) motoring and 44.8 kw (60 hp) absorbing.

Electrical configuration

The basic electrical configuration for this test is given in Figure 5.4.3.

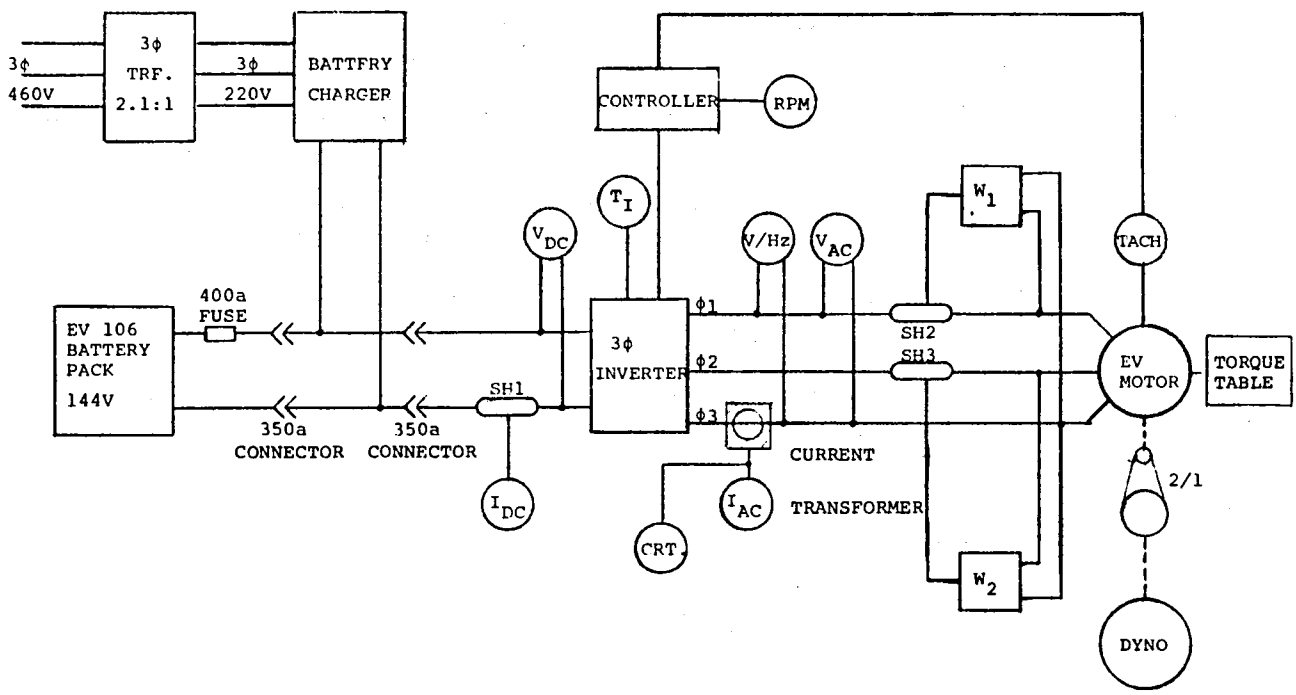

5.4.1 Electrical Configuration

The battery charger was used to provide a controlled dc bus voltage so that system efficiency could be evaluated at various speed and load conditions while holding average bus voltage constant. Current shunts were T&M coaxial shunts, accurate to 0.02% of full scale. The motor power was measured with Clarke-Hess model 255 wattmeters (W1, W2).

Test Data and Instrumentation

Figure 5.4.2 shows the data that was gathered on these tests along with the appropriate transducers and instrumentation that were used to collect data. The combined accuracy of the various transducers and instruments permitted the determination of inverter efficiency, motor efficiency and overall system efficiency to 2% of motor rated horsepower.

Inverter And Motor Efficiency Tests

The purpose of these tests was to optimize the system efficiency as a function of V/Hz, slip, and wave shape over the system operating range for selected motor torques and speeds. The steady-state combination motor and inverter efficiency was determined for as many variations of the above parameters as possible. Optimal operating conditions were used in programming of the controller microprocessor for use in the "Normal" mode of operation. This determination was made by adjusting V/Hz, slip, and wave shape to get minimum bus current for each condition.

The resulting motor efficiency for the optimal motor and inverter operating conditions is given in Figure 5.4.3.

The optimum wave shape (as explained by a parameter called notch number explained in Section 7.1) was a compromise for both the motor and the inverter, because, although increasing notch number benefits motor efficiency, inverter efficiency falls.

The optimum V/Hz vs. motor torque for various speeds is shown in Figure 5.4.4. The advantage of decreasing V/Hz below the motor rated V/Hz at low torque was verified on this test.

Variable Measured	Symbol		Accuracy
Rotor Speed	rpm	HP5301A Counter	0.02% of input +0.005% of range
DC Bus Volts	V D.C.	8600A DMM	0.02% of input +0.005% of range
	SH1	T&M coaxial shunt #F-10,000-40	0.1%
Motor Torque	T	Lebow Torque table	0.1% F.S. or 0.75 in-lb.
		Daytronic strain gage data module #878	0.05% F.S.
		Daytronic strain gage data module #870	0.05% F.S.
		Daytronic torque readout #890	0.02% F.S. ± digit
Volts/Hz	V/Hz	Eaton V/Hz meter	±1 digit
Motor Amps	I A.C.	Pierson current transformer	0.1%
		#301 x Hewlett Packard voltmeter #HP427A	2% F.S., 10 Hz-100 KHz
Motor Line Volts	V A.C.	Hewlett Packard voltmeter #HP427A	2% F.S., 10 Hz-100 KHz
Ø 1-3 watts	W1	Clark-Hess digital wattmeter	±0.4% F.S. ±0.2% V.A. @ 30 Hz-50 KHz
	W1E	Eaton wattmeter	0.5%
	SH2	T&M coaxial shunt #F10,000-40	0.1%
Ø 2-3 watts	W2	Clark-Hess digital wattmeter	±0.4 of F.S. ± 0.2% V.A. @ 30 Hz-50 KHz
	W2E	Eaton wattmeter	0.5%
	SH3	T&M coaxial shunt #F10,000-40	0.1%
Temperature		Doric thermocouple switch #ESC-24-IL	N.A.
Inverter		Doric thermocouple indicator #D5350T3	R.F. solution 0.1° stability
Motor		Type I	0.025°F/°F
Oil		Type K thermocouple	+0.6°F
Motor Winding	Temp.	Leeds & Northrup Kelvin bridge #4285	±100
Oil Flow		Dwyer Visi-float Flowmeter VFB	3% F.S.
Peak Currents	Crt.	Nicolet explorer oscilloscope	
Frequency Spectra	-	HP Fourier Analyzer #5451C	See Manual

Figure 5.4.2. Motor and Inverter PWM Tests

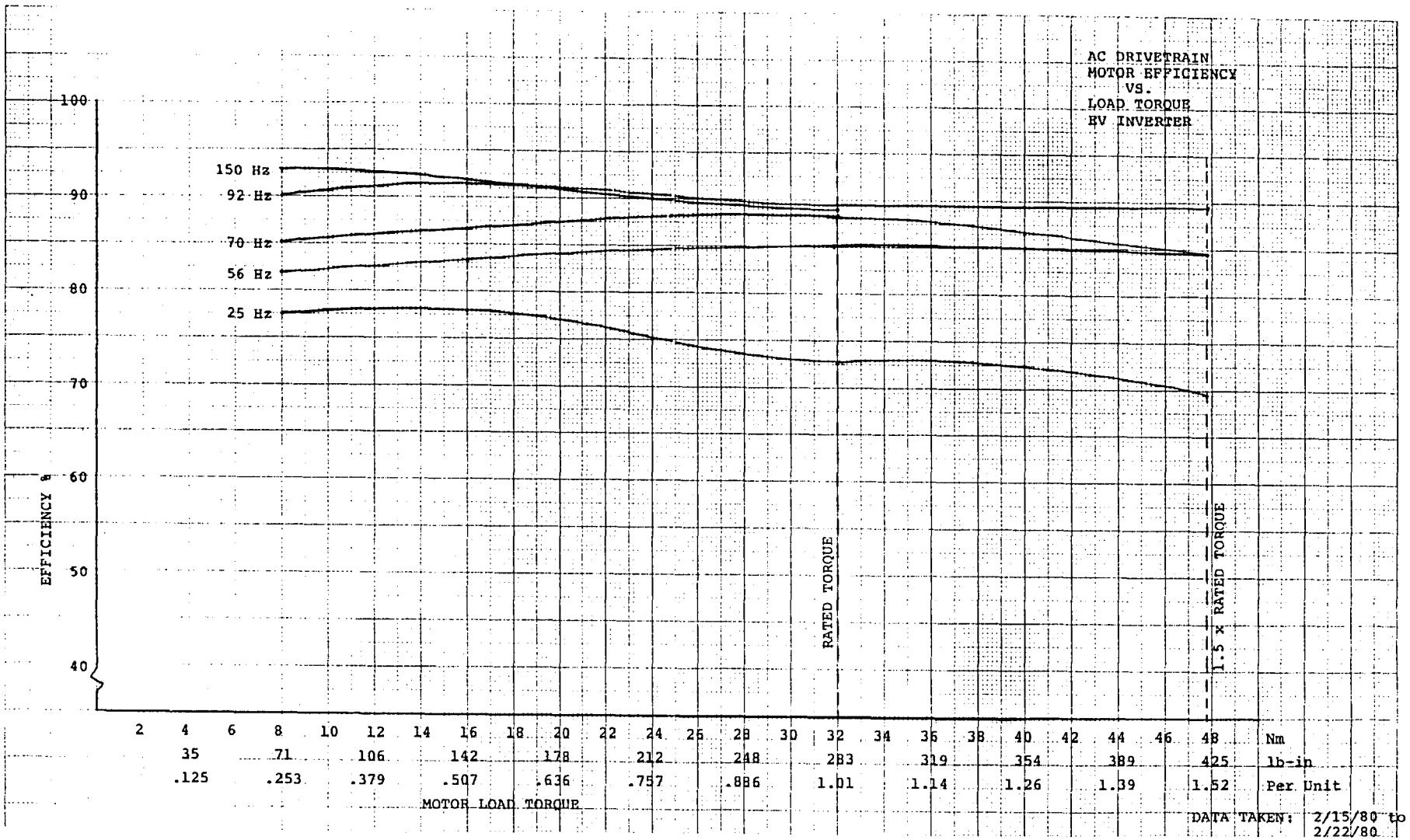

Figure 5.4.3 Optimal Motor and Inverter Operating Conditions

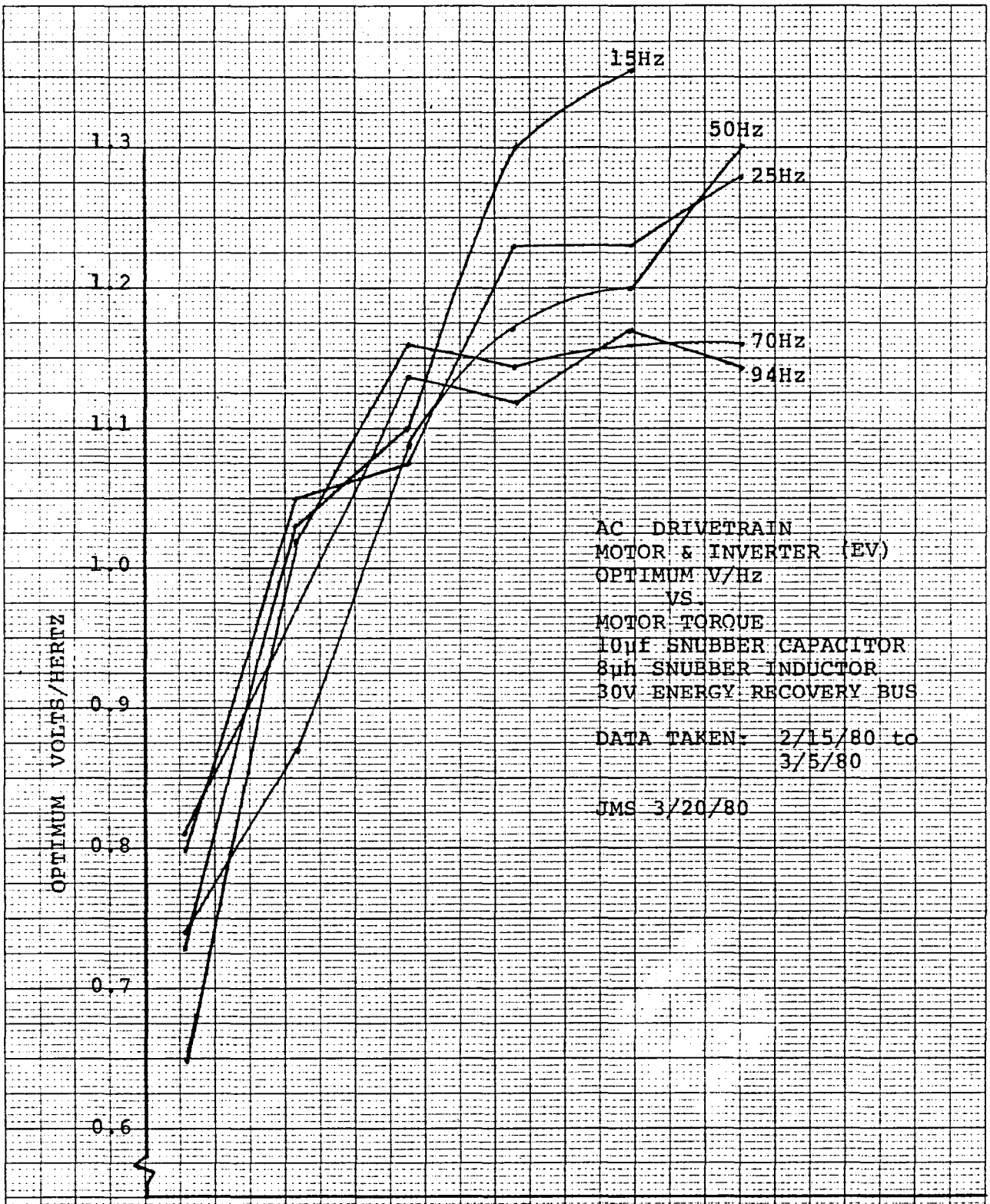

Figure 5.4.4 Optimum V/Hz vs. Motor Torque - Motoring

Motor Thermal Tests

This test was run to ensure that the motor could meet its one hour continuous thermal rating at rated torque. Tests were run at base speed and below in order to compare the square wave results with PWM operation. The test procedure for this test was as follows:

1. The oil flow was set to 1.9 liters/min. (cold).

2. The following data was recorded before starting up the motor: oil flow, input oil temperature, output oil temperature, motor case temperature, room temperature, and motor winding resistance.

3. Starting with a cold motor, operating at 30 Hz, 1.07 V/Hz and rated torque, the following data was immediately recorded: oil inlet and outlet temperature, ambient temperature, motor case temperature, transistor temperature, and notch number. The notch number was selected from previous data to minimize dc bus current.

4. The motor was operated under the above conditions for 30 minutes, and while motor was still running, all above data was recorded.

5. The motor was then shut down immediately, and winding resistance was measured.

6. After letting the motor cool down to ambient, the above procedure was repeated except the motor was run for 1 hour instead of 30 minutes.

The above procedure was repeated for 60 Hz and 94 Hz operation.

Figure 5.4.5 shows the temperature rise of the stator winding for this test as determined by the resistance measurement.

The PWM thermal tests indicate that voltage harmonic losses are not excessive. The losses introduced by the low order harmonic (5th and 7th) are usually most significant since the rotor presents a low inpedance path to these harmonic voltages. The effect of higher order

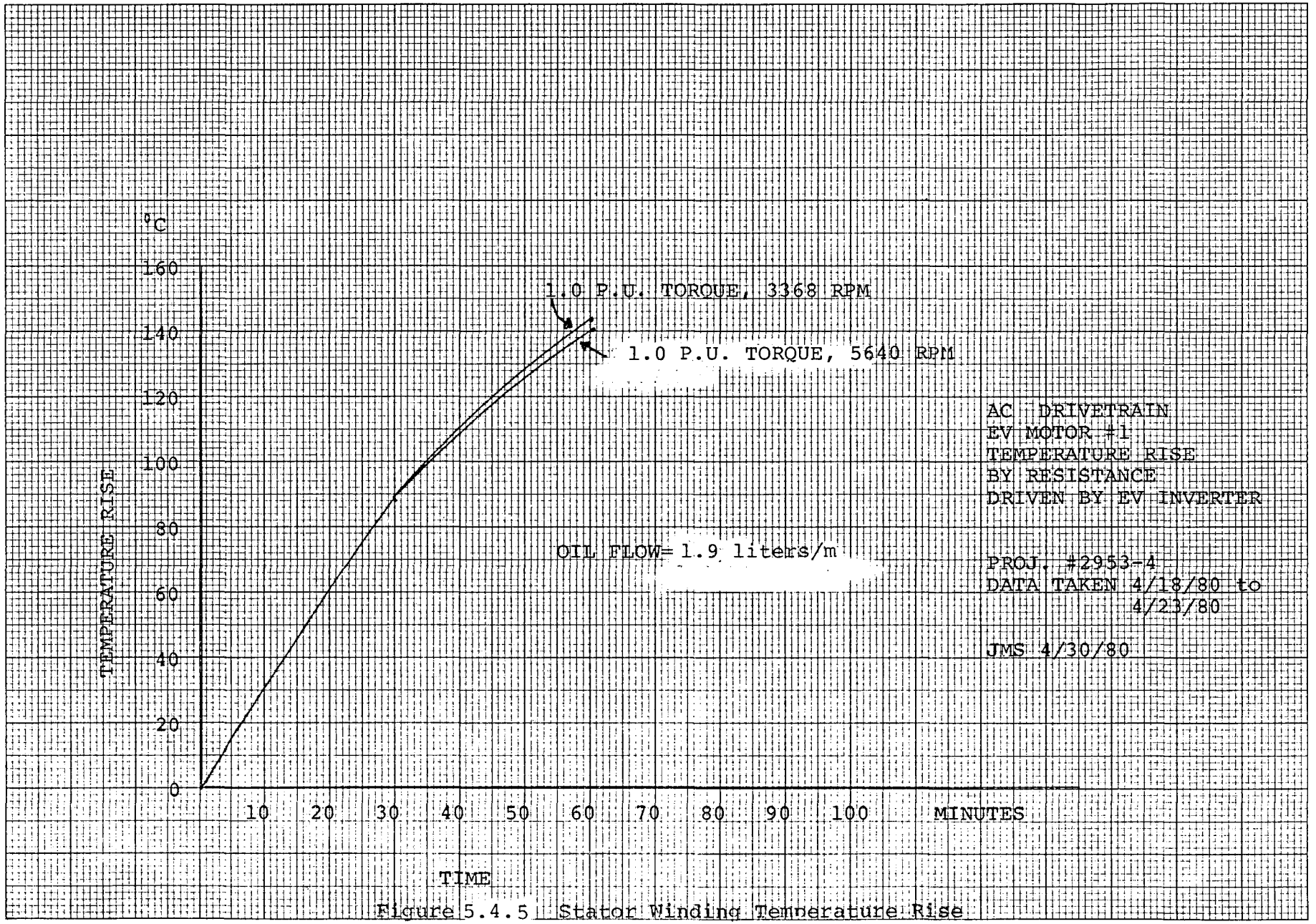

Figure 5.4.5 Stator Winding Temperature Rise

harmonics generally decreases as the inverse square of the harmonic number. A quality factor

$$Q = \sum_{N=2}^{\infty} \left(\frac{V_N}{N}\right)^2$$

may be defined for any applied waveform where V_N is the harmonic voltage of the Nth harmonic. Total RMS current is defined as

$$I_{RMS} = \sqrt{I^2 Fund + \left(\frac{1}{X_2}\right)^2 Q}$$

where X_2 is the fundamental locked rotor impedance, and I Fund is fundamental current.

Proportion of Losses Carried by the Oil

The Dexron #2 oil temperature rise through the machine at 1.9 liters/min. for the full load 100 Hz test was 12.5°C. Since the energy loss being carried away by the oil during a minute is rise times flow times specific heat,

12.5°C x 0.0315 liters/sec. x 0.75 kg/liter x 2097 joules/kg/°C = 619 watts,

and since the calculated machine dissipation is 4250 watts, the result suggests that only a small fraction (0.147) of the heat loss is being carried away by the oil in this first generation sample. Perhaps the oil is serving to balance the internal temperature rises.

5.5 Conclusions

This ac traction motor may be characterized as a motor capable of operating at a constant efficiency of around 85% at speeds and torque above 25% of rated value. This should aid in obtaining a high overall system efficiency on many driving cycles.

Improvements to this motor could be made in future development to provide better efficiency, cooler operation, lighter weight, and lower manufacturing costs.

Efficiency can be improved by providing more stator winding area, utilizing a better grade of steel and/or thinner laminations, and designing for lower slip operation. A motor designed with these improvements would require custom punchings which provide a larger winding window and slightly smaller air gap diameter. The rotor bars could be specially shaped to increase harmonic impedance and the rotor should be flame treated to open any eddy current paths caused by machining burrs. A machine designed to these conditions has a predicted sine wave efficiency of 91% at rated torque, 60 Hz, hot. This represents a 3.5% efficiency increase over the first prototype.

The use of fins and forced air could improve the motor heat transfer rates and temperature, but this introduces weight and complexity. Therefore, an improved oil heat transfer scheme is recommended. Cooling the housing before entering the motor would be proposed. Projections indicate an internal temperature rise for sine wave operation of 45°C.

The 66.8 kg (147 lb.) motor weight may be reduced by utilizing an aluminum housing and end bells, by utilizing a custom motor shaft of reduced diameter and by punching holes in the rotor laminations where there is no magnetic flux. A weight of 50-55 kg (110-120 lbs.) should be obtainable.

6. INVERTER

6.1 Introduction

This section presents the design and development information and test results for the power inverter section of the ac drivetrain. Subjects covered in this section are

- Inverter power requirements and transistor selection
- Power circuit design and snubber requirements
- Transistor base drive requirements
- Drive protection schemes
- Snubber energy recovery methods
- Test results and inverter performance
- Considerations for future improvements.

The basic inverter schematic is shown in Figure 6.1.1. In addition to the main transistor switching elements, the schematic shows the following:

- Inductive and capacitive snubber elements around each transistor, which are used to reduce transistor turn-on and turn-off stress.

- A "back" or "flywheel" diode connected antiparallel to each transistor for carrying motor current when both transistors in a leg are turned off.

- A base drive circuit for each transistor used to supply transistor base drive power and switching, and to provide fast, local protection for the transistors.

- An energy recovery circuit for recovering energy stored in the snubber inductors.

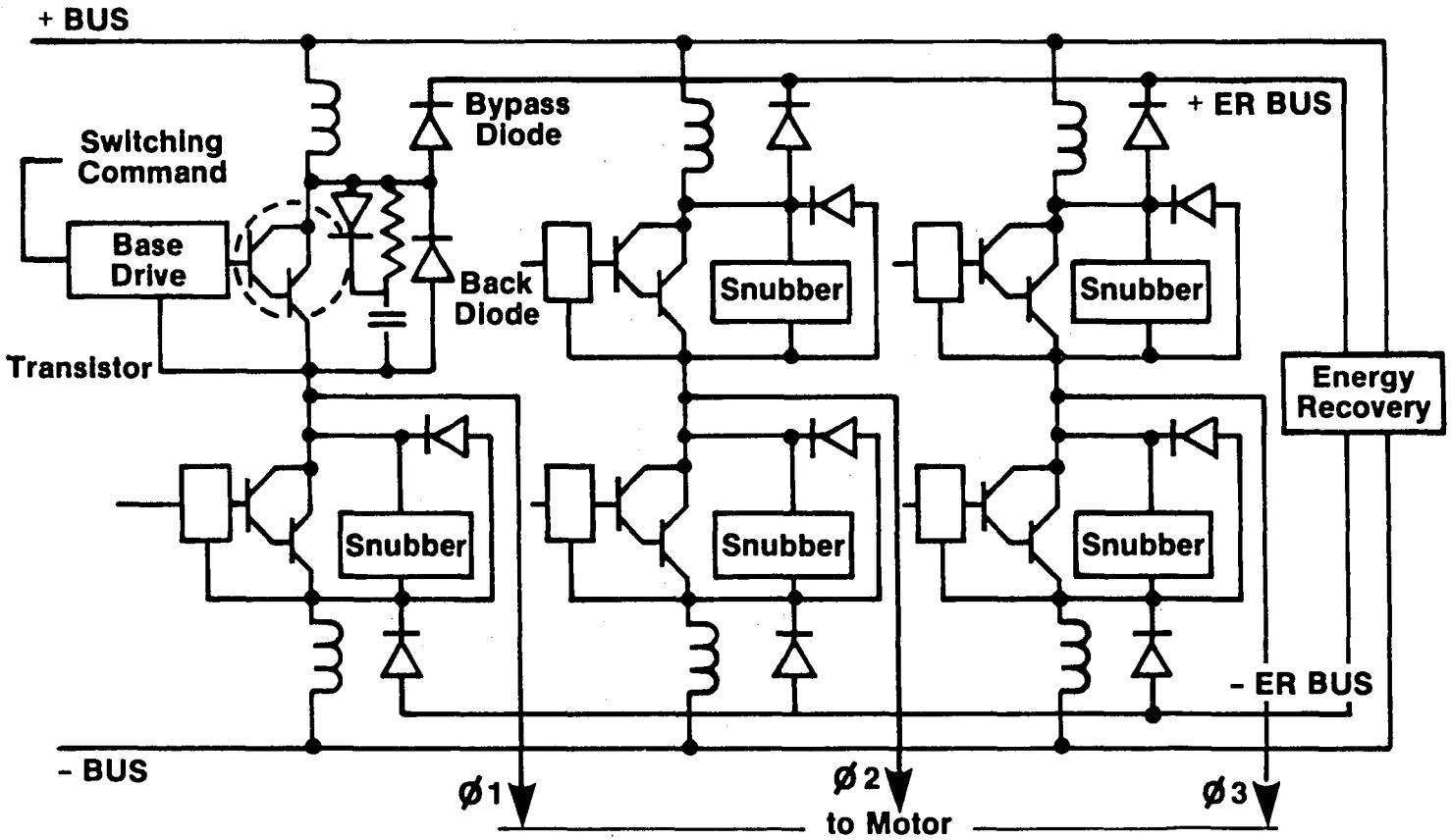

Figure 6.1.1 Inverter Schematic

6.2 Background

Upon receipt of this contract, a breadboard of the power inverter already had been built. Thus, a first cut at the major design and development tasks had been completed at the contract initiation date. These tasks included the following:

- Decision on a transistorized PWM approach and transistor selection based upon expected power levels.
- Design of inverter bridge circuitry, base drive circuitry with protection logic, and energy recovery circuit.
- Testing of a single inverter leg on a passive load.
- Buildup of a complete inverter prototype.

Although designed and built, the inverter had been tested at the component level only, and had not actually driven a motor. Thus, although the base drive circuitry had undergone extensive testing to ensure adequate base current under extreme battery voltages, and the inverter protection circuitry had been tested for proper voltage thresholds and noise immunity, there remained major system considerations and concepts that had not been tested. The following is a description of the inverter at the start of the contract.

Initial Design Considerations

Pulse width modulation was chosen to control motor voltage because of its ease in connecting to a battery source. Alternative approaches, such as variable dc link voltage, require a front-end chopper and a large bus filter and make regeneration awkward. In contrast, PWM is inherently regenerative and requires a relatively small bus filter. In addition, the generation of complex PWM waveforms is fairly easy with the microprocessor interface.

Transistors were chosen over SCR's as the main switching elements because they do not require commutation circuitry, and they offer the possibility of operating at a higher switching frequency than with SCR's. Although high power transistor costs are now prohibitively high, the promise of future low cost transistors and the above advantages justified their selection as the switching elements in this prototype. The advantage of the elimination of SCR commutation elements is somewhat offset by the large snubber components that were ultimately required, and by the energy recovery circuit on this inverter. However, it is predicted that these snubber components can be greatly reduced and the energy recovery circuit simplified or eliminated in future inverters.

Transistor Selection and Inverter Sizing

Drive transistor power handling capability is based upon calculations of expected motor current at peak torque output (see Figure 6.2.1). These calculations show that, for a 144 volt bus, peak currents of 500 amperes are possible at peak motor torque. The Toshiba 2SD648 monolithic power Darlington with a sustaining voltage of 300 volts and a peak pulsed current rating of 600 amperes, was the only available transistor that could meet these requirements at the time.

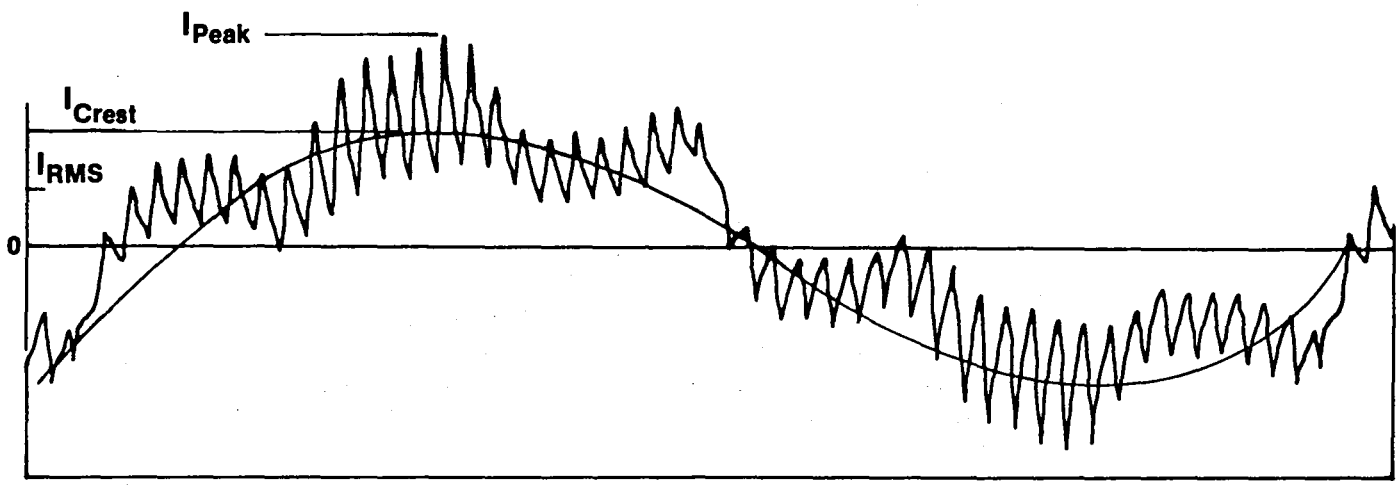

Figure 6.2.1 Motor Current Definitions

Drive Protection Schemes

Protection of the inverter transistors at the base drive level (local protection) was included in the design for protective functions needing a faster response than possible with microprocessor level protection. The protective functions on the original drive were as follows:

1. A "V_{CE} sense" comparator for each transistor for detecting a short circuit across that transistor or failure of that transistor to turn off. V_{CE} sense comparator outputs on complementary transistors in each inverter leg were coupled through opto-isolators in order to prevent a transistor from turning on if its complement failed to turn off or was shorted.

2. A negative current sense comparator. This comparator was intended to detect current in the antiparallel back diode of each transistor. Detection of negative current around a transistor prevents that transistor from turning on, thus conserving base drive power. This sensor was also needed in conjunction with the above V_{CE} sense comparator in order for the V_{CE} sense logic to distinguish between a failed or shorted transistor and a transistor with a conducting back diode.

3. Peak current limiter. An active current limit sensor for each transistor was included to turn off a transistor immediately if an overcurrent condition is detected.

Base Drive Power

Each of the six base drives has its own isolated dc-to-dc power supply for base drive and logic power. The independent supplies eliminate any leg-to-leg interference, and provides power section flexibility during development. The base drive power supplies are capable of supplying up to 6 amps of base current to any transistor. These supplies are capable of operating between a 160 and 94 volt battery input voltage. A negative supply is capable of sinking up to 5 amps base current for short duration at transistor turn-off in order to reduce transistor storage time.

Snubber Requirements and Energy Recovery Circuitry

Inductive and capacitive elements around each transistor are included for load line shaping during transistor switching. Requirements for both capacitive and inductive snubbers are interrelated in the PWM inverter as follows. Capacitive snubbers are needed due to stray wiring inductances and the need to prevent transistor second breakdown or overvoltage during turn-off, and these in turn lead to the need for snubber inductors to prevent large current inrush to the capacitive snubbers at turn-on. This current inrush can occur in a PWM inverter because the drive transistors are forced to turn on when the back diodes of their complements are conducting and, thus, the snubber capacitors across these back diodes will be discharged. Another requirement for the snubber inductors arises from the need for a di/dt limit for the transistors during short circuit conditions. Without this di/dt limit, the peak current of the transistor could be exceeded during a short circuit before the transistor's storage time has passed.

The energy recovery circuit is included as a means of recovering trapped snubber inductor energy. At transistor turn-off, this trapped energy is dumped onto an alternate

bus through bypass diodes where it can be either dissipated or returned back to the battery by a dc-dc converter. By recovering this trapped energy, it is possible to save more than one kilowatt of inverter power under extreme motor operating conditions.

6.3 Design Evolution Through Hardware Testing

Inverter development during this contract was concentrated in the following areas

1. Transistor safe switching loci and snubber design.
2. Drive local protection strategies.
3. Energy recovery converter.
4. Drive current limit methods.

These areas of development are discussed in the following paragraphs.

Transistor Safe Switching Locus

In order to achieve safe switching of the output transistors, it was necessary to solve problems related to packaging and snubber circuit design. The importance of packaging in high power transistor circuits cannot be overemphasized. During this development work, a complete redesign of the inverter package was required in order to shorten snubber and energy recovery circuit wire lengths. Figure 6.3.1 shows the transistor voltage and current turn-off waveform before repackaging of the inverter.

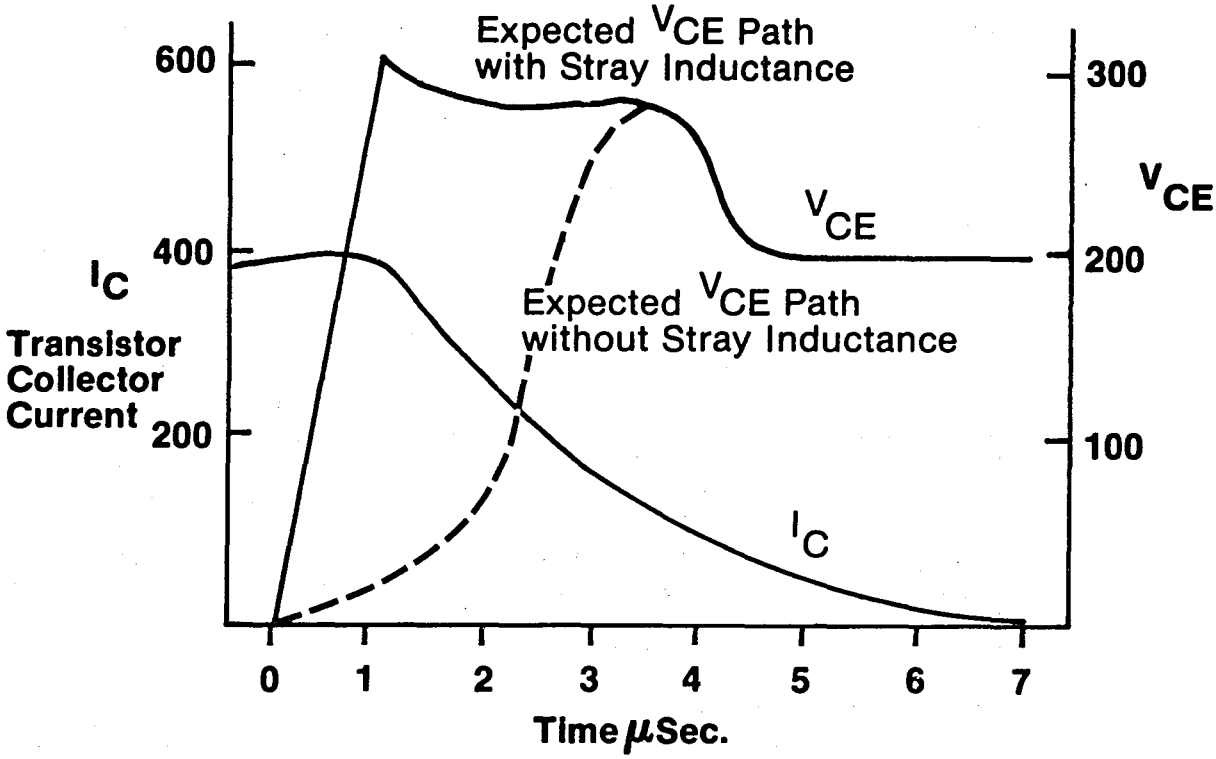

Figure 6.3.1 Transistor Turn-off Before Repackaging Inverter

It is seen that the fast voltage rise caused by the stray wire inductances is a serious deviation from the desired voltage path that would occur if stray inductances were eliminated. The above switching locus for I_C and V_{CE} was outside the transistor's safe operating area (SOA) and resulted in transistor failures. In the final inverter package, all wire lengths to snubber capacitors were kept below 5 cm. In addition, it was necessary to distribute capacitors along the energy recovery bus bars in order to provide a short, non-inductive path for the snubber inductor trapped energy at transistor turn-off.

Snubber Capacitor Energy Recovery

One leg of the original inverter circuit is shown in Figure 6.3.2. This configuration used one snubber capacitor for each leg.

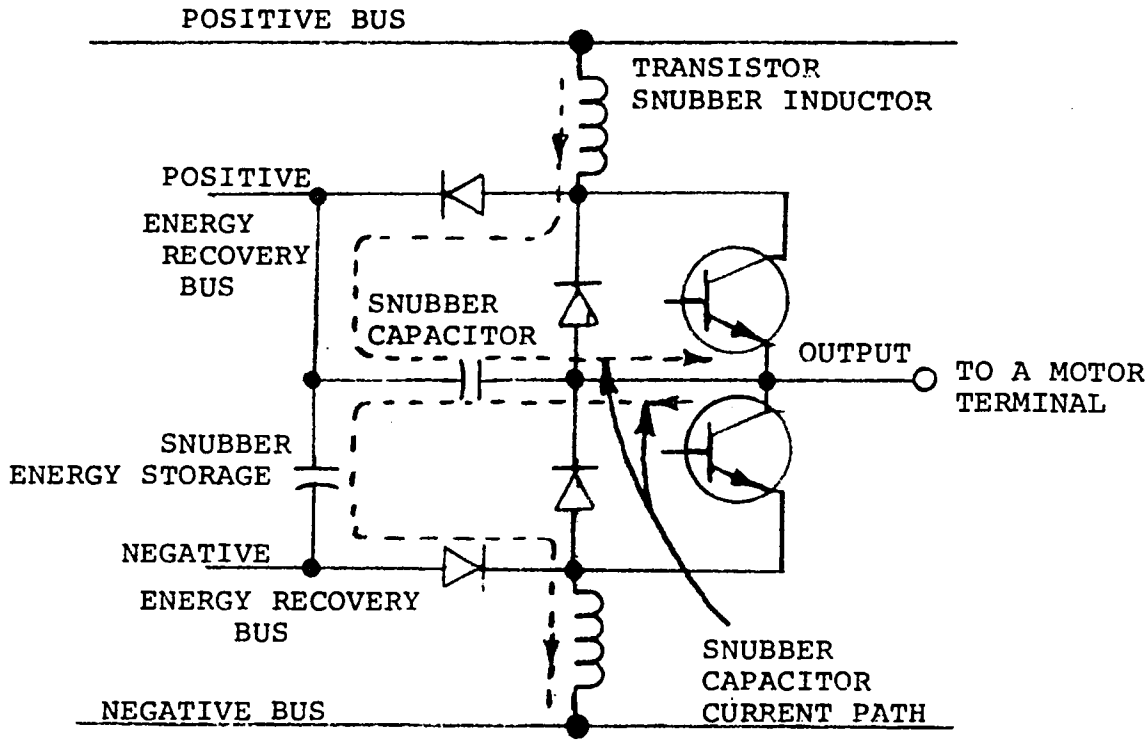

Figure 6.3.2 Power Circuit Schematic, One Inverter Leg

It can be seen from the figure that the current path through the snubber capacitor is always between the motor and the dc power source. In this design, snubber capacitor energy is transferred onto the energy recovery bus during transistor switching where it can be converted back to battery power. This approach was an attempted improvement over conventional snubber arrangements in which all of the stored snubber energy is dissipated at transistor turn-on.

A problem in this circuit was that excessive ringing occurred between the inductive and capacitive snubber elements when switching. This ringing had the effect of cancelling out some of the power conservation advantages of the circuit and was thought to have been related to motor current waveform stability problems that were also occurring at that time. An additional power loss in this circuit occurred at transistor turn-off because the transistor V_{CE} had to rise to the energy recovery voltage before the snubber capacitor could start conducting. Figure 6.3.3 is a transistor turn-off waveform for this circuit showing the ringing problem and the extra switching loss described above.

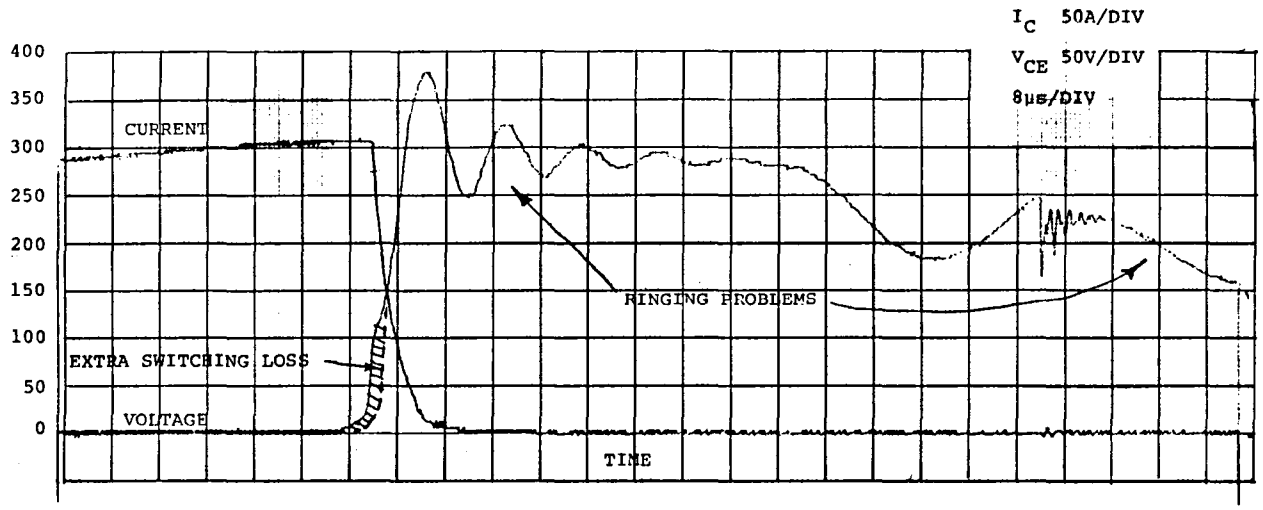

Figure 6.3.3 Transistor Turn-off Waveform

Conventional Snubber Configuration

Other variations of the above inverter configuration were attempted with marginal success in order to preserve the capacitive energy recovery feature, but break up the ringing paths. This concept was eventually abandoned in favor of the conventional snubber arrangement as shown in Figure 6.3.4.

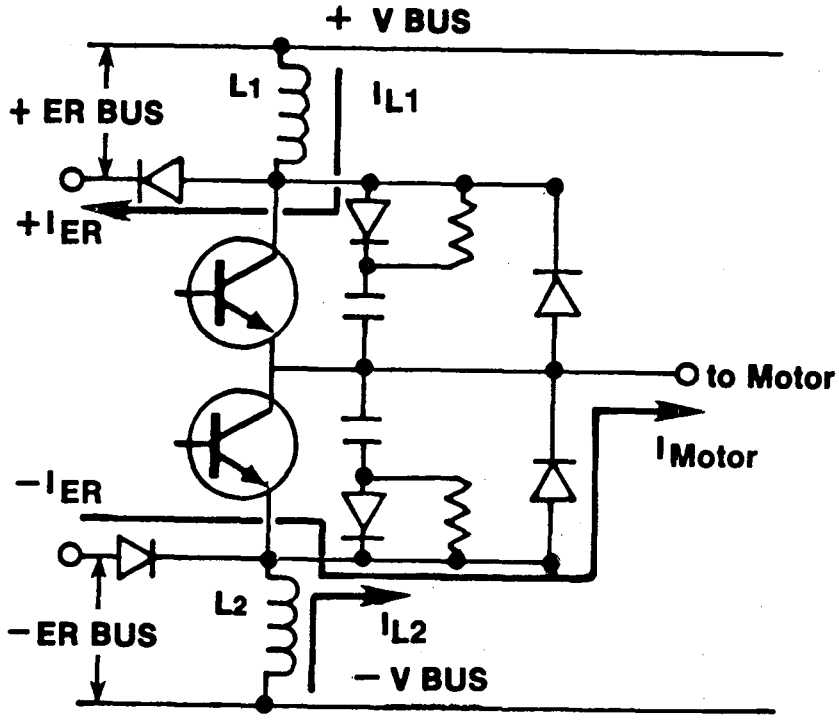

Figure 6.3.4 One Leg of Final Inverter Configuration

A transistor turn-off waveform for the final inverter configuration is shown in Figure 6.3.5.

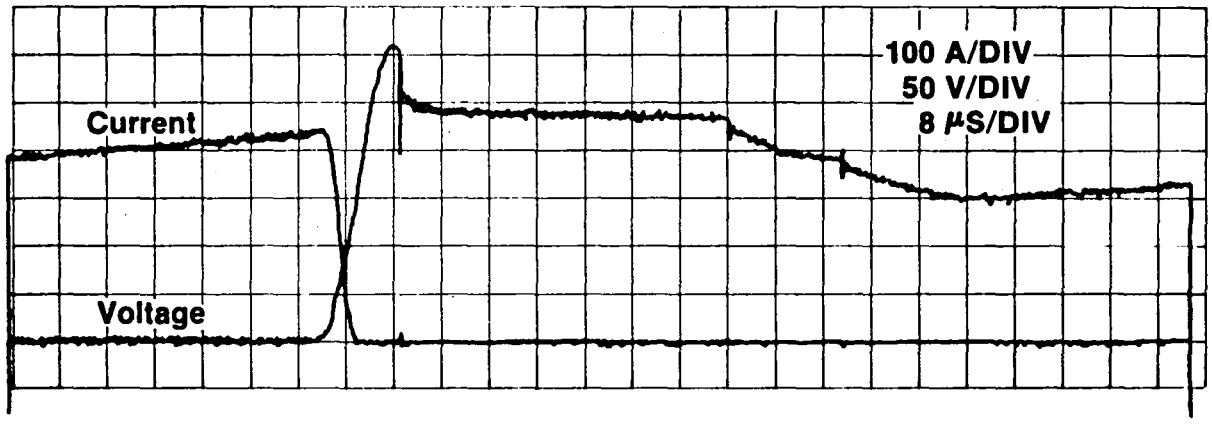

Figure 6.3.5 Transistor Turn-off Waveform .

The transistor load line for the above waveform is shown with the Toshiba repetitive safe operating area in Figure 6.3.6.

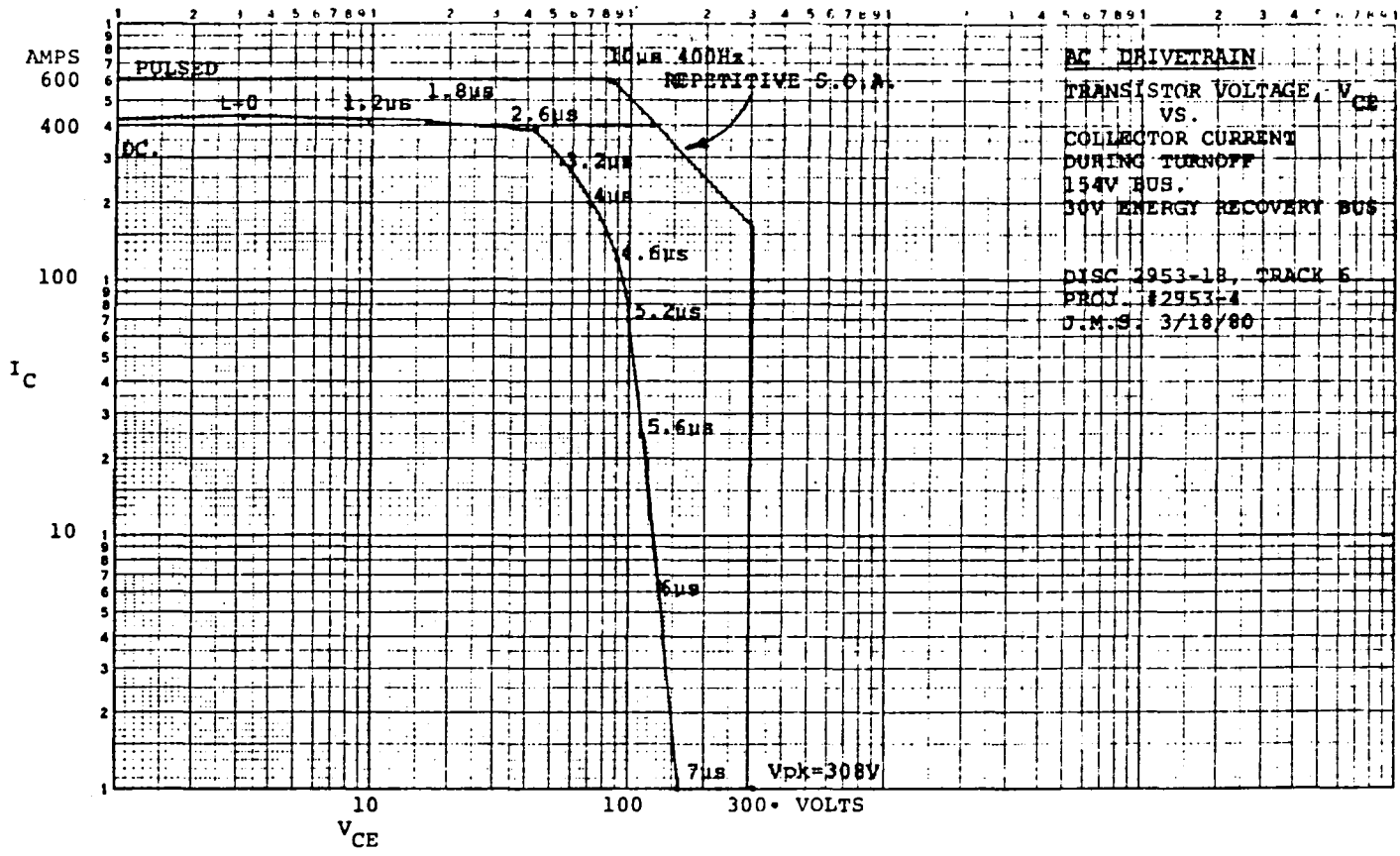

Figure 6.3.6 Transistor Turn-off Load Line

It can be seen from the above load line that the transistor switches well within the Toshiba safe operating area and that, in fact, the snubber capacitors are oversized for the inverter. However, examination of Figure 6.3.5 shows that the peak transistor turn-off voltage is near the V_{CE} sustaining voltage of 300 volts. This peak voltage is caused by stray wire inductance that remains even after repackaging the inverter. When the equation,

$$W = \frac{1}{\sqrt{LC}} \text{ , or } \frac{T}{2} = \pi\sqrt{LC}$$

where W is frequency in rad/s, T/2 describes the duration of the voltage peak, and L and C are the stray wire inductance and snubber capacitance (10 µf), respectively, is

solved for L, it is found that a stray inductance of only 0.25 microhenries would cause this voltage overshoot. As further significant reduction of stray inductance would be extremely difficult, and as transistors with greater voltage margin were not yet available, the only viable alternative for staying within the transistor's voltage rating was the use of power zeners, or use of oversized snubbers.

It was decided to use oversized snubbers on this drive because the added cost of power zeners on all six transistors was judged prohibitive. It is predicted that future, higher voltage transistors will allow snubber capacitor size to be significantly reduced without the need for power zeners.

Load lines taken with smaller snubber capacitors have shown that the existing capacitors could be cut at least in half if they were not required to reduce the peak voltage overshoot. The final value for the snubber capacitor was 10 microfarads.

Failed Transistors

During the inverter development, many transistor failures were encountered. Because of the high cost of these devices, and because of previous inexperience in dealing with transistors at this power level, considerable effort was expended categorizing the failure modes and investigating their causes. Photomicrographs were taken of failed transistor substrates as part of this effort.

The transistor failures can be grouped as follows:

1. Switching out of safe operating area. This failure mode has been discussed in the section on snubbers. Repackaging of the inverter eliminated this problem. A photomicrograph of a transistor subjected to this failure mode is shown in Figure 6.3.7.

2. Negative current too high. This type of failure occurs when the internal back diode in the transistor attempts to conduct more than its share of motor current. Normally, the external back diode (connected in parallel to the internal one) conducts virtually all of this current; however, cases were noted in which the internal back diode, which has a 12 ampere rating, had in excess of 60 amperes of current. At first, this problem was attributed to faulty mounting of the external back diode, but it is now believed that some of the transistors had lower than normal forward drop in their back diodes and that these failures were unavoidable. A photomicrograph of this type failure is shown in Figure 6.3.8. The indicated area shows the location of the internal back diode that failed.

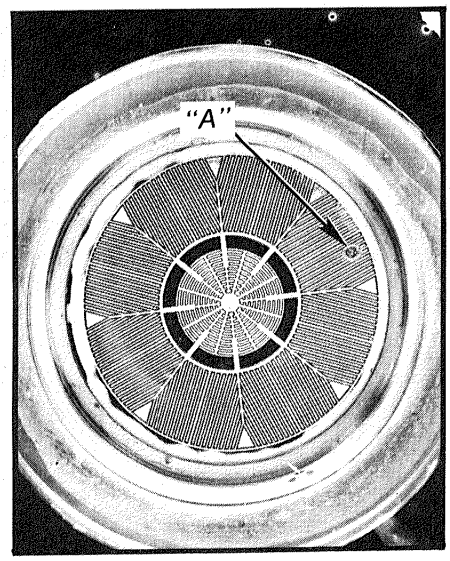

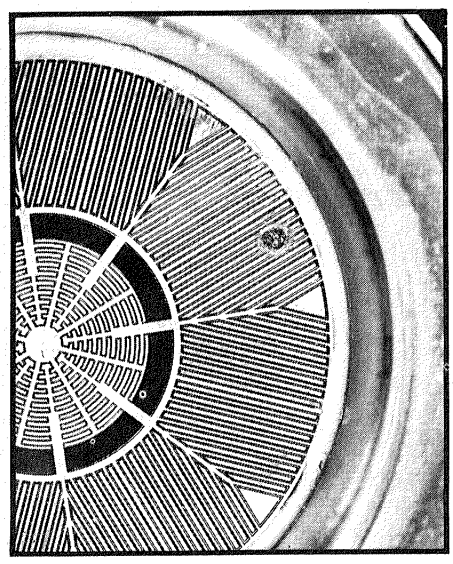

Detail of "A"

Figure 6.3.7
Photomicrograph of Second Breakdown Failure

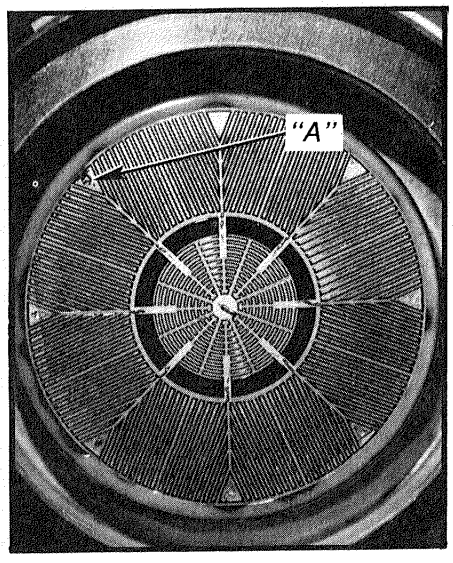

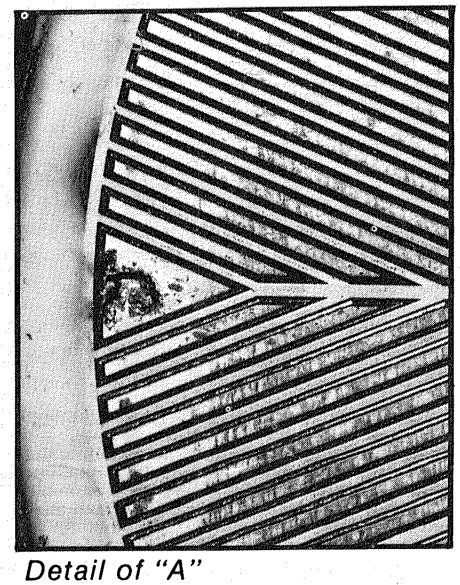

Detail of "A"

Figure 6.3.8
Photomicrograph of Reverse Diode Failure

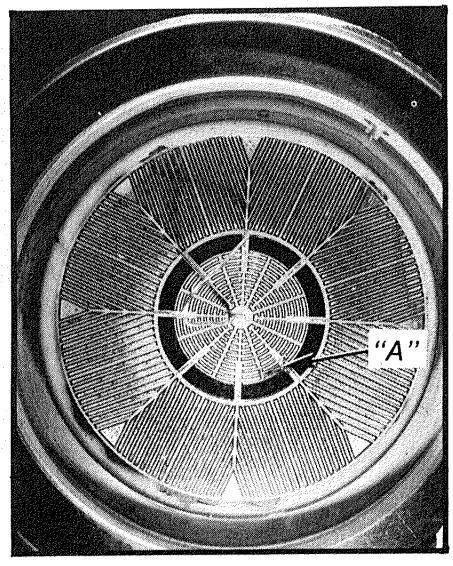

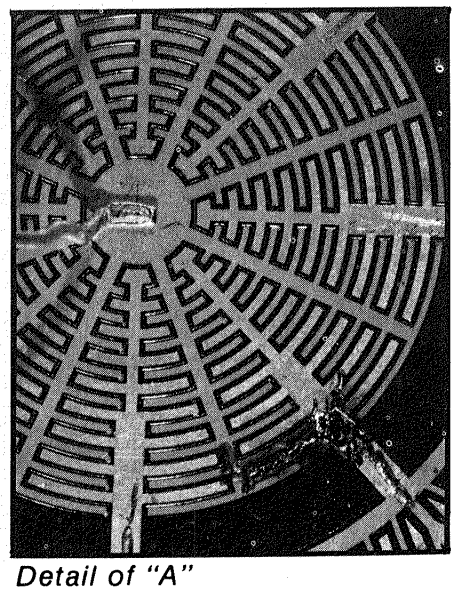

Detail of "A"

Figure 6.3.9
Photomicrograph of Collector-Base Short

3. Incorrect protection logic. These failures were related to the sense logic in the base drive circuit.

4. Transistor mounting. It is believed at least one failure was caused by incorrect transistor mounting in which the heat sink centering pin was out of line. This led to unequal current sharing over the active area and to hot spots. Other mounting failures were suspected but not proven.

5. Wiring mistakes. Some failures were caused by mistakes in wiring: base emitter leads reversed, incorrect fixes on base drive protection logic, broken wire to current limit sensor, etc. Figure 6.3.9 is a photomicrograph of a transistor whose collector-base terminals were inadvertently shorted.

All failures in the Toshiba transistors resulted in a collector-to-emitter short circuit. This failure mode was an important consideration in the overall drive protection logic, which is aimed at protecting the complement of a failed transistor. Failure modes, such as an open collector-emitter which could occur in other types of transistors, would place stress on the base drive circuit and would require a different protection approach. Future inverter designs must consider the failure modes of the transistor being used in its drive protection schemes.

Overall, the Toshiba 2SD648 Darlington Power Transistor proved to be a reliable device when driven within its ratings and safe operating area. Its thermal performance was excellent and its losses acceptable. Its disadvantages relative to EV inverter application are low switching speed and cost.

6.4 Test Results

The following is a summary of performance tests that were run on the inverter during this contract.

1. Motor line current and voltage. Figure 6.4.1 shows motor line current and line-to-line voltage at various speed and torque conditions. Included are two operating conditions for regenerative braking. Overall motor and inverter performance was acceptable.

2. Peak currents. Figure 6.4.2 is a plot of the peak motor current vs. motor output torque for various motor speeds. It can be seen that for 1.5 rated motor torque, the peak current is within the current limit setting of 460 amperes. The peak inverter current is the limiting factor in motor torque output capability. Above base speed (94 Hz), peak currents begin to fall.

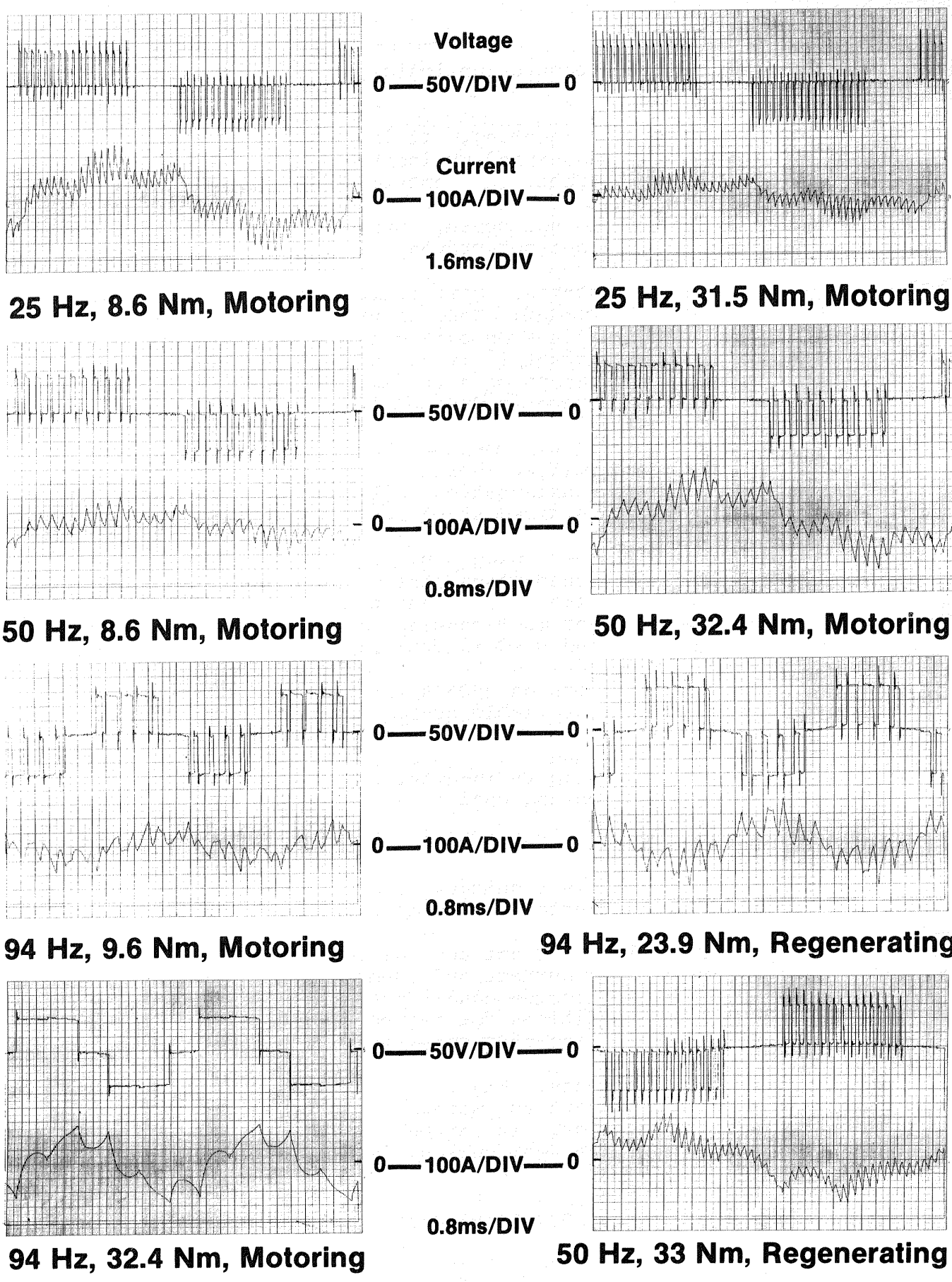

Figure 6.4.1 Motor Line-Line Voltage and Motor Current for Various Operating Conditions

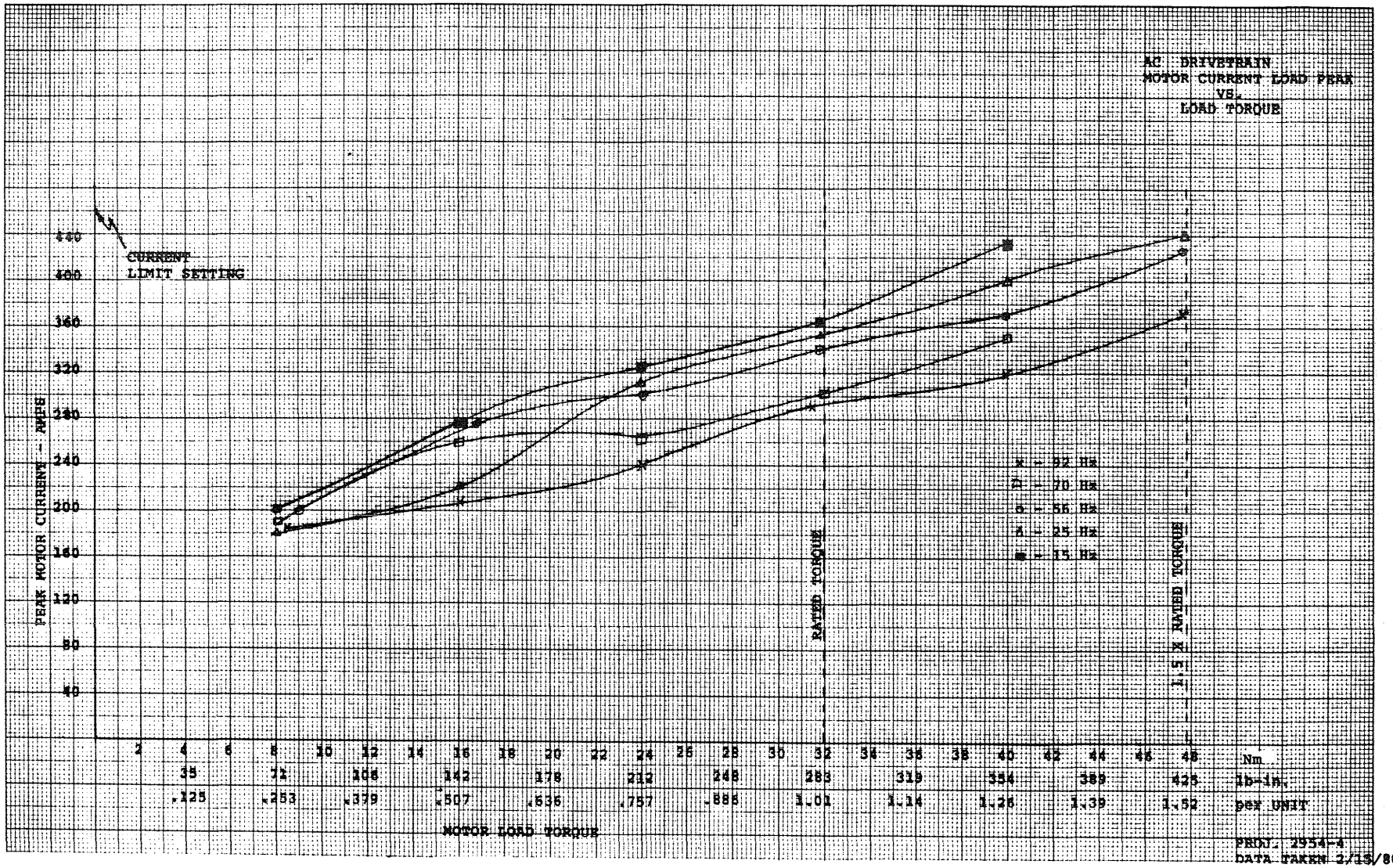

Figure 6.4.2 Motor Current Load Peak vs. Load Torque

3. Inverter efficiency. The test setup and instrumentation used is given in Section 9. Figure 6.4.3 is a plot of inverter efficiency vs. motor torque for various motor speeds. This plot shows a reasonably acceptable efficiency at high power levels, but at low motor speed and torque levels, inverter efficiency shows room for improvement.

Figure 6.4.4 shows the estimated losses in the principle inverter components for various inverter power levels. The component losses in the inverter are a function, not just of power level, but also of transistor switching rate. This effective switching rate is derived from the motor stator frequency, f, and the PWM notch number, n, by the relation, (2n + 1)f. Thus, the snubber capacitor power losses are calculated as

$$P_{loss} = K(2n + 1) \times f \times C \, V^2_{bus}/2$$

where K accounts for the voltage rise above V_{bus} at turn-off, and C is the snubber capacitor value.

Stator Frequency (Hz)	Inverter Power In (kw)	Inverter Power Out (kw)	Inverter Efficiency	Total Inverter Losses (kw)	Snubber Cap Loss (kw)	Snubber Ind. Internal Loss (kw)	Energy Recovery Loss (kw)	Transistor & Diode Conduction Loss (kw)	Base Drive Loss (kw)	Transistor Switching Losses
15	3.47	2.28	66%	1.19	0.277	0.427	0.10	0.340	0.13	0.065
25	6.8	5.08	75%	1.72	0.430	0.452	0.20	0.487	0.13	0.101
50	11.58	9.72	84%	1.86	0.496	0.574	0.20	0.474	0.13	0.116
70	15.41	13.16	85%	2.25	0.596	0.51	0.30	0.580	0.13	0.134
94	22.19	20.84	94%	1.35	0.075	0.470	0.051	0.580	0.13	0.044

Figure 6.4.4 Summation of Estimated Inverter Power Losses at Various Inverter Power Levels

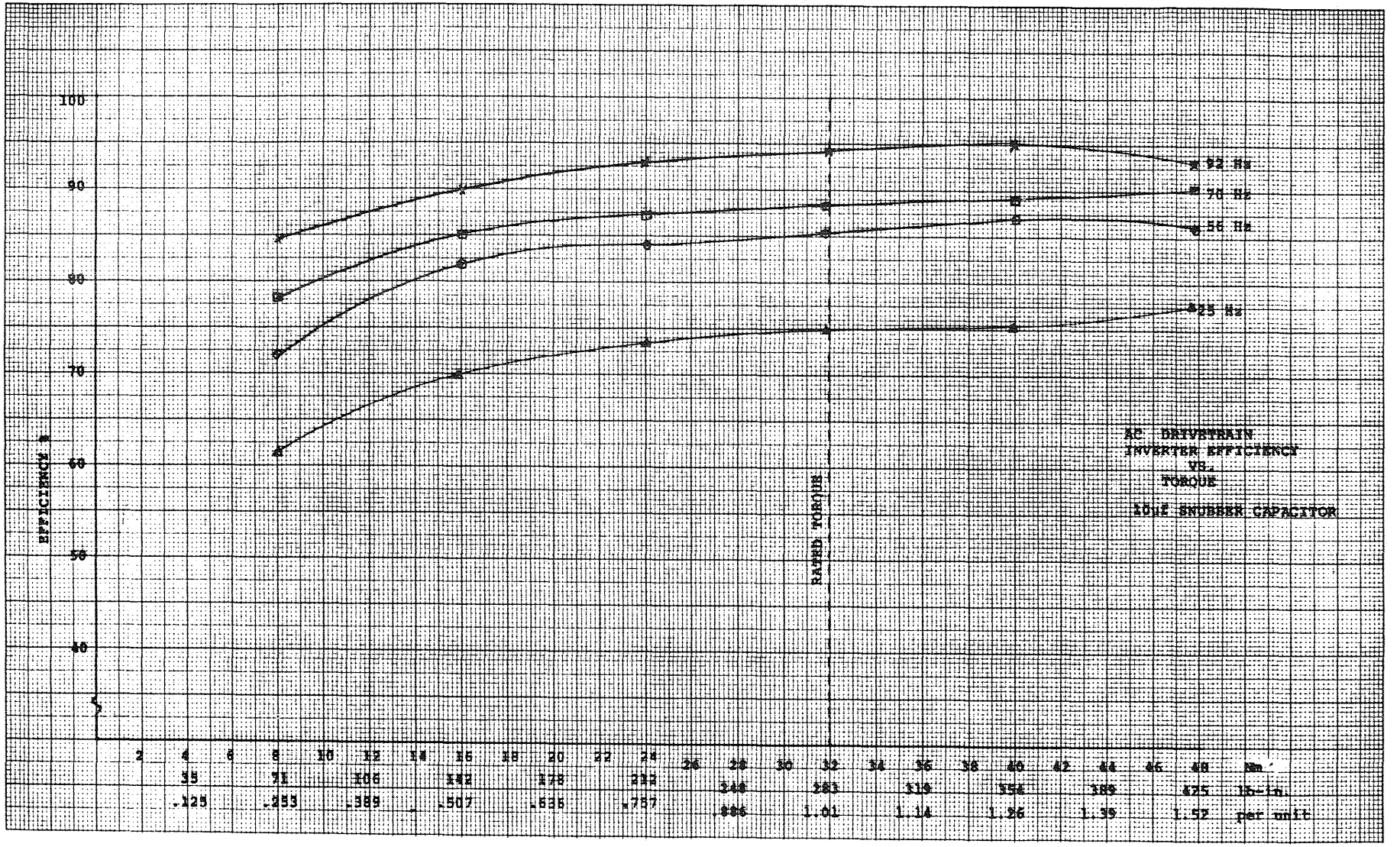

MOTOR LOAD TORQUE

Figure 6.4.3 Inverter Efficiency vs. Motor Torque

Referring to the itemized losses in Figure 6.4.4, it is predicted that future inverter efficiency can be improved as follows:

a. Snubber capacitor losses can be reduced proportionately to the reduction in the size capacitor required. With the availability of a higher voltage transistor, these losses can be cut at least in half. Figure 6.4.5 shows inverter efficiency test results with the snubber capacitor reduced by half.

b. Snubber inductor internal losses are composed of conduction I^2R losses, proximity, and skin effect losses. It is believed that these losses can be reduced by improving the inductor's physical design (increased stranding, cross-sectional area, improved geometry, etc.).

c. Energy recovery circuit losses were calculated by estimating the power loading on this circuit from the snubber inductors and assuming a conversion efficiency for converting this power back to the battery. Possible loss reduction in this area can be achieved by reduction in snubber inductor size or other means to reduce the power input to this circuit.

d. Transistor and diode conduction losses were calculated from the motor RMS current and an assumed voltage drop of 1.4 V across these devices. These losses could be reduced by raising the battery operating voltage in order to reduce the motor RMS current.

e. Transistor switching losses are related to inverter switching frequency, transistor turn-off time, and snubber values. These losses can be reduced by reducing transistor turn-off time. However, if snubber capacitors are reduced, then these losses may increase. Snubber capacitors need to be sized to optimize total switching losses.

f. Base drive losses are most significant at low power levels. These losses can be reduced by improved power distribution schemes and by improved base drive circuitry.

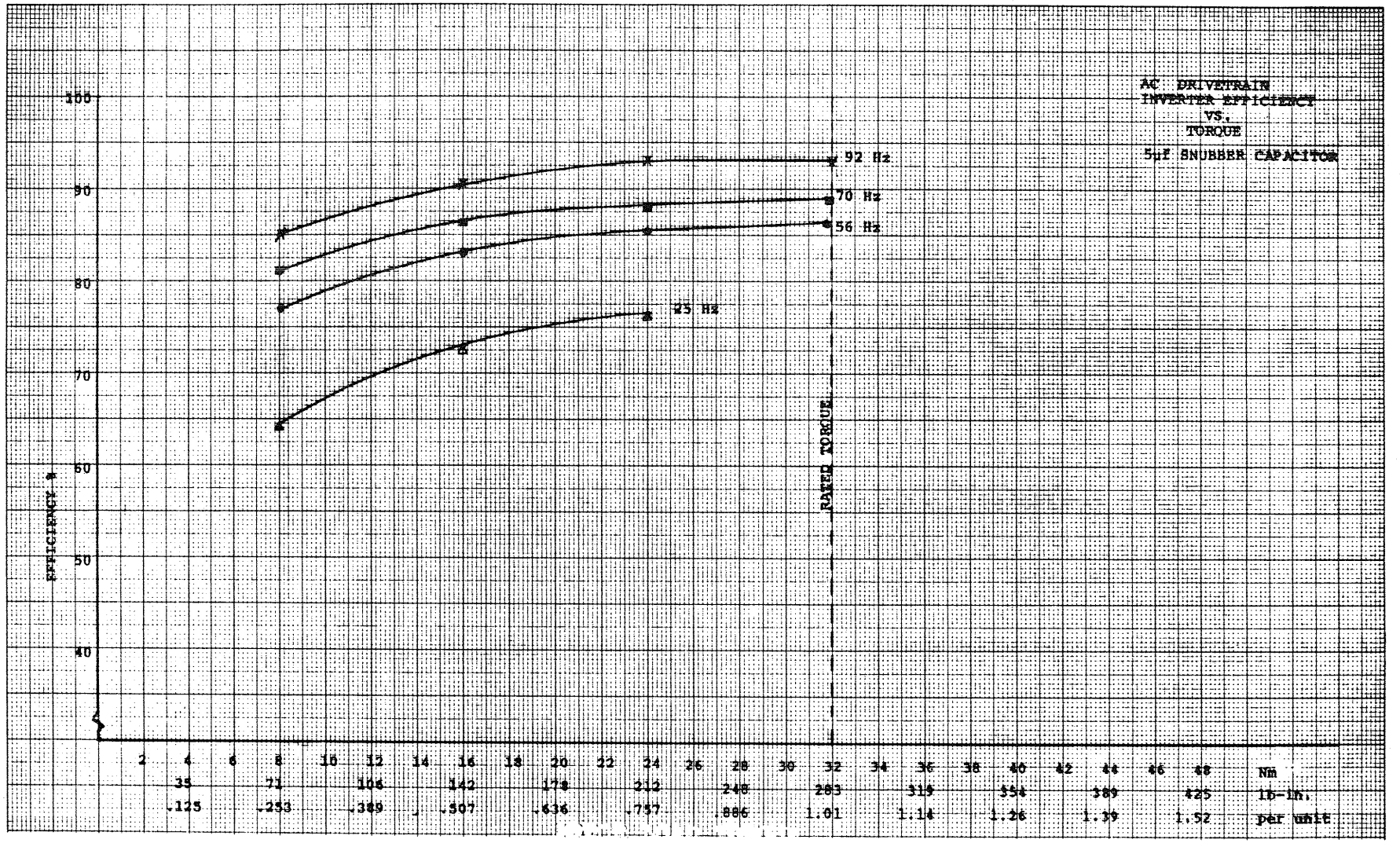

MOTOR LOAD TORQUE

Figure 6.4.5 Inverter Efficiency Test Results

4. Inverter thermal performance. Tests on the final inverter package at motor peak load and switching frequency revealed that at no time did the output transistor's heat sink temperature exceed 48°C. The energy recovery transistor peak heat sink temperature was 26°C. These relatively low temperatures indicate an overdesigned inverter cooling capability and, thus, indicate the possibility of reducing the inverter package size.

6.5 Discussion of Results and Future Improvements

The following points can be made on the status of the existing inverter and on goals for future inverters for electric vehicle applications:

1. The basic concept of a three-phase, PWM transistor inverter at the power level required for electric vehicle applications has been demonstrated. Before this concept is economically feasible, the cost of high power transistors must be drastically reduced. One possible method of obtaining greater transistor utilization, and thus lower transistor costs per inverter, is by running the inverter in continuous peak current limit when high torque is needed.

2. Efficiency. The inverter efficiency was sufficiently high at peak power output to make the total ac system efficiency comparable with dc systems. However, the inverter efficiency was low at reduced speed and torque and needs to be improved on future inverters.

   Improvements in inverter efficiency are possible by reducing capacitor and inductor snubber size, optimizing snubber inductor physical construction, improving base drive power design and distribution, and by selecting a higher battery voltage.

3. Inverter power rating. The inverter peak power level was sufficient for obtaining 1.5 times rated motor torque, which is marginal for meeting 1800 kg. vehicle acceleration goals. In a future inverter, this torque level should be pushed to 1.8 times rated motor torque. The limiting factor for peak power on the present inverter is the peak current rating of the Toshiba transistors.

4. Energy recovery. The energy recovery circuit was valuable for improving efficiency, but was overly complicated and would be economically unfeasible. An effort is needed to simplify or eliminate the need for this circuit.

7. CONTROLLER

7.1 Design Considerations

Any vehicle-mounted control logic must be rugged, free of delicate adjustments, and free of excessive temperature drift.

All operator interaction with the drive is through the controller. The transaxle shift point is completely under controller control.

The functional model contains diagnostic and status displays and several "dummy" control inputs for development purposes. It consists of a card rack and control panel. It bears no resemblance to a future vehicle-mounted unit. A single 12 vdc power input is required. The controller is seen at the lower right side of Figure 9.1.2.

The primary operator input is a torque demand (+ or -). The motor control strategy is based upon a slip control scheme where an absolute slip command (+ or -) is added to rotor frequency, yielding the desired stator frequency. A slip control method was chosen because it tends to give a stable, well-defined system response. The slip loop is tight without microprocessor sampling delays. The slip operating range is $\pm$ 8 Hz to provide plenty of experimental margin over the $\pm$ 3.5 Hz motor slip range.

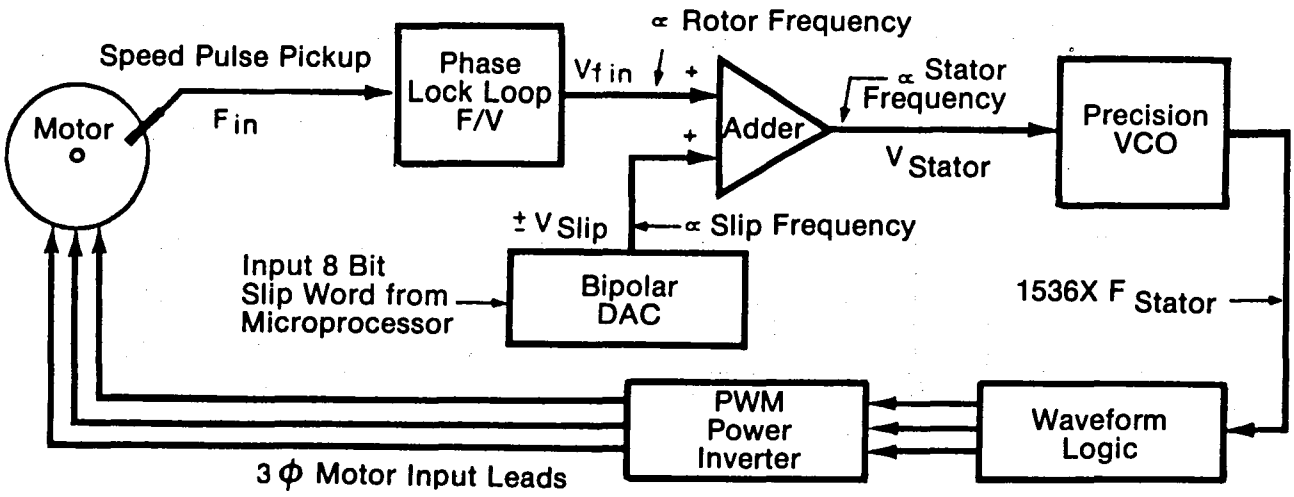

Fig. 7.1.1. Slip Control Scheme

Resolution to the slip digital-to-analog converter (DAC) is 0.0625 Hz. For the 0-150 Hz stator frequency range, this resolution has given smooth control. Rotor speed is detected by a magnetic pickup sensing a 60-tooth gear. A phase locked loop (PLL) acts as a frequency-to-voltage (F/V) converter. The DAC output voltage (+ or -) representing slip command is then added to the speed voltage. The sum is a voltage proportional to stator frequency. This voltage is applied to a precision voltage-to-frequency converter (VCO) which outputs a multiple of the stator frequency. Eventually this signal is transformed to stator frequency. Linearity and temperature stability have been obtained over a 10°C to 53°C range, which is satisfactory for the first model.

Both rms motor voltage (or current) and slip must be controllable in order to control torque efficiently in an adjustable speed induction motor drive.

Many modulation strategies are available for achieving rms voltage control. A method called "Center 60° notching" was chosen for one overriding reason...the fundamental component of the rms motor voltage is directly proportional to the duty cycle within the notch over the full duty cycle range (Figure 7.1.2a) (Ref. 3 and 4). Figure 7.1.2b shows 0% duty cycle, or 0 motor voltage. Figure 7.1.2c shows 100% duty cycle (no notch at all), or max motor voltage. Figure 7.1.2d is an example of a 2-notch waveform giving 50% duty cycle.

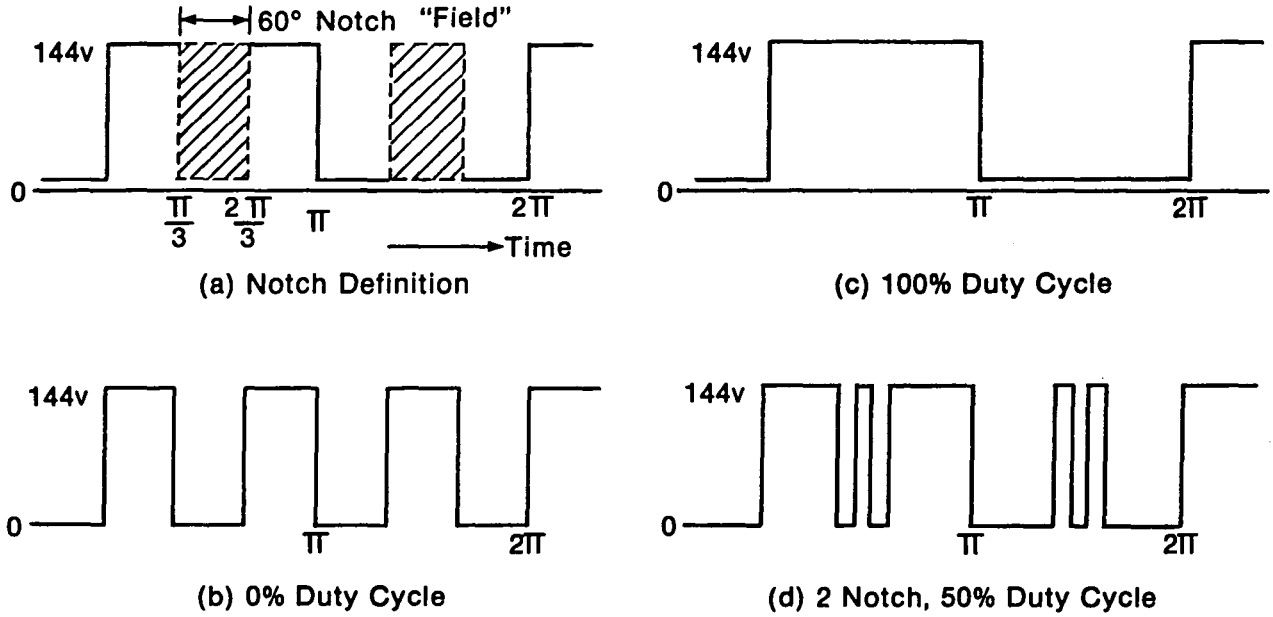

All Waveforms are a Typical Line-To-Negative DC Bus Voltage

Figure 7.1.2. Idealized PWM Voltage Waveform Examples

Each motor line-to-line voltage is the sum of two line-to-bus voltages. The line-to-bus voltages are always phased 120° apart. Half wave and quarter wave symmetry are maintained to prevent even harmonics and dc bias in the net motor current.

Center 60° notching allows a simple control of motor voltage. By varying the number and width of the notches, peak and harmonic currents can be minimized over the speed/torque range. Also, reducing V/Hz (motor voltage ÷ stator frequency) below rated at light loads increases efficiency significantly by reducing magnetizing current losses.

The software calculates the optimum V/Hz and slip, subject to programmable limits, to achieve the demand torque. From the simplified induction motor torque equation

$$\text{Torque} = (K)(\text{SLIP})(\text{V/Hz})^2, \text{ where}$$
$$K = \text{motor and scaling constant,}$$

it is clear that a given torque can be achieved by an infinite number of slip-V/Hz combinations. The processor uses empirically derived tables to pick the optimum pair. The selection is complicated by the fact that overall electrical efficiency is the product of inverter and motor efficiencies, so an optimum for the motor (i.e., low harmonic losses) is not necessarily an optimum for the inverter (i.e., low switching losses). For example, at a given speed and torque, the motor may want to see a 70% duty cycle at 1 Hz slip and 8 notches to minimize harmonics. However, overall efficiency may peak at 80% duty cycle at 0.8 Hz slip and 6 notches due to decreased inverter switching losses. The V/Hz and slip schedules must be fitted to the particular motor and inverter pair.

Since the nominal 144 vdc bus really varies from 160V to 94V as the battery discharges and load changes, the controller senses bus voltage and automatically compensates duty cycle to maintain the proper V/Hz. There are also numerous rate and over-limit constraints in software to prevent overstress. A special slip-V/Hz algorithm is used at start-up speeds to compensate for the large contribution of stator resistance to overall stator impedance.

Slip is calculated each loop of the program and simply strobed as a byte to the DAC (Figure 7.1.1). The waveform shape (determines voltage) is also calculated each loop, but it is used in a different fashion. If the microprocessor were to issue base drive commands in real time, the interrupt overhead needed for synchronization would be excessive. Therefore, the scheme shown in Figure 7.1.3 is used. The processor divides one motor cycle (360°) into 512 x 3 = 1536 parts. The notch pattern

is generated by assigning each part a 1 or 0. Thus, waveform resolution is one part in 1536. The processor serially clocks this string of 1536 bits into a buffer shift register. When the register is full, a ready command is used. Upon receiving a sync pulse derived from the stator frequency, the buffer register serially transfers the data to the main shift register at 1536 X stator frequency. Once the main register has the new waveform, it recirculates until the buffer is once again full with an update. The main shift register is always clocked at 1536 X stator frequency, the signal from the output VCO (Figure 7.1.1).

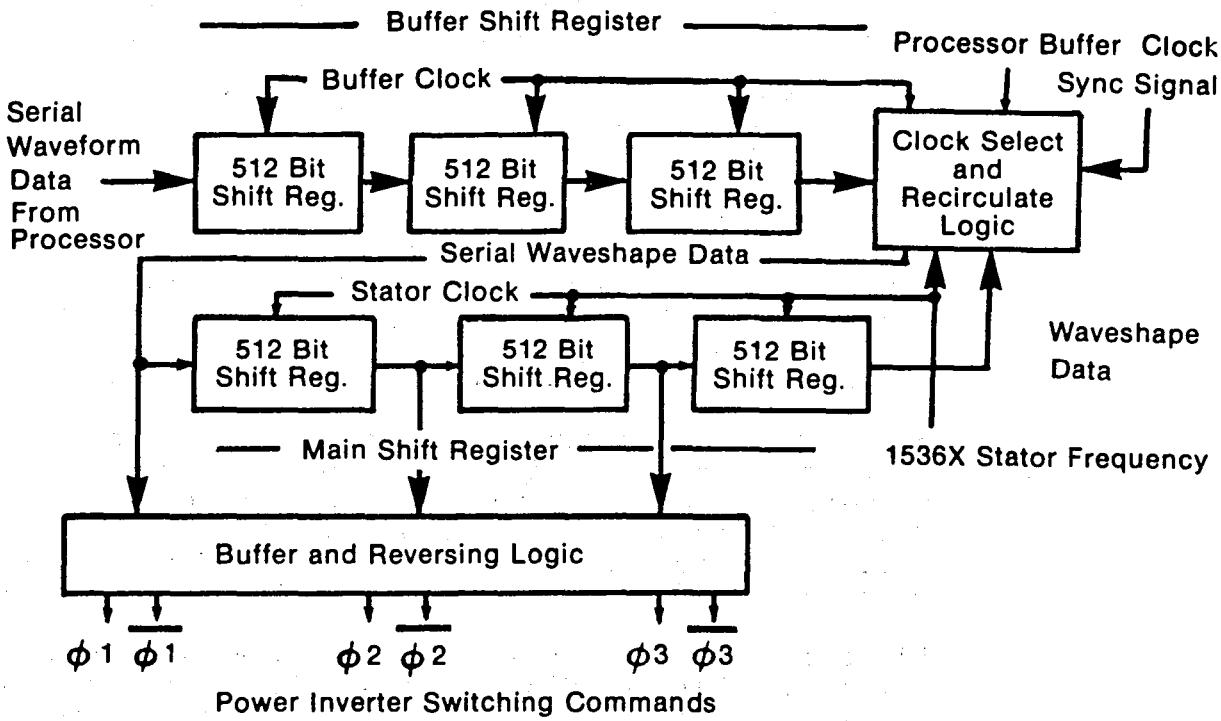

Figure 7.1.3. Waveform Shift Register Arrangement

The main shift register is composed of 3 512-bit registers. Thus, by simply tapping off the register outputs, the 3 inverter leg phases spaced 120° apart are obtained. Reverse rotation is achieved electrically by interchanging the Ø2 and Ø3 register outputs with logic gates.

This circuit has worked well, yielding good resolution and complete computer control of waveshape.

A 16-channel single-chip multiplexer/ADC provides new processor input data (speed, accel/decel commands, temperatures, etc.) once each program loop. Therefore, the overall vehicle control is a sampled data system (about 38 Hz sample rate). But the critical inner slip loop for the motor is continuous. This was deemed necessary to achieve stable response to random road load torque perturbations.

7.2 Hardware Description (Functional Prototype)

The ac EV drive controls are contained in an enclosure approximately 22" wide x 14.5" deep x 12" high. The controller comprises an operator control panel, a panel for system signal input, power input and test points, a dc power converter, and card cage with wire wrap boards containing hardware for controller functions.

The operator control panel includes an 18-character diagnostic readout display, simulated temperature inputs, and controls for drive operation in normal operating mode and manual mode for engineering development.

The input and test point panel contains power input jacks and a test point matrix for various engineering measurements. This panel also contains connectors for system sensor inputs, inverter drive signals output, and remote driver control inputs.

The dc power converter takes the supplied 12 dc voltage input and converts it to the proper voltage levels for the controller circuitry.

There are six wire wrap boards in the controller. Each has a main function it performs.

Appendix D contains hardware and software details.

7.3 Test Setups and Results

Tests were made to verify that the PWM waveforms had correct timing and proper signal levels. Oscilloscope traces were recorded showing that these output waveforms had the proper level and timing.Final controller calibration and checkout tests are also described in this section.

Tests were also performed to check and calibrate the system input sensors into the controller. These sensors included dc bus voltage, dc bus current, and motor, battery case and inverter heat sink temperatures.

1. DC bus voltage - Measured voltages were applied to the sensor, and the resulting controller readouts were recorded. Accuracy was within $\pm$ 1 volt over the operating range (see Figure 7.3.1).

2. DC bus current - Measured voltages were applied to the sensor to simulate the voltage across a 200 amp/50 mv shunt. The resulting current readouts were recorded. Accuracy was within $\pm$ 4 amps over a -400 to +400 amp range (see Figure 7.3.2). Operating sensitivity of the controller readout is 4 amps.

3. System temperatures - The three temperature sensors were placed in a temperature chamber. With temperature ranging from 0° to 100°C, the output resistance of each sensor was recorded. These resistances were then used as simulated inputs into the controller.

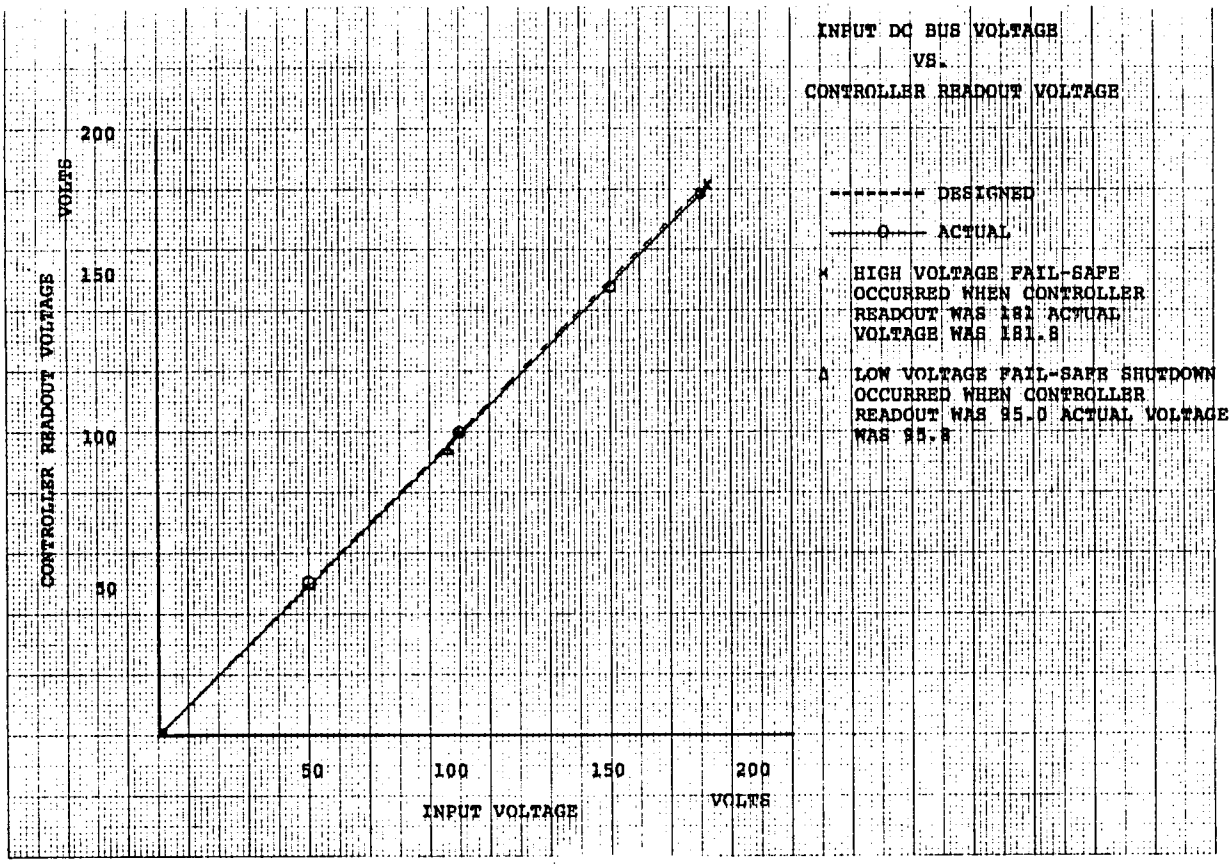

Figure 7.3.1 Bus Voltage Readout Cal Curve

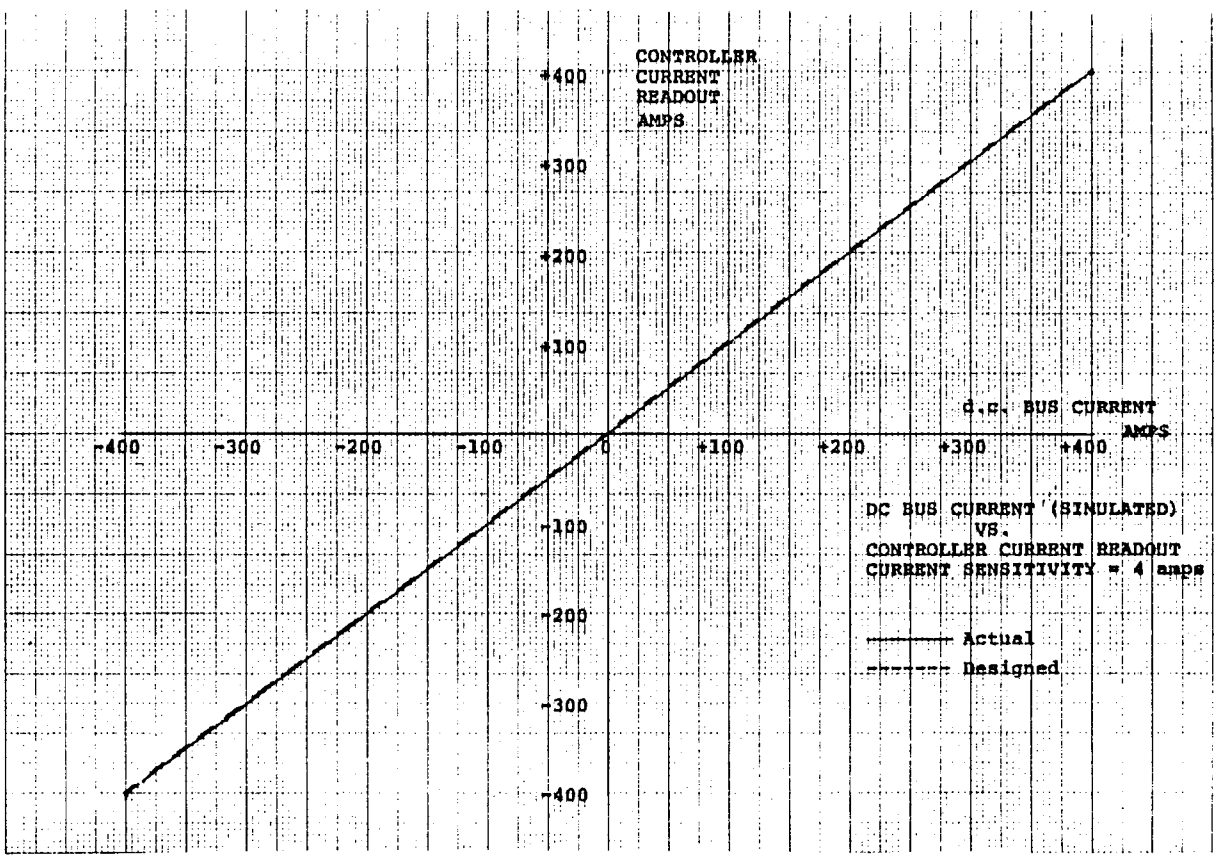

Figure 7.3.2 Bus Current Readout Cal Curve

The graph of equivalent temperature vs. controller temperature readout can be seen in Figure 7.3.3. These readouts were within ±4°C of actual temperature over the range of interest, adequate for the limit functions for which the temperatures are used.

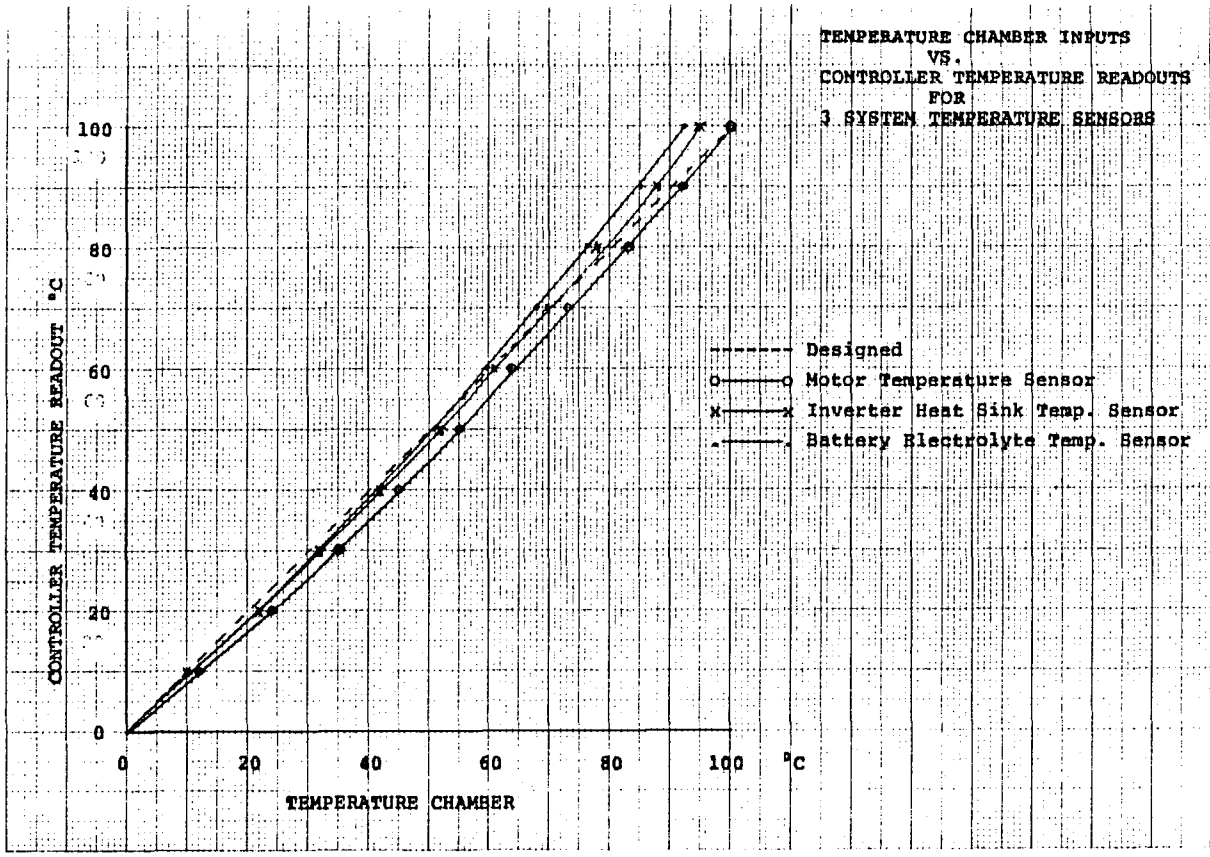

Figure 7.3.3 Temperature Readout Cal Curves

A test was performed to ensure that the controller would output the proper drive signals to the inverter. Recorded oscilloscope traces (of Forward and Reverse mode) show that drive signals were in proper timing sequence, with phases two and three interchanged when in Reverse.

Microprocessor response times were measured to determine the maximum rate at which the voltage waveform could be updated to the buffer shift registers. The measurements revealed the worst case maximum update rate to be 29 msec.

Another test was performed to ascertain the stability over time of the stator frequency circuit at room temperature, 5° and 50°C. The test setup with the controller in the temperature chamber is shown in Figure 7.3.4. At room temperature, 27°C, an input frequency was supplied to the

controller to produce an output reference frequency of 100 kHz. The differential output frequency was measured at fixed time intervals for several hours. The reference frequency remained constant within ±0.1%. At 50°C the frequency went up from the reference frequency approximately 2%. At 5°C the frequency was up approximately 2.5%.

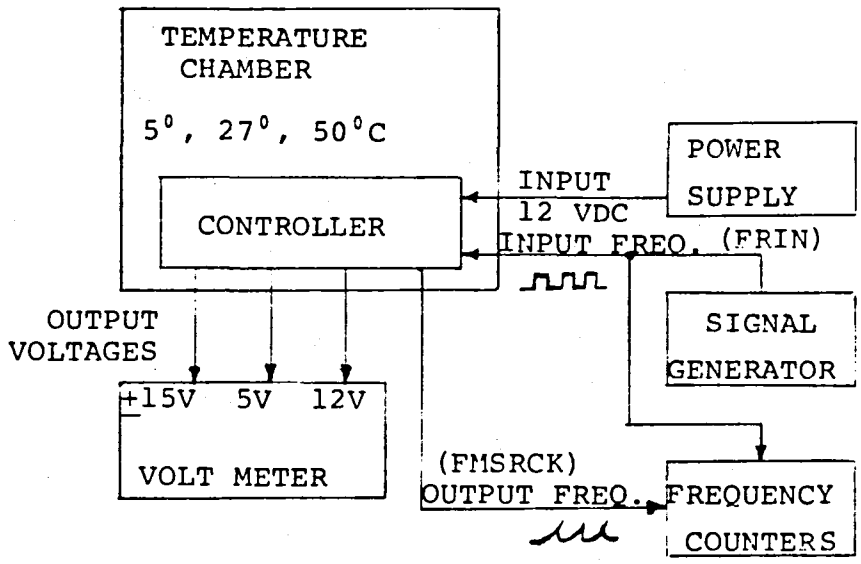

Figure 7.3.4 Controller Frequency Stability Temperature Chamber Test Setup

A final calibration and controller diagnostic operation check was performed before shipment. This final test included a calibration of the speed feedback circuit, the slip circuit, and the motor speed input circuit. The voltage outputs, +5 volts and ±15 volts, were measured and found to be within 1% of nominal. All controller diagnostics were checked and found to be operating correctly. The fault shutdown and warning code words were all tested and were operating properly.

7.4 Discussion of Results

The output waveform and microprocessor response time tests showed the controller to be operating as it was designed. The tests were run previous to system operation to ensure proper system operation.

The system sensor input tests of dc bus voltage, bus current and temperature showed that all inputs and readouts were within design tolerance.

The instability of the controller output frequency vs. temperature change can be accounted for by the characteristic X7R capacitor that was used in the circuit. The drop in capacitance at 5°C and 50°C would account for the rise in frequency. To stabilize the frequency over the temperature range, a temperature stable capacitor should be used.

7.5 Possible Improvements

There are several major improvements envisioned for EV control. These improvements evolved from shortcomings noticed in this prototype. One improvement is a change in the slip generating scheme. Presently the slip is strobed as a digital word to a DAC (digital-to-analog converter) and the output voltage summed with a motor speed proportionate voltage. This scheme works well but requires initial pot calibration, and offsets occur due to circuit drifting. The new scheme will eliminate the digital-to-analog conversion.

The motor speed measurement circuit shows another area for improvement. The present circuit is good at high speeds, but at low speeds the voltage output of the phase-locked loop becomes ragged with considerable ripple. This represents a problem for low speed control. The new scheme will measure motor speed in two different ways to optimize resolution with a given pulse rate: one for high speed, and one for low speed.

A third improvement is the method of waveform generation to the transistor base drives. The present method uses large shift registers which are becoming obsolete. This method inputs new waveforms serially into the shift registers. The three taps on the shift registers for the three phases do not see a wave change simultaneously. This has the drawback of entering current imbalances into the motor, though very slight. The new method proposes to replace the shift registers with RAM.

Diagnostic and test provisions will be expanded in a new design. The prototype diagnostics were so useful that a more extensive setup is planned for future designs.

The ac controller circuits used in the prototype are compatible with these objectives once some straightforward improvements are made.

8. TEST FRAME AND BATTERY RACK

This description consists of the following basic categories: mechanical hardware and electrical controls and instrumentation.

8.1 Mechanical Hardware

The basic mechanical components used on the test frame are described below. The ac induction motor was coupled to a hollow reaction torque sensor which was used to accurately measure the motor torque. The torque sensor was then bolted to the transaxle housing, while the motor shaft was attached to the upper Morse HY-VO(R) timing chain sprocket through a set of pilot bearings and a shaft extension. A motor support bearing was placed on the motor shaft opposite the transaxle to support and steady the weight of the motor.

This method of mounting and measuring the motor torque was chosen for two main reasons. The first advantage in this type of sensor was that there was no speed limitation which would have hampered an in-line torque sensor due to the 9000 rpm motor speed. The second advantage was that the pulsing torque sometimes transmitted by the motor shaft would fatigue an in-line torque sensor. The pulses felt by the reaction type sensor would be dampened through the inertia of the motor housing.

The rating of the torque sensor was chosen with two criteria in mind: accuracy and overload protection. The rating of the torque sensor (2000 lb-in) provided accurate torque reading through the entire range ($\pm$2.0 in-lb). The overload protection was approximately 4.76:1. This protection was needed in the shift sequencing tests, as well as normal overload protection.

The transaxle was modified for the dynamometer tests. These modifications included pressure and temperature taps. Pressure gauges were installed at the pump, high clutch, low clutch, and lubrication lines. Thermocouples were installed to measure temperature at the sump and case hot spot. The case hot spot was determined to be near the clutch packs. The differential of the transaxle was replaced with a straight-through shaft for the dynamometer tests. This allowed the power to flow through one output shaft. This means that any torque readings on the output shaft were twice the value that each wheel would normally feel, and that the differential carrier and planet gear losses would not be included in the efficiency readings taken on this setup. However, the omitted losses would only be significant if the vehicle were in a sharp turn.

The hydraulic system for the drivetrain prototype is best seen by reviewing the hydraulic schematic (Figure 4.1.5). The system pressure was supplied with a roller pump which was driven from 12 V dc battery power. The output of the pump was fed into the shift control valve, clutches, chain lubrication lines, motor lubrication, and cooling inputs. The motor cooling and lubrication fluid entered through the tap ports and exited from the front of the motor. The fluid was not drained through the chain case as originally planned due to excess churning losses which would result from fluid accumulating in the chain housing area.

The above mentioned mechanical items were shipped to LeRC as deliverables of the contract. The hardware was mounted to the bedplate and to the main angle bracket. The additional equipment described below was used at ERC for their in-house test program: the transaxle output shaft was coupled to a Lebow in-line torque sensor (#1248-10K). This was used to measure the output torque; the sensor had a range of 10,000 lb-in. and an accuracy of $\pm$ 0.1% ($\pm$10 in-lb). The torque sensor was then coupled to a speed increaser which increased the speed 6:1 and decreased the torque 6:1. This was necessary to match the speed-torque characteristics of the dynamometer. The dynamometer was a 45 hp driving and 60 hp absorbing dc machine (General Electric #7142019) and was used to apply the load to the system. The speeds of the system were monitored by magnetic speed pickups which were placed on the ac motor shaft and the dc dynamometer shaft. This summarizes the main mechanical items which were used on the test frame.

Battery Rack

The battery rack used for this project was constructed from an angle iron frame, 0.25 in.-thick bottom plate, poster board sides, and a set of casters on the legs. The batteries used in this system were EXIDE EV 106's. The inter-battery connections were kept as short as possible and were made with a maximum size wire in order to minimize the losses through the connections. A fuse connection was made on the input and output main power lines to guard against possible fault conditions and to satisfy general safety requirements.

8.2 Electrical Controls & Instrumentation

The electrical hardware for the system can be classified in two categories: power equipment and instrumentation equipment. The power equipment was located in one enclosure, while the instrumentation was located in the other enclosure. The power enclosure contained the contactors, relays, and safety circuits that were required for safety at LeRC, as well as the Eaton Engineering & Research Center. The major components contained in this

enclosure are described as follows with their respective purposes: the main power contactor (600 amp, 150 Vdc) was used as the 144 V battery power shutoff for the system. The control relays, fuses, and safety circuits were used in conjunction with the contactor to provide system control as well as meet safety requirements. Attached to this enclosure was a small enclosure which housed the coaxial current shunts. The shunts were used in the current measurements of the motor and the dc bus.

The instrument enclosure contained the measuring equipment and connection points used to instrument the motor and transaxle. The instrument cables were isolated from the power cables in order to minimize noise pickup. This enclosure contained all of the terminal strips necessary to secure the wires and interface with the NASA Road Load Simulator. The strips were arranged for torque, speed, temperature, and various other voltage and current measuring outputs of the sensors. Also contained in this enclosure were two wide-band Clarke-Hess wattmeters which were used for motor input power measurements.

Other electrical equipment contained on the main test frame included the prototype power inverter and 12V battery and charger assembly. The power inverter was oriented so the length of the 144 V battery leads would be minimized. The battery and charger were located on the test frame and were used to power the motor controller, (located off-frame), hydraulic pump, the control solenoids of the transaxle shifting circuit, and the test frame safety circuits.

Other electrical instrumentation used in conjunction with the test frame but not shipped to LeRC are described below. These were signal conditioners for the transducers, speed readouts, and temperature conditioning equipment. The torque sensor signals were conditioned with Daytronic 878 torque conditioners. The full-scale accuracy of the units was 0.1%. The thermocouples (Type J) used to monitor the temperature were conditioned with an 810 Daytronic signal conditioner which had a full-scale accuracy of $\pm 1.0°$. The speed readout used was an AIRPAX (Part No. 76l400110) with a full-scale accuracy of 0.1%.

Appendix E describes the test frame operating procedure. Appendix F covers the test frame safety features.

9. SYSTEM TESTS

9.1 Introduction

This section details the results of the final system test phase of the ac drivetrain prior to delivery to LeRC. The overall system test frame as delivered to LeRC is shown in Figures 9.1.1 through 9.1.3. This test phase was intended to provide the final integration of the major components into the total ac drivetrain and to characterize this total system under its full range of operating conditions.

A summary of the tests that were performed in this phase is as follows:

1. Efficiency maps were generated for each major component and for the overall system. These maps were obtained in both low gear and high gear throughout the system speed- torque envelope for both motoring and regenerating. Test results showed that these efficiencies were close to values obtained during the component tests. Combined inverter/motor/transaxle efficiency peaked at 82% for an axle speed of 755 rpm and 328 Nm torque output.

2. The dynamic performance of the system was characterized, and adjustments needed to stabilize the system were made. No stability problems were apparent after tuning the system, and since the dynamometer inertia for this test was only 40% of a 1364 kg vehicle inertia, no stability problems are anticipated on a vehicle.

3. Thermal data for the inverter, motor and transaxle were taken at a spectrum of operating conditions.

   Tests showed that after one hour of running at rated torque, the induction motor was the only component that approached its thermal rating. Overall, the system met the one-hour performance specification.

4. Vibration sensing tests on the system were made at various operating points. Noise tests were not run due to test setup limitations. The vibration test results did not reveal any major problems; however, vehicle test verification is required.

5. The performance of the torque and speed overload cutouts and recovery capability were verified.

   After some adjustment the system was found to respond gracefully to these overloads.

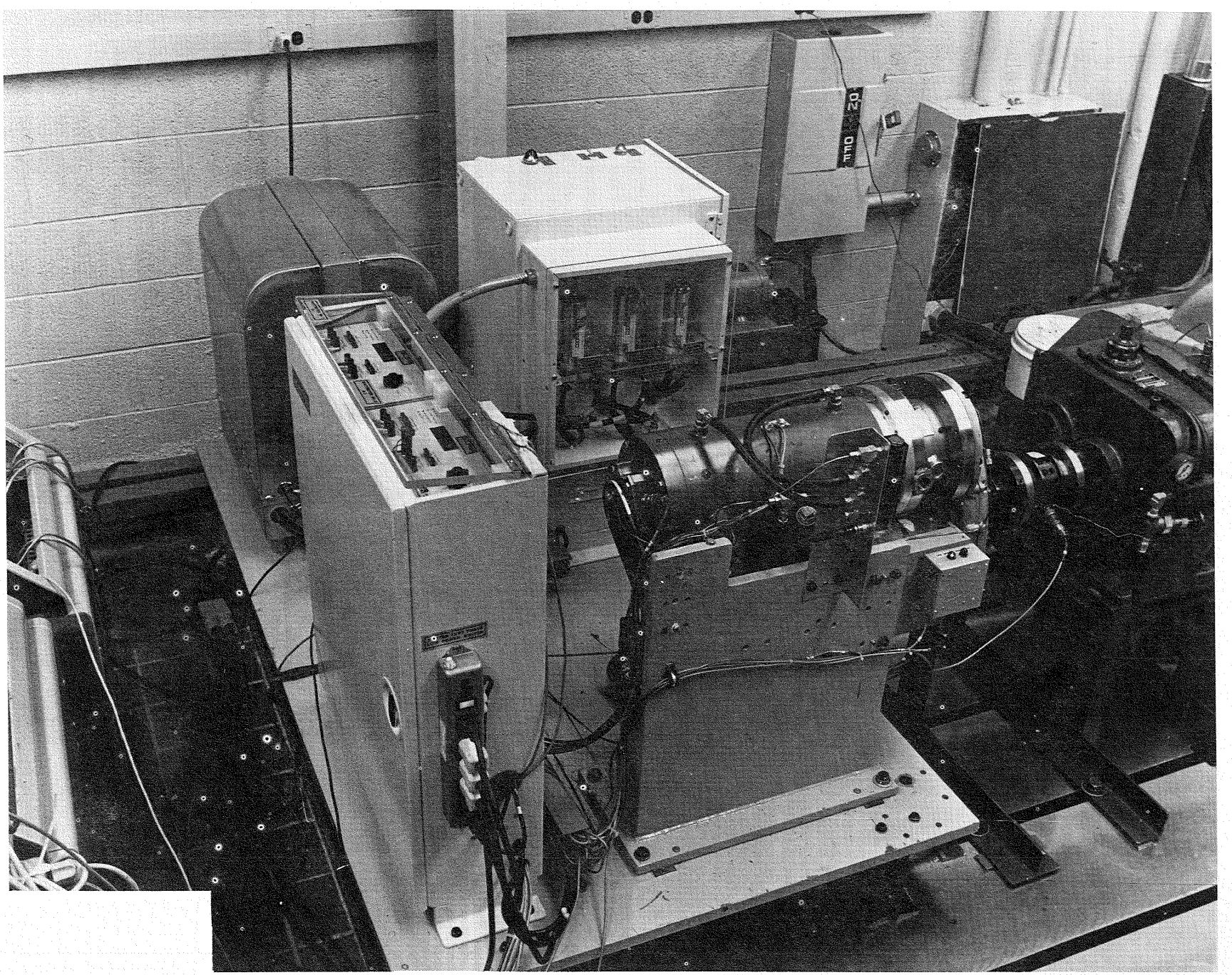

Figure 9.1.1 Overall Test Frame Configuration

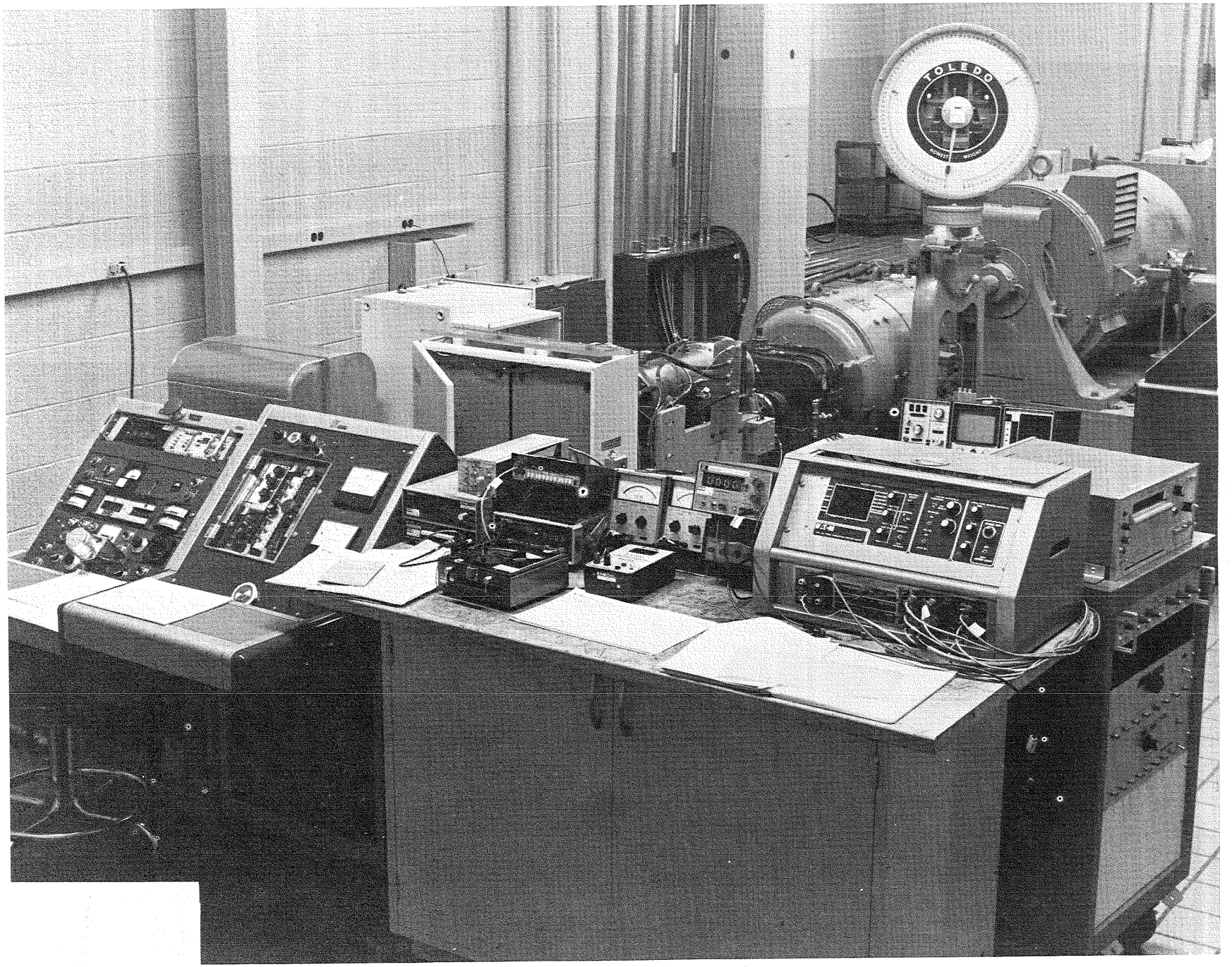

Figure 9.1.2 Dynamometer Test Setup with Instrumentation

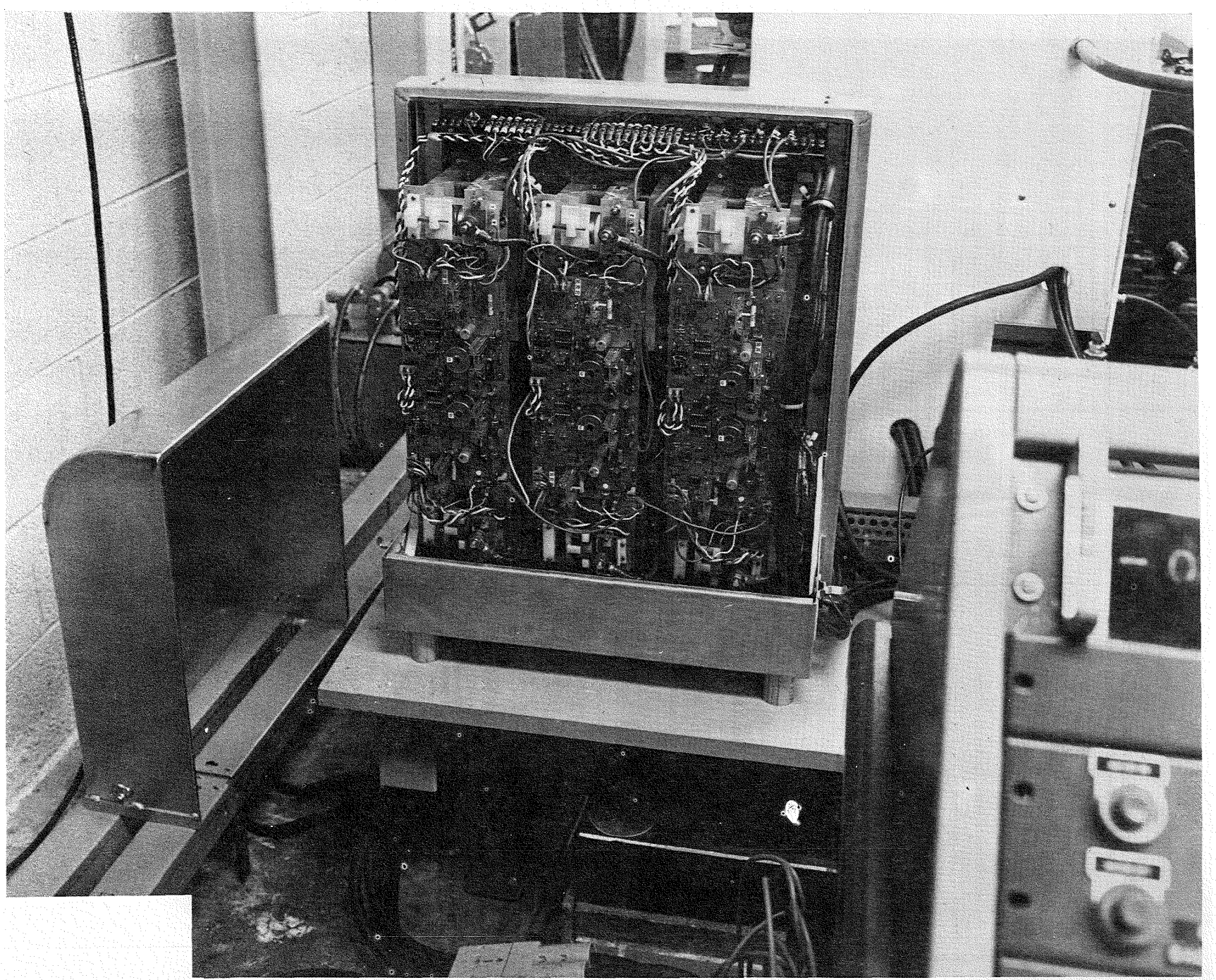

Figure 9.1.3 Power Inverter Mounted on Test Frame

6. The gearshift sequence was refined, and the shift points were optimized for efficiency and performance. Further work is needed on the gearshift sequence to obtain a smoother shift. However, the existing shift was judged adequate for use on the test frame.

7. The V/Hz map for the normal mode was checked for conformance with optimum values of V/Hz that were determined in the contract Task III. In order to conform to predetermined optimal values, it was necessary to compensate the motor slip as a function of motor temperature and to change a constant in the formula for calculating V/Hz.

8. Tests for graceful drive shutdown were run by introducing intentional failures. The drive survived without damage the types of failures that were forced upon it.

9. A final performance envelope for system torque versus speed was made for high and low gear. The motor torque was found to exceed the goal of 1.5 rated torque from 1200 to 4800 rpm. Rated torque was reached at 600 rpm, 0.7 rated torque being achieved at standstill.

10. Coast and regeneration performance tests were run, including a 10% downhill grade simulation test. These tests showed that at the vehicle speed of 80.5 km/hr. required for the test, the maximum torque available in regeneration was 27 Nm, which is equivalent to holding zero speed down a 1.4% grade. The 10% downhill grade test was run in low gear at an equivalent vehicle speed of 45.9 km/hr. In low gear, enough torque was developed in regenerative braking to hold constant vehicle speed.

11. No load tests were conducted to determine the drive-train losses due to windage and friction. Difficulty in reading the torquemeter at low torque levels resulted in inaccuracies in the data on this test.

9.2 Test Setup

Mechanical Configuration

The ac drivetrain was installed in the test frame that was delivered to LeRC. The basic mechanical configuration for this system is given in Figure 9.2.1. (Refer also to Section 8.1.)

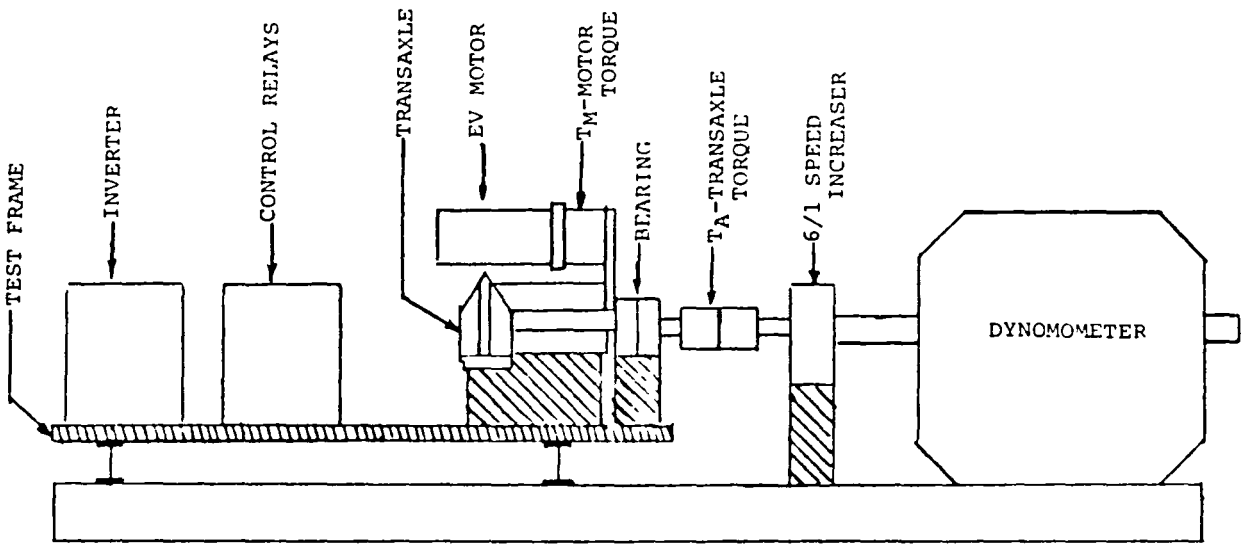

Figure 9.2.1 Mechanical Configuration

Electrical Configuration

The basic electrical configuration for this test is given in Figure 9.2.2. A battery charger was used for running extended tests, which would have otherwise run down the EV 106 batteries before the tests could have been completed.

Inverter dc power was determined from the dc voltage and current measurements. Motor ac power was measured with Clarke-Hess wattmeters using the two-wattmeter method. All current measurements were made with T&M coaxial shunts. A more detailed electrical schematic of the test frame has been submitted under another portion of this contract.

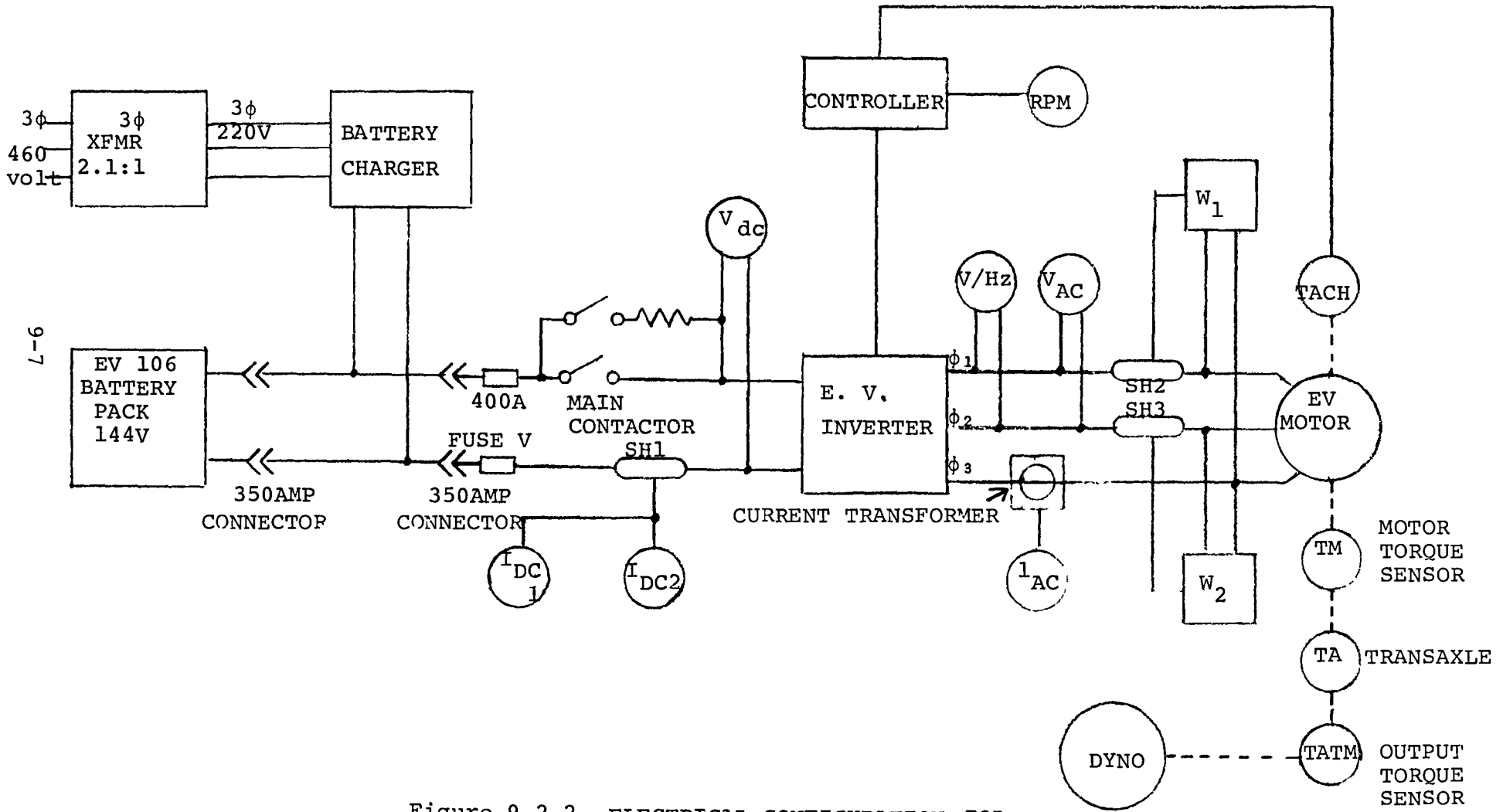

Figure 9.2.2 ELECTRICAL CONFIGURATION FOR FINAL AC DRIVETRAIN TESTING

Variable Measured	Symbol	Instrument	Accuracy
Motor Speed	rpm	Hewlett-Packard 5301A Counter	0.02% of input + 0.005% of range
DC Bus Volts	VDC	Fluke 8600A DMM	0.02% of input + 0.005% of range
DC Bus Amps	SH1	T&M coaxial shunt #F10,000-40	0.02% of input
	IDC1	DORIC Model K6 DORIC Model 100	
	IDC2	Sensitive research Inst. DC Voltmeter #HS 943668	1% f.s.
Motor Torque	TM	Lebow hollow reaction torque sensor #2404-2K Daytronic strain gage data module #878 Daytronic torque readout #890	0.1% f.s. or 2 lb/in 0.05% f.s. 0.02% f.s. $\pm$ 1 digit
Transaxle Torque	TA	Lebow rotary torque sensor #1248-25K Daytronic strain gage data module #878 Daytronic torque readout #890	0.1% f.s. or 25 lb/in 0.05% g.s. 0.02% f.s. $\pm$ 1 digit
Phase 1-3 Watts	W1	Clark-Hess Digital Wattmeter	$\pm$ 0.4% f.s. $\pm$ 0.2% VA at 30 Hz to 50 KHz
	SH2	T&M coaxial shunt #F10,000-40	0.02% of output
Phase 2-3 Watts	W2	Clarke-Hess Digital Wattmeter	$\pm$ 0.4% f.s. $\pm$ 0.2% VA at 30 Hz to 50 KHz
	SH3	T&M coaxial shunt #F10,000-40	0.02% of output
Volts/Hz	V/Hz	Eaton V/Hz meter	0.01 V/Hz
Motor line-line volts	VAC	Hewlett-Packard multimeter #4274	2% f.s. 10 Hz-100 KHz
Motor line amps	IAC	Hewlett-Packard multimeter #4274	2% f.s. 10 Hz-100 KHz
Temperature - all measurements		Type J thermocouple Daytronic thermocouple module #810	$\pm$ 2°C
Oil Flow Rate		Dwyer Visifloat Flowmeter	$\pm$ 3%

Figure 9.2.3. Test Instrumentation

Test Data and Instrumentation

Figure 9.2.3 shows the data that were gathered on these tests, along with the appropriate transducers and instrumentation that were used to collect the data. In addition to the measurements necessary for determining component power levels and component and system efficiencies, instrumentation was provided for measuring motor, controller, and battery voltage and currents, and the temperatures of critical components. The specifications on the combined accuracy of the various transducers and instruments was sufficient for the determination of the component efficiencies and the overall efficiency to within 2% of the rated power output of the system.

9.3 Efficiency Tests

These tests measured the efficiencies of the major components and of the total system over the torque-speed range of the system. Data were generated for use in computer simulations for determining system efficiency over a standard drive cycle. For these tests the system was put in normal mode to simulate true operating conditions.

To be as realistic as possible, tests were run for motor temperature from 25°C to 110°C. The battery charger was turned on in order to permit continuous testing; however, the charger voltage was not set higher than what would have been expected from the EV 106 batteries for a particular torque and speed. Efficiency results do not include losses from the transaxle oil pump (75 watts), inverter cooling fans (160 watts), logic controller (12 watts), or 12-volt battery charger. The cooling fans were greatly oversized.

Component efficiency maps of the motor and the inverter have been presented in previous sections. Figure 9.3.1 shows the combined motor and inverter efficiency over the motor speed torque range, Figures 9.3.2a through 9.3.2h show transaxle low and high gear efficiency in its speed and torque range, and Figure 9.3.3 shows the combined motor/inverter/transaxle efficiency for a 1364 kg vehicle over the speed and torque range of the vehicle.

Results of the motor and inverter efficiency tests were almost identical to previous results taken in Task III when the system operation was being optimized with V/Hz, slip, and notch number variations.

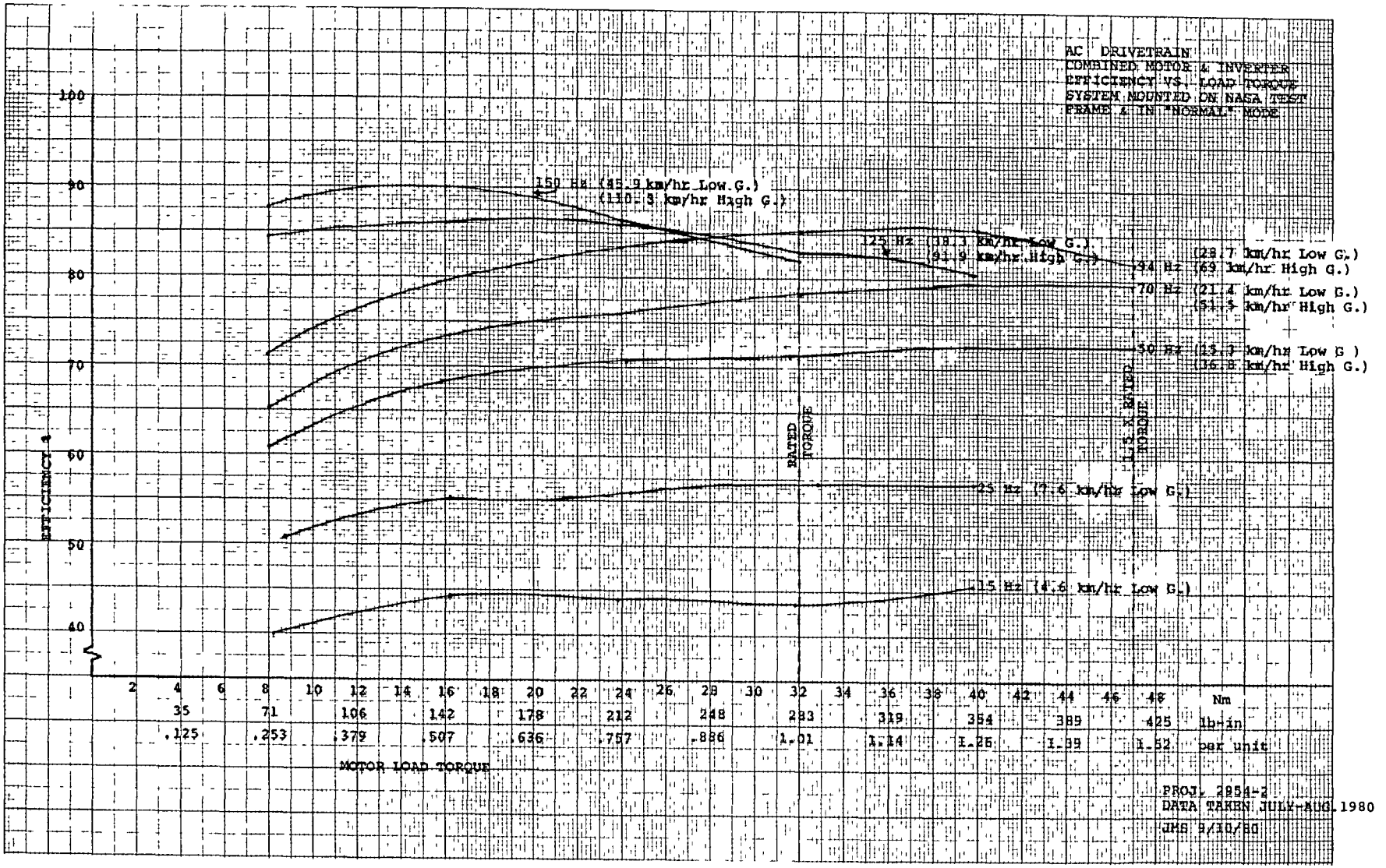

Figure 9.3.1 Combined Motor & Inverter Efficiency vs. Load Torque

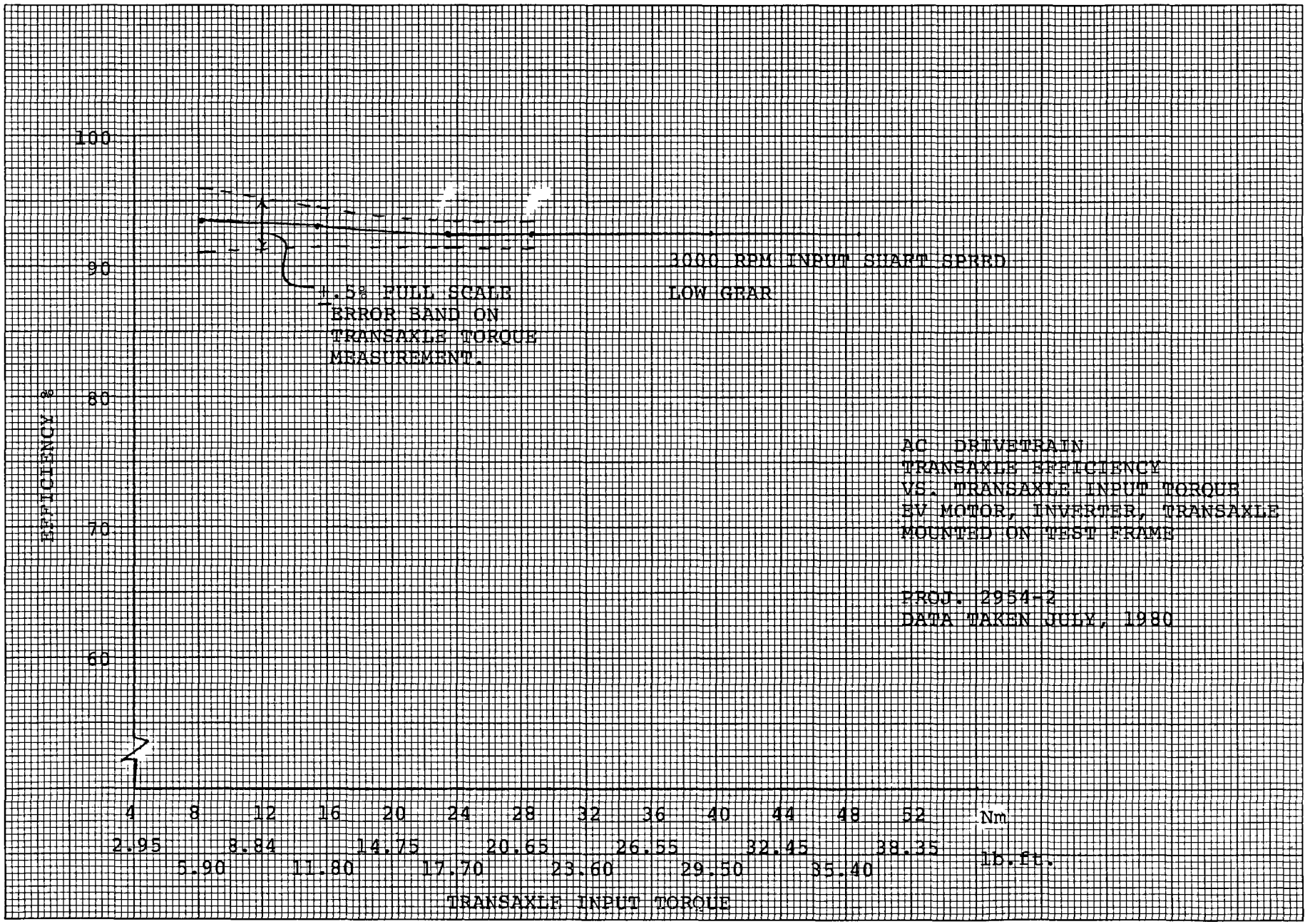

Figure 9.3.2a Transaxle Efficiency vs. Input Torque

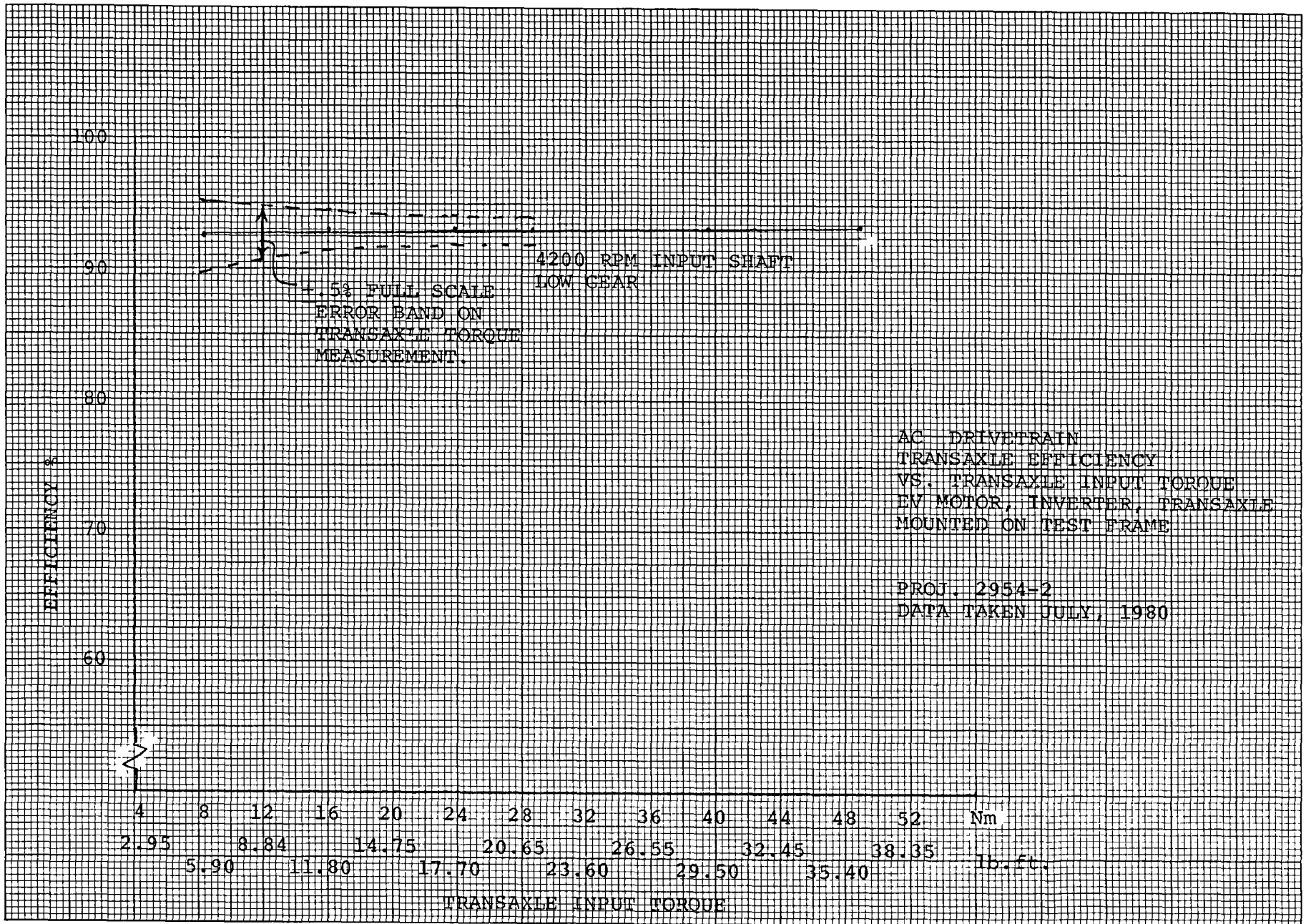

Figure 9.3.2b Transaxle Efficiency vs. Input Torque

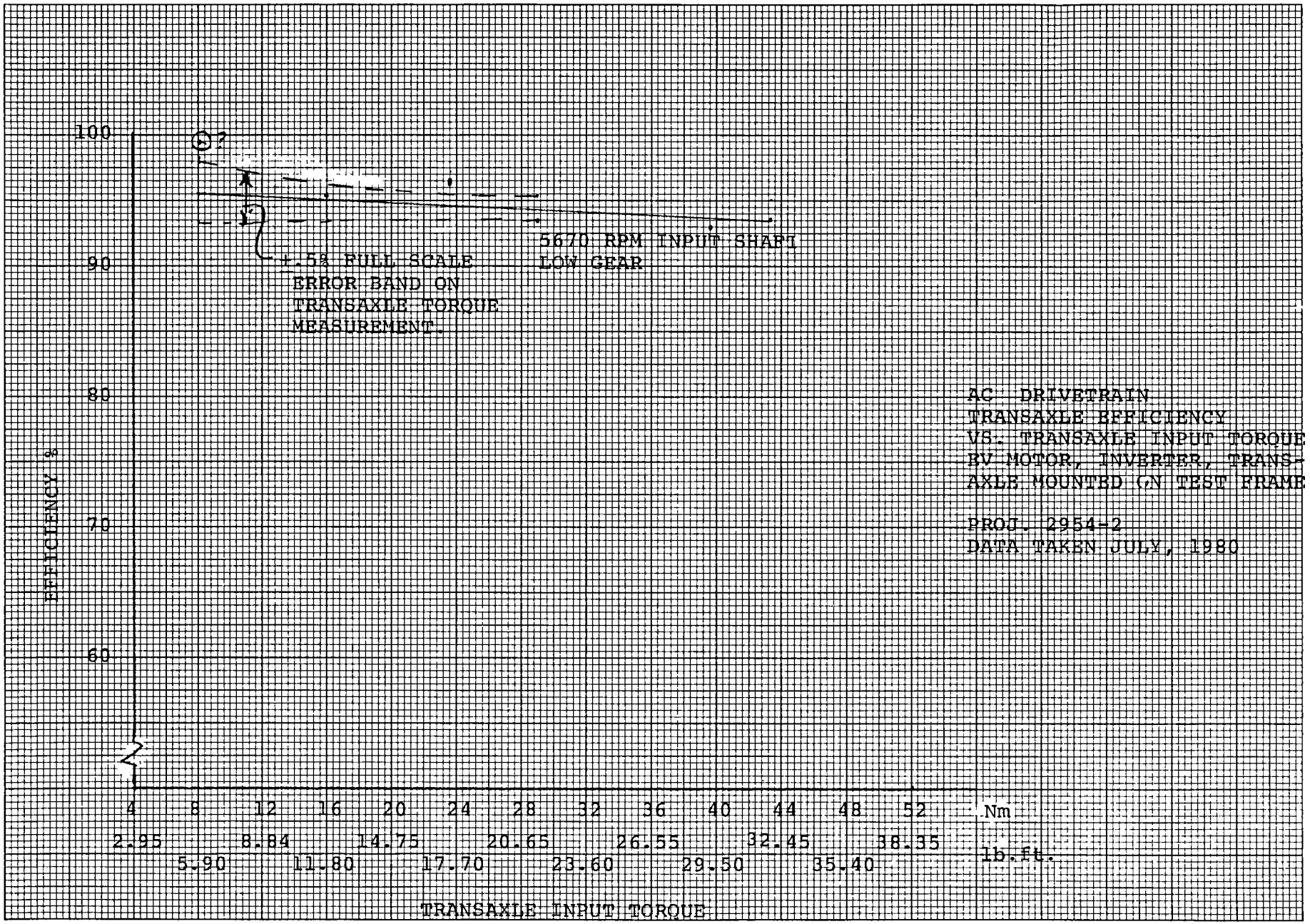

Figure 9.3.2c Transaxle Efficiency vs. Input Torque

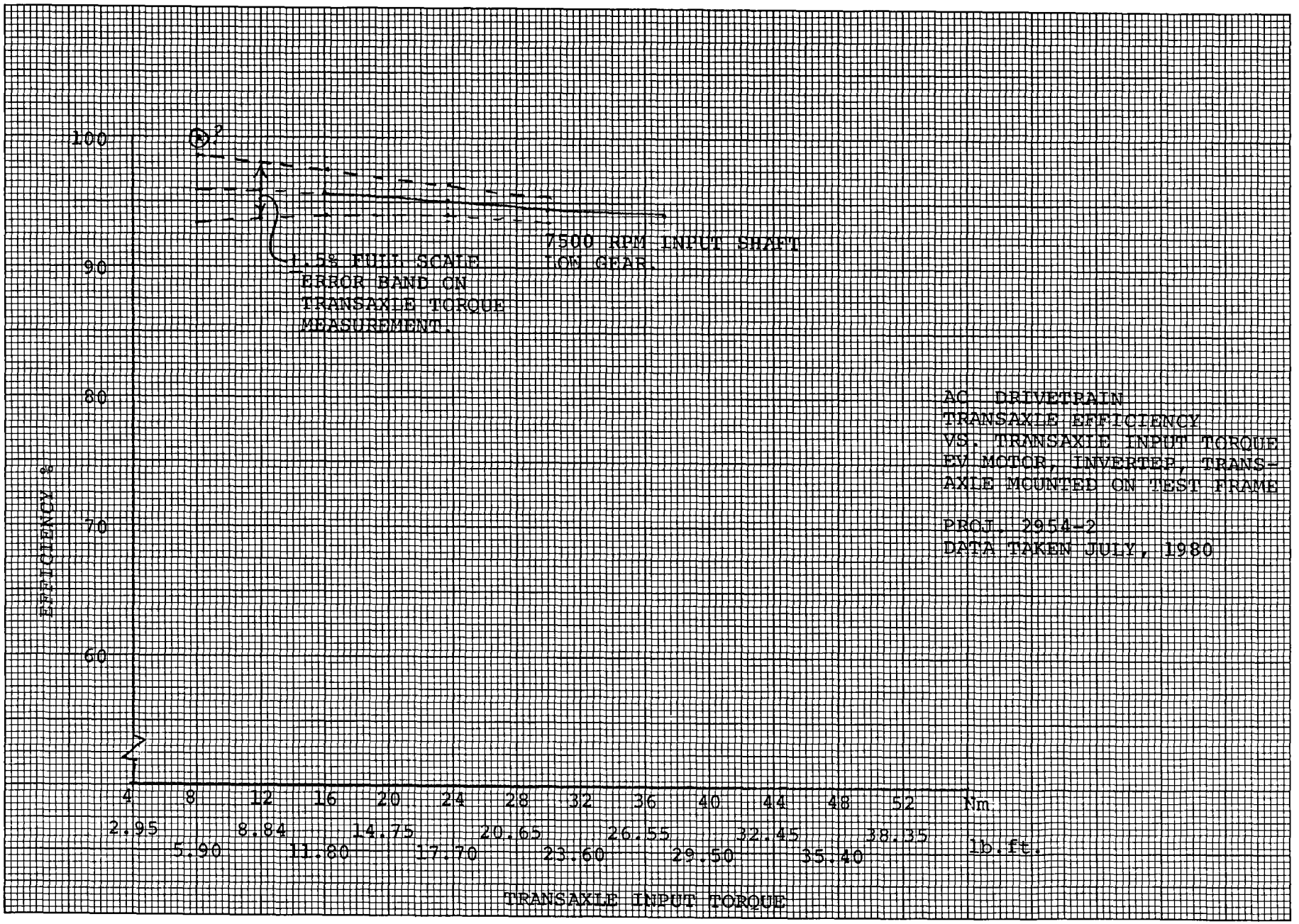

Figure 9.3.2d Transaxle Efficiency vs. Input Torque

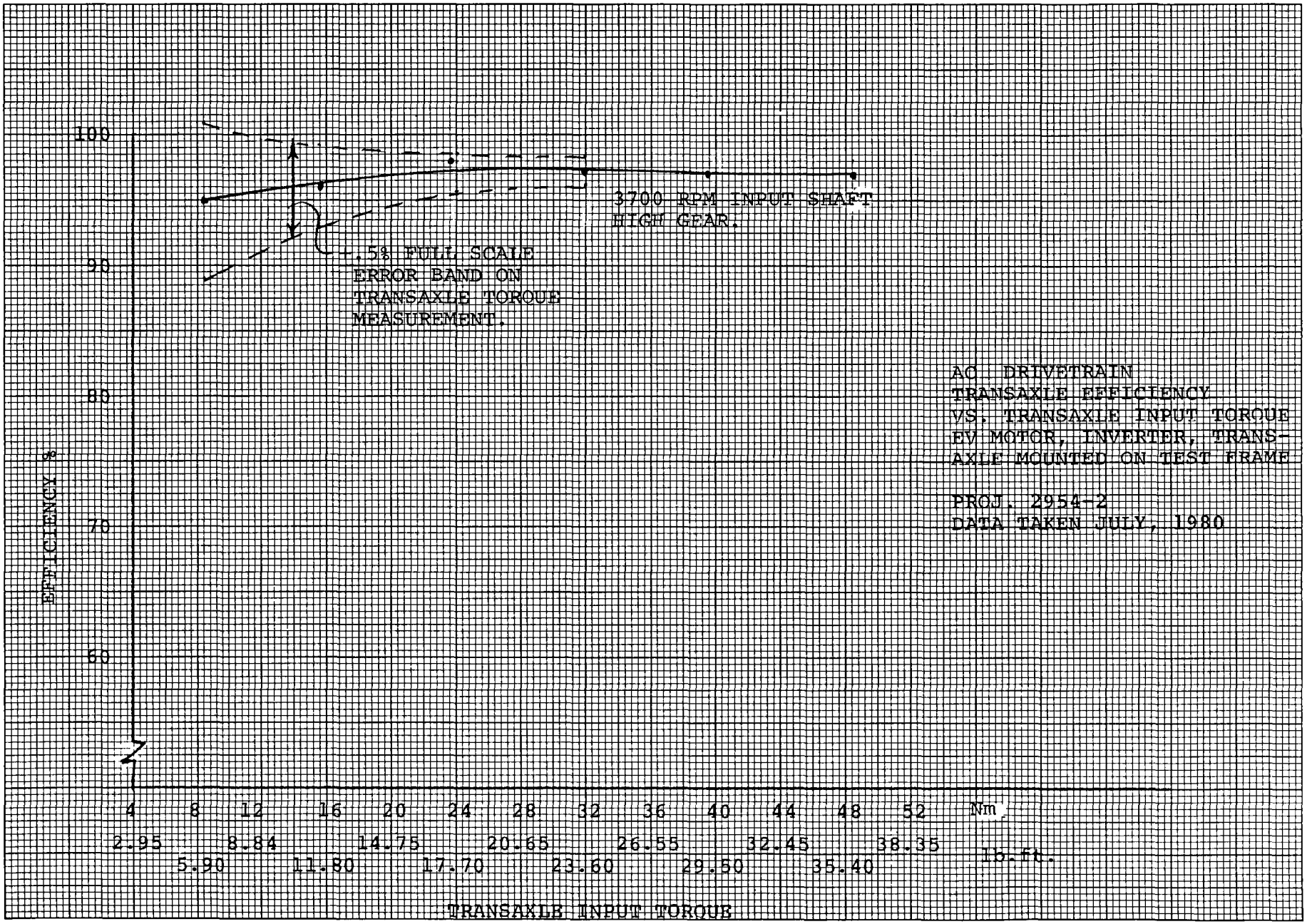

Figure 9.3.2e Transaxle Efficiency vs. Input Torque

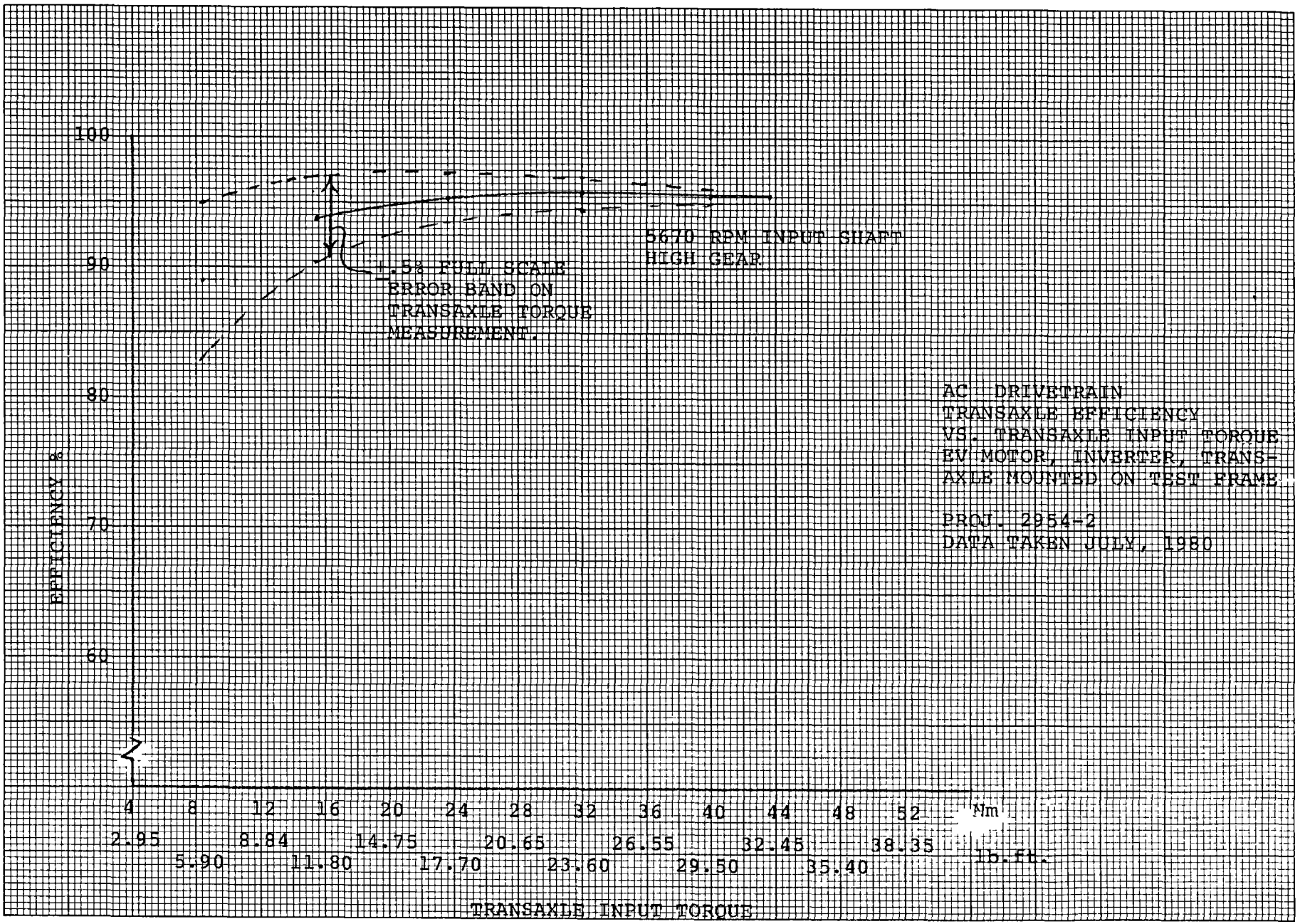

Figure 9.3.2f Transaxle Efficiency vs. Input Torque

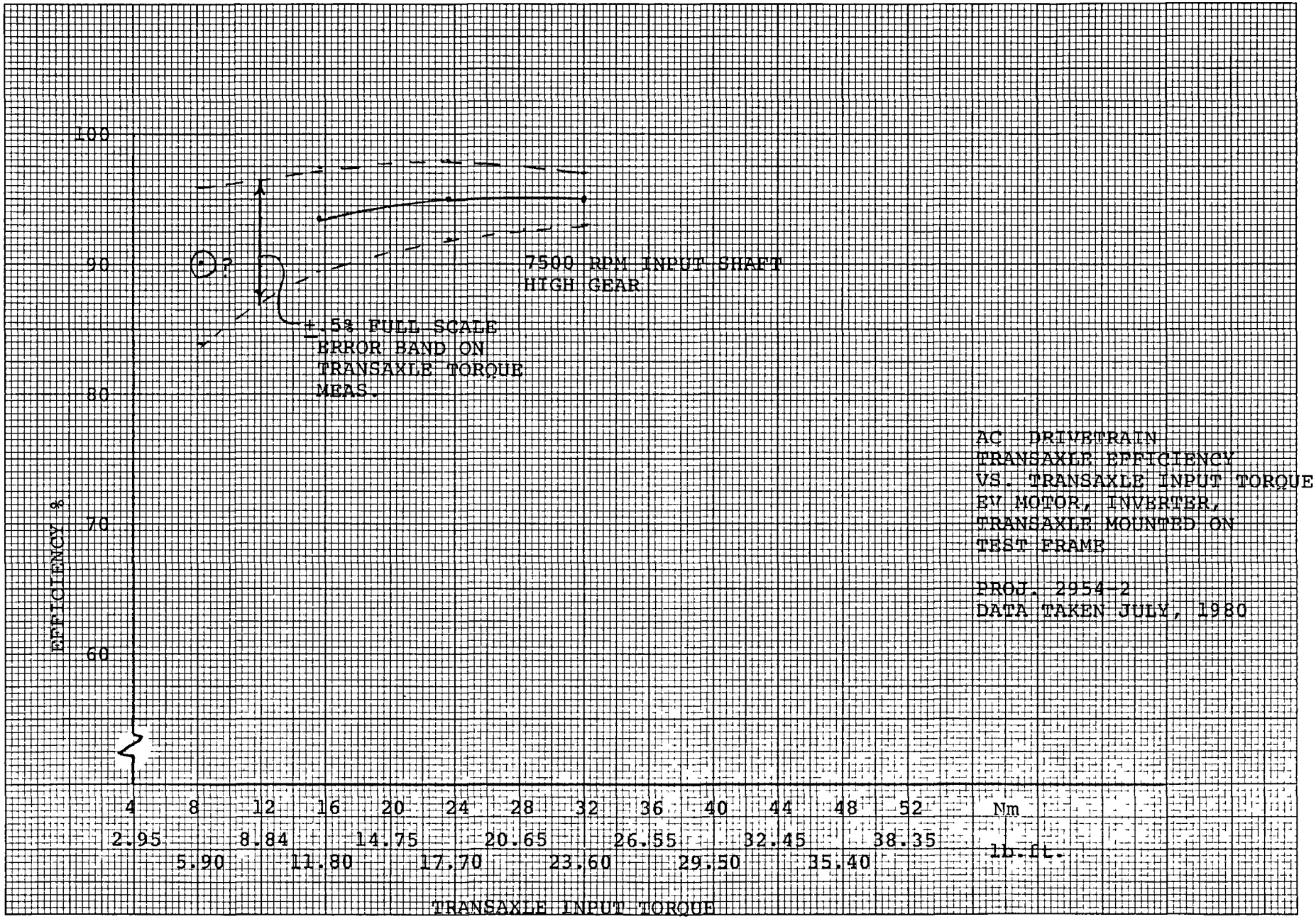

Figure 9.3.2g Transaxle Efficiency vs. Input Torque

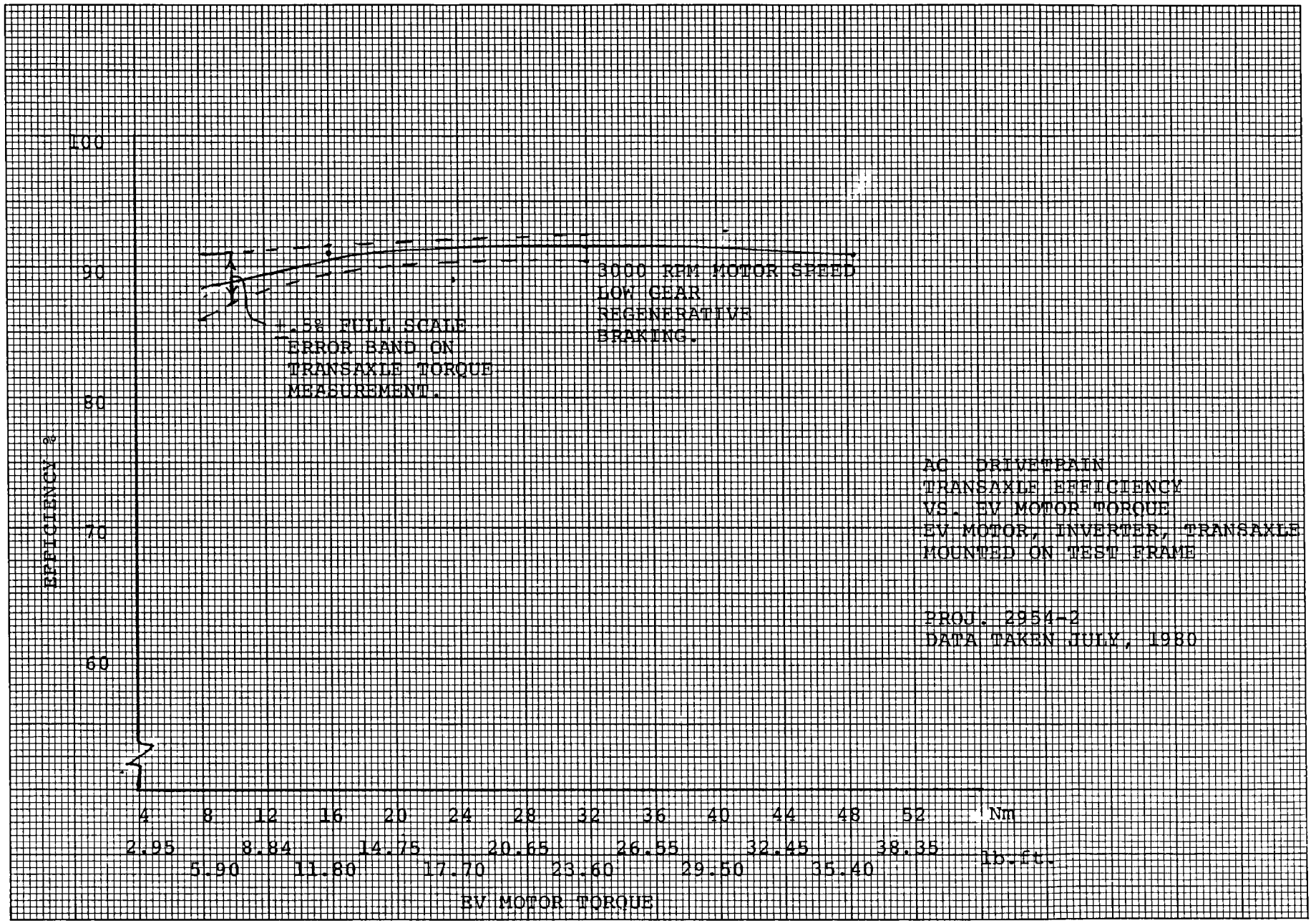

Figure 9.3.2h Transaxle Efficiency vs. Input Torque

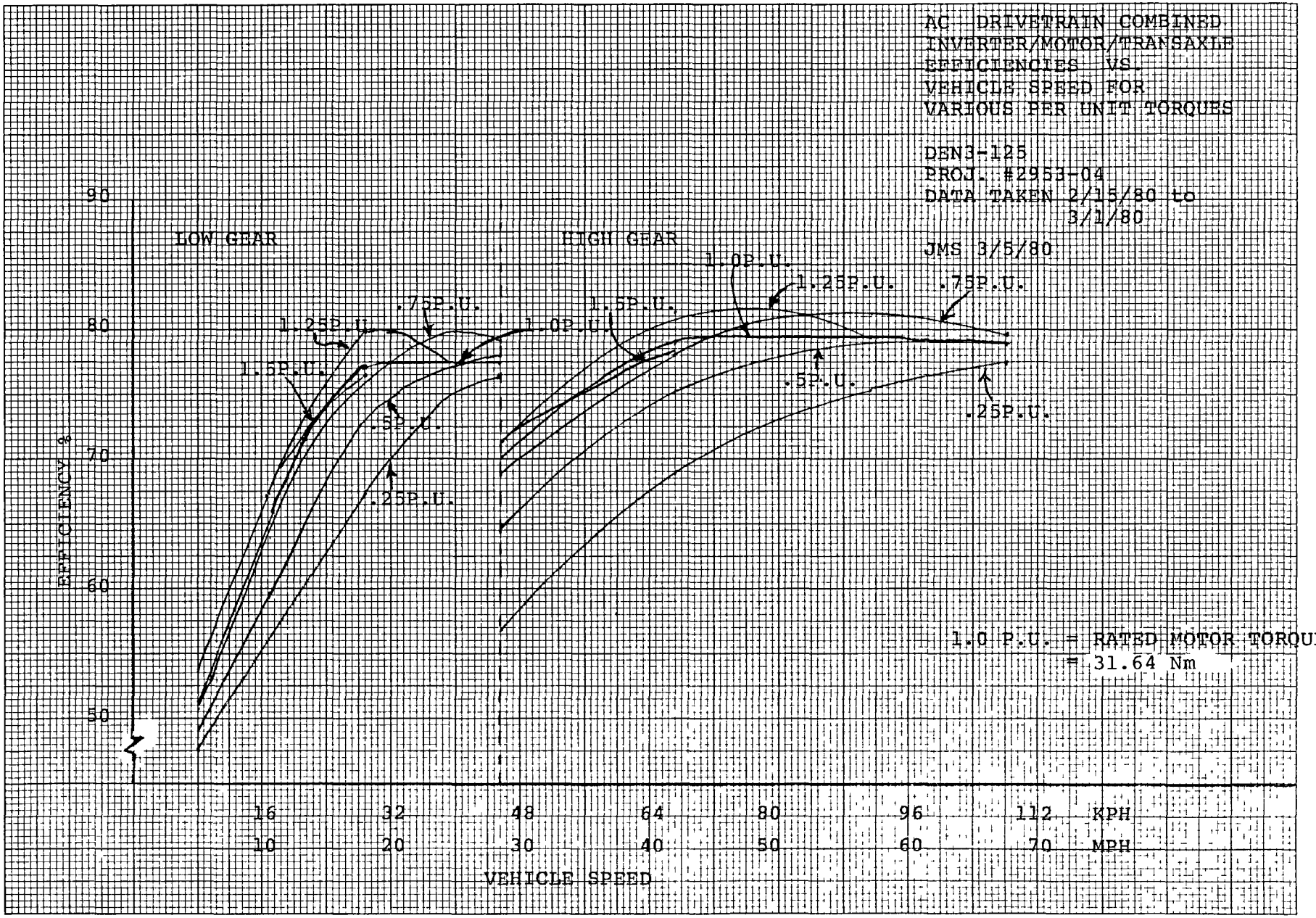

Figure 9.3.3 Combined Inverter/Motor/Transaxle Efficiencies

At high torque levels, the transaxle efficiency data was close to previous results, but efficiency errors were apparent at low transaxle torque due to problems encountered with the transaxle output torque sensor. The effect of a ±0.5% of full scale 814 Nm (600 lb.-ft.) error in transaxle output torque measurement is shown by dashed lines about the transaxle efficiency curves. These dashed lines indicate the low level of confidence that can be placed in the transaxle efficiency data at low torque levels.

The falloff in both overall system efficiency and the combined motor and inverter efficiency at low torque reflects the poor inverter efficiency under low torque conditions.

Figure 9.3.4 shows the combined motor and inverter efficiency in the regenerative braking mode. These efficiencies are lower than the motoring efficiencies for the same motor torque, because of the lower power level.

Figure 9.3.5 shows the combined motor/inverter transaxle efficiency in the regenerative braking mode.

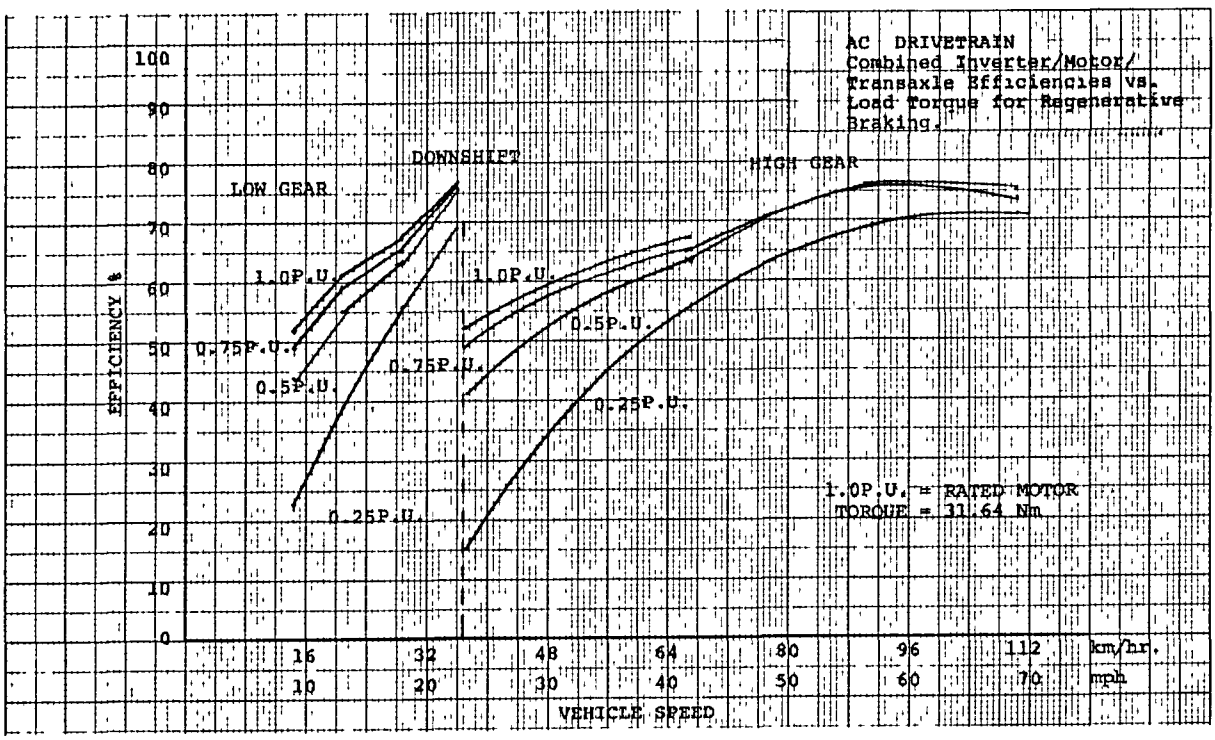

Figure 9.3.5 Combined Inverter/Motor/Transaxle Efficiencies

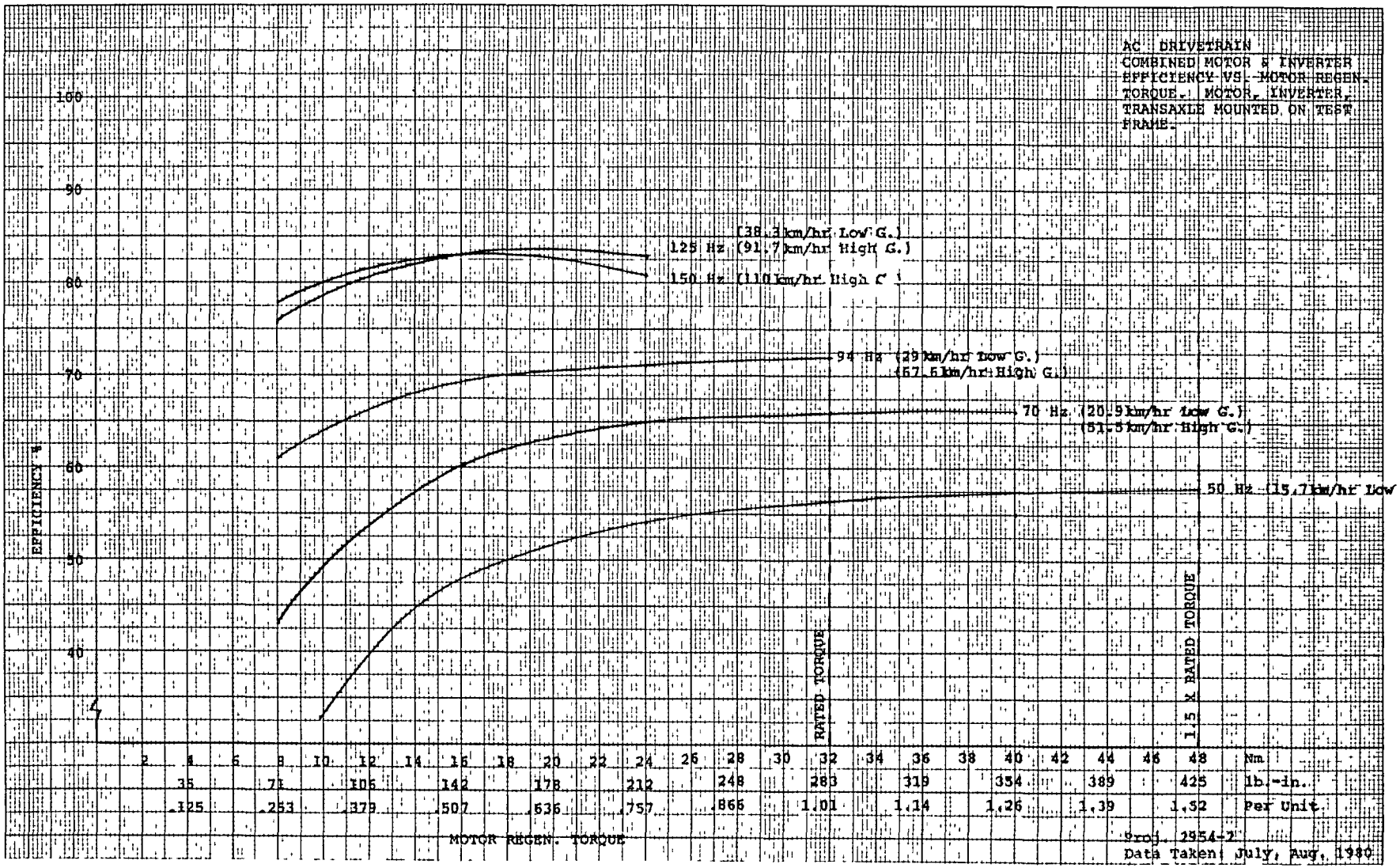

Figure 9.3.4 Combined Motor/Inverter Efficiency Regen. Braking Mode

9.4 System Dynamic Performance

The purpose of this test was to verify the stability of the system over its operating range, and to document its transient response to step changes in torque demand.

Stability Tests

Figure 9.4.1 shows the test setup that was used for the stability test. With this setup the system was run under no-load and loaded conditions at motor speeds from 900 rpm to 9000 rpm. Frequency response plots of both torque and speed to slip impulses were made with the fourier analyzer.

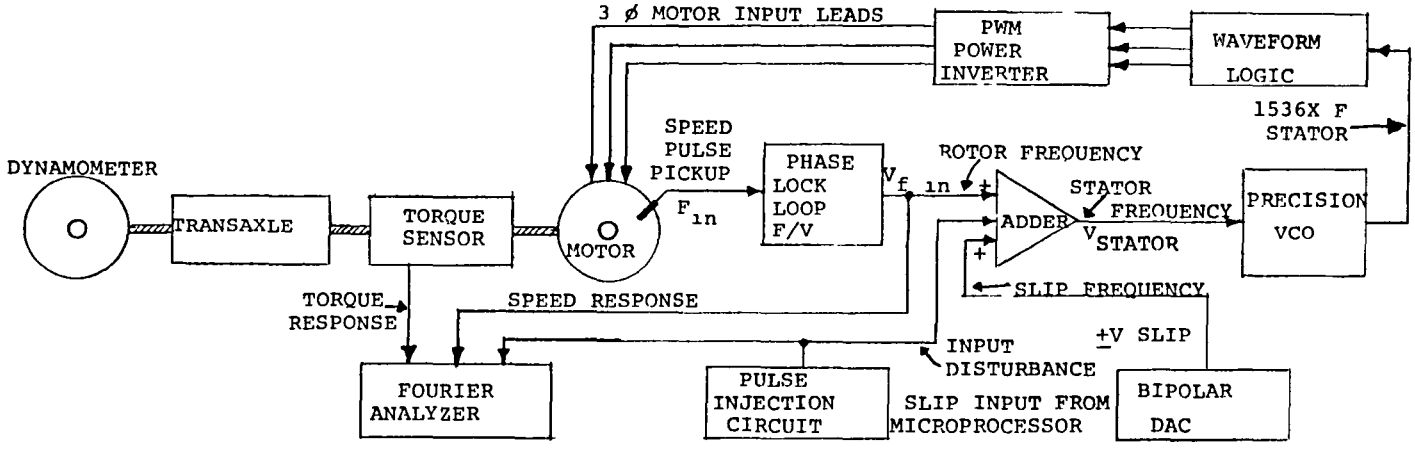

TEST SETUP FOR INJECTING DISTURBANCE INTO SLIP CONTROL LOOP

Figure 9.4.1 Stability Test Setup

Figure 9.4.2 shows a typical torque response to a slip disturbance, and Figure 9.4.3 shows the corresponding motor speed response under the identical conditions of 75 Hz and zero torque. Note that the horizontal perturbation scale is X 10^{-2}. Amplitude and phase are separately graphed.

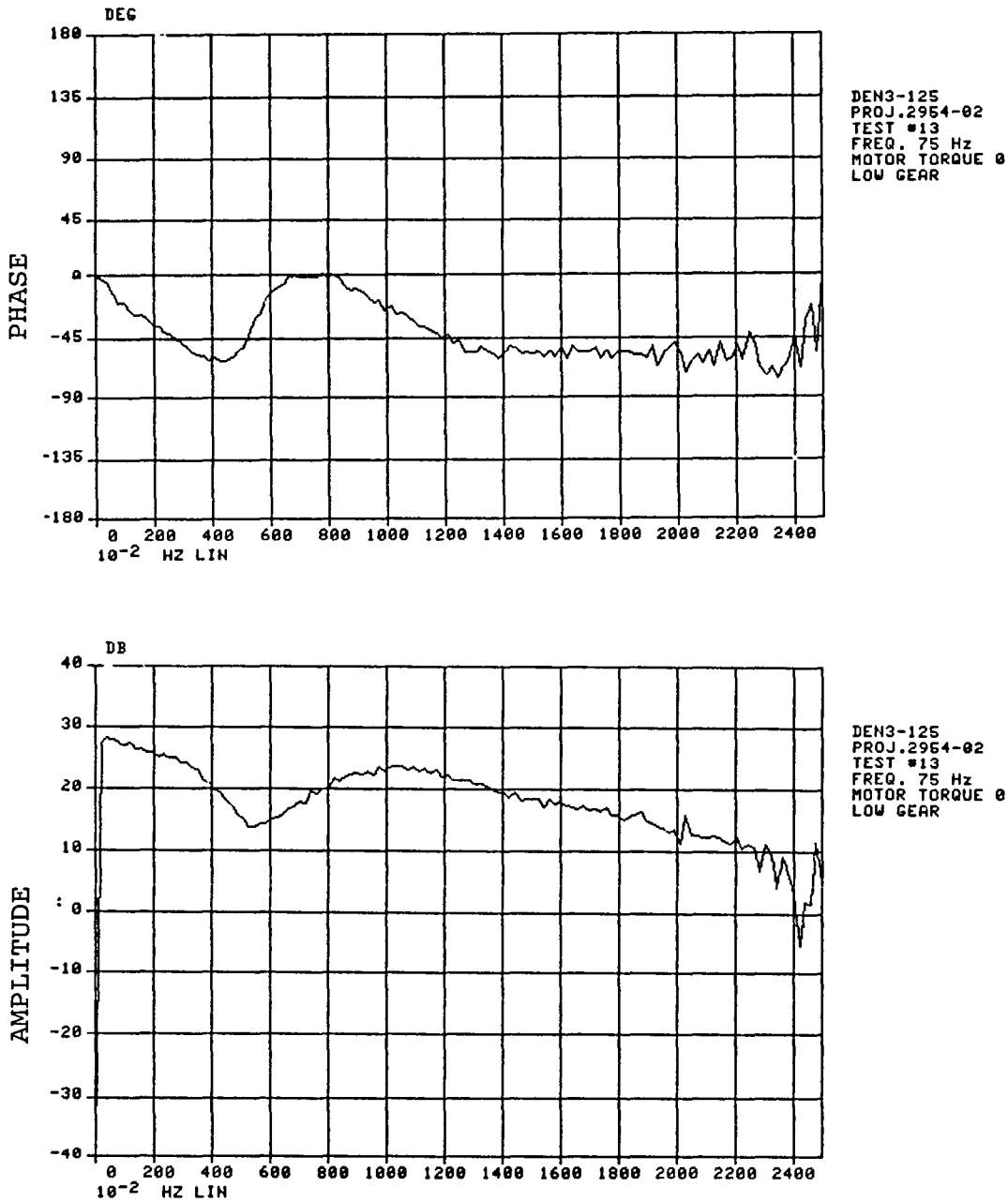

Ø db = Ø.6 Nm Motor Torque per Hz Slip

Figure 9.4.2 System Torque Response to Slip Disturbance

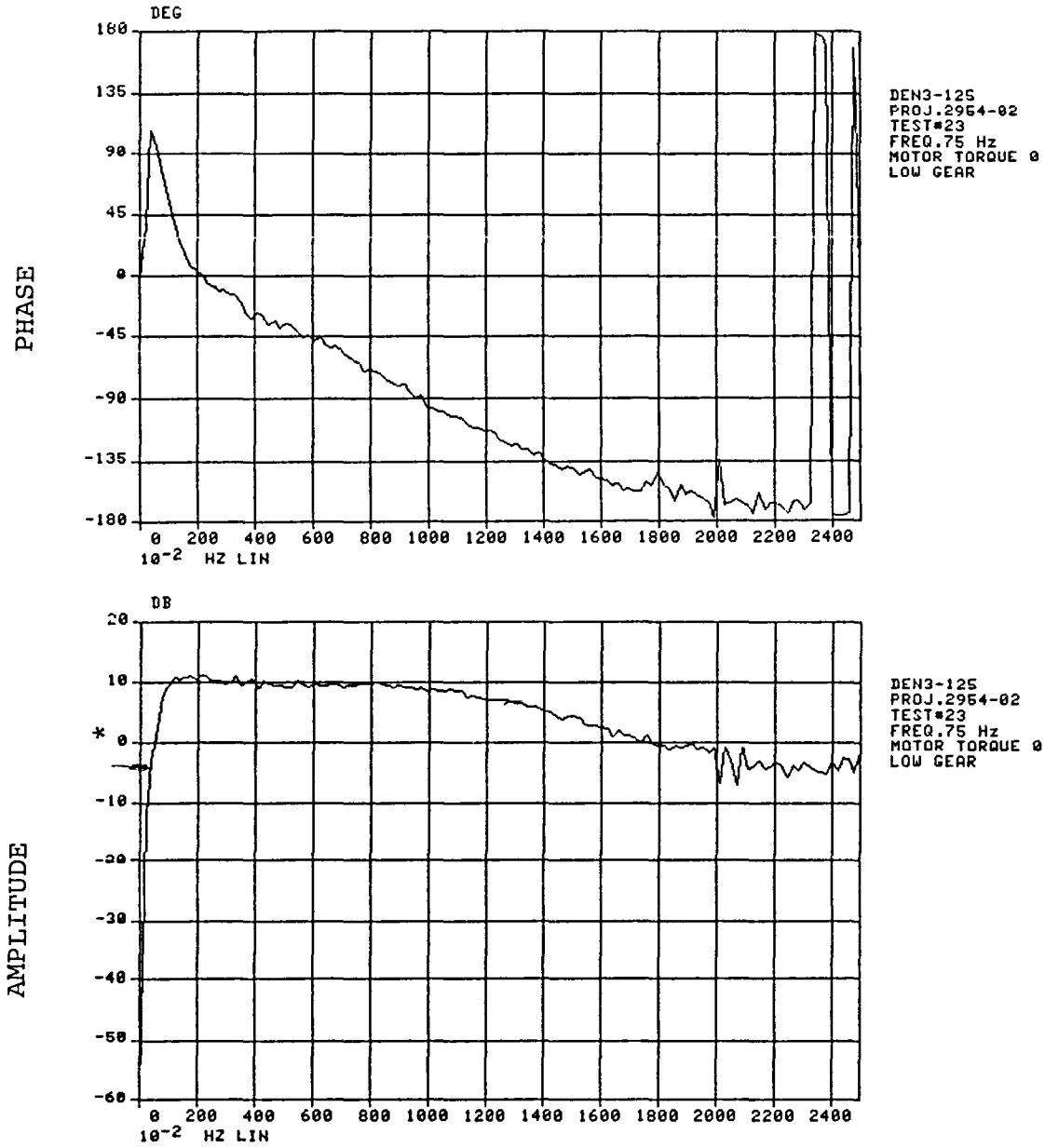

*Ø dB = 1 Hz Stator Frequency per Hz Slip

Figure 9.4.3 System Speed Response to Slip Disturbance

It is seen from the figures that no system resonances exist. Identical tests at other operating speeds also revealed no resonances. The system speed bandwidth is determined from the speed response to be about 10 Hz for the dynamometer inertia, which has been measured at about 40% of a 1,364 kg equivalent vehicle inertia. As the equivalent vehicle inertia is higher, it is believed that the vehicle bandwidth will be reduced and that no stability problems will be encountered on the vehicle.

Transient Response Tests

For this test a multi-channel light beam recorder was used for recording motor speed, motor torque, slip, motor current, and torque demand.

With the system initially at rest, a step torque demand was input to the system, and the system was permitted to accelerate through the gearshift range to top speed. The initial startup was jerky and was related to offset errors and instability problems in the slip control circuit near zero speed. The offset errors were corrected by a design change in the analog voltage-to-frequency converter; however, this correction was not made in time to fully document the better results before the test frame was shipped.

The startup problems were inherent to the use of the phase-locked loop in the slip control. In the future, it is intended to change the startup strategy whereby the rotor frequency signal will be locked out until the system gets started. However, time constraints prevented the inclusion of this improvement in the first generation system.

Once the motor speed was raised above 500 rpm, the system accelerated smoothly to top speed. Figure 9.4.4 is an oscillogram showing the step response to the torque demand input once the system is running. It can be seen that good response is achieved at 3600 rpm. Response becomes marginal at very slow speeds. It is believed that existing performance is adequate for testing on the road load simulator.

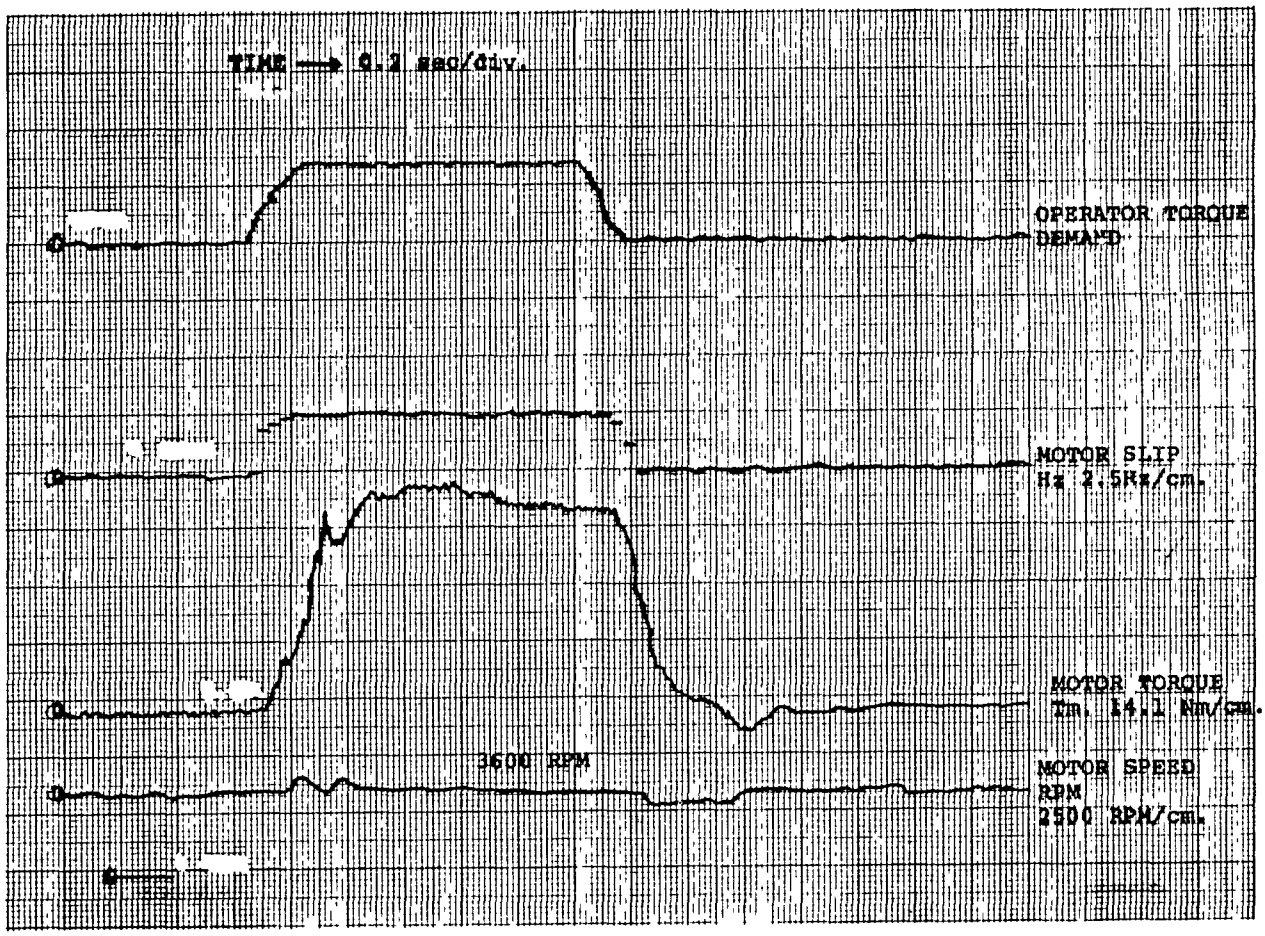

Figure 9.4.4 Motor Torque Response to Step Input

9.5 Temperature Effects

The purpose of this test was to determine the temperature rise of system components, and to evaluate the oil cooling system while running the system continuously at various power levels. In addition, the effect of temperature on system efficiency was measured. For this test, the same data was taken as for the efficiency test. This data included motor inlet and outlet oil temperature, inverter main transistor heat sink temperature, and energy recovery transistor heat sink temperature.

The system was set up as close as possible to actual operating conditions: closed oil cooling system, enclosure mounted on the inverter, and inverter fans running. One-hour continuous running was done for the following conditions:

1. 3600 motor rpm, 50% rated motor torque
2. 3600 motor rpm, rated motor torque
3. 1800 motor rpm, rated motor torque
4. 5640 motor rpm, rated motor torque

Figures 9.5.1 through 9.5.4 show the temperature rise of various components and the component efficiencies vs. time for these tests. It is seen that the only component that approaches its thermal rating is the motor. The overall system cooling capacity was judged adequate. It is also seen that component efficiencies do not change significantly as a function of temperature. Calculations show combined motor and inverter efficiency do not typically change more than 2% over the temperature range.

9.6 Noise and Vibration Tests

The purpose of this test was to obtain an indication of possible noise and vibration problems that may exist in the system. Test setup inadequacies (dynamometer noise, etc.) prevented the running of a meaningful noise test, and the vibration tests that were made have questionable applicability to the automobile environment. However, it was shown that no significant resonances exist in the test frame setup.

9.7 Torque and Speed Overload Performance

The purpose of this test was to evaluate system performance during system torque and speed overloads.

For both torque and speed overload tests a multi-channel light beam recorder was used for monitoring motor speed and torque, transaxle torque, slip, motor current, and torque demand.

Difficulties in controlling the speed of the test frame/dynamometer combination with both units in torque regulation prevented the running of the test exactly as planned (25 Hz to 150 Hz in 25 Hz steps). However, a verification of the ability of the system to respond gracefully to torque overloads was obtained as follows:

1. For both the dynamometer and test frame initially at constant speed and in torque regulation, the dynamometer torque is raised higher than the transaxle torque.

2. The system is observed to gradually slow down with increasing motor torque. The slip control easily follows the speed change to keep constant torque.

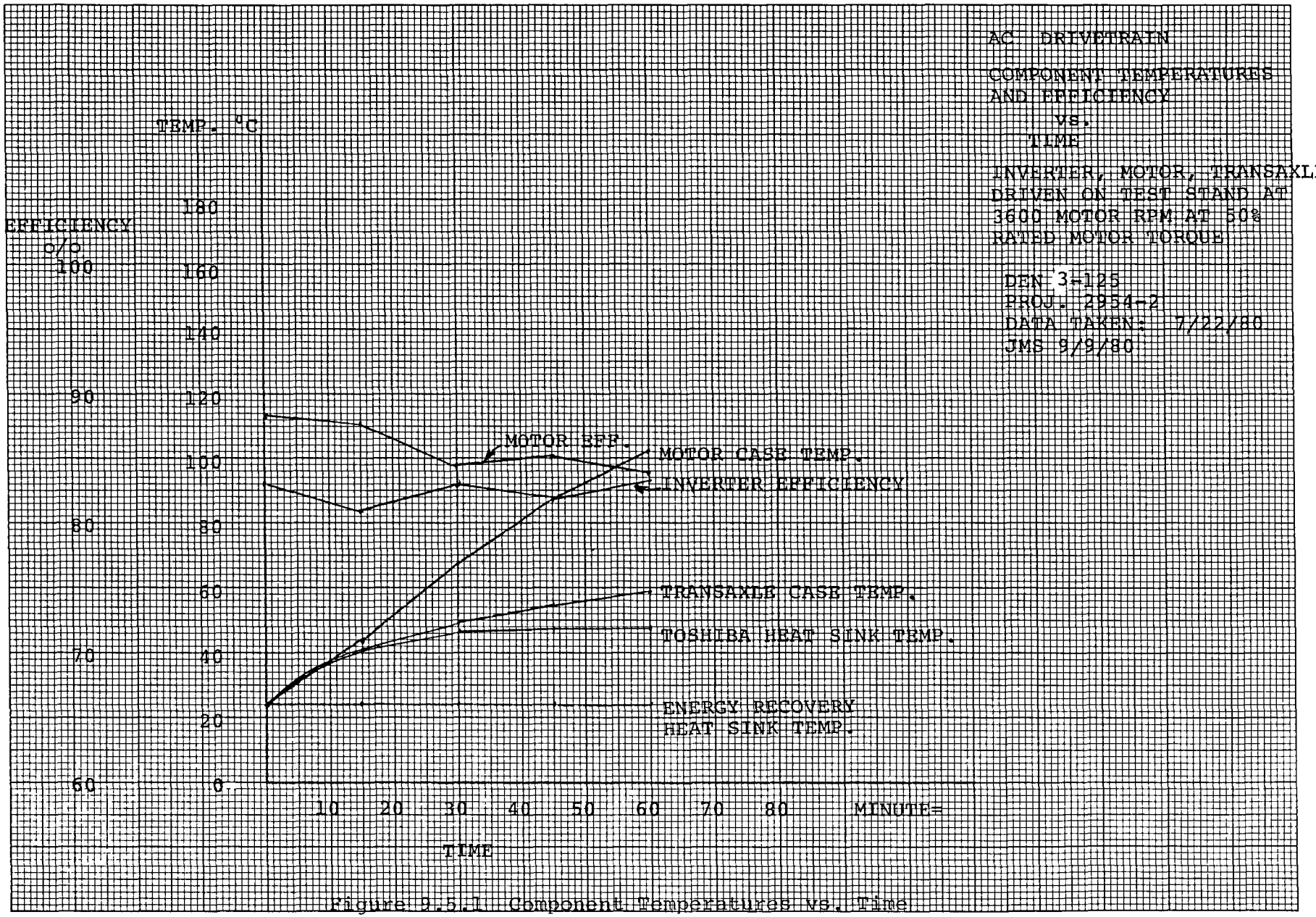

Figure 9.5.1 Component Temperatures vs. Time

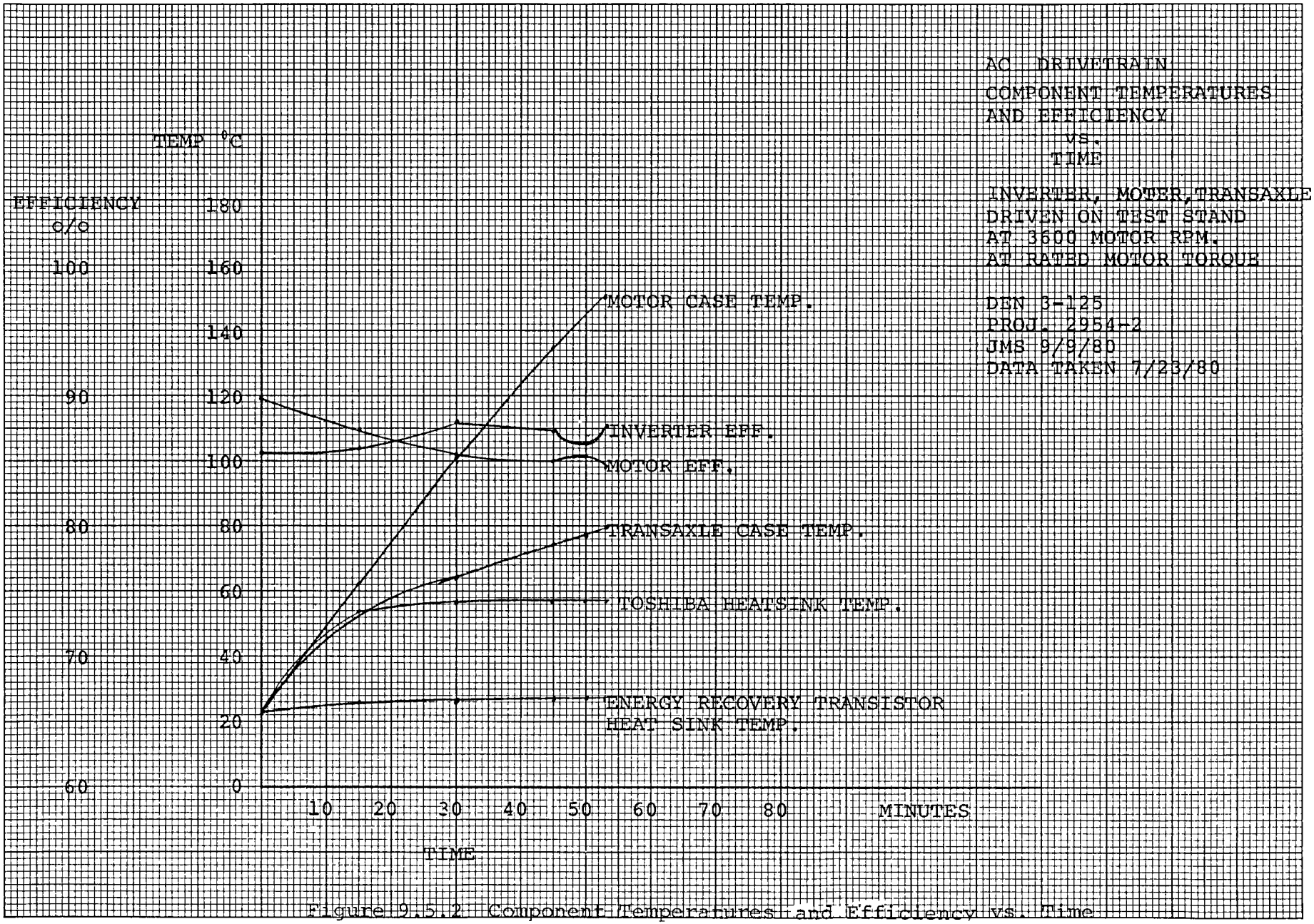

Figure 9.5.2 Component Temperatures and Efficiency vs. Time

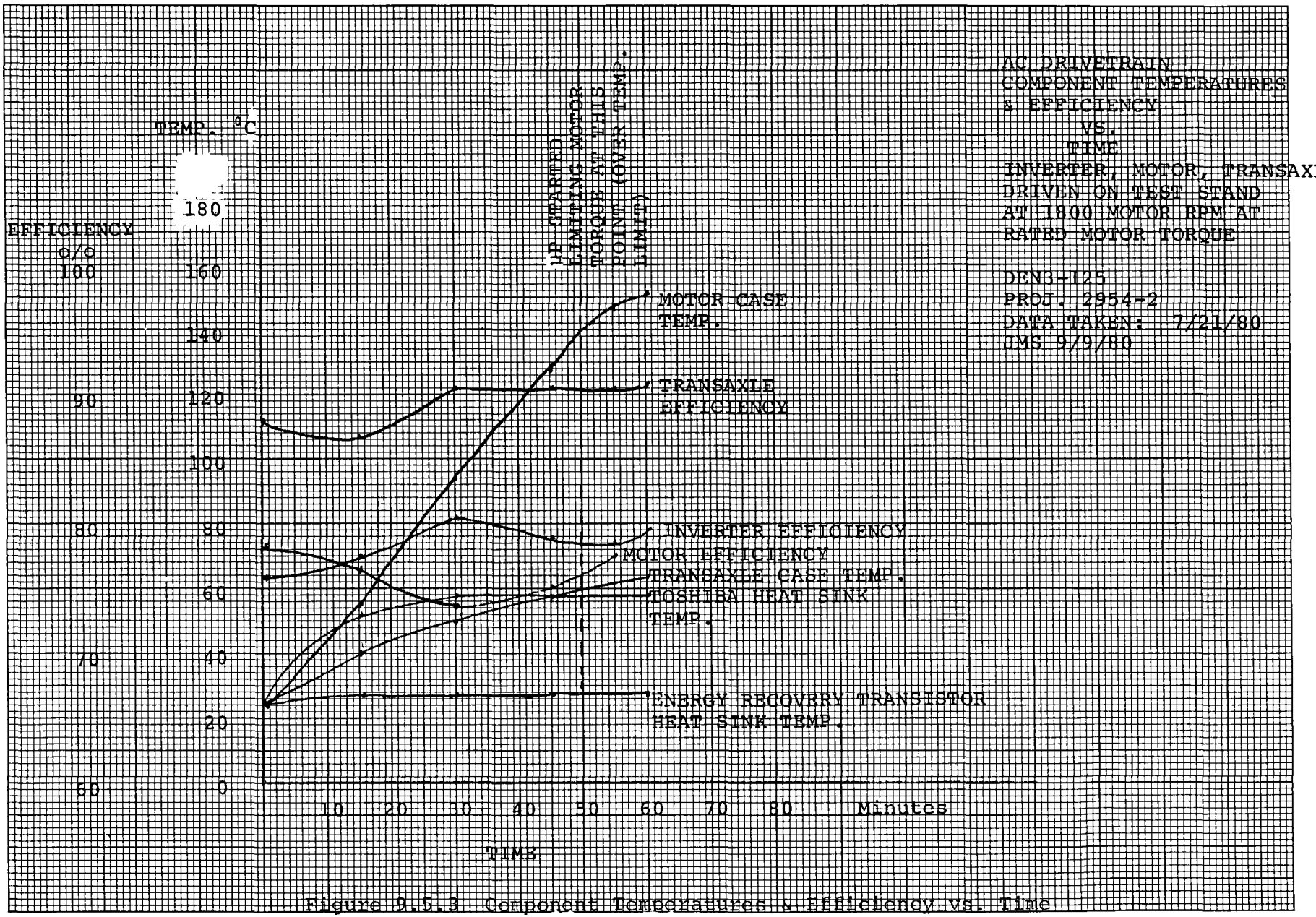

Figure 9.5.3 Component Temperatures & Efficiency vs. Time

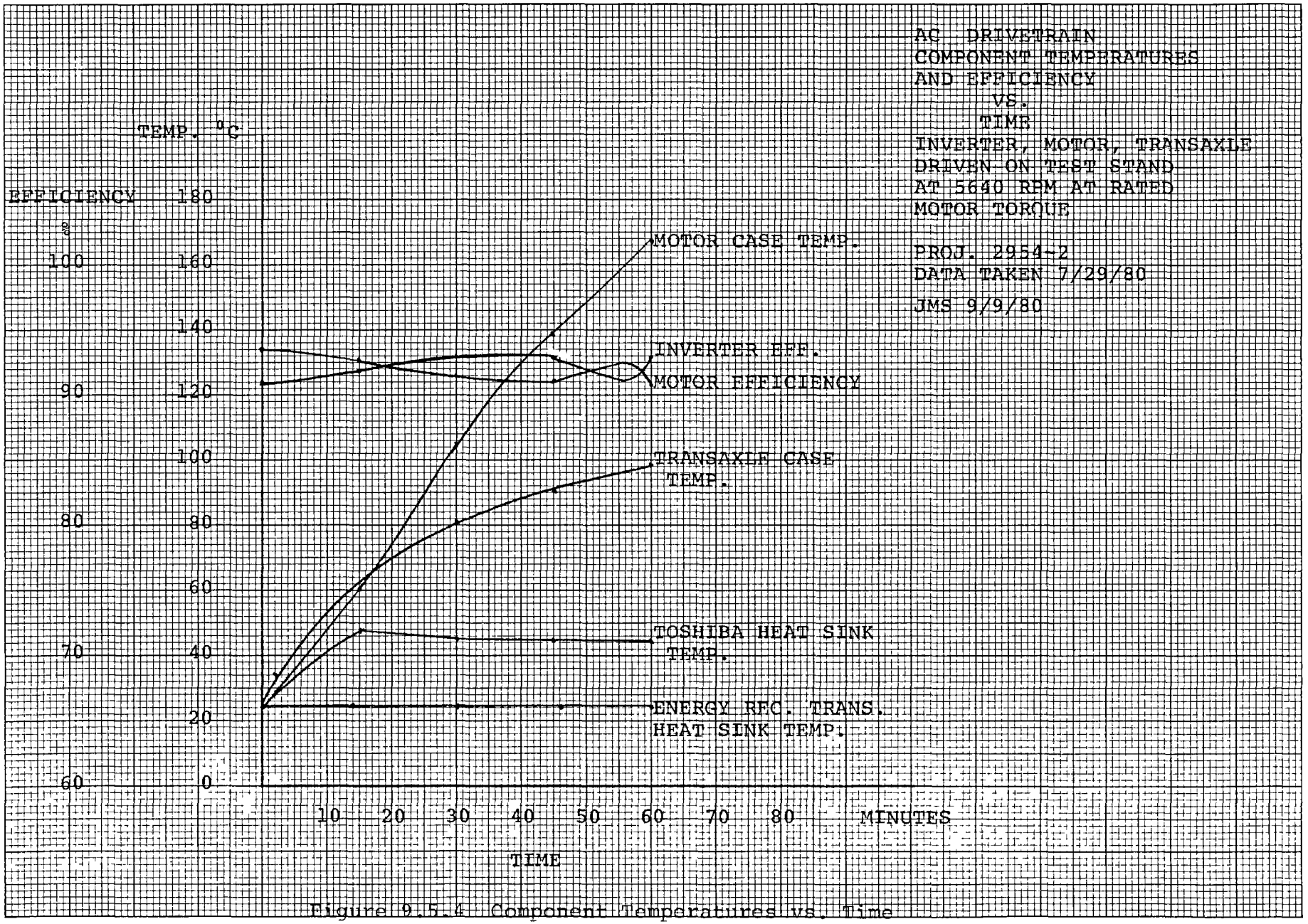

Figure 9.5.4 Component Temperatures vs. Time

3. Upon decreasing dynamometer torque, the system speed again increases smoothly.

Figure 9.7.1 shows this sequence; however, a slight torque oscillation is noted at zero motor rpm which is related to previously discussed problems at system startup from zero speed.

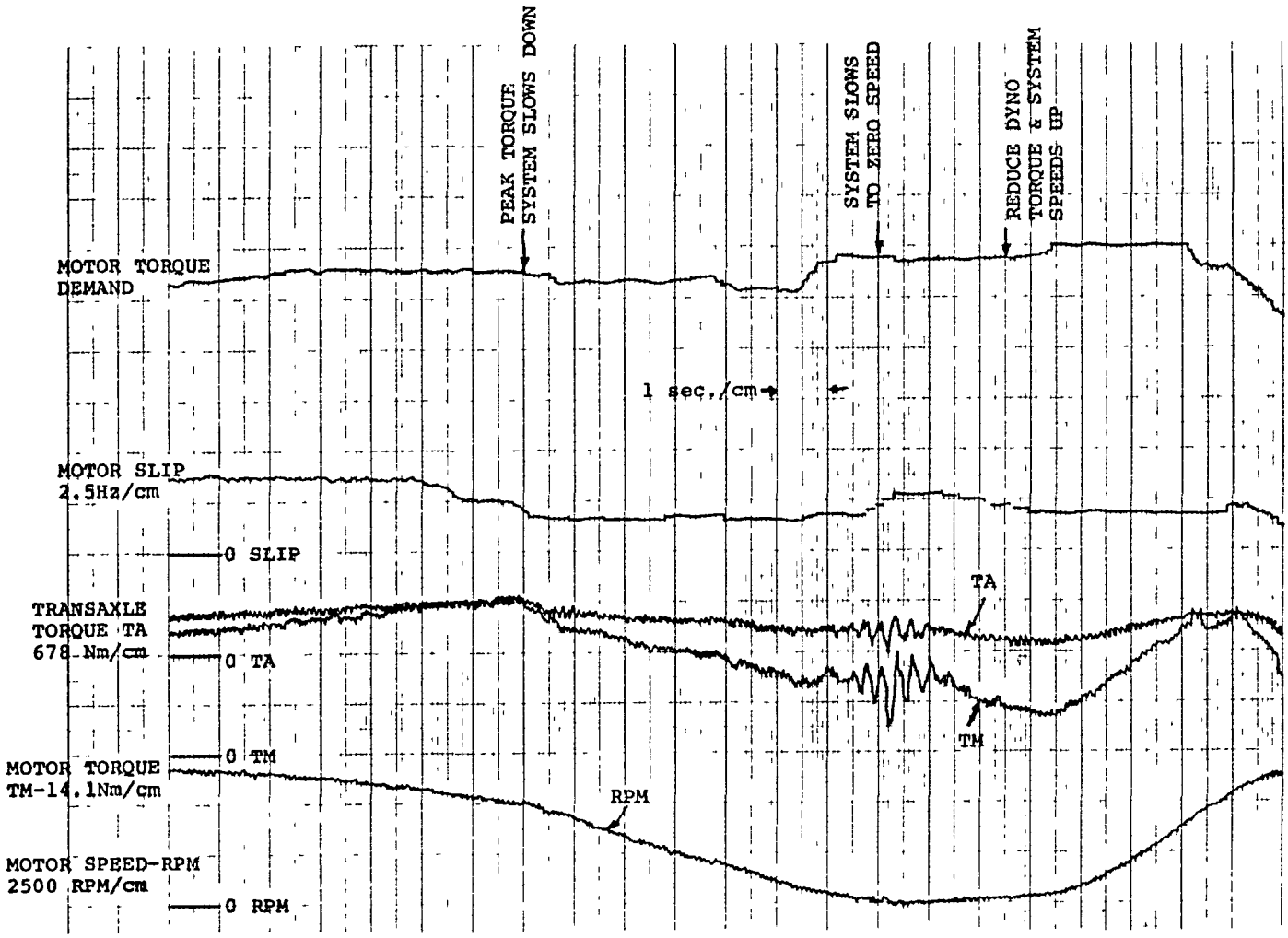

Figure 9.7.1 System Recovery from Torque Overload

The speed overload performance was verified after a digital filter was placed into the μP slip control algorithm to prevent rapid changes in slip that were causing instability.

For this test, the following sequence was observed:

1. With dynamometer in speed regulating mode and the test frame in a motoring condition, the dynamometer speed is increased beyond the top motor speed of 9000 rpm.

2. At 9000 rpm the motor torque limit is gradually reduced until, at 9600 rpm, the system goes into regeneration.

3. As the speed increases beyond 9600 rpm, the regeneration torque increases proportionately unless an overvoltage condition is detected which will shut the system down. This overvoltage shutdown was previously observed to occur at about 160 volts.

9.8 Shift Sequence Refinement and Testing

The purpose of this test was to achieve stable operation of the system during the gearshifting sequence. Adjustments were needed to both the controller and the transmission to attain this goal. The shift points were selected to optimize system efficiency.

An oscillograph showing the upshift sequence is shown in Figure 9.8.1. This sequence is described as follows:

1. Upon reaching the upshift speed of 9000 motor rpm, the controller issues the command to disengage the clutches.

2. After a fixed time delay to allow the clutches to disengage, the motor slip immediately goes negative, and a regenerative torque is applied to the motor. The high gear hydraulic solenoid is energized, although its clutch takes several hundred milliseconds to engage.

   The regenerative torque slows the disengaged motor to 3750 rpm in approximately 600 ms.

3. Upon recognizing that the motor speed is approximately synchronous with that required for high gear, the controller reduces the motor slip to zero until the total time allowed for the shift has elapsed.

4. At the end of this predetermined shift time, the controller looks at torque demand and adjusts its torque to that level.

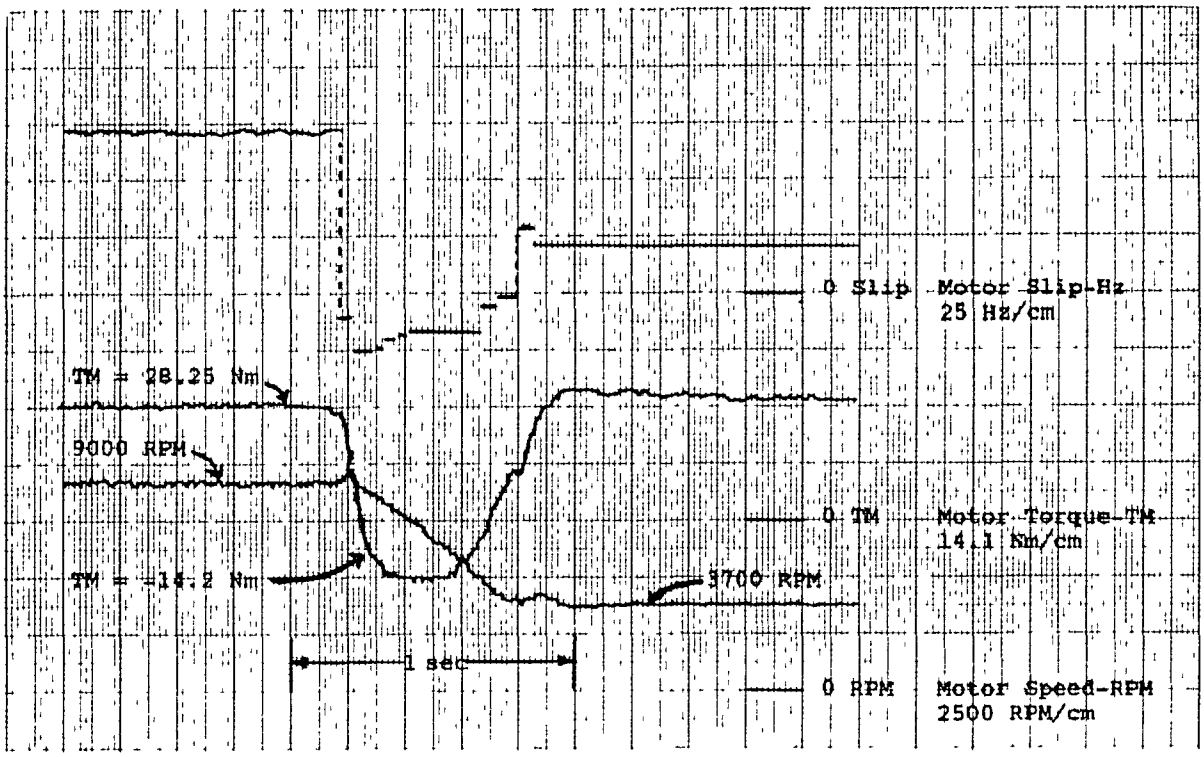

Figure 9.8.1 Transaxle Upshift Sequence

The above sequence proved effective for obtaining a fast shift without severe strain on the transaxle clutches, and it is believed that this shift is adequate for transaxle testing. However, this shift is too rough for an automobile. Further refinements are needed in the timing of the clutch solenoids and in the above control strategy to smooth out the upshift.

The downshift sequence is similar to the upshift sequence, but in the opposite direction. Upon issuing a shift command and delaying a fixed time for the clutches to disengage, the motor torque is increased to accelerate the motor to 2.4 times the high gear speed. When this speed is reached, the controller looks at torque demand and adjusts torque accordingly. The downshift speed of 3000 motor rpm is chosen to introduce hysteresis between the upshift and downshift points.

9.9 Final Programming of Slip/Duty Cycle Over Operating Range

The purpose of this test was to ensure that the V/Hz levels achieved by the system with the controller in the "Normal" mode agree with the optimum values. Most of the data necessary for this test was obtained from data taken during the efficiency measurement tests without running additional tests.

Figure 9.9.1 shows the V/Hz levels measured with the system in the "Normal" mode. When compared with the optimum V/Hz values obtained previously (Figure 5.4.4), it is seen that the "Normal" mode V/Hz values do not exactly follow the optimized values. However, a comparison of the combined motor and inverter efficiency measurements for both cases showed that the "Normal" mode operation produces efficiencies within $\pm$ 2% of the optimized efficiencies. Thus, it was determined that "Normal" mode selection of V/Hz and slip over the operating range was satisfactory, and further programming to improve efficiency was not necessary.

9.10 Intentional Failures and Graceful Drive Shutdown

The purpose of this test was to evaluate the drive protection and graceful shutdown capability during failures of various components. Specific failures evaluated were as follows:

1. Overtemperature, overspeed, and over/undervoltage conditions.
2. Loss of speed sensor.
3. Loss of base drive signals.
4. Loss of main bus power under load.
5. Loss of energy recovery circuit
6. Loss of controller power

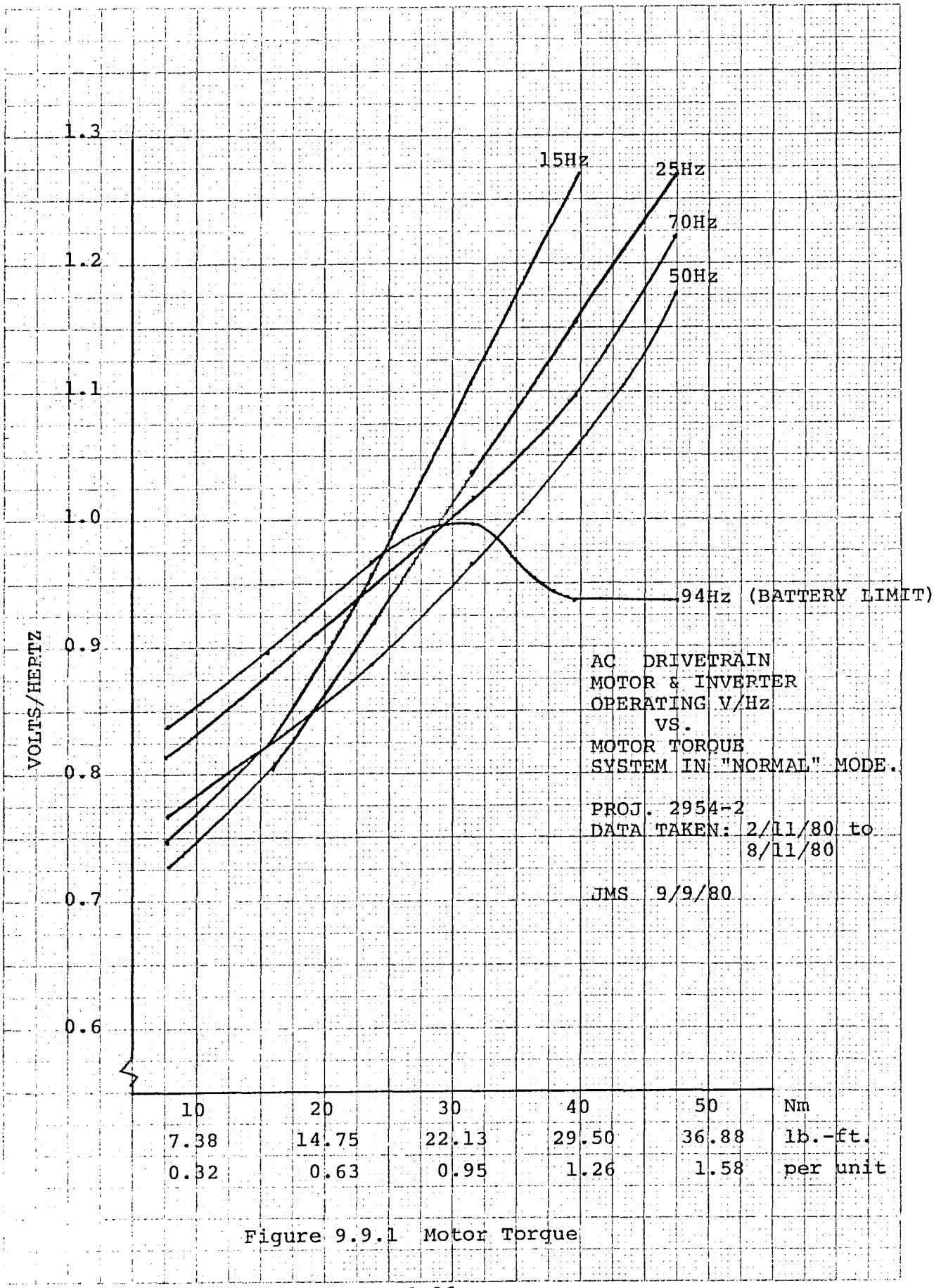

Figure 9.9.1 Motor Torque

The results of the above intentional failure tests follow:

1. Overtemperature. The overtemperature tests were done by connecting potentiometers in place of the thermistors that are used to sense battery temperature, main transistor heat sink temperature, and motor temperature. The actual temperature dialed in to the system was determined from the controller readout. During these tests, it was found that the following temperatures caused the controller to stop the motor:

Battery Temperature	81°C
Transistor Heat Sink	94°C
Motor Case	171°C

   In addition, it was verified that, as the motor case temperature rises above 94°C, the controller starts cutting back allowable torque under 1.5 rated torque to prevent the cutout temperature from being reached.

2. Overvoltage/Undervoltage. The overvoltage cutout was verified with the system in regeneration: it was observed that the controller automatically limits regenerative braking torque in order to hold the bus voltage under 160 volts. When the voltage rises above 165 volts, the inverter cuts out. The low voltage cutout was previously verified during the battery rundown test to shut the motor off at 94 volts.

3. Overspeed. This test was done under Section 9.7, "Torque and Speed Overload Peformance." Results are presented in that section.

4. Loss of Speed Sensor. For this test the motor pulse tachometer sensor was abruptly disconnected at various motor speeds. The drive was observed to shut down smoothly.

5. Loss of Base Drive Signals. With the system running at various torques and speeds, the base drive command connector from the controller was abruptly disconnected from the inverter. For each torque and speed level, the drive was observed to gracefully enter a single phasing condition at reduced motor torque. No failures in the system occurred during the running of these tests.

6. Loss of Main Bus Power. For this test an extra switch was needed to defeat the inherent system protection which automatically shuts the controller off if the main contactor is opened. With this protection disabled, the system had to rely on the controller's internal low voltage monitor to shut the motor down. This low voltage monitor was previously verified to trip the motor out at 94 volts. With this setup for various speed and torque levels, the main contactor was opened. Oscillograms of bus voltage and motor current taken during this sequence showed that no overvoltage problems are encountered under these conditions. In all cases run, the system shut down gracefully without failures.

7. Loss of Energy Recovery Circuit. Any voltage rise in the energy recovery circuit above a threshold level immediately trips out the system. The reliable operation of this failsafe shutdown without failures in the inverter was verified repeatedly during the test program. Thus, it was decided that a special test of this function was not needed during this phase.

8. Loss of Controller Power. This test is a verification of the ability of the controller to power down without uncontrolled firing of the output transistors. This test was done by turning the test frame off with the system running. This test was run successfully with no failures in the system.

9.11 Drive Performance Testing

The purpose of this test was to document the drive performance under the following simulated driving conditions, assuming a 1818 kg vehicle:

1. Constant vehicle speeds of 0 to 88.5 km/hr. on a flat surface.

2. Constant vehicle speeds of 0 to 51.5 km/hr. on a 4% uphill grade.

In addition, a final speed torque envelope for the system was documented.

Figure 9.11.1 shows the combined motor/inverter/transaxle efficiencies for driving on a flat surface and for a 4% grade. It is seen that there is poor efficiency at low speed, which is due principally to poor inverter efficiency. The 4% grade efficiency is higher than 0 grade because the system is working closer to rated torque.

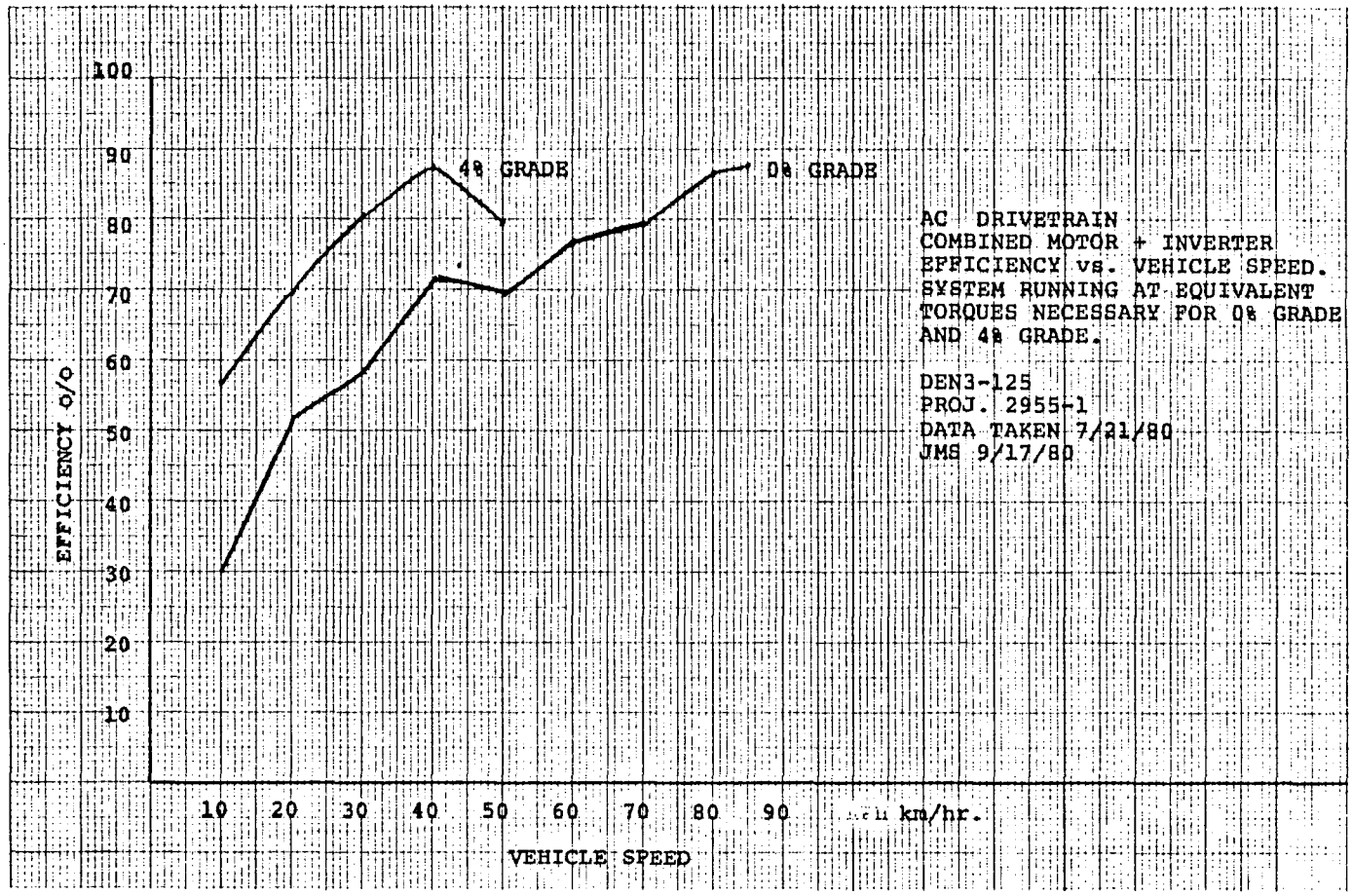

Figure 9.11.1 Combined Motor/Inverter Efficiency vs. Vehicle Speed

Figure 9.11.2 shows the motor/inverter speed-torque envelope with the system in the "Normal" mode. It is seen that the system exceeds the goal of 1.5 rated torque between 20 and 80 Hz stator frequency. However, the goal of rated torque at zero motor speed is not attained, and the system was battery limited at 150 Hz. With the battery charger supporting the battery voltage at top speed, it was previously demonstrated that the goal of rated torque at 150 Hz can be met. Figure 9.11.3 shows the speed-torque envelope with the system in regenerative braking. The regenerative braking peak power is limited by the peak voltage allowable on the inverter.

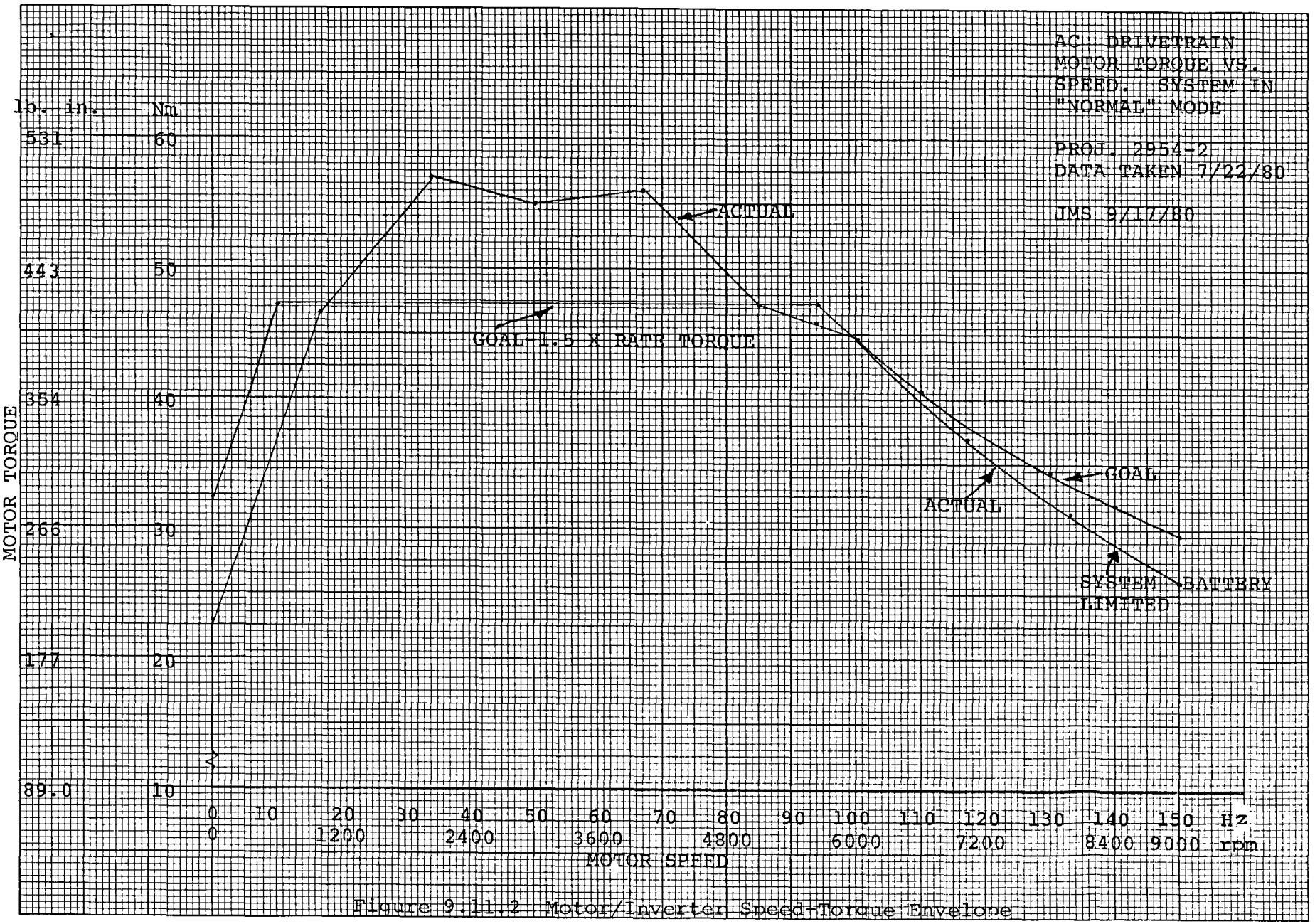

Figure 9.11.2 Motor/Inverter Speed-Torque Envelope

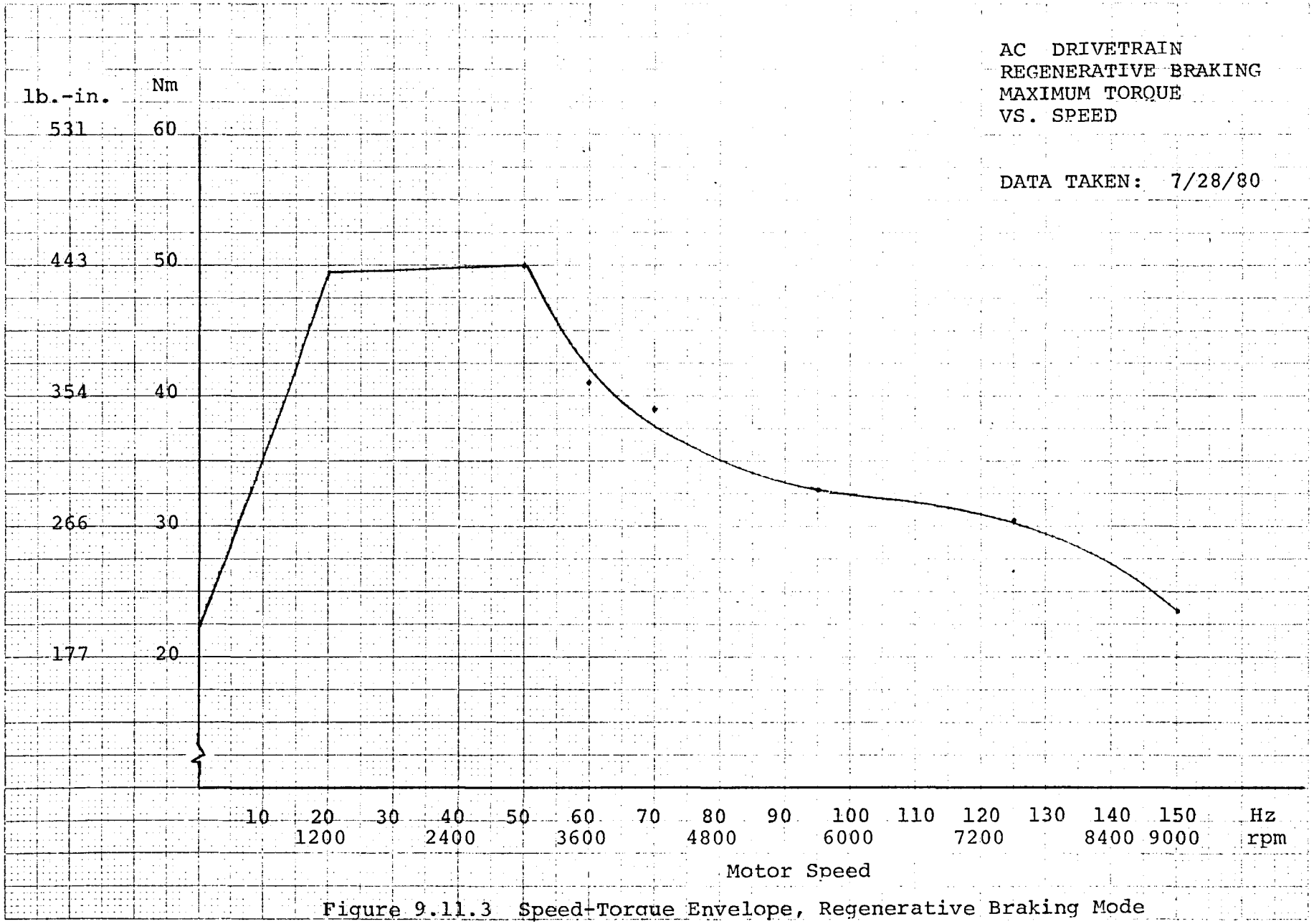

Figure 9.11.3 Speed-Torque Envelope, Regenerative Braking Mode

9.12 Coast Performance and Downhill Grade Simulation

The purpose of this test was to document the drive performance under the equivalent driving condition of coasting down a 10% grade at 80.5 km/hr. The drive was to be in regenerative braking, and no speed increase in the system was allowed. An 1818 kg vehicle was assumed for this test.

It had been determined that at the vehicle speed of 80.5 km/hr. required for the test, the maximum torque available in regeneration was 27 Nm, which is equivalent to holding zero speed down a 1.4% grade. The 10% downhill grade test was run in low gear at an equivalent vehicle speed of 45.9 km/hr. In low gear, enough torque was developed in regenerative braking to hold constant vehicle speed on a 10% grade.

Data taken for both of the above conditions is given in Figure 9.12.1.

Motor RPM	Battery Volts	Battery Amps	Motor Torque	Transaxle Torque	Motor Eff.	Inverter Eff.	Transaxle Eff.	Total Eff.
6640	156.8	92	25.6 Nm	208 Nm	0.86	88.0	97.5	73.8
9006	158.0	98	19.3 Nm	384 Nm	0.85	94.6	98.8	79.4

Figure 9.12.1 System Coast Performance

9.13 No Load Tests

The purpose of this test was to determine the drivetrain losses due to windage and friction. The degree of oil viscous friction in the oil cooled motor was to be estimated by spinning the drive with the oil lines first connected and then disconnected. Difficulty in reading the torque sensors at low torque levels resulted in inaccuracies in the data on this test.

For both high and low gear, the motor torque ranged between 0 and +0.06 Nm with the oil lines connected. The test was not repeated with the oil lines disconnected because of these low torque readings. The transaxle torque ranged from 0.12 Nm at 1000 RPM to 0.8 Nm at 6000 RPM and increased almost linearly with speed. However, low confidence is placed in these low readings which are less than 2% of the full-scale torque sensor output.

9.14 Vehicle Performance Predictions

Vehicle performance calculations at the beginning of the program indicated that a two-speed transaxle would sufficiently extend the performance spectrum to provide acceptable top speed capability at the high speed end of the spectrum and reasonable grade climbing ability at the low speed end. Acceleration performance was not approximated at that time due to insufficient definition of some drivetrain parameters.

Subsequent hardware development testing provided a more precise indication of the torque capacity of the ac motor. Acceleration performance was then computed for two gross vehicle weights, namely 1360 kg (3000 lbs) and 1810 kg (4000 lbs), based on intermittent, 150% rated torque capacity of the ac motor. Grade performance, however, was computed on the basis of continuous, rated torque capability. The results are graphically presented in Figures 9.14.1 and 9.14.2.

Also explored at that time were acceleration and grade performance of the same two GVW vehicles with single reduction gearing, and alternately, with 3-speed and 4-speed transaxles. Ratios were selected to provide approximately the same top speed in each case. Ratio steps were narrowed in the multiratio arrangements in order to minimize running of the motor in the top third of its speed range, where its torque output is declining. A one-second shift time was assumed for each shift. A 3.26:1 final drive ratio was used with the 1360 kg (3000 lbs) GVW vehicle, and 3.67:1 ratio with the 1810 kg (4000 lbs).

The results are listed in Figure 9.14.3 confirming the correctness of the earlier decision to use a two-speed transaxle in the prototype design. Acceleration performance is not substantially improved by adding one or more ratios. Grade performance is improved beyond requirements, hence the extra cost does not seem justified at this stage of development. Future vehicle testing may indicate a need for a smaller ratio step in order to minimize drive line torque disturbances and provide acceptable shift smoothness, but no compelling evidence for this exists.

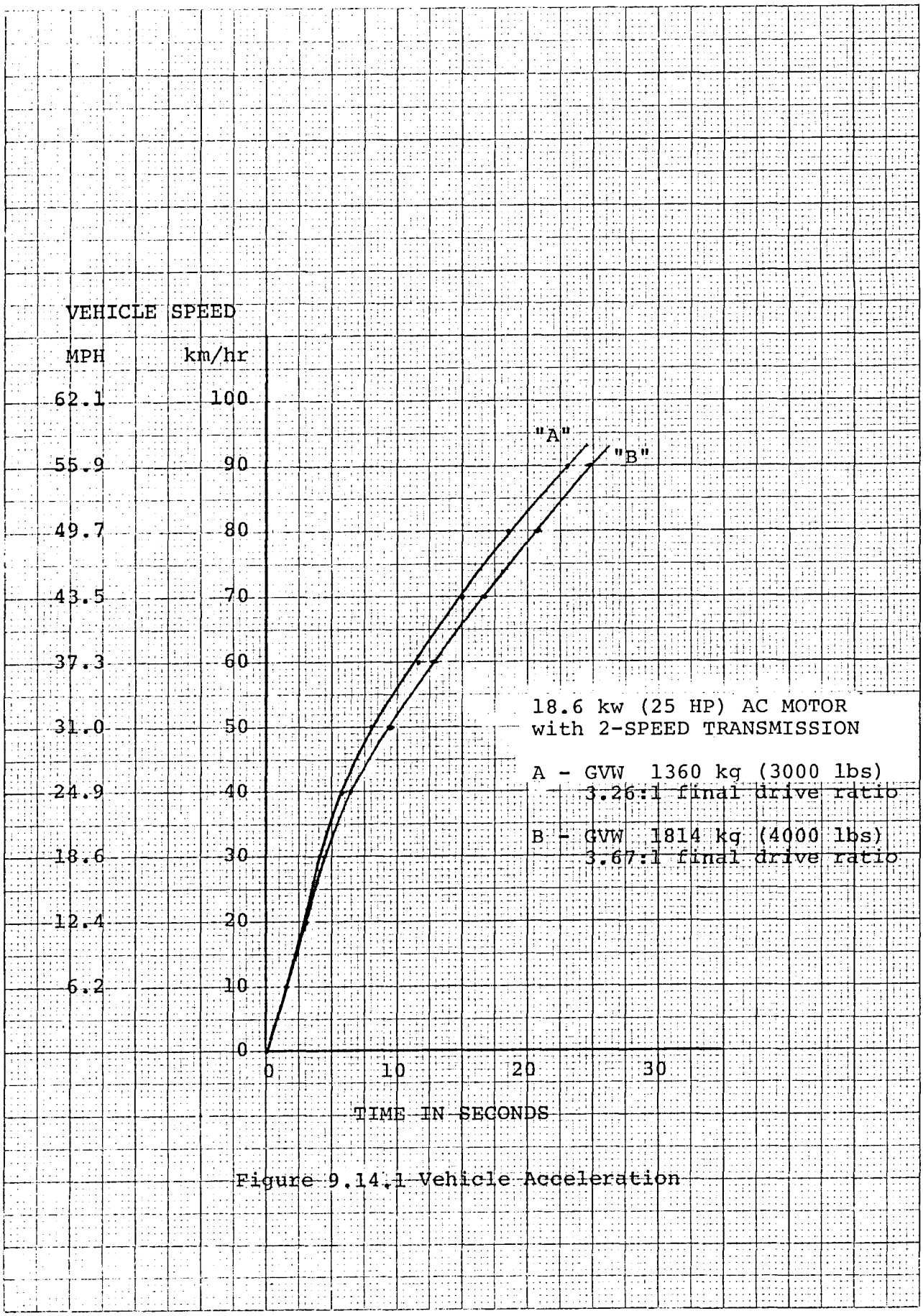

Figure 9.14.1 Vehicle Acceleration

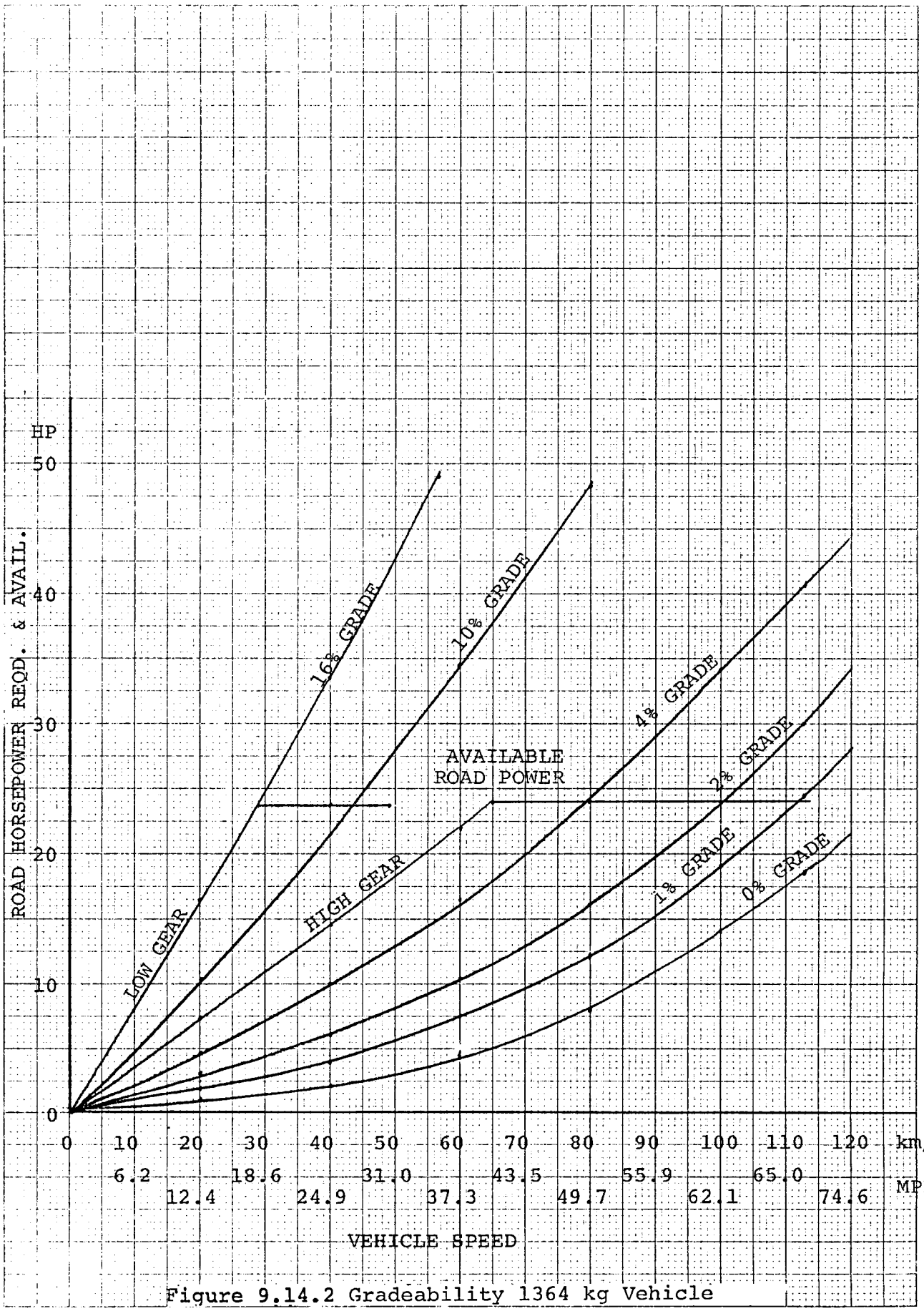

Figure 9.14.2 Gradeability 1364 kg Vehicle

NO. OF RATIOS		1-SPEED		2-SPEED		3-SPEED		4-SPEED		DESIRED	
GVW#		3000	4000	3000	4000	3000	4000	3000	4000	3000	4000
ACCELERATION SEC.											
0 - 48.3 km/h											
0 - 30 mph		12.6	15.2	7.9 (1 sec.)	9.8	7.1 (1 sec.)	8.8	7.4 (2 sec.)	9.0	6.2	9.2
0 - 88.5 km/h											
0 - 55 mph		25.5	32.2	22.4 (1 sec.)	27.0	20.5 (2 sec.)	26.7	20.8 (3 sec.)	27.0	19.0	25.0
40 - 89 km/h											
25 - 55 mph		15.0	19.6	16.7	20.8	14.7	20.0	15.8	21.0		
				Shift times (in parentheses) are included in the totals.							
SPEED											
ON 4% GRADE	kph	109.4	94.93	105.0	94.93	109.0	94.93	108.6	94.93	77.23	51.49
FOR 1 MIN.	mph	68.0	59.0	65.3	59.0	67.8	59.0	67.5	59.0	48.0	32.0
ON 4% GRADE	kph	80.45	67.26	79.48	67.26	80.45	67.26	80.45	67.26		
CONTINUOUS	mph	50.0	41.8	49.4	41.8	50.0	41.8	50.0	41.8		
ON LEVEL GRADE	kph	112.63	100.56	112.63	100.56	112.63	100.56	112.63	100.56	104.59	93.32
	mph	70.0	62.5	70.0	62.5	70.0	62.5	70.0	62.5	65.0	58.0
GRADEABILITY											
%, MAX.											
(FOR 2 MINUTES)		11.0	9.0	22.0	20.0	31.0	27.0	40.0+	40.0		

C_D = 0.3 A = 20.0 ft^2 1.86 m^2 RR = 10.5 in. 26.7 cm ROLL. RESIST. 8.1 kg/1000 kg GVW

Figure 9.14.3 Predicted Vehicle Performance, Electrical Vehicle, ac Drivetrain

9.15 Discussion of Results

The following is a summary of the most important test results in this section:

1. Efficiency. Although the peak system efficiency of 82% is acceptable for an electric vehicle, the efficiency at low power levels is limited by poor inverter efficiency and needs improvement. Prospects for improving inverter efficiency are given in Section 6 and motor efficiency in Section 5.

2. Dynamic performance. Overall system stability was acceptable for tests run with 40% vehicle inertia. No problems are foreseen with the actual vehicle inertia. Startup problems exist around zero speed which must be corrected in the future. However, performance is believed to be adequate for testing on LeRC Road Load Simulator.

3. The one-hour, rated torque, thermal rise of the system is acceptable. System efficiency was fairly constant over the temperature range.

4. The gearshift sequence is believed to be adequate for testing on the LeRC Road Load Simulator. However, shifting is too rough for an automobile, and needed improvements will be implemented during the course of track testing.

5. The system has fair immunity to overloads and intentional failures. However, more extensive testing will be required for a vehicle.

6. The motor/inverter speed-torque goals were met or exceeded except at zero motor speed, where the goal of rated torque was missed by 29%. The creep speed goal of 1 mph, however, was nearly met at 96% rated torque.

10.1 Modeling Approach

The computer simulation of the Eaton ac propulsion system consisted of three primary computer models: a detailed model of the primary inverter components, a detailed model of the induction machine, and a model of the total propulsion system installed in a vehicle.

The inverter was modeled by including its basic components such as transistors, diodes, resistors, capacitors, etc., in a state variable model, using the SPICE2[5] circuit analysis program. The detail and accuracy was sufficient to evaluate design changes such as alternative transistors, controller strategy and waveform notch schemes.

The induction machine was modeled using frequency domain analysis of an induction motor driven by a PWM wave. Custom computer software was developed to compute the motor losses due to waveform notch scheme variations. The induction motor simulation included modeling of the rotor's nonlinear frequency dependence and accurately modeled the effects of higher order harmonics. The simulation also included the capability to produce motor voltage and current waveforms. This simulation enabled the evaluation of new motor designs and aided in sizing of inverter components.

A quasi-steady state model of the total ac propulsion system in a vehicle was developed using the Boeing Computer Services HEAVY[6] program. The propulsion system model included a simplified battery model, inverter, motor, and transaxle models consisting of efficiency maps, and an overall vehicle model.

These three simulation capabilities were used to analyze and evaluate design modifications intended to improve inverter, motor, and overall propulsion system performance. The results of these analyses have been used in the revision of the propulsion system design and will continue to be used as the design evolves.

10.2 Motor Model Development

The study of the induction motor and drive system shown in Figure 10.2.1 was done using steady state motor analysis. The effects of various PWM waveshapes on motor efficiency and current waveshapes were studied with an analysis consisting of two parts. The first stage performs a Fourier analysis of the PWM wave of interest to find its harmonic content. The harmonic components of the voltage waveshape are then applied to a frequency-dependent induction machine equivalent circuit. The model predicts complex currents, torque contributions, volts/hertz, slip (with load effects), and efficiency at every harmonic.

The motors studied are balanced three phase induction machines. The assumption is made that the system operates as a balanced three-phase system. Also, as is common practice, the assumption is made that the induction motor can be represented by a linear model. These assumptions allow the schematic of Figure 10.2.2 to be drawn. Using these assumptions the motor phase to -VBUS waves of Figure 10.2.3 can be analyzed to give the phase to neutral wave of Figure 10.2.4 by:

$$V_{N,-VBUS} = 1/3\ (V_{\phi 1,-VBUS} + V_{\phi 2,-VBUS} + V_{\phi 3,-VBUS})$$

so

$$V_{\phi 1,N} = V_{\phi 1,-VBUS} - V_{N,-VBUS}$$

$$= 1/3\ (2\ V_{\phi 1,-VBUS} - V_{\phi 2,-VBUS} - V_{\phi 3,-VBUS})$$

Again, since the model is linear the phase to neutral voltage wave can be broken into its Fourier components as

$$V_{\phi 1,N}\ (M) = 1/3\ \ [2V_{\phi 1,-VBUS}(M) - V_{\phi 2,-VBUS}(M) - V_{\phi 3,-VBUS}(M)]$$

where M is the harmonic number, and $V_{\phi,-VBUS}(M)$ represents the phasor quantity at the Mth harmonic obtained by Fourier analysis of the phase to -VBUS wave. Knowing

$$V_{\phi 1,-VBUS}(M) = [V_{\phi 1,-VBUS}(M)]\ 1\ \underline{/0}$$

$$V_{\phi 2,-VBUS}(M) = [V_{\phi 1,-VBUS}(M)]\ 1\ \underline{/-M2\pi/3}$$

and

$$V_{\phi 3,-VBUS}(M) = [V_{\phi 1,-VBUS}(M)]\ 1\ \underline{/+M2\pi/3}.$$

The above expression for $V_{\phi 1,N}$ can be written as

$$V_{\phi 1,N}(M) = 1/3\ V_{\phi 1,-VBUS}(M)\ (2\underline{/0} - 1\ \underline{/-M2\pi/3} + 1\ \underline{/+M2\pi/3})$$

Performing phasor analysis, it can be shown[7] that the phase shift has the effect of eliminating the frequencies which have harmonic numbers M,

$$M = 3N,\ N = 1,\ 2,\ 3,...$$

causing negative phase rotation for frequencies with harmonic numbers M,

$$M = (3N - 1),\ N = 1,\ 2,\ 3,...$$

and not changing frequencies with harmonic numbers M,

$$M = (3N - 2),\ N = 1,\ 2,\ 3,...$$

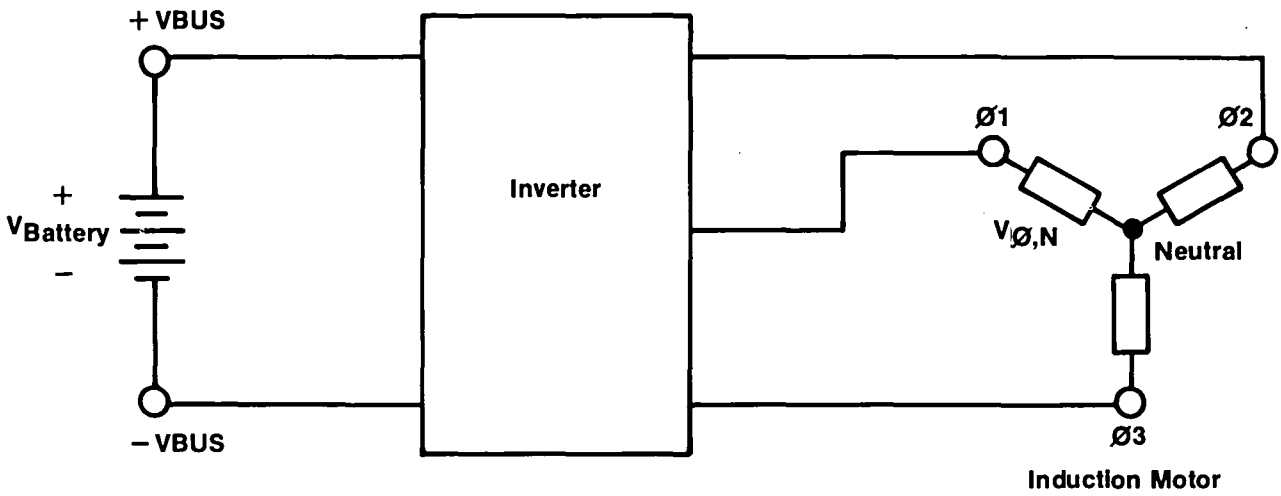

Figure 10.2.1 Drive System Schematic

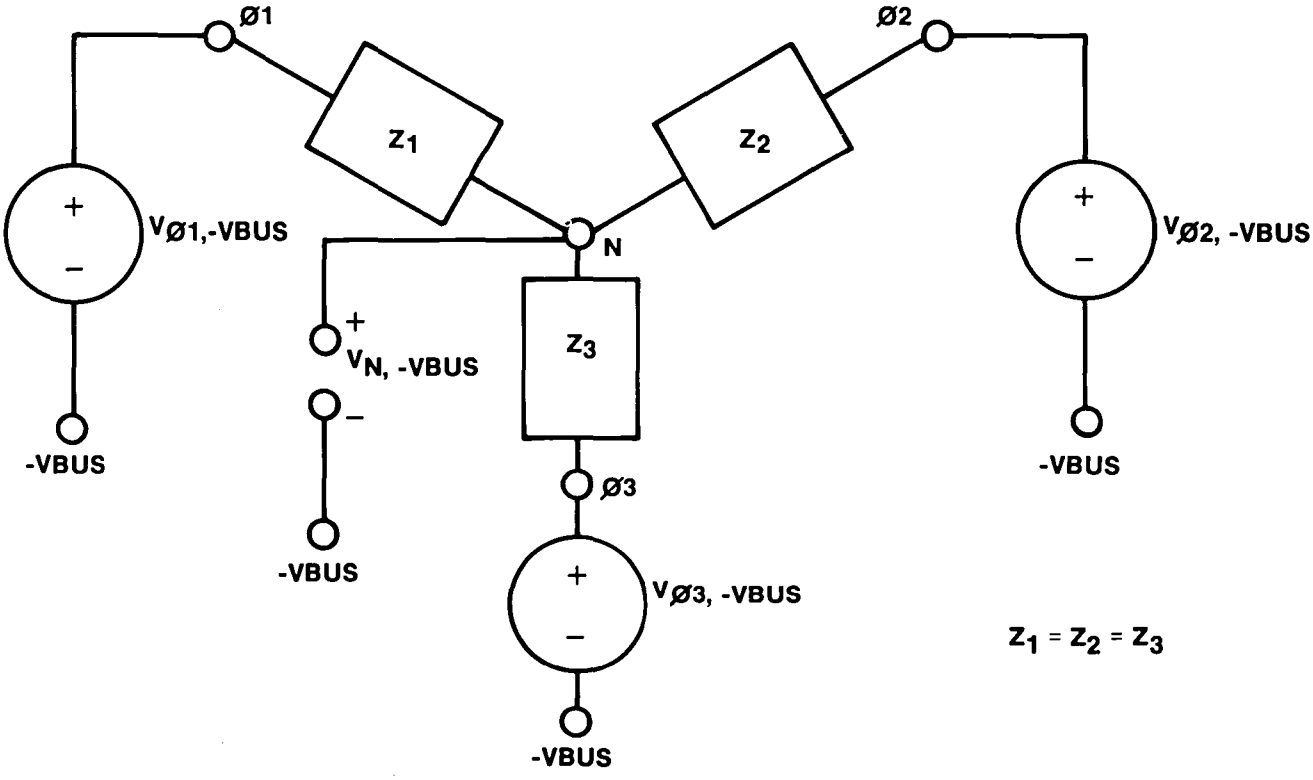

Figure 10.2.2 Linear Representation of Balanced Three Phase Motor

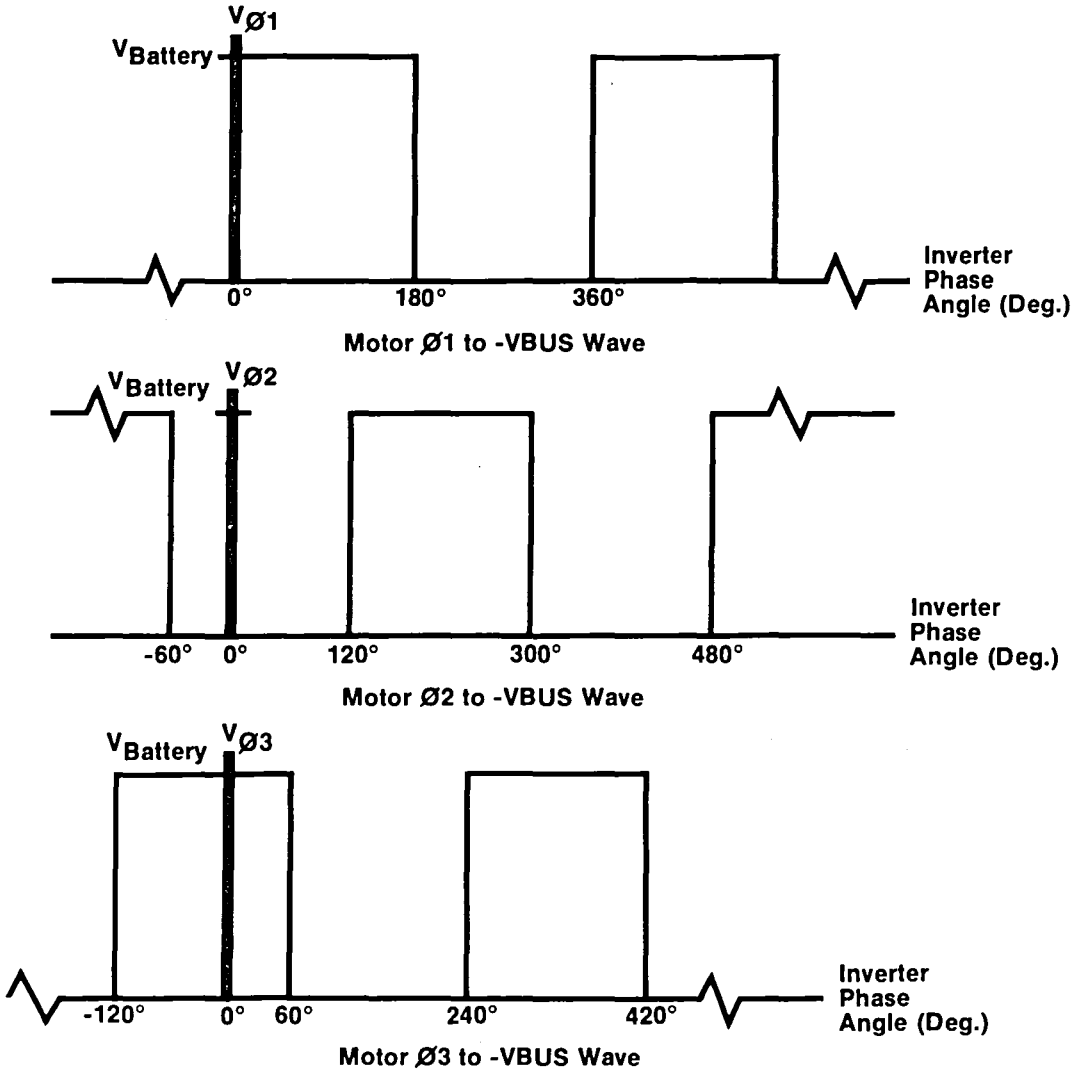

Figure 10.2.3 Motor Phase to -VBUS Waveshapes

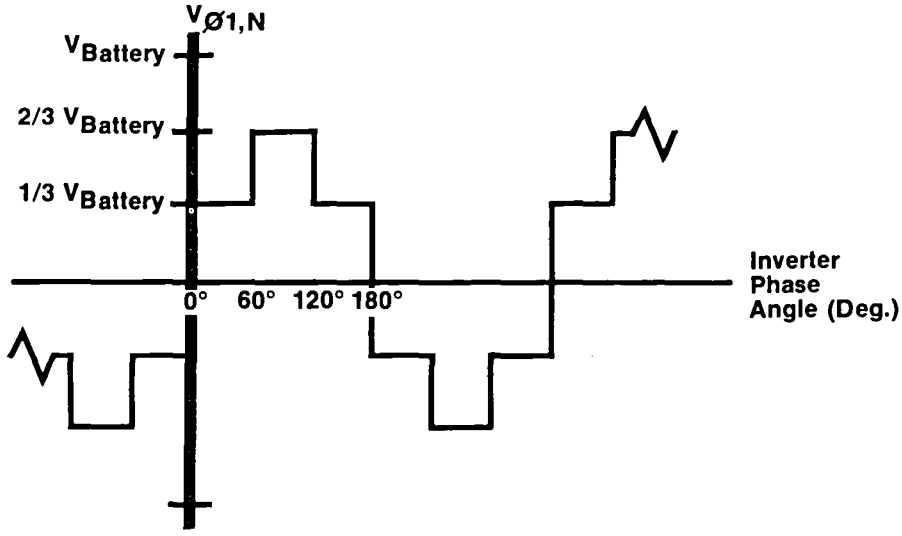

Figure 10.2.4 Motor Phase to Motor Neutral Waveshape

Thus, the phase to neutral wave has the same Fourier content as the phase to -VBUS wave with the triplen harmonic components eliminated and the change of rotation in other harmonics noted above. This allows Fourier analysis of the phase to -VBUS wave, a much simpler task than analysis of the phase to neutral wave. The analysis software solves the Fourier integral in closed form and stores the resultant harmonic voltage amplitudes. All harmonic components with peak voltage magnitudes greater than 0.1% of the bus voltage are retained for the analysis, and others of lesser magnitude are neglected. The fundamental frequency component is always retained for analysis. The harmonics retained are tabulated with their frequency information, voltage magnitude and sense of rotation and are then passed to the second stage of the analysis.

The second stage of simulation applies every significant voltage harmonic to an appropriate steady state induction machine equivalent circuit. By analyzing every voltage individually, an equivalent circuit, appropriate for that frequency, can be used with parameters that reflect the frequency dependence of the motor.

Superposition is then used to reconstruct the net effect of the whole PWM wave.

The circuit used for analysis of the fundamental component is shown in Figure 10.2.5.

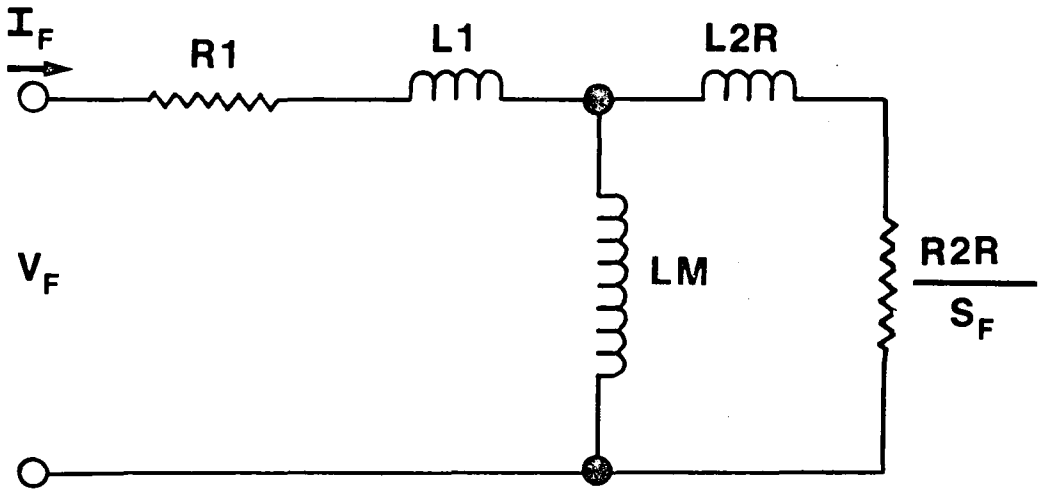

Figure 10.2.5 Fundamental Equivalent Circuit

V_F is the PWM voltage wave fundamental component, as determined by the Fourier analysis, and I_F is the resultant fundamental current. R1 and L1 comprise the stator impedance. The core loss equivalent resistance is large and is therefore omitted. LM is the magnetizing reactance. Rotor quantities are referred to the stator. L2R and R2R comprise the running rotor impedance. The running rotor impedance is used for analysis of the fundamental component since it is the impedance for the slip frequency, which is what the rotor sees. The load is simulated by S_F, the slip at the fundamental.

As part of this study, two motors were analyzed; the 100 V motor and a proposed 133 V motor. The values used in the analysis of the 100 V motor were those calculated from the motor test performed at ERC, and they are shown in Figure 10.2.6.

Frequency = 94 Hz		
Stator Resistance	R1	= 0.0113 Ω
Stator Leakage Reactance	X1	= 0.0247 Ω
Stator Leakage Inductance	L1	= 41.82 μH
Magnetizing Reactance	XM	= 1.204 Ω
Magnetizing Inductance	LM	= 2038. μH
Rotor Leakage Running Reactance	X2R	= 0.0321 Ω
Rotor Leakage Running Inductance	L2R	= 54.35 μH
Rotor Resistance Running	R2R	= 0.00806 Ω

Figure 10.2.6 Fundamental Equivalent Circuit Parameters for 100 V Motor

The values used in the analysis of a proposed 133 V motor were taken from motor design sheets and are shown in Figure 10.2.7.

Frequency = 94 Hz		
Stator Resistance	R1	= 0.01451 Ω
Stator Leakage Reactance	X1	= 0.0439 Ω
Stator Leakage Inductance	L1	= 74.35 μH
Magnetizing Reactance	XM	= 2.187 Ω
Magnetizing Inductance	LM	= 3703. μH
Rotor Leakage Running Reactance	X2R	= 0.05122 Ω
Rotor Leakage Running Inductance	L2R	= 86.72 μH
Rotor Resistance Running	R2R	= 0.011097 Ω

Figure 10.2.7 Fundamental Equivalent Circuit Parameters for 133 V Motor

The individual harmonic voltages (V_H) are separately applied to a frequency-dependent equivalent circuit shown in Figure 10.2.8.

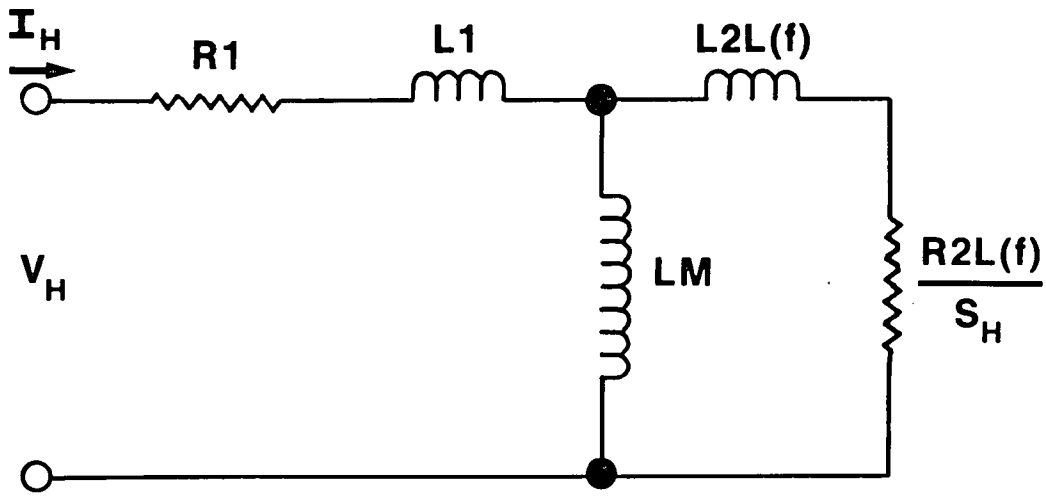

Figure 10.2.8 Harmonic Equivalent Circuit

As is the practice in this type of analysis, the assumption is made that the parameters of the model are independent of frequency except for the rotor impedance.[8] Thus, the values used for Rl, Ll, and LM at the harmonics are the same as the fundamental frequency model. The slip at the harmonic used for the model is given by

$$S_H = \frac{M - 1. + S_F}{M}$$

for positive rotating waves, and

$$S_H = \frac{M - 1. - S_F}{M}$$

for negative rotating waves where M is the harmonic number and S_F is the slip at the fundamental. Note that this equation for the slip does include load effects.

The frequency-dependent rotor quantities, R2L(f) and L2L(f), are modeled by piecewise linear approximations to empirical data. Measurements to determine the rotor impedance dependence on frequency were made on the 100 V motor at ERC with a Hewlett-Packard Fourier analyzer. The data retained after data reduction is shown in Figures 10.2.9 and 10.2.10. The quantities shown are referred to the stator. As shown in Figures 10.2.9 and

10.2.10, the data has a large error band, but a definite trend is apparent. The scattering of the data may be due to stray capacitance in the measurement setup, as phase information is very critical in these measurements. From this data the curves in Figures 10.2.11 and 10.2.12 were derived. Curve #1, in both Figures 10.2.11 and 10.2.12, was drawn so that it was bounded by the greatest number of experimental points. Curve #2, in both Figures 10.2.11 and 10.2.12, was drawn through the upper bounds of the experimental points. Curve #3, in both Figures 10.2.11 and 10.2.12, was drawn through the lower bounds of the experimental points. Then, a best-case/worst-case analysis was run. As expected, there was a large difference in the harmonic losses predicted by the model during the above analysis. Experimental results indicated that Curve #3 in Figure 10.2.11 should be used since comparison of the trial analysis with experimental results showed that the rotor resistance did not rise as fast as shown in Curves #1 and #2. Curve #1 in Figure 10.2.12 was chosen to approximate the rotor leakage inductance frequency dependence because this curve was bounded by the most number of experimental points. Both of the chosen curves were then biased through the 100 V motor design locked rotor impedance values at 94 Hz. The locked design values were used since a locked rotor sees full frequency and thus the design data gives a known impedance at the specified frequency. The values used were R2 = 0.0141 Ω at 94 Hz and L2 = 44.2 μH at 94 Hz. The resultant curves are shown in Figures 10.2.13 and 10.2.14.

In a study of the 100V motor initial runs were made with these curves. When compared with experimental results, analysis of the motor current waveshapes showed that the motor harmonic currents predicted were slightly larger than the actual currents measured. It was then postulated that the rotor inductance curve selected dropped off too fast with frequency. To demonstrate this, runs were made with a constant rotor leakage inductance at all harmonic frequencies of 54.35 μH, the running value. These runs clearly constituted a best-case analysis, since the rotor reactance was too high at high frequencies, resulting in reduced harmonic currents. Therefore, a compromise curve was postulated where the rotor inductance did not drop as quickly at high frequencies. This curve for the 100 V motor, which passes through the point described by the running rotor inductance of 0 Hz, 54.35 μH is shown in Figure 10.2.15. Further correlation with experimental data showed that the resistance did not rise as fast as had been postulated. Investigation showed that the curve in Figure 10.2.16 gives results that match the experimentally measured peformance of the 100 V motor. This is demonstrated in section 10.3.

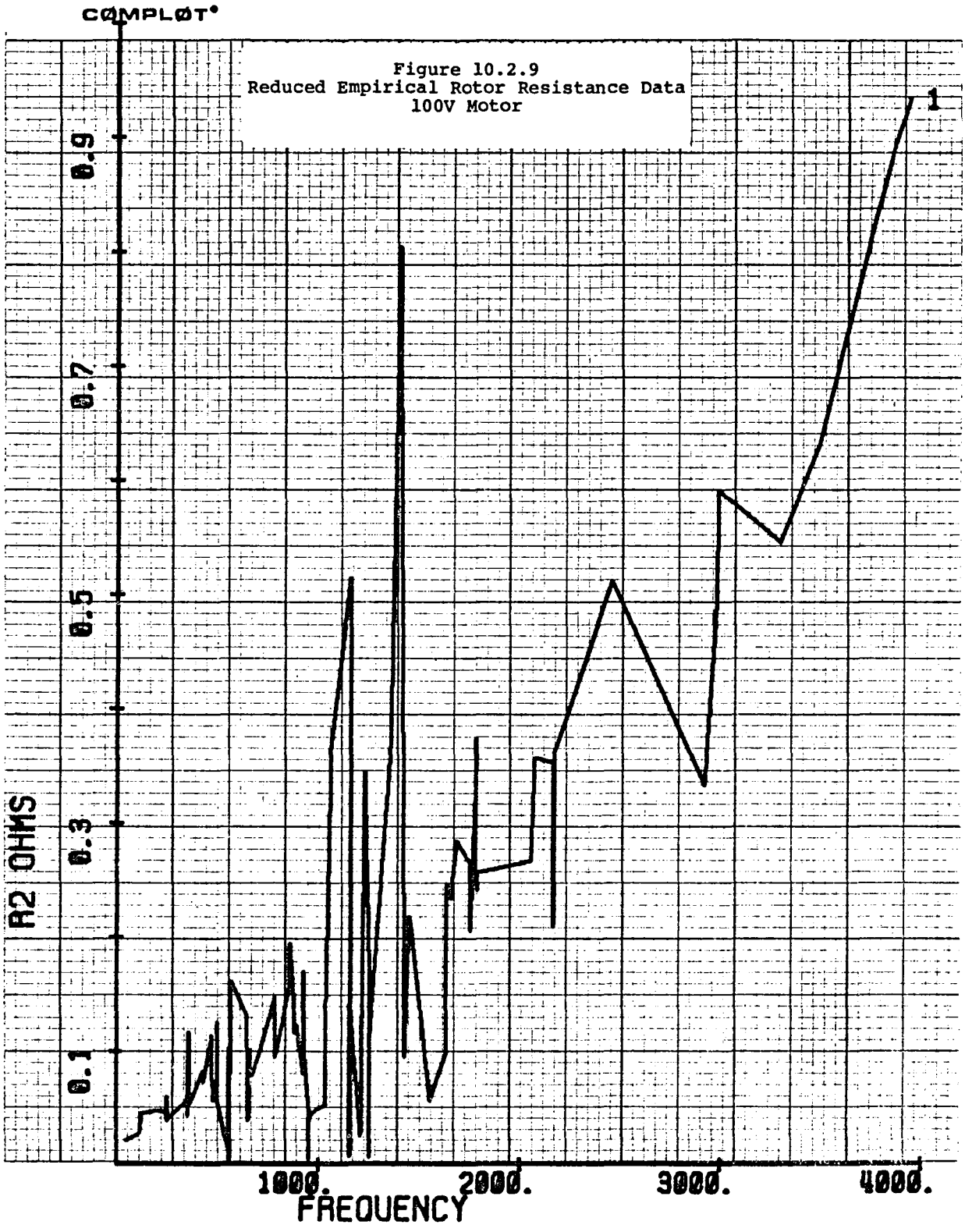
COMPLØT*
Figure 10.2.9
Reduced Empirical Rotor Resistance Data
100V Motor
R2 OHMS
0.9
0.7
0.5
0.3
0.1
1000.
2000.
3000.
4000.
FREQUENCY
1

Figure 10.2.10
Reduced Empirical Rotor Inductance Data
100V Motor

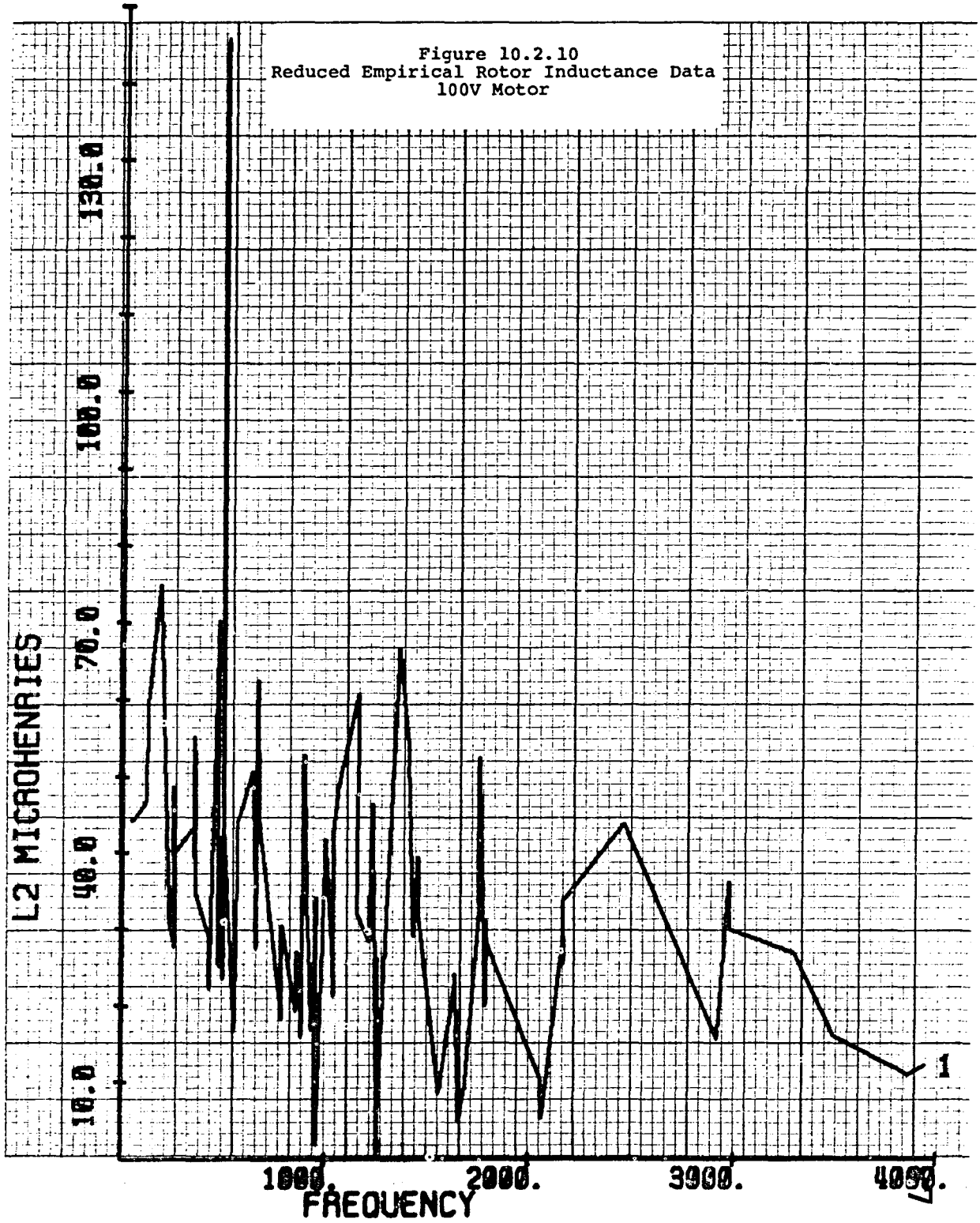

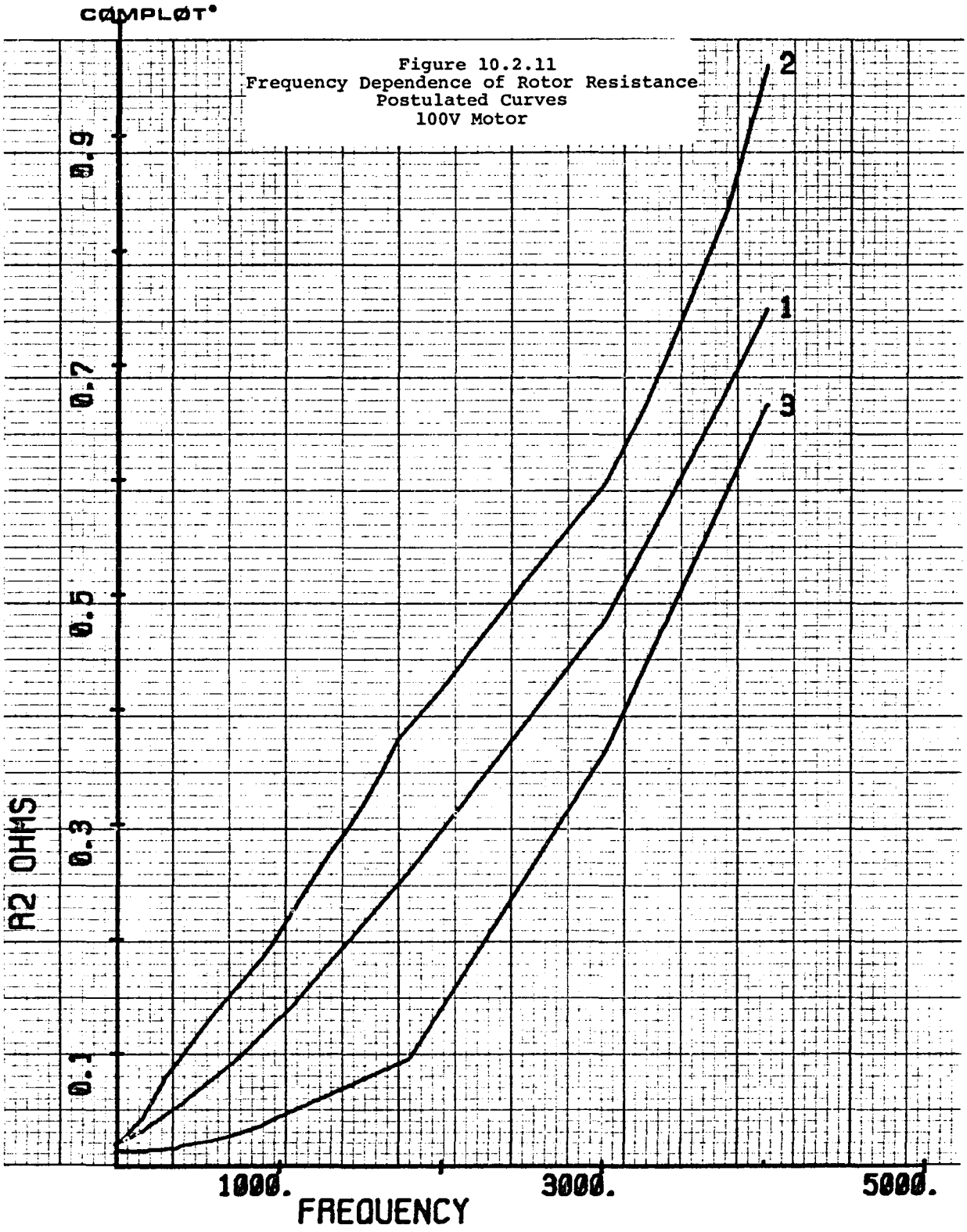
COMPLOT
Figure 10.2.11
Frequency Dependence of Rotor Resistance
Postulated Curves
100V Motor
2
1
3
0.9
0.7
0.5
0.3
0.1
R2 OHMS
1000.
3000.
5000.
FREQUENCY

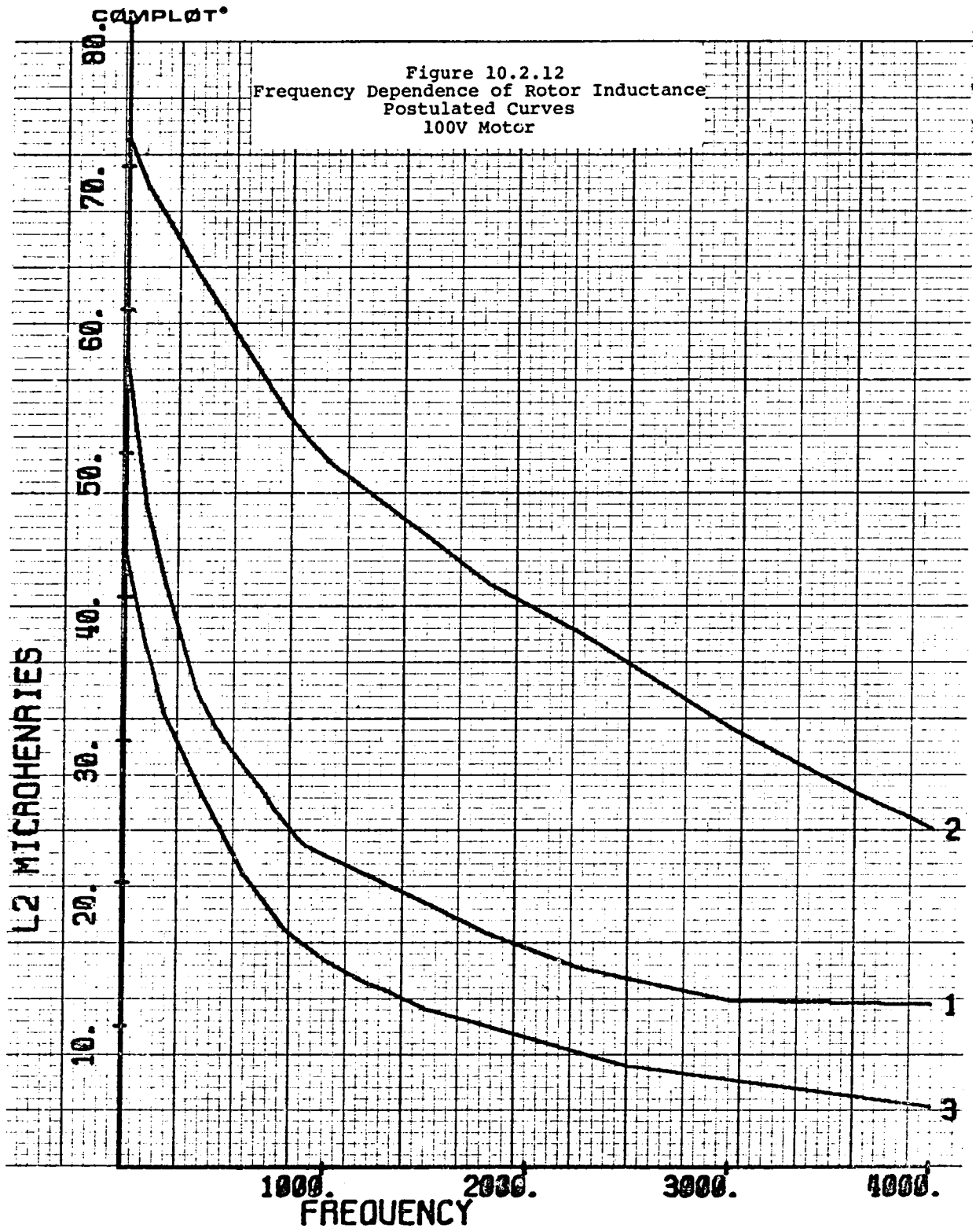
COMPLOT®
Figure 10.2.12
Frequency Dependence of Rotor Inductance
Postulated Curves
100V Motor
L2 MICROHENRIES
80.
70.
60.
50.
40.
30.
20.
10.
1000.
2000.
3000.
4000.
FREQUENCY
1
2
3

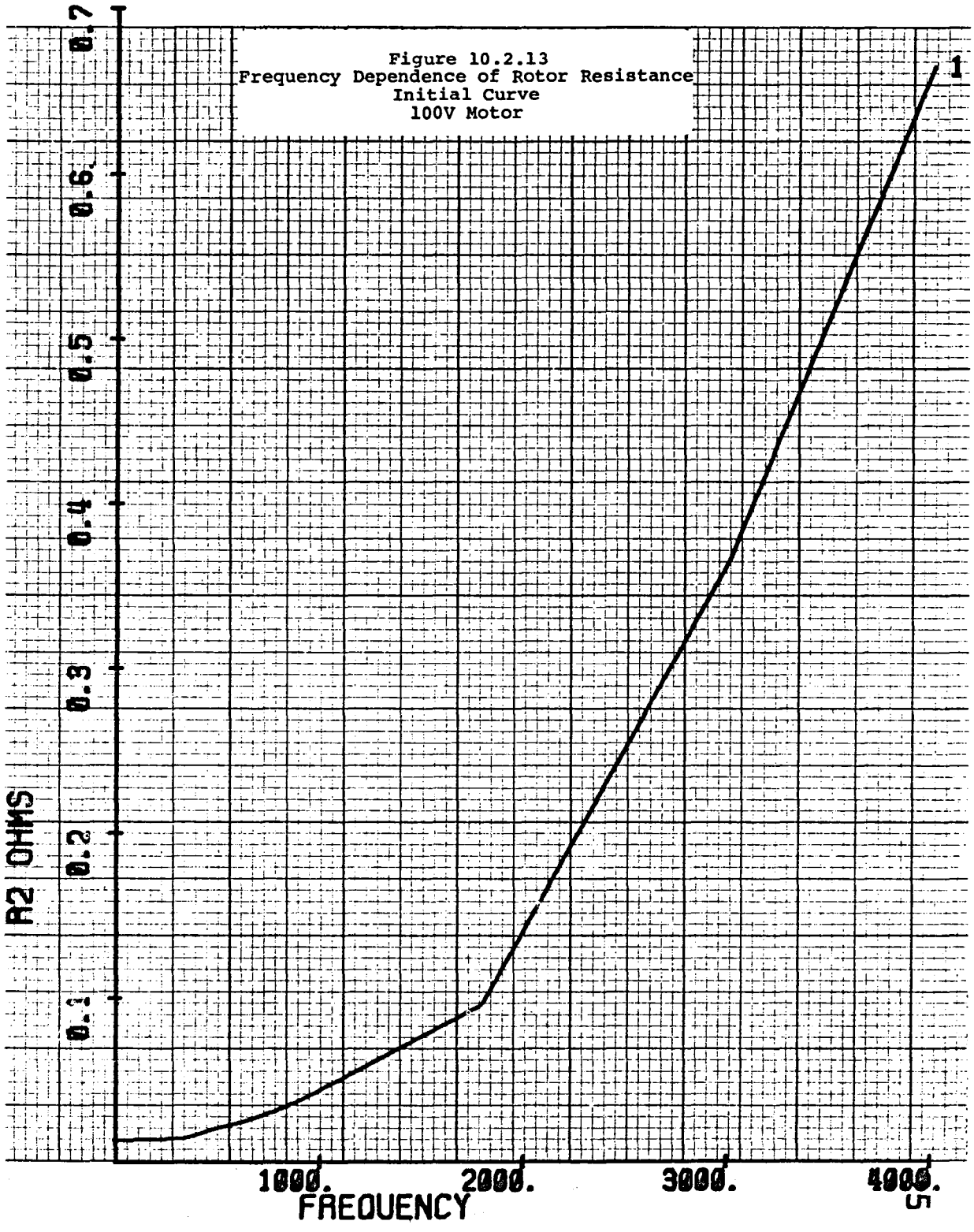
Figure 10.2.13
Frequency Dependence of Rotor Resistance
Initial Curve
100V Motor
R2 OHMS
0.7
0.6
0.5
0.4
0.3
0.2
0.1
1000.
2000.
3000.
4000.
FREQUENCY
1
5

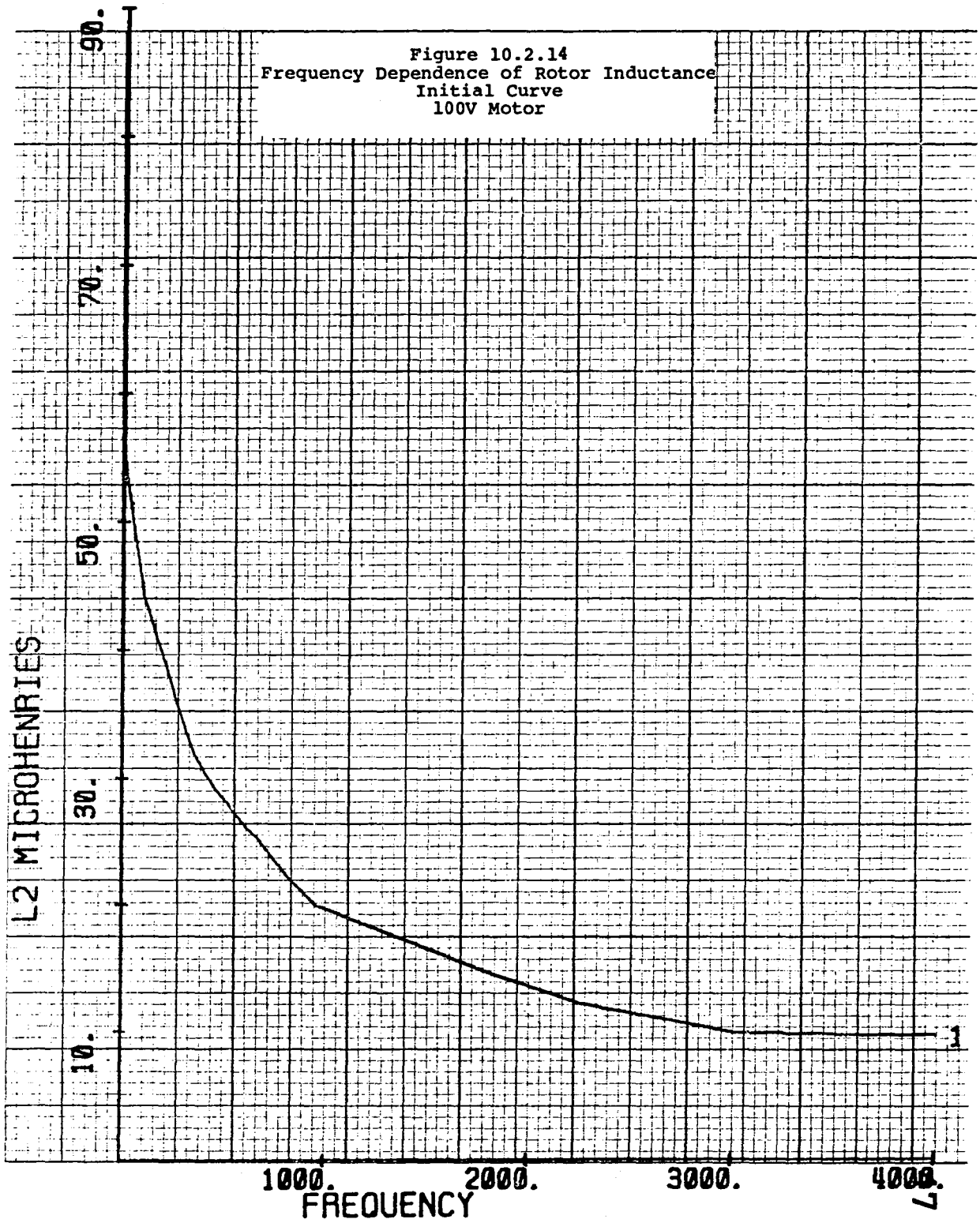

Figure 10.2.14
Frequency Dependence of Rotor Inductance
Initial Curve
100V Motor

The curves used in analysis of the 133 V motor were developed in a similar fashion. The analysis began by taking the shape of the curves used for the 100 V motor shown in Figures 10.2.13 and 10.2.14 and biasing them through the locked rotor values predicted by the proposed 133 V motor design. (That is, R2 = 0.01555Ω and L2 = 77.72 μH at 94 Hz.) This resulted in the curves shown in Figures 10.2.17 and 10.2.18. These curves were found to be too steep at the high frequencies also. A reasonable assumption is to postulate that the frequency dependence of the 133V motor has the same functional dependence ratioed by the increase in the stator turns ratio.

$$R2_{133\ V}(f) = \frac{\text{Motor Design } R2_{133\ V}}{\text{Motor Design } R2_{100\ V}} \times R2_{100\ V}(f)$$

$$L2_{133\ V}(f) = \frac{\text{Motor Design } L2_{133\ V}}{\text{Motor Design } L2_{100\ V}} \times L2_{100\ V}(f)$$

where $R2_{133\ V}$ and $L2_{133\ V}$ comprise the rotor impedance for the 133 V motor, $R2_{100\ V}$ and $L2_{100\ V}$ comprise the rotor impedance of the 100 V motor, and $R2_{100\ V}(f)$ is the final piecewise linear approximation to rotor resistance as a function of frequency of the 100 V motor described above (shown in Figures 10.2.15 and 10.2.16). The resultant curves shown in Figures 10.2.19 and 10.2.20 were the curves used in the analysis of the 133 V motor performance. The ratio of design parameters $R2_{133\ V}$ to $R2_{100\ V}$ gives the increase in the turns ratio of the 133 V motor over the 100 V motor, through which the rotor is reflected to the stator.

An accurate method of modeling stray losses at the harmonics was not obtained. Instead, the windage, friction, eddy current, and iron losses were modeled as a constant 400 w at all speeds and torques. The value chosen was a typical number taken from motor tests performed at the manufacturing division. This estimate is proper at the higher torque levels but the loss is too high at the lower torque levels. Thus the efficiencies predicted at the lower torque levels are lower than the empirical data shows. Efficiency calculations are accurate over most of the range of motor operation. There is need for further development of an accurate model for stray loss prediction.

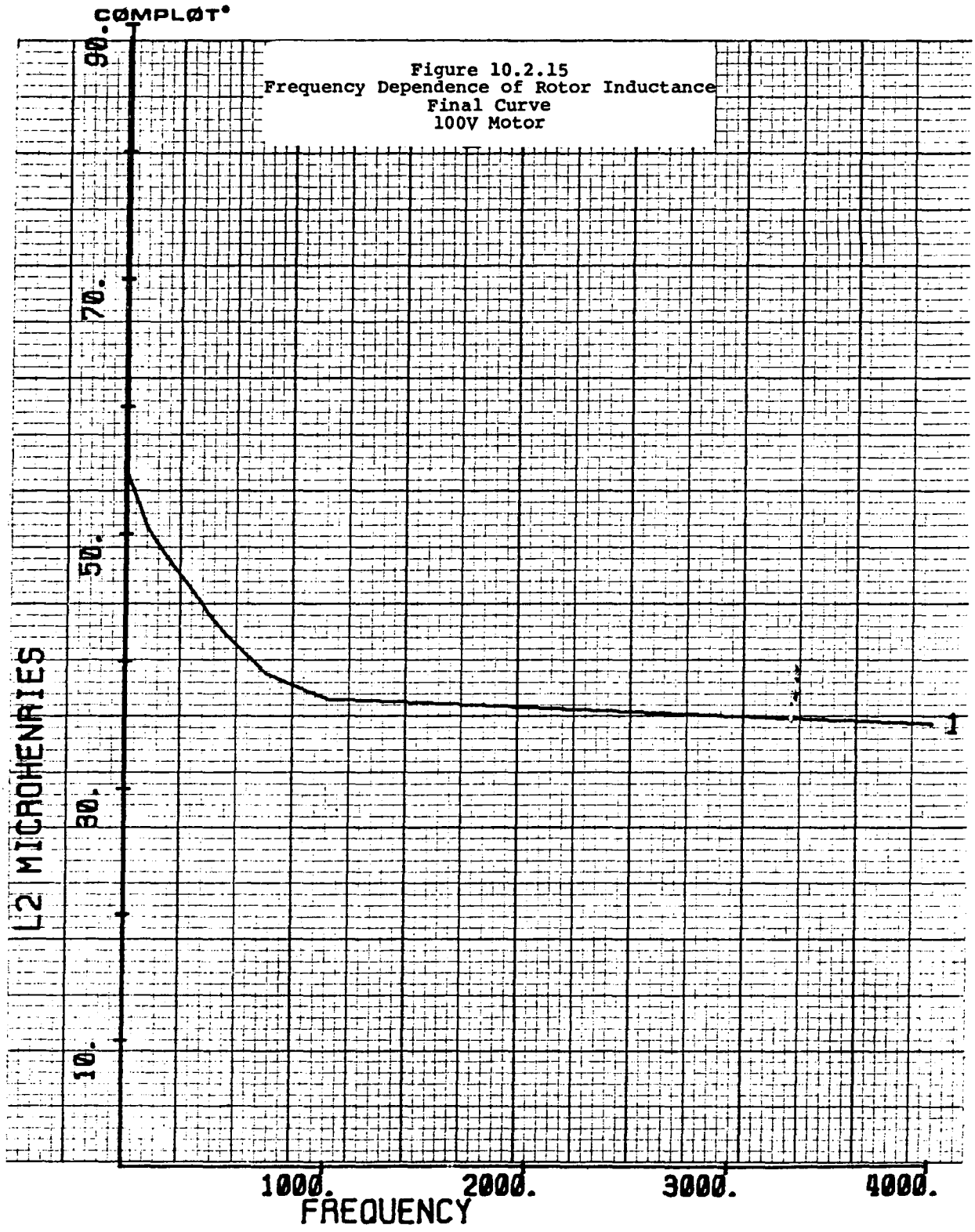

Figure 10.2.15
Frequency Dependence of Rotor Inductance
Final Curve
100V Motor

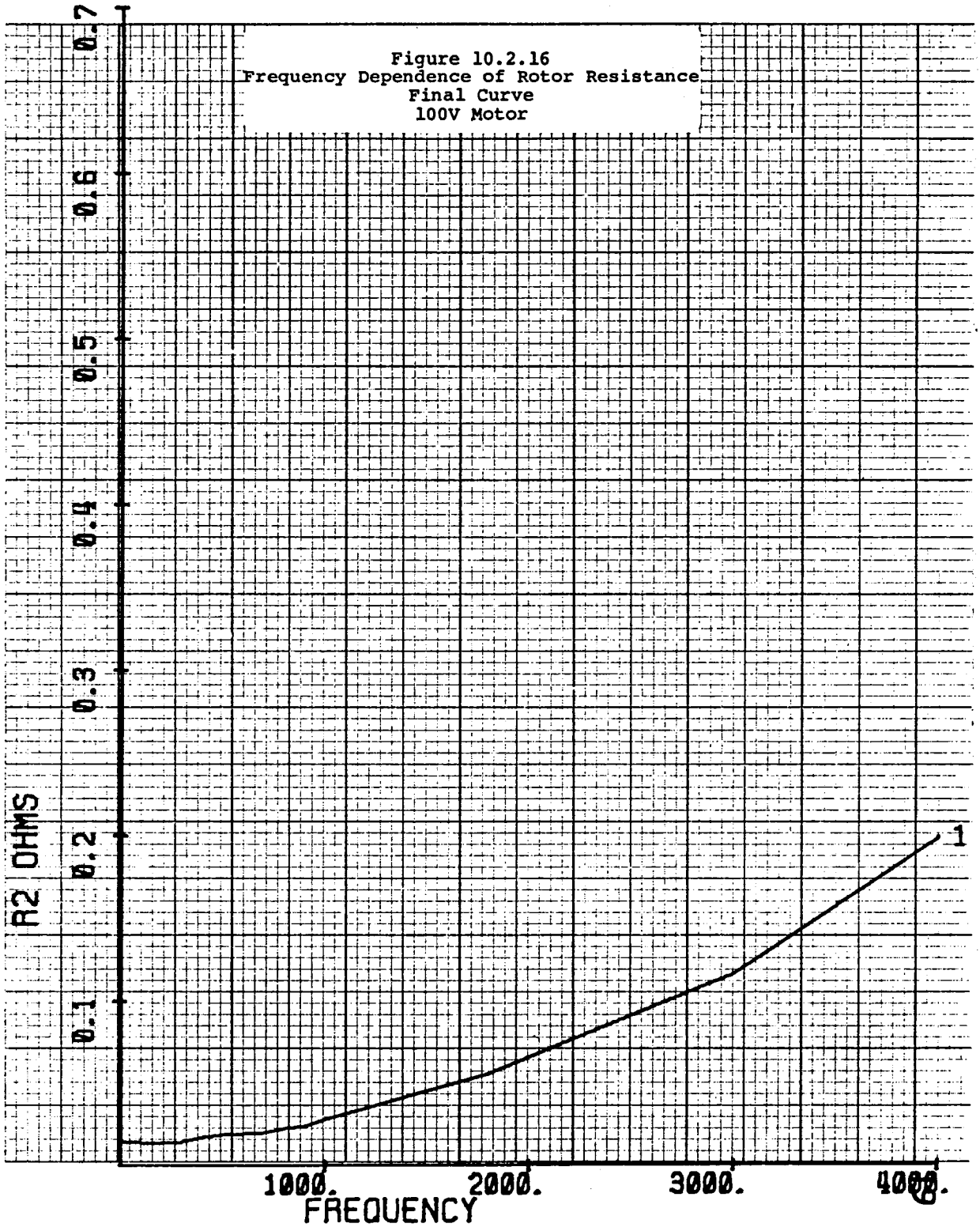
Figure 10.2.16
Frequency Dependence of Rotor Resistance
Final Curve
100V Motor
R2 OHMS
0.7
0.6
0.5
0.4
0.3
0.2
0.1
1000.
2000.
3000.
4000.
FREQUENCY
1

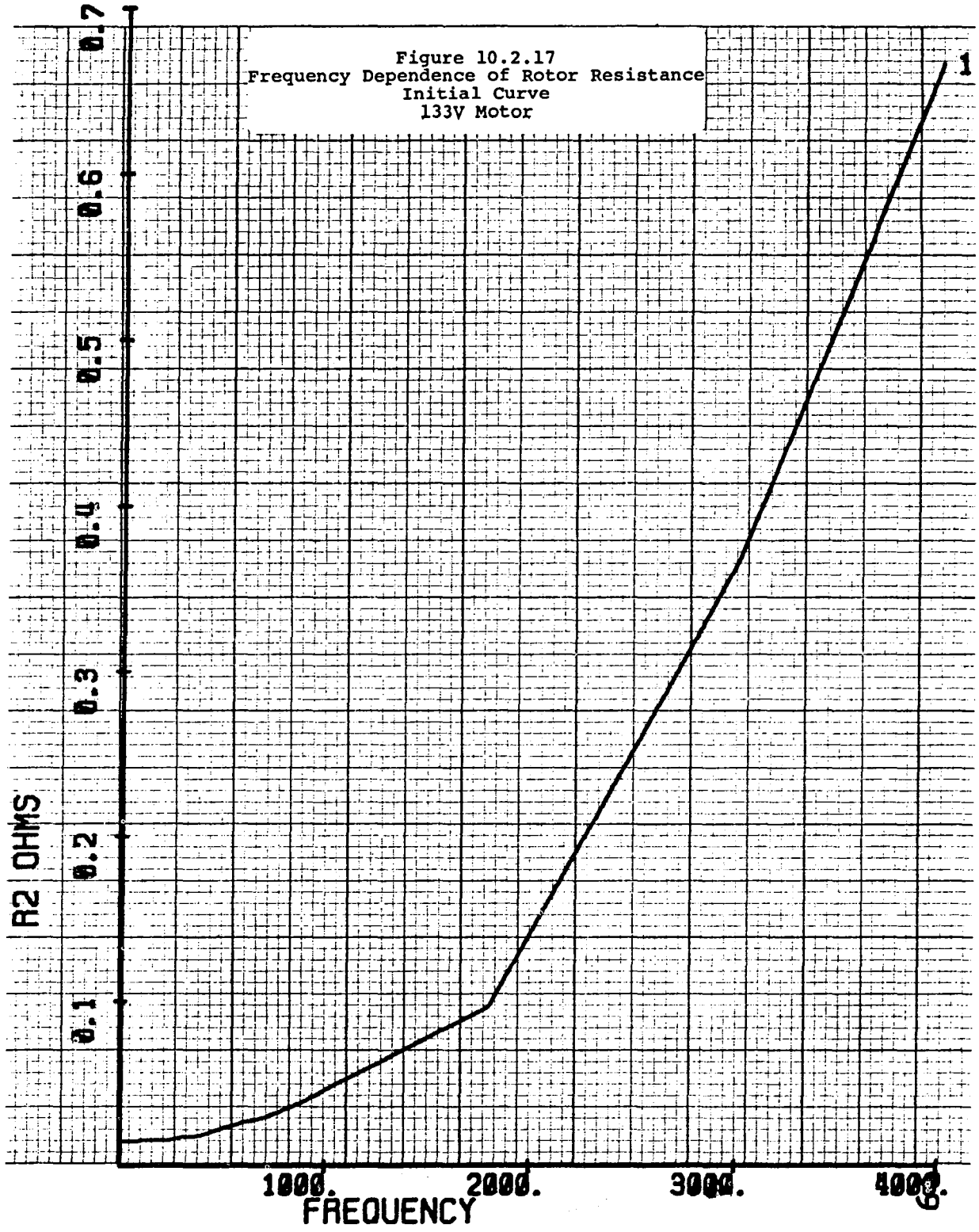
Figure 10.2.17
Frequency Dependence of Rotor Resistance
Initial Curve
133V Motor
0.7
0.6
0.5
0.4
0.3
0.2
0.1
R2 OHMS
1000.
2000.
FREQUENCY
1

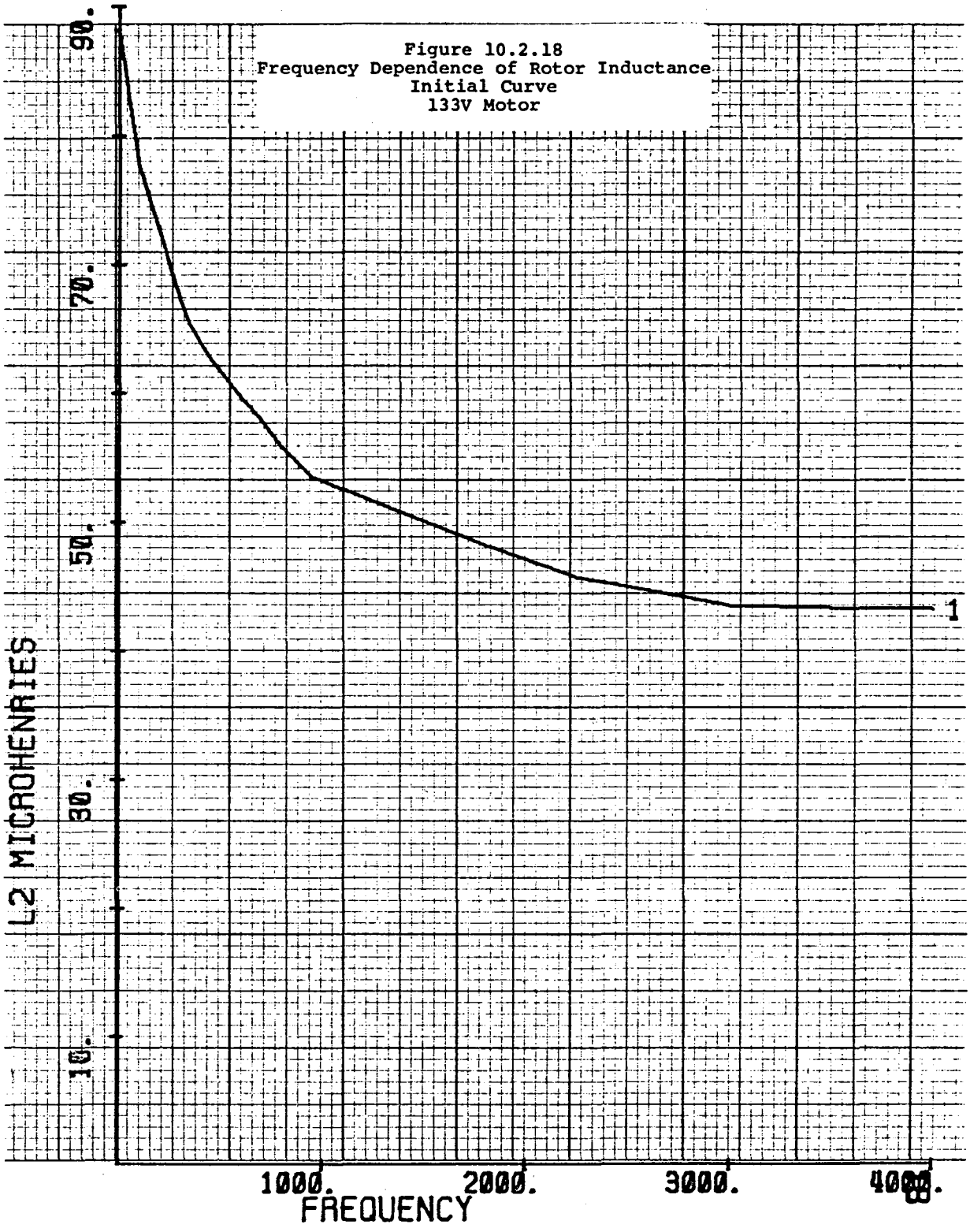

Figure 10.2.18
Frequency Dependence of Rotor Inductance
Initial Curve
133V Motor

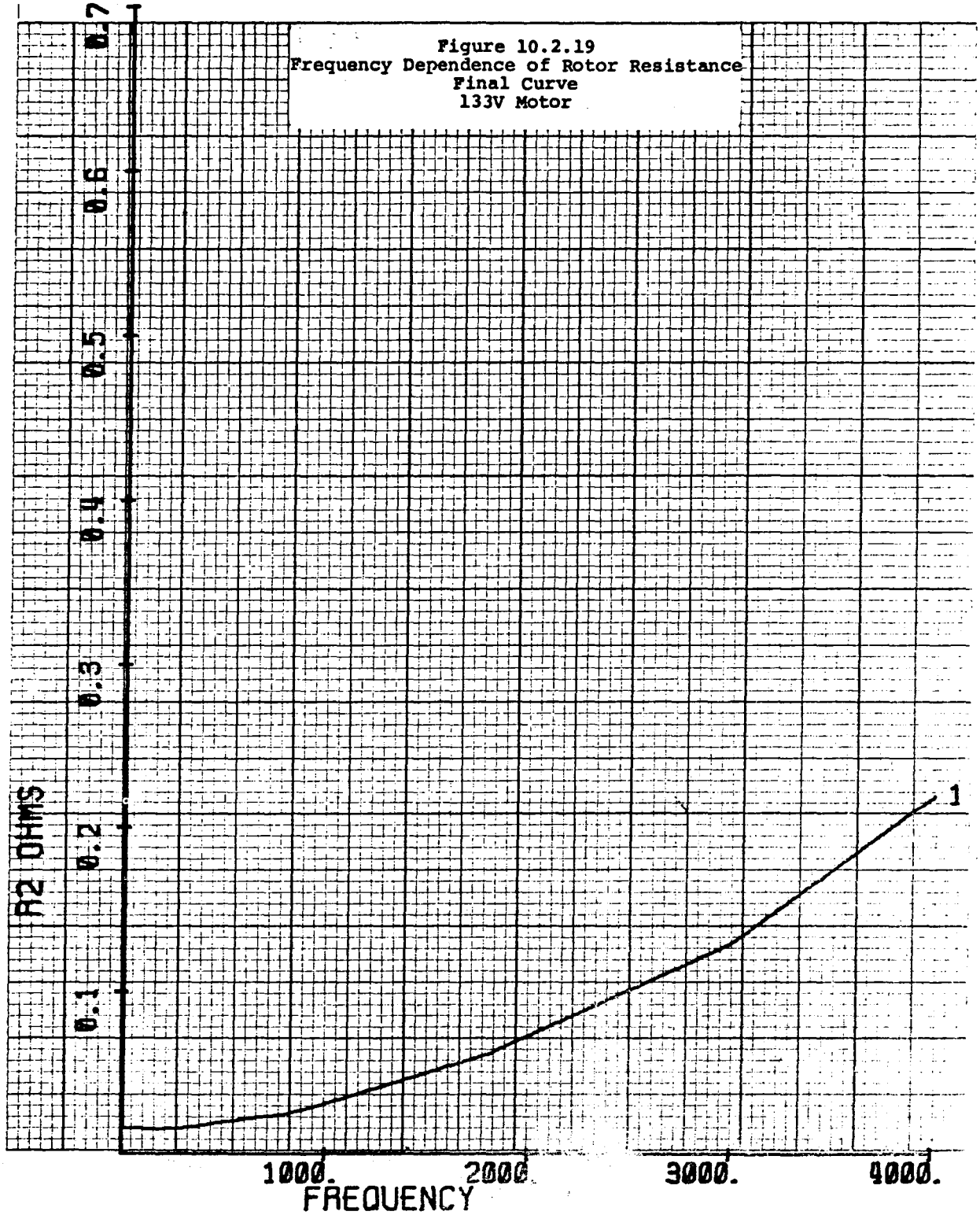
Figure 10.2.19
Frequency Dependence of Rotor Resistance
Final Curve
133V Motor
R2 OHMS
0.7
0.6
0.5
0.4
0.3
0.2
0.1
1000.
2000.
3000.
4000.
FREQUENCY
1

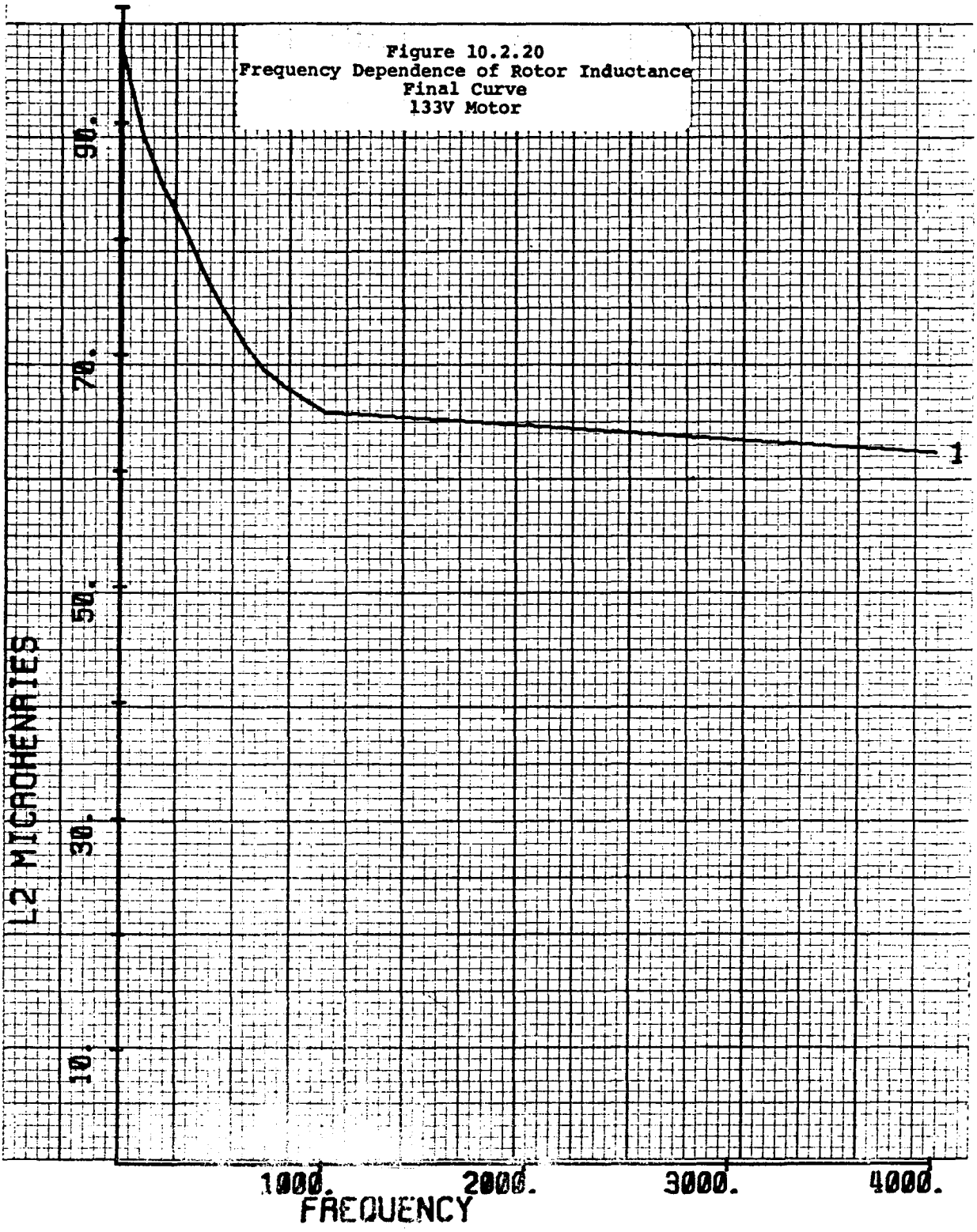
Figure 10.2.20
Frequency Dependence of Rotor Inductance
Final Curve
133V Motor
L2 MICROHENRIES
90.
70.
50.
30.
10.
1
1000.
2000.
3000.
4000.
FREQUENCY

Analysis Input

The analysis uses two forms of input. The motor-forcing function is entered through program interaction with the user. The motor equivalent circuit description is file driven, allowing for easy entry of motor design changes. That is, by simply changing storage files on the computer, different motors can be modeled. The program interacts with the user to enter the PWM waveform in terms familiar to an electronic engineer. The analysis assumes that the PWM waveshape is described by an odd function. An odd function is a periodic function, f(t) with period τ, for which $f(t) = -f(-t)$. The waveform description required is that of the phase to -VBUS PWM wave. The simulation allows the user to enter the phase to -VBUS PWM waveshapes with notches anywhere in the 0° to 180° range (the 180° to 360° wave is then specified automatically since the wave is an odd function). The transitions at switching time are assumed to be instantaneous. Analysis is performed for any number of notches. Notch placement description is simplified if the wave has half-wave symmetry. A periodic function, f(t) with period τ, which has half-wave symmetry has the property that $f(t) = -f(t + \frac{1}{2}\tau)$. The user also enters the PWM wave fundamental frequency, battery voltage, and motor slip. The number of harmonics to be analyzed is user selectable up to 200 harmonics.

The parameters for harmonic motor equivalent circuit description are stored in three computer storage files and are used automatically by the program. One file contains the frequency dependent rotor resistance data. A second file contains the frequency dependent rotor leakage inductance data. A third file contains the motor primary resistance, primary leakage inductance, mutual inductance, fundamental frequency rotor impedance, a fixed loss constant, series choke impedance, and motor equivalent circuit base quantities. These files can be changed to model different motors, allowing design changes to be analyzed easily.

Analysis Output

Output for the harmonic motor analysis is available in two forms. A tabular summary is automatically generated and printed when the analysis is run. Also, computer storage files are automatically created by the analysis with tabulated voltage and current magnitude vs. phase angle. These storage files can be easily post-processed into graphical form.

The tabular summary reports the user input and pertinent analysis output in a complete readable format. The output is titled by a 72-character heading entered by the

user at run time. Program input, including battery voltage, fundamental frequency, series choke value, and a complete PWM wave description, are summarized in a header block on the printed output. User entered titles from the motor description files are also printed in the header block, allowing easy identification of the particular motor design analyzed. The main body of the printed output reports the following quantities both in per-unit values (familiar to power engineers) and engineering units (watts, volts, amps, etc.) at every significant harmonic frequency: harmonic number, frequency, slip, complex (real and imaginary) voltage, primary impedance, mutual impedance, secondary impedance, terminal impedance, complex primary current, complex mutual current, complex secondary current, complex secondary voltage, mechanical power output, complex power transferred across the air gap, complex power input, power loss in the primary, power loss in the secondary, volts/hertz, and efficiency. These tables are used to analyze how notch scheme variations change the power spent at each harmonic frequency. Because some of the harmonics have negative rotation the torque contributions at these harmonics are actually destructive to the net torque output. This is clearly reported in the tabular output. Another use of this output was in devising notch schemes which pushed the harmonic power out to higher frequencies. The output indicated the power levels, and thus losses were lower at the higher frequencies, due to the increased rotor impedance.

Summaries of net motor performance at the end of the printed output report the following quantities in both per-unit values and engineering units: complex electrical power drawn, power factor, motor slip, mechanical speed, mechanical output torque, complex current drawn, current magnitude, power loss in the primary, power loss in the secondary, total copper power loss, fixed losses, total power loss, motor terminal volts per hertz, mechanical power output, motor efficiency, and peak motor current. These summaries report the net motor performance for the notch scheme entered by the user. The summaries allow the engineer to be sure that the operating point (V/Hz, torque output, speed) analyzed is what was intended. The summaries give a clear, concise report as to what the motor performance (efficiency, net torque, current losses) is for the notch scheme described.

The analysis also produces several tabular files which can easily be post-processed by a plotting routine into computer generated plots of instantaneous voltage and current waveforms. A plot of the user input phase to -VBUS voltage forcing function is available. A PWM wave with three notches in the center 60° is shown in Figure

10.2.21 as a typical output. This plot is reconstructed directly from the user input and gives the user a graphical verification of the applied waveform. A plot of the phase to neutral voltage waveform is also available. The phase to neutral wave for the typical run cited above is plotted in Figure 10.2.22. This plot is reconstructed from the voltage harmonics generated by the Fourier analysis and three-phase analysis of the user input wave. This plot allows verification of the voltage applied to the motor equivalent circuit by comparison with pen recordings made on the actual system hardware. A useful tool produced by the analysis is the plot of instantaneous motor current during the cycle. The resultant current from the typical run is plotted in Figure 10.2.23. This plotting capability has aided in verification of the motor model. The plot of instantaneous motor current has also proved to be a valuable design tool by predicting peak motor currents and current waveshapes for any PWM voltage scheme applied to the motor terminals. These current predictions were then used to size inverter components.

Conclusion

The harmonic motor model for motor steady-state performance analysis with PWM forcing functions was developed and refined through correlation with experimental data. Copper losses are accurately predicted at all frequencies. This model's modular construction allows easy comparison of different motor designs and accurate harmonic analysis of all odd function PWM control schemes. The harmonic model accurately predicts voltage and current waveshapes. Motor peak and rms current predictions were used to redesign PWM schemes for reduced peak currents. The motor current predictions were also used to size inverter components.

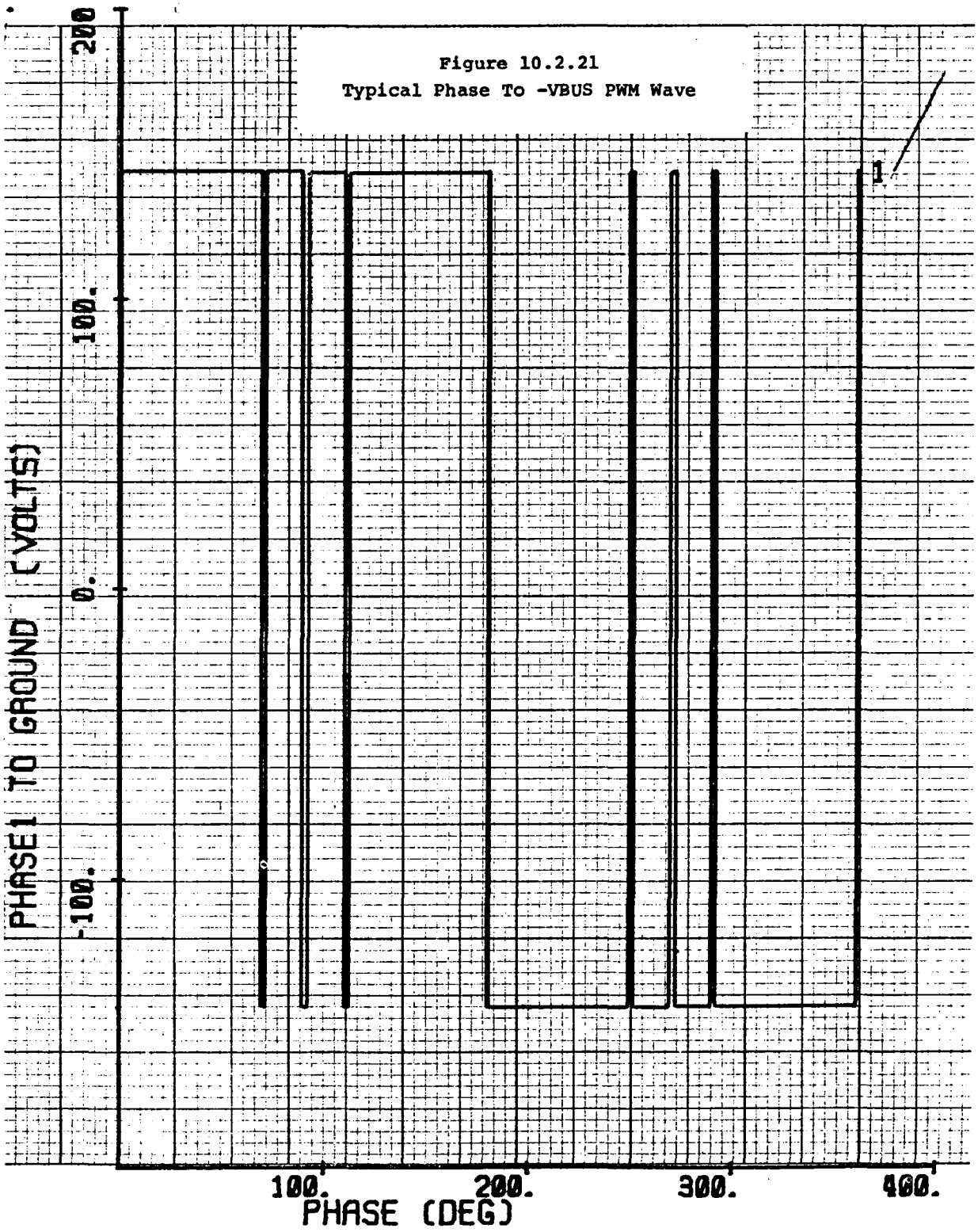

Figure 10.2.21
Typical Phase To -VBUS PWM Wave

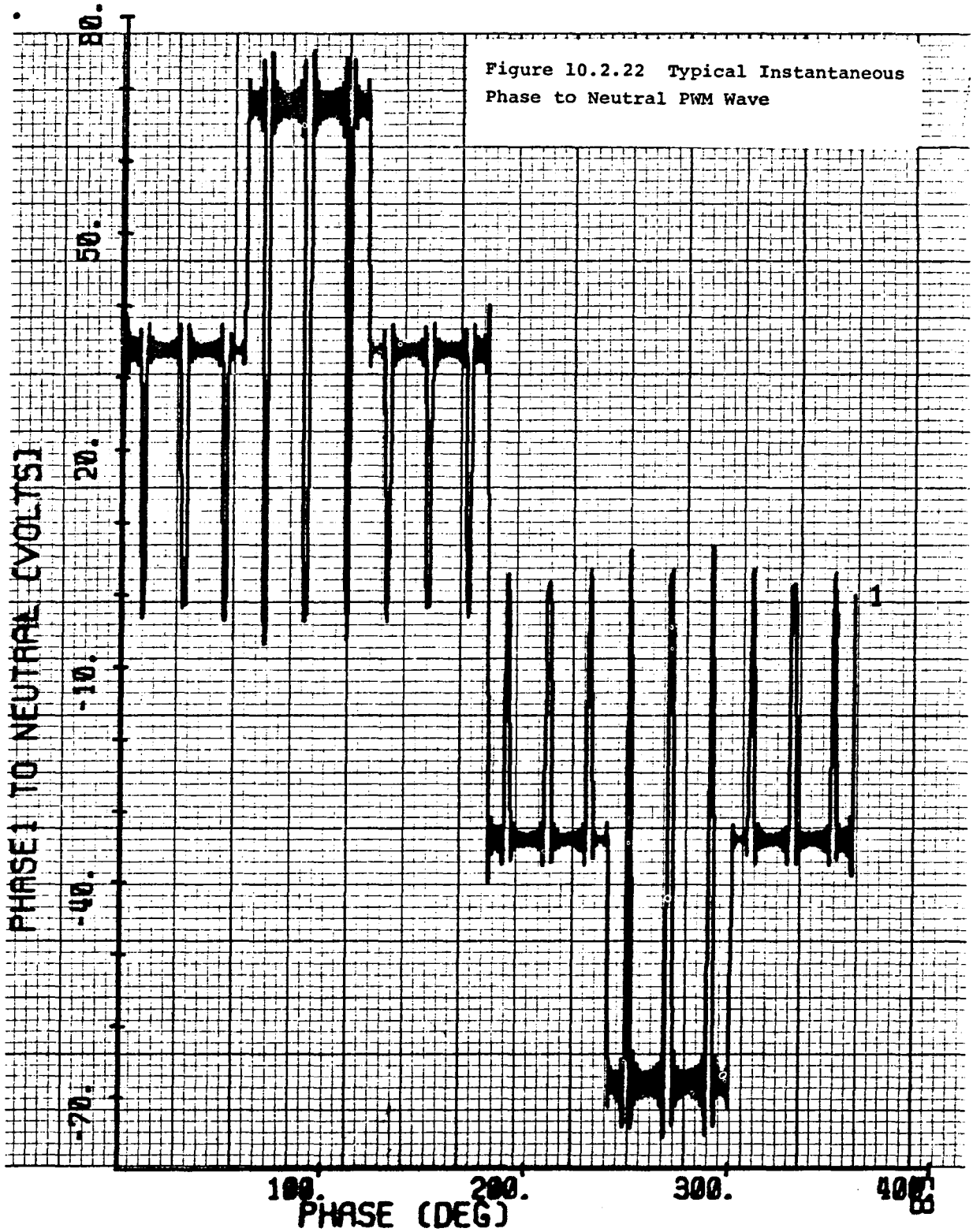

Figure 10.2.22 Typical Instantaneous Phase to Neutral PWM Wave

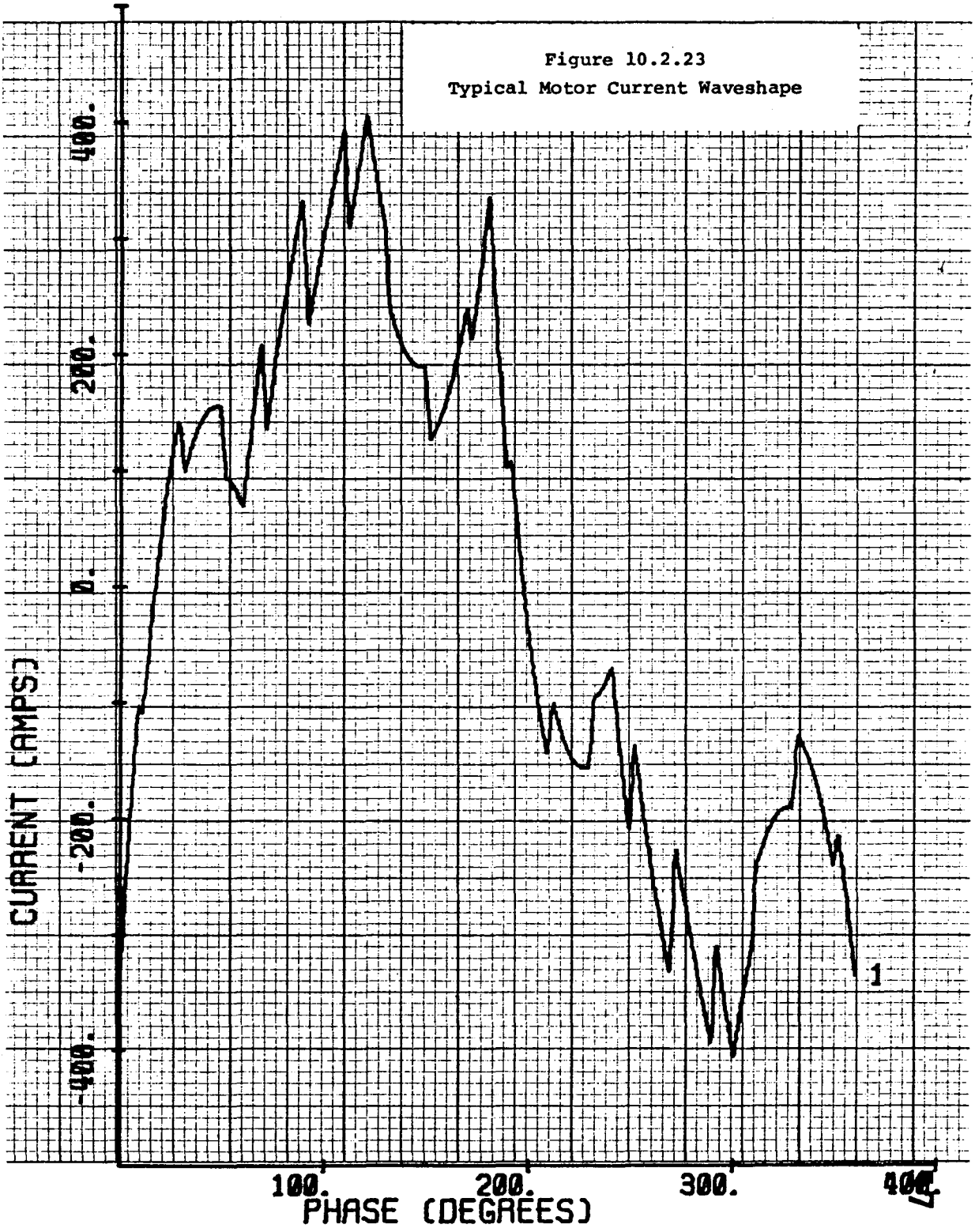

Figure 10.2.23
Typical Motor Current Waveshape

10.3 Motor Harmonic Analysis Performed with Computer Simulation

The steady-state ac motor simulation described in Section 10.2 is being used as a basis for developing notch schemes and for comparing motors having different voltage ratings. The notch scheme study will continue in order to develop an alternate PWM approach that will reduce harmonic losses. A study on the existing center 60° notch scheme has been performed which compares motor harmonic losses as a function of notch number. In addition, a comparison of motor harmonic losses and efficiencies has been done for the existing EV motor (100 V motor) connected to a 144 V bus and a proposed higher voltage motor (133 V motor) connected to a 192 V bus. The above evaluations were based upon the motor I^2R losses due to harmonic currents (harmonic copper losses).

The first step in the harmonic analysis was aimed at validation of the motor model. This validation was intended to verify the capability of the computer simulation to accurately predict motor peak and rms current, motor torque, and motor efficiency. Computer simulations of the existing 100 V motor were run under identical V/Hz, slip, and notching schemes that were run with the physical system on the test stand. An example of the simulation capability to duplicate motor currents is shown in Figure 10.3.1, which compares actual motor current and computer-predicted motor current. The close correlation of peak currents can be seen in this figure. Further verification of the simulation's current prediction capability can be obtained by plotting peak motor currents vs. torque at selected motor speeds. Figure 10.3.2 compares actual and simulated peak motor current vs. torque at 70 Hz stator frequency. Again it is seen that close agreement is obtained.

Figure 10.3.3 is a comparison of actual and predicted motor efficiency vs. torque at 70 Hz. It can be seen that close agreement is obtained at high torque levels, but that the predicted efficiency is lower than measured at low torque levels. Possible sources of the disagreement at low torque levels are errors in empirical data caused by wattmeter readings taken for motor operation at 10% of full scale on the wattmeter. Other sources for the disagreement at low torque levels are the motor model unknowns related to uncertainties in modeling iron loss, eddy current loss, and stray loss vs. torque and frequency. The degree of this uncertainty could cause a discrepancy of the magnitude seen in Figure 10.3.3. It was concluded that the computer predicted efficiencies were accurate enough for making comparative evaluations of motors and notching schemes, since copper losses, which are the major source of the losses, are predicted accurately.

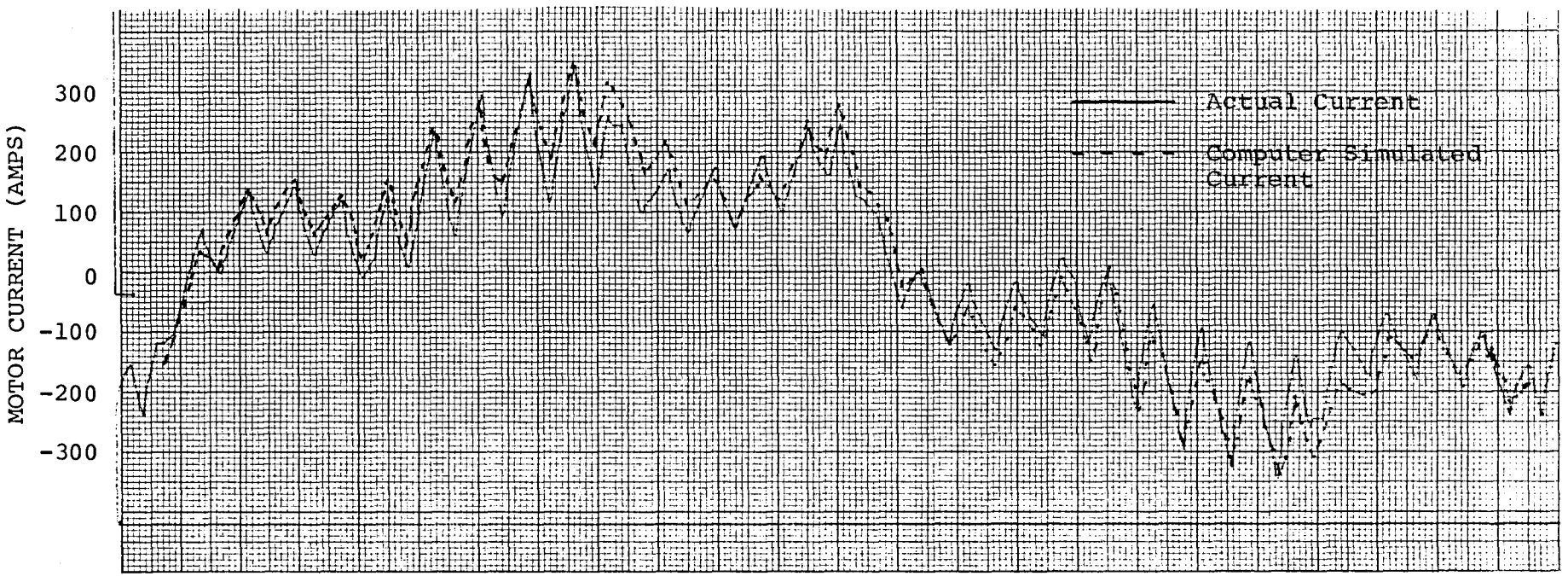

Figure 10.3.1
Comparison of Empirical and Motor Model
Computer Simulated Motor Current Waveshapes

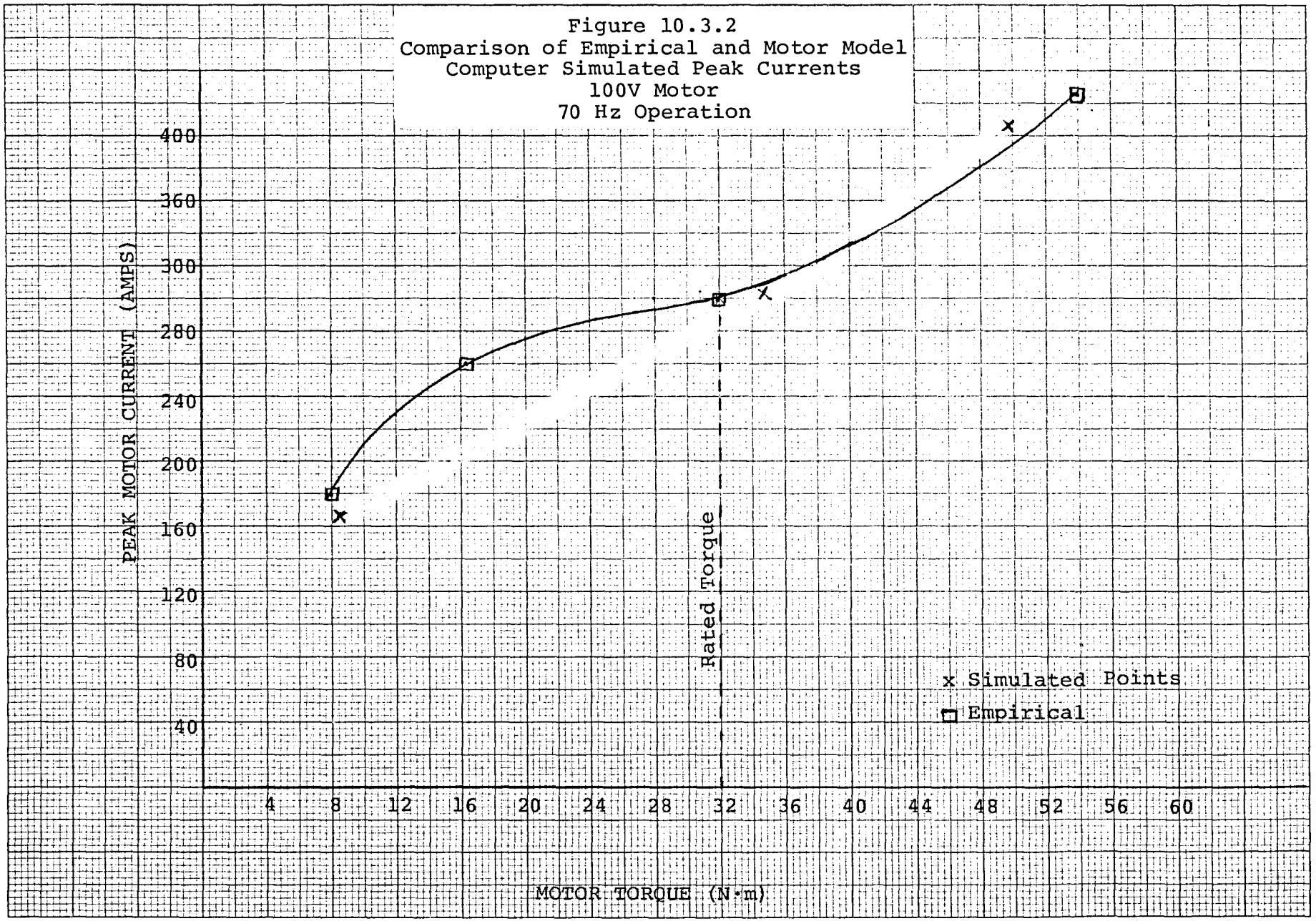
Figure 10.3.2
Comparison of Empirical and Motor Model
Computer Simulated Peak Currents
100V Motor
70 Hz Operation
PEAK MOTOR CURRENT (AMPS)
400
360
300
280
240
200
160
120
80
40
4
8
12
16
20
24
28
32
36
40
44
48
52
56
60
MOTOR TORQUE (N·m)
Rated Torque
x Simulated Points
Empirical

Figure 10.3.3
Comparison of Empirical and Motor Model
Computer Simulated Efficiencies
100V Motor

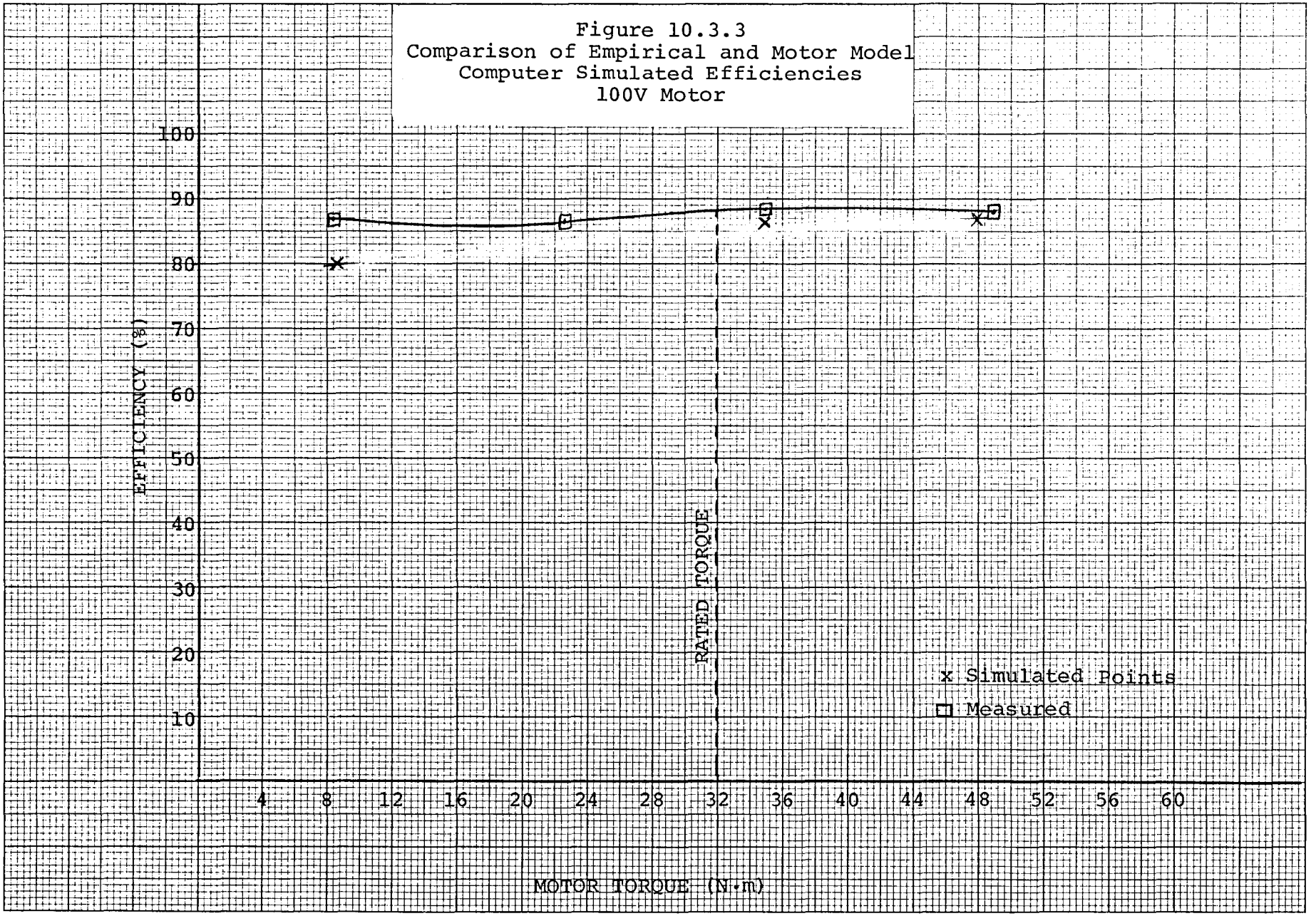

Comparison of Bus Voltages

The motor simulation was used for making comparisons between motors operating on a 144 V and a 192 V bus. Results of these comparisons are being used as a consideration in selecting the battery voltage for future systems. Figure 10.3.4 is a comparison between the 100 V motor operating on a 144 V bus and a proposed 133 V motor operating on a 192 V bus. This comparison was based upon the efficiency and harmonic copper losses in the two motors as a function of notch number for a center 60° notch scheme. A description of this notch scheme is given in section 7. It can be seen that the 133 V motor has a higher efficiency and lower harmonic loss for any notch number used over the full torque speed range.

Motor Current Prediction

With use of a 133 V motor, operating on a 192 V bus, it is necessary to predict the peak and rms motor currents for this configuration in order to size the inverter components. Figure 10.3.5 shows the predicted motor currents vs. torque for the 133 V motor. Comparison with Figure 10.3.2 shows that the motor peak currents can be reduced by about 150 amps by using the higher voltage system.

Summary

The motor steady-state, ac simulation has been a useful tool for comparing motors and optimizing notch numbers. Continued use of this simulation is expected in the Phase 2 program in order to improve notch schemes and to optimize system operating conditions.

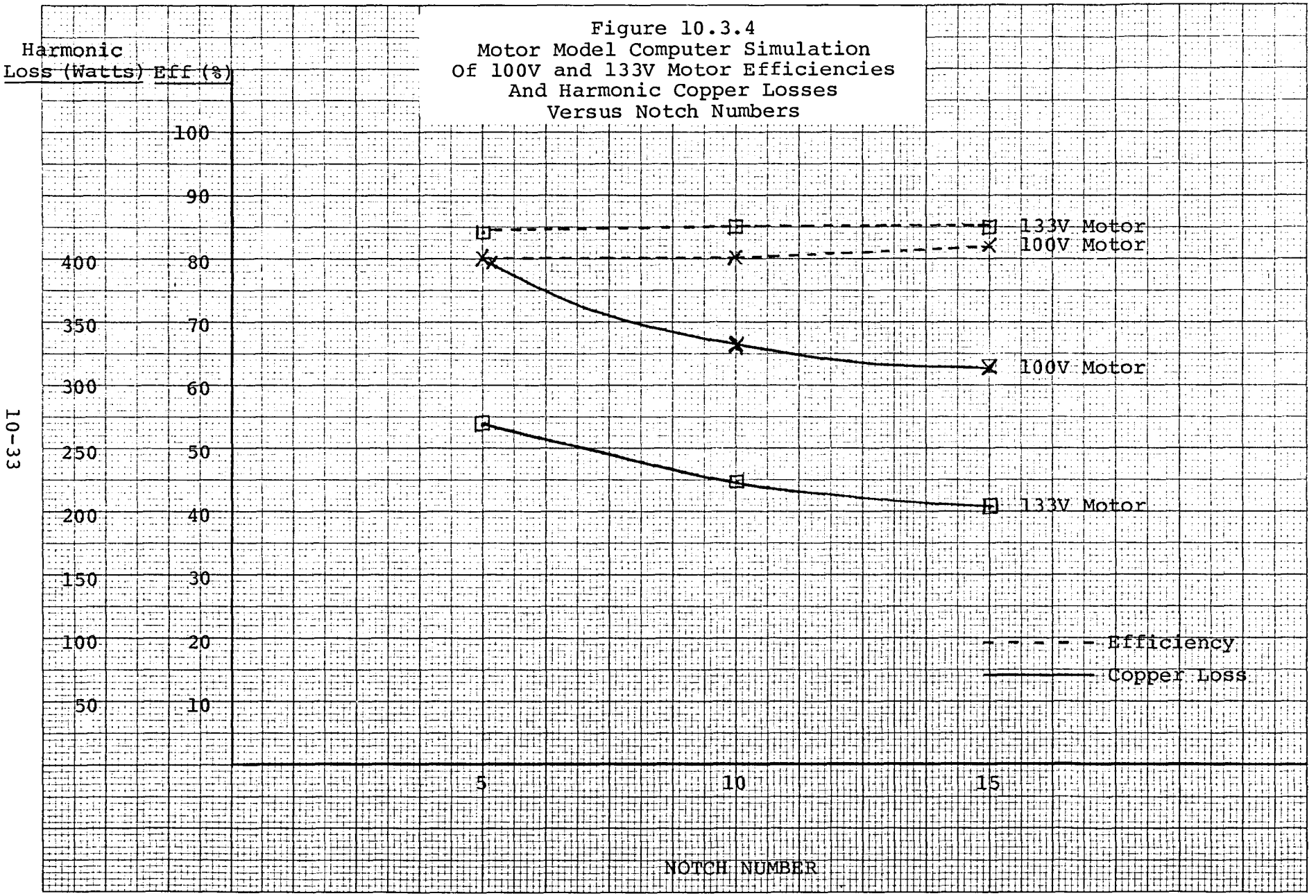
Figure 10.3.4
Motor Model Computer Simulation
Of 100V and 133V Motor Efficiencies
And Harmonic Copper Losses
Versus Notch Numbers
Harmonic
Loss (Watts)
Eff (%)
400
350
300
250
200
150
100
50
100
90
80
70
60
50
40
30
20
10
5
10
15
NOTCH NUMBER
133V Motor
100V Motor
100V Motor
133V Motor
Efficiency
Copper Loss

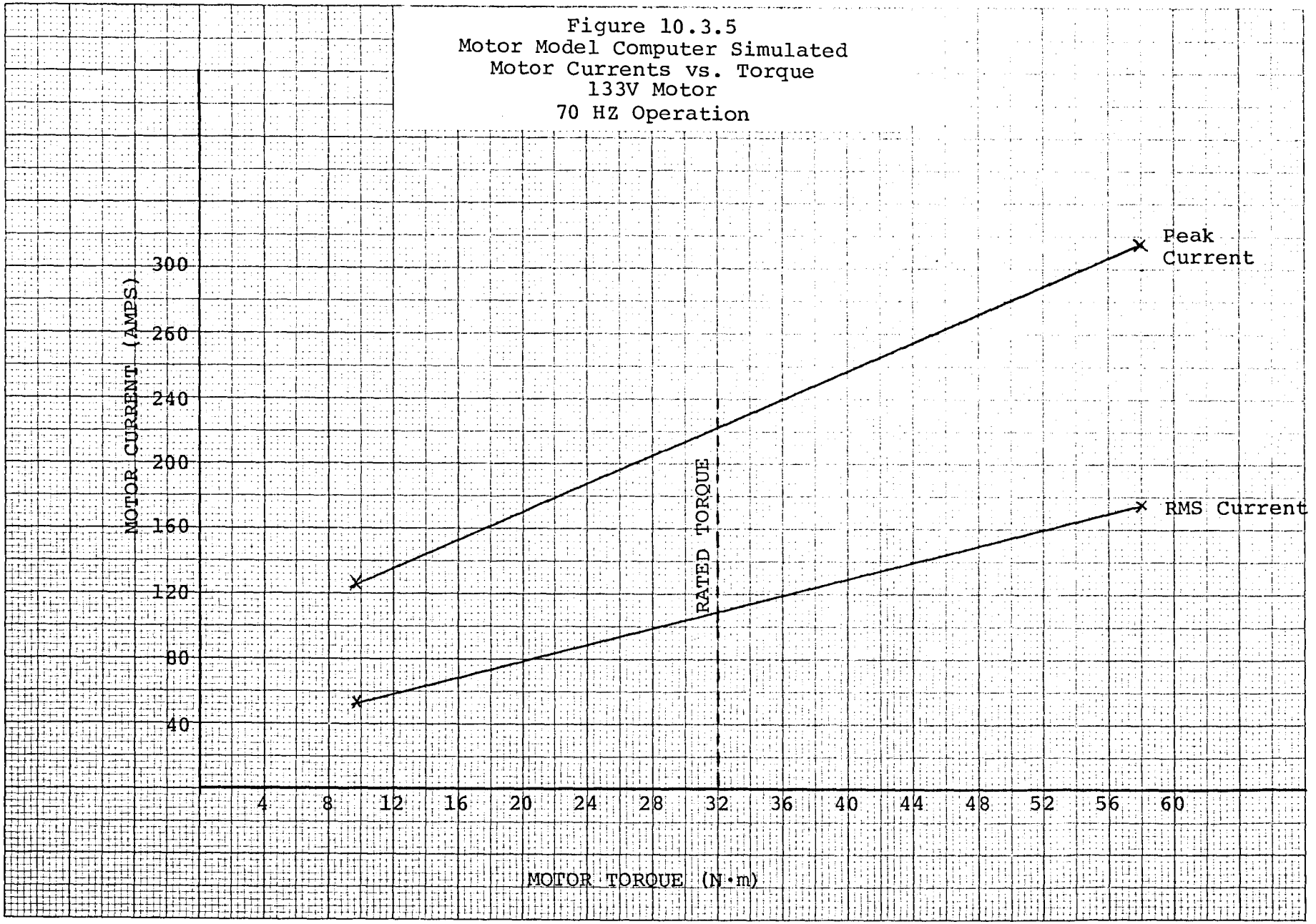
Figure 10.3.5
Motor Model Computer Simulated
Motor Currents vs. Torque
133V Motor
70 HZ Operation
MOTOR CURRENT (AMPS)
300
260
240
200
160
120
80
40
4
8
12
16
20
24
28
32
36
40
44
48
52
56
60
MOTOR TORQUE (N•m)
RATED TORQUE
Peak
Current
RMS Current

10.4 Inverter Model Development

The overall objective of any simulation effort is to obtain accurate and useful results at a reasonable cost. There are several methodologies that can be used to obtain this objective, each with its own particular advantages and disadvantages. Examples of such methods include linearization models, analog computer models, analog-digital hybrids, and state variable time response analysis[9,10].

The state variable approach was used in this simulation effort over the possible methods for several reasons.

1. The availability of circuit analysis programs to perform state variable time response analysis (eg., SPICE2, SCEPTRE).

2. The capability of such programs to accurately model the dynamic characteristics of solid state devices.

3. The ease with which a model can be modified, either slightly or radically, from component changes to circuit redesign.

4. Detail of any electrical system can be modeled as simply or in as much detail as desired.

The intent of the simulation was not only simply to duplicate the current design and to study its operation in detail but to evaluate alternative solid state devices, evaluate controller strategies and notch schemes, evaluate different operating voltages, evaluate different circuit configurations, and determine the power losses of the inverter for each of these various conditions.

Initially, development of the simulation model was done using both the SPICE2 and SCEPTRE programs. The reason for the co-development of the model with both programs was the trade-off between the more efficient (less computer CPU time) analysis capability of SPICE2 versus the broader capabilities of SCEPTRE. The input methods of each program are similar enough to each other so as not to cause much of a burden initially to use both programs. As the development continued, one would be chosen over the other either for computational efficiency or extensive capability, whichever was deemed most important to the success of the analysis.

Solid State Device Model Development

The modeling of standard electric components such as capacitors, resistors, inductors, and current and voltage sources is a straightforward task. The development of solid state device models of transistors and diodes, on the other hand, is a considerably more difficult task. For the inverter simulation, models of the power transistors and diodes were developed for both the SPICE2 and SCEPTRE programs.

Transistor Model Development

The transistor model used was the modified Gummel-Poon model for the Bipolar Junction Transistor (BJT) used in the SPICE2 program[5,11,12]. The model included 40 parameters to describe a BJT with the importance of each parameter dependent upon the purpose of the model or conditions in which it is to be used. Similar parameters are required for the modified Ebers-Moll model for the SCEPTRE program[13,14]. Although some nomenclature is different between the two models, the parameters of each can basically be derived from the other. The procedures required in the development of such a model are well documented in the literature[14,15].

The first step in the development of the model was to determine the dc characteristics of the transistor. The values of the dc parameters were either derived from the manufacturers data sheets or determined from laboratory tests.

One difficulty encountered in the model development of high power devices is that the BJT transistors typically consist of Darlington pairs. The Darlington must either be modeled as a single BJT or as two BJT's, making the testing of the device considerably more difficult or impossible. The model developed for this simulation was a single BJT model which then caused the test procedures outlined for standard BJT's to be more difficult and the results of the tests difficult to interpret.

Once the initial dc parameters were estimated, a preliminary transistor model was included in the test circuit model illustrated in Figure 10.4.1. The test circuit simulation was then used to fine tune the BJT model to meet, as nearly as possible, the typical manufacturer's specifications. The dc performance of the model is compared to manufactured data in Figure 10.4.2. The correlation is not exact, partly due to the single BJT model of the Darlington pair but the results were considered to be sufficiently accurate to obtain realistic performance from the overall inverter model.

Figure 10.4.2 Toshiba Transistor 2SD648 I_C Versus V_{CE}

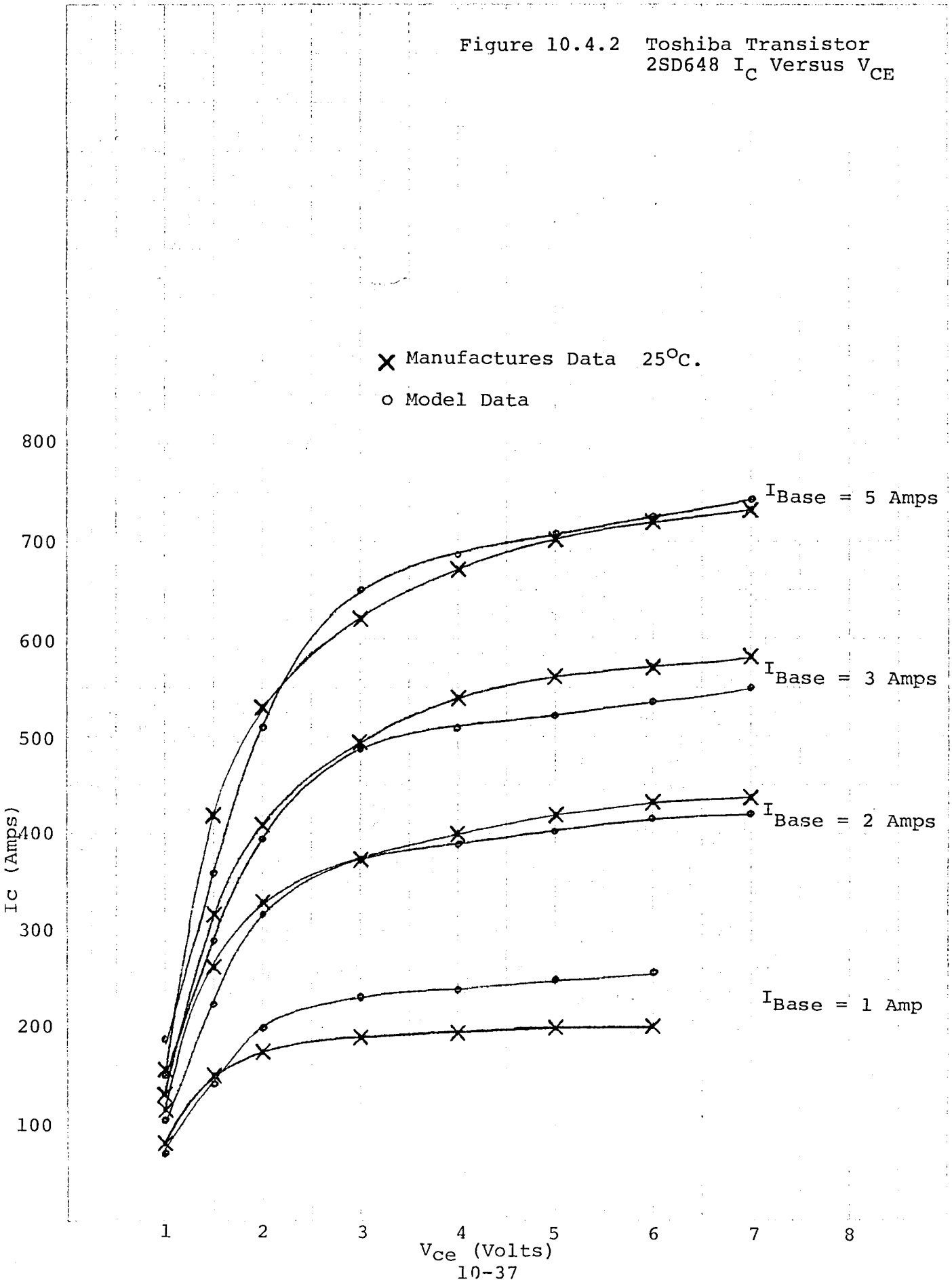

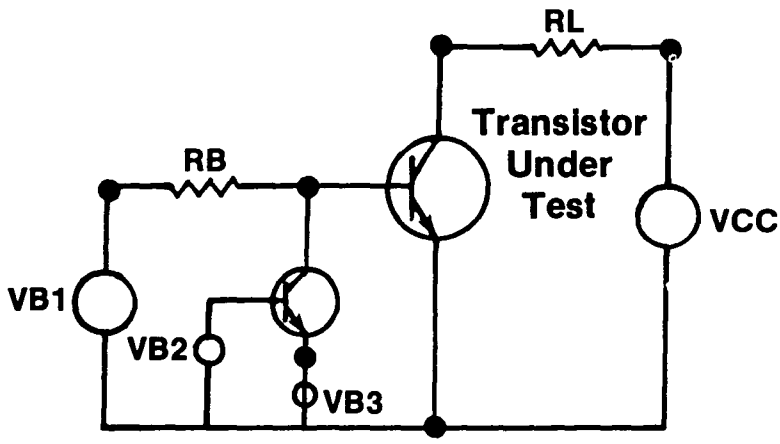

Figure 10.4.1 Transistor Test Circuit

The determination of the parameters to model the transient, large-signal characteristics of the transistor was achieved in a similar fashion. Laboratory tests were performed and preliminary values for the parameters were derived. A test circuit model was again used to fine tune the transient characteristics of the model. The final parameter values for the transistor model are given in Figure 10.4.3.

The average rise, storage, and fall times for the actual transistor in a circuit similar to the test circuit model are, according to manufacturers specifications, 0.5 μs, 11 μs, and 2.5 μs, respectively. The empirically derived transient parameters were modified slightly to match these average specifications. The performance of the transistor model in the inverter is compared to actual transistor performance in a later section (refer to Figures 10.4.23 and 10.4.24).

Diode Model Development

The model used for the inverter diodes had been developed in analysis work prior to this task. The parameters of the G.E. A397 diode are listed in Figure 10.4.4 for the SPICE2 diode model.

Figure 10.4.3 Modified Gummel-Poon BJT Parameters[5,11]

Toshiba 29D648

	Name	Parameter	Units	Value
1	IS	transport saturation current	A	.0025
2	BF	ideal maximum forward beta	-	900
3	NF	forward current emission coefficient	-	10
4	VBF	forward Early voltage	V	37
5	IBF	corner for forward beta high current roll-off	A	220
6	ILE	B-E leakage saturation current	A	.0001
7	NLE	B-E leakage emission coefficient	-	15
8	BR	ideal maximum reverse beta	-	2
9	NR	reverse current emission coefficient	-	12
10	VBR	reverse Early voltage	V	37
11	IBR	corner for reverse beta high current roll-off	A	200
12	ILC	B-C leakage saturation current	A	.001
13	NLC	B-C leakage emission coefficient	-	12
14	RB	zero bias base resistance	Ohms	.0005
15	IRB	current where base resistance falls halfway to its min value	A	infinite
16	RBM	minimum base resistance at high currents	Ohms	RB
17	RE	emitter resistance	Ohms	.0005
18	RC	collector resistance	Ohms	.0005
19	CJE	B-E zero-bias depletion capacitance	F	24E-8
20	VJE	B-E built-in potential	V	0.7
21	MJE	B-E junction exponential factor	-	0.4
22	TF	ideal forward transit time	sec	6.7E-8
23	XTF	coefficient for bias dependence of TF	-	0
24	VTF	voltage describing VBC dependence of TF	V	infinite
25	ITF	high-current parameter for effect on TF	A	0
26	PTF	excess phase at freq=1.0/(TF*2PI) Hz	deg	0
27	CJC	B-C zero-bias depletion capacitance	F	30E-8
28	VJC	B-C built-in potential	V	0.7
29	MJC	B-C junction exponential factor	-	0.4
30	CDIS	fraction of B-C depletion capacitance connected to internal base node	-	1
32	CJS	zero-bias substrate capacitance	F	14E-12
33	VJS	substrate junction built-in potential	V	0.75
34	MJS	substrate junction exponential factor	-	0
35	TB	forward and reverse beta temperature exponent	-	0
36	EG	energy gap for temperature effect on IS	eV	1.11
37	PT	temperature exponent for effect on IS	-	3
38	KF	flicker-noise coefficient	-	0
39	AF	flicker-noise exponent	-	1
40	FC	coefficient for forward-bias depletion capacitance formula	-	0.5

	Name	Parameter	Units	Value
1	IS	saturation current	A	2.875E-4
2	RS	onmic resistance	Ohm	.000431
3	N	emission coefficient	-	2.59
4	TT	transit-time	sec	2.54E-7
5	CJO	zero-bias junction capacitance	F	3.8E-9
6	PB	junction potential	V	0.75
7	M	grading coefficient	-	0.38
8	EG	activation energy	eV	1.11
9	PT	saturation-current temp. exp	-	3.0
10	KF	flicker noise coefficient	-	0
11	AF	flicker noise exponent	-	1
12	FC	coefficient for forward-bias depletion capacitance formula	-	0.5
13	BV	reverse breakdown voltage	V	infinite
14	IBV	current at breakdown voltage	A	1.0E-3

Figure 10.4.4 Diode Model[5,11]

Modeling the Inverter

The development of the inverter model consisted of an effort to maintain as much detail of the inverter as possible while at the same time maintaining reasonable computer run times. Since in any circuit analysis the run time is highly dependent upon circuit topology, initial steps were taken to determine the degree of detail that should be included in the inverter.

The first step was the development of a model of one leg of the inverter supplying a pure, inductive load, representing a simple motor model. Initial results from this 1/3 size simulation indicated that modeling the entire inverter was economically feasible.

The next step involved modeling the entire inverter. As much of the circuitry as possible was omitted from two of the legs to simplify the model and still maintain proper operation. A two-phase (transformed from three phases) model of a high slip motor was then incorporated into the model. Results of this simulation indicated that this model, once refined, would be sufficiently accurate and still economical.

The model was then refined to include an accurate representation of the low slip motor of the actual drive system (refer to Figure 10.2.6 for parameter values). The reduced response time of the low slip motor resulted

in an approximate four-fold increase in required computer run time. Therefore the full inverter model was reduced to include one detailed leg with the remaining two legs represented simply with voltage sources. This final model is illustrated in Figure 10.4.5 and was the one used for the remaining inverter analysis. The SPICE2 input listing for the inverter at one operating point is given in Figure 10.4.6.

Although this simplification resulted in a compromise of inverter model detail, the output which resulted correlated well with experimental data. Since computational efficiency did prove to be important, the SPICE2 program was henceforth used exclusively. The computer run time on a VAX 11/780 for the inverter model at three different operating conditions is given in Figure 10.4.7.

Configuration	CPU Time (Min:Sec)
94 Hz 0 Notches 1 cycle	8:8
70 Hz 5 Notches 1 cycle	26:17
27 Hz 8 Notches 1 cycle	49:40

Figure 10.4.7 Computer Run Time Examples (VAX 11/780 COMPUTER)

Primary Inverter Components

As discussed above, the reduction of the inverter model resulted in detailed modeling of only one inverter leg. As shown in Figure 10.4.5 all components including the transistors, diodes, capacitors, etc., for one entire leg were included. Stray inductance of the snubber capacitor, diode, and transistor base leads were also modeled. The values of these stray inductances were determined from experimental data and refined through correlation with detailed transistor switching waveforms.

Transistor Base Drives

Piecewise linear voltage sources with series resistances were used to simulate the transistor base drives. Initial efforts to include the current sense override circuitry which insures the transistors are not switched when reversed biased were unsuccessful. A simple MOSFET model was inserted in series with the base drive voltage sources. The MOSFETS were then driven with voltage sources, dependent upon transistor bias. The resulting fluctuations of the MOSFET drive sources caused instability of the MOSFET operation and the scheme was eliminated. The effect was finally simply modeled with a 10 microsecond delay between the turn-off of one and the

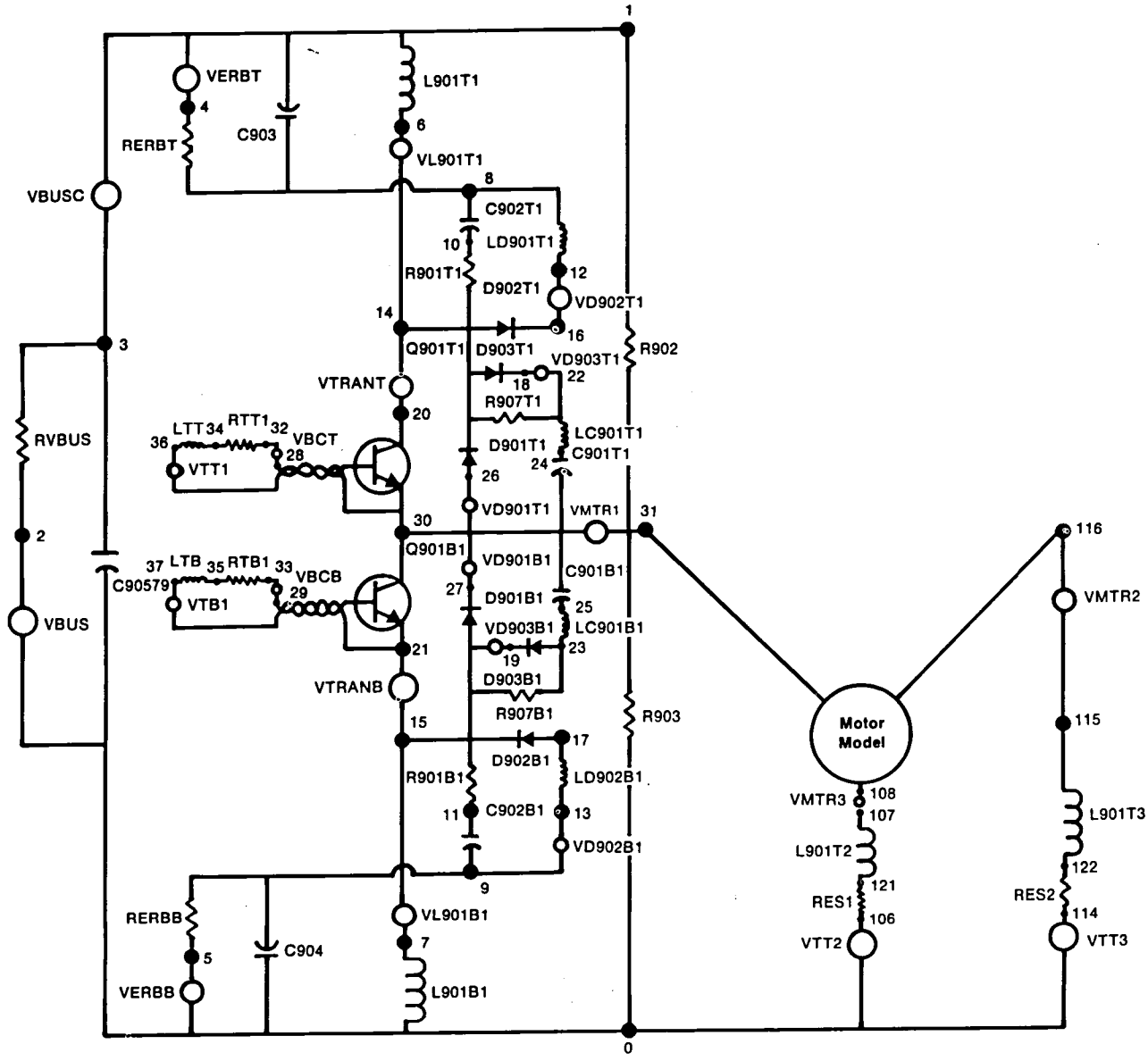

Figure 10.4.5 Inverter Model - One Detailed Leg

```
INVERTER MODEL - DEN3-125
*
* STATOR FREQUENCY = 94.6 HZ
* DUTY CYCLE = 1.0
*
* - - VOLTAGE SOURCES - -
*
VBUS        2     0     144.0
VERBT       4     1     30.0
VERBB       0     5     30.0
*
* - - CAPACITORS - -
*
C905T9      3     0     35000UF
C903        1     8     3500UF
C904        9     0     3500UF
C902T1      8     10    .047UF
C902B1      11    9     .047UF
C901T1      24    30    10UF
C901B1      30    25    10UF
*
* - - RESISTORS - -
*
RVBUS       3     2     .045
RERBT       4     8     .001
RERBB       9     5     .001
RTT1        34    32    1.0
RTB1        35    33    1.0
R901T1      10    14    50
R901B1      15    11    50
R907T1      14    22    2
R907B1      15    23    2
R902        1     31    5000
R903        31    0     5000
RES1        106   121   .045
RES2        114   122   .045
*
* - - INDUCTORS - -
*
L901T1      1     6     8UH
L901B1      7     0     8UH IC=274.99
L901T2      121   107   8UH IC=8.63
L901T3      122   115   8UH IC=266.36
LTT         36    34    .5UH
LTB         37    35    .5UH
LD902T1     8     12    .4UH
LD902B1     17    13    .4UH
LC901T1     22    24    .5UH
LC901B1     25    23    .5UH
*
* - - DIODES - -
*
D902T1      14    16    DIODM1
D902B1      17    15    DIODM1
D903T1      14    18    DIODM1
D903B1      23    19    DIODM1
D901T1      26    14    DIODM1
D901B1      15    27    DIODM1
*
```

Figure 10.4.6 SPICE2 Input Listing of the Inverter Model

```
* - - TRANSISTORS - -
*
Q901T1     20    28    30    TRANSM1
Q901B1     30    29    21    TRANSM1
*
* - - CURRENT SHUNT VOLTAGE SOURCES - -
*
VBUSC      3     1     0
VL901T1    6     14    0
VL901B1    7     15    0
VBCT       32    28    0
VBCB       33    29    0
VTRANT     14    20    0
VTRANB     21    15    0
VD902T1    16    12    0
VD902B1    9     13    0
VD903T1    18    22    0
VD903B1    19    15    0
VD901T1    30    26    0
VD901B1    27    30    0
VMTR1      30    31    0
VMTR2      107   108   0
VMTR3      115   116   0
*
* - - MODEL DEFINITIONS - -
*
.MODEL DIODM1 D
+ IS=2.875E-4
+ RS=.000431
+ N=2.59
+ TT=2.54E-7
+ CJO=3.8E-9
+ M=.38
+ PB=.75
.MODEL TRANSM1 NPN
+ BF=900
+ JS=.0025
+ JLE=.0001
+ VBF=37
+ JBF=220
+ NLE=15
+ RB=.0005
+ RE=.0005
+ RC=.0005
+ NF=10
+ NR=12
+ BR=2
+ JLC=.001
+ VBR=37
+ JBR=200
+ NLC=12
+ CJE=24E-8
+ VJE=.7
+ MJE=.4
+ CJC=30E-8
+ VJC=.7
+ MJC=.4
+ CJS=14E-12
+ TR=1.2E-5
+ TF=6.7E-8
*
```

Figure 10.4.6 Cont'd. Input Listing of the Inverter Model

```
* - - MOTOR MODEL - -
*


*      STANDARD DESIGN
*      94.6 HZ SLIP=1.32HZ
*
EA 200 210 POLY(3) 31 220 108 220 116 220
+  0. .816497 -.408248 -.408248
EB 205 211 POLY(2) 108 220 116 220
+  0. .707107 -.707107
H1 0 204   POLY(2) VEB VH2
+  0. 1.2918 1.323
H2 209 0   POLY(2) VEA VH1
+  0. 1.2918 1.323
F1 31 220  VEA .816497
F2 108 220 POLY(2) VEA VEB
+  0. -.408248 .707107
F3 116 220 POLY(2) VEA VEB
+  0. -.408248 -.707107
RM1 200 201 .00906
RM2 203 212 .00702
RM3 205 206 .00906
RM4 208 213 .00702
LM1 201 202 40.3UH IC=-336.76
LM2 202 203 53.3UH IC=-258.22
LM3 202   0 2204UH IC=-78.54
LM4 206 207 40.3UH IC=-182.15
LM5 207 208 53.3UH IC=-179.55
LM6 207   0 2204UH IC=-2.599
VEA   0 210 0
VEB   0 211 0
VH1 204 212 0
VH2 209 213 0
RN1  31 220 100
RN2 108 220 100
RN3 116 220 100
*
* - - END MOTOR MODEL - -
*
*
* - - OUTPUT CONTROLS - -
*
.PRINT TRAN
*
* - - ANALYSIS CONTROLS - -
*
.TRAN .0002 .011 0.0 .000005 UIC
.OPTIONS ABSTOL=.01 VNTOL=.01 RELTOL=.001
+ LIMPTS=1000000
+ ITL5=50000
+ ITL4=30
+ ITL1=300
+ GMIN=1E-15
*
```

Figure 10.4.6 Cont'd. Input Listing of the Inverter Model

```
* - - INITIAL CONDITIONS - -
*
.IC
* IC AT TIME = 0.00000E+00
+ V(1       )= 0.14648E+03 V(2       )= 0.14400E+03
+ V(3       )= 0.14648E+03 V(4       )= 0.17648E+03
+ V(5       )=-0.30000E+02 V(6       )= 0.14648E+03
+ V(7       )= 0.00000E+00 V(8       )= 0.17659E+03
+ V(9       )=-0.30030E+02 V(10      )= 0.12444E+03
+ V(11      )= 0.00000E+00 V(12      )= 0.17659E+03
+ V(13      )=-0.30030E+02 V(14      )= 0.14648E+03
+ V(15      )= 0.00000E+00 V(16      )= 0.17659E+03
+ V(17      )=-0.30030E+02 V(18      )= 0.14563E+03
+ V(19      )= 0.00000E+00 V(20      )= 0.14648E+03
+ V(21      )= 0.00000E+00 V(22      )= 0.14563E+03
+ V(23      )= 0.42254E-05 V(24      )= 0.14563E+03
+ V(25      )= 0.42254E-05 V(26      )= 0.73900E+02
+ V(27      )= 0.73900E+02 V(28      )= 0.61969E+02
+ V(29      )=-0.39976E+01 V(30      )= 0.73900E+02
+ V(31      )= 0.73900E+02 V(32      )= 0.61969E+02
+ V(33      )=-0.39976E+01 V(34      )= 0.69900E+02
+ V(35      )=-0.40000E+01 V(36      )= 0.69900E+02
+ V(37      )=-0.40000E+01 V(106     )= 0.00000E+00
+ V(107     )= 0.60760E+02 V(108     )= 0.60760E+02
+ V(114     )= 0.14400E+03 V(115     )= 0.87297E+02
+ V(116     )= 0.87297E+02 V(121     )= 0.60760E+02
+ V(122     )= 0.87297E+02 V(200     )=-0.10501E+00
+ V(201     )= 0.00000E+00 V(202     )= 0.00000E+00
+ V(203     )= 0.00000E+00 V(204     )= 0.15630E+00
+ V(205     )=-0.18764E+02 V(206     )= 0.00000E+00
+ V(207     )= 0.00000E+00 V(208     )= 0.00000E+00
+ V(209     )= 0.14090E+02 V(210     )= 0.00000E+00
+ V(211     )= 0.00000E+00 V(212     )= 0.15630E+00
+ V(213     )= 0.14090E+02 V(220     )= 0.62349E+02
*
* - - TRANSISTOR CONTROL VOLTAGE SOURCES - -
*
*     TSTRT   =  0.00000E+00
*     FREQ    =  0.94600E+02
*     ON VOLT =  0.60000E+01
*     OFF VOLT= -0.40000E+01
*     DELAY   =  0.10000E-04
*     RISE T  =  0.10000E-05
*     CYCLES  =     3
*     NOTCHES =     0
*
*
VTT1 36 30 PWL(  0.0000000E+00 -0.4000000E+01  0.5000000E-05 -0.4000000E+01
+              0.6000000E-05  0.6000000E+01  0.5280413E-02  0.6000000E+01
+              0.5281413E-02 -0.4000000E+01  0.1057083E-01 -0.4000000E+01
+              0.1057583E-01 -0.4000000E+01  0.1057682E-01  0.6000000E+01
+              0.1585124E-01  0.6000000E+01  0.1585224E-01 -0.4000000E+01
+              0.2114165E-01 -0.4000000E+01  0.2114665E-01 -0.4000000E+01
+              0.2114765E-01  0.6000000E+01  0.2642206E-01  0.6000000E+01
+              0.2642306E-01 -0.4000000E+01
+ )
VTB1 37 21 PWL(  0.0000000E+00 -0.4000000E+01  0.5285413E-02 -0.4000000E+01
+              0.5290413E-02 -0.4000000E+01  0.5291412E-02  0.6000000E+01
+              0.1056583E-01  0.6000000E+01  0.1056683E-01 -0.4000000E+01
+              0.1585624E-01 -0.4000000E+01  0.1586124E-01 -0.4000000E+01
+              0.1586224E-01  0.6000000E+01  0.2113665E-01  0.6000000E+01
+              0.2113765E-01 -0.4000000E+01
+ )
VTT2 106 0 PWL(  0.0000000E+00  0.0000000E+00  0.3523608E-02  0.0000000E+00
+              0.3528608E-02  0.0000000E+00  0.3529608E-02  0.1440000E+03
+              0.8804022E-02  0.1440000E+03  0.8805021E-02  0.0000000E+00
+              0.1409443E-01  0.0000000E+00  0.1409943E-01  0.0000000E+00
+              0.1410043E-01  0.1440000E+03  0.1937485E-01  0.1440000E+03
+              0.1937585E-01  0.0000000E+00
+ )
VTT3 114 0 PWL(  0.0000000E+00  0.1440000E+03  0.1756804E-02  0.1440000E+03
+              0.1757804E-02  0.0000000E+00  0.7047217E-02  0.0000000E+00
+              0.7052217E-02  0.0000000E+00  0.7053216E-02  0.1440000E+03
+              0.1232763E-01  0.1440000E+03  0.1232863E-01  0.0000000E+00
+              0.1761804E-01  0.0000000E+00  0.1762304E-01  0.0000000E+00
+              0.1762404E-01  0.1440000E+03  0.2289845E-01  0.1440000E+03
+              0.2289945E-01  0.0000000E+00
+ )
.END
```

Figure 10.4.6 Cont'd. Input Listing of the Inverter Model

turn on of the other transistor. The accuracy of this simplification proved to be adequate for overall inverter model performance. The application of the SCEPTRE program would have been advantageous in this case where special purpose devices, such as current sensing devices, may be included.

Energy Recovery Bus (ERB)

The inclusion of the detail of all the components of the energy recovery bus was not feasible. The ERB was modeled simply by resistance and voltage sources to provide the proper 30 volt offsets. The current ERB consists of a considerable number of components, and a conserted effort will need to be made for its redesign. This redesign effort is beyond the scope of this analysis and will be addressed in future work.

Battery Pack

The battery pack of the system was modeled with a voltage source and series resistance. The value of the voltage source was 144 volts, representing a fully charged state. The resistance value was obtained from experimental battery data given in Figure 10.4.8.

Initial Conditions Model

A simple model including the two phase motor model driven by piecewise-linear voltage sources was used to develop initial conditions for the larger inverter model. This simplified model is illustrated in Figure 10.4.9 with the SPICE2 input listing for one operating condition given in Figure 10.4.10. This simplified model would be simulated through several cycles of operation, allowing any transients to die out. The results from this simulation would then be used to generate initial conditions for the inverter model basically devoid of transients.

Later in the development of the motor analysis program, a capability was added to that program to output motor model inductor currents at any chosen point in time. These then could be used as initial conditions for the inverter resulting in a considerable reduction in required effort.

Correlation of Inverter Model Results

The correlation of the results of the inverter simulation with experimental data consisted of two basic aspects: one, the comparison of the transient voltage and current waveforms of the various inverter components; and two, comparison of the power losses of various inverter components.

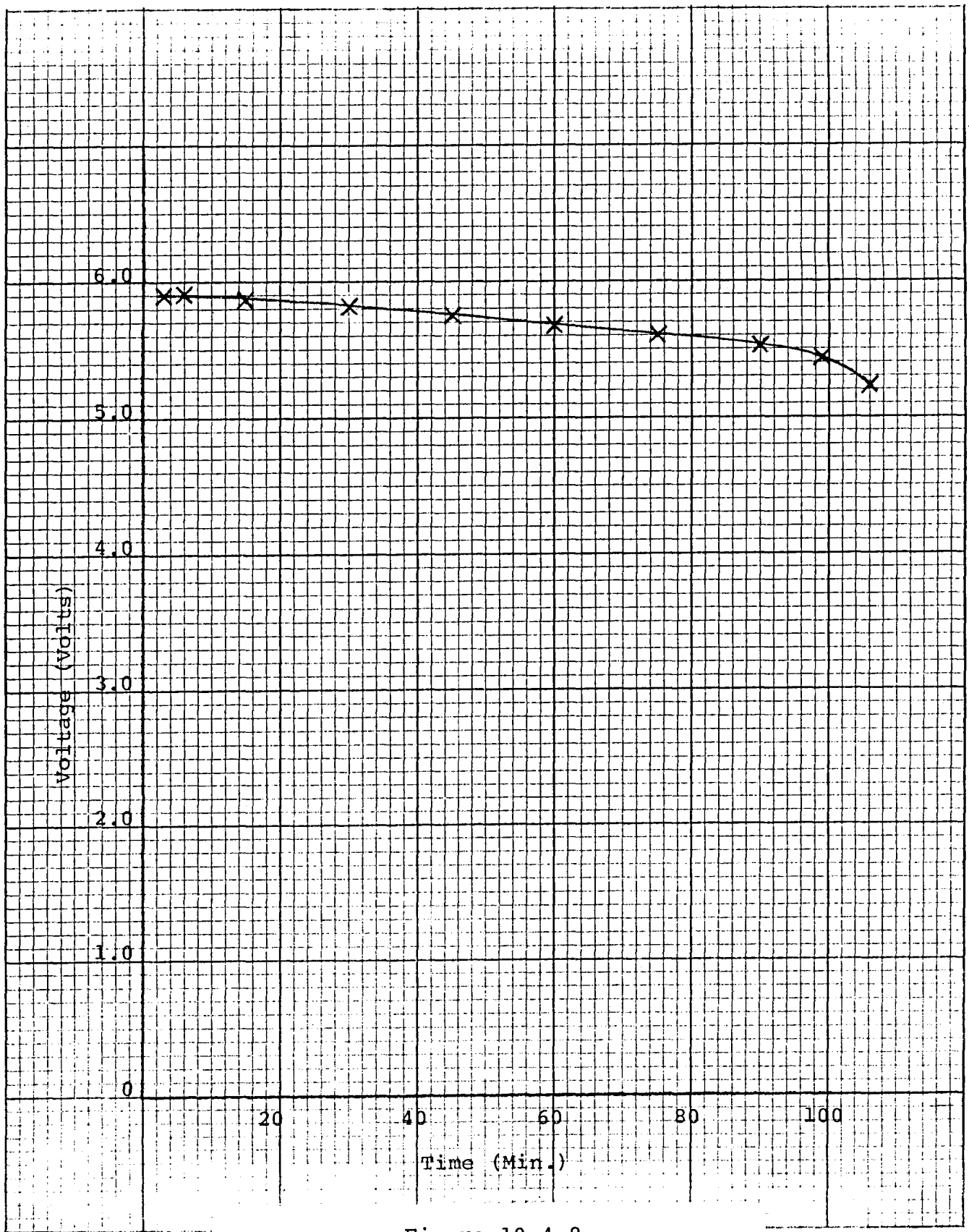

Figure 10.4.8
EV-106 75 AMP
Discharge at 27°C.

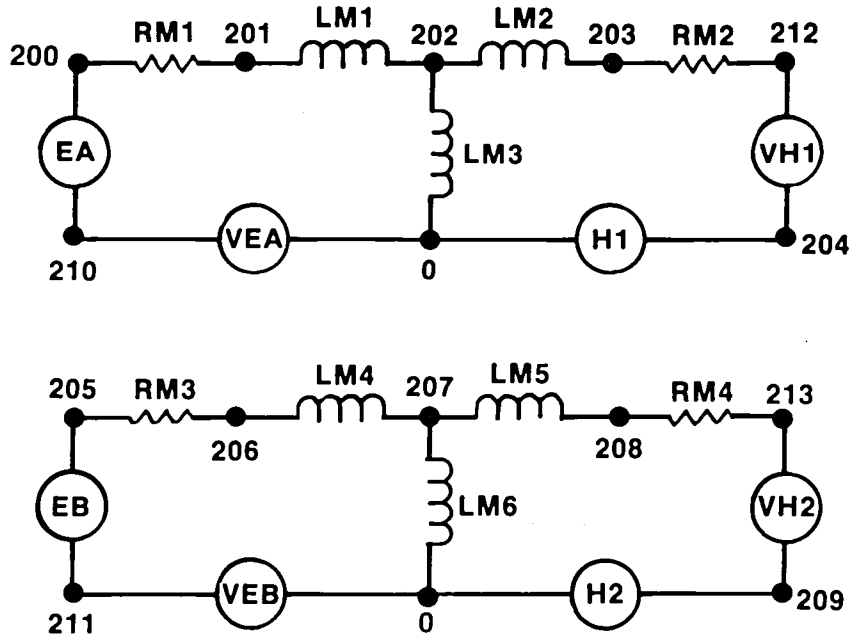

$$EA = \sqrt{2/3}\, V_{RN1} - 1/2\sqrt{2/3}\, V_{RN2} - 1/2\sqrt{2/3}\, V_{RN3}$$

$$EB = \frac{\sqrt{2}}{2} V_{RN2} - \frac{\sqrt{2}}{2} V_{RN3}$$

$$H1 = L_M W_R I_{VEB} + L_R W_R I_{H2}$$

$$H2 = L_M W_R I_{VEA} + L_R W_R I_{H1}$$

$$F1 = \sqrt{2/3}\, I_{VEA}$$

$$F2 = -1/2\sqrt{2/3}\, I_{VEA} + \frac{\sqrt{2}}{2} I_{VEB}$$

$$F3 = -1/2\sqrt{2/3}\, I_{VEA} - \frac{\sqrt{2}}{2} I_{VEB}$$

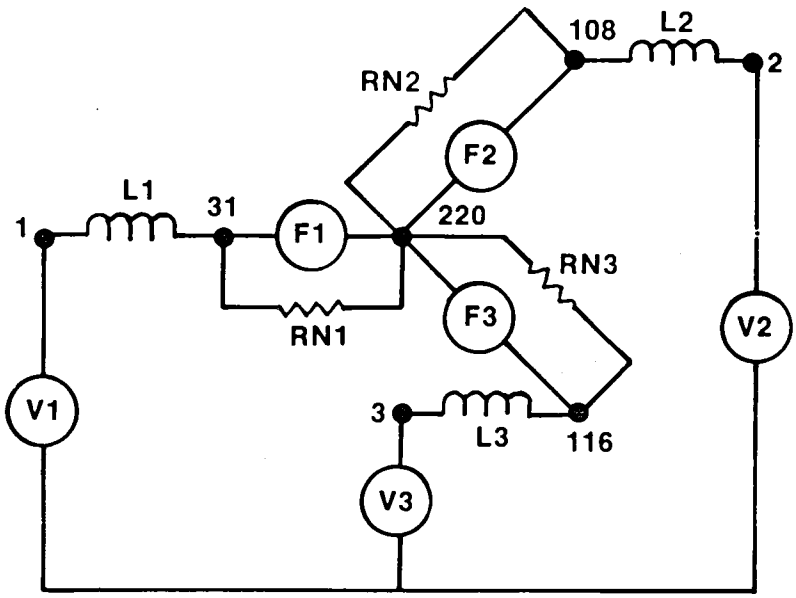

Figure 10.4.9 Motor Model with Simplified Inverter

Figure 10.4.10 SPICE2 Input Listing of Simplified Inverter Model with the Motor Model

```
SIMPLIED INVERTER WITH MOTOR - DEN3=125
*
* SIMPLIFIED MODEL USING ELEMENTAL
* VOLTAGE SOURCES FOR THE INVERTER
* TO GENERATE INITIAL CONDITIONS
*
* - - INVERTER - -
*
L1 4  31 8UH IC=-169,9
L2 5 108 8UH IC=59,69
L3 6 116 8UH IC=110,2
RE1 1 4 ,045
RE2 2 5 ,045
RE3 3 6 ,045
*
* - - MOTOR MODEL - -
*
*     NEW MOTOR DESIGN
*     70,0 HZ  SLIP=0,43 HZ
*
EA 200 210 POLY(3) 31 110 108 110 116 110
+  0, ,816497 -,408248 -,408248
EB 205 211 POLY(2) 108 110 116 110
+  0, ,707107 -,707107
H1 0 204   POLY(2) VEB VH2
+  0, 1,618791 1,6566981
H2 209 0  POLY(2) VEA VH1
+  0, 1,618791 1,6566981
F1 31 110  VEA ,816497
F2 108 110 POLY(2) VEA VEB
+  0, -,408248 ,707107
F3 116 110 POLY(2) VEA VEB
+  0, -,408248 -,707107
RM1 200 201 ,01451
RM2 203 212 ,0111
RM3 205 206 ,01451
RM4 208 213 ,0111
LM1 201 402 74,36UH
+ IC=-208,02
VLM1 402 202 0
LM2 202 403 86,72UH
+ IC=-152,87
VLM2 403 203 0
LM3 202  404 3703,3UH
+ IC=-55,142
VLM3 404 0 0
LM4 206 407 74,36UH
+ IC=-35,59
VLM4 407 207 0
LM5 207 408 86,72UH
+ IC=-34,35
VLM5 408 208 0
LM6 207  409 3703,3UH
+ IC=-1,24
VLM6 409 0 0
VEA  0 210 0
VEB  0 211 0
VH1 204 212 0


VH2 209 213 0
RN1  31 110 1000
RN2 108 110 1000
RN3 116 110 1000
*
* - - END MOTOR MODEL - -
*
```

Figure 10.4.10 SPICE2 Input Listing of Simplified Inverter Model with the Motor Model (cont'd.)

```
* - - ANALYSIS CONTROLS - -
*
.PLOT TRAN V(1) I(V1)
.TRAN .002 .043 0.0 .00002
+ UIC
.OPTIONS ABSTOL=.01 VNTOL=.01 RELTOL=.001
+ ITL5=50000
+ ITL4=20
+ ITL1=300
*
* - - INITIAL CONDITIONS - -
*
.IC
* IC AT TIME = 0.42840E-01
+ V(1       )= 0.00000E+00 V(2       )= 0.00000E+00
+ V(3       )= 0.19200E+03 V(4       )= 0.76454E+01
+ V(5       )=-0.26860E+01 V(6       )= 0.18704E+03
+ V(31      )= 0.10188E+02 V(108     )=-0.22066E+01
+ V(110     )= 0.63931E+02 V(116     )= 0.18402E+03
+ V(200     )=-0.65906E+02 V(201     )=-0.62888E+02
+ V(202     )=-0.33946E+02 V(203     )=-0.98875E+00
+ V(204     )= 0.70815E+00 V(205     )=-0.13168E+03
+ V(206     )=-0.13116E+03 V(207     )=-0.10815E+03
+ V(208     )=-0.83850E+02 V(209     )=-0.83469E+02
+ V(210     )= 0.00000E+00 V(211     )= 0.00000E+00
+ V(212     )= 0.70815E+00 V(213     )=-0.83469E+02
+ V(402     )=-0.33946E+02 V(403     )=-0.98875E+00
+ V(404     )= 0.00000E+00 V(407     )=-0.10815E+03
+ V(408     )=-0.83850E+02 V(409     )= 0.00000E+00
*
* - - TRANSISTOR CONTROL VOLTAGE SOURCES - -
*
*     TSTRT    =  0.00000E+00
*     FREQ     =  0.70000E+02
*     ON VOLT  =  0.19200E+03
*     OFF VOLT=  0.00000E+00
*     DELAY    =  0.10000E-04
*     RISE T   =  0.10000E-05
*     CYCLES   =     4
*     NOTCHES  =     5
*
*   WIDTH          DEGREE
*  0.48000E+01 0.63600E+02
*  0.48000E+01 0.75600E+02
*  0.48000E+01 0.87600E+02
*  0.48000E+01 0.99600E+02
*  0.48000E+01 0.11160E+03
*
V1 1 0 PWL(  0.0000000E+00  0.0000000E+00  0.5000000E-05  0.0000000E+00
+            0.6000000E-05  0.1920000E+03  0.2523809E-02  0.1920000E+03
+            0.2524809E-02  0.0000000E+00  0.2713286E-02  0.0000000E+00
+            0.2714286E-02  0.1920000E+03  0.3000000E-02  0.1920000E+03
---- ETC. ----
V2 2 0 PWL(  0.0000000E+00  0.0000000E+00  0.1528561E-03  0.0000000E+00
+            0.1538564E-03  0.1920000E+03  0.3233328E-03  0.1920000E+03
+            0.3243331E-03  0.0000000E+00  0.6290469E-03  0.0000000E+00

+            0.6300472E-03  0.1920000E+03  0.7995237E-03  0.1920000E+03
---- ETC. ----
V3 3 0 PWL(  0.0000000E+00  0.1920000E+03  0.2375952E-02  0.1920000E+03
+            0.2376952E-02  0.0000000E+00  0.4914761E-02  0.0000000E+00
+            0.4915761E-02  0.1920000E+03  0.5085238E-02  0.1920000E+03
+            0.5086238E-02  0.0000000E+00  0.5390952E-02  0.0000000E+00
---- ETC. ----
.END
```

Transient Waveforms Correlation

The results from three analyses are given in the following figures to illustrate the comparison of model and actual voltage and current waveforms.

The first case illustrates the inverter operating at 25.7 Hz with 8 notches under low load. The transistor voltage, current, snubber inductor current, and motor currents are compared with similar experimental waveforms in Figures 10.4.11-10.4.14, respectively. The transistor, inductor, and motor currents of the analysis are in all cases somewhat lower than the experimental data, but overall waveforms correlate very well. The slight differences in peak values are due to factors such as duty cycle, differences in loading applied to the inverter from the motor model as compared to the actual motor, and the existence of some transients due to errors in the initial conditions.

Transistor voltage and current, inductor current, and motor current waveforms for the second case are given in Figures 10.4.15-10.4.18, respectively. This case simulated the inverter operating at 47.9 Hz with 5 notches in a regenerative mode. The same observations as above apply here. The overall waveforms compare very well with the differences in peak values due to the same causes as mentioned above. Note the different duty cycles when comparing the inductor and motor currents in Figures 10.4.17 and 10.4.18.

The third case includes waveforms of the inverter operating at 94.6 Hz in quasi-square wave mode. The transistor voltage and current, inductor current, and motor current waveforms are compared in Figures 10.4.19-10.4.22, respectively. Again, the overall waveform shapes compare quite favorably with experimental measurements.

Detailed transistor voltage and current waveforms through one notch are compared to actual data of the inverter in Figures 10.4.23 and 10.4.24. The overall waveshapes compare favorably and indicate the adequacy of the transistor and overall inverter models, and the detail of operation that can be observed with the simulation.

Component Power Loss Correlation

The second aspect of correlation was the comparison of overall power loss in the components of the inverter. The accurate evaluation of component power loss is crucial to the evaluation of inverter design changes which are made with intent to improve operating efficiency.

Figure 10.4.11
Inverter Transistor Voltage

Measured (Top)
Frequency = 25.7
Notches = 8

Simulated
Frequency = 25.7
Notches = 8

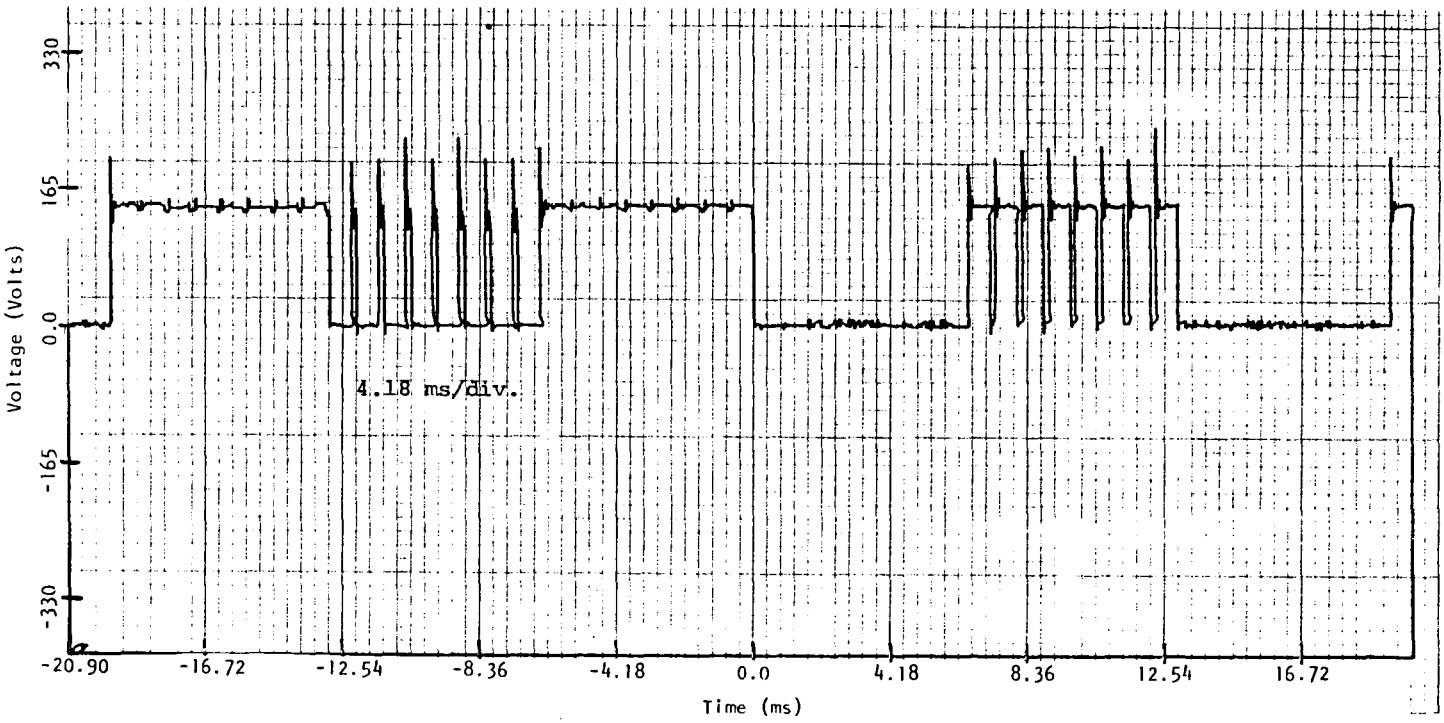

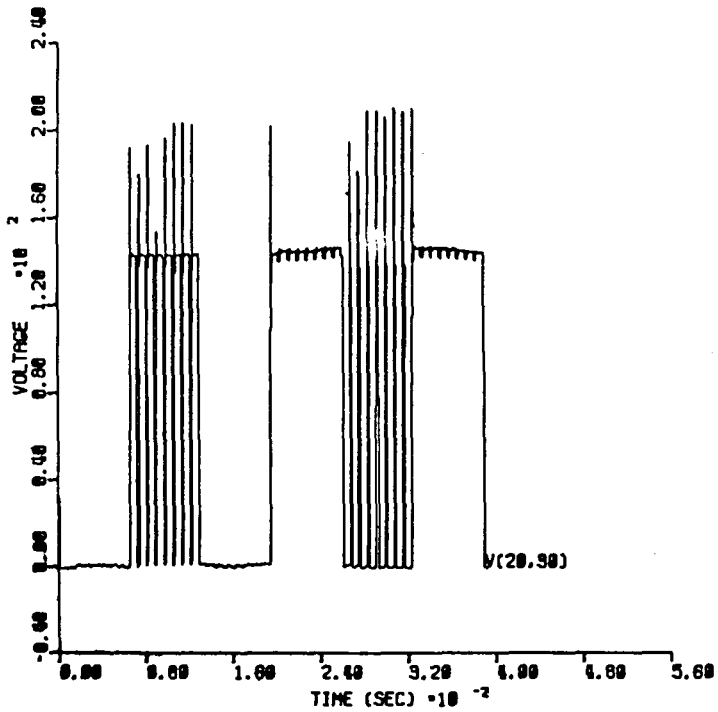

Figure 10.4.12
Inverter Transistor Current

Measure (Top)
Frequency = 25.7
Notches = 8

Simulated
Frequency = 25.7
Notches = 8

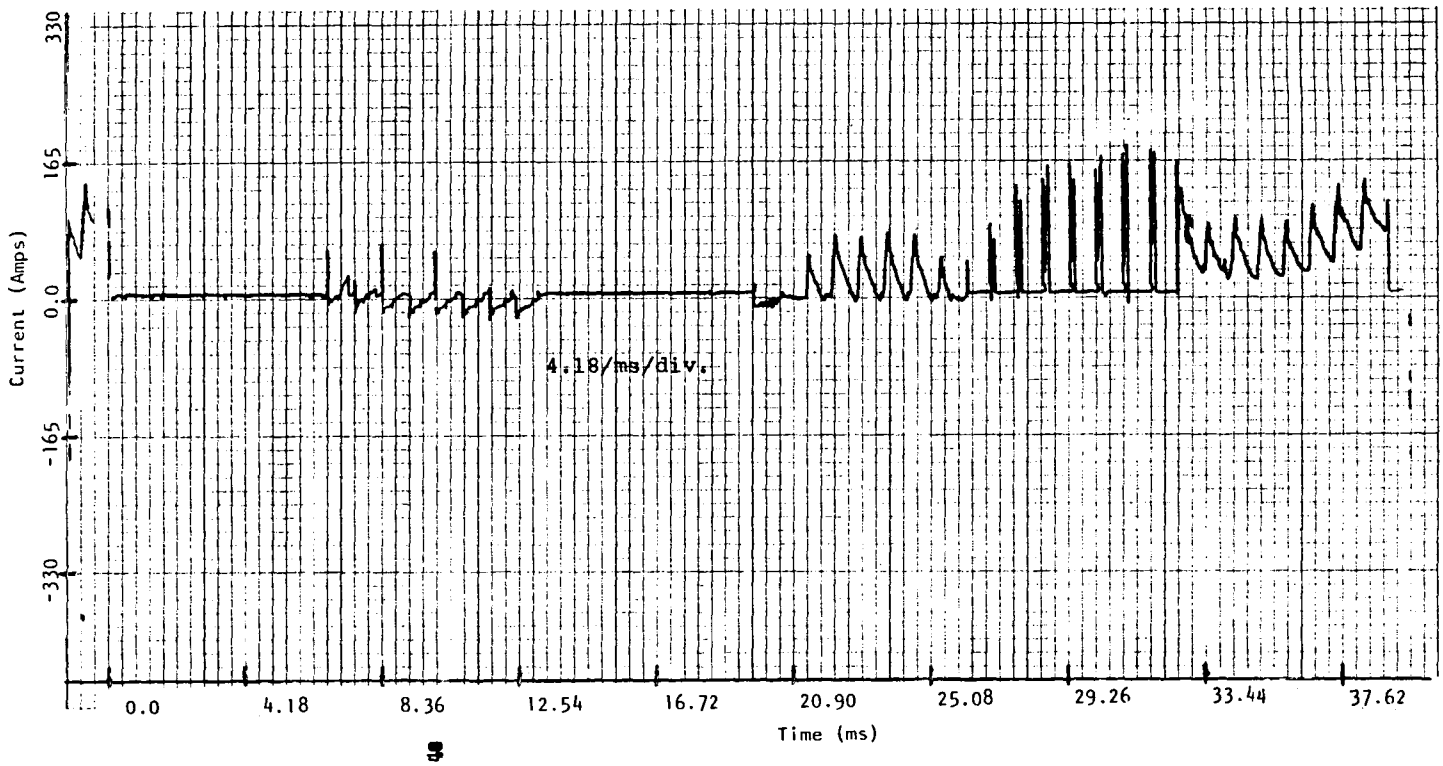

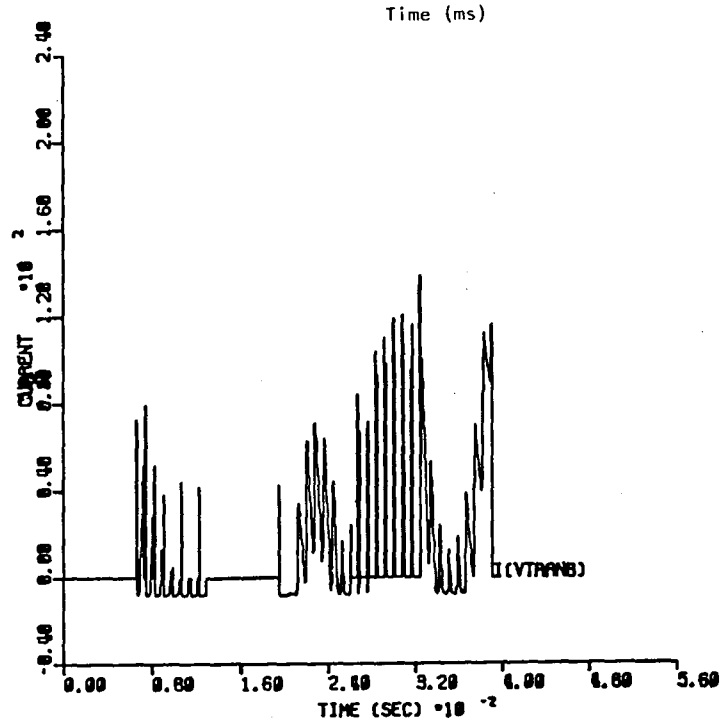

Figure 10.4.13
Inverter Inductor Current

Measured (Top)	Simulated
Frequency = 25.5	Frequency = 25.7
Notches = 8	Notches = 8

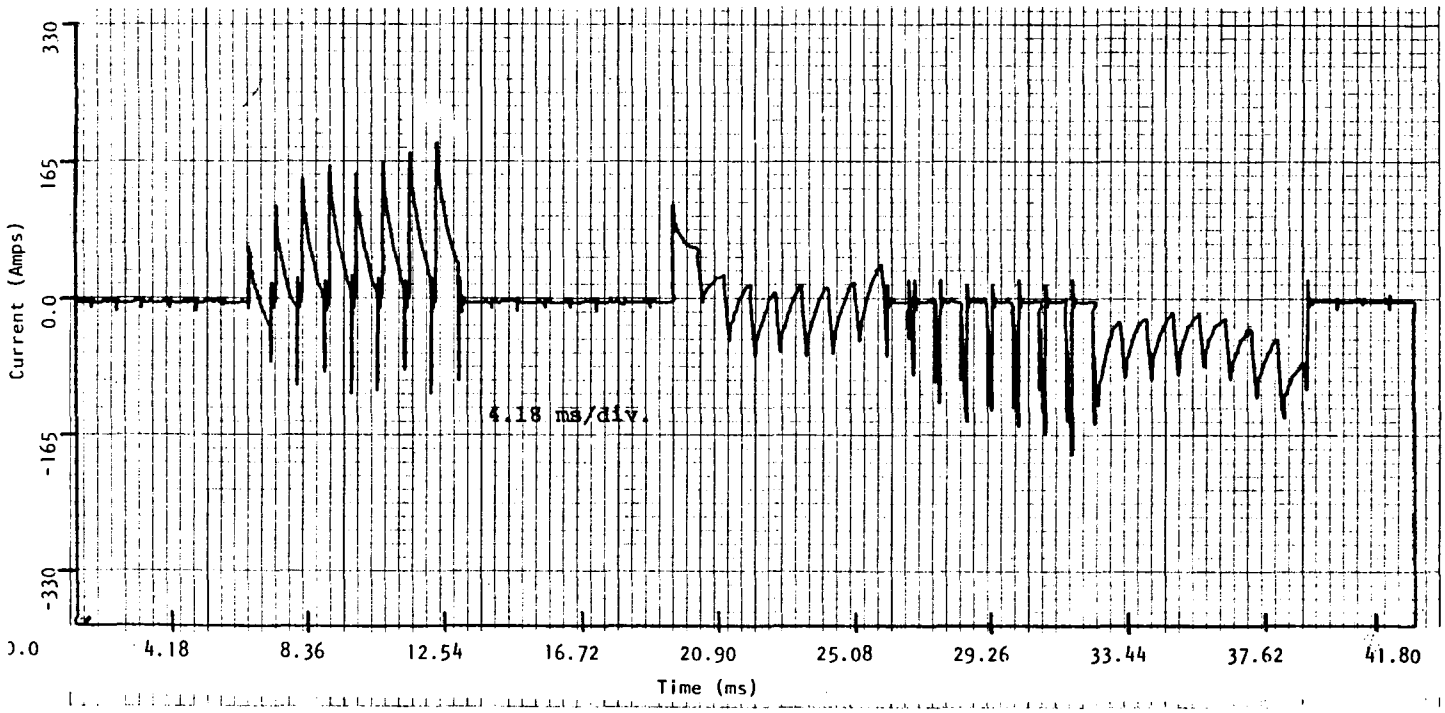

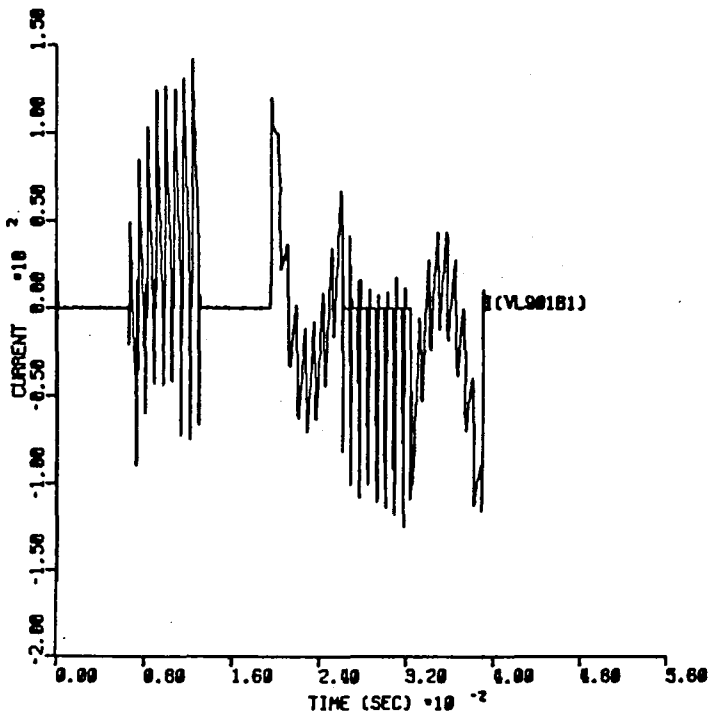

Figure 10.4.14
Motor Current

Measured (Top)
Frequency = 25.6
Notches = 8

Simulated
Frequency = 25.7
Notches = 8

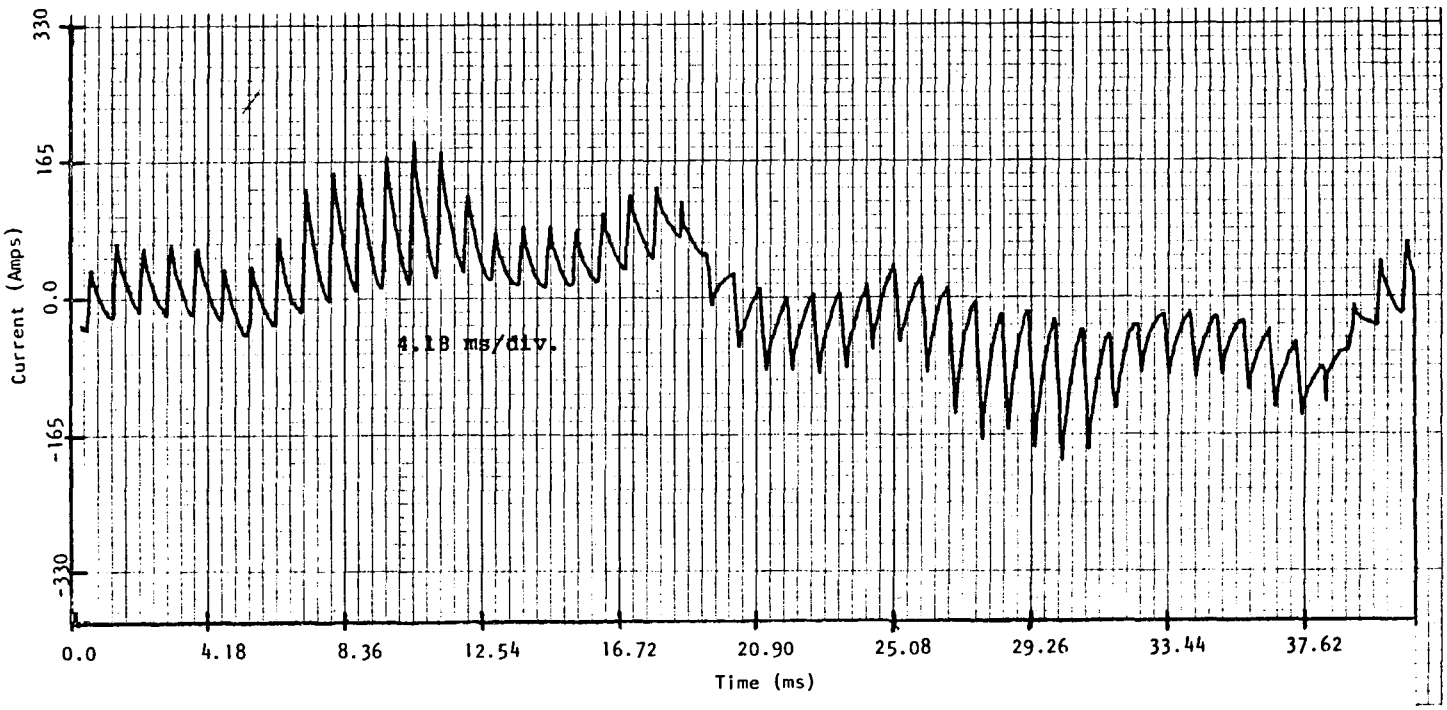

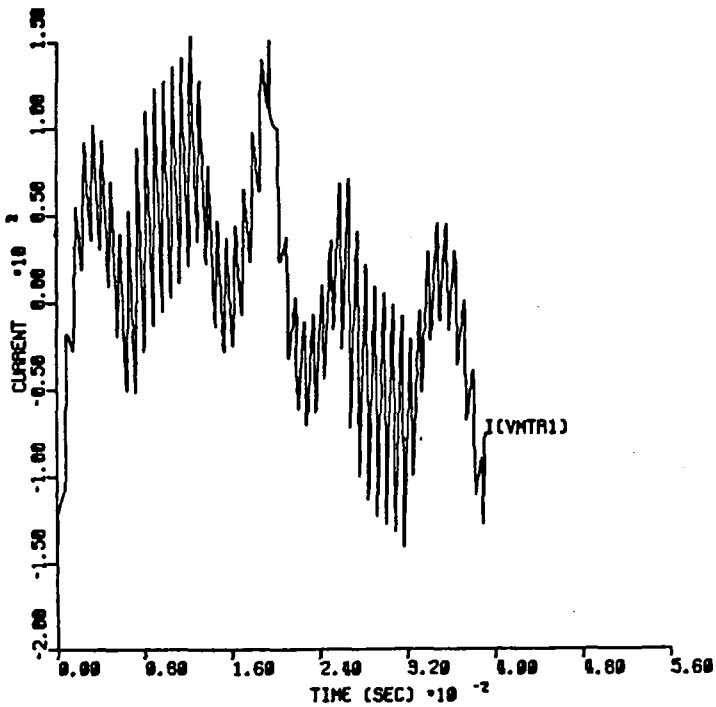

Figure 10.4.15
Inverter Transistor Voltage - Regen
Measured (Top) Simulated
Frequency = 47.9 Frequency = 47.9
Notches = 5 Notches = 5

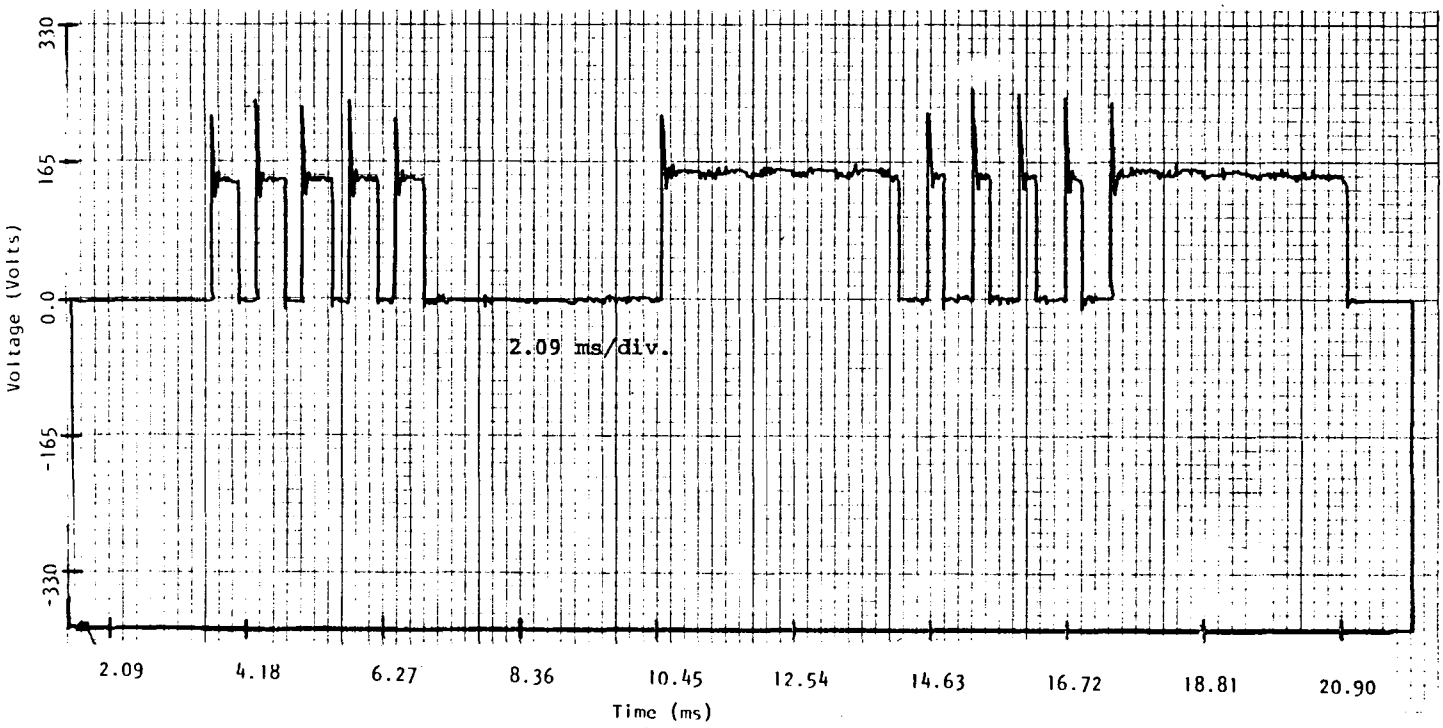

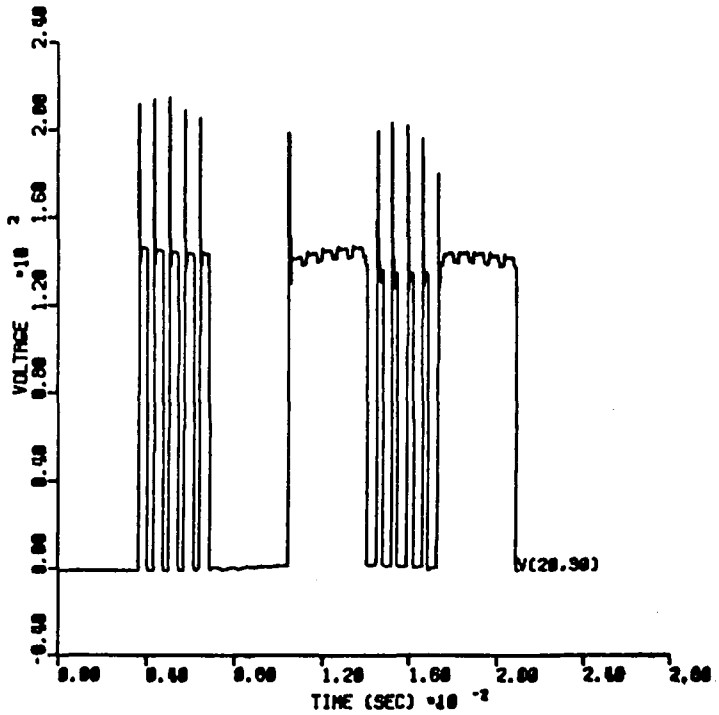

Figure 10.4.16
Inverter Transistor Current - Regen
Measured (Top) Frequency = 47.9 Notches = 5
Simulated Frequency = 47.9 Notches = 5

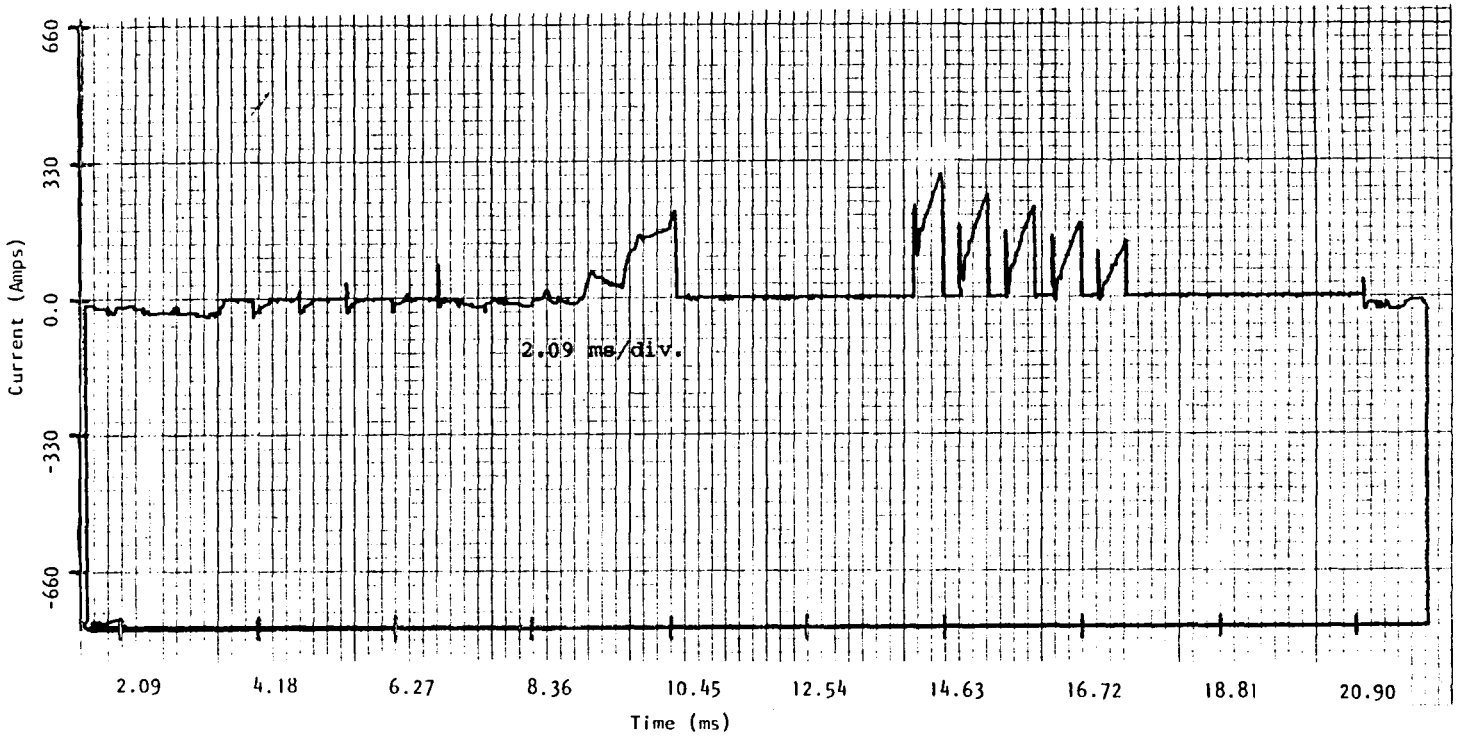

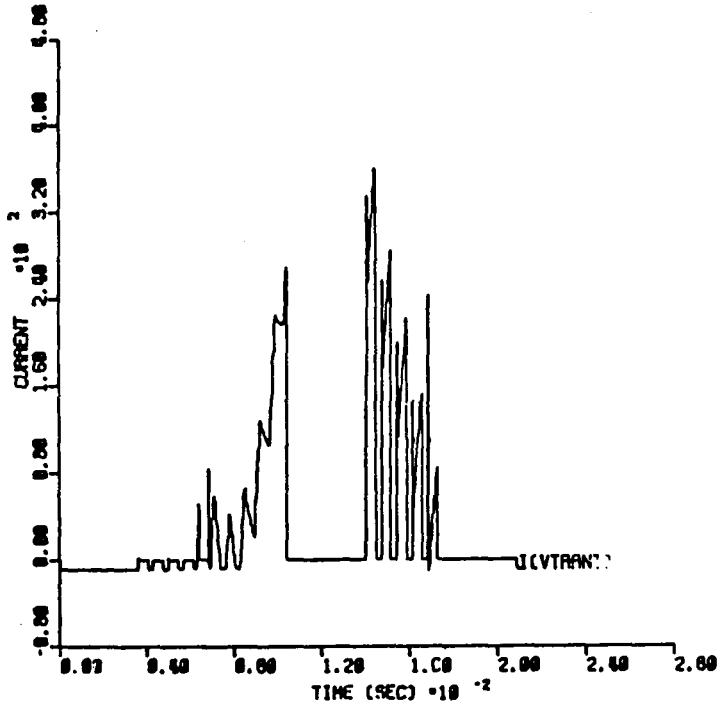

Figure 10.4.17
Inverter Inductor Current - Regen

Measured (Top)	Simulated
Frequency = 48.1	Frequency = 47.9
Notches = 8	Notches = 5

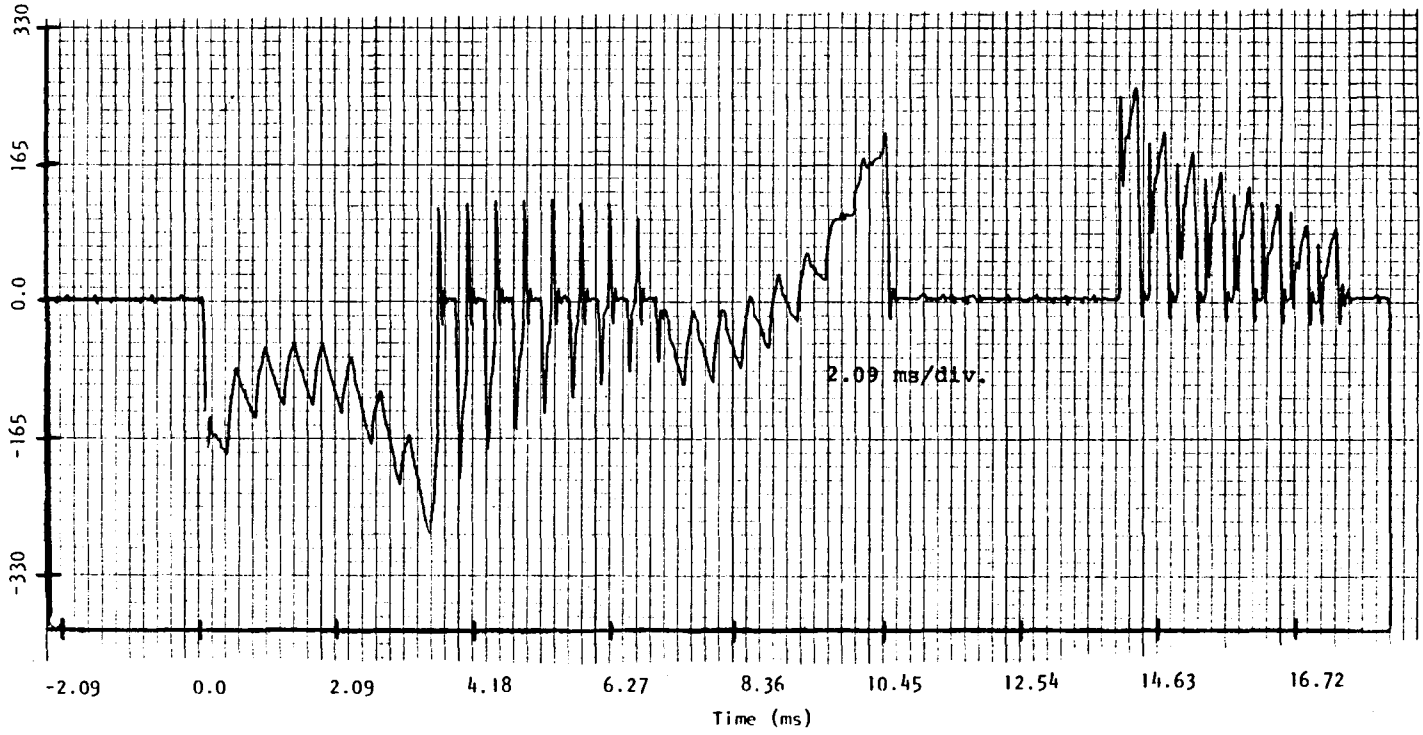

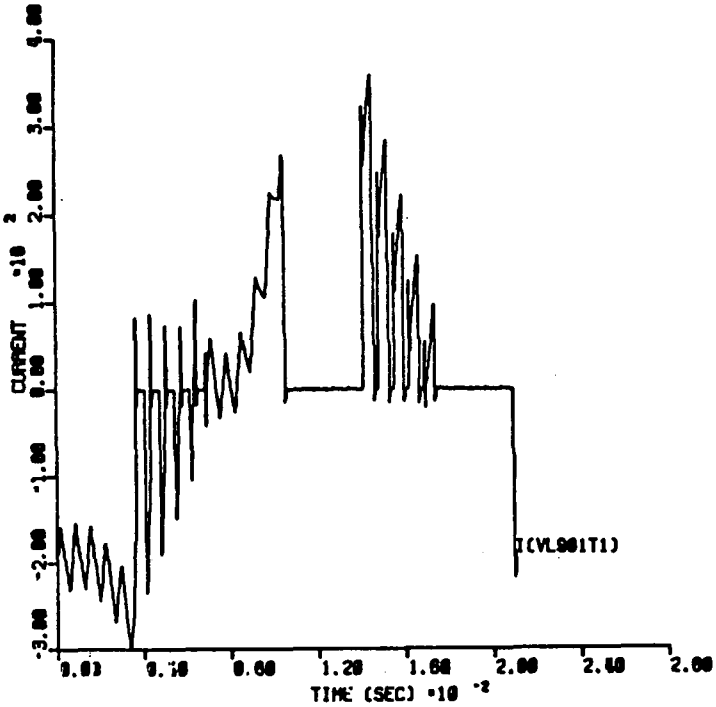

Figure 10.4.18
Motor Current - Regen

Measured (Top)
Frequency = 48.6
Notches = 8

Simulated
Frequency = 47.9
Notches = 5

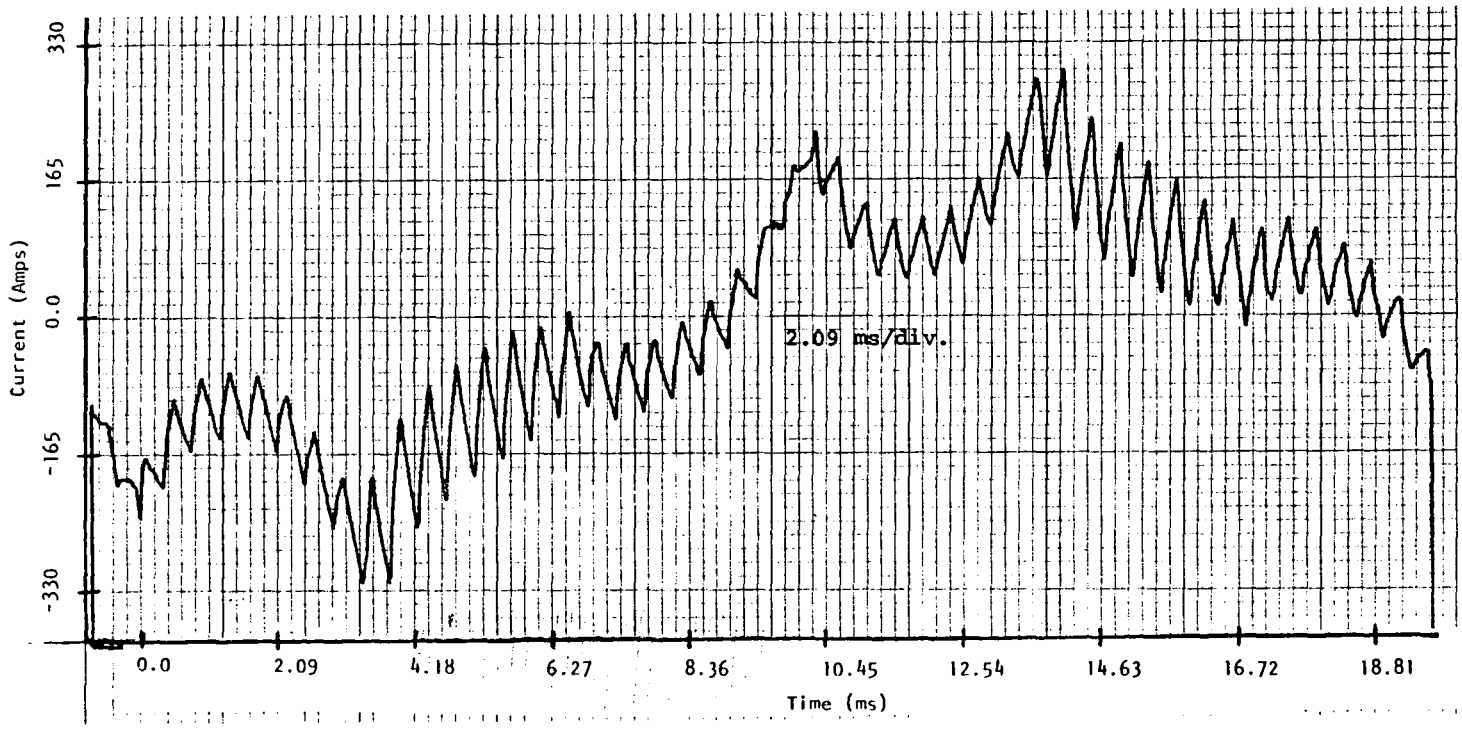

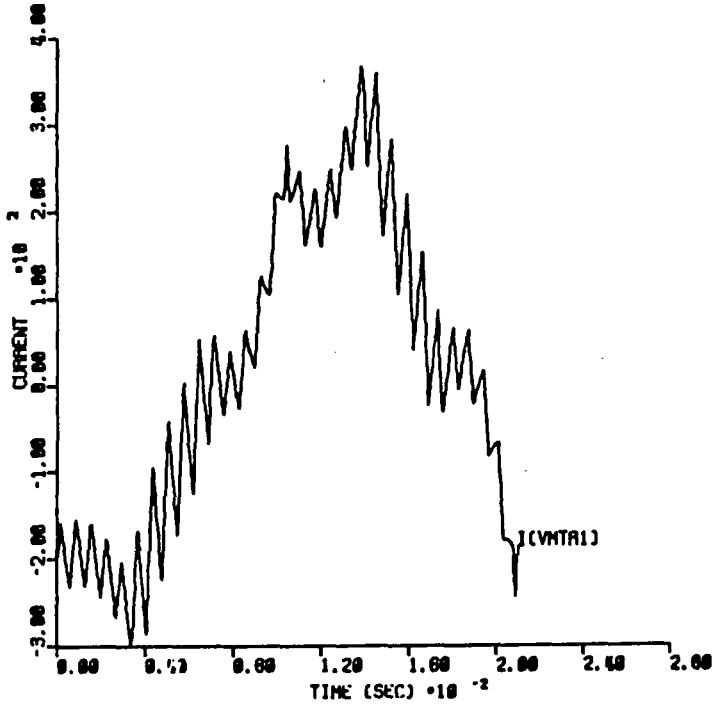

Figure 10.4.19
Inverter Transistor Voltage

Measured (Top)
Frequency = 94.6
Notches = 0

Simulated
Frequency = 94.6
Notches = 0

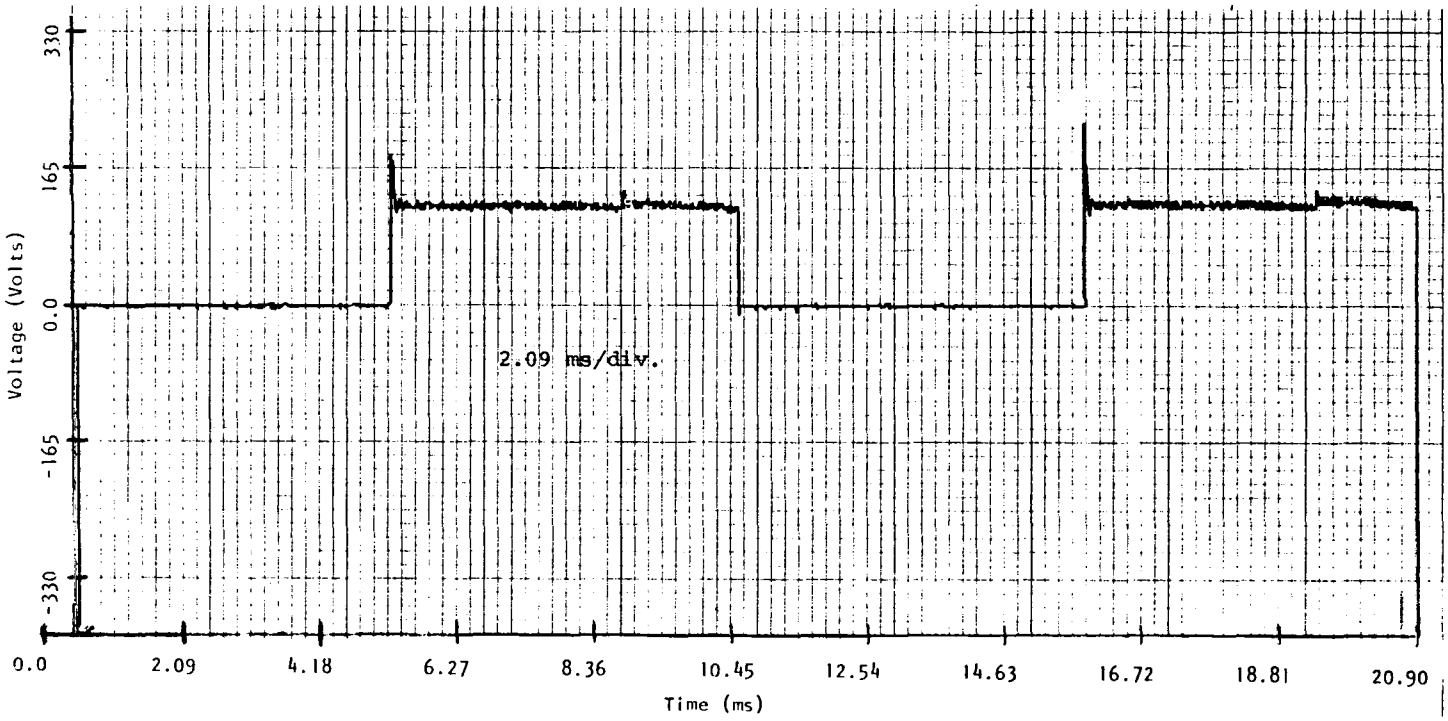

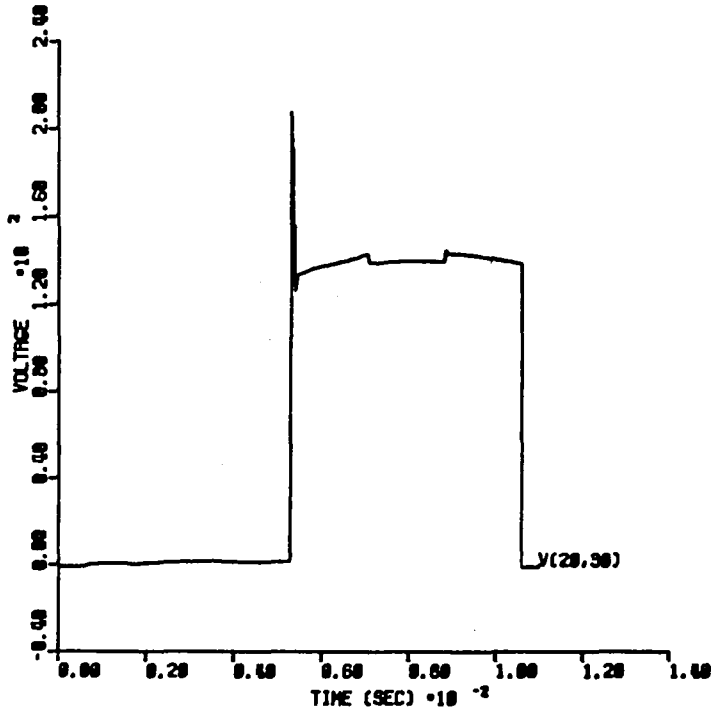

Figure 10.4.20
Inverter Transistor Current

Measured (Top)	Simulated
Frequency = 94.6	Frequency = 94.6
Notches = 0	Notches = 0

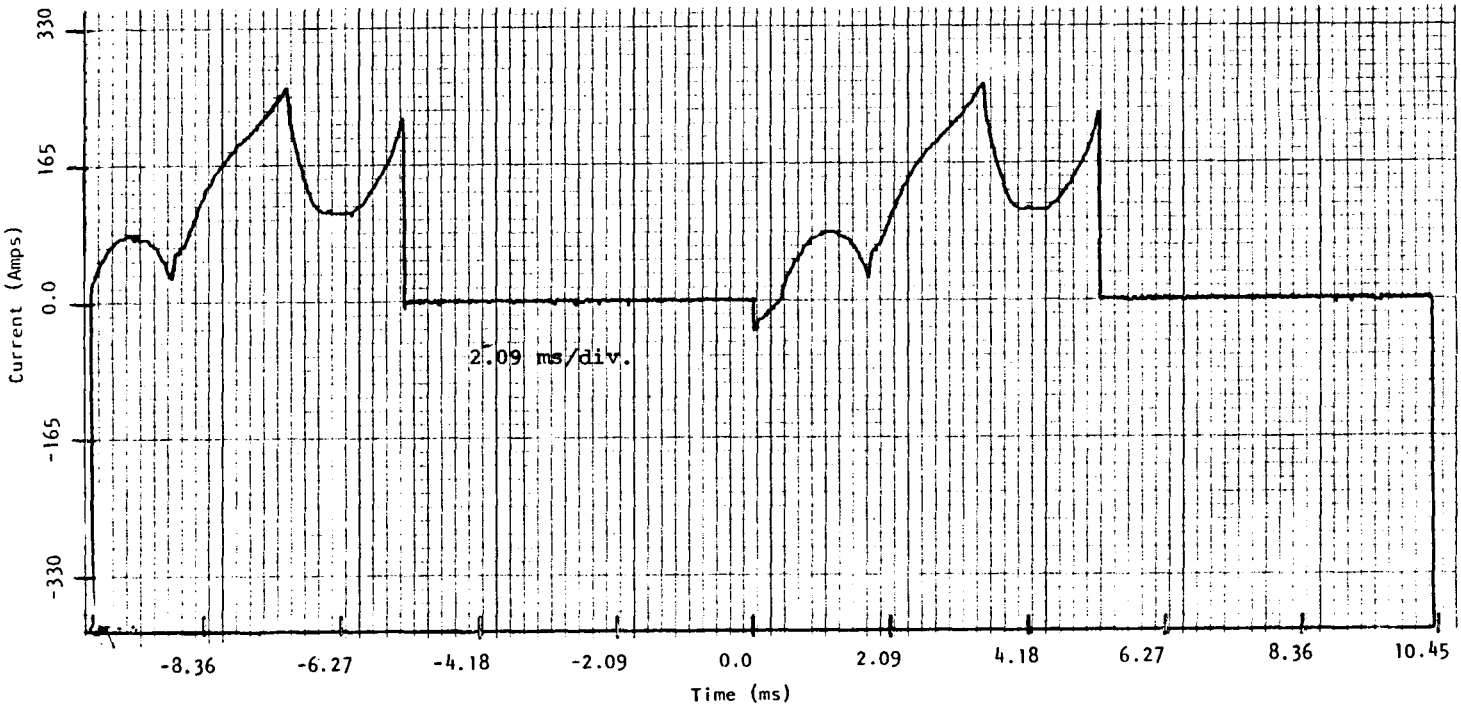

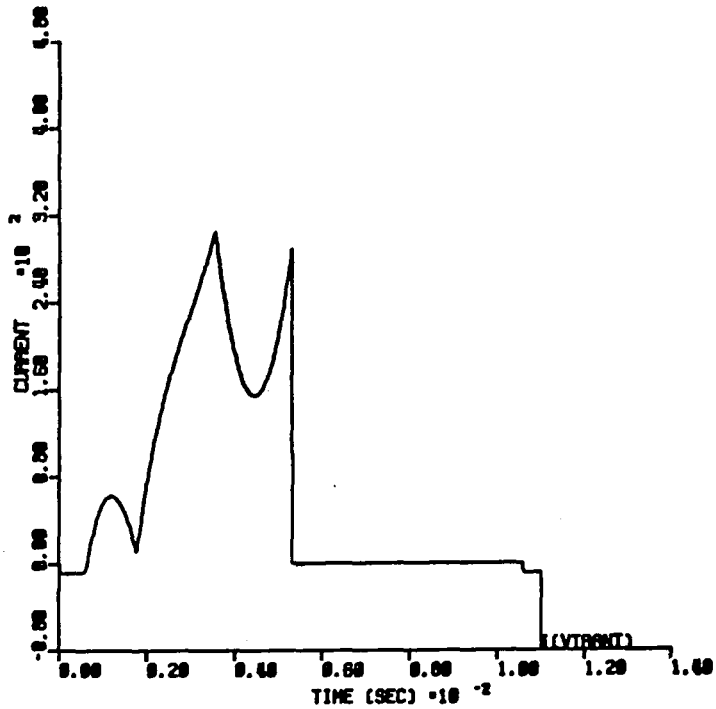

Figure 10.4.21
Inverter Inductor Current

Measured (Top)
Frequency = 95.3
Notches = 0

Simulated
Frequency = 94.6
Notches = 0

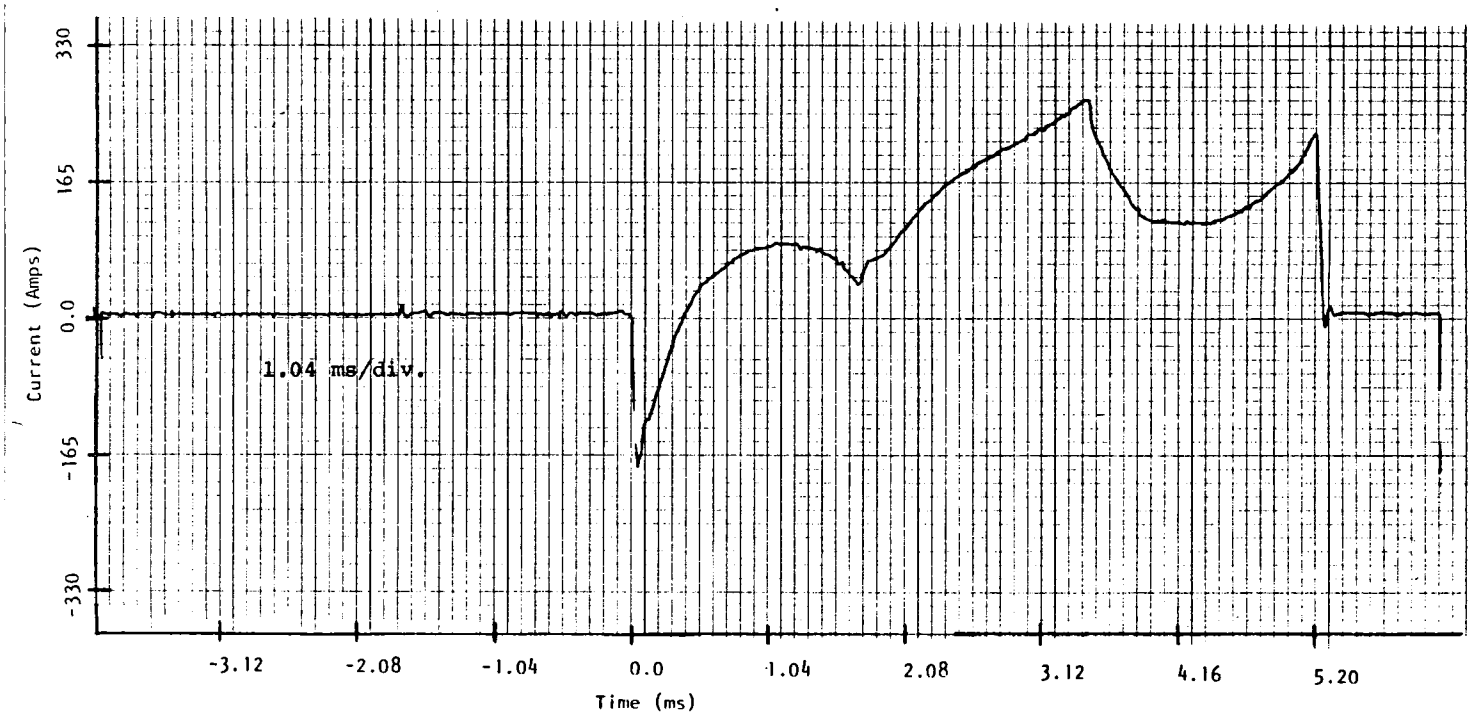

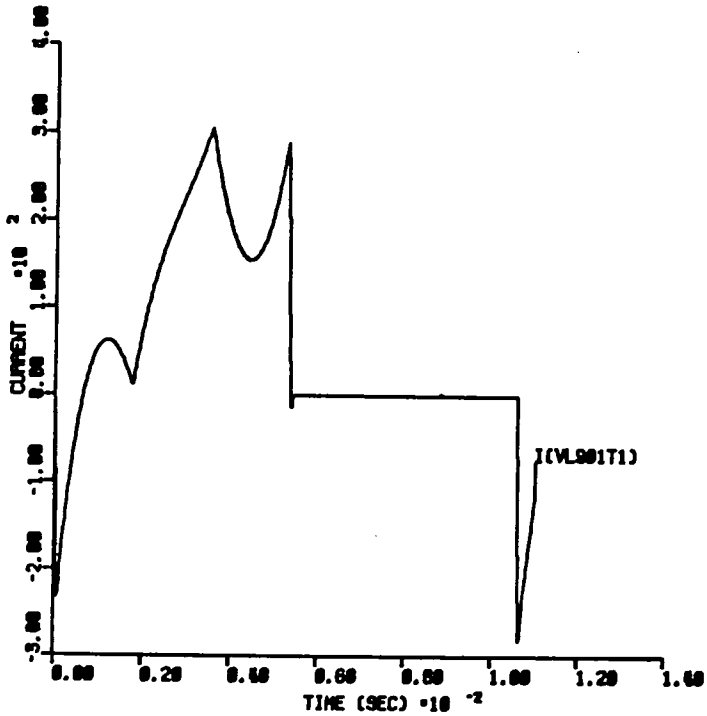

Figure 10.4.22
Motor Current

Measured (Top)
Frequency = 94.6
Notches = 0

Simulated
Frequency = 94.6
Notches = 0

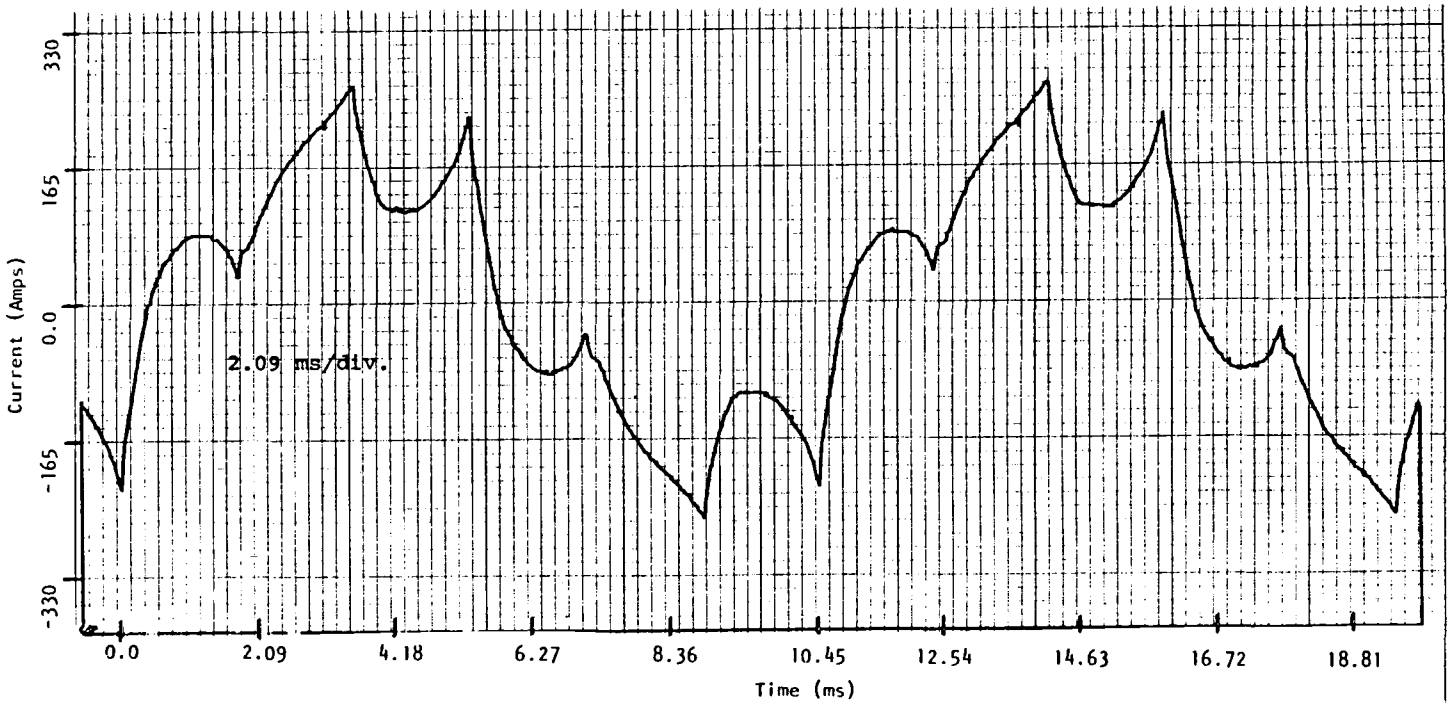

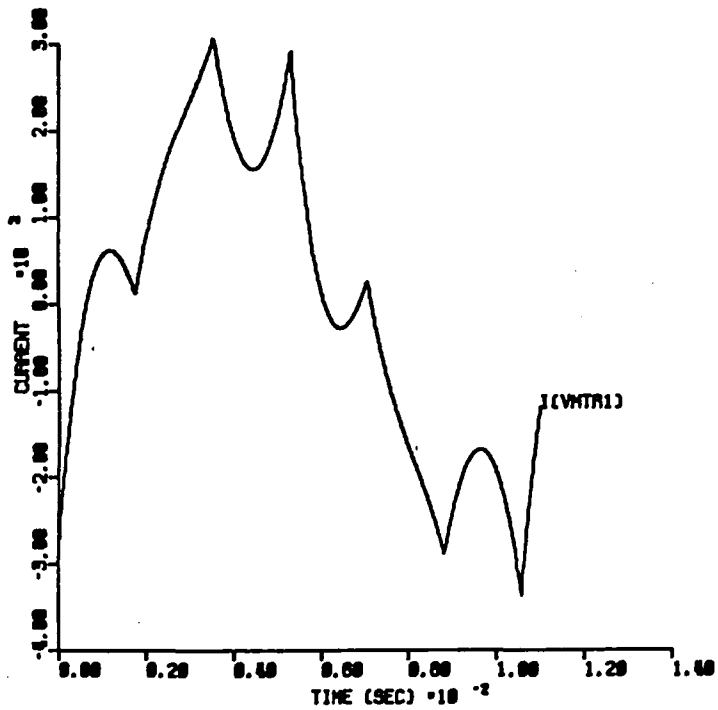

Figure 10.4.23
Inverter Transistor Voltage - One Notch
Measured (Top) Simulated
Frequency = 25.7 Frequency = 70
Notches = 8 Notches = 5

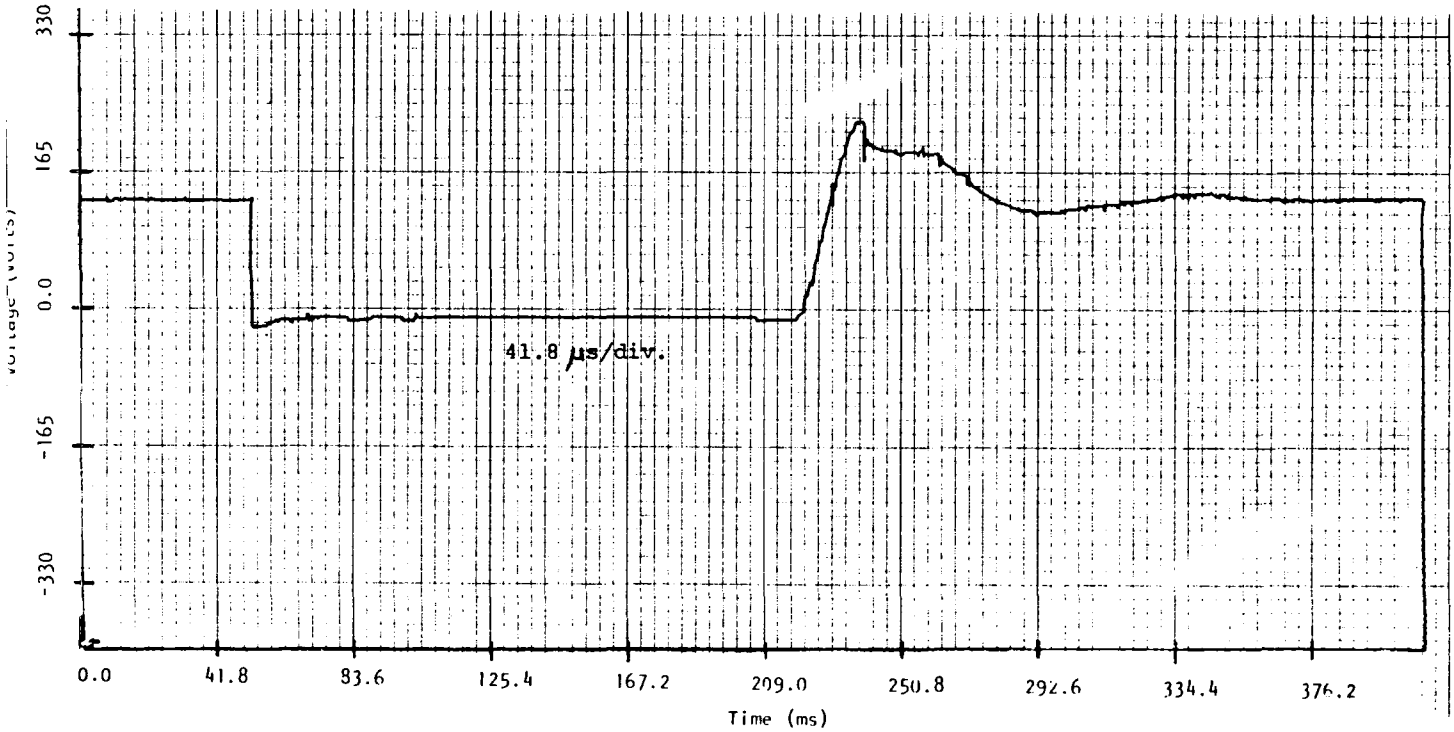

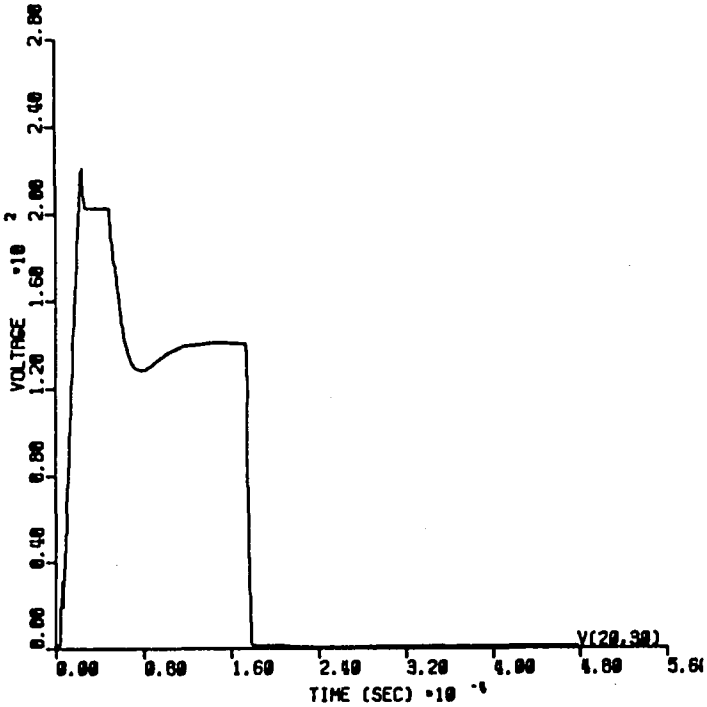

Figure 10.4.24
Inverter Transistor Current - One Notch
Measured (Top) Frequency = 25.7 Notches = 8
Simulated Frequency = 70 Notches = 5

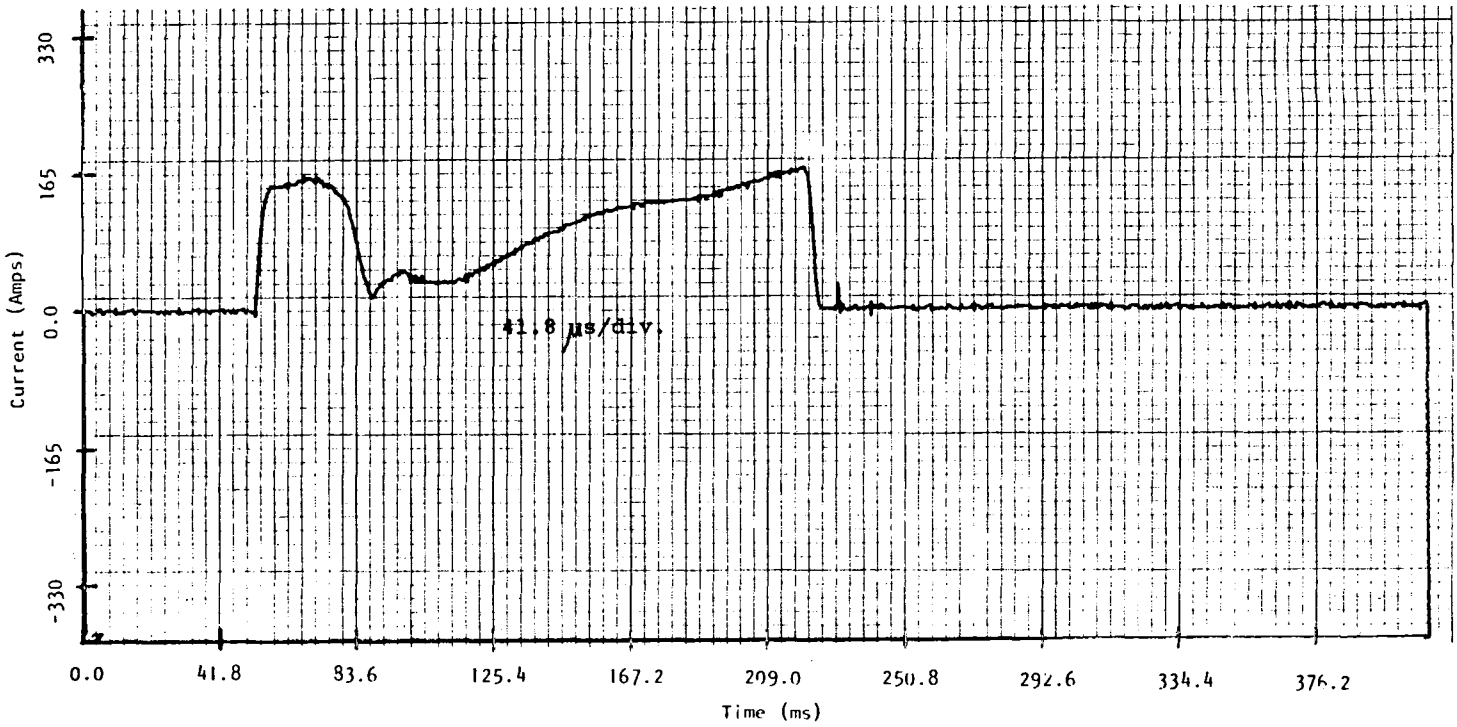

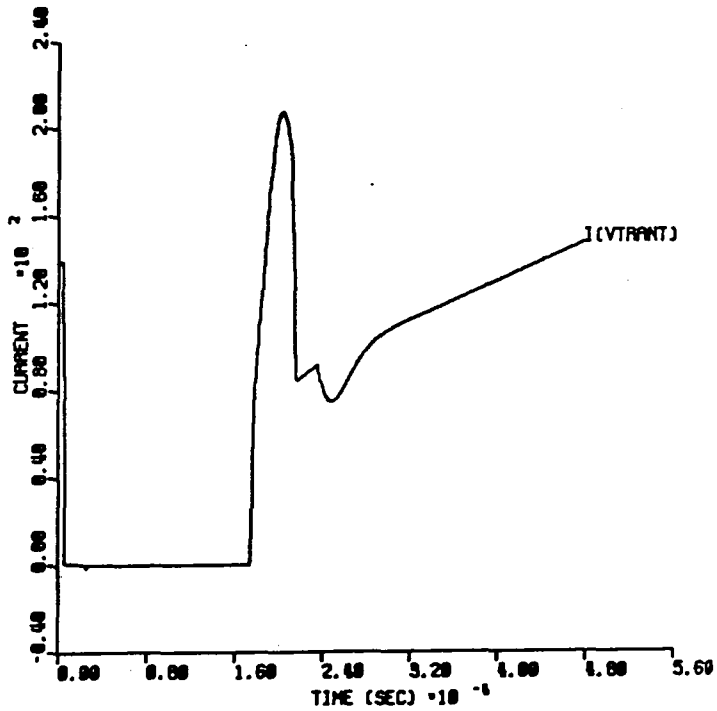

Three operating conditions for the inverter are used for comparative purposes and are summarized in Figure 10.4.25 along with the results from the model and experimental measurements. The formulas used to calculate the losses of the components from the experimental data are given at the bottom of the table. It should be noted that the energy recovery bus losses for the model were also calculated using Equation 3. All other model losses were determined by direct summation of the instantaneous power loss of a component through one cycle of operation.

In the comparison of power loss results, a primary difficulty occurs in determining the snubber inductor conduction losses. Unfortunately, these losses were not determined experimentally and the analytical estimation of Litz wire inductor losses is quite difficult. This problem was circumvented to some extent for the experimental results by calculating all other known losses and attributing the remaining losses to be primarily inductor conduction losses. Although this did not alleviate the problem for the analytical results, they were nevertheless calculated using a similar procedure. In each case, the losses due to each component were summed and the total then subtracted from the average total losses of the corresponding experimental component. The results give a good indication as to the overall correlation of the simulation and experimental results.

The losses due to the inductors could have been determined accurately in the analysis if the frequency dependency of the inductor resistance was known or had been determined experimentally as was the motor inductance and resistance values in the motor analysis section. With this relationship known, the inductor losses could be applied in a post-simulation analysis procedure; i.e., the frequency content of the inductor currents could be determined through a Fourier analysis of the simulation results and the losses then determined.

When comparing the results of the analysis and experimental data, the approximations required in the use of the formulas must be considered. As an example, the experimental transistor conduction losses must be determined based upon an estimate of the transistor saturation voltage. Figure 10.4.26 gives the manufacturer's data of saturation voltage versus collector current for various base drive currents. Based upon this data, the saturation voltage for the 95 Hz range was assumed to be 1.15 volts, 0.9 volts for the 70 Hz range, and 0.95 volts for the 25 to 35 Hz range. Similar approximations are required for the other calculations such as average peak current at transistor turnoff, etc. Given these considerations, the overall experimental and analytical results compare quite closely.

	Frequency (Hz)	Inverter Power In (kw)	Inverter Power Out (kw)	Inverter Efficiency (%)	RMS Current (amps)	Total Inverter Losses (kw)	Snubber Cap Loss (kw)	Snubber Inductor + Misc. Losses (kw)	Energy Recovery Loss (kw)	Transistor & Diode Conduction Loss (kw)	Base Drive Loss** (kw)	Transistor Switching Losses (kw)
Actual	95.8	22.02	20.29	92.1	141	1.73	0.071	1.011	0.024	0.486	0.130	0.008
Actual	96.4	27.73	26.01	93.8	173	1.72	0.067	0.877	0.037	0.597	0.130	0.012
Model	94.6	22.70	20.98*	92.4*	172	1.725*	0.075	0.833*	0.028	0.600	0.130	0.009
Actual	70.9	5.52	4.19	75.8	62	1.33	0.516	0.477	0.028	0.167	0.130	0.012
Model	70.0	6.18	4.85*	78.5*	79	1.33*	0.537	0.336*	0.054	0.255	0.130	0.018
Actual	27.3	4.86	3.22	66.2	94	1.64	0.375	0.786	0.054	0.268	0.130	0.027
Actual	35.3	5.86	4.27	72.8	96	1.59	0.485	0.604	0.070	0.274	0.130	0.027
Model	27.0	5.32	3.71*	69.7*	101	1.615*	0.315	0.787*	0.054	0.309	0.130	0.020

Equations: 1) Snubber Cap Loss = $K(2N + 1)\, f\, c\, v_{bus}^2/2$ (refer to p. 6-20)

2) Transistor Conduction Loss = $I_{RMS}\, V_{CE}$

3) Energy Recovery Loss = $(1 - ERB_{eff})\, L \frac{I^2}{2} (2N + 1)\, f$

4) Transistor Switching Loss = $(2N + 1)\, [I^2\, t_s^2/(24C)]$

*Since snubber inductor ac resistance is unknown, these values were calculated using snubber inductor losses deduced from experimental data.

N = notch number
f = frequency
C = snubber capacitance
I_{RMS} = RMS current
V_{CE} = transistor saturation voltage
ERB_{eff} = energy recovery efficiency
L = snubber inductance
I = current
t_s = switching time as defined in Ref. 16

**Taken from Figure 6.4.4.

Figure 10.4.25 Summary of Actual Versus Simulated Inverter Losses

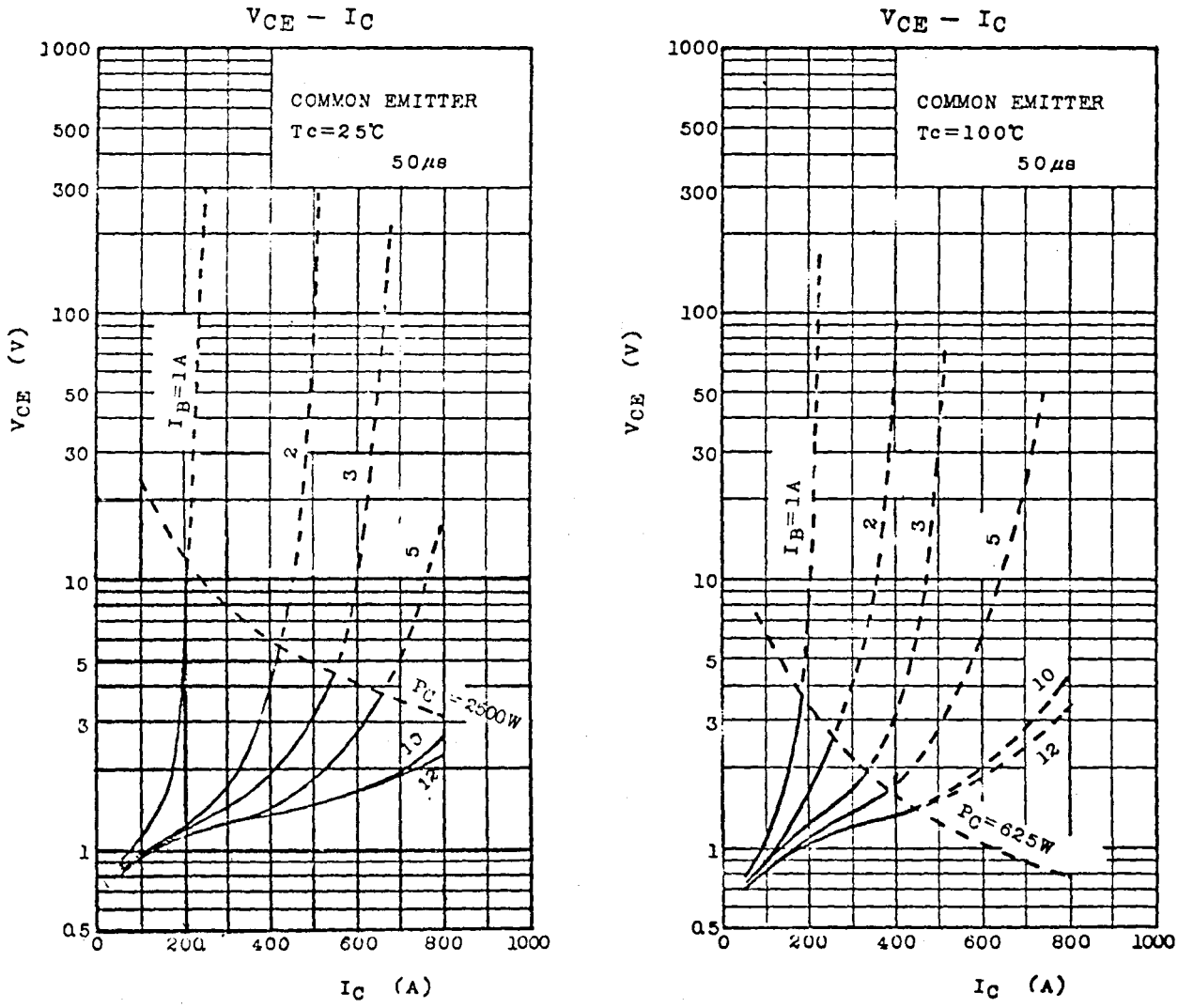

Figure 10.4.26 Toshiba Transistor 2SD648 V_{CE} Versus I_C Manufactures Technical Data

10.5 Inverter Model Results

Experimental and analytical results show (see Figure 10.4.23) that the three primary causes of power loss in the inverter are snubber cap losses, transistor & diode conduction, and snubber inductor conduction losses. The proportion of total power loss of each component varies depending upon the operating conditions. Under higher power and speed 85% of the losses can be caused by transistor and inductor conduction where as at lighter loads this percentage may drop to somewhat below 50%. At high speed and high load (e.g., quasi-square wave operation) the snubber cap losses are negligible, whereas at lower power levels, they can account for 40% of the inverter losses. Since these three loss components comprise over 85% of the total inverter losses, the inverter model was used to investigate modifications to reduce them. The operating point chosen for comparative purposes was 70 Hz stator frequency at low load. This could represent cruising conditions and is not the most efficient operating point for the inverter.

The snubber cap losses can be reduced by reducing the capacitor values. The currently designed snubber caps are oversized to minimize transistor failures, and could be reduced to gain some efficiency. A transistor with higher voltage capability, however, would return the largest benefit in permitting the snubber capacitors to be significantly reduced.

The first configuration analyzed (case 1) represented the operation of a high voltage transistor with operating characteristics similar to the current transistor. The transistor was accompanied with a reduction in the snubber caps to 2 μf compared to previous values of 10 μf and a snubber resistance value of 5 ohms compared to the previous value of 2 ohms.

The second configuration analyzed (case 2) addressed the reduction of both transistor and inductor conduction losses. This was achieved through an increase in the bus voltage to 192 volts which also implies an increase in the number of batteries which must now be contained in the vehicle. Again, the configuration included a high voltage transistor and the same change in snubbers as indicated in the case above. Also included in this case was a model of a motor designed to operate at higher volts/hz. The motor parameters are outlined in the motor analysis section. (See Figure 10.2.7.)

The third configuration was an outgrowth of the motor analysis, which indicated that an increase in notch numbers could increase motor efficiency by approximately 1%. This configuration was analyzed to see if an

increase in notch number would cause power loss increases in the inverter which would more than offset the increased efficiency of the motor.

Analysis Results

The power loss results of the three cases are summarized in Figure 10.5.1 along with the current design as the base of comparison. The transistor current and voltage, inductor current and motor current waveforms are given in Figures 10.5.2 to 10.5.17, for reference. Figure 10.5.1 compares only the three primary power loss contributions; i.e., snubber capacitor, transistor conduction, and inductor conduction losses. The inductor losses in each case are approximated by using a 0.02 ohm ac resistance value. This value was chosen based upon the results in Figure 10.4.23.

A dramatic improvement is seen in case 1 with the reduction of the snubber capacitor losses. As mentioned before, with operating conditions of low load where snubber capacitor losses can make up 40% of the total losses, the result could reduce total power loss by nearly 20%. However, this gain is lost under higher load/speed operating conditions.

The greatest improvement resulted with case 2 which does not exhibit quite the improvement in snubber cap losses as in case 1 but significant reductions are made in conduction losses. It should be noted that in this case the improvements will be even greater under higher load conditions, and reduction in total power loss could reach 40%.

Finally the results of case 3 would indicate that an increase in notch number would negatively affect the inverter performance to eliminate any gains obtained in motor efficiency. However, a range of operating conditions should be investigated before reaching a final conclusion.

The improvements due to a high voltage transistor accompanied with higher bus voltage is amplified if the conduction losses are corrected based upon inverter power level. This has been done in Figure 10.5.18 for cases 1 and 2. The snubber losses are kept the same in both cases but the conduction losses ratioed up or down dependent upon power level, to more nearly approximate the current design operating conditions. The results indicate considerable improvement for the higher bus voltage configuration. The reduction in power loss under conditions when conduction losses approach 85% could improve inverter efficiency by as much as 43%, and approach an improvement of 20% when snubber losses account for the greater part of the loss.

	Frequency (Hz)	Inverter Power In (kw)	Notch Number	RMS Current (Amps)	Snubber Cap Losses (kw)	Transistor Conduction Losses (kw)	Snubber* Inductor Losses (kw)	Total Primary Losses (kw)	Percent of Current Design
Current Design	70	6.177	5	78.8	0.537	0.246	0.388	1.171	100
Case 1	70	5.374	5	74.5	0.102	0.240	0.330	0.672	57
Case 2	70	6.975	5	65.7	0.168	0.213	0.258	0.639	55
Case 3	70	8.037	10	66.1	0.315	0.279	0.262	0.856	73

* Losses approximated by using an ac resistance value of 0.02 ohm based upon average losses of Figure 10.4.23

Figure 10.5.1 Summary of Primary Losses of Improved Inverter Designs

Figure 10.5.2 Current Inverter Design at 70 Hz Transistor Voltage

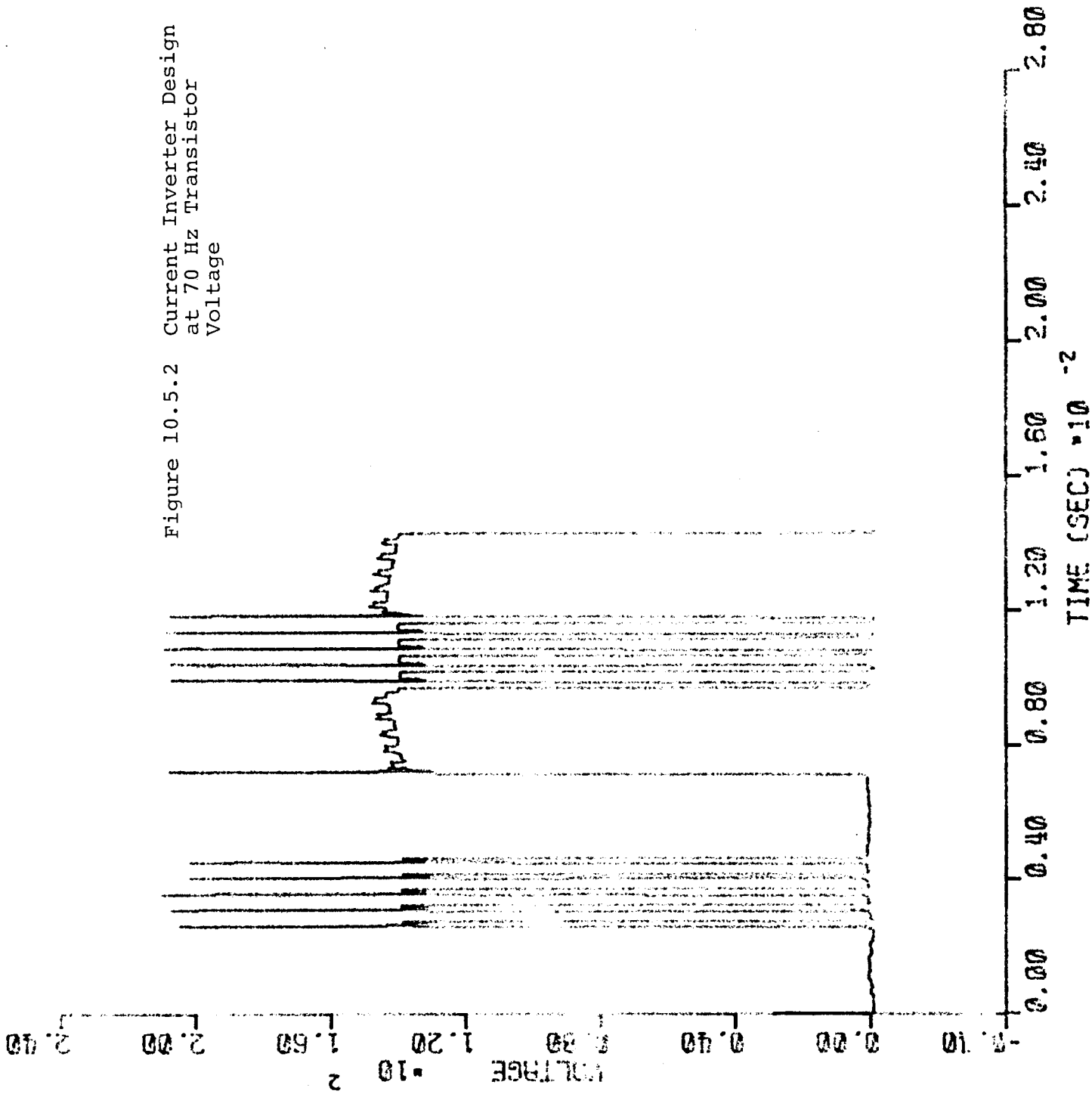

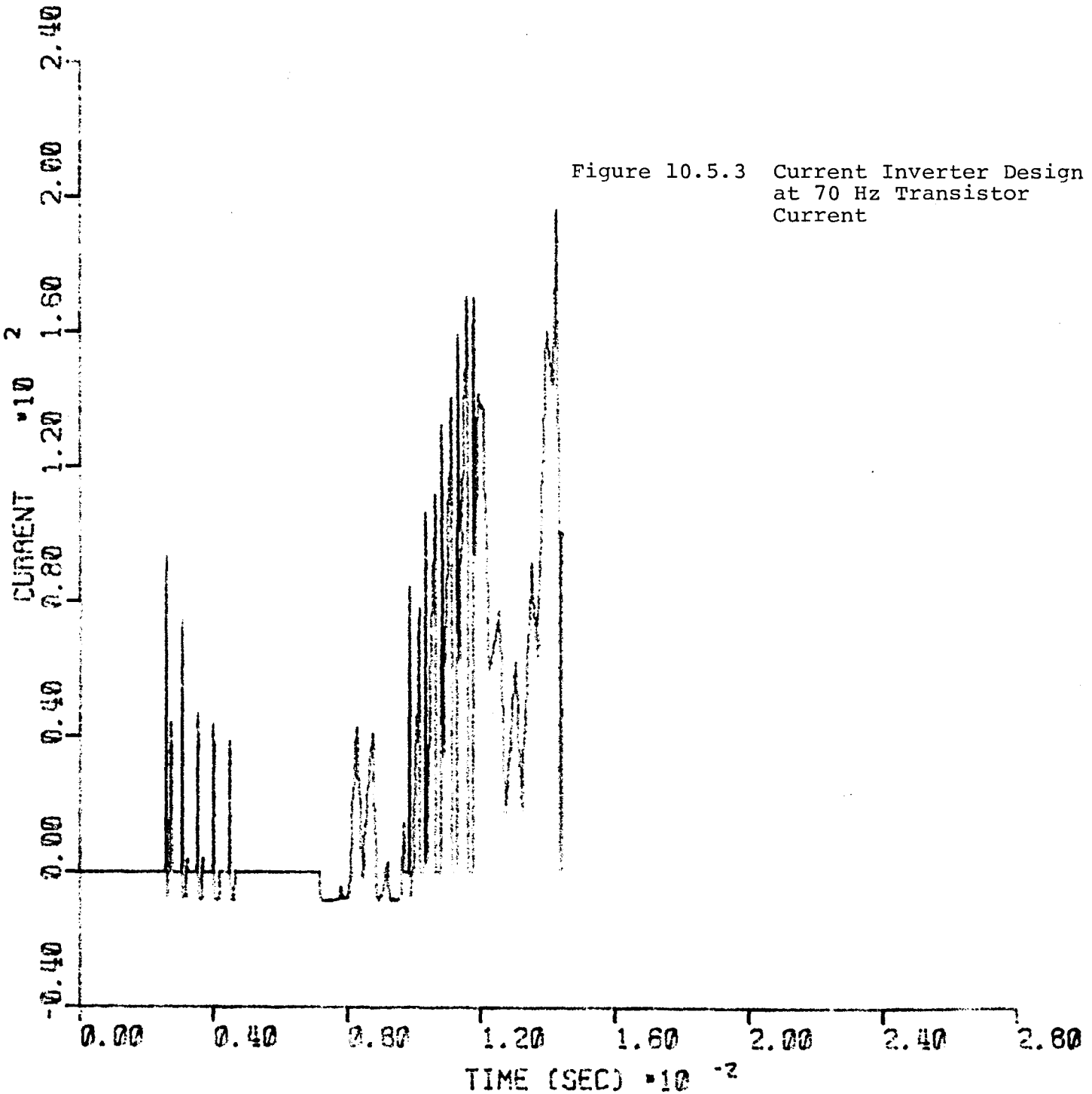

Figure 10.5.3 Current Inverter Design at 70 Hz Transistor Current

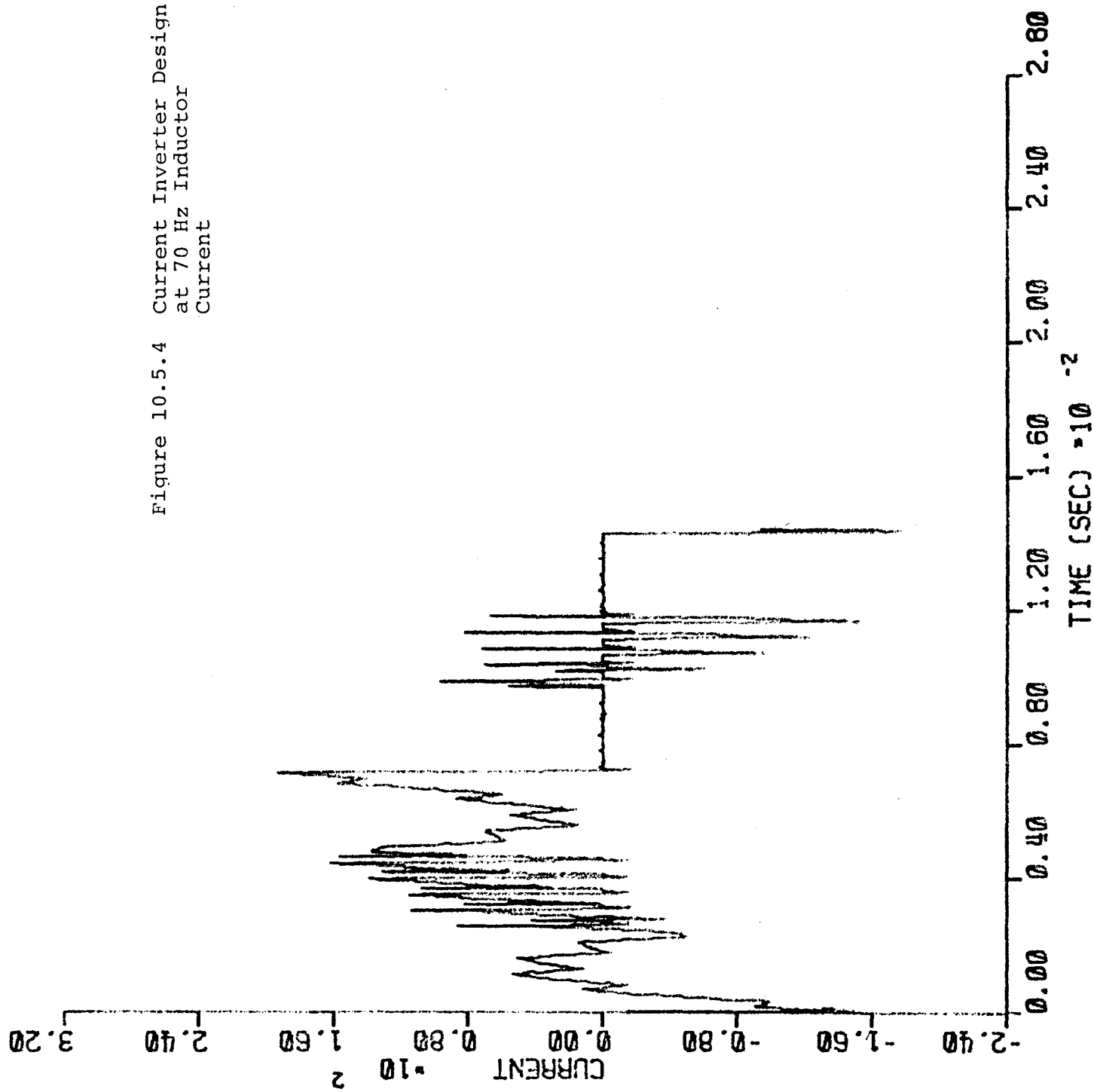

Figure 10.5.4 Current Inverter Design at 70 Hz Inductor Current

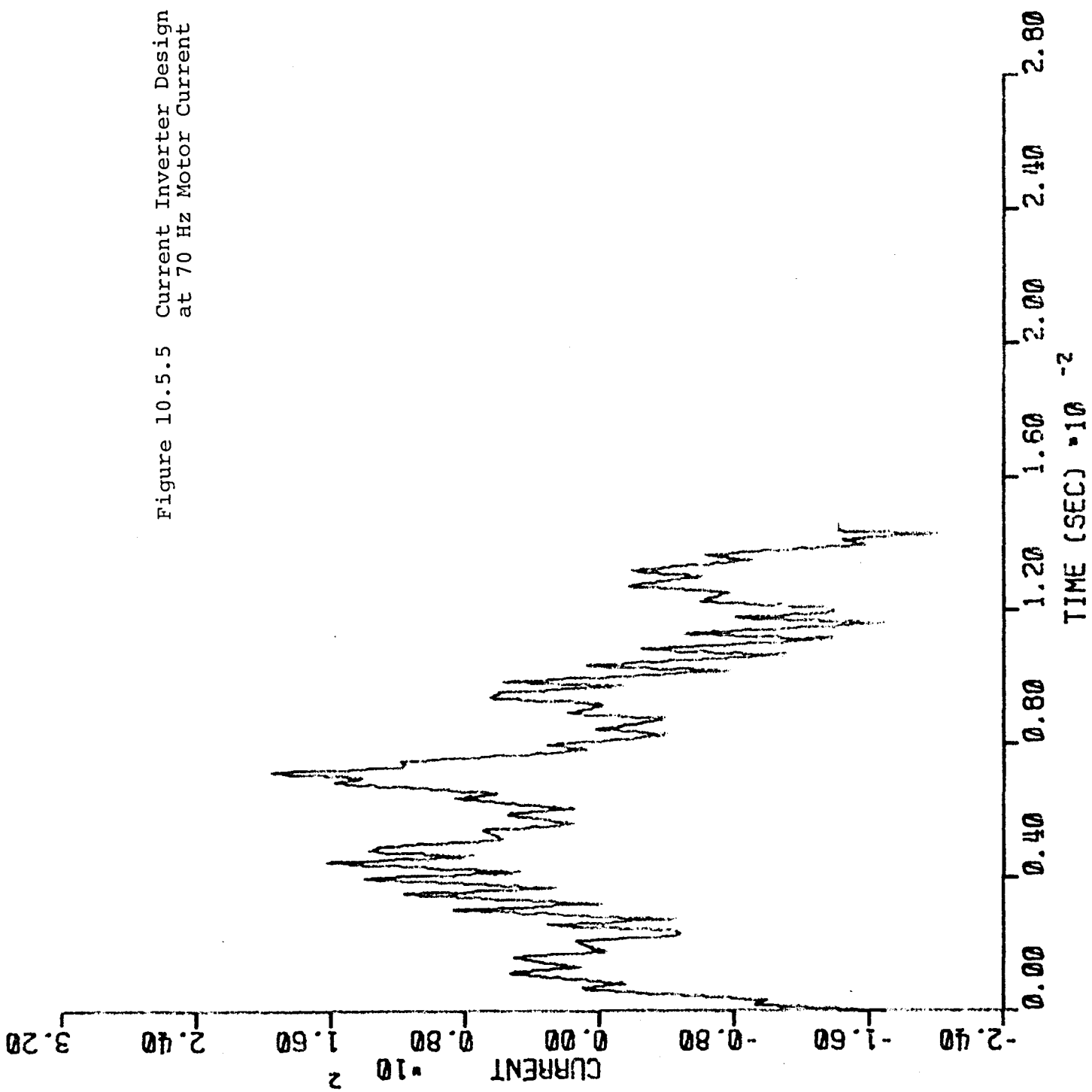

Figure 10.5.5 Current Inverter Design at 70 Hz Motor Current

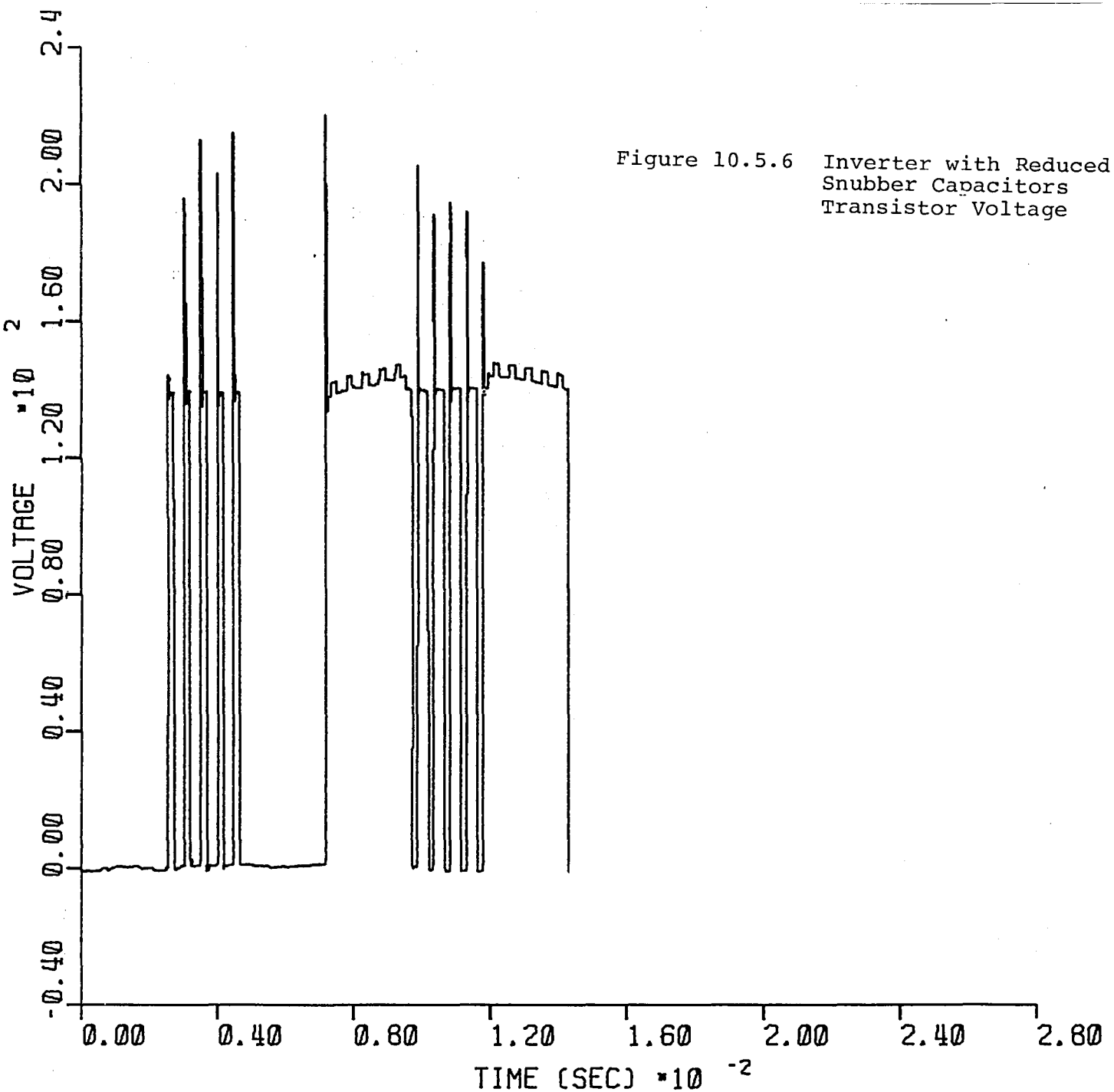

Figure 10.5.6 Inverter with Reduced Snubber Capacitors Transistor Voltage

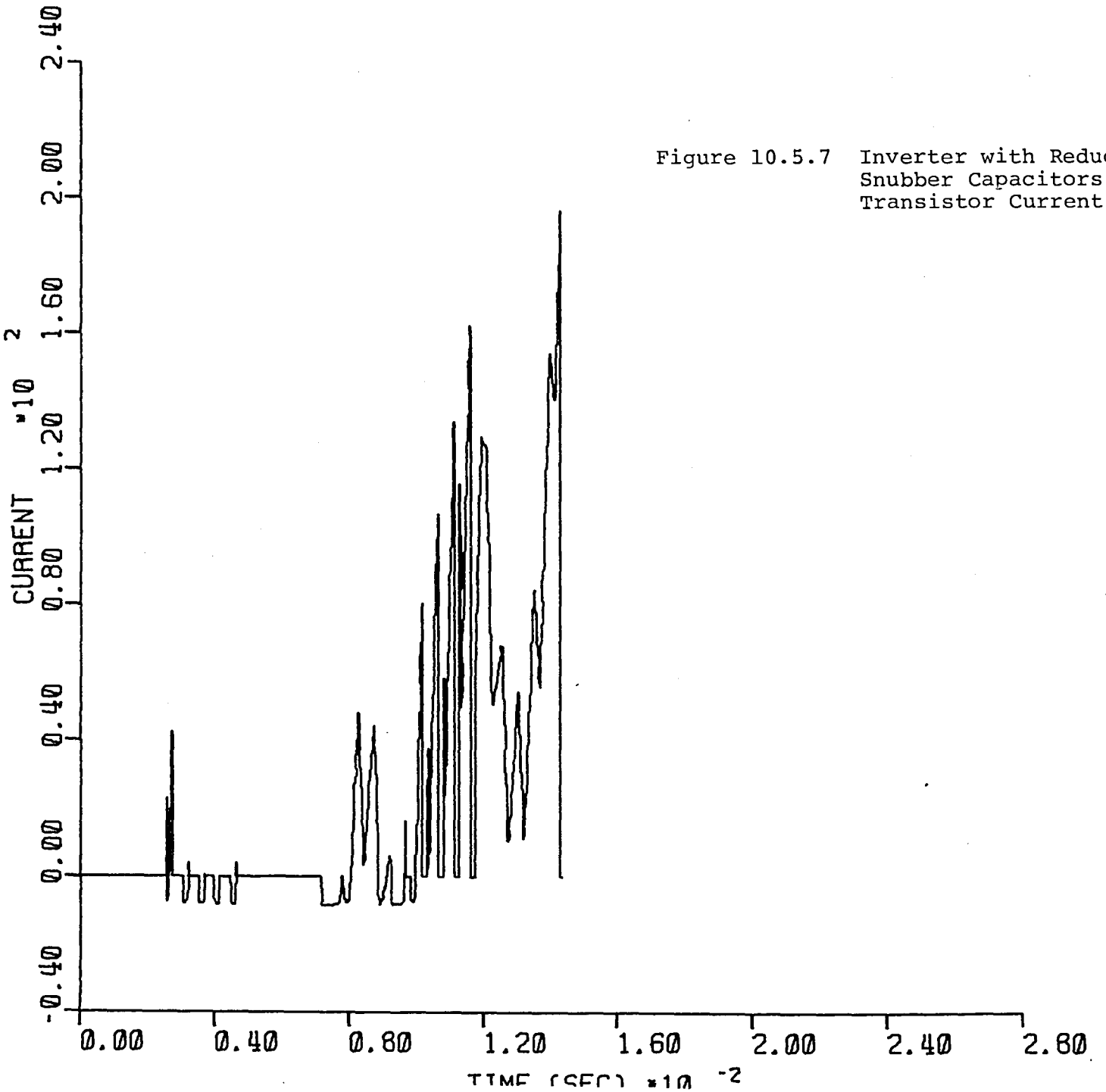

Figure 10.5.7 Inverter with Reduced Snubber Capacitors Transistor Current

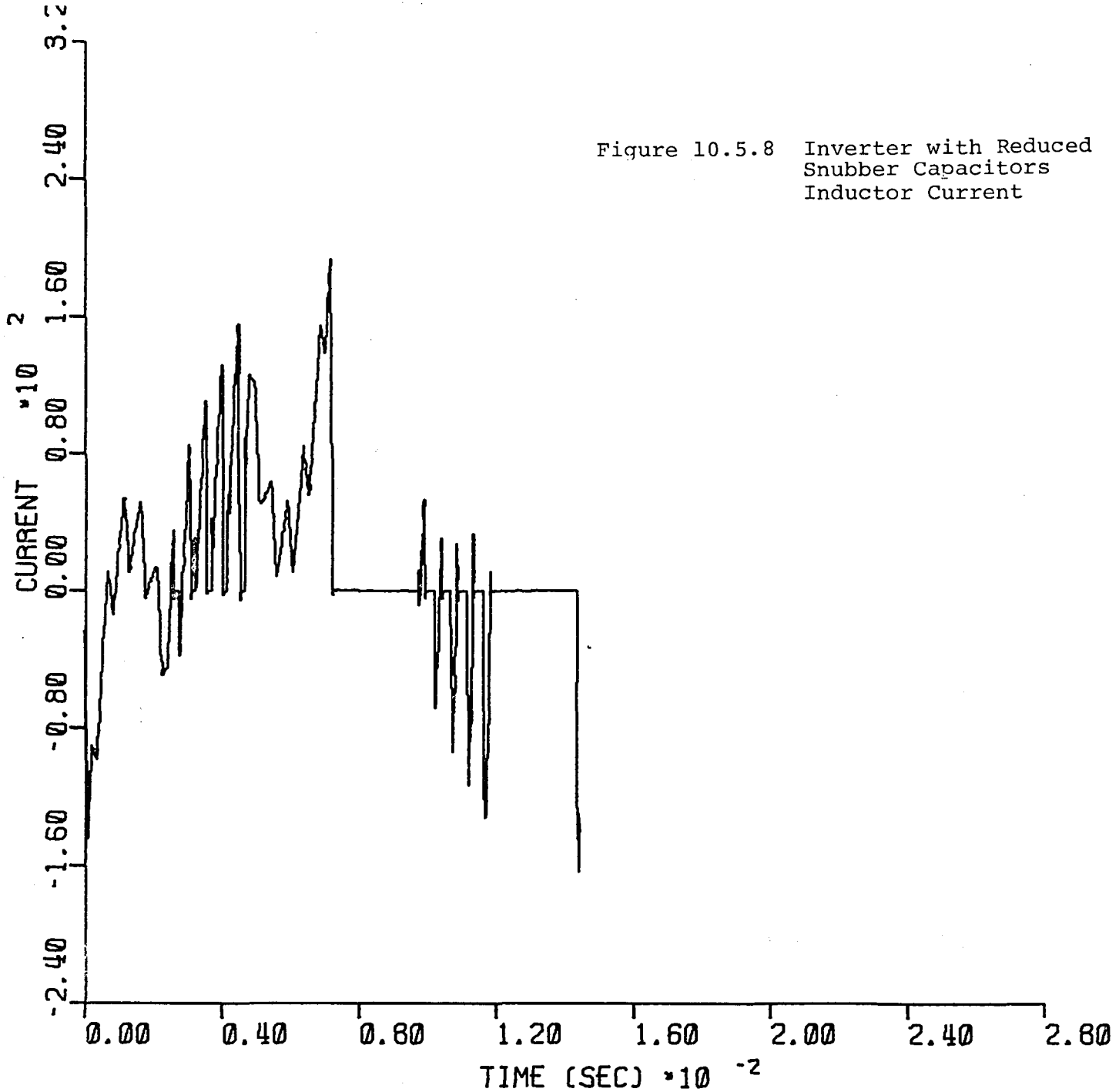

Figure 10.5.8 Inverter with Reduced Snubber Capacitors Inductor Current

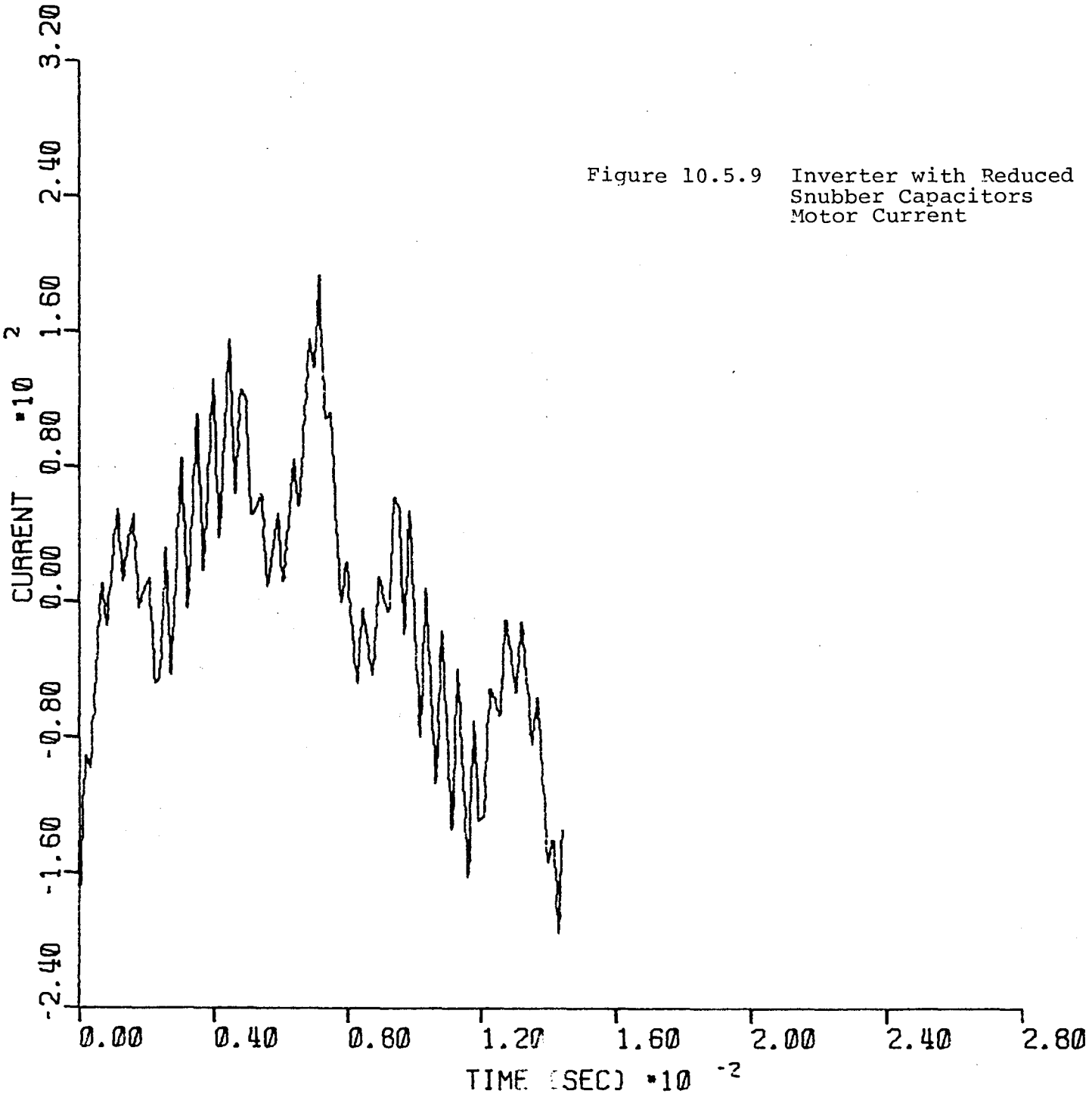

Figure 10.5.9 Inverter with Reduced Snubber Capacitors Motor Current

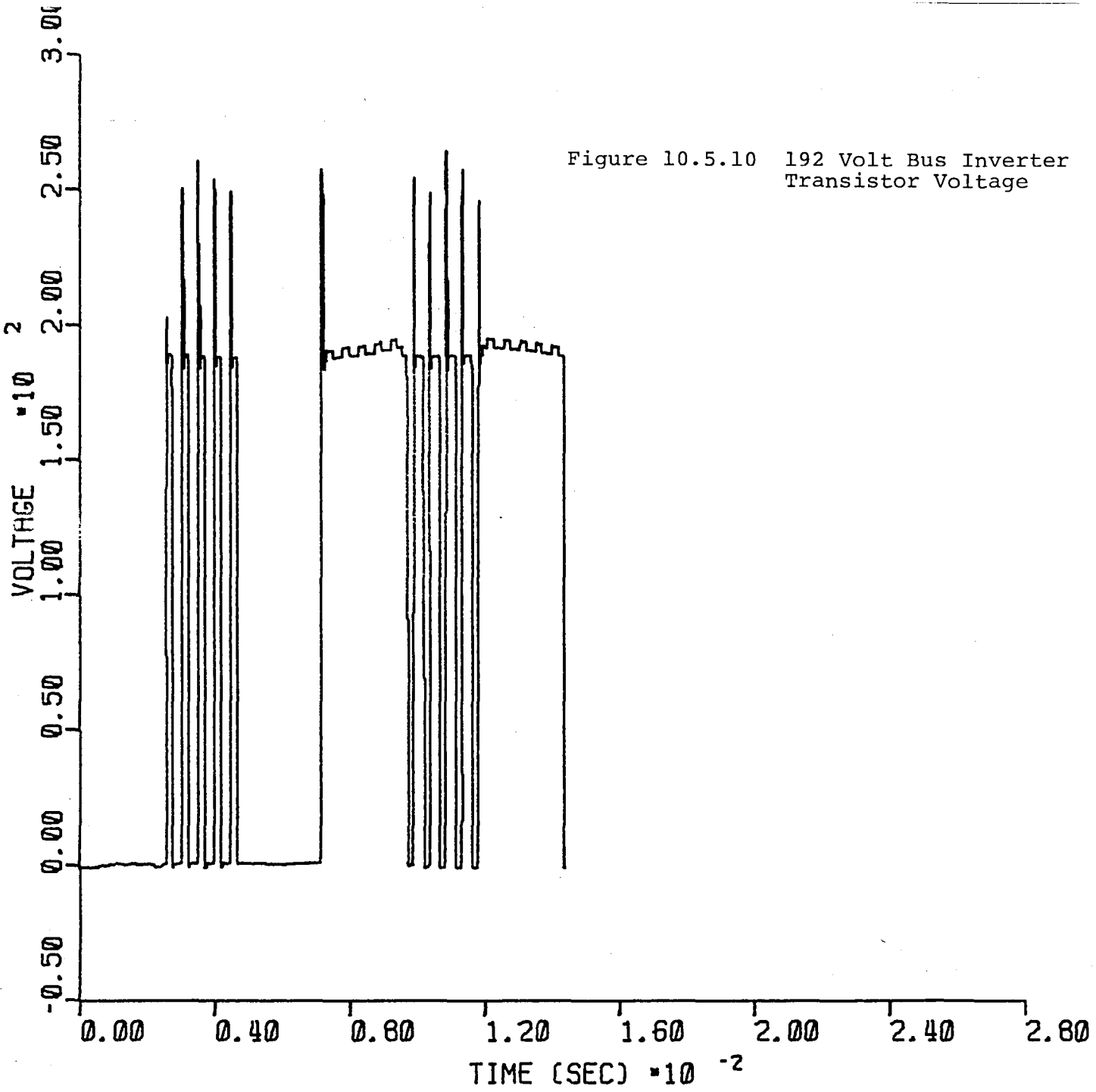

Figure 10.5.10 192 Volt Bus Inverter Transistor Voltage

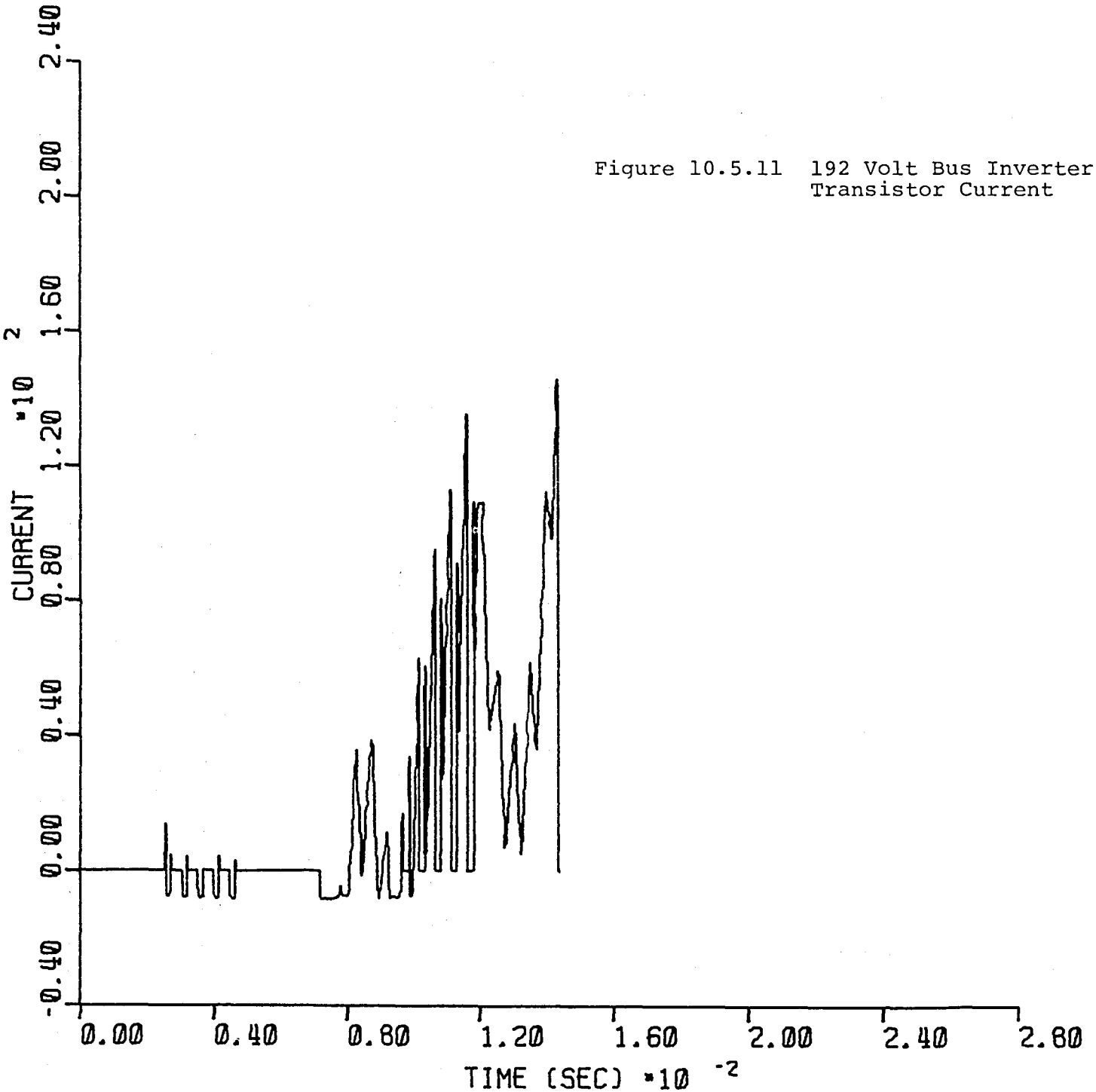

Figure 10.5.11 192 Volt Bus Inverter Transistor Current

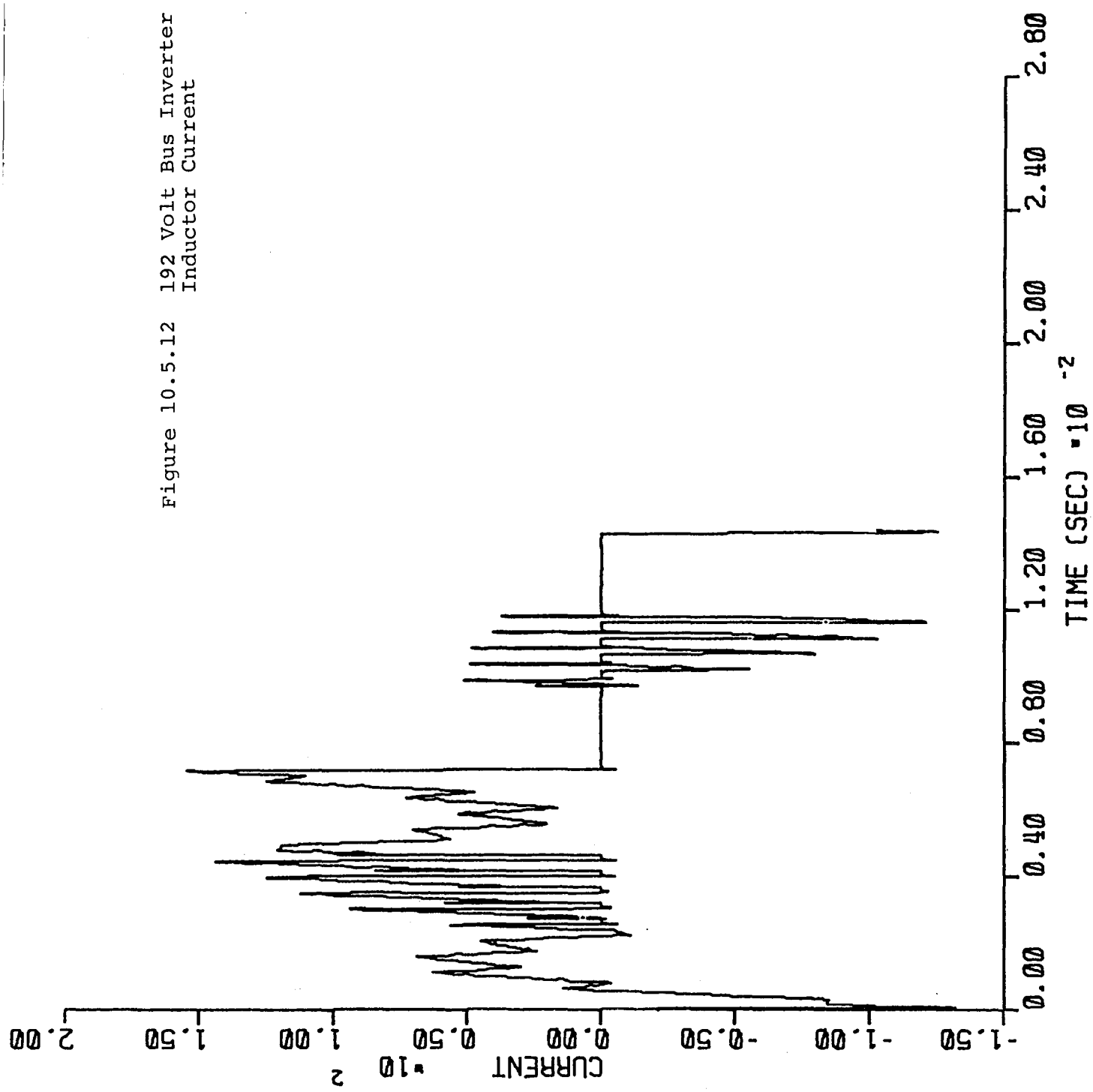

Figure 10.5.12 192 Volt Bus Inverter Inductor Current

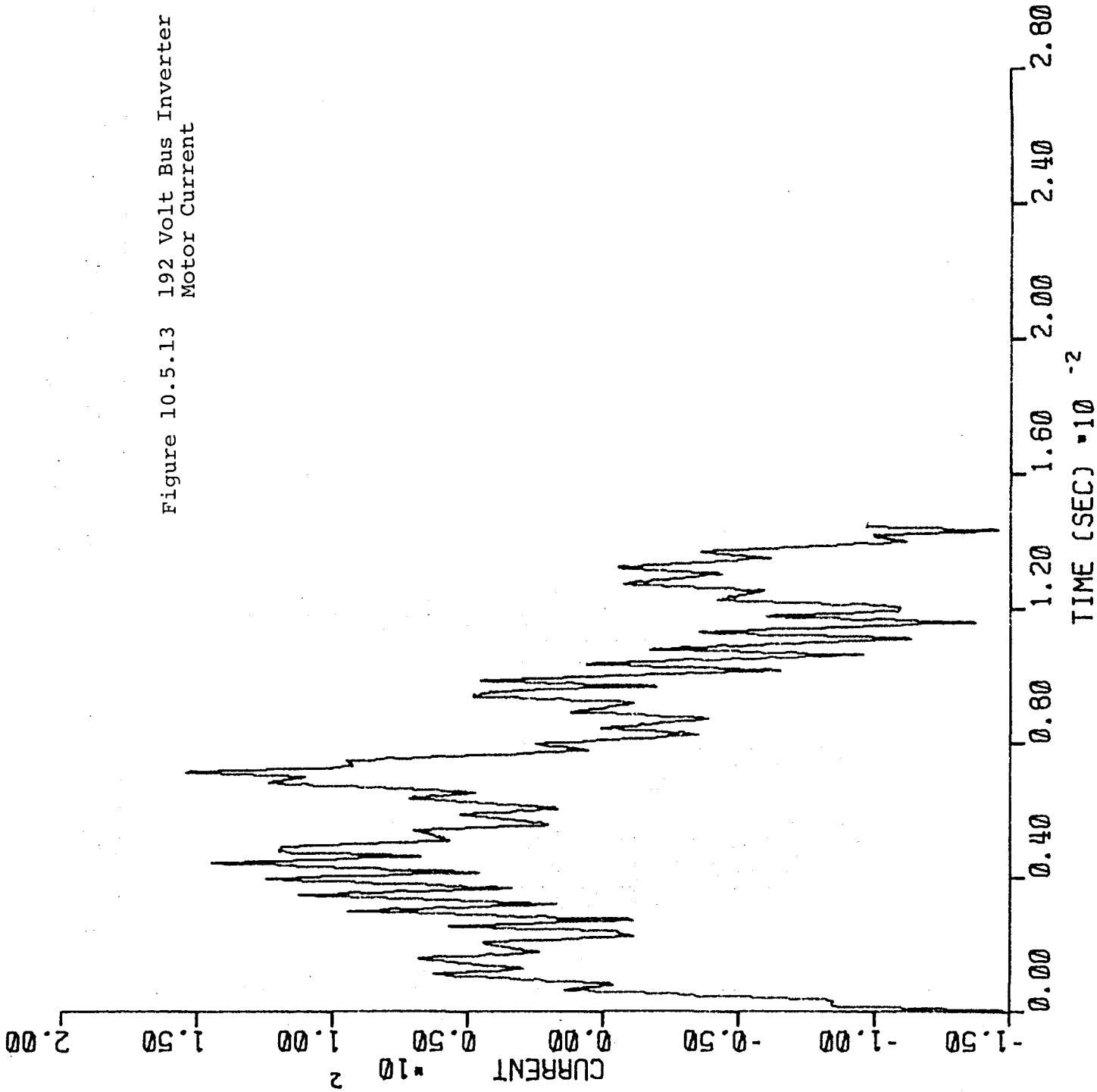

Figure 10.5.13 192 Volt Bus Inverter
Motor Current

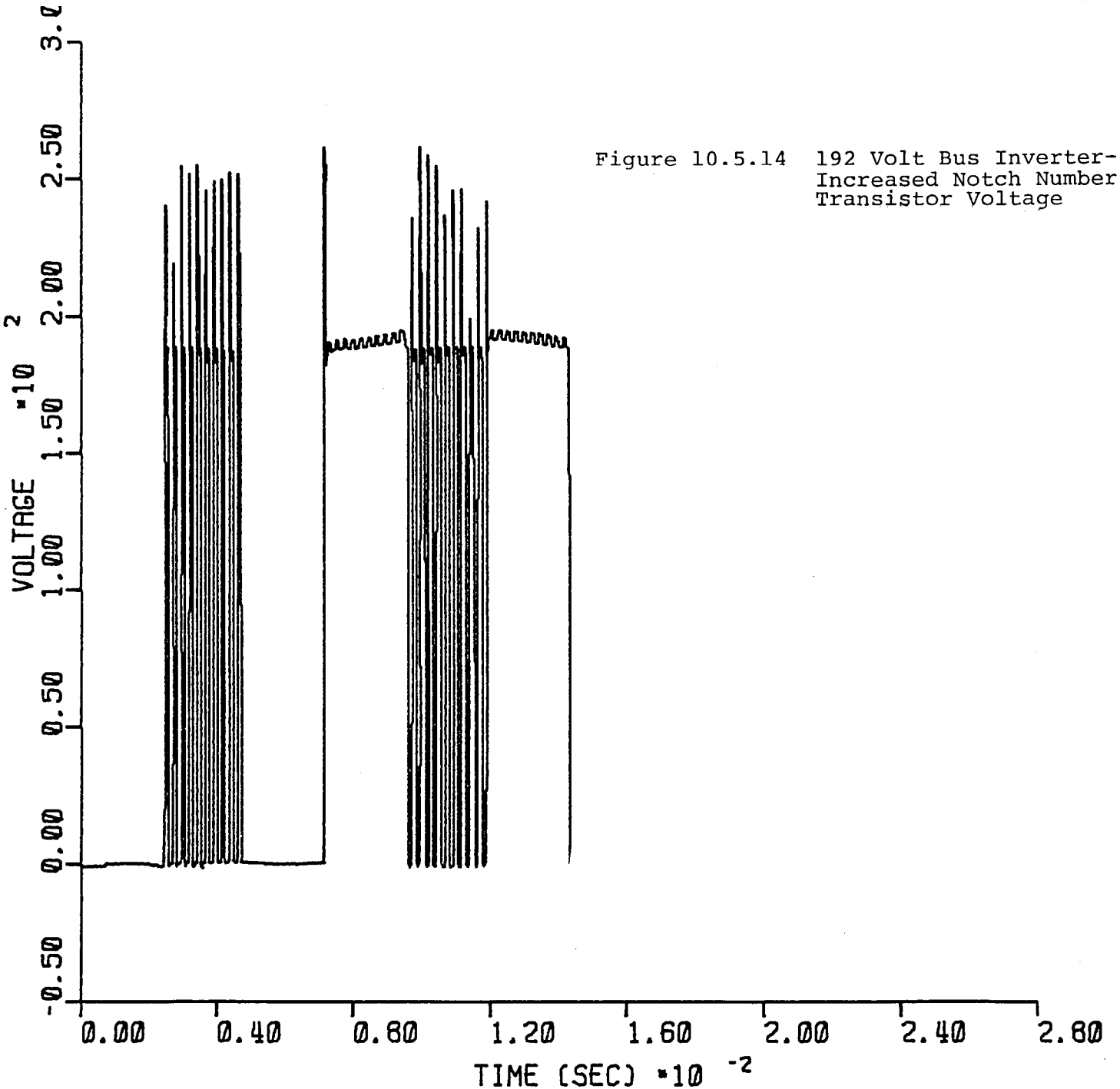

Figure 10.5.14 192 Volt Bus Inverter-Increased Notch Number Transistor Voltage

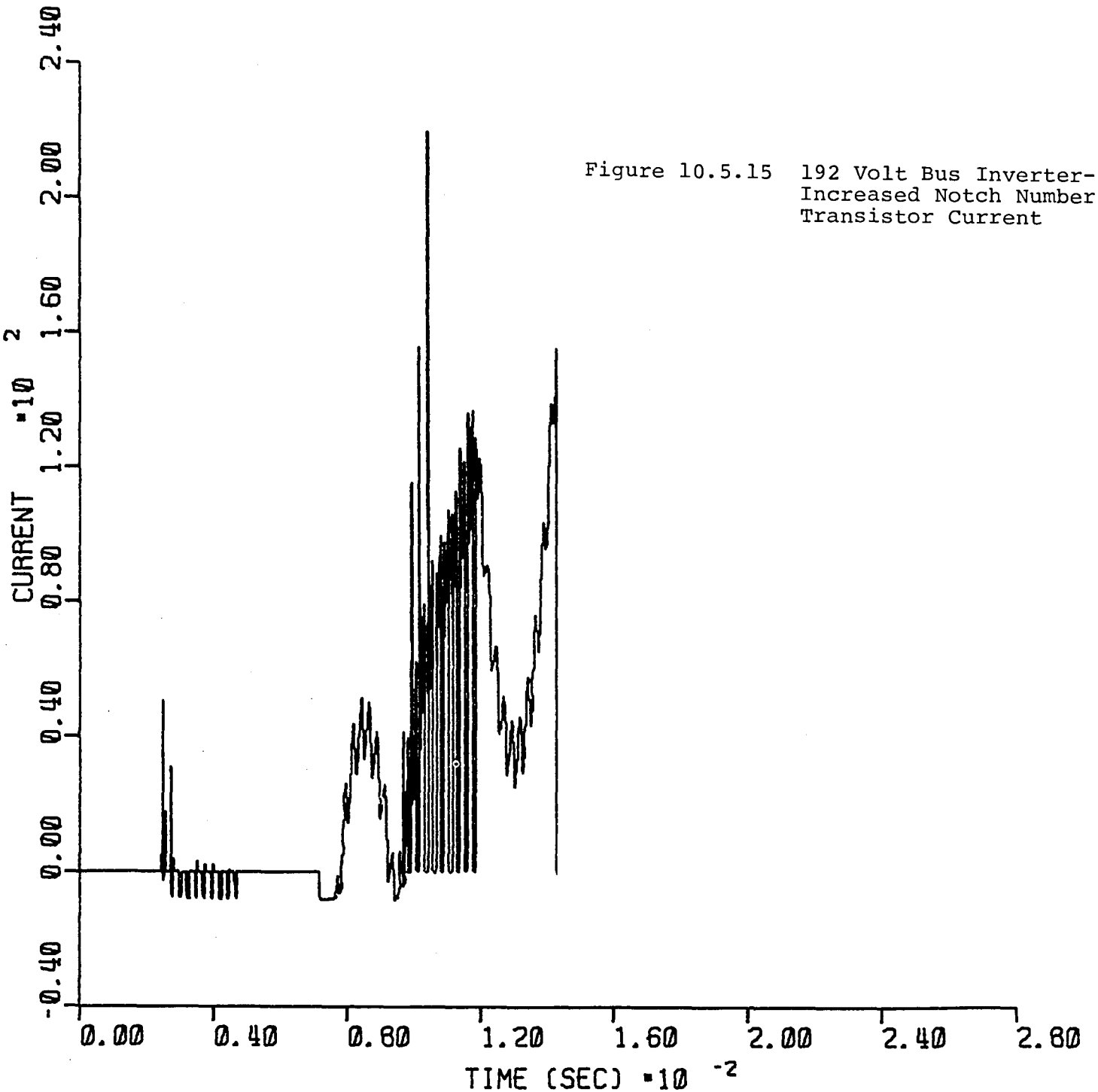

Figure 10.5.15 192 Volt Bus Inverter-Increased Notch Number Transistor Current

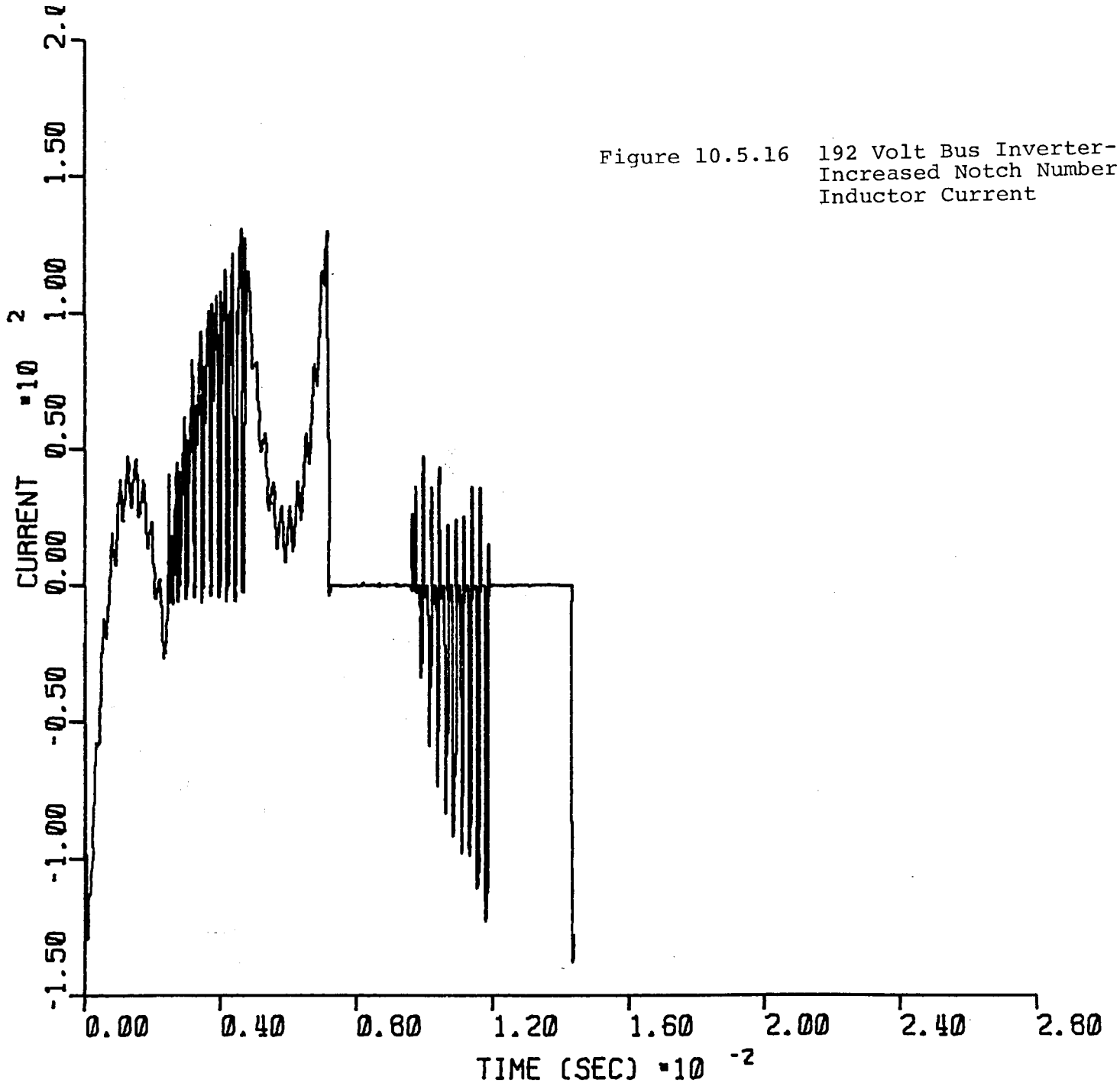

Figure 10.5.16 192 Volt Bus Inverter-Increased Notch Number Inductor Current

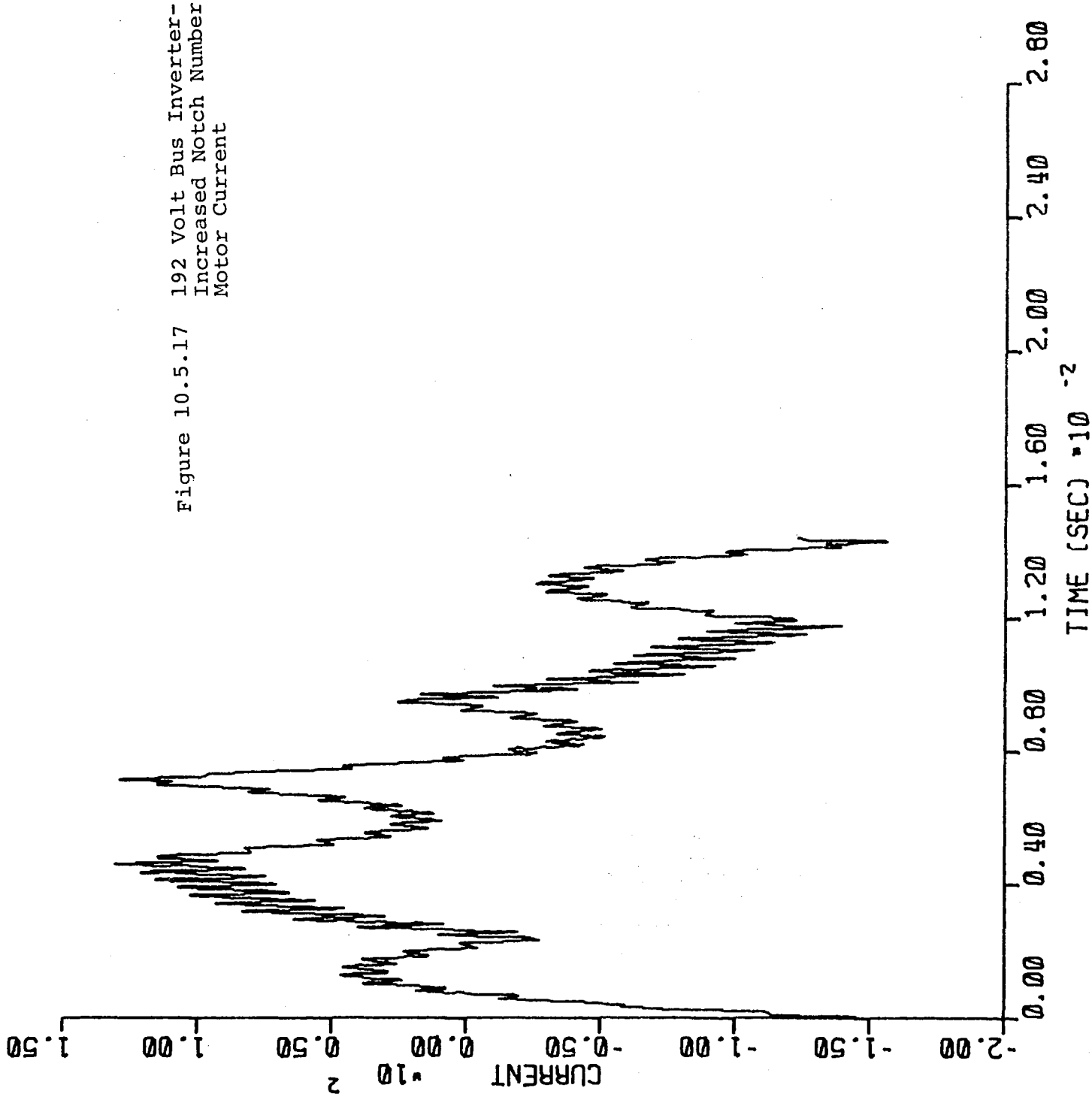

Figure 10.5.17 192 Volt Bus Inverter-Increased Notch Number Motor Current

The gain in inverter efficiency with the higher voltage must be weighed against the increase in battery weight and the packaging consideration involved.

	Snubber Cap Losses (kw)	Transistor Conduction Losses (kw)	Snubber Inductor Losses (kw)	Total Primary Losses (kw)	Percent of Current Design
Current Design	0.537	0.246	0.388	1.171	100
Case 1	0.102	0.276	0.379	0.757	65
Case 2	0.168	0.189	0.228	0.585	50

Figure 10.5.18 Conduction Losses Corrected to Current Design Based Upon Inverter Power Level

Concluding Remarks on Inverter Analysis

The cases investigated indicate a clear improvement in inverter efficiency over all operating ranges can be obtained with higher operating voltage. Further improvements are foreseen in other design changes which will be considered in the future. Though larger improvements may not be made in inverter efficiency, there are other gains to be made in packaging and cost reduction through redesign. One consideration which was not undertaken here is the redesign of the current energy recovery bus. The current configuration is too complex to analyze in concurrence with the inverter model but it is recognized that design improvements can be made. Another design consideration is the filter capacitors which if reduced in size can reduce packaging requirements.

10.6 Vehicle Model Development

The Boeing Computer Services HEAVY program was the computer simulation program used to study the Eaton induction machine, drive, and transaxle performance in a vehicle. Eaton co-developed the induction machine and inverter models with Boeing by providing empirical drive performance data, formulating drive system simulation concepts and debugging the overall vehicle system simulation.

Motor and inverter data was collected at ERC using the test setup described in Section 9. The data collected was posted on the Eaton VAX computer system and was reduced to give the following parameters at every operating point: test number index, motor temperature, transistor temperature, motor output speed, DC bus voltage, DC bus current, motor torque, power input to the motor, volts per hertz, rms voltage, magnitude into motor, rms current magnitude into motor, stator frequency, microcomputer control quantities (hexidecimal command slip, command duty cycle), transaxle gear number, actual motor slip, DC bus power, inverter power output, motor power output, inverter efficiency, motor efficiency and total drive efficiency.

Several data reduction schemes were implemented to interpret this data for different phases of this study. The original intent was to organize this data in tabular form and transmit the pertinent tables to Boeing. It was found that these tables did not represent maps that were smooth enough for use in the analysis. It was then decided to plot the data by hand using engineering knowledge of the drive system hardware to interpret the data and draw the curves. This resulted in the following families of curves:

Figure 10.6.1
Traction induction motor efficiency as a function of motor torque and rotor speed

Figure 10.6.2
Traction induction motor volts/hertz as a function of motor torque and rotor speed

Figures 10.6.3 & 10.6.4
Traction induction motor slip as a function of motor torque and rotor speed

Figure 10.6.5
Traction induction motor current as a function of motor torque and rotor speed

FIGURE 10.6.1
TRACTION INDUCTION MOTOR
EFFICIENCY VS. TORQUE AT
VARIOUS MOTOR OUTPUT SPEEDS

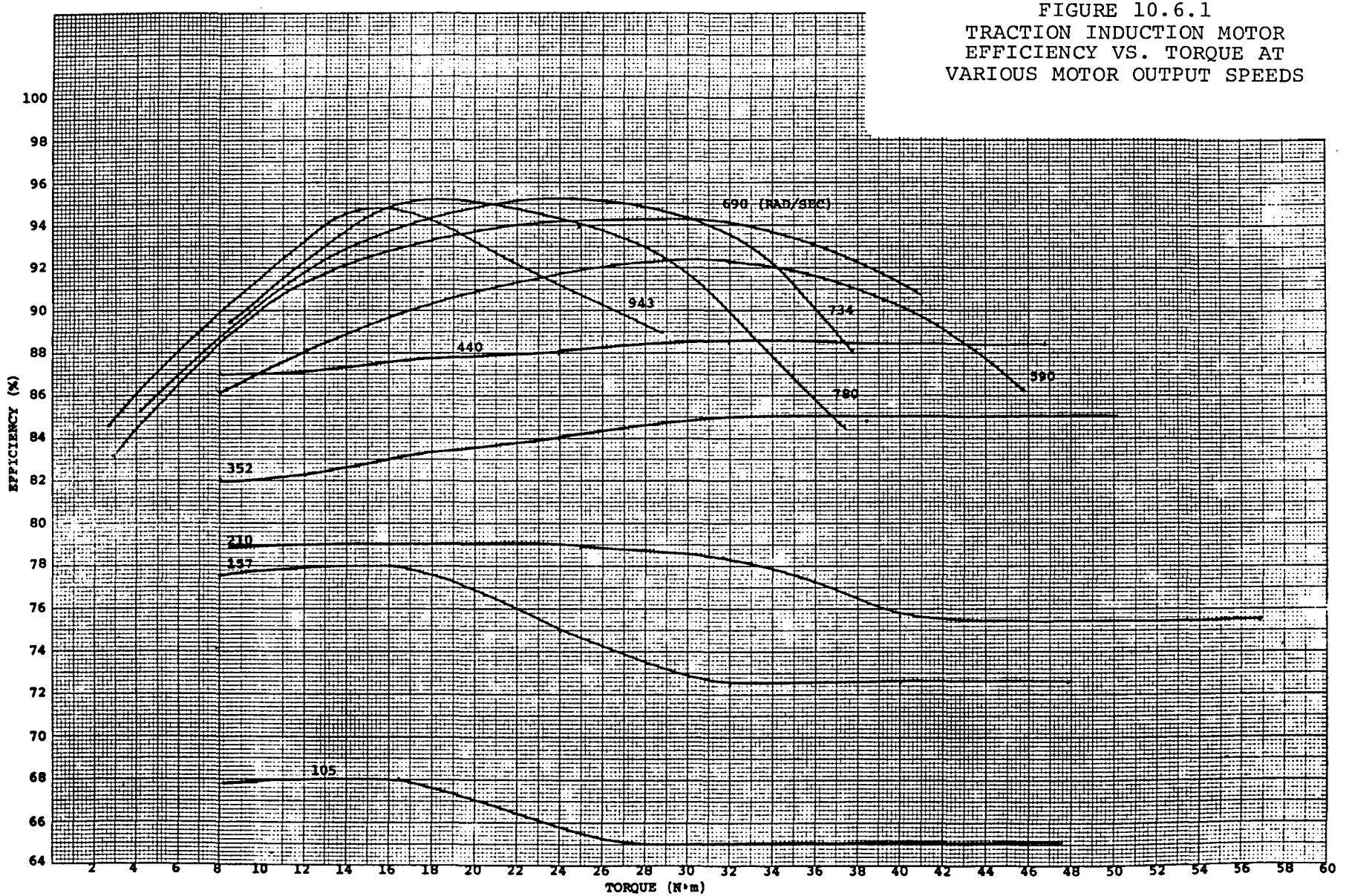

FIGURE 10.6.2
TRACTION INDUCTION MOTOR
V/HZ RATIO VS. TORQUE AT
VARIOUS MOTOR OUTPUT SPEEDS

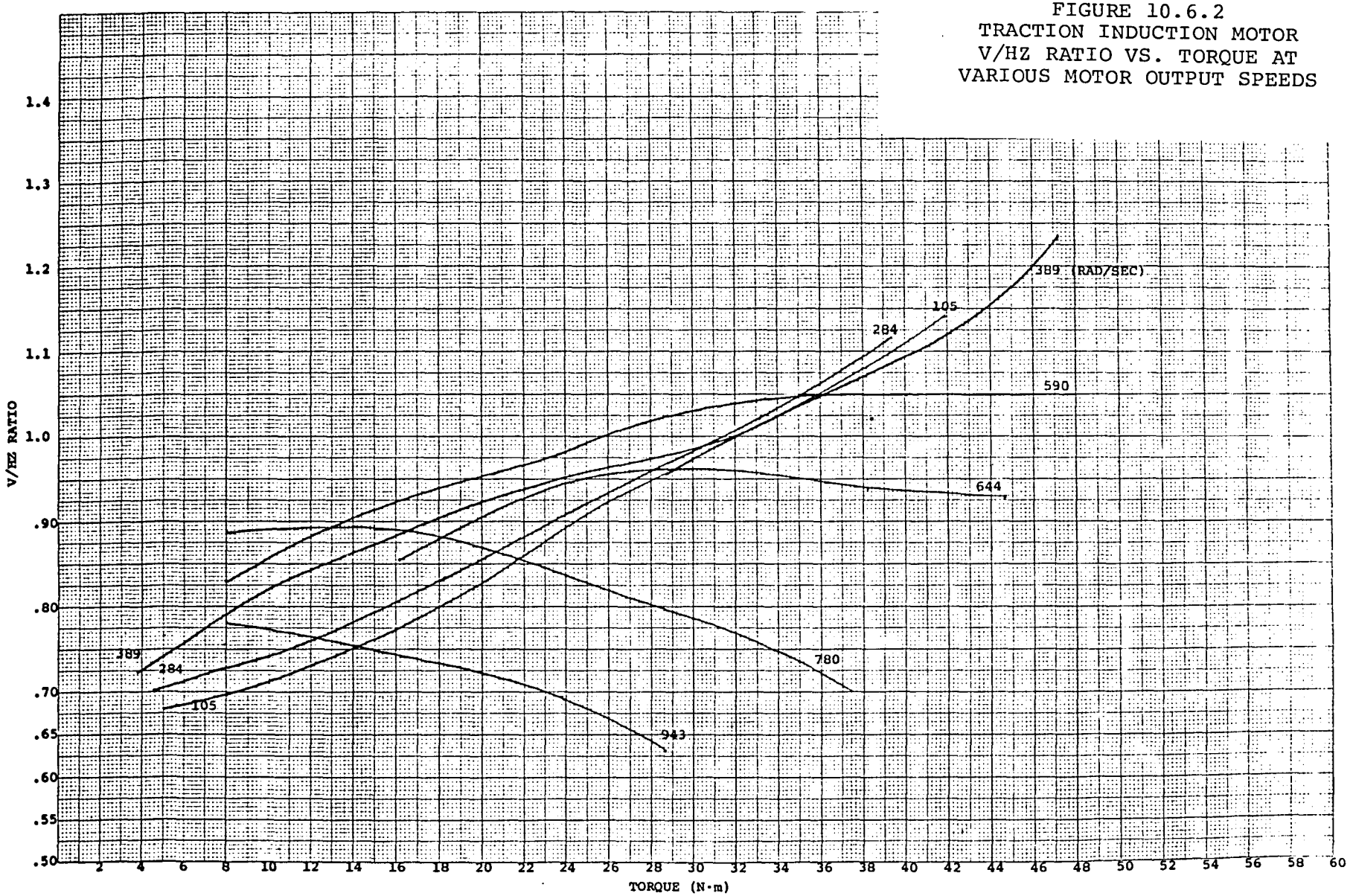

FIGURE 10.6.3
TRACTION INDUCTION MOTOR
SLIP VS. TORQUE AT
VARIOUS MOTOR OUTPUT SPEEDS
(GRAPH #1 OF 2)

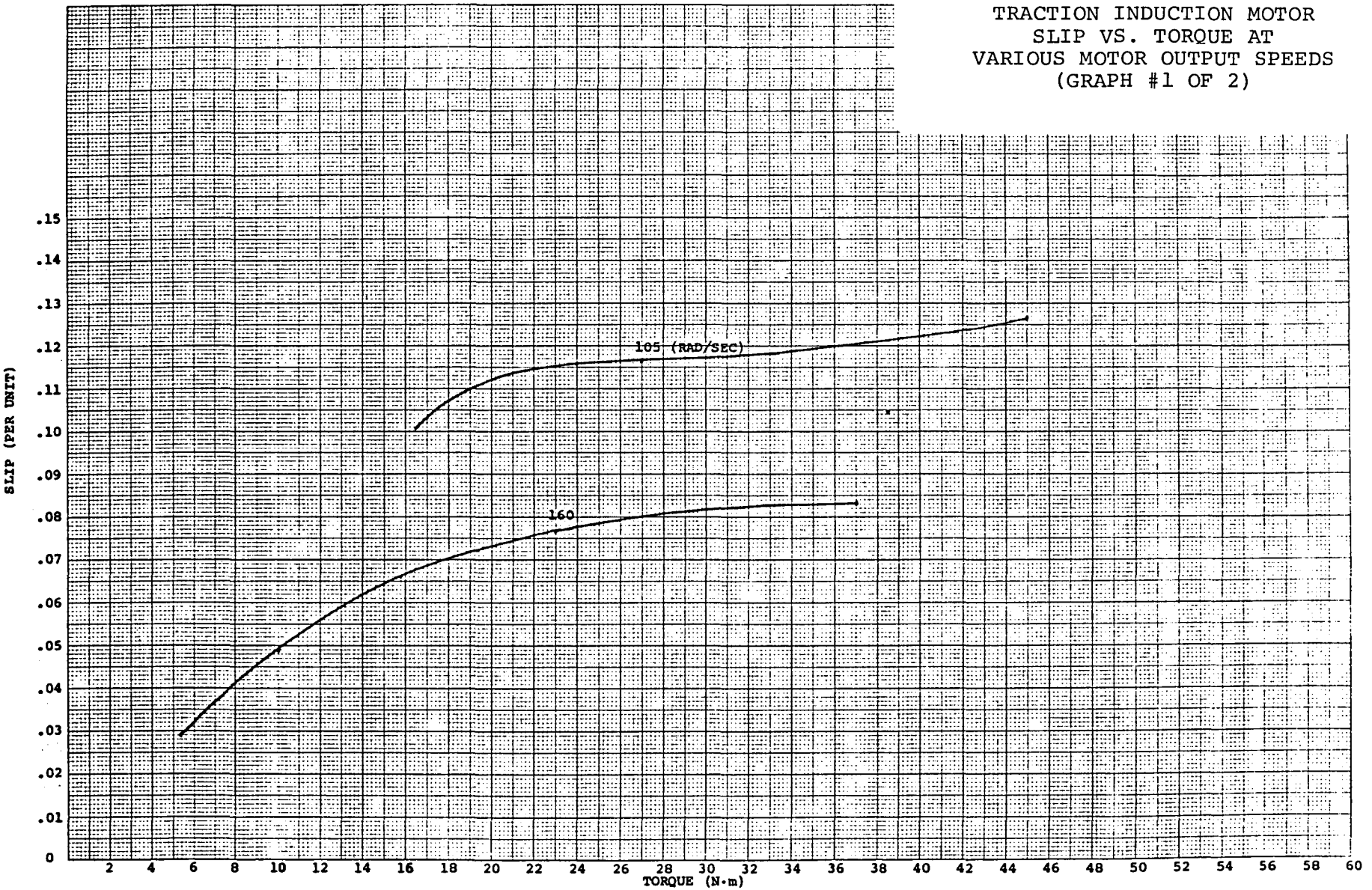

FIGURE 10.6.4
TRACTION INDUCTION MOTOR
SLIP VS. TORQUE AT
VARIOUS MOTOR OUTPUT SPEEDS
(GRAPH #2 OF 2)

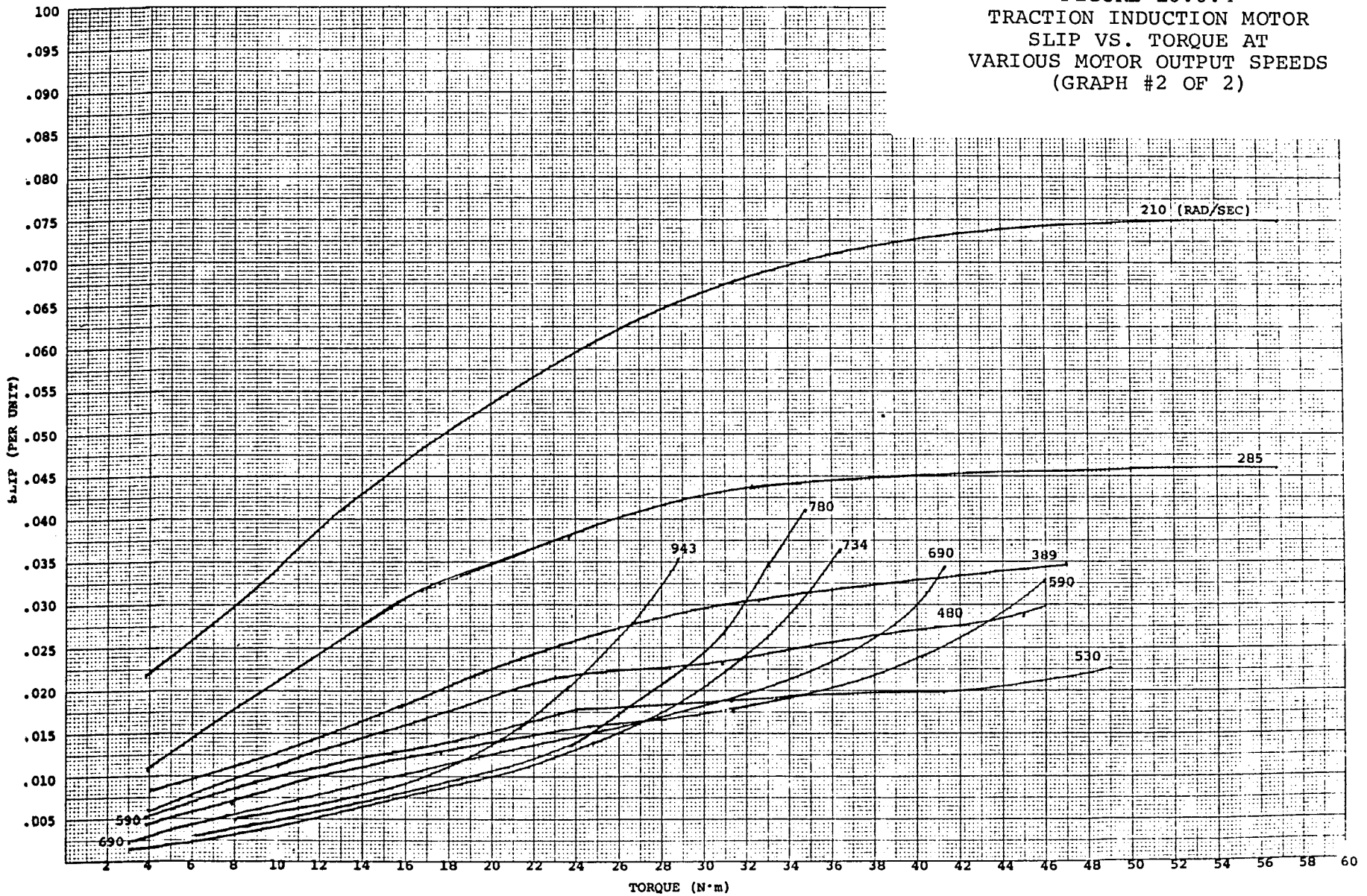

FIGURE 10.6.5
TRACTION INDUCTION MOTOR
CURRENT VS. TORQUE AT
VARIOUS MOTOR OUTPUT SPEEDS

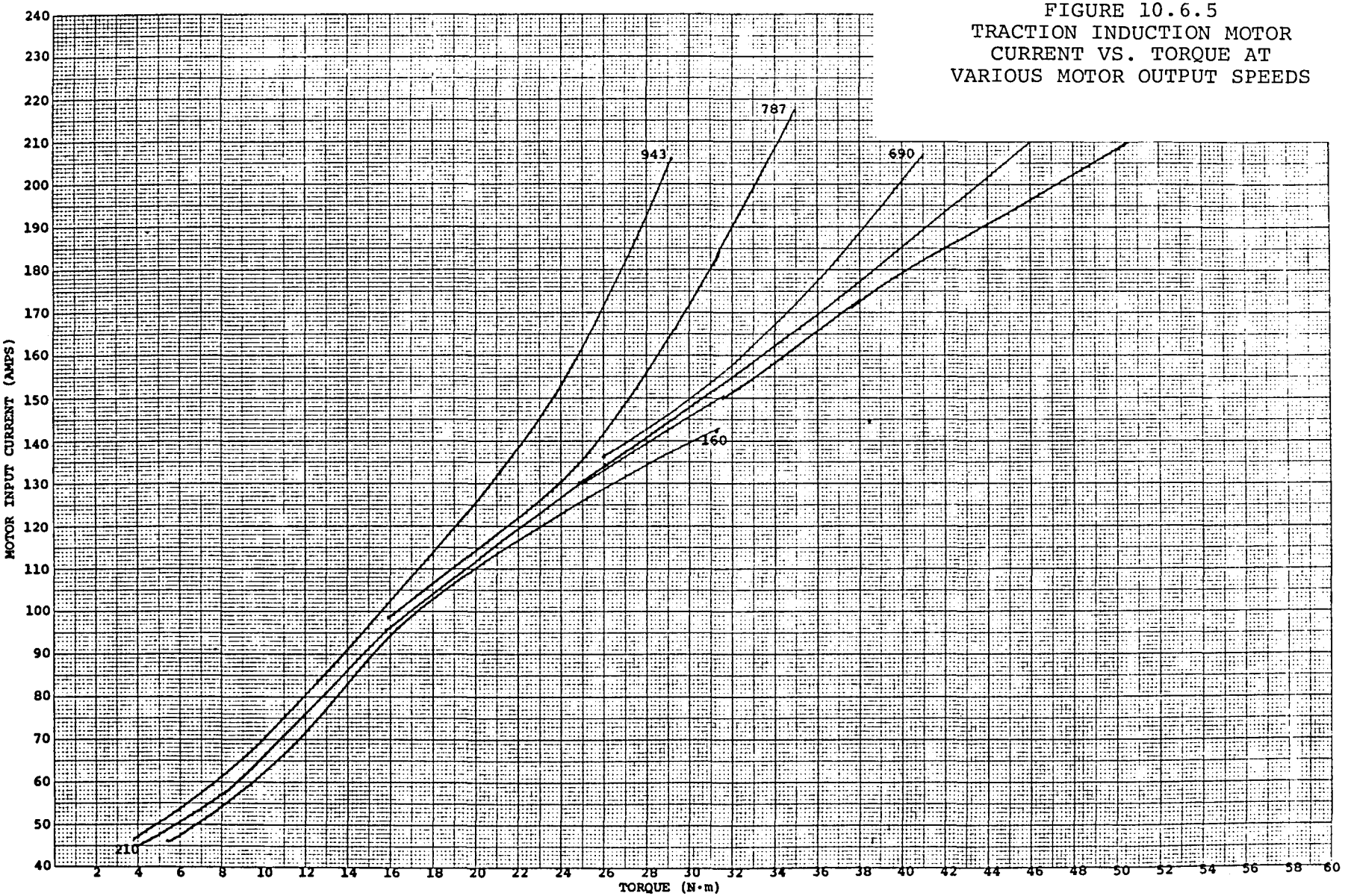

Figure 10.6.6
Regeneration induction motor efficiency as a function of motor torque and rotor speed

Figure 10.6.7
Regeneration induction motor volts/hertz as a function of motor torque and rotor speed

Figures 10.6.8 & 10.6.9
Regeneration induction motor slip as a function of motor torque and rotor speed

Figure 10.6.10
Regeneration induction motor current as a function of motor torque and rotor speed

Figures 10.6.11 & 10.6.12
Traction inverter effeciency as a function of output current and fundamental frequency

Figure 10.6.13
Traction inverter power loss as a function of DC bus current and fundamental frequency

Figures 10.6.14 & 10.6.15
Traction inverter DC bus current as a function of current output and fundamental frequency

Figure 10.6.16
Traction inverter power loss as a function of current output and fundamental frequency

Figure 10.6.17
Regeneration inverter efficiency as a function of output current and fundamental frequency

Figure 10.6.18
Regeneration inverter power loss as a function of DC bus current and fundamental frequency

Figure 10.6.19
Regeneration inverter DC bus current as a function of current output and fundamental frequency

Figure 10.6.20
Regeneration inverter power loss as a function of current output and fundamental frequency

These curves were mailed to Boeing Computer Services where they were digitized and entered into the Boeing computer network. Data is read from these three-dimensional families of curves in the following manner: given two system operating points, eg., torque and speed or current and frequency, the simulation finds the four

FIGURE 10.6.6
REGENERATION INDUCTION MOTOR
EFFICIENCY VS. TORQUE AT
VARIOUS MOTOR OUTPUT SPEEDS

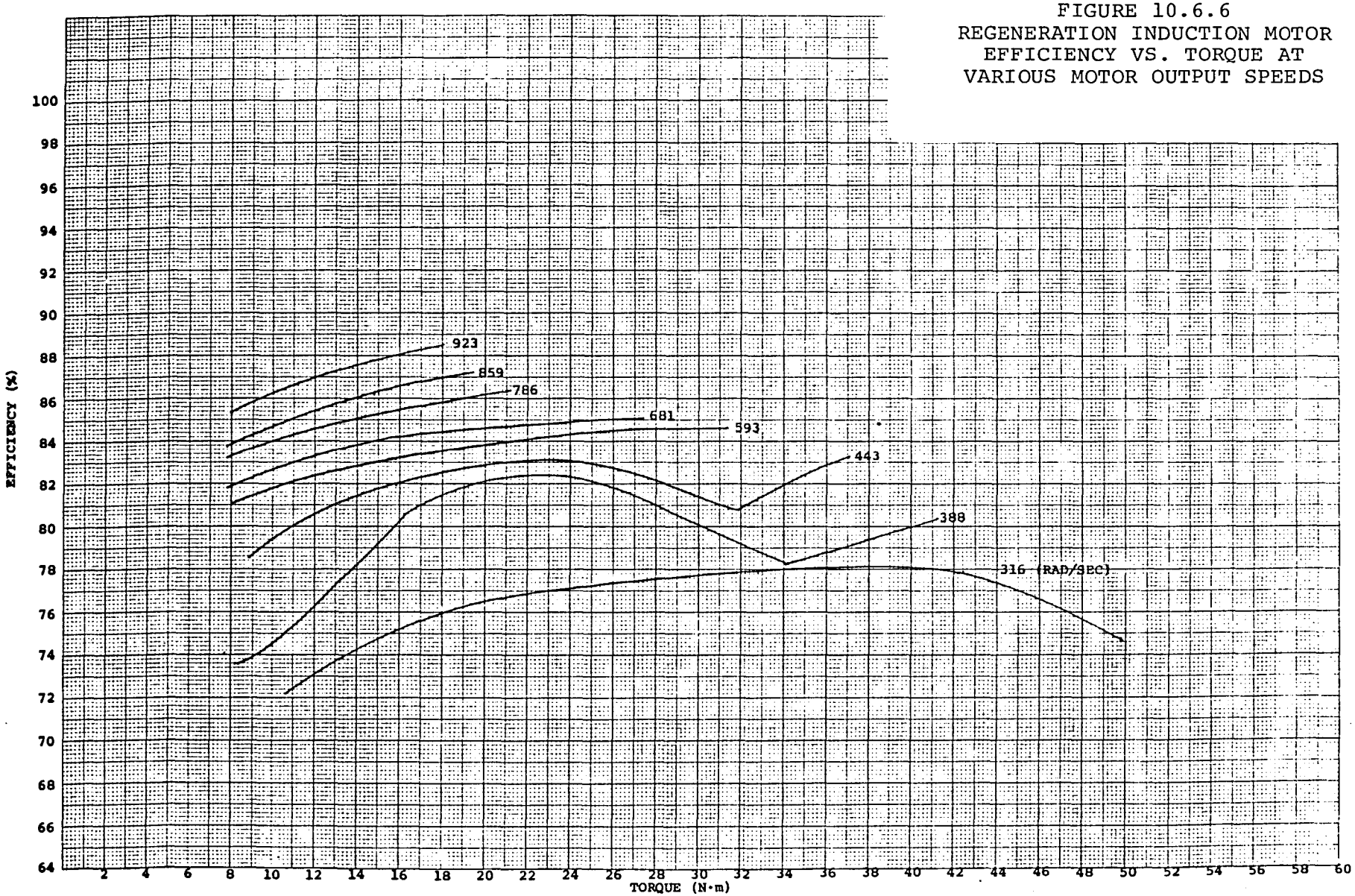

FIGURE 10.6.7
REGENERATION INDUCTION MOTOR
V/HZ RATIO VS. TORQUE AT
VARIOUS MOTOR OUTPUT SPEEDS

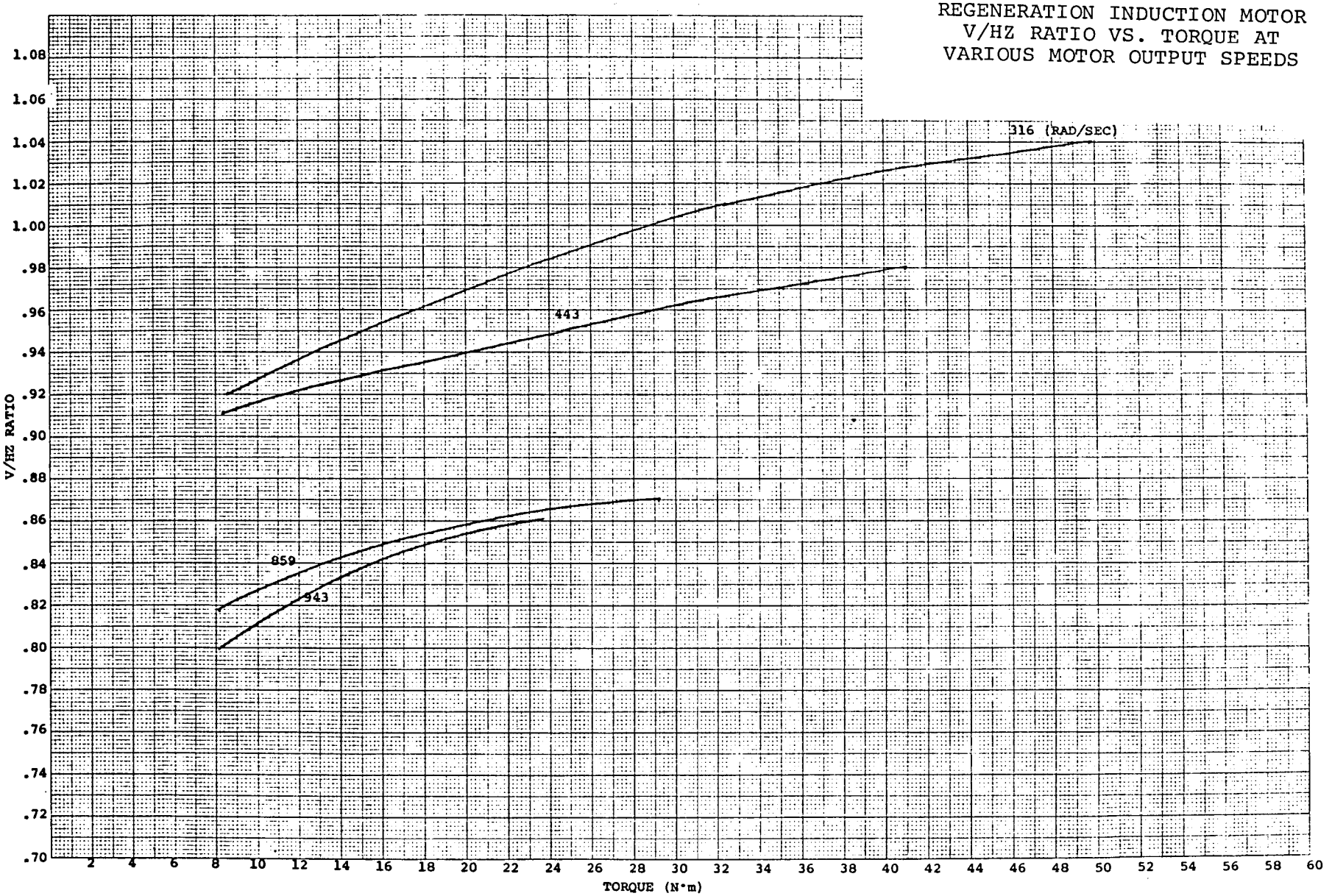

FIGURE 10.6.8
REGENERATION INDUCTION MOTOR
SLIP VS. TORQUE AT
VARIOUS MOTOR OUTPUT SPEEDS
(GRAPH #1 OF 2)

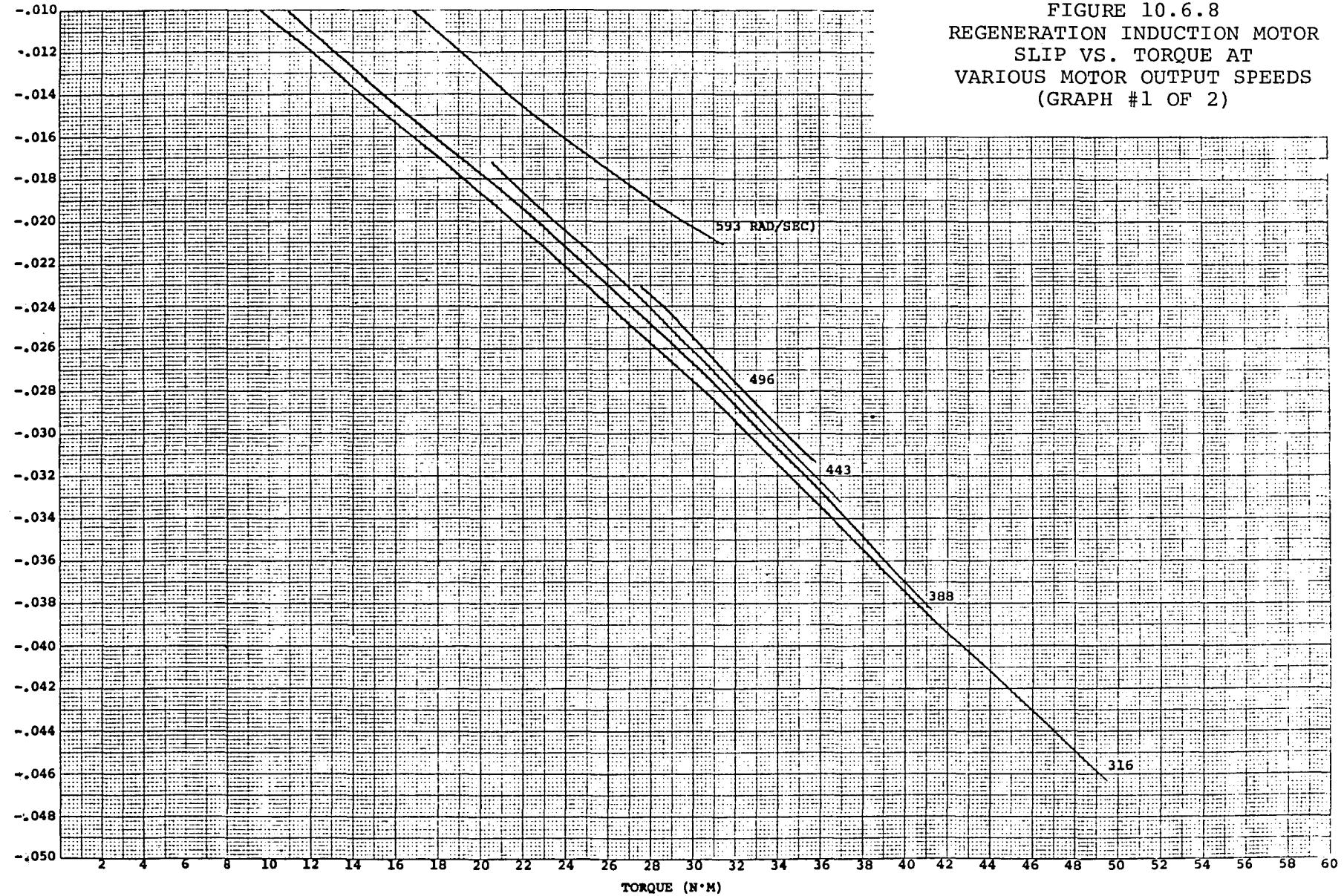

FIGURE 10.6.9
REGENERATION INDUCTION MOTOR
SLIP VS. TORQUE AT
VARIOUS MOTOR OUTPUT SPEEDS
(GRAPH #2 OF 2)

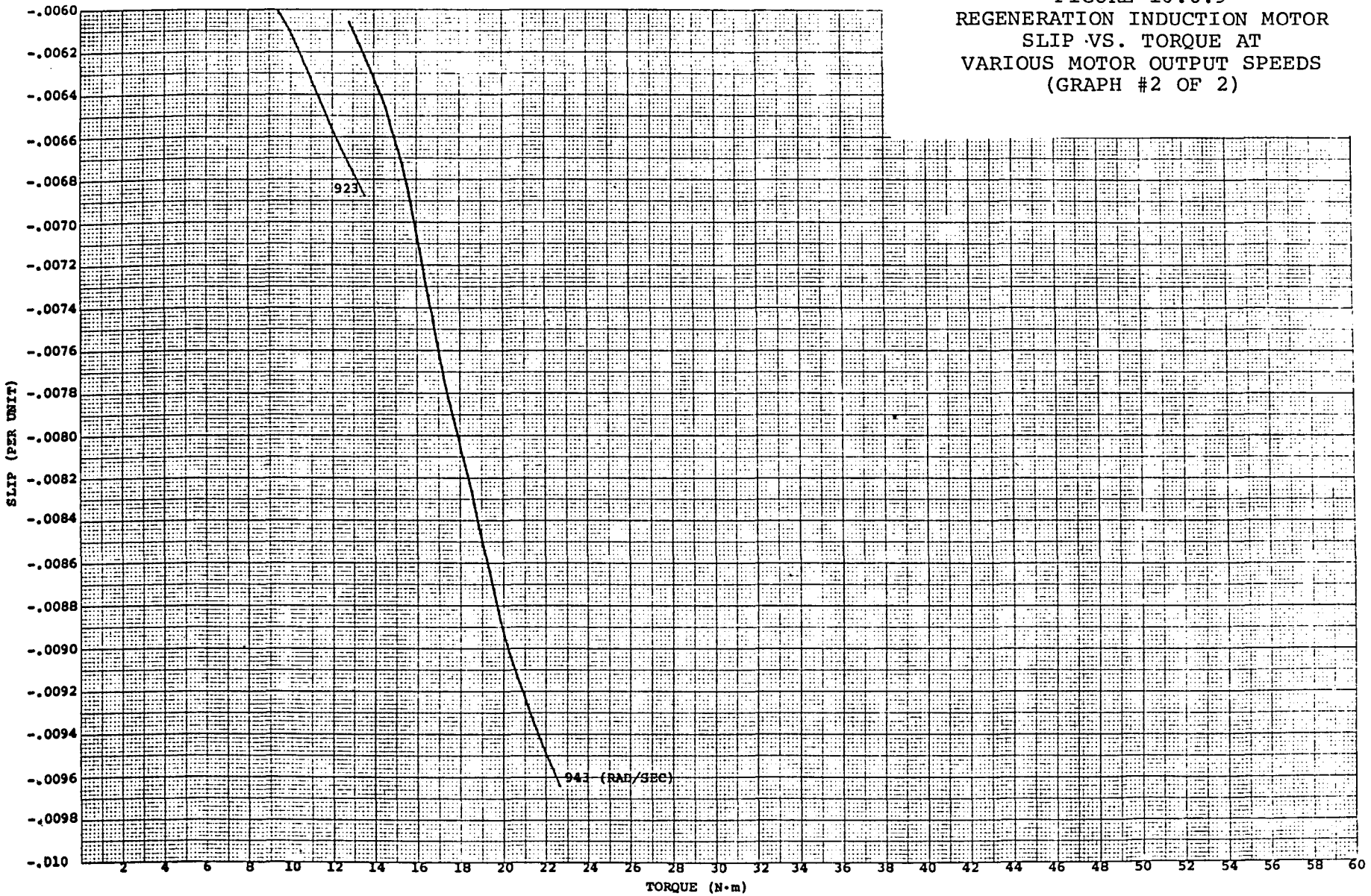

FIGURE 10.6.10
REGENERATION INDUCTION MOTOR
CURRENT VS. TORQUE AT
VARIOUS MOTOR OUTPUT SPEEDS

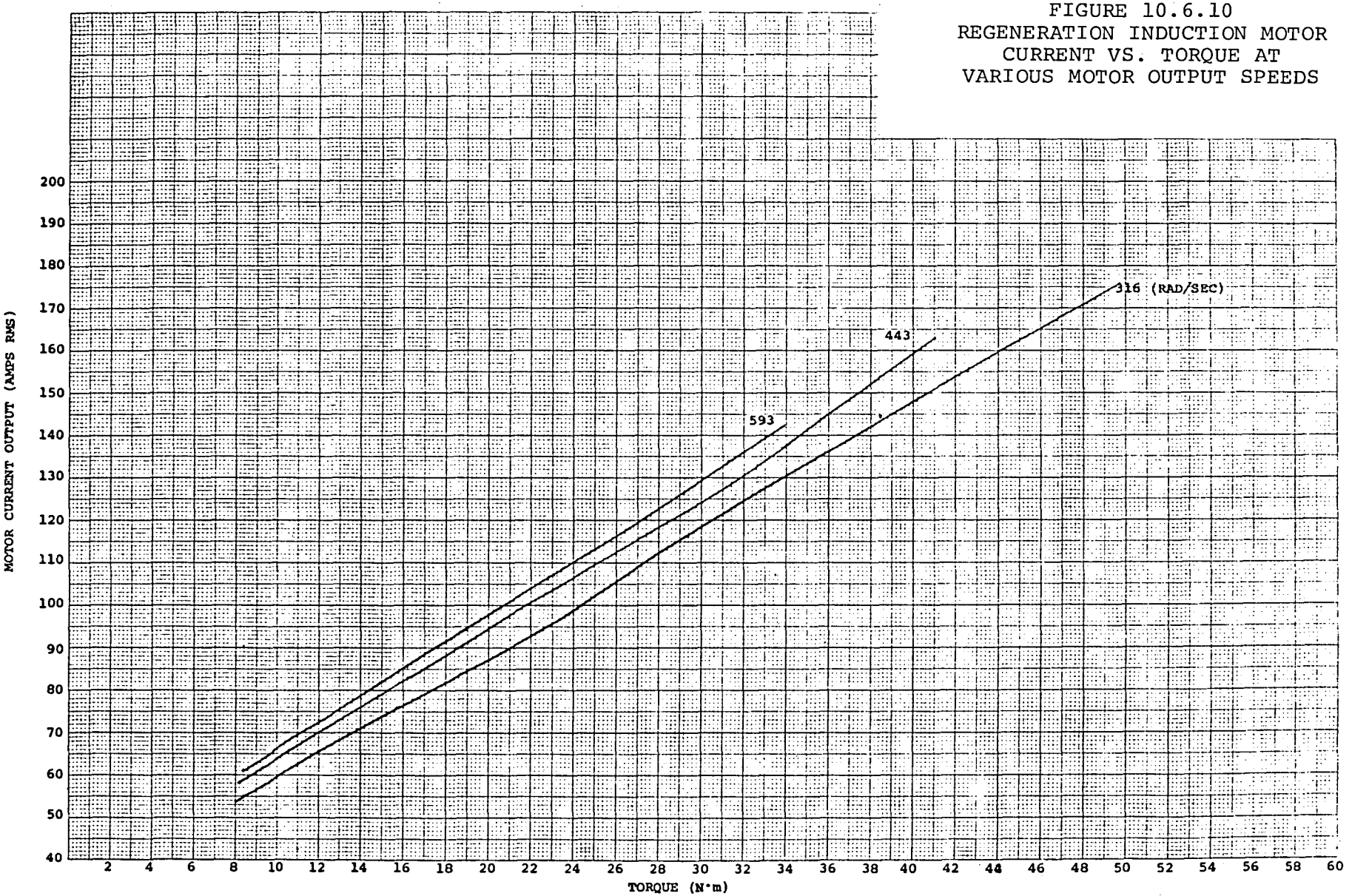

FIGURE 10.6.11
TRACTION INVERTER
EFFICIENCY VS. OUTPUT CURRENT AT
VARIOUS INVERTER FREQUENCIES
(GRAPH #1 OF 2)

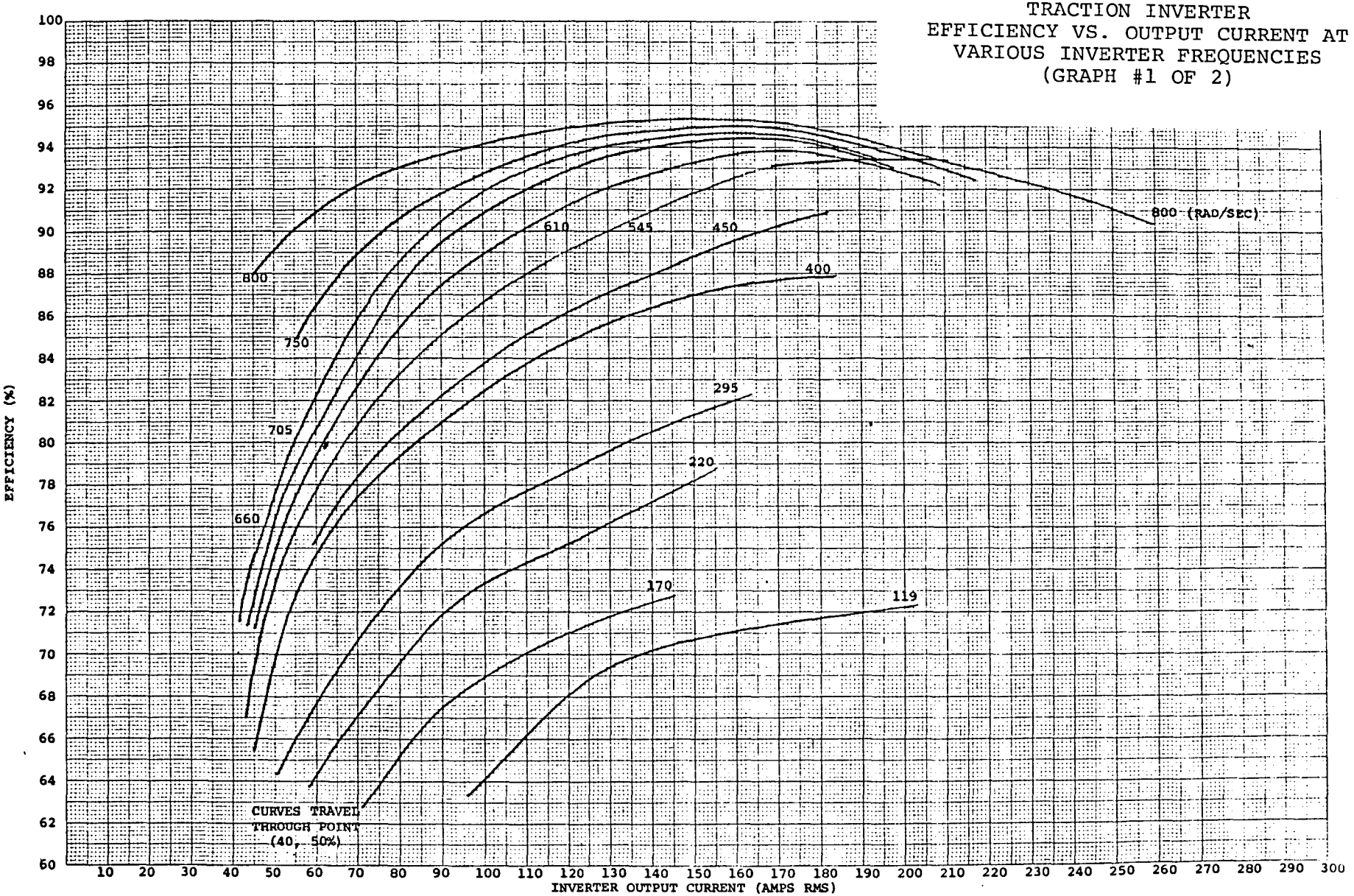

FIGURE 10.6.12
TRACTION INVERTER
EFFICIENCY VS. OUTPUT CURRENT AT
VARIOUS INVERTER FREQUENCIES
(GRAPH #2 OF 2)

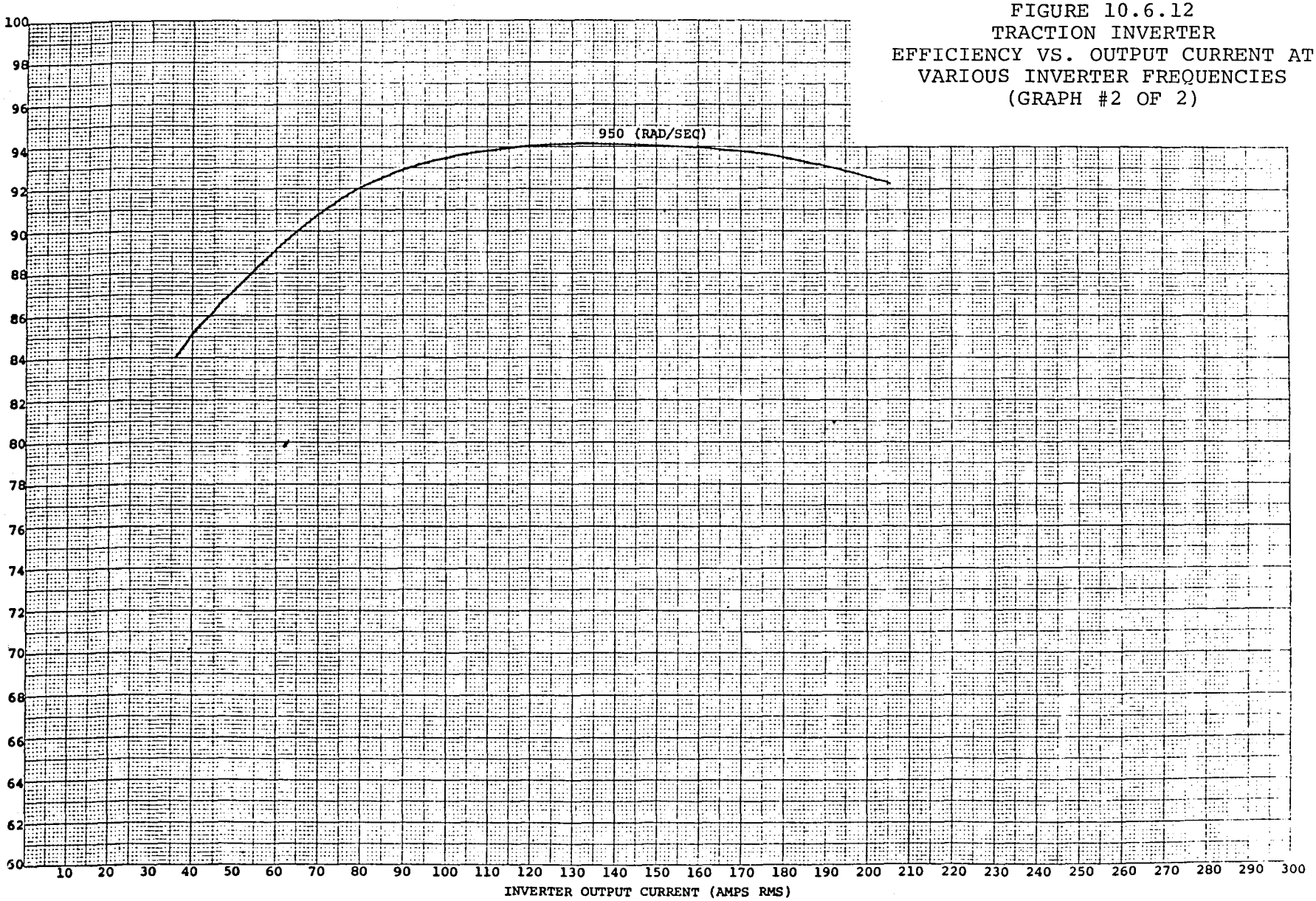

FIGURE 10.6.13
TRACTION INVERTER
POWER LOSS VS. INPUT CURRENT AT
VARIOUS INVERTER FREQUENCIES

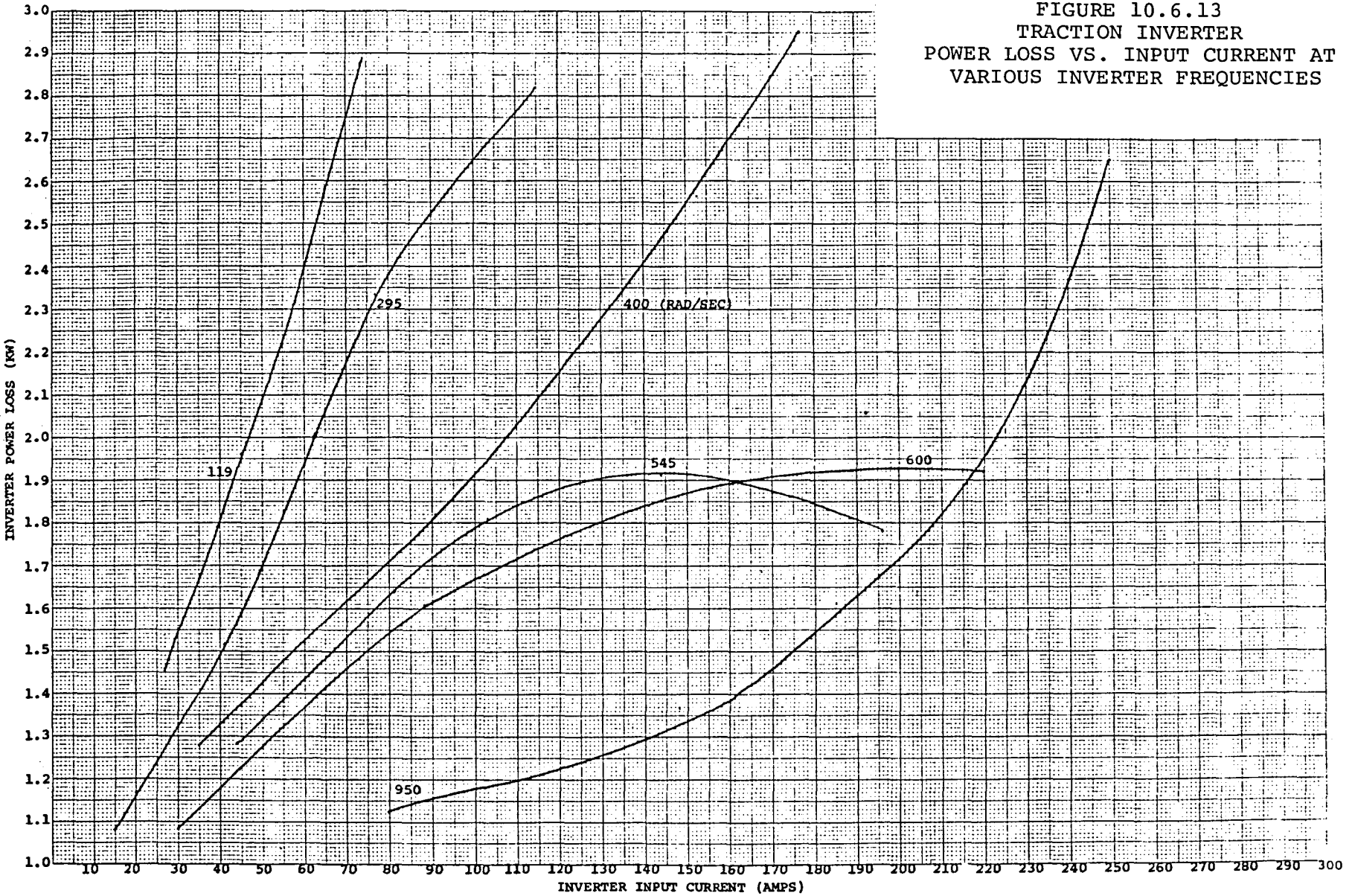

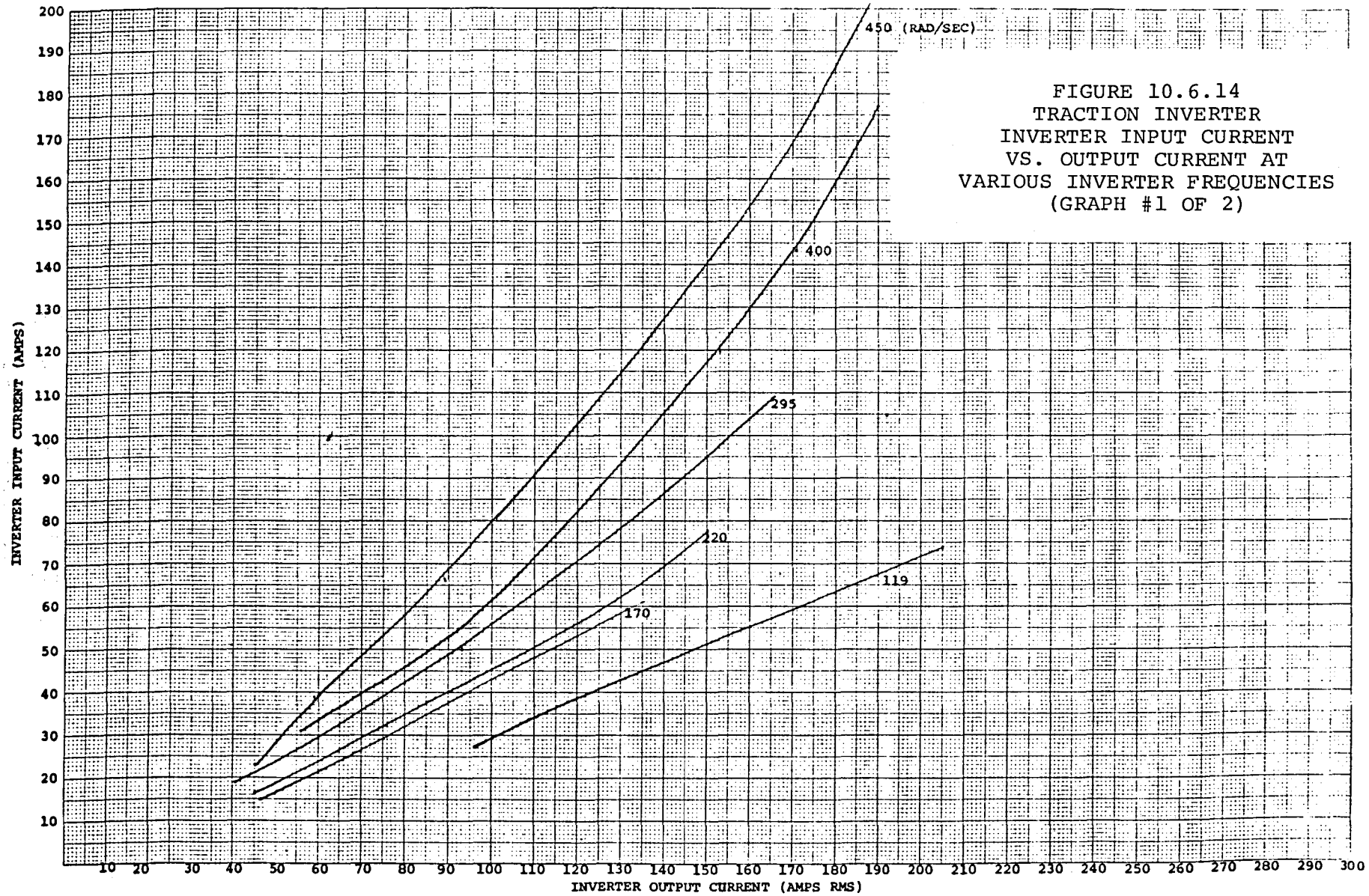

FIGURE 10.6.14
TRACTION INVERTER
INVERTER INPUT CURRENT
VS. OUTPUT CURRENT AT
VARIOUS INVERTER FREQUENCIES
(GRAPH #1 OF 2)

FIGURE 10.6.15
TRACTION INVERTER
INVERTER INPUT CURRENT
VS. OUTPUT CURRENT AT
VARIOUS INVERTER FREQUENCIES
(GRAPH #2 OF 2)

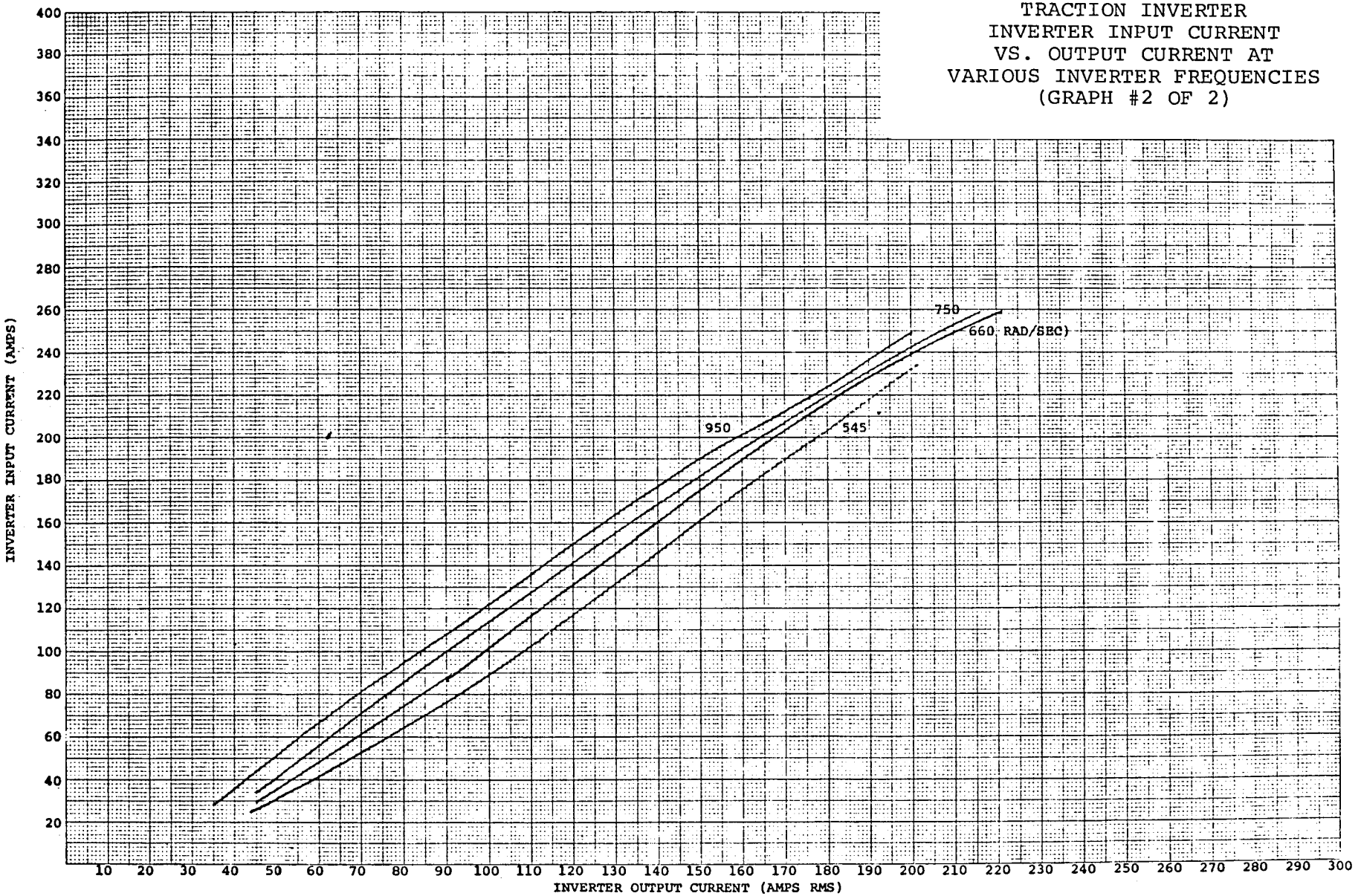

FIGURE 10.6.16
TRACTION INVERTER
POWER LOSS VS. OUTPUT CURRENT AT
VARIOUS INVERTER FREQUENCIES

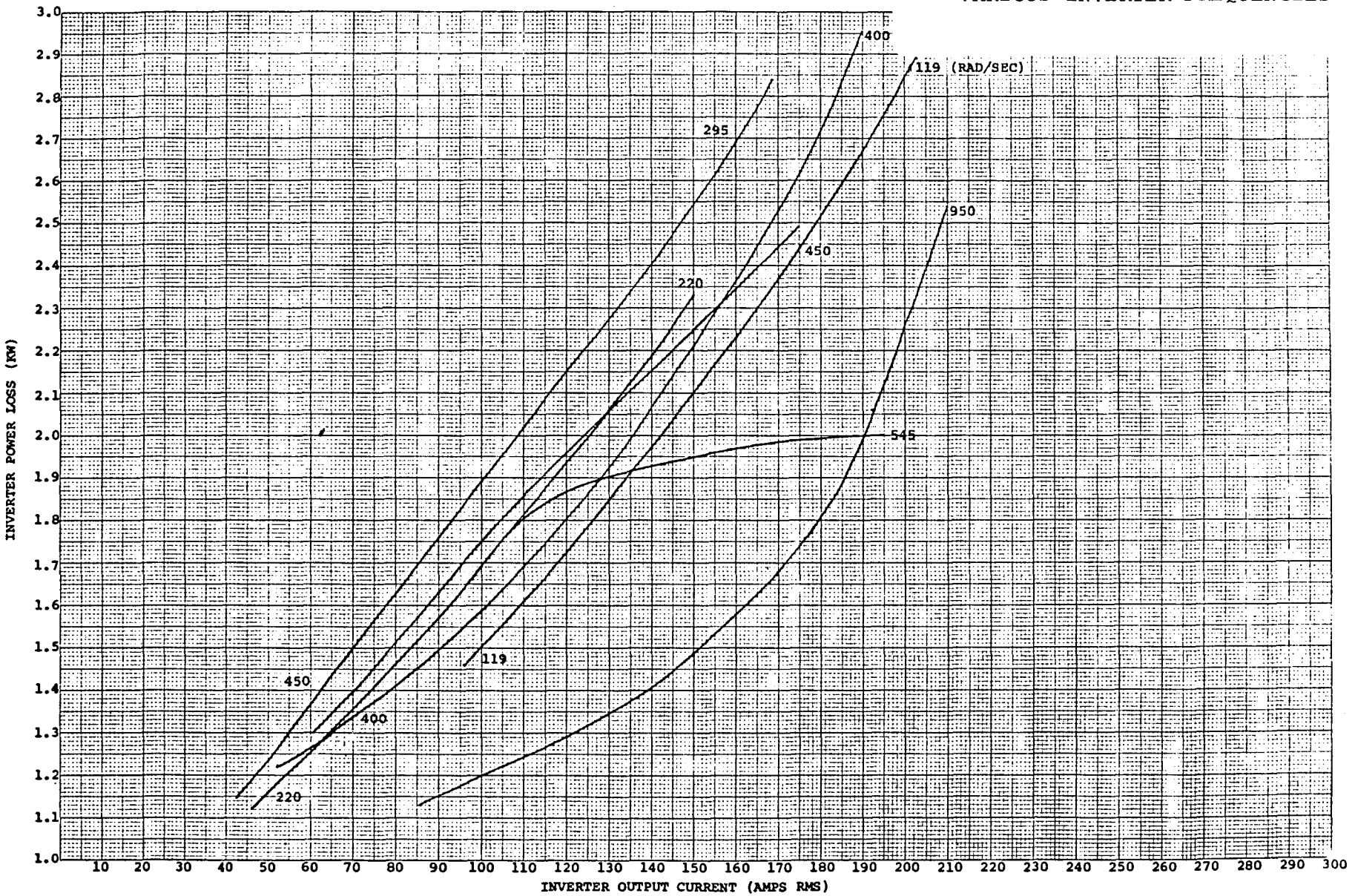

FIGURE 10.6.17
REGENERATION INVERTER
EFFICIENCY VS. OUTPUT CURRENT OF
VARIOUS INVERTER FREQUENCIES

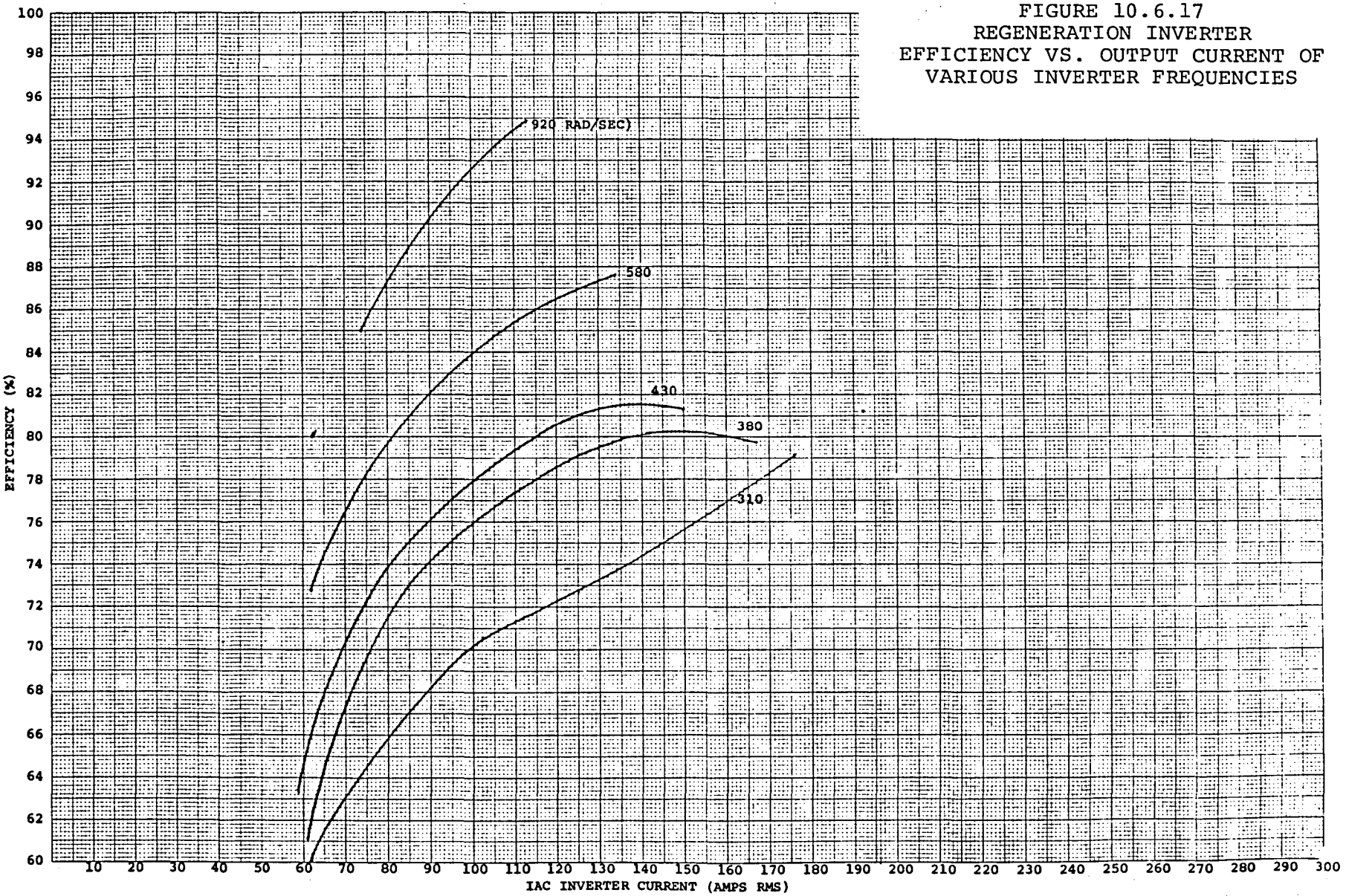

FIGURE 10.6.18
REGENERATION INVERTER
POWER LOSS VS. INPUT CURRENT AT
VARIOUS INVERTER FREQUENCIES

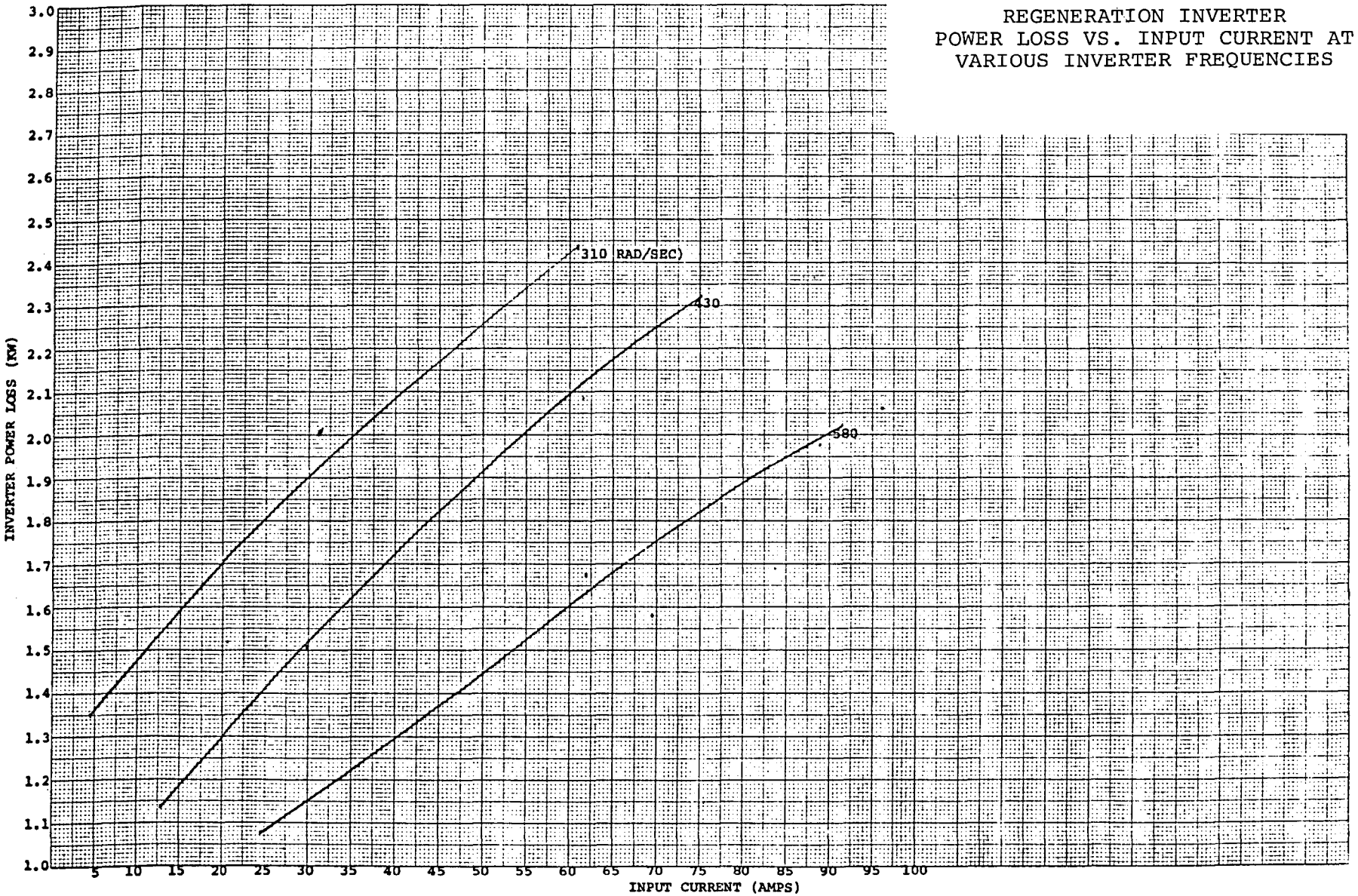

FIGURE 10.6.19
REGENERATION INVERTER
INPUT CURRENT VS. OUTPUT CURRENT AT
VARIOUS INVERTER FREQUENCIES

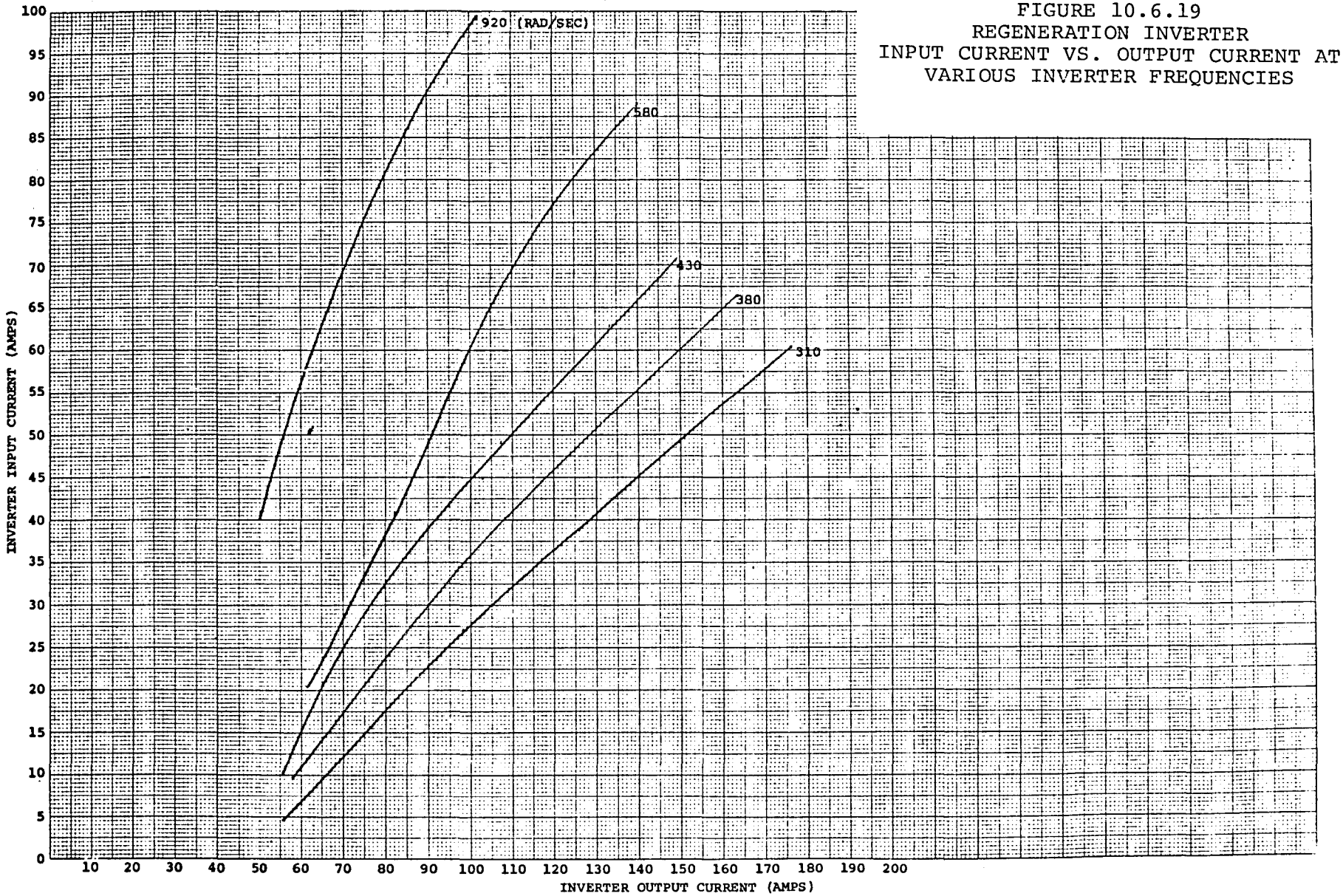

FIGURE 10.6.20
REGENERATION INVERTER
POWER LOSS VS. OUTPUT CURRENT AT
VARIOUS INVERTER FREQUENCIES

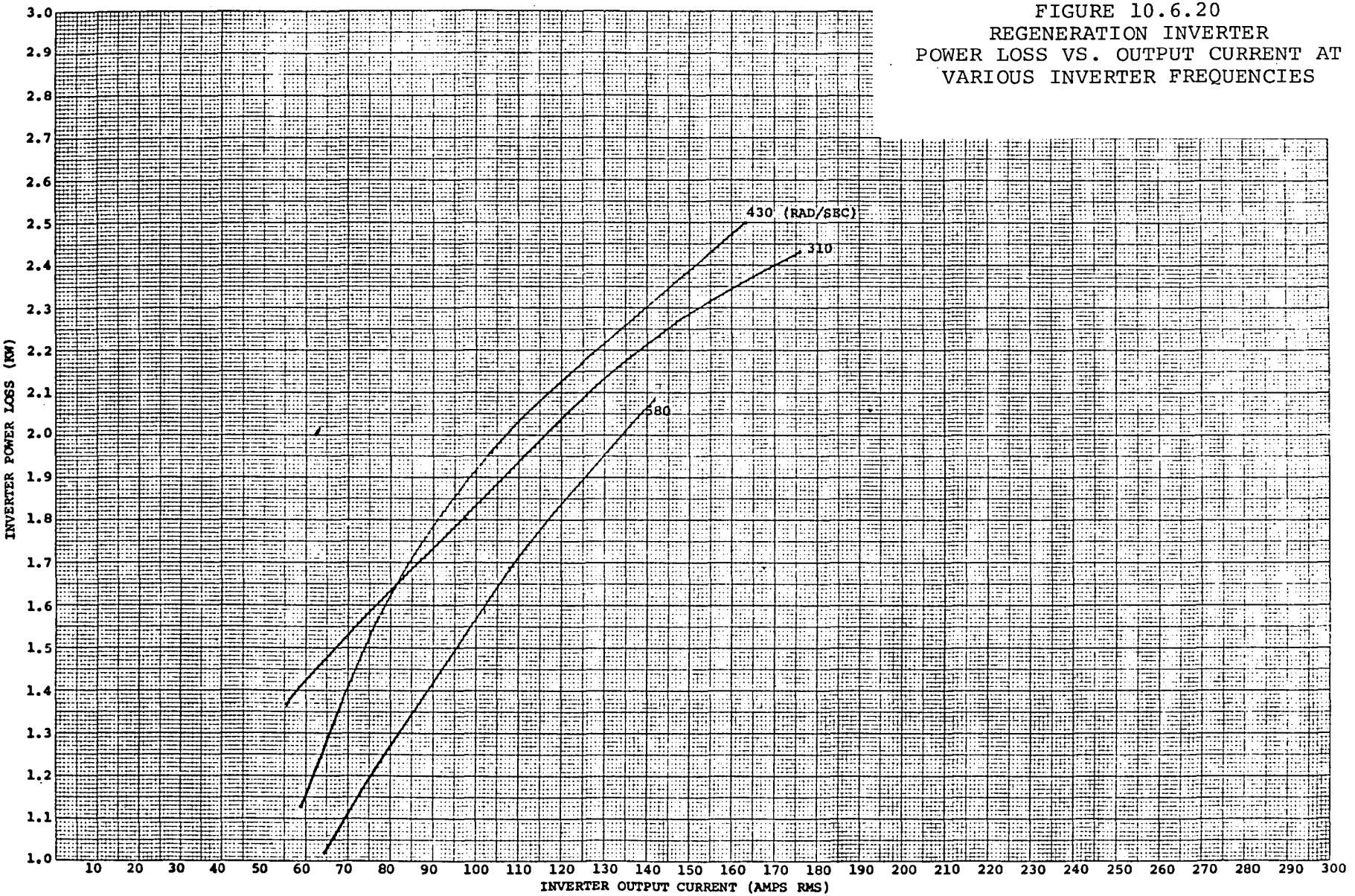

data points bracketing the known operating condition, then uses a two-dimensional linear interpolation to find the unknown operating condition, e.g., slip or efficiency on V/Hz.

Acceptable simulation of drive performance was obtained with the HEAVY package by implementing the following scheme. The HEAVY simulation uses an "upstream" calculation alternated with a "downstream" calculation until all system state variables have converged (downstream calculation is calculation in the direction of energy flow).[6] In the upstream pass, the induction machine component receives a torque request from the fixed ratio transmission. Knowing the present output shaft speed, the model finds the slip that would be commanded by the controller if the torque request were met by using the data in Figures 10.6.3 and 10.6.4 (Figures 10.6.8 and 10.6.9 for regen. mode). Then, knowing the slip and output shaft speed, the model calculates the frequency command to the inverter. The volts/hertz ratio that would be commanded if the torque request were met is found from the data in Figure 10.6.2 (Figure 10.6.7 for regen. mode) and is commanded to the inverter. The inverter model, knowing the present output current and frequency request, gets the battery current that would be drawn if the request were met using the data in Figures 10.6.14 and 10.6.15 (Figures 10.6.19 for regen. mode). The battery and inverter components form an implicit loop.[6]

In the downstream pass, the inverter output frequency is set equal to the command frequency. Knowing the DC bus current and operating frequency, the inverter finds the power loss from the data in Figure 10.6.13 (Figure 10.6.18 for regen. mode). The power loss is then represented by a DC voltage drop as

$$V_{loss} = P_L / I_{IN}$$

where P_L = power loss as above and I_{IN} = inverter input current.

The commanded rms output voltage is calculated by

$$V_{rms} = V_{HC} \cdot F$$

where V_{HC} = volts/hertz ratio commanded and F = output frequency.

If the state of charge of the battery allows the terminal voltage to be set high enough, it is set at the requested value. If the terminal voltage cannot be set high enough, it is set to the maximum voltage available given by

$$V_O = (V_{bus} - V_{loss}) \frac{\sqrt{6}}{\pi}$$

where V_O = voltage out inverter (V_{rms}) and V_{bus} = DC bus voltage.

The motor model then calculates the actual volts/hertz ratios that this voltage represents and finds the torque that results from this ratio at the present output shaft speed. This resultant torque is passed to the fixed ratio transmission. At this point one pass through the drive loop has been completed. Passes are made upstream and downstream until all the vehicle system state variables converge.[6] Motor efficiency, motor current, and inverter efficiency are found from the data in Figures 10.6.1, 10.6.5, 10.6.11 and 10.6.12 (Figures 10.6.6, 10.6.10 and 10.6.16 for regen. mode), respectively. These quantities are for output only and are not used in the drivetrain calculations.

The Eaton transaxle was modeled with the HEAVY simulation using the fixed ratio transmission component. Power loss was represented as a torque loss which is a function of torque input and output speed. The transmission ratios were taken from the experimental data reported in Section 4. This data, transmission shift points, and other pertinent vehicle information used in the simulation is tabulated in Figure 10.6.21.

Minimum battery operating voltage	94 VDC
Number of EV106 battery cells	72
Weight of inverter and controller	50 kg
Weight of induction machine and cables	57.5 kg
Inertia of induction machine	0.0129 kgm^2
Weight of transaxle	39 kg
Inertia of transaxle	0.002202 kgm^2
Transmission gear ratio low gear	19.8
Transmission gear ratio high gear	8.23
Transmission output speed for positive acceleration shift up point	47.6 rad/sec
Transmission output speed for negative acceleration shift down point	38.17 rad/sec
Vehicle weight without propulsion system and batteries	617 kg
Battery weight	707.8 kg
Payload (2 passengers)	136 kg
Tire radius	0.2667 m
Rolling resistance	0.011
Aerodynamic drag (D_dA)	0.784 m^2
Total vehicle weight with payload	1,607 kg

Figure 10.6.21 Vehicle Simulation System Parameters

10.7 Vehicle Model Results

The HEAVY vehicle simulation described above is a useful tool for energy use comparisons of system effects for vehicle and component design changes. The model has been used to investigate gear ratio changes, shift point changes, and control scheme improvements.

The vehicle simulation compared well with a hand calculation made from efficiency estimates over a J227a/D cycle (Figure 10.7.1). The hand calculation predicted that the vehicle with the 100 V motor would need 168.05 watt-hours at the wheels and draw a net of 204.98 watt-hours (regen. included) from the battery to complete a single J227a/D cycle. This is an efficiency of 82.0%. The HEAVY vehicle model predicted the 100 V motor drive system would need 159.54 watt-hours at the wheels and draw a net of 197.81 watt-hours (regen. included) from the battery to complete a single J227a/D cycle. This is an efficiency of 80.6%. This close agreement shows that the vehicle model is certainly an acceptable model of energy consumed by the vehicle in meeting a J227a/D driving cycle. (The above vehicle simulation run will be cited hereafter as the base case.)

Vehicle simulations were run with different transmission ratios. A run was made with a 25% lower gear ratio in both gears. Although the vehicle still met the J227a/D cycle command speeds, it used a net energy of 208.50 watt-hours to complete a single cycle.

This demonstrates that this lower gear ratio would result in the vehicle using 5.4% more energy than the base case. This would translate to 5.4% less range for the vehicle. (To be conservative, in range estimates one must truncate to the lower number of integral cycles since energy use during a cycle is not linear.) A run was also made with 25% higher gear ratios in both gears. Again, the vehicle met the demands of the J227a/D cycle. The net energy drawn with this vehicle was nearly the same as the base case, but more energy was drawn from the battery and more was regenerated to it. These higher power levels (rate of energy transfer) result in less efficient battery charging, leaving the state of the battery predicted by the averaging model after one J227a/D cycle slightly lower than the base case. This, of course, results in less range for the vehicle. The above results show the present gear ratios are near optimum performance as set with the system studied. Note that no attempt was made to investigate the smoothness of these shifts with these gear ratios. The model does not include enough detail for an analysis of smoothness to be quantitatively accurate.

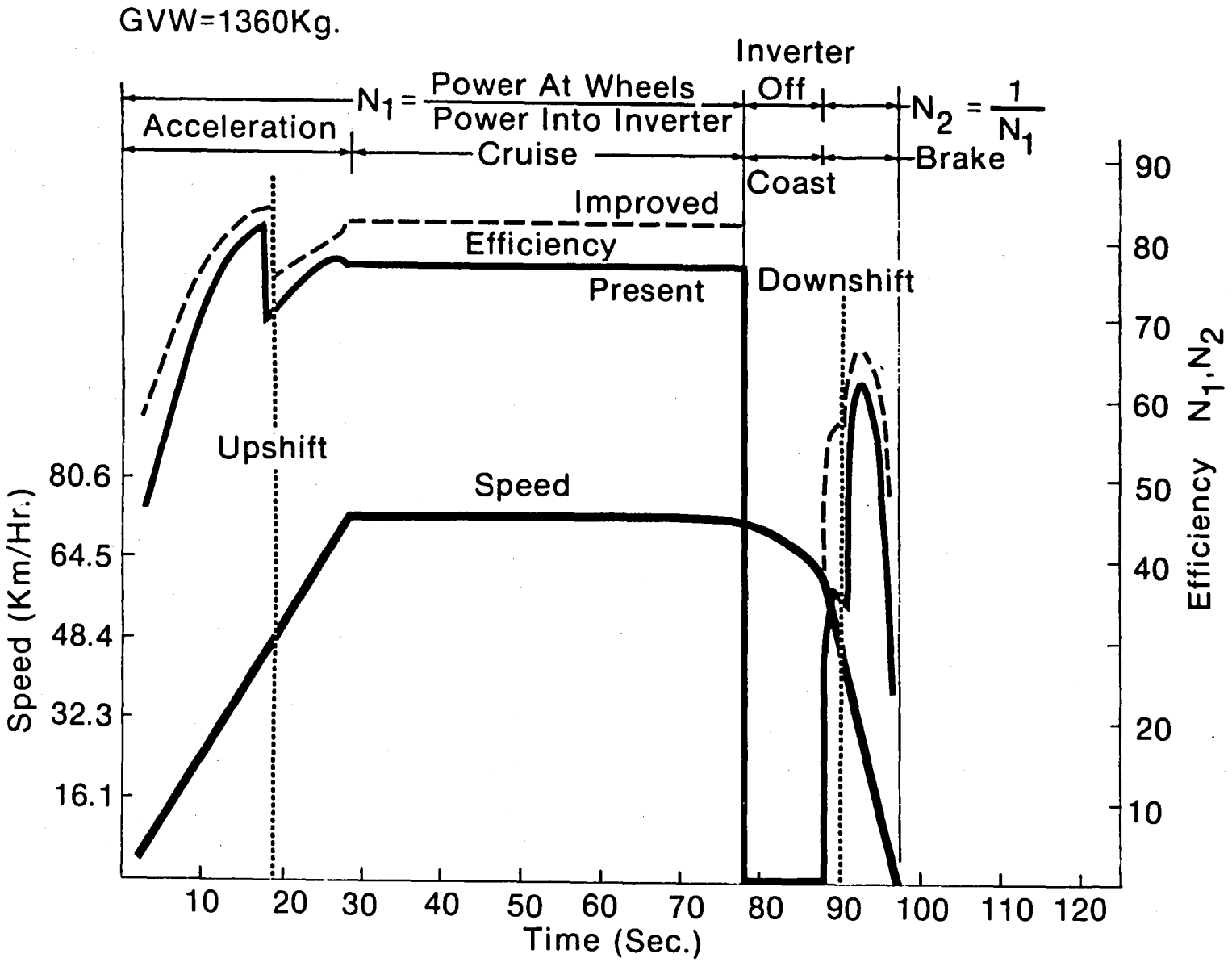

Figure 10.7.1 Efficiency over SAE J227a/D Cycle

Another set of simulations were run with different transmission shift points. The nominal shift point for first to second in the base case was a motor speed of 150 Hz. The nominal shift point for the downshift from second to first in the base case was at a motor speed of 50 Hz. A simulation with 25% higher shift points was run, i.e., a shift up with motor speed at 187.5 Hz and a downshift at 62.5 Hz. This run showed a net energy of 193.42 watt-hours were drawn from the battery. This run also showed that the energy out of the battery was slightly better than the base case by 0.5 watt-hours. This result occurred because the system was allowed to run to its high torque speed points, where the system efficiencies are greater, before shifting. The higher downshift allowed 41 watt-hours more to be regenerated to the battery, resulting in an improvement of 2.2% energy use over a single J227a/D cycle. This result occurs because the higher downshift point allows greater torques, and thus currents, to be used while in lower gear.

An improved center 60° notching scheme was investigated using the motor and inverter models discussed in Sections 10.1-10.4. The improved scheme consisted of placing more notches in the center 60°, keeping the V/Hz the same. This resulted in pushing the harmonic voltage components to higher frequencies. Since the motor has a higher impedance at high frequency, the currents, and thus the losses, are reduced. The inverter, on the other hand, incurs more switching and snubber capacitor losses at the high frequencies. The trade-off is very close to even, but some small improvement was accomplished at low torque levels. The net drive efficiency improvement was about 1% at low torque levels. This was modeled with the vehicle simulation using Fortran statements to increase the torque produced by the motor by 1% for torque requests below 16 newton-meters. This run showed that the vehicle used a net of 197.80 watt-hours to complete a J227a/D cycle. This is a marginal improvement over the base case and would not add to the range of the vehicle.

Conclusion

The HEAVY vehicle model predicts energy use of a cycle accurately enough to make comparative studies of system changes. This study showed that there is some range improvement possible by changing the transmission shift points. The vehicle transmission ratios are near optimum efficiency points in the present design. Controller schemes investigated so far show only a marginal net improvement, trading off any gains made in motor efficiency with additional losses in the inverter.

10.8 Battery Charger

A proposed battery charging scheme is shown in Figure 10.8.1. This charger employs a full wave, phase controlled rectifier to regulate the battery charging current from the ac line. Inductor L1 is used to limit the charge current when the rectified voltage is significantly greater than the battery voltage.

Charging current will be sensed by the microprocessor controller, which will then issue the appropriate phase commands to the phase-controlled rectifier through gate drive circuits.

The electronic portion of this circuit is inexpensive since only the phase controlled rectifier need be added to the system. The control electronics already exist in the inverter controller. The largest and heaviest component in the system is the series inductor L1, which will be in the order of 2 mh to 5 mh.

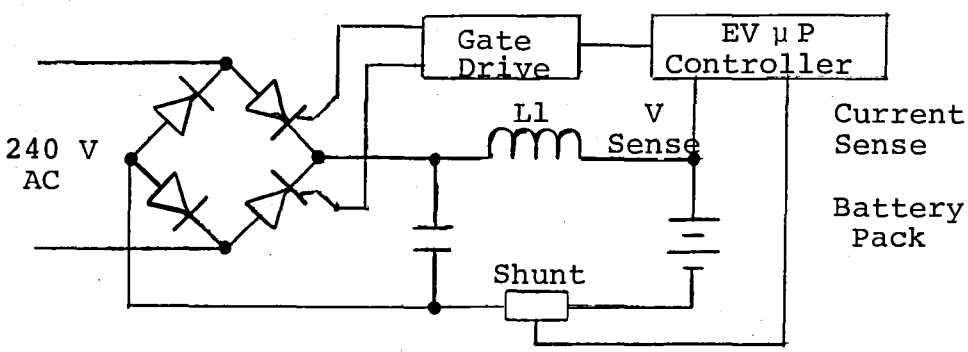

Figure 10.8.1 Battery Charger Scheme

Battery Charger Analysis and Results

The battery charger design was briefly analyzed to determine the inductance required to keep charger peak currents to an acceptable level. A schematic of the model of the battery charger is given in Figure 10.8.2.

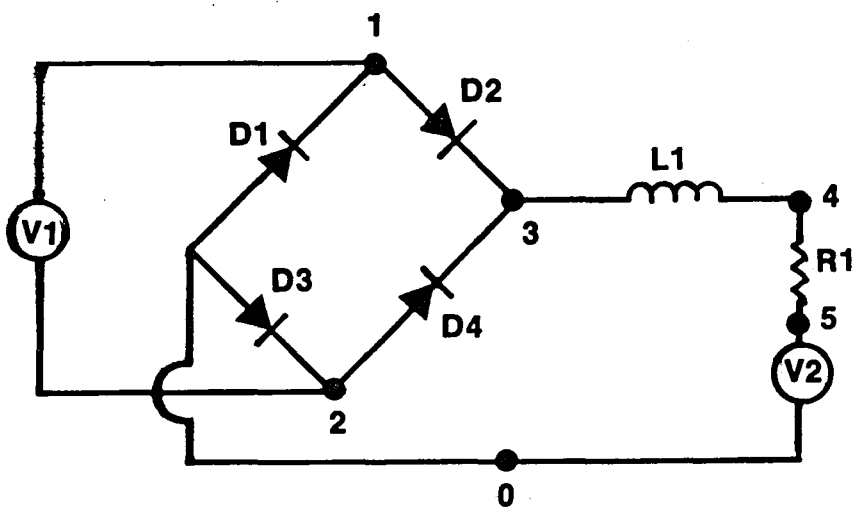

Figure 10.8.2 Battery Charger Model

The operating condition represents full duty operation. It should be noted that the microprocessor would normally control the duty cycle to maintain the proper average voltage dependent upon the battery state of charge. An initial valve of 2.653 mh was used with resulting peak current waveforms given in Figure 10.8.3. The value of the inductance was then increased in 5.300 mh which resulted in a more acceptable peak current magnitude of 60 amps as shown in Figure 10.8.4. It is realized that this design is simplified and results in packaging and weight additions.

Future considerations will focus on improvements in battery charger design accompanied with a comprehensive redesign of the energy recovery bus.

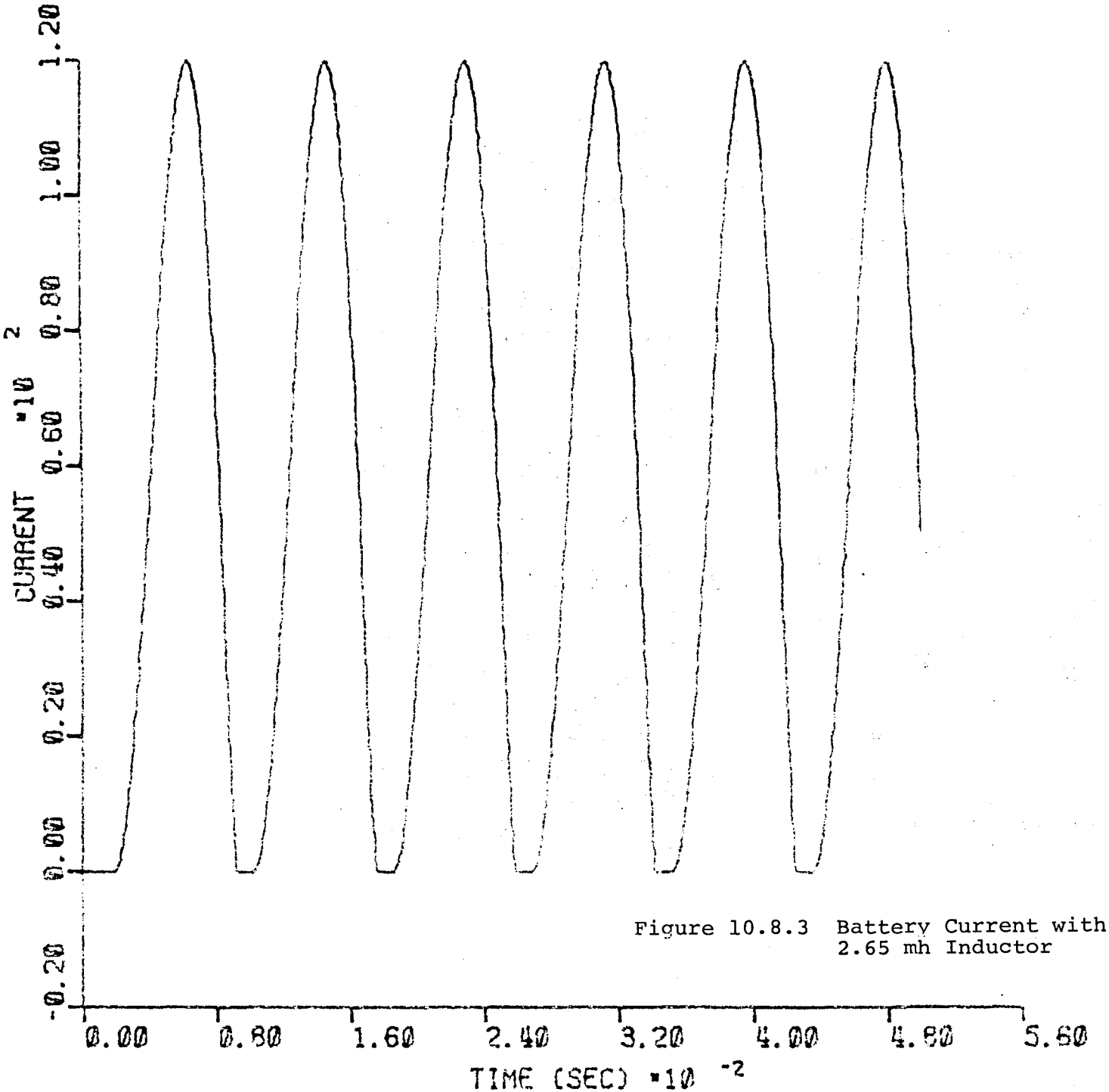

Figure 10.8.3 Battery Current with 2.65 mh Inductor

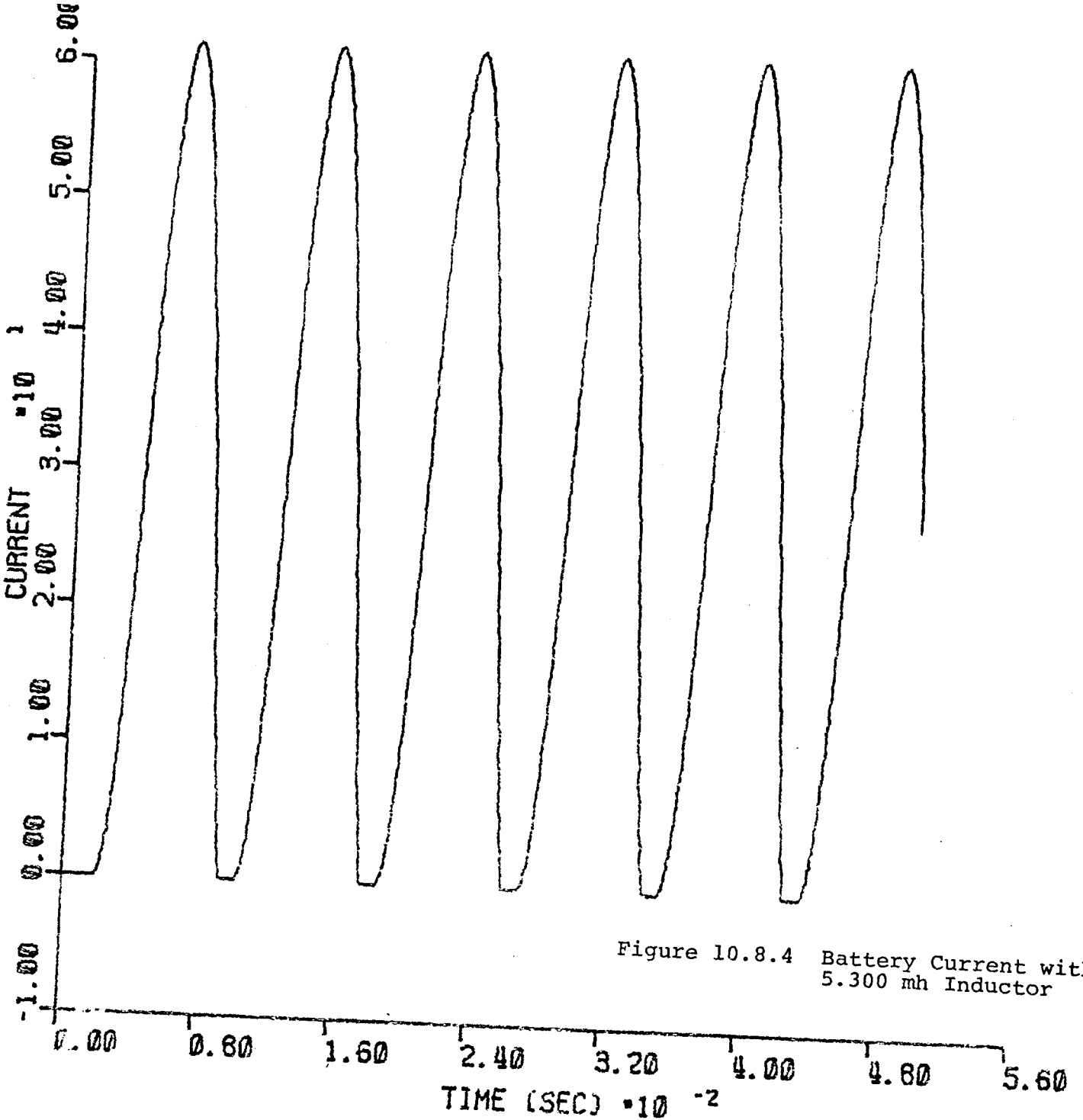

Figure 10.8.4 Battery Current with 5.300 mh Inductor

11. RELIABILITY AND MAINTAINABILITY

11.1 Reliability Model and Prediction

The reliability system model for the electric vehicle drive system is shown in Figure 11.1.1. The figure presents a serial reliability model which infers that the failure of any one (or more) of the "blocks" will fail the system.

The level of the reliability analysis was selected to be consistent with the developmental efforts of the electrical vehicle drive system. The system model was developed to supply an appropriate level of detail to provide a meaningful analysis of the system. Therefore, in some instances the "blocks" represent a singular component failure mode, while in other instances the "blocks" represent entire circuitry which supplies or performs a particular function. Additional descriptive summaries for related "blocks" (functions/components) have been noted above the associated blocks (i.e., primary power, analog circuitry, etc.). The solid blocks represent required deliverable hardware, while the dashed blocks represent nonrequired, supplied hardware. All blocks with numbers indicated at the bottom were considered in this initial reliability analysis. The numbers ("λ_i" numbers) given for each block represent associated failure rates per 10^6 operational hours. A discussion of the failure rates is given in section 11.2.

Previously it was stated that the failure of any one or more "blocks" would fail the system. What is meant by this is that the criteria assumed for successful system operation can no longer be met should one or more of the components or circuits represented by the various blocks fail. The success criteria for this initial analysis was defined to be the ability to accomplish the driving cycle defined by SAE-J227a, Schedule D. Therefore, with this criteria, the reliability system model represents an "operational" reliability model versus a more encompassing "hardware" reliability model which would include all hardware whose failure would result in a corrective maintenance action. Thus, circuitry which could fail and not prevent system operation, as defined above, is excluded from the reliability system model. An example of this type of excluded hardware is dedicated diagnostic circuitry.

The reliability system model depicted in Figure 11.1.1 was utilized to perform the initial reliability prediction. The failure rates for the electronic components were generated utilizing MIL-HDBK-217B, Reliability Prediction of Electronic Equipment. Due to the developmental phase of the system design, the parts count reliability

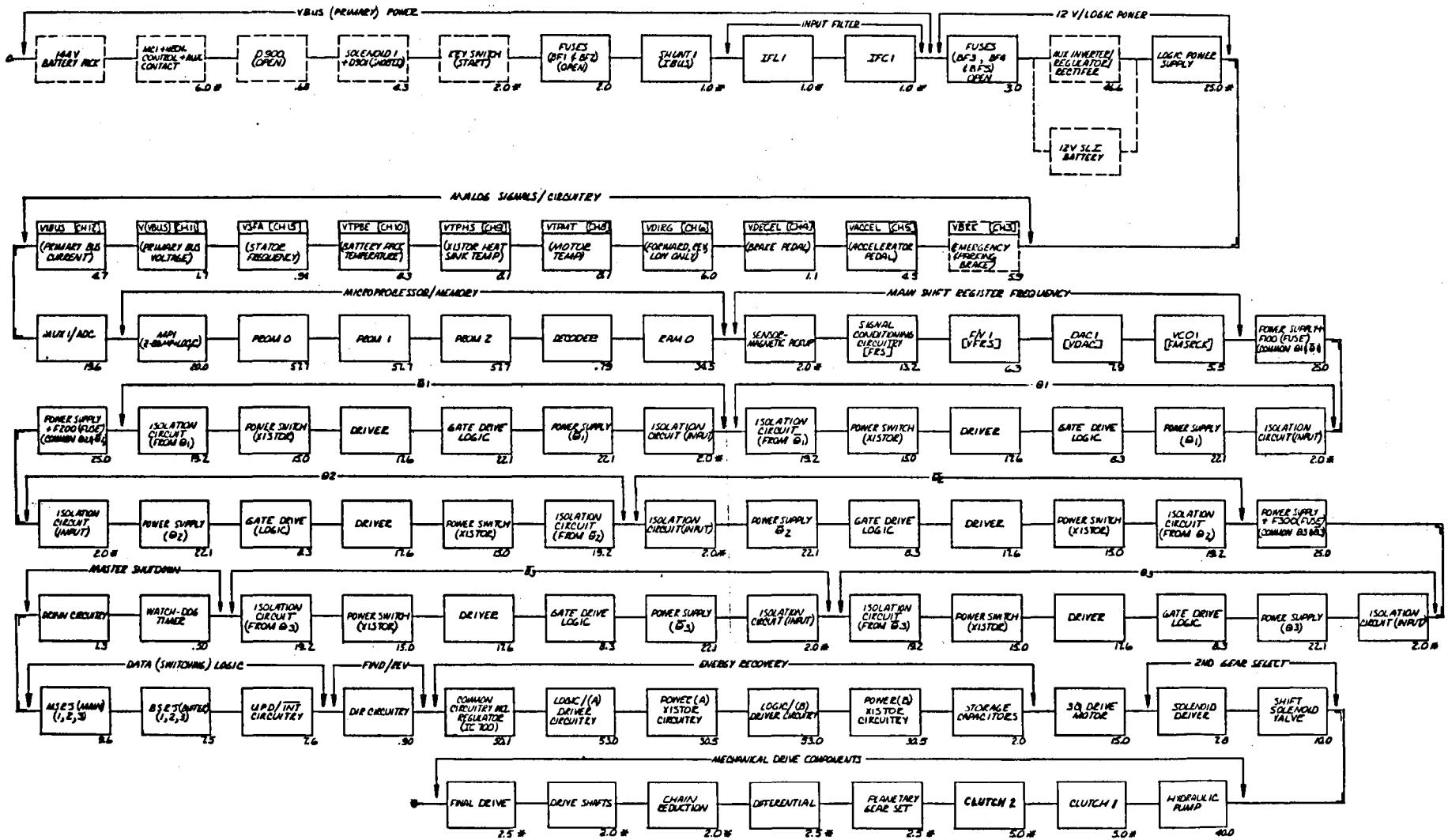

FIGURE 11.1 RELIABILITY SYSTEM MODEL
(ELECTRIC VEHICLE DRIVE SYSTEM)

prediction method was utilized as opposed to the detailed part stress analysis prediction method. The prediction assumed a ground-mobile environment and a Class C quality level. This is a very conservative approach for the electronic circuitry. The "blocks" on Figure 3.2.1, representing circuitry, were utilized as a system, in that it was assumed that all failure modes of each component comprising the system would result in system failure; which in turn would cause a failure of the electric vehicle drive system. Future detailed reliability analyses performed at the component level would include only the applicable components and component failure modes which would result in a failure of the operational success criteria. For example, consider several RF filter capacitors. If one of them fails-shorted, this would result in a system failure; however, if one of them fails open, there will be a slight reduction in RF filtering, but the system operational criteria will probably still be met. Thus, a detailed reliability model/prediction would probably only consider the shorted failure mode, or depending on the RF testing results, consider the open failure in parallel with the probability of being exposed to RF at a sufficient level to fail the operational criteria. The failure rate utilized in this prediction includes any failure of the capacitor.

The failure rates for the nonelectronic components were obtained from NPRD-1, Nonelectronic Parts Reliability Data, supplied by the Reliability Analysis Center of Rome (N.Y.) Air Development Center. The failure rates given with an asterisk (*) note that an engineering estimate/judgment was made in determining the rate given. The resulting rates are felt to be reasonable until actual test data is available.

The reliability system model is a series model. Therefore, the reliability product rule can be utilized to predict the reliability of the system:

$$R_{system} = \prod_{i=1}^{n} R_i$$

where n = the number of components in the system and
R_i = the reliability of the i^{th} component.

Considering that the majority of the system components are electronic and that the reliability of the system is being determined, an exponential failure distribution was assumed. Therefore, the initial predicted reliability for the electric vehicle drive system, as shown in Figure 11.1.1, for one year of operation is

$$R_{system} = \prod_{i=1}^{n} e^{-[(\lambda_i)\ (269 \text{ operating hours})]}$$

λ_i = failure rate of i^{th} component

Note: 269 operating hours per year was determined in Section 11.3.

$R_{system\ (1\ year)} = 0.694$ $\quad MTBF_{system} = 737$ operating hours

This states that, conservatively, the initial reliability prediction indicates that there is a 69.4% chance of operating the electric vehicle drive system for one year without failure, where failure is defined as being unable to accomplish the driving cycle by SAE-J227a, Schedule D.

Figure 11.1.2 is provided to indicate the relative contribution of the various system components to the total system unreliability (i.e., probability of failure). For instance, the switching transistors and their associated circuitry (i.e., power supplies, isolation circuitry, drivers, and logic) are initially predicted to account for 42.8% of the total probability of system failure. The ranking points to system areas where extra design and component selection care will be required during design refinements.

11.2 Failure Modes and Effect Analysis

The initial failure modes and effects analysis was performed at the level indicated by the reliability system model shown in Figure 11.1.1. Thus, in some instances the FMEA addresses component failure modes (i.e., a diode failing open or shorted), while in other instances the FMEA addresses subsystem failure modes. Subsystems refer to the blocks on Figure 11.1.1 representing circuitry groupings which supply or perform a particular function. The failure modes for the subsystems addressed the final function or signal supplied by the subsystem. The types of system failure modes considered were no output, signal failing "high" (highest possible positive voltage), or signal failing "low" (zero or lowest possible negative potential). The failure modes of the various components comprising the subsystem which would result in the subsystem failure mode were not investigated in this FMEA. Future detailed FMEA's would address subsystem component failure.

Appendix A presents the actual FMEA including the initial probability of occurrence factors and severity factors for each failure mode. The product of the probability of occurrence and the severity factor results in the criticality index for each failure mode. The results of the FMEA are discussed utilizing the resulting criticality indexes and the severity factors.

	($x10^{-6}$ Hours)	MTBF (Hours)	% Contribution	Cumulative % Contributions
Switching Transistors and Associated Circuitry	580.20	1724	42.8	42.8
Microprocessor and Memory Circuitry	228.39	4378	16.8	59.6
Energy Recovery Circuitry	219.10	4564	16.1	75.7
12 V Logic Power	73.60 (46.6)	13587	5.4	81.1
Mechanical Drive Components	61.5	16260	4.5	85.6
Analog Circuitry	49.34	20268	3.6	89.2
Main Shift Register Frequency Circuitry	34.9	28653	2.6	91.8
Data Switching Logic	24.7	40486	1.8	93.6
MUX 1	19.6	51020	1.4	95.0
VBUS Primary Power	17.98 (12.98)	55617	1.3	96.3
2nd Gear Select	17.8	57180	1.3	97.6
3Ø Motor	15.0	66667	1.1	98.7
Auto-Shutdown Indicator Circuitry	12.1	82645	0.9	99.6
Master Shutdown Circuitry	1.8	555556	0.1	99.7
Direction Circuitry	0.90	1111111	-	

NOTE: Numbers in parentheses are the failure rates for nonrequired Eaton-supplied components.

Figure 11.1.2 - System Ranking

The initial FMEA on the electric vehicle drive system has revealed several failure modes which have been assigned high (9 or 10) severity factors. Severity factors 9 or 10 indicate injury is possible. To direct the review of the FMEA, the results are presented by indicating the failure modes which have a severity factor of 10 first, followed by the failure modes with a severity factor of 9, and then the components/subsystems with the highest total criticality index. (Criticality index is the product of severity factor times failure rate.)

Severity Factors

The following severity factors were utilized in the FMEA:

Factors	
1	Insignificant impact on system operation or performance
2*	Degradation in system performance; system operation not affected
3	Degradation in system operation; no component damage or injury likely
4	Partial loss of system operational selection options; full system operation still possible
5**	Only partial system operation available
6***	System inoperable; no component damage or injury likely
7	Incorrect system operation; component damage possible
8	System inoperable; component damage possible
9	Incorrect system operation; component damage unlikely; injury possible
10	Incorrect system operation; component damage likely; injury possible

*Performance = quality of operation; function/component still operates.

**Partial system operation indicates loss of one or more operational drive modes - 1st, 2nd or R (Reverse), or system is unable to obtain proper operational speeds.

***System inoperable = unable to start vehicle; loss of all forward drive options; or loss of all drive options.

The assignment of the severity factors in this initial FMEA assumes that failure modes which result in indeterminate or erratic system operation may result in the vehicle being involved in an accident and personal injury. Future, more in-depth, FMEA's may conclude that a less severe factor is appropriate; however, an initial FMEA should consider the most severe factor that is deemed possible based on the level of the analysis performed.

Severity Factor = 10

There are two failure conditions which were assigned a severity factor of 10. The first condition concerns the loss of the speed signal or subsequent related signals, which would result in sudden downshifting of the vehicle if it is at highway speed. The second failure condition concerns the reverse direction select circuitry which could fail and allow the vehicle operator to select "reverse" but result in unexpected forward vehicle motion. The associated failure modes are summarized below.

Component/Subsystem Failure Mode	Effect
Output of stator frequency circuitry (channel 15) fails open or shorts	If vehicle in 2nd gear with accelerator depressed will immediately downshift to 1st gear resulting in possible component damage and possible accident.
Rotor speed sensor output is open or shorted	Same as above.
No output from Rotor Frequency signal conditioning circuitry	Same as above.
Reverse direction circuitry output is open	Vehicle motion is forward when reverse is selected, possible component damage and injury.

Severity Factor = 9

There are several failure conditions which are assigned a severity factor of 9. However, the effects of the various failure modes can be grouped into failure effects, the first effect being that system operation is erratic or indeterminate, and the effect is the inability to select "neutral." The associated failure modes are summarized as follows.

Component/Subsystem Failure Mode	Effect
An input channel fails with a negative potential	Multiplexer operates erratically, resulting in undesired/indeterminate system operation.
Incorrect output from analog multiplexer	Indeterminate system operation.
Incorrect output from microprocessor	Same as above.
Incorrect output from program memories (PROM's) "0," "1," or "2"	Same as above.
Incorrect output from address decoder	Same as above.
Incorrect output from random access memory (RAM) "0"	Same as above.
Incorrect output from waveform generation circuit	Same as above.
Hydraulic gearshift solenoids fail "on"	Unable to select neutral.
Hydraulic gearshift solenoid drives fail "on"	Same as above.
Clutch 1 or clutch 2 fails "on"	Same as above.

Highest Criticality Indexes

The criticality index is the product of the probability of occurrence and the severity factor. A ranking of the components or subsystems which have the highest criticality indexes, regardless of the severity factor, was prepared. An additional step was to combine (add) the criticality indexes of similar components or subsystems. These combinations will assist in placing the system elements in the proper perspective for review. The ranking of combined criticality indexes is presented below.

Component/ Subsystem	Total Criticality Index
Proms "0," "1," and "2"	1305.0
Power supplies for six main transistors	795.6
Energy recovery driver circuitry	636.0
Drivers for six main transistors	633.6
Drive power transistors	540.0
Energy recovery transistors	391.2
Auxiliary inverter	326.2
Random Access Memory	310.5
Common energy recovery circuitry	300.6

Probability of Occurrence

The occurrence factors utilized in the FMEA represent the probability of the component failure mode occurring per 10^6 hours of system operation. The factors were calculated utilizing MIL-HNBK-217B, Reliability Prediction of Electronic Components. The criteria utilized in the various component equations were as follows:

1. Ambient temperature - 60°C
2. Quality levels
   - Transistors - Plastic
   - Relays - Lower level
   - IC's - Commercial plastic
   - Diodes - Plastic
   - Capacitors - Estab. rel. (ER)
   - Resistors - Non-ER
   - Microprocessor - Class C, MIL-STD 883
3. Application - Ground mobile

The factors resulting from this criteria resulted in very conservative probability of occurrences. It is anticipated that actual system testing will result in at least an order of magnitude improvement in the IC and microprocessor factors. The reason for this estimate is that present component manufacturing and screening techniques should result in a significant improvement in "commercial grade" components. The occurrence factors should be interpreted as "worst case" factors.

As stated earlier, the FMEA addresses subsystem failure modes and component failure modes. The failure rates calculated for the components were apportioned to the failure modes of the components, based on historical data indicating the relative percentage of failures which resulted in the various failure modes. The failure rates calculated for the subsystems were apportioned equally to the various subsystem failure modes. The equal apportionment is due to the subsystems being comprised of numerous components whose failure modes result in combinations too numerous to determine the resulting subsystem failure mode percentages.

Recommendations

The recommended actions applicable to this preliminary FMEA are as follows:

1. Review all failure modes which have been assigned a severity factor of 9 or 10. The review should be conducted regardless of the assigned occurrence factors. The reason for this recommendation is to ensure that all failure modes which may result in injury are reviewed. The review should be aimed at downgrading the severity factors by further analysis to prove the high severity factor is not applicable or by considering possible design modifications.

2. Investigate/develop automatic self-checking routines to minimize the system utilization of incorrect signal/command outputs.

3. Investigate self-checking circuitry to note abrupt loss of speed signal (or subsequent related signals) once vehicle is in 2nd gear, to prevent sudden downshifting (perhaps remaining in 2nd gear).

4. Reconfigure Direction Select circuitry to alleviate possibility of failure resulting in forward motion when reverse is selected.

5. Review the gear select solenoids and associated circuitry to minimize/eliminate the possibility of a single failure resulting in an inability to select neutral. Every effort should be made to allow the selection of neutral by the vehicle operator. Selection of neutral and actually being in gear as a result of a failure unknown to the vehicle operator is a highly undesirable condition, and efforts should be expended to minimize its occurrence.

6. Similar to (5) above, review clutch 1 and clutch 2 hardware to assure the possibility of either clutch "failing on" is minimized/eliminated.

A recommendation concerning the criticality index ranking will be deferred until a later analysis. Addressing the six recommendations stated above will result in changes to the criticality index ranking. In addition, circuitry simplifications as part of the normal development process will reduce the probability of occurrence factor and, thus, the criticality index. At this stage, the criticality index ranking should serve as a guide indicating candidates for possible design review/simplification.

11.3 Reliability and Maintainability Goals

The Contract Statement of Work (SOW) alludes to a 10-year, 100,000-mile life for the complete electric vehicle drive system, which infers an average of 10,000 miles per year. Since the initial and future reliability predictions will utilize failure rates based on operating hours, 10,000 miles per year must be transformed to an equivalent number of operating hours per year. This transformation was accomplished by determining a representative driving cycle. The driving cycle utilized is defined by SAE J227a, Schedule D. Utilizing the velocities, acceleration times and incremental times given for Schedule D, it was determined that the total distance traveled in one driving cycle was approximately one mile. Therefore, in one year 10,000 driving cycles occur, with each having a duration of approximately 122 seconds. This yields

[10,000 driving cycles] x [122 seconds/cycle] x [1 hour/3600 seconds] = 339 hours/year for total driving cycles

The system is not operating during the idle phase of the driving cycle; therefore, the operating hours per year are [339 hours/year] x [122-25/122] = 269 operating hours/year.

These operating hours per year will be utilized to perform the reliability prediction discussed in a future section.

Anticipating possible future testing of the mechanical drive components separately from the electronic components, it was decided to develop separate reliability goals for the mechanical and electronic components. Based on past experience with mechanical drive mechanisms, a goal for the mechanical drive components of 0.90 reliability for 2690 hours (10 years) of operation was assigned. This means that 90% of the mechanical drivelines survive 2690 hours of operation.

Developing a goal for the electronic/electrical components is more difficult, for there is no previous experience to draw upon. The electronic/electrical system is basically a "nonforgiving" system when compared to present gasoline-powered drive systems. The electronic/electrical system essentially has two states: operative vs. nonoperative. This translates to most failures requiring maintenance to regain an operational condition as opposed to improving performance, as is the case in many maintenance actions in gasoline-powered drive systems. Considering the initial reliability prediction developed in Section 11.1., an optimistic goal of 0.70 reliability for ten years has been initially assigned to the electronic/electrical system. Achievement of this goal will require an order of magnitude improvement over the initial predicted reliability for the electronic/electrical components. Based on the conservative nature of the prediction, future detailed reliability analyses, possible selective higher reliability and/or limited redundant components, etc., it is felt that this is a reasonably attainable goal.

The initial total electric vehicle drive system goal, obtained by combining the mechanical and electronic/electrical goals, is 0.63 for ten years of operation. This goal may be revised as the system design develops. Presently the goal is optimistic in nature based on the level of analyses performed to date.

Summary

Reliability Goals for Ten Years

Mechanical Drive Components	0.90
Electronic/Electrical Components	0.70
Total Drive System	0.63

Equally important as reliability goals are maintainability goals. Considering both goals at the design development phase assists in developing a final design that is reliable and easily maintainable once a failure occurs. As with the reliability goals, separate maintainability goals have been developed for the mechanical and electronic/electrical components. These are shown on the following page.

Summary

Maintainability Goals

	Isolation Time	Repair Time
Mechanical Drive Components	0.25 hour	1 hour
Electronic/Electrical Components	0.25 hour	1 hour

The interpretation of these goals is as follows:

Isolation Time - The maximum time to isolate the cause of a failure to the lowest level replaceable component.

Repair Time - The maximum time to remove and replace the failed lowest level replaceable component and then verify the drive system is operational.

Naturally, at this stage of development there are many unanswered questions impacting maintainability. These questions refer to

- Defining "lowest replaceable components"
- "Built-in" diagnostic requirements
- Packaging of drive system
- Packaging of drive system within the vehicle
- Development of necessary diagnostic/test equipments
- Financial goals/requirements

However, recognizing that these questions will be resolved in the future, the initial review of the design indicates that these appear to be realistic goals.

12. COST CONSIDERATION

12.1 Cost Analysis

Any high volume cost estimate on a complex product which is still in the early development stage must be viewed with a "grain of salt." The approach used here was to use low volume cost estimates of the present prototype propulsion system as a base. From that base, engineering judgments pertaining to likely cost reductions of a refined production design at 10,000 and 100,000 units per year were made. The resulting costs were then compared to those obtained by plugging in system weight and power to cost estimating formulae from References 17 and 18. Finally, the results were compared with the cost goals of the Federal Electric Vehicle Commercialization Project Plan.

The following assumptions and procedures were used:

- All costs were adjusted to 1980 dollars.
- It is Eaton's policy to release only OEM cost, not manufacturing cost. Therefore, any formula-generated manufacturing costs were adjusted by a reasonable mark-up factor to yield OEM cost. Acquisition and Life Cycle costs are addressed in the next section.
- Relatively "soft tooling" was assumed for the 10,000/year estimates. "Hard tooling" and highly automated electronics fabrication was assumed for the 100,000/year estimate.
- R & D and tooling costs were assumed to be written off and were not included.
- System costs were broken down into four parts: transaxle, motor, inverter, and controller. Operator controls and sensors were included in the controller cost. The on-board charger would share many inverter components, and was lumped in with inverter cost. Throughout this analysis, no vehicle-related or battery-related costs were considered, since only the components mentioned above are under the purview of this project. It is assumed the ac system will impact the vehicle by being 10 to 20% lighter than a well-designed dc system of equivalent power. Battery utilization will be similar to a good, unbuffered dc propulsion system with a multi-speed transmission.

Figure 12.1.1 summarizes the results. Three different costs for the six main power transistors were carried through to demonstrate the system price sensitivity to this item. The ac Propulsion System will be very

Figure 12.1.1 System OEM Cost Estimate Summary

COMPONENT	Quantity/Year ($K = 1 \times 10^3$)	Cost To OEM 1980 $	Comments
Transaxle			
Eaton	10K	820	Soft tooling, many purchased parts, hand assembly,
	100K	350	hard tooling, custom parts, much jig fixturing
NASA LeRC	"Large"	270	
JPL	at least 300K	120	
MOTOR			
Eaton	10K	440	Soft tooling, much hand assembly
	100K	250	hard tooling, automated assembly and testing.
NASA LeRC	"Large"	300	
JPL	at least 300K	300	
ac INVERTER (NOTE 4)			
Eaton, main power transistors @ $100 ea.	10K	1050	Assumes transistor pricing passes directly
	100K	930	through to OEM cost.
50	10K	750	
	100K	630	
40	10K	690	
	100K	570	
ac CONTROLLER (NOTE 5)			
Eaton	10K	370	
	100K	250	
ac INVERTER + CONTROLLER (NOTE 7)			
Eaton, main power transistors @ $100 ea.	10K	1420	
	100k	1180	
50	10K	1120	
	100K	880	
40	10K	1060	
	100K	820	
NASA LeRC	"Large"	1480	
JPL	at least 300K	1120	
PROPULSION SYSTEM Totals:			
Eaton, main power transsitors @ $100 ea.	10K	2680	
	100K	1780	
50	10K	2380	
	100K	1480	
40	10K	2320	
	100K	1420	
NASA LeRC	"Large"	2050	
JPL	at least 300K	1540	

NOTES:

1. All amounts adjusted to 1980 dollars.
2. "NASA LeRC" refers to estimates computed from Ref. 17
3. "JPL" refers to estimates computed from Ref. 18
4. Inverter cost includes on-board charging components.
5. Controller cost includes contactors, operator controls, and sensors.
6. To convert NASA LeRC and JPL manufacturing costs to OEM costs, a sales and administration factor of 1.25 and profit factor of 1.12 (12%) was used.
7. The NASA LeRC and JPL cost formulae use the term "controller" to refer to both the high power inverter and logic controller together as a single component.
8. R & D prototype testing, and tooling costs are not included in estimates.

competitive with an equivalent dc system (with transmission) if power transistor prices drop below $100 each. At present, the 1,000-10,000 piece price for the Toshiba 2SD-648 Darlington used in the prototype is $209.00. The 60,000 piece price (10,000 inverters @ 6 devices/inverter) is estimated at $180.00 (Toshiba did not quote above 10,000).

Several new suppliers are entering the high power transistor market as industrial demand grows rapidly. One promising entry could yield a piece price of $150.00 in volume by 1982. Overall the transistor cost outlook continues to improve.

The 1986 DOE propulsion system cost goal (as of 10/80) is $80.00 per rated kilowatt (1977 dollars). Adjusted to early 1980 dollars, the goal is about $106.00 per rated kilowatt. The weight goal is 7 kg per rated kilowatt. To meet these goals, a 19 kw (25.5 hp) rated drive would need to retail for $2014.00 and weigh 133 kg. (293 lb).

Present projections for the Eaton ac Propulsion system give an overall weight (including on-board charger, operator controls, auxiliary contactors) of 154 kg (339 lb.), or 16% over the goal. However, it should be noted that by a modest increase of rated power to 22 kw (29.5 hp), the goal is achieved. A reasonable markup from OEM cost to sticker retail price is 1.3, assuming the vehicle manufacturer (OEM) installs the propulsion components as a finished, purchased, package. Applying this factor, the estimated OEM propulsion system price goal is $2014/1.3 = $1550. Referring to Figure 12.1.1, it is seen that the Eaton system could meet that goal in 100,000 annual quantities if the main power transistors come down in the $60.00 range. In a more reasonable 10,000 annual quantity, it is highly unlikely the cost goal can be met; even at $50.00 per transistor, the OEM cost estimate is $2380.00.

12.2 Life Cycle Cost Estimate

The life cycle cost of an item refers to the total cost the consumer incurs in using the item over its useful life. It consists of two major pieces: acquisition and ownership costs. Acquisition cost ("first cost") is the retail price. In that price is reflected development, testing, material, tooling, manufacturing, distribution, and marketing costs, along with profit. In the case of a vehicle, the cost of financing and the negative salvage cost is sometimes lumped into acquisition cost. For an automobile, ownership costs consist of maintenence costs, repair costs, replacement tires and accessories costs, insurance, registration and licensing,, fuel, parking fees, tolls, etc. For an EV, battery amortization is a

large chunk of the ownership costs. See Reference 5 for a good summary of Life Cycle Cost methodology.

In this analysis, only that portion of life cycle cost attributable to the propulsion system will be considered. Moreover, only maintenence and repair costs on the propulsion system will be considered in ownership cost, since the other factors are common to any EV and also outside the focus of this project. The ac system efficiency is comparable to a good dc system, so there is negligible recharge energy cost difference.

Life Cycle Cost for the propulsion system will be defined as:

$$LCC = \frac{\text{Propulsion system retail cost + total repair \& maint. cost}}{161{,}000 \text{ km}} \$/km$$

(1980 dollars)

As shown in the previous section, transistor cost has a strong effect on retail cost. Retail cost will again be set at 1.3 X OEM cost.

Engineering judgements on the "typical," "average" repair and maintenance costs of each propulsion system component are given in Figure 12.2.1. A ten year, 161,000 km life is postulated.

A conservative operating hours estimate for the transaxle

is $\frac{161000 \text{ km}}{30 \frac{\text{km}}{\text{hr}}} = 5360$ hrs.

Much of this time would be spent in a low torque, low stress regime. The operating hours are well within the present life expectations of quality seals, bearings, and gears. Only the parking latch mechanism and high speed chain are listed in Figure 12.2.1, and even these components could very well last 10 years if not abused.

It is not unreasonable to assume zero maintenence on the motor. Industrial ac induction motors easily outlive the required vehicle life. To achieve full motor life, the bearings must be properly lubricated and the stator winding insulation temperature rating must not be exceeded. The motor temperature sensor helps ensure the latter requirement. Motor failure should be so rare that it has negligible impact.

Inverter repair represents the highest cost item, but also is highly uncertain. There are no certain wear out mechanisms in solid-state parts over the ten year period, but the random failure rate is not zero. Also, unusual failures, such as due to a lightning-induced power line surge

Figure 12.2.1 Propulsion System Life Cycle Cost

COMPONENT	Repair/Maintenance Description	Frequency	Cost Per Time (parts + labor) $	Lifetime Total Cost $
Transaxle	Change Oil	once over life	15	15
	Replace first-stage chain	once over life	50	50
	Replace parking latch mechanism	once over life	60	60
Motor	None expected			0
Inverter	Replace main drive transistor w/integral diode	twice over life	90	180
	Repair/Replace base drive board	twice over life	40	80
	Replace a large filter capacitor	once over life	30	30
	Replace a snubber cap or resistor	three times over life	30	90
Controller	Replace contacts on main contactor	once over life	30	30
	Repair/replace accel/decel signal senders	once over life	50	50
	Repair main logic board or solenoid driver	twice over life	60	120
	Replace one of several protection fuses	once/2 years	10	40
			Total	745
			Life Cycle Cost *	0.023$/km
				0.037$/mi

*Assume propulsion system retail cost is $3000.

during charging, an insulation defect, an inadvertant short between power phases, or an infant mortality, will take their toll in the real world. It is cost prohibitive to design and test to aerospace rigor. The life cycle cost estimate attempts to form a reasonable average based on industrial experience.

The system contains a power contactor and operator controls. These parts have lifetimes within the vehicle lifetime, and as such show up in Figure 12.2.1. The protection fuses will occasionally blow due to fatigue or a momentary fault. Such a fault need not do damage to other parts.

The total propulsion system life cycle cost estimate is $0.023/km (retail price of system assumed $3000). It has wide variability due to the random nature of the most expensive failures.

For comparison, life cycle cost as defined earlier was derived from the cost estimating formulae given in References 17 and 18. The NASA LeRc figure is $0.022/km (no distinction between ac and dc systems is made). The JPL figure is also $0.022/km. Purchase price dominates all these estimates.

13. CONCLUSIONS

This report describes work relating to the development and testing of an ac propulsion system for an electric vehicle. The system consists of a 2-speed automatic transaxle, 18.6 kw ac induction traction motor, 30 kw inverter, and overall logic controller.

The important conclusions are listed below.

1. The system concept is technically feasible.

2. Presently available transistors, although expensive, can reliably handle the main switching task in a PWM inverter.

3. A multi-speed transmission pays large dividends in reducing weight and cost in both the motor and inverter for a given over-the-road performance.

4. The ac approach has comparable efficiency to that of known, good dc systems.

5. For a feasible ac system using transistors at rated 19 kw, higher battery voltage leads to system advantages. A voltage of 108V is not practical. A 144V bus is the minimum recommended. New designs should consider higher voltages.

6. Overall system cost is very sensitive to main transistor cost. Transistors in the $60.00 range are needed to compete with comparable dc systems on first cost.

APPENDIX A

FAILURE MODES, EFFECTS, AND CRITICALITY ANALYSIS

Failure Modes, Effect, and Criticality Analysis

Project Description: Electric Vehicle Drive System

Date:

Page 1 of 17

Revision Date:

DWG. NO. 48804, SHEETS 1 & 2

Engineer:

Component	Component Function	Failure Mode	Effect of Failure	Cause of Failure	Occur	Severity	Detection	Criticality Index	Remarks
MC1 + Mechanical Linkage	Mechanically applies/removes primary battery voltage to drive system	Fails in "off" position	Unable to apply primary voltage to system. System inop.	. Broken contact . Broken pedal linkage	3.0	6		18.0	
		Fails in "on" position	Unable to remove battery voltage. Batteries will discharge continuously.	. Pedal linkage broken/jammed	3.0	6		18.0	
Diode D900	Battery polarity check failsafe prevents application of battery voltage if battery cables are reversed (i.e. ground positive)	Open	Unable to energize solenoid 1; unable to apply primary battery voltage, system inop.		.7	6		4.2	
		Shorted (open)	Loss of battery polarity check/failsafe. Will burn open after shorting.		2.7	1		2.7	
Solenoid 1	Permits pedal to control the application and removal of primary battery voltage	Fails "on"	Unable to open MC1 once MC1 is in "on" position. Batteries will discharge continuously.	. Plunger jammed . Broken return spring	.8	6		4.8	
		Fails "off"	Unable to close MC1. Once MC1 is in "off" position, unable to apply primary battery voltage. System inop.	. Open/shorted coil . Plunger jammed	.8	6		4.8	
Diode D901	Provide discharge path for solenoid 1 when deenergized	Shorted (open)	See solenoid 1 - fails "off." If remains shorted, will probably blow open after shorting.		2.7	2		5.4	
		Open	Loss of discharge path for solenoid 1. Arcing in key switch.		.7	2		1.4	
Key Switch	Turns solenoid 1 on and off	Fails in "start" position	See solenoid 1 - fails "on" Unable to remove key		.7	8		4.2	

Form E30-80 (Rev. 11/79)

Printed in U.S.A.

Failure Modes, Effect, and Criticality Analysis

Date | Page 2 of 17

Project Description: Electric Vehicle Drive System

Revision Date | DWG. NO. 48804, SHEETS 1&2

Engineer

Component	Component Function	Failure Mode	Effect of Failure	Cause of Failure	Occur	Severity	Detection	Criticality Index	Remarks
Key Swtich (Cont'd)		Fails in "off" position	. See solenoid 1 - fails "off"		.7	6		4.2	
		Fails in "on" position	. See solenoid 1 - fails "off" . Unable to remove key		.7	6		4.2	
Fuse BF1	+ Primary BUS circuit protection from excess current	Open	+ BUS is opened. Loss of primary battery voltage. System inop.		1.0	6		6.0	
Fuse BF2	- BUS circuit protection from excess current	Open	- BUS (V common) is opened. Loss of primary battery voltage. System inop.		1.0	6		6.0	
Shunt 1	Allow sensing of BUS current (+ BUSS and - BUSS)	Open	- BUS is opened. Loss of primary battery voltage. System inop.		1.0	6		6.0	
1FL1 Input Filter inductor	Reduce ripple current	Open	Loss of primary battery voltage to system. System inop.		.5	6		3.0	
		Shorted	Increase in ripple current		.5	1		.5	
1FC1 Input Filter	Reduce fluctuations in primary voltage	Shorted	See 1FL1 - open BF1 and/or BF2 will open		.5	6		3.0	
		Open	Loss of primary voltage filtering		.5	1		.5	
Fuse BF3	+ Secondary BUS (aux.) inverter) circuit protection	Open	Loss of "switched" 12V; logic power. System inop.		1.0	6		6.0	
Fuse BF4	- Secondary BUS (aux. inverter) circuit protection	Open	See BF3 - open		1.0	6		6.0	

Failure Modes, Effect, and Criticality Analysis

Date | Page 3 of 17

Project Description: Electric Vehicle Drive System

Revision Date | DWG. NO. 48804, SHEETS 1, 2 & 12

Engineer

Component	Component Function	Failure Mode	Effect of Failure	Cause of Failure	Occur	Severity	Detection	Criticality Index	Remarks
Fuse BF5	Provides reference for VBUS/IBUS measurements. Protects logic common from large fault currents on primary bus	Open	Loss of reference. VBUS/IBUS signals will float. Possible auto shutdown if "float" reaches limits.		1.0	6		6.0	
Diode D902	Provides discharge path for solenoid 2 when deenergized.	Shorted (Open)	Loss of "switched" 12V logic power. System inop. If it remains shorted, will probably blow open.		2.7	2		5.4	
		Open	Insignificant effect.		.7	1		.7	
Solenoid 2	Prevent removal of key unless primary battery voltage is removed. Mandatory reminder to "turn off" batteries.	Fails "off"	Key can be removed with primary battery voltage still applied to system. Batteries would continuously discharge unless contactor pedal depressed.		.8	2		1.6	
		Fails "on"	Unable to remove key. System still operational.		.8	1		.8	
Auxiliary Inverter/ Regulator/ Rectifier Circuitry	Converts primary battery voltage (144VDC) to a regulated 13VDC	Open	Loss of "switched" 12V; loss of logic power. After 12V battery discharges below 9V, then system inop.		23.3	6		139.8	
		Shorted	BF3 or BF4 should open. Loss of "switched" 12V. Loss of logic power. System inop. Component damage likely.		23.3	8		186.4	
Logic Power Supply	Provides power to logic circuitry. Converts 13VDC input to +5VDC, +15VDC, -15VDC	Open (5V)	Loss of logic power, loss of base drive. Auto shutdown. System inop.		4.2	6		25.2	
		Shorted (5V)	Loss of base drive, auto shutdown. Circuit protection within power supply.		4.2	6		25.2	

Form 839-00 (Rev. 11/79)

Printed in U.S.A.

Failure Modes, Effect, and Criticality Analysis

Project Description: Electric Vehicle Drive System

Date | Page 4 of 17

Revision Date | DWG. NO. 48804, SHEETS 1, 2 & 4

Engineer

Component	Component Function	Failure Mode	Effect of Failure	Cause of Failure	Occur	Severity	Detection	Criticality Index	Remarks
Logic Power Supply (cont'd)		Open (+15V)	Loss of "fwd" direction, loss of battery, transistor, and motor over-temperature protection. Loss of all analog circuits. System inop.		4.2	6		25.2	
		Short (+15V)	See open (+15V) circuit protection within power supply.		4.2	6		25.2	
		Open (-15V)	Loss of "rev" direction auto shutdown due to TPBE, TPHS, and TPMT, indicating over-temperature condition. Loss of all analog circuits. System inop.		4.2	6		25.2	
		Short (-15V)	See short (-15V) circuit protection within power supply.		4.2	6		25.2	
VBRK (Channel 3) circuitry	Prevents system operation (forward/reverse motion) if either parking brake or emergency brake is on. Provides indicating signal to μ processor.	Fails "on" (indicates brakes applied).	System inop.; unable to move in forward or reverse.		3.0	6		18.0	
		Fails "off" (indicates brakes released).	Unable to obtain acceptable speed. Excessive heat generated due to movement if brakes applied.		3.0	5		15.0	
VACCEL (Channel 5) circuitry	Provides acceleration request signal to μ processor as a function accelerator pedal movement/position.	Fails "open" (maximum acceleration exceeded).	Auto-shutdown of system when VACCEL exceeds 4.5 VDC.		2.3	6		13.8	
		Fails "closed" ("0" acceleration position).	Unable to accelerate.		2.3	5		11.5	

Failure Modes, Effect, and Criticality Analysis

Date | Page 5 of 17

Project Description: Electric Vehicle Drive System

Revision Date: DWG. NO. 48804, SHEETS 3 & 4

Engineer

Component	Component Function	Failure Mode	Effect of Failure	Cause of Failure	Occur	Severity	Detection	Criticality Index	Remarks
VDECEL (Channel 4) Circuitry	Provides deceleration signal to μprocessor as a function of brake pedal movement position	Fails "open" (maximum deceleration exceeded)	Auto-shutdown of system when VDECEL exceeds 4.5 VDC		.6	6		3.6	
		Fails "closed" ("0" deceleration position)	Loss of regenerative braking. Hydraulic braking still operative		.6	1		.6	
VDIRG (Channel 6) Circuitry	Provides direction request signals (forward, reverse, or lo only) to μprocessor	Fails "open"	Only "lo gear only" direction signal is available - loss of "forward & reverse"		3.0	5		15.0	
		Fails "closed"	Continuously in forward or reverse depending on which "closed" position is failed		3.0	5		15.0	
VTPMT (Channel 8) Circuitry	Provides motor stator temperature. Signal to μprocessor.	Fails "high" condition (open)	Indicates maximum motor temperature exceeded. Auto-shutdown of system initiated.		4.0	6		24.0	
		Fails "low" condition	Loss of motor temperature monitoring. Possible overheating of motor.		4.0	1		4.0	
VTPHS (Channel 9) Circuitry	Provides power switching transistors heat sink temperature indicating signal to μprocessor	Fails "high" condition (open)	Indicates maximum heat sink temperature of switching transistors is exceeded, auto-shutdown is initiated.		4.0	6		24.0	
		Fails "low" condition-0-	Loss of over-temperature protection for power switching transistors. Over-temperature condition will result in loss of transistor(s).		4.0	1		4.0	
All Input Channels	Possible failure mode which is possible on any input channel.	Fails with negative potential	MUX 1 operates irratically, undesired system operation.		.5	9		4.5	

Form E30-80 (Rev 11/78)

Printed in U.S.A.

Failure Modes, Effect, and Criticality Analysis

Date | Page 6 of 17

Project Description: Electric Vehicle Drive System

Revision Date | DWG. NO. 48804, SHEET 3

Engineer

Component	Component Function	Failure Mode	Effect of Failure	Cause of Failure	Occur	Severity	Detection	Criticality Index	Remarks
VTPBE (Channel 10) Circuitry	Provides primary batteries electrolyte temperature indicating signal to μprocessor	Fails -"high" condition (open)	Indicates maximum battery temperature is exceeded. Auto-shut-down is initiated.		4.1	6		24.6	
		Fails "low" condition	Loss of over-tempera-ture protection for primary batteries. Over-temperature con-dition will result in loss of the affected battery(s).		4.1	1		4.1	
V(VBUS) (Channel 11) Circuitry	Provides primary BUS voltage indicating signal to μprocessor	Fails-"high" condition	Indicates maximum BUS voltage exceeded. Auto-shutdown initiated.		.8	6		4.8	
		Fails-"low" condition	Indicates BUS voltage is below minimum acceptable voltage. Auto-shutdown initiated.		.8	6		4.8	
VIBUS (Channel 12) Circuitry	Provides primary BUS current indicating signal to μprocessor	Fails-"high" condition	Indicates maximum positive BUS current is exceeded. Auto-shutdown initiated.		2.4	6		14.4	
		Fails-"low" condition	Indicates maximum negative BUS current is exceeded. Auto-shutdown initiated.		2.4	6		14.4	
VSFA (Channel 15) Circuitry	Provides motor stator frequency indicating signal to μprocessor	Open (fails low)	Loss of stator freq. input to processor. Slip pull-out occurs. If vehicle in 2nd gear, immediate downshift to 1st gear, possible damage to drive system compon-ents.		.5	10		5.0	
		Shorted (GND)	See "open."		.5	10		5.0	

Failure Modes, Effect, and Criticality Analysis

Date | Page 7 of 17

Project Description: Electric Vehicle Drive System

Revision Date: DWG. NO. 48804, SHEETS 4 & 5

Engineer

Component	Component Function	Failure Mode	Effect of Failure	Cause of Failure	Occur	Severity	Detection	Criticality Index	Remarks
MUX 1 w/ADC	Multiplexes and converts analog transducer signals to digital signals which serve as primary data inputs to μ processor	No output	Loss of all data input to processor, no update, auto-shutdown Due to failsafe limits.		9.8	6		58.8	
		Input channel fails with negative potential	MUX 1 operates irratically; undesired system operation.						
		Incorrect output (line fails high or low)	Possible: 1. false or no warning 2. unwanted or no auto shutdown 3. incorrect operation μ processor issues commands based on incorrect data		9.8	9		88.2	
MP1 μ Processor and Control Logic Circuitry	Provides master control function for system operation. Major functions are to generate: . slip command . direction signal . warning signals . initiate auto-shutdown . control power transistor duty cycle . shift command	Incorrect output(s)	. Possible auto-shutdown if no update supplied . Incorrect/undesired system operation . Unwanted or no auto-shutdown . False or no warnings . Incorrect slip command . Unwanted or no shift command . Incorrect power Xistor(s) duty cycle		10.0	9		90.0	
		No output	Auto-shutdown of drive due to no update from μ processor		10.0	6		60.0	
PROM "O"	Provide permanent storage for portion of control system operating program.	Incorrect output (output fails high or low)	Incorrect/undesired system operation, processor issues incorrect commands		29.0	9		261.0	
		No output	Auto-shutdown of system		29.0	6		174.0	

Failure Modes, Effect, and Criticality Analysis

Date | Page 8 of 17

Project Description: Electric Vehicle Drive System

Revision Date: Dwg. No. 48804, Sheets 5, 8, & 9

Engineer

Component	Component Function	Failure Mode	Effect of Failure	Cause of Failure	Occur	Severity	Detection	Criticality Index	Remarks
PROM "1"	See PROM "0"	See PROM "0"	See PROM "0"						
PROM "2"	See PROM "0"	See PROM "0"	See PROM "0"						
Decoder (IC258)	Controls operation of memory chips (PROMS and RAMS) by selecting appropriate chip as directed by μprocessor	Incorrect output	Data processed by wrong memory chip resulting in incorrect/ undesired system operation.		.8	9		7.2	
RAM "0"	Provides temporary data storage during operation of control system program	Incorrect output	Incorrect/undesired system operation μprocessor issues incorrect commands		34.5	9		310.5	
Sensor - Magnetic Pickup	Provide rotor speed signal	Open	"0" speed indication, if accelerator is depressed, system will downshift, possible damage to drive system components. System will shut down as soon as accelerator released.		1.0	10		10	
		Shorted	See "open"		1.0	10		10	

Failure Modes, Effect, and Criticality Analysis

Date | Page 9 of 17

Project Description: Electric Vehicle Drive System

Revision Date: Dwg. No. 48804, Sheets 7, 8, & 9

Engineer

Component	Component Function	Failure Mode	Effect of Failure	Cause of Failure	Occur	Severity	Detection	Criticality Index	Remarks
FRS Signal Conditioning Circuitry	Converts sinusoidal speed signal from sensor to output pulses and doubles the frequency	No ouptut	See sensor - open		6.6	10		66	
		Incorrect frequency output	Incorrect inverter slip and duty cycle resulting in incorrect motor torque		6.6	5		33	
F/V 1 Circuitry (VFRS)	Converts FRS signal to analog voltage which varies as a function of the rotor frequency	No output	See FRA--no output		3.2	10		32	
		Incorrect output voltage	Incorrect inverter duty cycle resulting in incorrect motor torque		3.2	5		16	
DAC 1 Circuitry (VDAC)	Converts digital slip command to analog voltage for summation with VFRS to generate stator frequency signal	No output	No motor torque generated. System inop. coast to stop, or use service brakes. No negative torque		4.0	6		24	
		Incorrect voltage output	Incorrect inverter slip resulting in incorrect motor torque		4.0	5		20	
VCO1 Circuitry (FMSRCK)	Converts stator frequency signal to clock pulses which allow serial transfer of power xistors' duty cycle data	No output	Unable to enter duty cycle data, lose stator freq., motor goes out of synch., system inop.		2.8	6		16.8	
		Incorrect freq. output	Incorrect inverter slip resulting in incorrect motor torque		2.8	5		14.0	
Power Supply Circuitry (Common to θ_1 & $\bar{\theta}_1$)	Generates DC voltages for θ_1 and $\bar{\theta}_1$ base drive circuitry	No output	Phase 1 (θ_1) leg of motor inoperative		12.5	6		75	
			Minimal torque, motor inoperative						

Failure Modes, Effect, and Criticality Analysis

Date

Page 10 of 17

Project Description: Electric Vehicle Drive System

Revision Date: Dwg. No. 48804, Sheets 6 & 7

Engineer

Component	Component Function	Failure Mode	Effect of Failure	Cause of Failure	Occur	Severity	Detection	Criticality Index	Remarks
		Incorrect oscillator operation (1/2 of oscillator inoperative)	1/2 of complementary power transistors inop. minimal motor torque, motor inoperative		12.5	6		25	
Power Supply Circuitry θ_1	Generates DC voltages (+5V, -5V, +13V) for θ_1 base drive circuitry	No output	θ_1 power switch inoperative (1/2 of complementary pair) motor inoperative due to loss of torque		22.1	6		132.6	
Input Isolation Circuit to θ_1	Provides isolation from input circuitry to enable θ_1 power transistor's emitter to be common to its base drive circuitry	Open	Loss of drive to θ_1 power switch, minimal motor torque, system inop.		1.0	6		6	
		Shorted (output low)	θ_1 (complementary power transistor) inop. due to constant θ_1 input signal, motor inop.		1.0	6		6	
Gate Drive Logic - θ_1	Provides turn-on signal to Q_1 driver when Q_1 power transistor is off (i.e. not conducting) and θ_1 "on" command present	Open (output to driver)	Q_1 power transistor will never be turned on, motor inop.		4.2	6		25.2	
		Open (output to θ_1 isolation CKT)	Single phasing results minimal motor torque, system inop.		4.2	6		25.2	
Driver - θ_1	Provides necessary turn-on power and duty cycle for θ_1 power transistor	No output	See θ_1 gate drive logic-"open"		8.8	6		52.8	
		Slow turn-off	θ_1 (complementary power transistor) "on" time altered, incorrect wave form developed for Phase 1, minimal torque, transistor overheats		8.8	6		52.8	

Form 838-00 (Rev. 11/79)

Printed in U.S.A.

Failure Modes, Effect, and Criticality Analysis

Project Description: Electric Vehicle Drive System

Date:

Revision Date: Dwg. No. 48804, Sheets 6 & 7

Engineer:

Component	Component Function	Failure Mode	Effect of Failure	Cause of Failure	Occur	Severity	Detection	Criticality Index	Remarks
Power Transistor θ_1	1/2 of complementary transistor pair which develops synthesized 3θ AC wave form to drive motor	Open	See θ_1 gate drive logic-"open"		3.0	6		18	
		Shorted	θ_1 hall switch current sensor should turn off θ_1 power transistor, minimal torque, motor inop.		12.0	6		72	
Isolation Circuit from θ_1 to θ_1	Provides isolation of θ_1 from θ_1 base drive circuitry	Open	θ_1 power transistor will not be allowed to turn on, motor inop.		9.6	6		57.6	
		Shorted (output low)	Incorrect Phase 1 wave form can occur, causing erratic operation of drive motor		9.6	3		28.8	
Input Isolation Circuitry to θ_1	Provides isolation from input circuitry to enable θ_1 power transistor's emitter to be common to its base drive circuitry	Open	Loss of drive to θ_1 power switch, minimal torque, motor inop.		1.0	6		6	
		Shorted (output low)	θ_1 (complementary power transistor) inop. due to constant θ_1 input signal, motor inop.		1.0	6		6	
Power Supply Circuitry θ_1	Generates DC voltages (+5V, -5V, +13V) for θ_1 base drive circuitry	No output	θ_1 power transistor inop. (1/2 of complementary pair) motor inop. due to minimal torque		22.1	6		132.6	

Failure Modes, Effect, and Criticality Analysis

Date | Page 12 of 17

Project Description: Electric Vehicle Drive System

Revision Date: Dwg. No. 48804, Sheets

Engineer

Component	Component Function	Failure Mode	Effect of Failure	Cause of Failure	Occur	Severity	Detection	Criticality Index	Remarks
Gate Drive Logic - $\overline{\theta}_1$	Provides turn-on signal to $\overline{\theta}_1$ driver when θ_1 power transistor is off and $\overline{\theta}_1$ "on" command is present	Open (output to driver)	$\overline{\theta}_1$ power transistor will never be turned on, motor inop.		4.2	6		25.2	
		Open (output to θ_1	Single phasing results minimal torque, motor inop.		4.2	6		25.2	
Driver - $\overline{\theta}_1$	Provides necessary turn-on power and duty cycle for $\overline{\theta}_1$ power transistor	No output	See $\overline{\theta}_1$ gate drive logic-"open"		8.8	6		52.8	
		Slow turn-off	θ_1 (complementary power transistor) "on" time altered, incorrect wave form developed for Phase 1, minimal torque, transistor overheats		8.8	6		52.8	
Power Transistor $\overline{\theta}_1$	1/2 of complementary transistor pair which develops synthesized 3θ AC wave form to drive motor	Open	See $\overline{\theta}_1$ gate drive logic "open"		3.0	6		18	
		Shorted	θ_1 hall switch current sensor should turn off θ_1 power transistor, minimal torque, motor inop.		12.0	6		72	
Isolation Circuit from θ_1 to $\overline{\theta}_1$	Provides isolation of $\overline{\theta}_1$ from θ_1 base drive circuitry	Open	$\overline{\theta}_1$ power transistor will not be allowed to turn on, motor inop.		9.6	6		57.6	
		Shorted (output low)	Negative V_{CE} sense circuit disabled on θ_1, incorrect Phase 1 wave form developed, erratic operation of drive motor		9.6	3		28.8	

Form 809-68 (Rev. 11/72) Printed in U.S.A.

Failure Modes, Effect, and Criticality Analysis

Project Description: Electric Vehicle Drive System

Date:

Page: 13 of 17

Revision Date:

Dwg. No. 48804, Sheets 5 & 11

Engineer:

Component	Component Function	Failure Mode	Effect of Failure	Cause of Failure	Occur	Severity	Detection	Criticality Index	Remarks
θ_2 Circuitry, Function, Failure Modes & Effects	are the same as θ_1 by symmetry								
$\overline{\theta}_2$ Circuitry, Function, Failure Modes & Effects	are the same as $\overline{\theta}_1$ by symmetry								
θ_3 Circuitry, Function, Failure Modes & Effects	are the same as θ_1 by symmetry								
$\overline{\theta}_3$ Circuitry, Function, Failure Modes & Effects	are the same as $\overline{\theta}_1$ by symmetry								
"Watch-Dog" Timer	Checks for the presence of a preiodic pulse from the microprocessor which is utilized as an indicator of proper microprocessor operation. If pulse disappears, drive is shut down	Undersized output	Drive signals inhibited inadvertently, drive motor is unwantedly disabled		.3	9		2.7	
		Fails to supply required shutdown output when needed	Loss of drive control, power transistors maintain existing duty cycle and drives remain enabled though shutdown is required, action by vehicle operator required		.3	7		2.1	
DRINH Circuitry (Master Inhibit Shutdown)	1) Inhibits logic drive signals when motor is at rest & no "accel" command is present	Undesired output	See "watch-dog" timer -At rest, motor shutdown not assured		.7	7		4.9	
	2) Provides circuitry for normal drive shutdown in response to failure detection	Fails to supply required output	-Unknown motor response on start-up ($\approx$ 50 ms) -Loss of normal drive shutdown capability,		.7	7		4.9	
	3) Issues command for neutral in transaxle		component damage likely if failure condition requires drive shutdown						

Failure Modes, Effect, and Criticality Analysis

Date | Page 14 of 17

Project Description: Electric Vehicle Drive System

Revision Date: Dwg. No. 48804, Sheet 11

Engineer

Component	Component Function	Failure Mode	Effect of Failure	Cause of Failure	Occur	Severity	Detection	Criticality Index	Remarks
MSR's (Main Shift Registers) 1, 2, & 3	Store and output present, real-time 30 PWM wave form	No output	Drive motor shutdown, system inop.		4.8	6		28.8	
		Incorrect output	Minimal torque, drive motor inop., possible high fault currents in transistors		4.8	8		38.4	
BSR's (Buffer Shift Registers) 1, 2, & 3	Accepts and stores new wave form from microprocessor, then updates MSR's when commanded	No output	MSR's - no output		3.8	6		22.8	
		Incorrect output	See MSR's-incorrect output		3.8	8		30.4	
UPD/$\overline{INT}$ Circuitry	1) Synchronize the loading of the new wave form from the BSR's to the MSR's	No UPD output	MSR's maintain existing wave form, eventually loss of drive control		2.5	6		15	
	2) Provides signal to the microprocessor that the BSR's are ready to receive updated wave form information	No $\overline{INT}$ output	Unable to update BSR's see UPD-no output		2.5	6		15	
		Incorrect output	Erratic drive operation		2.5	9		22.5	
DIR Circuitry	Translates vehicle operator commands (Fwd., Rev., Lo only) to 3 different voltage levels	Open (Fwd.)	Results in "lo only" output command		.5	5		2.5	
		Open (Rev.)	Results in "lo only" output command, (i.e. Rev. selected, vehicle motion is Fwd. instead		.5	10		5	
30 Drive Motor	Provide mechanical power to provide vehicle motion	No	Loss of vehicle motion capability, system inop.		15.0	6		90	

Failure Modes, Effect, and Criticality Analysis

Project Description: Electric Vehicle Drive System

Date:

Revision Date:

Dwg. No. 48804, Sheets 13 & 14

Engineer:

Component	Component Function	Failure Mode	Effect of Failure	Cause of Failure	Occur	Severity	Detection	Criticality Index	Remarks
(A) Power Transistor Circuitry Including Storage Capacitors	+BUS/switching transistor for the primary winding of the energy recovery system transformer	Open	+Battery BUS voltage increases resulting in the voltage sensing circuit inhibiting the complementary power transistors, drive system shutdown		16.3	6		97.8	
		Shorted	(B) Power transistor would not operate resulting in the -battery BUS voltage increasing, voltage sensing circuit would inhibit the complementary power transistors, drive system shutdown		16.3	6		97.8	
(A) Driver Circuitry	Provides base drive current and duty cycle for (A) power transistor	No output	See (A) power transistor "open"		53.0	6		318	
(B) Power Transistor Circuitry Including Storage Capacitors	-BUS/switching transistor for the primary winding of the energy recovery system transformer	Open	-Battery BUS voltage increases resulting in the voltage sensing circuit inhibiting the complementary power transistors, drive system shutdown		16.3	6		97.8	
		Shorted	(A) Power transistor would not operate resulting in the +battery BUS voltage increasing, voltage sensing circuit would inhibit the complementary power transistors, drive system shutdown		16.3	6		97.8	
(B) Driver Circuitry	Provides base drive current and duty cycle for (B) power transistor	No output	See (B) power transistor "open"		53.0	6		318	

Failure Modes, Effect, and Criticality Analysis

Date | Page 16 of 17

Revision Date

Project Description: Electric Vehicle Drive System

Dwg. No. 48804

Engineer

Component	Component Function	Failure Mode	Effect of Failure	Cause of Failure	Occur	Severity	Detection	Criticality Index	Remarks
Common Circuitry Including Regulator	Provides power and control for (A) & (B) power transistors' base drive circuits - 20 KHZ at a 45% duty cycle	No output	Voltage sensing circuits will inhibit the complementary power transistors resulting in the shutdown of the drive system		50.1	6		300.6	
Solenoid Valve (Double-Acting Solenoid)	Selects neutral, 1st (lo), or 2nd gear (hi) depending whether the solenoids are on or off:	"Lo" solenoid fails	Unable to select 1st gear (lo)		2.5	6		15	
	"Lo" solenoid on= 1st gear	"Lo" solenoid fails on	1st gear selected continuously, possible drive system damage if "hi" solenoid is turned on; unable to select neutral or 2nd gear		2.5	9		22.5	
	"Hi" solenoid on= 2nd gear	"Hi" solenoid fails	Unable to select 2nd gear (hi)		2.5	5		12.5	
	"Lo" & "Hi" solenoids off= neutral	"Hi" solenoid fails on	2nd gear selected continuously, possible drive system damage if "lo" solenoid is turned on; unable to select neutral or 1st gear		2.5	9		22.5	
Solenoid Drivers "hi" & "lo"	Provides power to activate shift solenoids	Open	See solenoid valve-fails off		7.8	6		46.8	
		Shorted	See Solenoid valve-fails on		7.8	9		70.2	
Hydraulic Pump	Provides hydraulic power for clutch activation	No output	Remains in neutral, loss of vehicular drive motion		40.0	6		240	

Failure Modes, Effect, and Criticality Analysis

Project Description: Electric Vehicle Drive System

Date | Page 17 of 17

Revision Date

Engineer

Component	Component Function	Failure Mode	Effect of Failure	Cause of Failure	Occur	Severity	Detection	Criticality Index	Remarks
Clutch 2	Locks up planetary gear set to select 2nd gear	Fails on	Unable to select neutral, some drive possible, minimal speed, 2nd gear selected at all times, frictional drag loss when Clutch 1 activated		2.5	9		22.5	
		Fails off	Unable to select 2nd gear		2.5	9		22.5	
Clutch 1	Energizes to activate planetary gear set to select 1st gear	Fails on	Unable to select neutral, 1st gear selected at all times, frictional drag loss when Clutch 2 activated		2.5	9		22.5	
		Fails off	Unable to select 1st gear, loss of vehicle motion		2.5	6		15	
Chain Reduction	Provides coupling of AC drive motor output to drivetrain speed reduction	Mechanical break	Loss of drive to wheels		2.0	6		12	
Differential, Final Drive and Drive Shafts	Transmits mechanical drive force to both axles	Jammed	Loss of drive to wheels, motor shutdown due to high current demand		3.5	6		21	
		Mechanical break	Loss of drive to wheels		3.5	6		21	
Planetary Gear Set	Provides required gear reduction ratios to permit 2-speed drive	Jammed	Loss of drive to wheels, motor shutdown due to high current demand		1.3	6		7.8	
		Mechanical break	Loss of drive to wheels		1.3	6		7.8	

APPENDIX B

TRANSAXLE OPERATION INSTRUCTIONS

Normal operation of the transaxle is automatically controlled from the ac motor controller system. Manual shifting of transaxle disk clutches is possible, but should be attempted only for diagnostic test purposes and then at low motor speeds and loads. A toggle switch on the small control panel near the transaxle is provided to switch clutch solenoids to either "MANUAL" or "AUTO" operation. This switch should be in the "AUTO" position for all normal operations. When both clutch indicator lights are off, the transmission is in neutral. When in "AUTO" mode, neutral is selected whenever the drive is below a low threshold speed and no acceleration command is present.

The lubricant-coolant in the transaxle is Dexron II, G.M.'s automatic transmission fluid. Its normal operating temperature is in the 66-82 degrees C (150-180 degrees F) range. Temperature should not be allowed to exceed 107 degrees C (225 degrees F) to avoid deterioration of the fluid. If the color of the fluid changes from the bright red to dirty brown, it should be replaced. Operating oil level with pump on is at the parting line between pan and main housing. The level can be checked by the sight tube provided. Drain and fill plugs are readily accessible.

Pump pressure is set for 3.4-4.5 bar (50-65 psi) range and read on a pressure gauge at pump outlet. It normally drops to 1.4-2.1 bar (20-30 psi) during clutch shifts, then recovers to full pressure in about two seconds. Much longer recovery times may indicate a deteriorated pump condition. Lube and cooling flow pressure is indicated on the second pressure gauge and should be approximately 0.34 bar (5 psi).

System pressure is adjustable. However, it should not be increased beyond the present 4.5 bar (65 psi) maximum, as pump performance may be adversely affected.

When in "MANUAL" mode, the gear clutch solenoids will follow the manual shift commands regardless of motor speed. Thus, a downshift (HI to LOW) could cause a drastic motor overspeed condition. Downshifting should only occur with the motor spinning at less than 3800 rpm in HI gear before the shift.

APPENDIX C

GEAR RATIO CALCULATION

The shape of the speed torque curve is determined by the system torque requirements and the mechanical two-speed reduction ratios. Different equations apply for the case of a system limited by the motor or limited by the inverter. The following variables are defined:

T_m - motor per unit breakdown torque
x - ratio of maximum motor speed to base speed
y - ratio of maximum design torque to base torque, T_b
R - ratio of high gear to low gear reduction
T_b - motor per unit base torque

The most basic consideration in selecting the gear ratio provides that the maximum power speed-torque curve for low gear intersect the maximum power speed-torque curve for high gear before the motor speed exceeds "x" times base speed.

For the case where the system is limited by motor breakdown torque, induction motor theory states that torque falls off as the inverse square of speed above base speed. Thus,

$$\frac{T_m R}{x^2} \leq y \qquad (1)$$

In cases where the system is inverter limited, there will always be a decrease in maximum available torque after the gear change. In this instance it becomes more important to return to the constant torque operating regime after the shift. The constraint is then

$$\frac{x}{R} < 1 \qquad (2)$$

and R may be chosen to maximize torque and provide a pieced-together approximation to a constant wheel horsepower characteristic.

For the initial system design, a motor limited system was envisioned where $T_m = 2$, and $y = 1.8$. The parameter x cannot reasonably exceed about 1.5 to 1.75. Within this range, the motor torque falls off inversely with speed as slip is allowed to increase toward the breakdown value.

From (1) $R \leq 0.9\ x^2$. The cruising torque of $T_c = T_b/x$ and gradability torque of $T_g = T_b y R$ are substituted in (1) as follows:

$$T_g = T_c x y R = (T_c y x^3)\ 0.9$$

Solving x to deliver the required torques gives

$$x = 1.59 \approx 1.6$$

Substituting $R \leq 0.9(1.6)^2$

$$R \leq 2.3$$

Because the system is, in fact, inverter limited and the motor breakdown limit is never reached, there is a greater than predicted available low gear torque at the maximum motor speed. Thus, a drop in available torque will occur after a low-to-high gear shift.

APPENDIX D - HARDWARE AND SOFTWARE DETAILS

The first board is the MICROPROCESSOR (μP) board. It contains the Z-80 microprocessor, the brains of the controller. A 2 MHz clock frequency is used for μP timing. This frequency is also divided down to supply the operating frequency for the analog-to-digital converter multiplexer circuit on the analog board and the calibration frequency used to calibrate slip and clock the waveform circuit when the vehicle is stopped. The "Master Reset" hardware on this board is used to reset the μP program on startup or after a shutdown fault.

The MEMORY board has three 2k x 8 EPROM's containing the μP program. It has one 256 x 8 RAM. The chip select logic is also on the board. Expansion space is decoded for up to two additional 0.25K RAM's.

The INVERTER INTERFACE board contains the shift registers and gates to supply the μP output waveform to the optically coupled inverter transistor base drives. The following expands on the explanation given in Section 7.1. The μP calculates the shape of the output waveform and inputs this shape bit by bit into the Buffer Shift Register, BSR, at the μP's own rate. When the BSR is full, the μP sends a signal to allow transfer to the Master Shift Register, MSR. The data transfer is initiated when a synchronizing signal indicating the beginning of a new phase of the motor waveform is received. At this instant the data starts transferring from the BSR to the MSR at a rate synchronous to stator frequency until the BSR is empty--one full wave cycle. The μP is given the signal that the BSR is ready for a new waveform input. During the waveform calculation and the BSR loading, the MSR is continuously recirculating its waveform synchronous to motor stator frequency.

The base drive command signals can be disabled manually or by the computer program. Manual disable is controlled by the switch on the controller labeled "Drivers." When in the "off" position, the signals are disabled. The computer can also disable the signals in the event of a shutdown fault or when motor speed drops below a cutoff point when coasting or decelerating.

The SPEED FEEDBACK board gets the motor speed signal through a magnetic pickup from the 60-tooth on the motor shaft. The board conditions this signal for input into a phase-locked loop (PLL). The conditioned signal also goes to a circuit to sense low rotor frequency. The low rotor frequency signal is used by an analog switch to choose between two filters for the PLL, one for high speed and one for low speed. The PLL voltage output is fed back through a precision voltage-to-frequency converter.

The voltage output is summed with the slip voltage which comes from a digital-to-analog converter. This summed voltage signal is fed into a voltage-to-frequency converter, and the output becomes the frequency of the MSR clock as described on the inverter interface board.

The speed feedback circuit is also designed to allow a calibration frequency signal to be input into the phase-locked loop instead of the motor speed signal. This calibration frequency is used to calibrate the slip and speed feedback circuits. There are four trim pots used to calibrate these circuits. The first is a trim pot to adjust the reference voltage on the slip DAC. The second is used to weight the amount of slip voltage output from the DAC with respect to the motor speed voltage. The third and fourth pots are used to get the correct multiple of frequency out to frequency in. Frequency out should equal 1536 x frequency in.

At one stage in development a speed loop circuit was designed to control speed in Manual mode. It was found that the test dynamometer could control the speed so the circuit was disconnected.

The ANALOG/MUX board contains a 16-channel multiplexed, analog-to-digital converter, ADC/MUX. The board contains conditioning circuitry to convert and interface the system input values to the 0 to +5.12 V required by the ADC/MUX. The sixteen inputs are defined as follows:

1. VAR0 - variable zero-channel select. Input is wiper voltage on controller potentiometer. Used in diagnostics.

2. VAR1 - variable one-channel select. Input is from a pot. Used in diagnostics.

3. VAR2 - variable two-channel select. Input is from a pot. Used in diagnostics.

4. VBRK - emergency or parking brake. Input is either on, 4.65 V, or off, 0 V, as determined by switch position.

5. VDECEL - decelerate demand. Input is wiper voltage on controller pot. Failsafe is 5.12 V input if potentiometer loses power. This signals the uP to shut down the drive.

6. VACCEL - accelerate demand. Similar to VDECEL.

7. VDIRG - direction and gear select. Input is tri-level voltage from switch on controller for Low (only), Reverse, and Normal (High-Low) select.

8. MODT - motor motion detect. Disconnected.

9. VTPMT - motor temperature sensor. Input is from floating temperature-sensitive resistor as feedback element in op amp circuit.

10. VTPHS - inverter transistor heat sink temperature sensor. Input same type as VTPMT.

11. VTPBE - battery electrolyte temperature sensor. Input same type as VTPMT.

12. VVBUS - dc bus voltage. Input is from voltage divider across dc voltage input line. A differential input is used for common mode immunity. Sensitivity is 1 volt/digital count. Controller ground is tied to bus ground.

13. VIBUS - dc bus current. Bipolar input is voltage across current shunt from dc current input line. It is scaled and conditioned through op-amp circuitry. Sensitivity is four amps/digital count.

14. VMSRNL - master shift register frequency null detector. Disconnected.

15. ERBOV - energy recovery bus overvoltage. Input is high-low signal from opto-isolator circuitry on energy recovery board. Signal low represents over-voltage fault.

16. VRFA - rotor frequency. Input is voltage signal from phase-locked loop on speed feedback board. It is proportional to rotor frequency.

The READOUT board contains three sets of hexadecimal read-out displays with decoding for diagnostics. Diagnostic output information is shown on these displays. The first pair in each row are the variable select code readouts. The second and third pair are for data display. Six LED's are on this board. The LED's are indicators for alarm shut-down faults and warnings, calibration frequency on, reverse, high gear, and μP enable of the base drive signals. The Manual/Normal select switch logic hardware is on this board.

Software Description

The control software was set up so that each main function was defined in a block or module. This setup allowed for ease of program writing, understanding, debugging, and testing. Each module was given a label with the prefix "M," followed by a mnemonic best describing the main function of the module. The program was written, debugged, and tested on a Tektronix 8002 development system and emulator for a Zilog Z-80 microprocessor. Each module was debugged and tested using simulated inputs on the development system before testing on the motor/inverter. These modules are linked together with connecting logic by the Executive software shown in the flowchart of Figure D.1. The control software is now described for each module of the Executive flowchart.

EV AC PROPULSION SYSTEM PROGRAM

EXECUTIVE FLOWCHART

LINKS MODULES TOGETHER WITH CONNECTING LOGIC

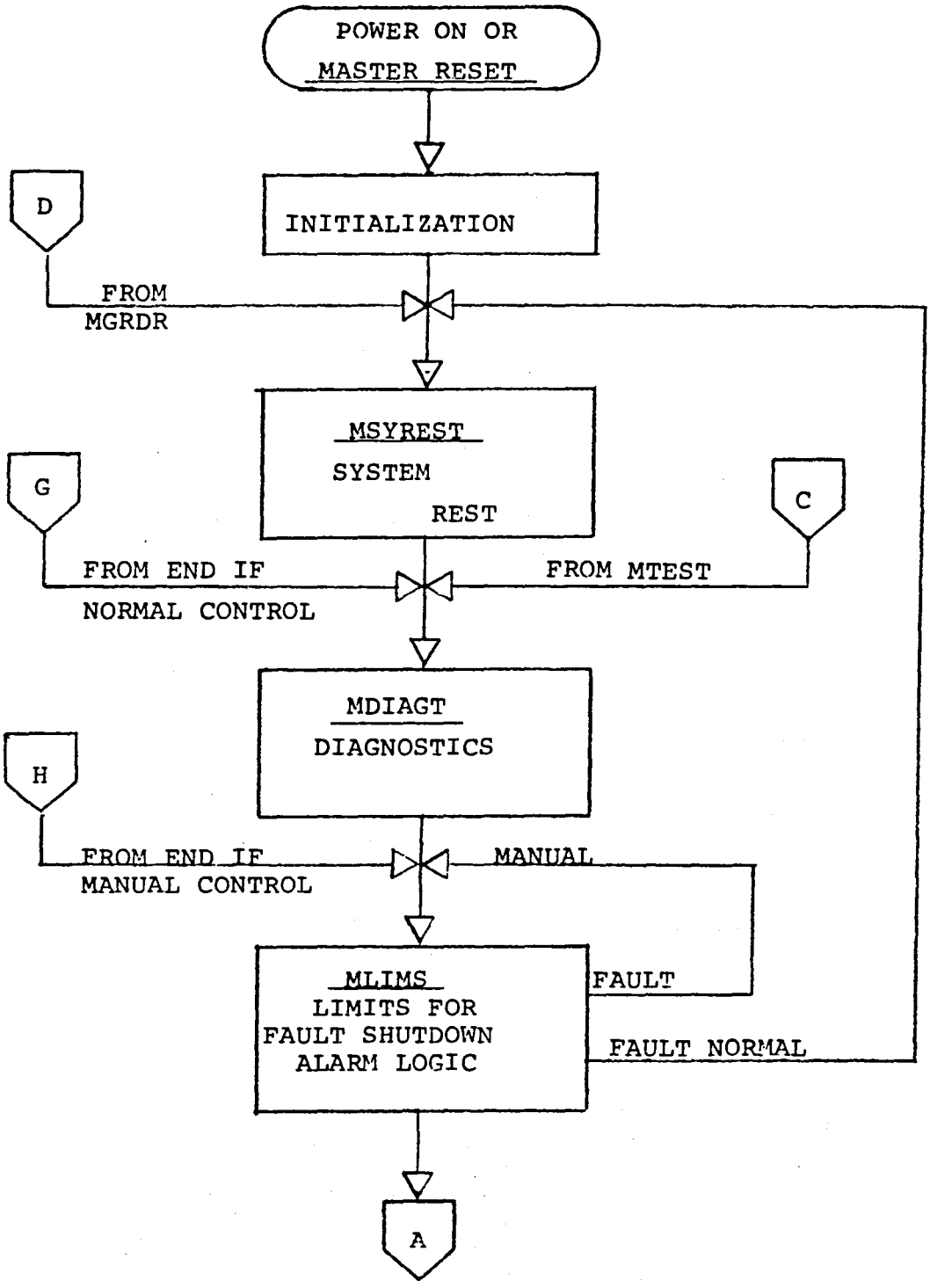

Figure D.1 Executive Flowchart

EV AC PROPULSION SYSTEM

EXECUTIVE FLOWCHART

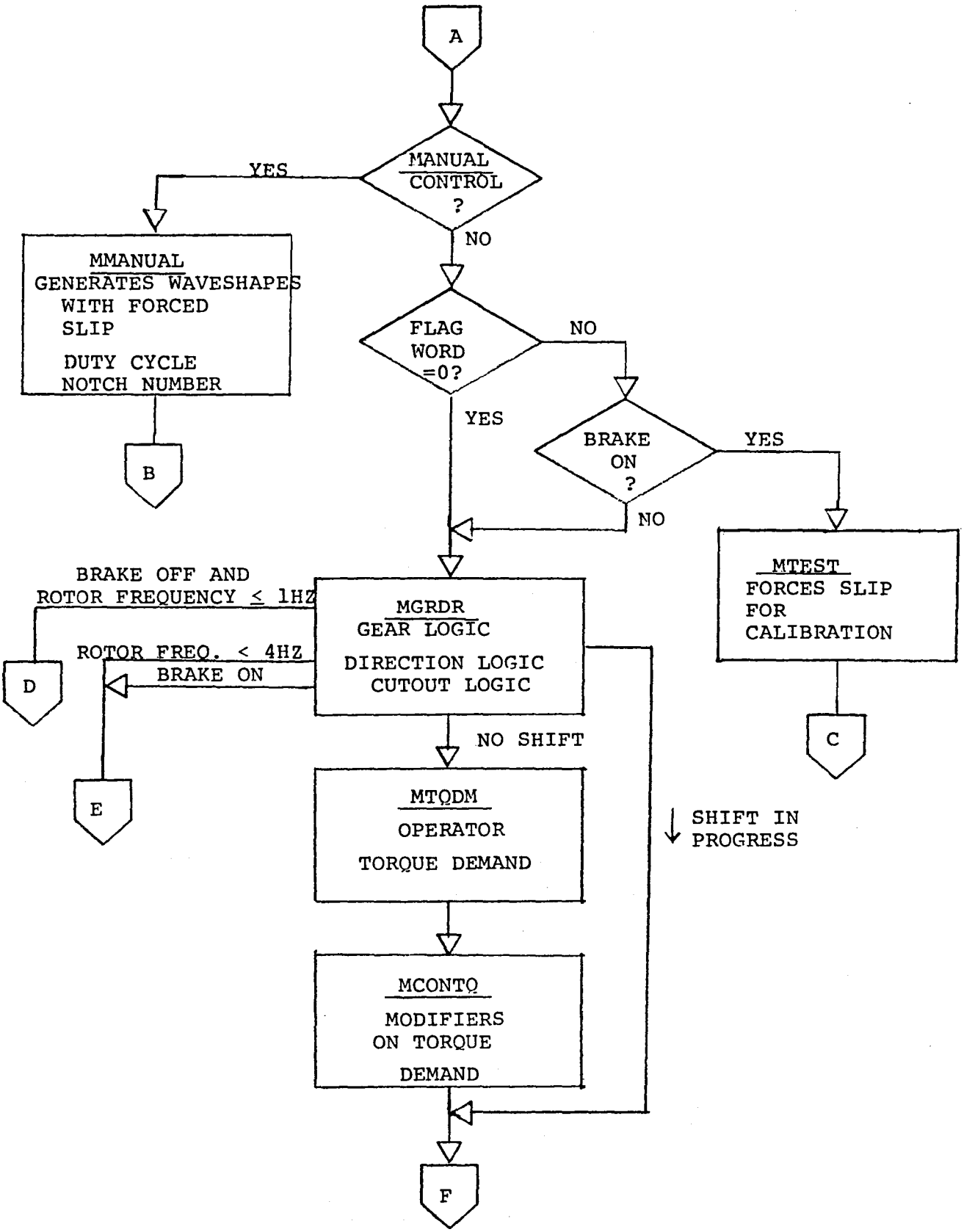

Figure D.1 (Cont'd)

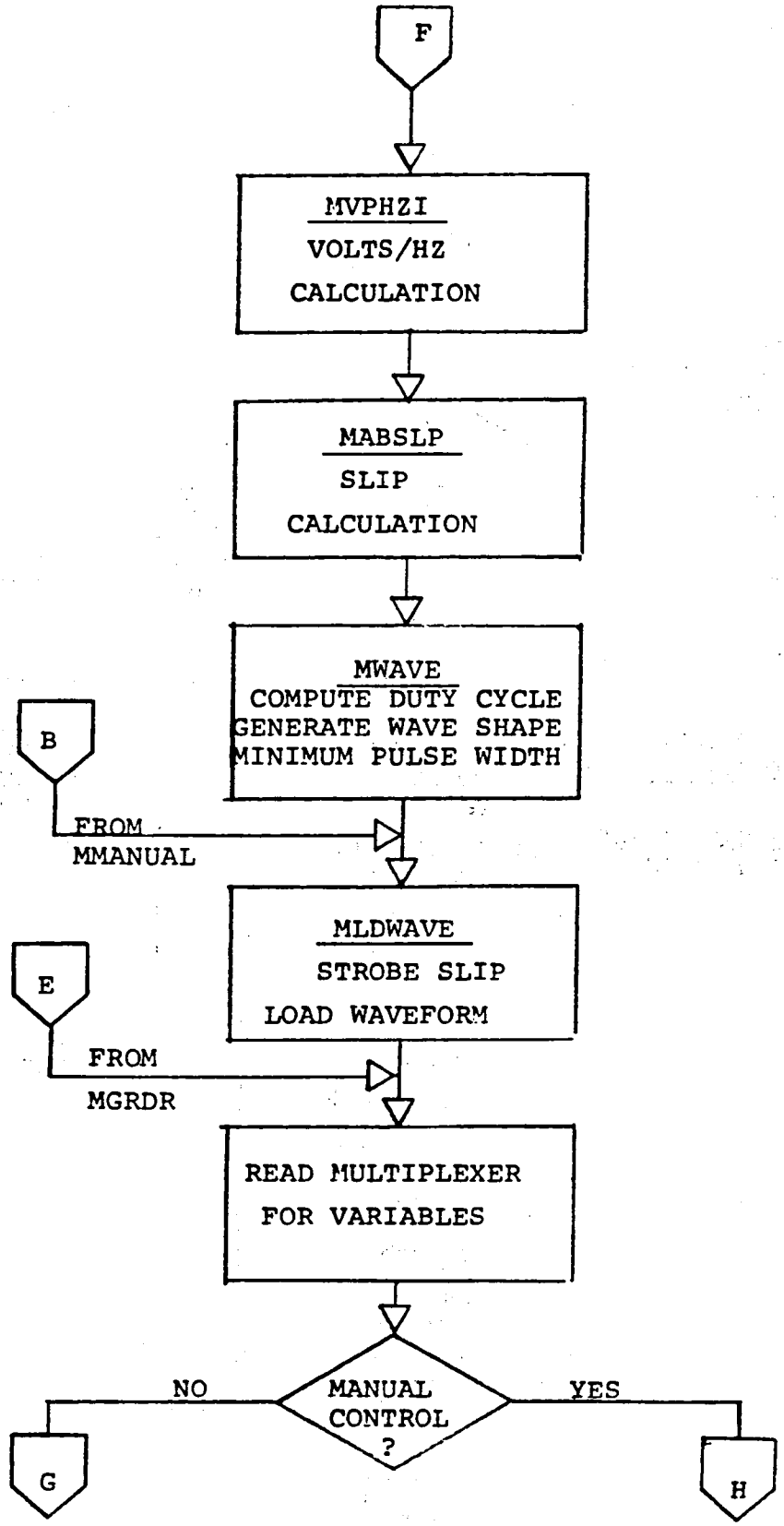

Figure D.1 (Cont'd)

Software Executive Flowchart Explanation

INITIALIZATION. The proper operating mode is set for the Z-80 microprocessor, and program variables are initialized.

MSYSREST - SYSTEM REST. The module is entered on system powerup, on a "Master Reset," when the drive is stopped or if a "Fault" shutdown occurs. A zero duty cycle voltage waveform is forced into the system shift registers, and inputs are read and stored.

MDIAGT - DIAGNOSTIC DISPLAY. Selected variables are transferred to the controller display readouts based on controller channel selection pots labeled VAR1 and VAR2. The readouts display data in hexadecimal values for engineering development or in decimal values (see Figure D.2). The readout also shows a "Flagword" based on a selection pot labeled VAR0. Flagword is a coded word used to force a slip value for calibration in MTEST. Duty cycle and slip in hexademical notation are also displayed. See Figure D.3.a for controller readout format.

DIAGNOSTIC READOUT LAYOUT FOR

NORMAL AND MANUAL MODES

VAR0	FLAG WORD status word	DUTY CYCLE hex (00-FF)	SLIP hex - 0 + (00-80-FF)
VAR1	CHANNEL NUMBER decimal	CHANNEL DATA	
VAR2	CHANNEL NUMBER decimal	CHANNEL DATA	

Figure D.3.a Diagnostic Readout Layout For Normal Mode

SLIP	SLIP (0.1HZ) decimal	A = + D = -	ROTOR FREQUENCY decimal
DUTCY	DUTCY CYCLE decimal %	A = + D = -	BUS CURRENT decimal (Amps)
MNOCH	NOTCH NUMBER decimal	BUS VOLTAGE decimal	(VOLTS)

Figure D.3.b Diagnostic Readout Layout For Manual Mode.

VAR1/VAR2			CHANNEL	DATA	SYMBOL DEFINITION	
	BCD	BINARY				
00		x	FLTS1	FLTO	Low Priority Fault	High Priority Fault
01		x		FLTXO		High Priority Fault
02		x	DSTAT	VBRK	Status Flags	Brake Voltage
03		x		VDIRG		Direction Voltage
04		x	ERBOV		Energy Recovery Bus Over Voltage	
05		x	CONTQ	TQDM	Final Control Torque	Torque Demand
06		x	CTQL1	CTQMIN	Torque Limit Due MT	Smallest Torque Temp.Limit
07		x	CTQL3	CTQL2	Torque Limit Due BE	Torque Limit Due HS
08		x	FLAGO		Conditional Flags	
09		x	NPW	NOCHF	Notch Pluse Width	Final Notch Number
10		x	ICTR	TQDM2	Bus Current Limit Counter	Final Torque Demand
11		x	ACCEL1	ACCELS	Digital ACCEL	Scaled ACCEL
12		x	DECEL1	ACCELS	Digital DECEL	Scaled DECEL
13		x	SLP3MX	ABSLPL	Slip Limit (Voltage)	Slip Limit (Speed)
14		x	ABSLP2	ABSLP6	Slip Limit (Overflow)	Offset Slip
15		x	ABSLP7	NOCHIN	Slip Limit (Speed)	Initial Notch Number
16		x	VPHZMX	VPHZAL	Volts/HZ Maximum	Volts/HZ Available
17		x	VPHZCH		Volts/HZ Chart	
18		1ST TWO DIGITS		2ND TWO DIGITS		
19				ALL FOUR DIGITS		
20	x			VPHZMX	Maximum Volts/HZ Demand	
21	x			VPHZAL	Volts/HZ Available	
22	x			VPHZCH	Volts/HZ Chart Demand	
23	x			FR	Rotor Frequency	
24	x			FS	Stator Frequency	
25	x					
26	x					
27	x			IBUS	Main Inverter Bus Current	
28	x			VBUS	Bus Voltage	
29	x			TPBE	Battery Electrolyte Temp. ^{0}C	
30	x			TPHS	Transistor Heat Sink Temp. ^{0}C	
31	x			TPMT	Motor Temp. ^{0}C	

Figure D.2 Channel Display Variables
In Normal Mode.

MLIMS - MAXIMUM LIMITS FOR TEMPERATURE, VOLTAGE AND CURRENT. Input sensor readings are checked to see if they have exceeded their limits (see Figure D.4). If a limit is exceeded, a high priority warning code word is set and the drive is shut down. If a high priority fault word or a low priority warning code word is set in the program, the appropriate LED will light on the controller display.

When Limits Are Exceeded The Drive Is Shutdown

Battery Case Temperature	>	80°C
Inverter Heat Sink Temperature	>	93°C
Motor Case Temperature	>	170°C
D.C. Bus Current	>	352 Amps
D.C. Bus Current	>	-352 Amps
D.C. Bus Voltage	>	180 Volts
D.C. Bus Voltage	>	96 Volts
Energy Recovery Bus Over Voltage	>	32 Volts

Figure D.4 Maximum Shutdown Limits in MLIMS.

The fault or warning can be determined by selecting the proper channel on VAR1 or VAR2 pots in NORMAL operating mode and using Figure D.5 (see following page) for code definition.

MMANUAL - MANUAL MODE. In MANUAL mode the microprocessor bypasses normal operation by allowing manual control input on Slip, Duty Cycle and Notch Number. The three values are input from pots on the controller labeled Slip, Dutcy, and Mnoch, respectively. Each value is displayed on the readout with Bus Current, Bus Voltage and Rotor Frequency as shown in Figure 7.4.3.b. Ranges of control inputs are -8.0 to 7.9 Hz Slip, 0 to 100% Duty Cycle (with FF representing 100%), and 0 to 31 Notches.

MTEST - SLIP TEST CALIBRATION. This module is used for slip frequency calibration. The inverter drivers are inhibited. It is entered as a result of Flagword (VAR0 pot) not being equal to zero with the emergency or parking brakes on. A forced calibration frequency is generated and can be measured on the test point matrix on the controller. By changing the Flagword code, fixed values of + and - slip can be added to the calibration frequency. This makes it possible to calibrate the slip circuit with only an external frequency counter.

FAULT WORD

FLTO -AP1 priority shutdown, branches to MSYREST

BIT
↓
0 = 1 Acceleration or Deceleration Demand Pot Voltage too high
1 = 1 battery electrolyte temperature too high
2 = 1 transistor heat sink temperature too high
3 = 1 motor stator temperature too high
4 = 1 +bus current too high
5 = 1 -bus current too high
6 = 1 +bus voltage too high
7 = 1 -bus voltage too low

FLTX0 -AP1 priority shutdown, branches to MSYREST

0 = 1 energy recovery bus over voltage

——Must be manually reset with MASTER RESET——

FLTS1 -AP2 low priority alarm warn

0 = 1 Torque demand input limited by temperature curves
1 = 1 bus current accel/decel limit
2 = 1 motor speed greater than 150 HZ
3 = 1 torque demand maximum rate of change exceded
4 = 1 parking or emergency brake on
5 = 1
6 = 1 at +/- slip limits
7 = 1 Decel slip limited by regenerative bus voltage

Figure D.5 Fault/Status Codes
(1 = Active State).

MGRDR - GEAR SHIFT, DIRECTION LOGIC, BRAKE CHECK. This module contains shift logic to control upshifts and downshifts and to determine when to shift. Gear select is done on the controller and allows Normal (automatic shift), Low-Only, and Reverse (Low-Only). Automatic shift points are set so that an upshift (Low to High gear) occurs when motor speed is greater than 9000 rpm. With the shift ratio at 2.4/1, the motor is slowed to 3750 rpm. For a downshift (High to Low gear) the shift occurs when motor speed is less than 3000 rpm and speeds the motor to 7200 rpm for low gear. This allows for shift hysteresis as shown in Figure D.6. With Low-Only selected, the uP will not let the motor shift into High gear. If Low-Only is selected while in High gear, the motor will not shift until motor speed is less than 3000 rpm. The uP will only allow shifting in and out of Reverse when the motor is stopped. Both High gear and Reverse are indicated by a corresponding LED on the controller.

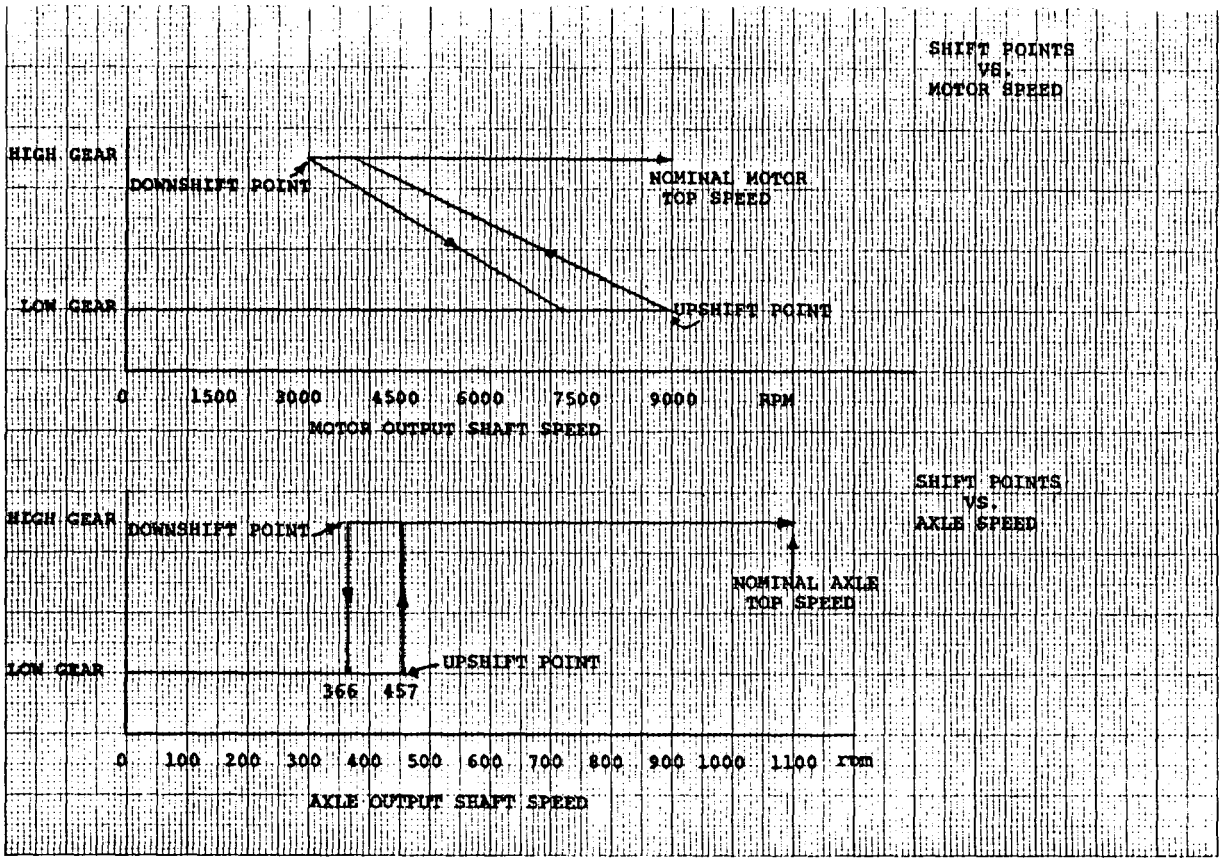

Figure D.6 Transaxle Shift Points

Also included in this module is an emergency and parking brake check. If the brakes are sensed "On," the drive is inhibited. If the motor is turning and the brakes are on, a low priority warning LED will be displayed on the controller.

If the motor speed is sensed below 4 Hz and there is no acceleration demanded, the drive is inhibited and will coast to a stop.

MTQDM - TORQUE DEMAND OPERATOR INPUT. This module reads and scales the acceleration and deceleration demand pots labeled "ACCEL" and "DECEL" on the controller. If either input exceeds a set limit, a fault word is set and the drive is shut down. If both inputs are active at the same time, the DECEL demand will always override.

MCONTQ - TORQUE DEMAND MODIFICATION CALCULATIONS. This module limits torque demand due to three parameters. The first limit is imposed due to critical system temperatures. Three temperatures are monitored: motor case (TPMT), inverter transistor heatsink (TPHS) and battery case (TPBE). The limiting curves are shown in Figure D.7.

Torque demand will be limited to the smallest of these limits. A second limit is due to excessive dc bus current. A dynamic limiter reduces torque demand in incremental steps as dc current is sensed above +260 amps or below -260 amps. The third limit is a rate of change constraint on the torque demand. This exists to smooth the effects of operator step inputs that could introduce current spikes to the system. This limit is bypassed in gear shift mode to allow for faster shifts.

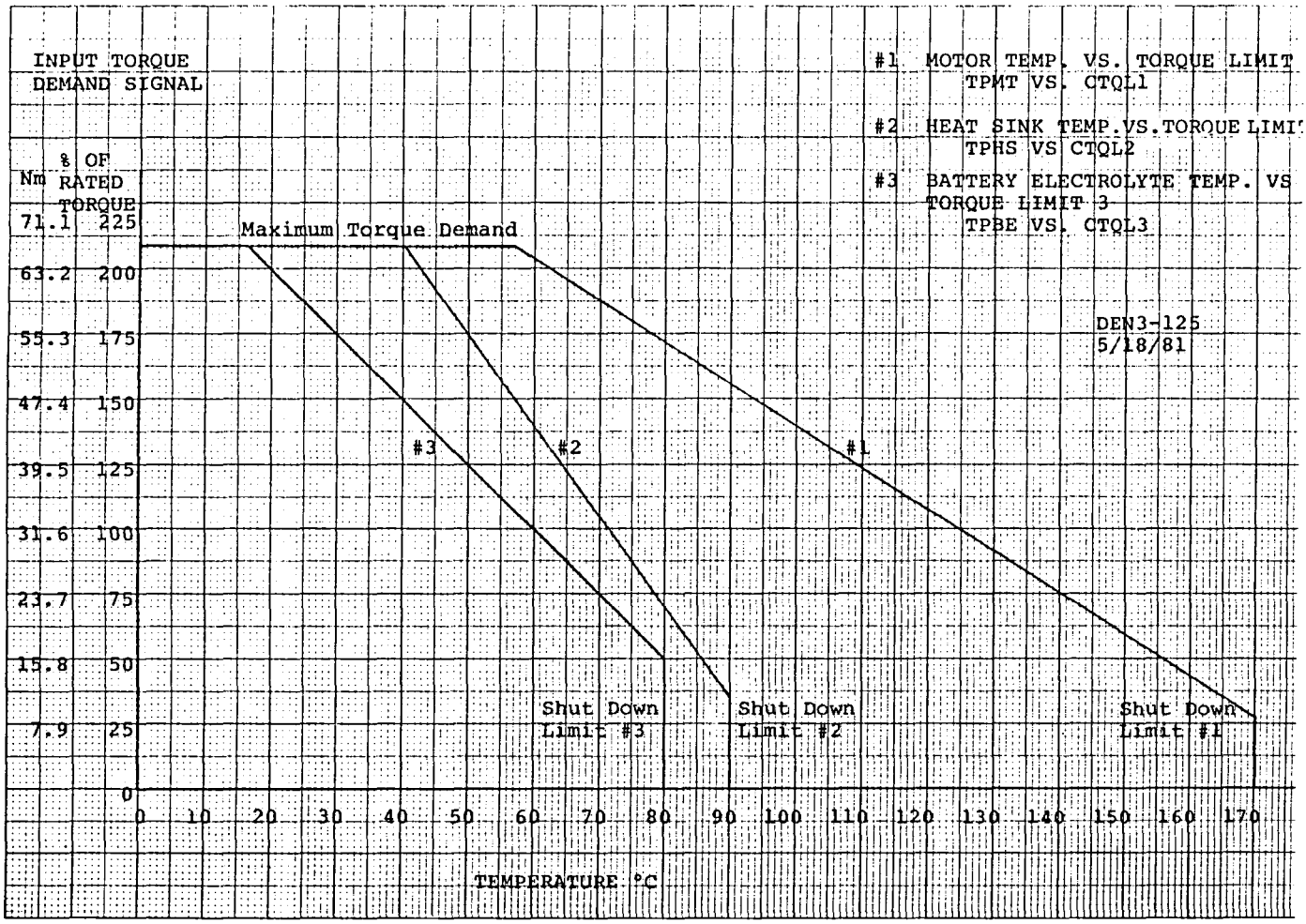

Figure D.7 Temperature Modifiers on Torque Demand.

MVPHZI - VOLTS/HERTZ DEMAND CALCULATION. This module calculates motor volts/Hz required to supply torque demand. The calculation is taken from the schedule shown in Figure D.8. This curve was obtained by fitting it to actual motor test data to obtain optimum efficiency in the normal operating region. The curve limits maximum volts/Hz as motor speed increases. As motor speed falls below 4 Hz, if torque demand is light, the curve allows volts/Hz to approach zero. At the same time it fixes slip to a specified level. This is done to improve low speed control and allow for smooth startups at light torque demands.

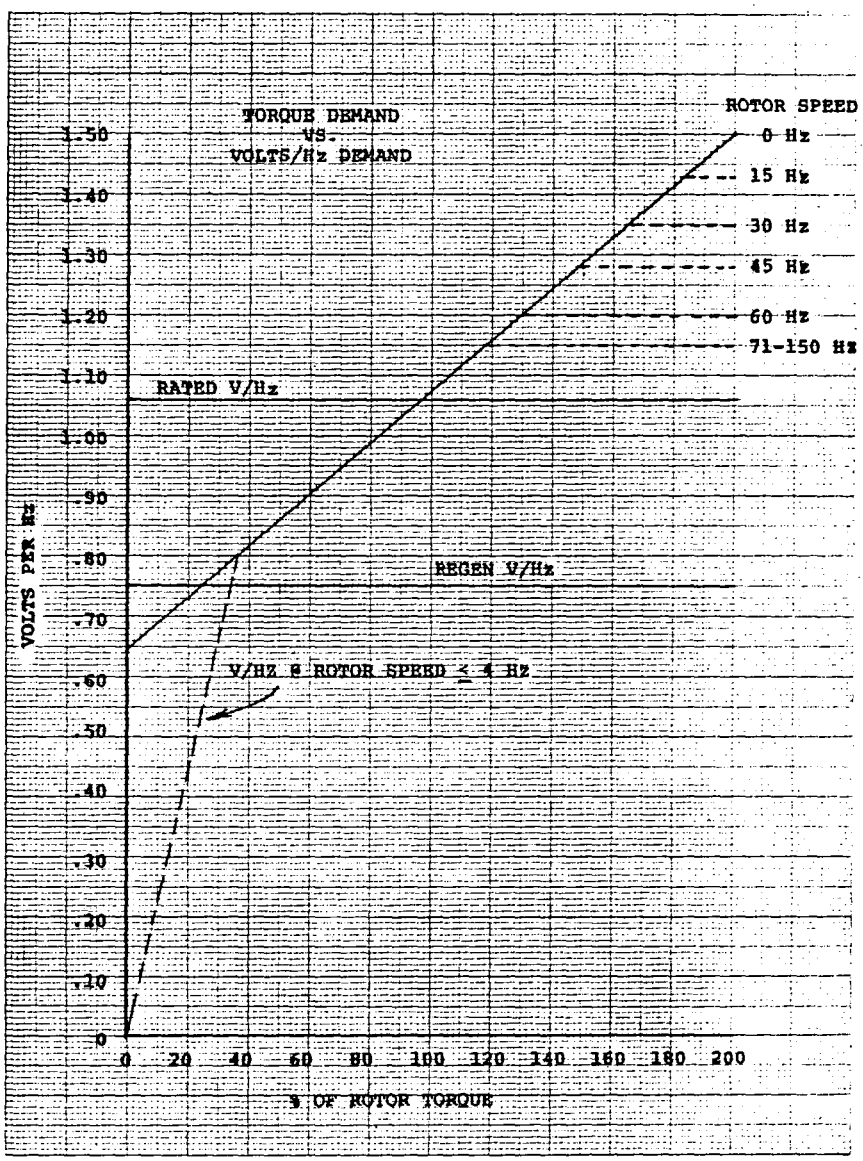

Figure D.8 Volts/Hz Schedule

Another factor used in determining volts/Hz is the amount of available volts/Hz due to increase in motor speed or decrease in dc bus voltage. As motor speed increases beyond these curves (Figure D.9), not enough volts/Hz are available. The torque demand must further be met by increasing slip. Thus, volts/Hz demand is limited to the volts/Hz available for proper calculation of slip.

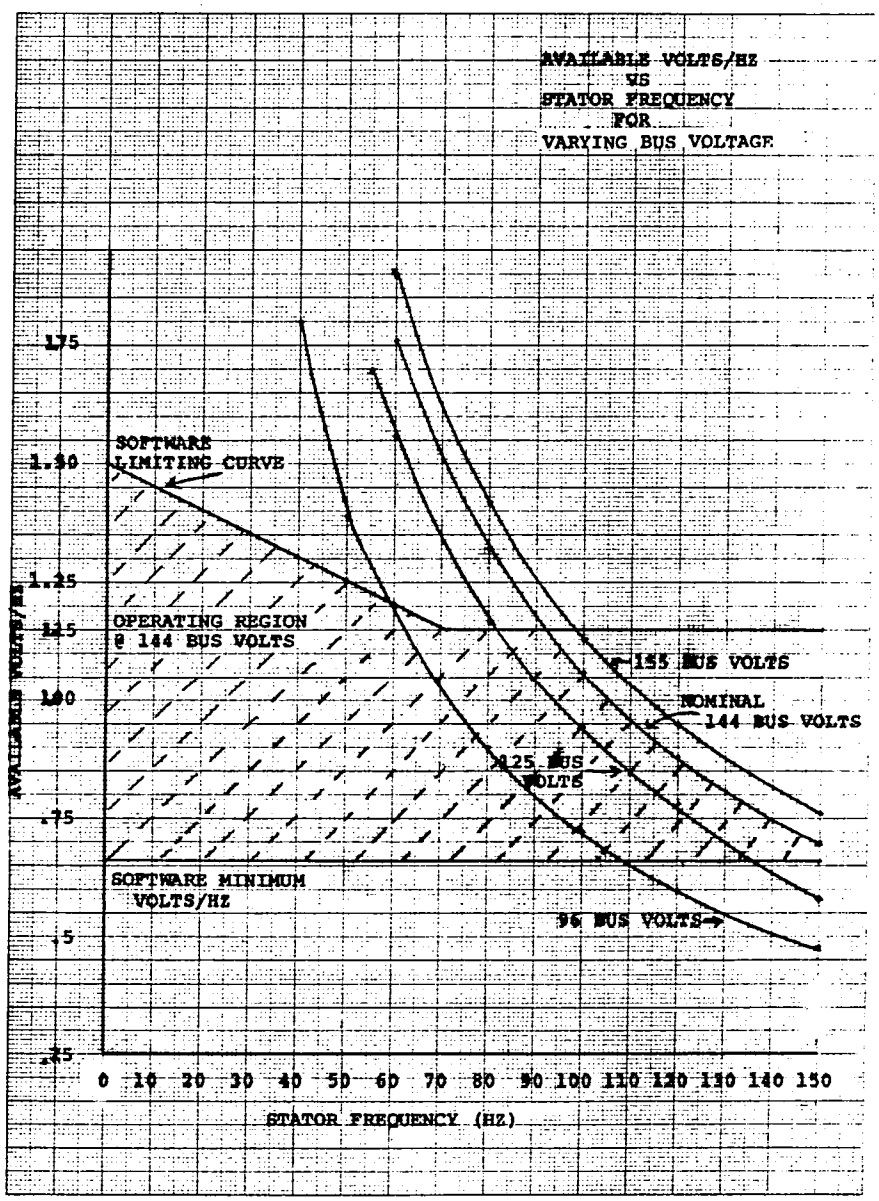

Figure D.9 Available Volts/Hz

MABSLIP - SLIP. Motor slip is calculated in this module as a bipolar digital word with an initial range of +7.9 Hz to -8.0 Hz in 0.0625 Hz increments. The equation used to determine slip is

$$\text{Slip} = \frac{(\text{Motor Scaling Constant})(\text{Torque Demand})}{(\text{Volts/Hz})^2}$$

where torque demand and volts/Hz are previously calculated values. The motor scaling constant has been determined from experimental data. Slip has several modifiers before its final output. The first modifier sets slip to a fixed value when motor speed is less than 4 Hz. This is done for smooth low speed control. It was verified during testing that motor temperature affected the slip needed to hold a constant torque. Motor temperature compensation was added based on test data. The data shows that as motor temperature rises, the amount of slip needed to hold torque constant rises proportionately, while speed and volts/Hz are held constant. The curve was normalized for 70°C operating temperature. Slip compensation for several torque demands is shown in Figure D.10.

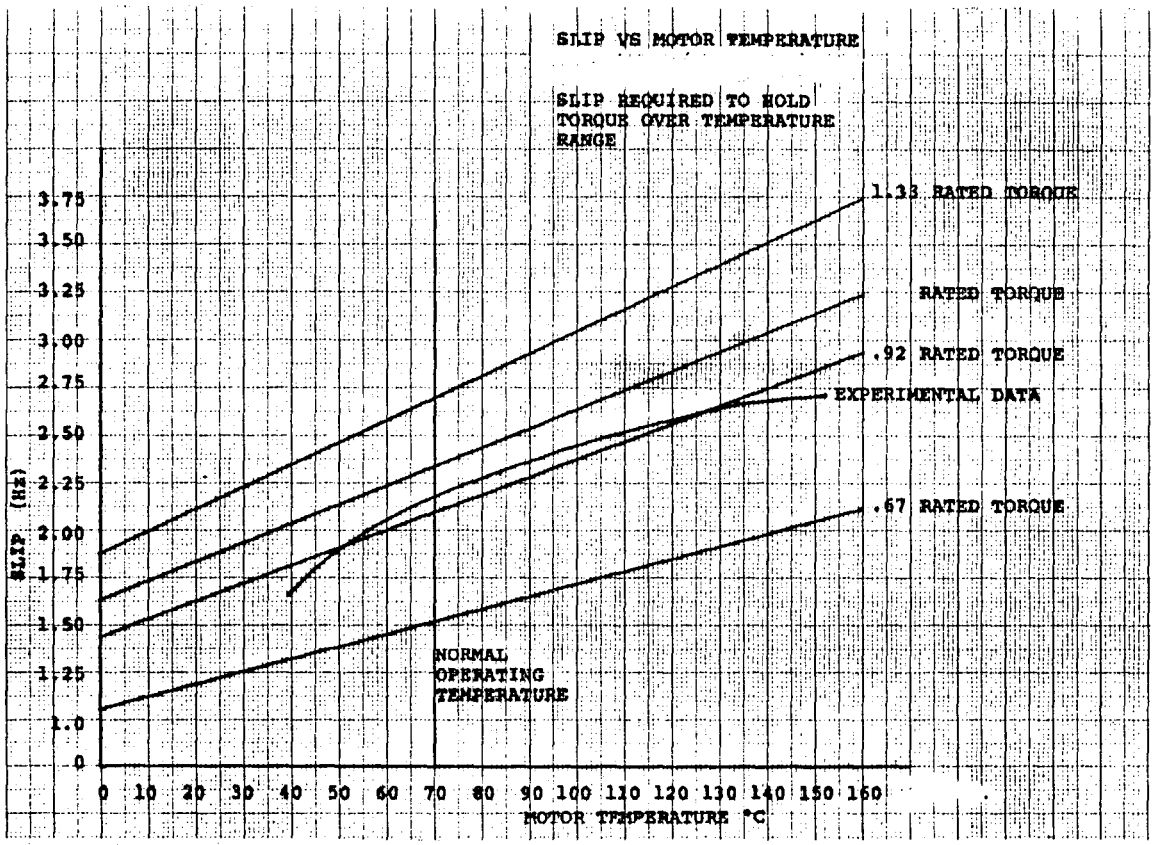

Figure D.10 Temperature Modifier On Slip

Bus voltage is also a modifier to slip. If the motor is in the regeneration mode (i.e., negative slip), bus voltage will rise. To keep this voltage from getting too high, the negative slip is limited by the curve shown in Figure D.11. The mechanical brakes are then required to slow the vehicle if more braking is required.

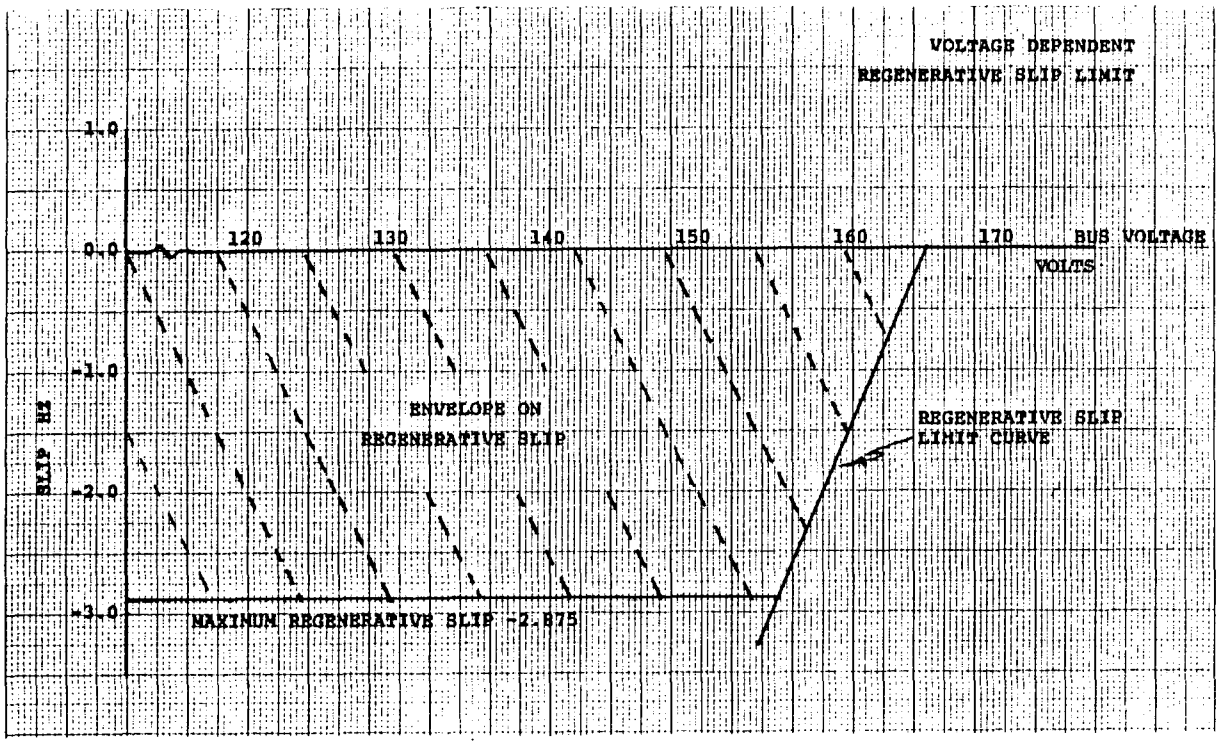

Figure D.11 Bus Voltage Modification On Negative Slip

Another modifier is the maximum speed constraint. If motor speed is sensed greater than 9000 rpm, the slip value is reduced according to a limiting curve. The slip will decrease to zero, and if the motor speed is still increasing will go into regenerative braking (see Figure D.12). A software stabilizing routine is used to limit the rate of change of the slip to minimize unwanted oscillations.

Final constraints on the slip are maximum positive and negative slip limits. Positive slip is limited to 4.0 Hz, and negative slip to -2.875 Hz.

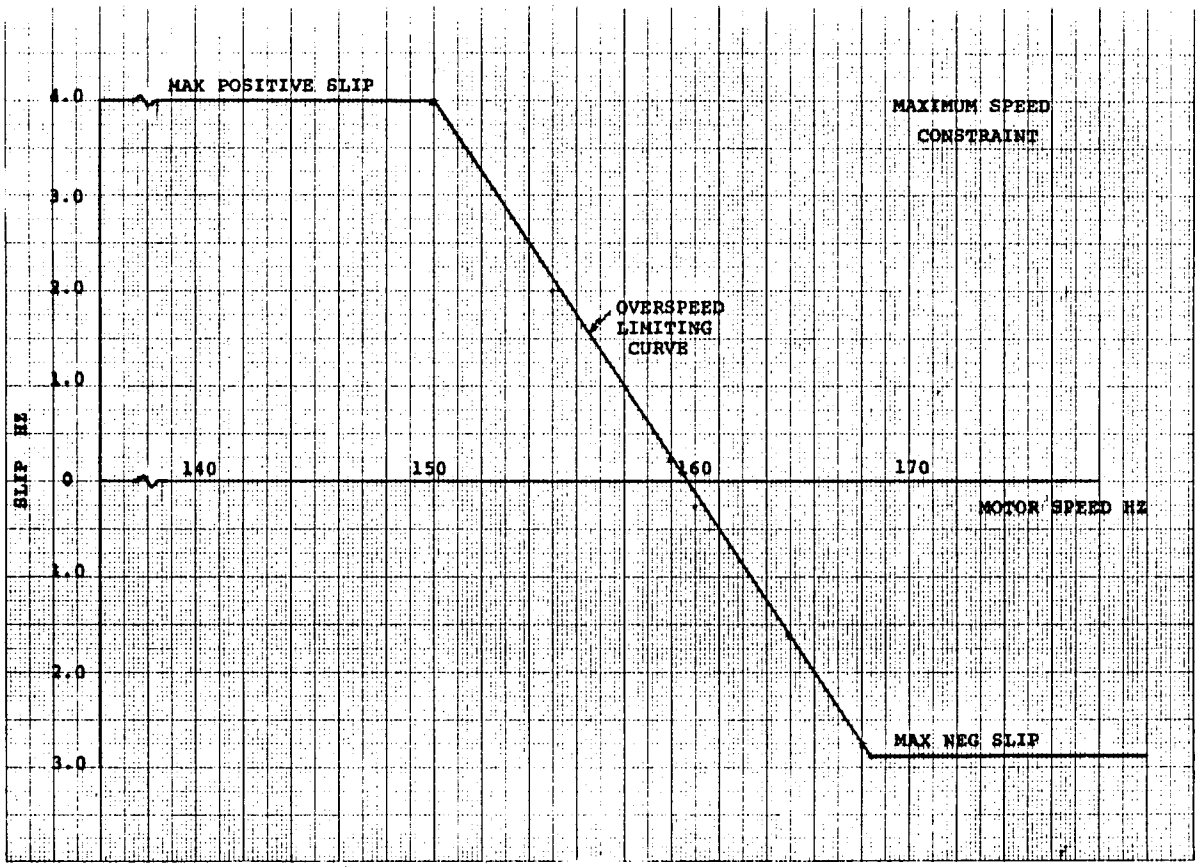

Figure D.12 Motor Speed Constraint Curve

MWAVE - WAVESHAPE CALCULATIONS. This module first calculates the voltage duty cycle to satisfy volts/Hz demand. The equation follows:

$$\text{Duty Cycle} = \frac{(\text{Stator Frequency}) \times (\text{Volts/Hz Demand})}{(\text{Voltage Scaling Constant}) \times (\text{Bus Voltage} - \text{Losses})}$$

The voltage scaling constant is used to relate bus voltage to the scaled voltage used in the volts/Hz demand calculation. Below 6 Hz stator frequency, the duty cycle rate of change is limited to smooth out rough startups. Once the duty cycle is found, the module proceeds to find the number of notches for the center 60° from a look-up table based on rotor frequency. The notch selection is based on experimental data to obtain optimum efficiency. (A small amount of hysteresis is added to this look-up process to avoid borderline switching between notches.) Using the duty cycle and number of notches, the module calculates the width of the notch pulses and the width between notch pulses. It checks to see if the notch pulse width is too narrow, eliminates a notch if it is, and recalculates the notch pulse width.

MLDWAVE - LOAD WAVE TO BUFFER SHIFT REGISTERS. This is the final module of the Executive flow chart. At this point the new digital slip word is output to the slip DAC. A new PWM voltage waveform is also ready for output to the buffer shift registers. If the external hardware has not generated an interrupt to signal that it is ready for new waveform data, it passes by the waveform load routine. If an interrupt has occurred, the hardware is ready for a new waveform. The new waveform is then output to the buffer shift registers, with the software making sure the waveform has quarterwave symmetry. At the end of its waveform output, the microprocessor accepts the sixteen input values from the ADC multiplexer.

The microprocessor then reads some critical inputs that may have been skipped if the interrupt signal was not received. These signals are rotor frequency, direction switch, brakes, acceleration pot, and VAR0 for calibration testing. The program then returns to its proper location, depending on whether in Manual or Normal mode.

APPENDIX E

OPERATING PROCEDURE FOR AC EV PROPULSION SYSTEM TEST FRAME

1. Check oil level in clear tube on transaxle. Proper oil level is up to split in castings between oil pan and transaxle housing. If oil level needs filling use DEXRON II ATF only.

2. Be sure water flow through oil cooler is on, if cooling is being used.

3. Turn "DRIVERS" switch to "OFF" at controller to keep inverter inhibited on power up.

4. Turn "MASTER TEST FRAME LINE POWER SWITCH" "ON" using switch on plug strip located externally on Instrumentation Enclosure. 110 VAC Powers:

   - 2 Clarke-Hess Wattmeters
   - fans for inverter cooling
   - 12 VDC battery charger
   - 144 VDC Power Enclosure safety circuitry

5. Connect 144 VDC Battery Cable, making sure plug is fully inserted.

6. Turn "CONTACTOR ENABLE" switch on top of Power Enclosure to "ENABLE." This switch allows 144 VDC contactor to be closed when a valid "START" command is present.

7. Make sure all shutdown mode N.C. contacts on safety shutdown line are closed. These are any safety contacts wired in series with "START" push button that will either prevent turn on or turn off controller and shutdown drive.

8. Press "START" Push Button. At this point the test frame drive system should be enabled, including:

   - Logic Power to Inverter, LED's on base drive board will be active.
   - 144 VDC Power to system; "CONTACTOR ON" light will come on after a short delay.
   - Transaxle oil circulation pump comes on. Check for oil flow on meter mounted on transaxle bracket.
   - Power to Controller, Diagnostic Display Panel will be lit.

If these conditions do not exist, check the following:

- 144 VDC Plug inserted fully
- 110 VAC present
- 12 VDC present
- any failsafe switches wired in the safety shutdown line external to the test frame.

9. Select "NORMAL" or "MANUAL" mode to operate in.

10. Making sure "DRIVERS" switch is "OFF," press "MASTER RESET" pushbutton on controller.

11. Making sure control knobs are in proper position for startup, turn "DRIVERS" switch to "ENABLE." Proper positions are:

    - in Manual Mode; "DUTCY" knob full CCW or = 00.
    - in Normal Mode; "ACCEL," "DECEL" and "VAR0" knobs full CCW.

    Drive is now ready to operate.

12. Upon APl shutdown or desire to change operating modes, slow motor to a stop and turn off "DRIVERS" switch. Repeat procedure from step 9.

    The drive may be shutdown at any time by turning the "DRIVERS" switch to "OFF." This will inhibit any further base drive signals to the inverter. The motor must come to a stop before enabling the inverter again.

APPENDIX F

SAFETY FEATURES OF AC PROPULSION SYSTEM ON TEST FRAME

Operating personnel safety has been approached at two levels: test frame features and propulsion system features.

Test Frame Safety Features

Test frame safety features are listed below:

1) A ground fault interruptor is in the 115 VAC feed line which powers several test frame auxiliary items. Any significant leakage to ground (shock hazard) trips the device and powers down the test frame. The line is also protected by a 15 amp breaker.

2) All 115 VAC and 144 VDC components are enclosed in metal cabinets.

3) A master disable switch on the test frame prevents system power-up from a remote location. This prevents any inadvertent start-up when someone is working on the test frame or the propulsion system.

4) A safety start-up/shutdown interlock circuit prevents start-up or shuts down the system under the following conditions:

   a) The main battery input connector is not completely mated with the battery cable.

   b) Momentary or continuous loss of 115 VAC test frame power. A manual restart is required after a momentary power loss.

   c) Any normally closed contact in the series string of contacts constituting the "STOP" circuit is opened. One NC contact in the string is the "STOP" mushroom button in the control room. Any other contacts can be wired in series at LeRC discretion. For example, signals representing road load simulator overspeed, over-temperature or torque non-compliance could drive small control relays (contacts rated 1a @ nominal 12 VDC) whose contacts are in series with the "STOP" circuit. Only a momentary open contact is needed to shut down the system.

   d) Loss of 12 VDC controller power.

5) Prominent indicator lamps on the test frame show operation status. The red lamp indicates the manual disable switch is OFF, and the main battery contactor can be actuated if no shut-down conditions exist. The green lamp indicates the main contactor is ON and 144 VDC is present on the test frame.

6) Both + and - battery bus lines are fused at 400 amp.

7) The 12 VDC battery supply is fused at 20 amp.

8) The safety circuit is fused. Any high current fault in the circuit itself causes the fuse to blow which shuts down the test frame in an orderly manner just as if the "STOP" button had been pressed.

9) The two Clarke-Hess wattmeters installed on the test frame are totally isolated from the frame ground (including the use of 2-prong adaptors in the plugs) with plastic standoffs. This is necessary to prevent any ground loops.

10) Labels warning of polarity and high voltage are posted on the test frame.

11) All power wires running around the test frame are well protected. All terminals are enclosed.

Propulsion System Safety Features

The propulsion system has numerous safety limits built into the controller software and hardware. The various items and their verification tests are summarized below:

1) Overtemperature - three critical temperatures, battery, motor, and transistor heat sink, are constantly being monitored by "tempistors" sensors. The three sensor inputs were simulated by potentiometers for testing. The tests show that as each temperature input was increased to its limit the torque capability of the drive was limited according to a fixed schedule for each. When the maximum temperature for each was reached the inverter was shut down and a fault word displayed. The maximum temperature shutdown limits are 170°C for the motor, 90°C for the heat sink, and 80°C for the batteries (measured at middle of battery pack).

2) Undervoltage - the voltage input signal was simulated for this test. When the voltage signal was brought below the minimum limit, 96 volts, the drive was shut down and a fault word displayed.

3) Overvoltage- this test verified that motor regeneration torque was reduced to hold bus voltage to 162 volts maximum. If a sudden overvoltage occurs the driver will shut down at about 165 volts.

4) Overspeed - this test verified that as motor speed increased past the maximum speed of 150 Hz, the torque is limited by decreasing slip. If speed continues to increse above 160 Hz, the slip goes negative to produce regen braking torque until bus voltage reaches its maximum 165 volts, at which point the drive shuts down.

5) Loss of speed sensor - this test verifies that when the speed sensor is disconnected the motor slows gracefully to a stop.

6) Loss of base drive signal - this test showed that with the loss of base drive signals to one leg the motor will operate in single phasing with reduced torque. No damage occurs.

7) Loss of main bus power - this test verified that the drive shut down smoothly when main bus power was removed with drive operating.

8) Loss of energy recovery circuit - this test verified that when power to the energy recovery circuit was removed the drive shut down smoothly.

9) Loss of controller power - this test verified that when power to the controller was removed the drive shut down gracefully.

10) DC bus overcurrent - using a simulated current input the shutdown limits on DC bus current were verified to be -352 amps and +352 amps. These are programmable as required.

11) Loss of energy recovery bus over voltage (ERBOV) signal - the ERBOV signal was simulated to verify that the drive shut down when the signal was brought low or disconnected.

12) Brakes - with either emergency or parking brake on, the drive will not be enabled. This was simulated with switches.

13) Accelerate or decelerate pot inputs - either pot turned past its maximum input limit, 4.5 volts, will shut down drive. This is equivalent to losing the ACCEL or DECEL commands from the driver acceleration or brake pedal respectively.

APPENDIX G - SYMBOL TABLE

alternating current	ac (a-c)
ampere	amp
British thermal units	Btu
centimeter	cm
digital to analog converter	DAC
degrees Celsius (centigrade)	°C
degrees Fahrenheit	°F
direct current	dc
farad	f
foot	ft
stator frequency	F.S.
hertz (cycle per second)	Hz
horsepower	hp
hour	hr
transistor collector current	I_C
inch	in.
inch-pound	in-lb
kilogram	kg
kilometer	km
kilovolt-ampere	kVA
meter	m
microprocessor	µP
miles per hour	mph
millimeter	mm
minute	min
ohm	Ω
phase-locked loop	PLL
pound	lb
pounds per square inch	psi
Pulse-Width Modulation	PWM
quasi-square-wave	QSW
radian	rad
revolutions per minute	rpm
silicon controlled rectifier	SCR's
Safe Operating Area	SOA
second	sec
tangent	tan
transaxle output torque meter	TATM
temperature	temp.
transistor under test	TUT
transistor collector to emitter voltage	V_{CE}
scaled rotor frequency voltage	VFRS
volt	V
watt	W

REFERENCES

1. "ac Propulsion System for an Electric Vehicle," Geppert, S., Proceedings Convergence '80, 9/15-18/80, Detroit, MI (DOE).

2. "Electric Vehicle ac Drive Development," Plunkett, Kliman, SAE 80061.

3. "PWM Inverter Induced Harmonic Effects in ac Motor," Frederick, W. and Klein F., IEEE IAS Paper #SPC-THU-AM 1007.

4. "A Pulse Width Modulated Three-phase Inverter," Dewan, S. B. and Forsythe, J. B., IGA Conference Record 1971.

5. "SPICE2: A Computer Program to Simulate Semiconductor Circuits," L. W. Nagel, Memorandum No. ERL-M520, May 9, 1975, University of California, Berkeley, Ca.

6. User's Guide to the Hybrid and Electric Advanced Vehicle Systems (HEAVY) Simulation, Hammond, R. A., R. K. McGehee, Boeing Computer Services Company, (Preliminary), 1980.

7. "Development of a Modulation Strategy for a PWM Inverter Drive," Kliman, G. B., A. B. Plunkett, IEEE Transactions on Industry Applications, Vol. 1A-15, No. 1, January/February, 1979.

8. Induction Machines, Alger, P. C., Gordon and Breach Science Publishers, 2nd Ed., New York, 1970.

9. "Simulating Power Electronic Systems - A New Approach," J. G. Kasakian, Proceedings of the IEEE, Vol. 67, No. 10, Oct. '79.

10. "Automatic Analysis of McMurray's PWM Inverters," G. Indri, P. Tenti, Alta Frequenza, Vol. XLVII-N.9, Sept. '78.

11. "SPICE Version 2F.1 User's Guide," A. Vladimirescu, A. R. Newton, D. O. Pederson, University of California, Berkeley, Ca.

12. "An Integral Charge Control Model of Bipolar Transistors," H. K. Gummel, H. C. Poon, The Bell System Technical Journal, May-June, 1970.

13. Extended SCEPTRE Volume I User's Manual, D. Becker, AFWL-TR-73-75, Vol. 1, Distributed by National Technical Information Service, June 30, 1974, U. S. Dept. of Commerce.

14. SCEPTRE: A Computer Program Circuit and Systems Analysis, J. C. Bowers, S. R. Sedore, Prentice Hall, Inc., Englewood Cliffs, New Jersey, 1971.

15. "Modeling the Bipolar Transistor," I. Getreu, Electronics, September 19, 1974.

16. "Selection of Snubbers and Clamps to Optimize the Design of Transistor Switching Converters," W. McMurray, IEEE Transactions on Industry Applications, Vol. IA-16, No. 4, July/August 1980.

17. "Impact of Propulsion System R&D on Electric Vehicle Performance and Cost," Schwartz, H. J. and Gordon, A. L., Paper delivered at EV EXPO '80, St. Louis, May 20-22, 1980.

18. "Electric and Hybrid Vehicle Cost Handbook," (Review Draft) #5030-182, Rev. A., Heft, R. C. and Heller, S. C., Jet Propulsion Laboratory, California Institute of Technology, Pasadena, California, January 1979.

19. "Near-Term Electric Vehicle Program Phase I, Final Report," Rowlett, B. H. et al, AiResearch Manufacturing Co. of California, August 1977, NTIS #SAN/1213-1, pp. 11-6-1 to 11-6-8.

1. Report No.	2. Government Accession No.	3. Recipient's Catalog No.
NASA CR-165480		

4. Title and Subtitle	5. Report Date
AC PROPULSION SYSTEM FOR AN ELECTRIC VEHICLE - PHASE 1 FINAL REPORT	August 1981
	6. Performing Organization Code: 778-36-06
7. Author(s): Steven Geppert	8. Performing Organization Report No.: ERC TR-8101
	10. Work Unit No.
9. Performing Organization Name and Address: Eaton Corporation, Engineering & Research Center, 26201 Northwestern Hwy., P. O. Box 766, Southfield, MI 48037	11. Contract or Grant No.: DEN 3-125
	13. Type of Report and Period Covered: Contractor Report
12. Sponsoring Agency Name and Address: U.S. Department of Energy, Office of Vehicle and Engine R&D, Washington, D.C. 20546	14. Sponsoring Agency ~~Code~~ Report No.: DOE/NASA/0125-1

15. Supplementary Notes

Final report. Report prepared under Interagency Agreement DE-AI01-77CS51044. Project Manager, R. F. Soltis, Transportation Propulsion Division, NASA Lewis Research Center, Cleveland, Ohio 44135.

16. Abstract

A functional prototype of an electric vehicle ac propulsion system was built consisting of a 18.65 kW rated (25 hp) ac induction traction motor, pulse-width modulated (PWM) transistorized inverter, two-speed mechanically-shifted atuomatic transmission, and an overall drive/vehicle controller. Total prototype system weight is 185 kg (407 lb.). Design considerations, developmental steps, and test results of individual components and the complete system on an instrumented test frame are described. Overall DC-to-mechanical system efficiency varied from 67% to 82% as axle speed/torque varied from 159 RPM/788 Nm to 755 RPM/328 Nm. Detailed computer models were developed for the inverter, motor, and a representative vehicle. Simulation results compared with experimental data are described. A preliminary reliability model and failure-modes-effects-analysis are given. The inverter cost is the primary challenge for this system's viability. A minimum nominal battery voltage of 144 volts is required for system feasibility.

17. Key Words (Suggested by Author(s))	18. Distribution Statement
Electric vehicle; Alternating current; Propulsion system; Drivetrain; Inverter	Unclassified - unlimited STAR Category 44 DOE Category UC-96

19. Security Classif. (of this report)	20. Security Classif. (of this page)	21. No. of Pages	22. Price*
Unclassified	Unclassified		

* For sale by the National Technical Information Service, Springfield, Virginia 22161

*USGPO: 1981 — 559-091/3213

End of Document